NARCCAP Model Assessment and Future Projections for the Southeast United States

by

Erik David Kabela

Bachelor of Science
Valparaiso University, 2004

Master of Science
Iowa State University, 2006

Submitted in Partial Fulfillment of the Requirements

For the Degree of Doctor of Philosophy in

Geography

College of Arts and Sciences

University of South Carolina

2012

Accepted by:

Gregory Carbone, Major Professor

Susan Cutter, Committee Member

Brian Habing, Committee Member

Cary Mock, Committee Member

Lacy Ford, Vice Provost and Dean of Graduate Studies

DEDICATION

This work is dedicated to my beautiful and loving wife, Megan, my daughter, Abigail, and my soon-to-be-born child for supporting me and continually sacrificing while I pursued by doctorate over the past four and a half years. This work is also dedicated to my parents, Dave and Joan Kabela, in recognition of their continued love, support, and words of encouragement.

ACKNOWLEDGEMENTS

First and foremost, I would like to thank my advisor, Dr. Greg Carbone, for his guidance, patience, and support throughout my time at the University of South Carolina, specifically (but not limited to) this research and the writing of this dissertation. His insights and words of encouragement have often inspired me and renewed my hopes for completing my graduate education. I would also like to thank my committee members for their efforts and contributions to this work and providing valuable lessons during coursework: Drs. Susan Cutter, Brian Habing, and Cary Mock. Thank my master's degree advisor from Iowa State University, Dr. Brian Hornbuckle, for his continued support while I sought my doctorate. Thank you to members, past and present, of the Carolinas Integrated Sciences and Assessment group for their continued curiosity, interest, and support in my doctoral research.

Thank you to management at the Savannah River National Laboratory who allowed modification of my work schedule so that I could pursue my doctorate. Specifically, I would like to thank Chuck Hunter for working through several issues and going to bat for me throughout my doctoral pursuit. Thank you to Dr. Steve Chiswell for always lending an open ear and allowing me to discuss thoughts, ideas, and frustrations. Steve's knowledge, expertise, and great sense of humor made coming to work an enjoyable experience. Thank you to Matt Parker for providing me a great mentor/mentee experience while at SRNL. Matt's guidance has helped to shape my personal and

professional goals, and for that, I am truly grateful. Many thanks go out to all the members of the Atmospheric Technologies Group and the SRS Emergency Management Section for all of their support, words of encouragement, and motivation.

I would like to thank my sister, Kerri, for her love and support, and always pushing me to be better at anything I am pursuing. Finally, I want to thank my parents-in-law, Dr. Vince and Susan Bolton, for all of their love, support, and words of encouragement.

ABSTRACT

Global climate models (GCMs) provide most climate change projections, but their coarse resolution must be downscaled to more local scales in order to conduct meaningful climate impact assessments. This dissertation investigates dynamically downscaled regional climate model (RCM) output from the North American Regional Climate Change Assessment Program (NARCCAP) in the Southeast United States. Analysis uses a suite of statistical measures to assess model skill in hindcasting minimum and maximum temperature and mean precipitation during an historical reference period, 1970-1999. It identifies model biases and sheds light on their causes. Most models demonstrated high skill for temperature during the historical period. Two outliers included two RCMs run using the Geophysical Fluids Dynamics Lab (GFDL) model as their lateral boundary conditions; these models suffered from a cold maximum temperature bias, attributed to erroneously high soil moisture. Precipitation skill showed mixed skill – relatively high when measured using a probability density function overlap measure or the index of agreement, but relatively low when measured with root-mean square error or mean absolute error, because several models overestimate the frequency of extreme precipitation events. Downscaling generally improves projections of minimum temperature and mean precipitation at local scales for RCMs run with the Community Climate Model (CCSM) and Candian Global Climate Model version 3

(CGCM3), while adding value for CCSM-based runs with respect to maximum temperature.

The historical analysis set the stage for interpreting future projections (2040-2069) of minimum and maximum temperature and mean precipitation change, and helps to quantify associated uncertainties in these scenarios. Projected minimum temperatures show an ensemble mean increase between 1° and 2°C in the winter and early spring, and an increase between 2° and 3°C for all other months. Maximum temperatures show an ensemble mean increase between 1° and 2°C in winter and early spring with increases between 2° and 4°C from mid spring through fall. Precipitation increases up to 10% in the eastern part of the region from late summer through early spring. Ensemble mean decreases of up to 10% occurred in January, April, June, and July. In western portions, precipitation increases up to 10% in January through March, May, August, September, and November with an up to 12% decrease in precipitation in March, May through July, and October. This work provides users of NARCCAP data with indepth validation of commonly used climate variables from several ensemble members against observations, determines the "value added" by RCMs in the downscaling process, and assesses atmospheric processes internal to each RCM which feed back into the climate system. Additionally, recommendations are made for selecting NARCCAP members based on the intended assessment by stakeholders of climate information. Lastly, this work serves as a template for the type of indepth analysis needed for climate models to provide added confidence in a models' ability to simulate all aspects of the climate system.

TABLE OF CONTENTS

LIST OF TABLES

LIST OF FIGURES

LIST OF SYMBOLS

Q_i	Amount of energy absorbed by the system (such as the atmosphere).
R	Amount of radiation emitted by the system.
C	Sensible heat flux.
λE	Latent heat flux.
S_{score}	Perkins' PDF-based model skill score.
n	Number of bins used to calculate the PDF in Perkins' skill score method. Number of values in Willmott's index of agreement and root mean squared error.
Z_m	Frequency of values in a given bun from the model
Z_o	Frequency of values in a given bin from the observed data.
d_r	Willmott's index of agreement.
P_i	Predicted values (model) used in Willmott's index of agreement.
O_i	Observed values used in Willmott's index of agreement.
$\bar{O}$	Observed mean used in Willmott's index of agreement.
$RMSE$	Root mean squared error.
MAE	Mean absolute error.
y_i	Observed values in RMSE and MAE calculations.
$\hat{y}_j$	Modeled values in RMSE and MAE calculations.

x	Represents a single NARCCAP ensemble member used to calculate the Euclidean distance in the hierarchical cluster scheme.
y	Represents another single NARCCAP ensemble member used to calculate the Euclidean distance in the hierarchical cluster scheme.
x_k	Raw data contained within x.
y_k	Raw data contained within y.
K	Number of geometric dimensions used to calculate the Euclidean distance in the hierarchical cluster scheme.
ΔT	Change in temperature from the historical reference period to the future.
T_{fut}	Future mean temperature.
T_{ref}	Historical reference period mean temperature.
ΔP	Change in precipitation from the historical reference period to the future.
P_{fut}	Future mean precipitation.
P_{ref}	Historical reference period mean precipitation.
$mean_w$	Weighted ensemble mean change for temperature and precipitation.
$mean_n$	Unweighted mean change from the n^{th} ensemble member.
w_n	Weight garnered from Perkins' skill score, Willmott's index of agreement, or RMSE.

List of Abbreviations

AR4 ..... IPCC Fourth Assessment Report

ASOS ..... Automated Surface Observing System

AU ..... Approximately Unbiased p-value

BP ..... Bootstrap Probability

CCSM ..... NCAR Community Climate Model

CDO ..... Climate Data Operators

CGCM3 ..... Canadian Global Climate Model version 3

CISA ..... Carolinas Integrated Sciences and Assessment

COTS ..... Commercial-Off-The-Shelf

CRAN ..... Comprehensive R Archive Network

CRCM ..... Canadian Regional Climate Model

DOE ..... Department of Energy

ECP2 .....Experimental Climate Prediction Center Regional Spectra Model version 2

ENSO ..... El Niño-Southern Oscillation

GCM ..... Global Climate Model

GFDL .....Geophysical Fluid Dynamics Laboratory

GrADS ..... Grid Analysis and Display System

HadHCM3..... Hadley Centre Climate Model version 3

IPCC..... Intergovernmental Panel on Climate Change

IQ ..... Inner-Quartile

LBC..... Lateral Boundary Conditions

LLNL ..... Lawrence Livermore National Laboratory

MAD ..... Mean Absolute Deviation

MAE..... Mean Absolute Error

MAGICC..... Model for the Assessment of Greenhouse-gas Induced Climate Change

mb ..... millibar

MM5 ..... Mesoscale Model version 5

MM5I ..... MM5 run by Iowa State University

MDS..... Multidimensional Scaling

NARCCAP..... North American Regional Climate Change Assessment Program

NARR ..... North American Regional Reanalysis

NCAR ..... National Center for Atmospheric Research

NCEP ..... National Centers for Environmental Prediction

netCDF..... network Common Data Format

NMDS..... Non-metric Multidimensional Scaling

PCMDI ..... Program for Climate Model Diagnosis and Intercomparison

PDF ..... Probability Density Function

PSU ..... Penn State University

RCM ..... Regional Climate Model

RCM3 ..... Regional Climate Model version 3

REA ..... Reliability Ensemble Averaging

RMSE ..... Root Mean Squared Error

SCENGEN ..... SCENario GENerator

SRES ..... Special Report on Emissions Scenarios

SS ..... Perkins' skill score

UQAM ..... Université du Québec á Montréal

US ..... United States

WCRP ..... World Climate Research Program

WGCM ..... Working Group on Coupled Modeling

WRF ..... Weather Research and Forecasting model

CHAPTER 1

INTRODUCTION

How skillfully can climate models simulate regional temperature and precipitation? What do climate models project for future regional temperature and precipitation in the Southeast United States? This dissertation addresses these questions, ones that decision makers increasingly face as they consider climate change impacts in their assessments. These are also questions asked by water resource managers (Vorosmarty, et al., 2000), agricultural engineers and farmers (Tubiello et al., 2007; Kruijt et al., 2008), and forest managers (Shem et al., 2010) when they want to gauge impacts of potential temperature or precipitation changes in order to make informed decisions regarding mitigation and adaptation actions. Officials with multiple scales of interest from local municipalities, to state decision makers, to regional and federal authorities all require information on future climate change to determine appropriate adaptive measures (Smith et al., 2009), calculate adaptive capacity (Brooks et al., 2005), and determine limits of adaptive capacity at their scale of interest (Adger et al., 2009) rather than attempting higher risk and higher cost mitigation efforts (Pielke et al., 2007). Additionally, the Intergovernmental Panel on Climate Change (IPCC) calls for reliable estimates of expected impacts under projected climate change while seeking to gain trust in climate models, improve decision scenarios, build awareness of issues surrounding future climate, and increase dialog between stakeholders with knowledge to share (such as researchers) and with the wider public (Parry et al., 2007). Central to the problem of

making adaptation policy, especially at the local scale, is the spatial resolution at which readily available climate change information is presented and the limited predictability of some relevant climate variables (Cutter et al., 2012). Most global climate models (GCMs) have spatial resolution of 100 kilometers or more – relatively coarse with respect to surface-based processes influenced by climate. Figure 1.1a provides an illustration of this point with the dark black box in the center of the image representing one grid point from a GCM.

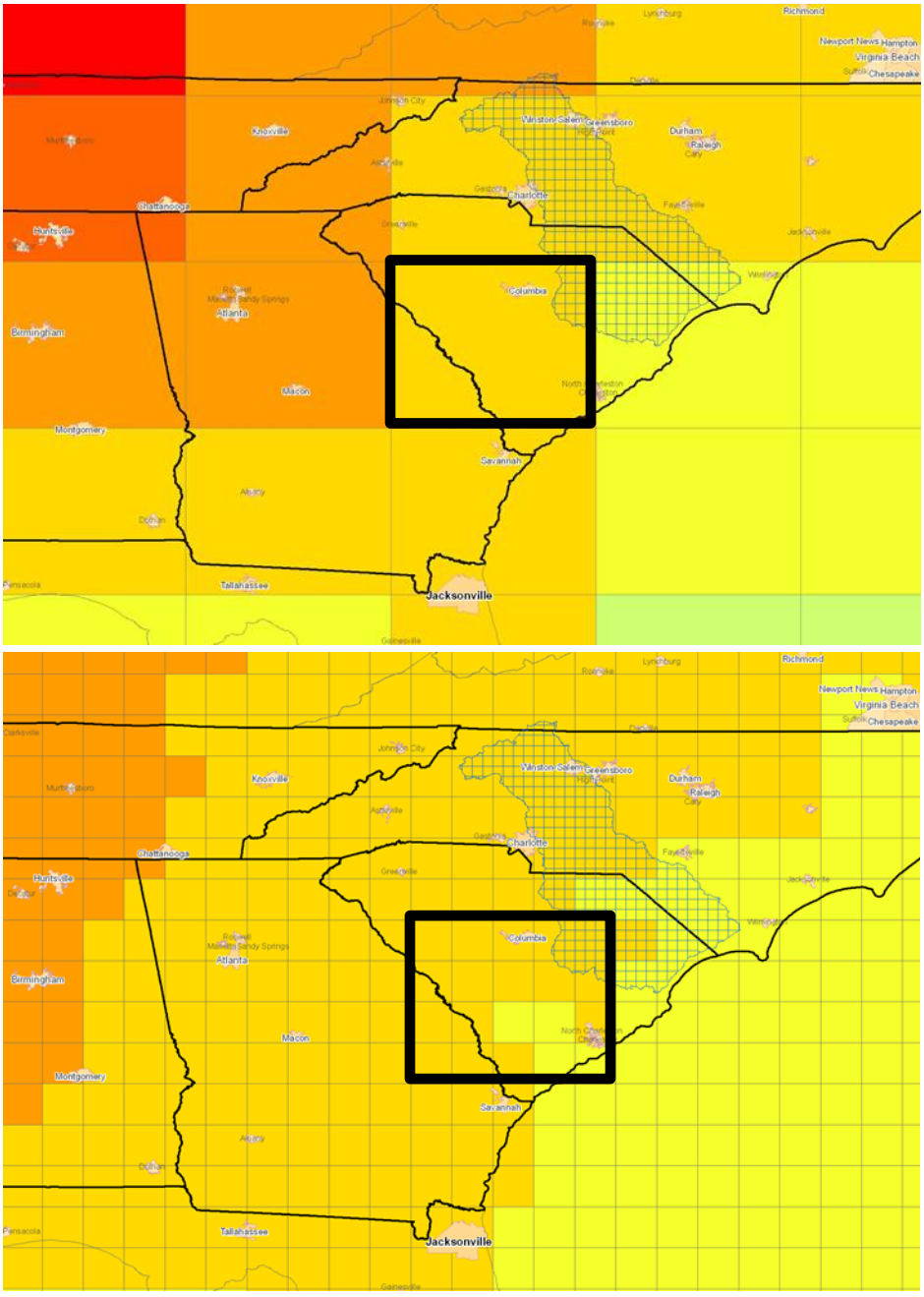

Figure 1.1. Example of grid resolution from a coarse resolution global climate model (a) and a high resolution regional climate model (b). The bold black box represents one grid point from the global climate model.

For this reason, two main types of "downscaling" are used to transfer GCM information to a local and appropriate scale. The first is a physical/dynamical approach

using regional climate models (RCMs) nested within, and driven by GCMs (e.g. Gao et al., 2011; Pan et al., 2011). The second is a statistical approach (e.g. Hewitson and Crane, 1996) wherein translation to local scales is based on the historical relationship between coarse GCM output and local-scale climatology. Figure 1.1b provides illustration of the resolution obtained through downscaling to higher resolution relative to GCM resolution. In this instance, twenty-times higher resolution (i.e., 20 RCM grid points are contained within one GCM grid) is achieved through the downscaling process with features such as coastlines and complex topography better resolved in comparison to GCMs. Most RCMs are run at resolutions of 25 to 50 kilometers and run with a one-way nested grid in which the large-scale GCM provides lateral boundary conditions (LBCs) for the smaller-scale RCM (Figure 1.2). This approach is called a one-way nested grid because the GCM provides boundary conditions to the RCM but the RCM does not feedback information to the GCM.

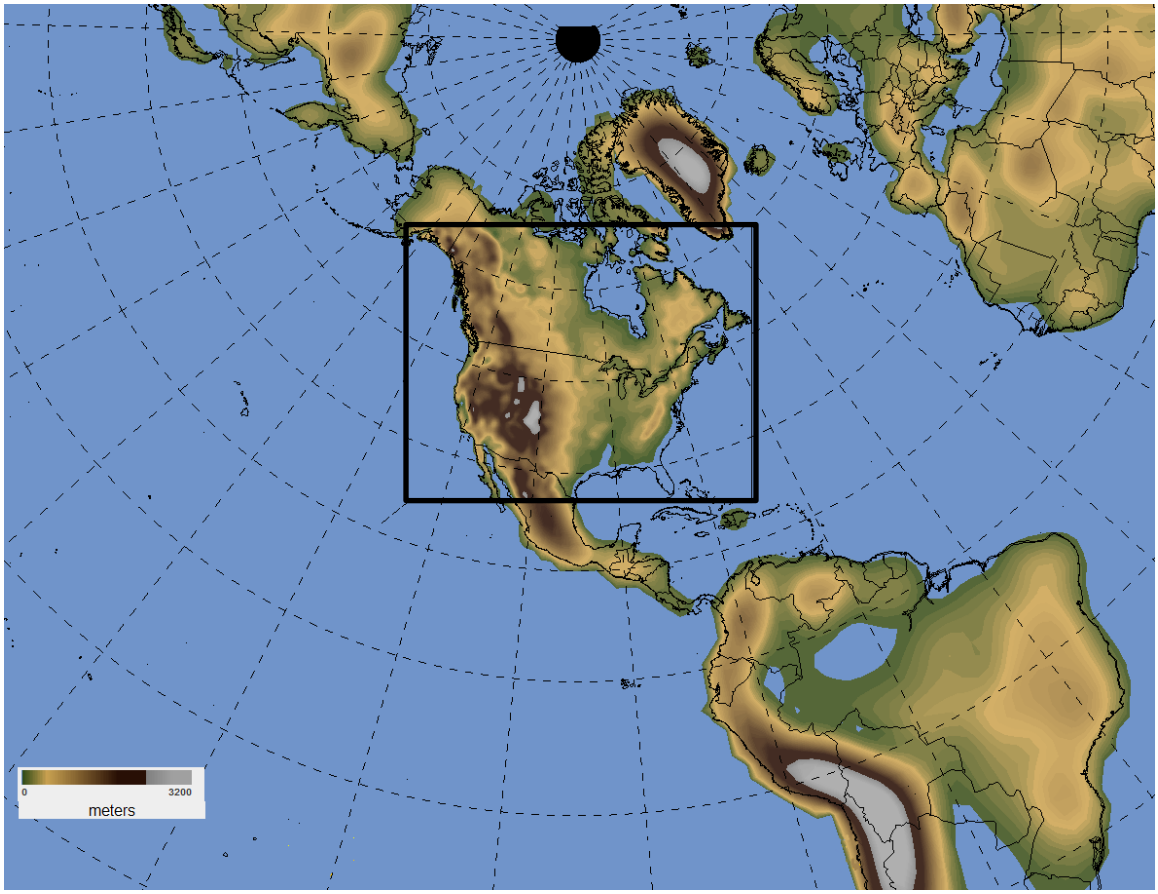

Figure 1.2. Representation of a regional climate model domain (black box) nested within a global climate model.

Regional scenarios from the RCMs are only as good as the GCM providing LBCs, accounting for the largest amount of uncertainty in climate change projections (Deque et al., 2007; Jacob et al., 2007). Additionally, each RCM differs in their physical handling of complex atmospheric processes, adding another layer of uncertainty to climate change projections at local scales, which according to Giorgi (2006), accounts for the second largest source of uncertainly. An example of this increased uncertainty occurs in the summer months when convective precipitation is the primary mode of precipitation and results from the differing cumulus parameterizations each RCM uses. Another

disadvantage of running RCMs is the high expense associated with model run-time and large amount of computational resources required to run the model. The main advantage of the RCM is its physically-based approach incorporating governing equations of conservation of momentum, mass, moisture, and energy, as well as the inclusion of surface processes and land-atmosphere interactions, processes which large-scale GCMs have difficulty resolving. This allows the model to produce results that are physically meaningful at a small scale.

Statistically downscaling GCM output requires deriving a relationship between a micro-scale observed variable from either a gridded dataset or raw surface station data to a GCM variable. For example, a relationship may be obtained between 500-mb geopotential height and observed surface temperature for the reference climate. A transfer function such as multiple linear regression (Kidson and Thompson, 1998; Zhang, 2005; Lim et al., 2007; Semenov and Stratonovitch, 2010) is used to find a relationship between the observed variable and GCM variable. Other examples of transfer functions include principal components analysis (Zorita and von Storch, 1998; Gangopadhyay and Clark, 2005), correlation analysis (Zorita and von Storch, 1998), analogue methods (Zorita and von Storch, 1998), and artificial neural networks (Zorita and von Storch, 1998). Once a relationship with a supporting transfer function is established, future GCM values are used to drive the relationship for future micro-scale climate. The advantage of this method is that, unlike dynamically downscaled approaches, statistically downscaling global climate models requires less time and computational hardware. The drawback of statistical downscaling is the relationship developed for the transfer function is based on the observed climate and may not be representative of future relationships.

1.1 RESEARCH QUESTIONS

Two general research questions structure the dissertation:

- How skillful are dynamically downscaled models in simulating minimum and maximum temperature and mean precipitation in the reference period (1970-1999) for the Southeast United States? What are their biases? Does downscaling provide "value added" at local scales?
- What are future projections (2040-2069) of minimum and maximum temperature and mean precipitation change for the Southeast United States?

Characterization of climate model forecast skill begins with determining how closely models output matches observations. Model skill matters to stakeholders utilizing climate model output for risk assessments of climate extremes from the local scale (Cutter et al., 2012) to the national scale. Assessing model skill, performing model validation, and determining model bias increases stakeholder's confidence in future projections (Seneniratne et al., 2012), provided the model performs well. Additionally, it is extremely important to determine if downscaling global climate model data adds value beyond using global climate model output directly. If information gleaned from a GCM provides skillful results, the need to further downscale this information is moot; however, if value is added through the downscaling process, the users of RCM output stand to benefit. Few prior studies have evaluated whether downscaling adds value to impact analysis. Castro et al. (2005) provides one of the first comprehensive reviews of assessing value added through dynamical downscaling with another recent study performing an assessment for Europe (Feser et al., 2011). Castro et al. (2005) define "value added" as the amount of additional information the RCM can provide beyond the highest resolved

wavelength of the global model. In other words, downscaling should improve the physical representation of the atmosphere at scales resolved by the RCM when compared to observations. Additionally, Castro defines the concept of "value retained", which describes how well the RCM maintains consistency with the large-scale behavior of the LBCs.

Within the last few months two studies by Di Luca have utilized the North American Regional Climate Change Assessment Program (NARCCAP; Mearns et al., 2009) data to determine if value is added (Di Luca et al., 2012a; Di Luca et al., 2012b) for a small number of the ensemble's members. Di Luca et al. (2012b) conclude that none of the five NARCCAP models used in their study provide physically significant improvement to winter-time temperature and only two models provide limited improvement in the summer for the Southeast U.S. For winter precipitation, only the RCM3-GFDL, RCM3-CGCM3, and CRCM-CGCM3 models provided improvement while the RCM3-GFDL and RCM3-CGCM3 provided improvement in summer-time precipitation, however, this improvement is limited to only the eastern portion of the region. Both Di Luca pieces point out that the potential value added through downscaling temperature and precipitation is mostly constrained to coastal regions and areas where complex topographic features (e.g., Appalachian and Rocky Mountains) have large influence on the local scale.

1.2 ESTABLISHING SKILL IN DOWNSCALING

A recent study by Schoof et al. (2009; hereafter, Schoof) aimed to determine which methods of downscaling (dynamical or statistical) were superior to the other and

which provided skillful and meaningful results for the Southeast U.S. Schoof produced hindcasts of mean temperature and precipitation using both downscaling approaches and found, overall, precipitation hindcasts were less skillful than temperature hindcasts. Skill was evaluated using the root mean square error of mean temperature and precipitation against climatological data. This result makes intuitive sense from the perspective that temperature is closely aligned with the prevailing meso- and synoptic-scale pattern, scales at which GCMs excel, and are better translated in a downscaling approach than the complex nature of precipitation initiation, especially convective precipitation initiation. Schoof found no indication that either method of downscaling provided a direct advantage over the other, a finding echoed by Murphy (1999). Although this dissertation does not incorporate statistically downscaled climate data, this work does utilize a multi-model ensemble of dynamically downscaled models, a recommended approach by Pierce et al. (2009) and Knutti et al. (2010) as best practices for presentation of regionally projected climate change scenarios.

Ensemble approaches to dynamically downscaled projections have mostly been confined to the European realm with the PRUDENCE (Christensen and Christensen, 2007) and ENSEMBLES (Hewitt and Griggs, 2004) projects as examples. In 2009, a consortium within North America developed a dynamically downscaled climate dataset dubbed the North American Regional Climate Change Assessment Program (NARCCAP). NARCCAP is an international program to produce high resolution climate change simulations in order to investigate uncertainties in regional scale projections of reference and future climate. Additionally, the project's aim was to generate climate

change scenarios for use in impacts research (NARCCAP webpage, http://www.narccap.ucar.edu/).

A number of publications have explored NARCCAP model output for various regions of the United States including the intermountain West (Wang et al., 2009), the southern Colorado Rockies (Rangwala et al., 2012), the Colorado River Basin (Gao et al., 2011), the upper-Mississippi River Valley (Takle et al., 2010), the Lake Winnipeg watershed (Shrestha et al., 2011), greater Vancouver, Canada area (Hambly et al., 2012), and a general analysis of the entire NARCCAP modeling domain (Schliep et al., 2009). One study used a small number of NARCCAP ensemble members to evaluate performance during a historical reference period for the Southeast U.S. (Shem et al., 2010). However, this study did not provide the breadth or depth needed to fully evaluate as many NARCCAP ensemble members as possible and provide comprehensive and detailed future climate model projections.

Work recently published by Sobolowski and Pavelsky (2012) evaluated six NARCCAP ensemble members for the Southeast United States during a historical reference period (defined by them as 1970-2000). Using the reliability ensemble averaging (REA) technique developed by Giorgi and Mearns (2003), Sobolowski and Pavelsky reduced uncertainty in future projections of seasonal temperature and precipitation by weighting projected change according to how skillful the models were in the reference period, accounting for model bias relative to observations, and determining how close future projections for each model was to the multi-model mean.

1.3 STUDY AREA

There are two drawbacks to Schoof's study which will be addressed in this dissertation: 1) Schoof's use of the states of Alabama, Georgia, and Florida to narrowly define the Southeast U.S. This dissertation will encompass what is traditionally thought as the Southeast U.S., which are the states of Alabama, Georgia, Mississippi, North Carolina, South Carolina, and Tennessee; and 2) Schoof utilizes only one dynamically and one statistically downscaled model.

Climatologically, the Southeast U.S. is classified as humid subtropical (Cfa) in the Köppen climate classification system, is characterized by hot, humid summers and cool winters. The coldest month's mean temperature is between -3°C and 18°C with the hottest month's mean above 22°C with no pronounced dry season (thus the "f" in "Cfa"). Winter rainfall is associated with large-scale driven storm systems with frequent passage of mid-latitude cyclones and associated wide-spread precipitation while the summer months are marked by convective (thunderstorms), locally-driven storms with an occasional tropical storm or hurricane impacting the region.

The Southeast United States is the focus region for this dissertation because results obtained from this work directly impact projects being conducted by the Carolinas Integrated Sciences and Assessment (CISA) team, whose focus is to work with a variety of stakeholders across North Carolina and South Carolina to incorporate climate information into water and coastal management and related decision-making processes. Efforts include working with decision makers on improving their adaptation to drought, linking climate variability to watershed, landuse, and coastal adaptation planning, and characterizing climate vulnerability in the region. A major area of CISA research centers

on watershed modeling, of which, NARCCAP dynamically downscaled information will be used to drive watershed models used to project impacts of climate change on water availability in the region. In addition to CISA-related efforts, other locations within the Southeast U.S. can use information gleaned from this work to aid in determination of water availability for medium and large metropolitan areas which rely on small watersheds for their water supply (Gavrilles, 2010) and energy needs (World Resources Institute, 2009).

Preliminary analysis conducted to gain familiarity with datasets and methods proposed as part of the dissertation work noted an east-west gradient in future mean temperature and precipitation projections across the Southeast U.S. Due to this gradient, the Southeast U.S. region defined above was split into two sub-regions. Further justification for aggregating the Southeast U.S. into two separate sub-regions accounts for meteorological and climatological micro-, meso-, and synoptic-scale patterns that impact the two sub-regions differently due to the influence of the Appalachian Mountains and Atlantic and Gulf Coasts. These regions are defined as the east region (Georgia, North Carolina, and South Carolina) and the west region (Alabama, Mississippi, and Tennessee). A similar, yet slightly different, east-west sub-division is noted in work conducted by Bukovsky (2011) in which she used NARCCAP data to calculate and categorize regions within the NARCCAP domain. Similar size sub-domains and subsequent analysis to those in this dissertation have been conducted for other regional climate model ensemble assessments (Kjellstrom et al., 2010).

Chapter 2 provides a detailed review of the dynamically downscaled multi-model dataset used for the research, including its creation and purpose, and specific information

related to emission scenario, GCMs used, and spatial and temporal resolution. Additionally, Chapter 2 details the steps taken to format the model data such that each model had the same geospatial projection, the four methods used to calculate model skill, how model bias was determined using multiple metrics, and whether downscaling provides value, the effective number of models needed from an ensemble. Finally, the chapter concludes with an explanation of how future projections of climate change were computed and presented.

Chapter 3 provides detailed analysis of model skill using four statistical measures and providing assessment of model biases. Further, the chapter determines if dynamically downscaling GCM data adds value to climate change projections at local scales over GCMs alone by calculating each of the four skill metrics for the driving GCMs and comparing the values to RCMs driven by each GCM during the reference period. Another aspect of this chapter provides insight into the effective number of models needed from the NARCCAP ensemble to provide meaningful climate change results while maintaining inter-model independence, an aspect several ensemble projects fail to achieve (Masson and Knutti, 2011).

Chapter 4 provides projections of future climate for minimum and maximum temperature, and mean precipitation. A series of tables and maps provide aspects of central tendency change from the ensemble. Additionally, spread about the mean and median will be presented in the form of standard deviation and the inner-quartile values (25^{th} and 75^{th} percentiles, respectively). Finally, ensemble projections will be provided from a smaller ensemble comprised of highly skillful models (determined by four skill metrics) and limited in number by findings about the effective number of models.

Chapter 5 provides summary, key findings, scientific merit and implications of this work to the field of climatology, and suggestions for future work.

CHAPTER 2

DATA AND METHODS

2.1 DATA

The increased need for local and regional climate change projections has fostered several collaborative partnerships to develop diverse downscaling techniques and provide relevant climate model output to decision makers (Stainforth et al., 2007). This dissertation used dynamically downscaled climate data from the North American Regional Climate Change Assessment Program (NARCCAP). Methods to compare observed gridded data to downscaled data for the reference climate involved both qualitative and quantitative methods of assessing spatial differences and model skill to replicate the reference climate, a common practice in climate research (Eum et al., 2012). Described within this section are the dynamically downscaled dataset and the gridded observed and reanalysis datasets used to validate the dynamically downscaled dataset.

2.1.1 DYNAMIC DOWNSCALING

In NARCCAP, investigators generated 50-km regional climate model output using six RCMs coupled with four global climate models as lateral boundary conditions (LBCs). The regional climate models save output approximately every 3-6 hours. Table 2.1 provides the acronyms, full names (with references), the modeling group responsible for providing output, and the GCMs used as lateral boundary conditions for each RCM. In addition to the eight models listed in Table 2.1, data from the Geophysical Fluid

Dynamics Laboratory (GFDL) model timeslice experiment is used to provide a third RCM run with the GFDL GCM. In the timeslice experiments, the atmospheric component of the GCM is run without the full-coupled ocean component of the model. Instead, the boundary conditions for sea surface and ice for the reference period runs are based on observed data, and boundary conditions for the future period runs are derived by perturbing the same observed sea-surface temperature and ice data by an amount based on the results of a lower-resolution run of the full GCM. Excluding the coupled ocean model allows the atmospheric model to be run at a much higher resolution (50-km in this case) because the computational requirements are much lower. This procedure is called a 'timeslice' experiment because it only simulates two slices of time, one for the present (1968-2000) and one for the future (2038-2070), skipping over the time between them. This method saves time and computational resources compared to the usual GCM computation methodology of running one simulation for 100 to 150 years.

Table 2.1. Acronyms, full names with references, and modeling groups of RCMs involved in NARCCAP and this dissertation.[1]

Regional Climate Model	Full name (Reference)	Modeling group	Lateral Boundary Conditions	Number found in percentile plots in Chapter 3
CRCM	Canadian Regional Climate Model (version 4.2.0) (Caya and Laprise, 1999)	Ouranos/UQAM	CCSM CGCM3	8 7
ECP2	Experimental Climate Prediction Center Regional Spectral Model (Juang et al., 1997)	University of California-San Diego / Scripps	GFDL	3
MM5I	MM5 – PSU/NCAR Mesoscale Model (version 5) (Grell and Stauffer, 1993)	Iowa State University	CCSM	1
RCM3	Regional climate model (version 3) (Giorgi et al., 1993)	University of California-Santa Cruz	CGCM3 GFDL	6 2
WRFG	Weather Research and Forecasting model (Leung et al., 2005)	Pacific Northwest National Laboratory	CCSM CGCM3	4 5

[1] Column 4 indicates the lateral boundary conditions (LBCs)/GCMs used to drive each RCM. Column 5 provides a reference to the number found on the percentile plots in Chapter 3.

The domain of each regional climate model includes the contiguous United States, Canada, and northern Mexico (Figure 2.1). Each model differs in expressions of dynamic processes, including cumulus parameterization, number of vertical levels within the model, dynamics packages, and land-surface process treatments. Table 2.2 provides a comprehensive breakdown of the characteristics of each NARCCAP ensemble member.

GCMs used as boundary conditions were generated for the International Panel on Climate Change's (IPCC) Fourth Assessment (IPCC, 2007) by the World Climate Research Program's (WCRP's) Working Group on Coupled Modeling (WGCM) and hosted on a server at Lawrence Livermore National Laboratory's (LLNL) Program for Climate Model Diagnosis and Intercomparison (PCMDI, 2010). For this dissertation, the lone NARCCAP RCM run with the HadCM3 GCM as its LBC was excluded because at of the time of analysis, no other NARCCAP model(s) utilized HadCM3's LBCs. To provide a consistent, meaningful, and robust analysis, it was important for multiple models to share the same LBCs.

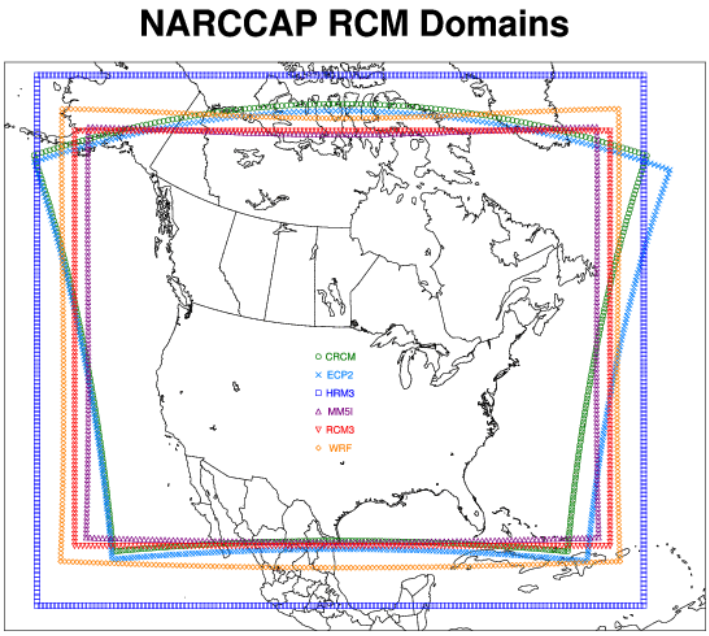

Figure 2.1. Modeling domain for each of the six NARCCAP regional climate models. Courtesy of the North American Regional Climate Change Assessment Program (www.narccap.ucar.edu). © UCAR

Table 2.2. Major characteristics of the regional climate models participating in NARCCAP and used in this dissertation.

Modeling Component	CRCM	ECP2	MM5I	RCM3	WRFG
Dynamics	Nonhydrostatic, Compressible	Hydrostatic, Incompressible	Nonhydrostatic, Compressible	Hydrostatic, Compressible	Nonhydrostatic, Compressible
Lateral Boundary Treatment	9 points (Davies 1976); spectral nudging of horizontal wind.	Perturbations relaxed at boundaries; spectral filter	4 points (linear relaxation)	12 points (exponential relaxation)	15 grid points (exponential relaxation)
Land Surface	CLASS	NOAH	NOAH	BATS	NOAH
Thermal/Water Layers	3/3	4/4	4/4	1/3	4/4
Vegetation Types	21 vegetation classes	13 classes	16 classes from USGS SiB model	19 classes	24 classes from USGS
Boundary Layer	Local K, gradient Richardson number formulation	Hong-Pan non-local K	Hong-Pan (MRF) countergradient, non-local K	Non-local K, countergradient flux	Yonsei Univ. (explicit entrainment)
Explicit Moist Physics	Removal of supersaturation	Removal of supersaturation	Dudhia simple ice	SUBEX, prognostic cloud water	Prognostic cloud liquid and ice, rain, snow
Cumulus Parameterization	Mass Flux	Simplified Arawaka-Schubert	Kain- Fritsch2 mass flux	Grell with Fritsch-Chappell closure	Grell
Number of Vertical Levels	29	28	23	18	35
Type of Vertical Coordinate	Gal-Chen scaled-height	Normalized pressure	Sigma	Terrain following	Terrain following
Original Grid Size	160 x 135	161 x 136	154 x 129	160 x 130	155 x 130
Length of Timestep	900 Seconds	100 seconds	120 seconds	150 Seconds	150 seconds

tasmin/tasmax Calculation	timestep	timestep	timestep	3-hourly	hourly
Spectral Nudging	Yes	Yes	No	No	No
Longwave Radiation Scheme	Morcrette (1984)	Chou and Suarez (1994)	RRTM	CCM3	CAM3
Shortwave Radiation Scheme	Fouquart and Bonnel (1980)	Chou (1992)	MM5 cloud scheme (not CCM2)	CCM3	CAM3
Uniform Aerosols?	No	Yes	Yes	Yes	Yes* *(ozone varies)

Modeling runs for NARCCAP were conducted for the "present climate" (1979-2004) with NCEP/DOE Reanalysis II data (Kanamitsu et al., 2002) as boundary conditions as Phase I of NARCCAP and another run in the reference climate (1968-2000) using four GCMs as LBCs comprised Phase II (Mearns et al., 2009). The NCEP/DOE Reanalysis II dataset provides the equivalent of observed data as boundary conditions for RCMs and allows for the assessment of uncertainties and bias from the RCMs alone. NARCCAP runs were also conducted for future climate (2038-2070) using the Special Report on Emissions Scenarios (SRES, Nakicenvoic et al., 2000) A2 emission scenario.

The A2 emission scenario is characterized by a world of heterogeneity with independently operating and self-reliant nations. Self-reliance is defined in terms of less emphasis on economic, social, and cultural interactions between regions. The population in the A2 scenario continuously increases with time, faster than the other emissions scenarios developed for the IPCC Third Assessment Report (IPCC, 2001). Lastly, the A2 emission scenario is characterized by slower and more fragmented technological changes and improvements to per capita income. Figure 2.2 illustrates the carbon dioxide emissions due to fossil fuels and deforestation, carbon dioxide concentrations, and global temperature change with respect to 1990 for the four emission scenarios (A2, B2, A1, and B1). Additionally, Figure 2.3 provides an illustration of the variables which factor into the emission scenarios and how each differs in their economic, environmental, global, and regional aspects.

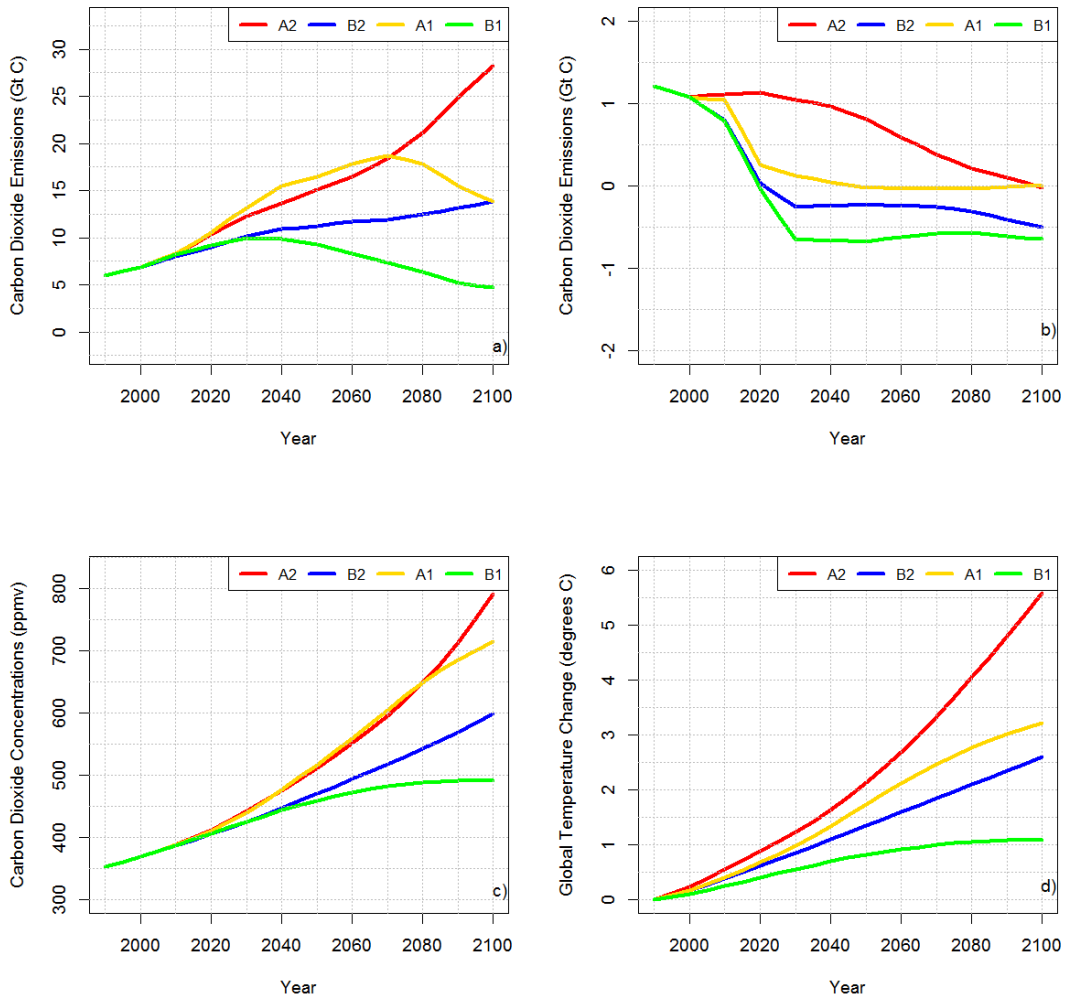

Figure 2.2. Illustration of carbon dioxide emissions from fossil fuels (a) and deforestation (b), atmospheric CO_2 concentrations (c), and global temperature change with respect to 1990 values (d) for the A2, B2, A1, and B1 emission scenarios. Graphics made based on data from the MAGICC/SCENGEN v 5.3 software (http://www.cgd.ucar.edu/cas/wigley/magicc/).

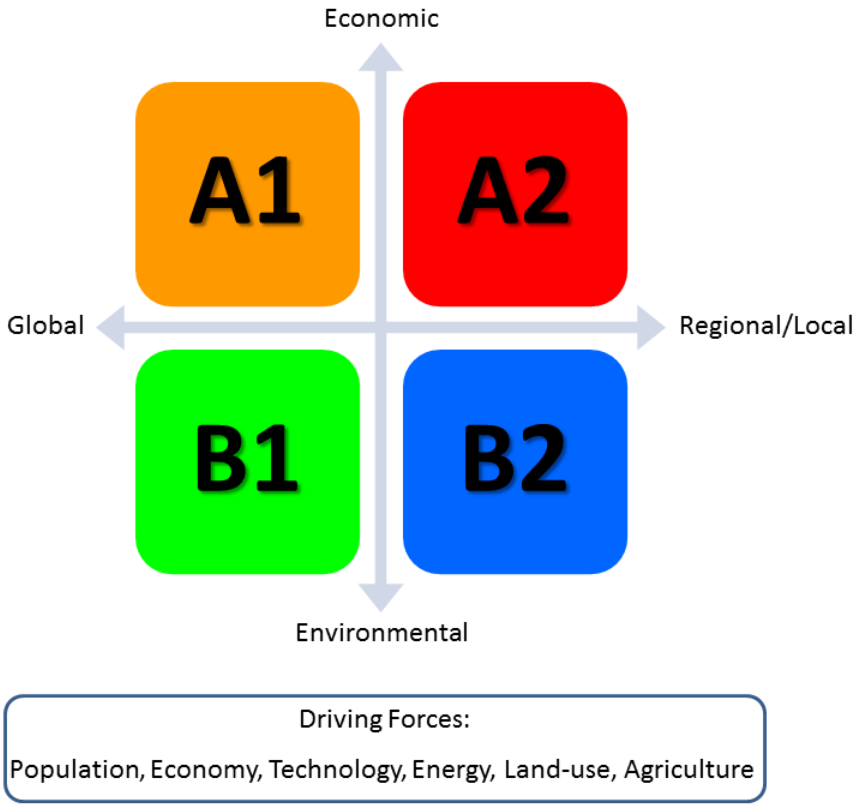

Figure 2.3. Illustration how each of the main SRES emissions scenarios differ from each other in terms of the economic, environmental, global, and regional aspects.

The A2 emission scenario provides projections at the higher end of the SRES scenarios. However, global greenhouse gas emissions from 2000 (when the SRES scenarios were reported) to present, match those observed, and the A2 emission scenario can be considered high-end only if change is not made in the current rate of fossil fuel consumption. Although the forthcoming 5th IPCC assessment (Johns et al., 2011) will include additional emissions scenarios, the A2 emission scenario is still considered among the highest. It also parallels observations during the past 15 years, instilling confidence that it may provide sound projections for future scenario years (2038-2070).

2.1.2 GRIDDED OBSERVED DATASET

A gridded meteorological dataset developed by the University of Washington (hereafter, Maurer dataset) serves as the observed dataset. It is described in Maurer et al. (2002) and available for download at http://www.engr.scu.edu/~emaurer/data.shtml. The Maurer dataset has daily temporal resolution of minimum and maximum air temperature and precipitation from 1950 to 1999 and a spatial resolution of 12 kilometers, covering a domain from 25.125°N to 52.875°N latitude and -124.625°E to -67.000°E longitude. Additionally, the Maurer dataset treats interactions at the land-atmosphere interchange in a way that is physically superior to reanalysis data. Accuracy in calculating land-atmosphere interactions and the energy budget contributes to model bias (a finding which is further explored in Chapter 3).

Unlike reanalysis data, the Maurer dataset does not employ the use of soil moisture ‘‘nudging’’ or adjusting, which results in failed closure of the surface water budget. Maurer et al. (2001) showed that the nonclosure term can be of the same order as other terms (e.g., runoff) in the surface water cycle. Although nudging in reanalysis data is designed to bring the model (especially atmospheric moisture variables) closer to observations, this is done at the expense of other components of the water budget, and complicates studies focused on the interaction and variability of water budget components at the land surface (like temperature and precipitation). Maurer et al. (2000, 2001) argue that physically-based land surface model forced with quality controlled surface variables produce better data for diagnosis of land surface water budget simulations.

2.1.3 GRIDDED REANALYSIS

The National Centers for Environmental Prediction's (NCEP) North American Regional Reanalysis (NARR; http://www.esrl.noaa.gov/psd/data/gridded/data.narr.html) supplements observations of variables not found in the Maurer dataset. It allowed systematic biases of the RCMs by examining variables that may affect temperature and precipitation. Variables from the reanalysis dataset ranged from micro-scale processes at the land-atmosphere interface (soil moisture content, latent heat flux, and sensible heat flux) and free atmosphere (total cloud cover) to meso- and synoptic-scale processes (500-mb height and sea-level pressure). Soil moisture content is expressed as a uniform thickness of water within the soil (in millimeters) and can be equated to the mass of water (in kilograms) contained within a specified area (in square meters) (Kabela, 2006). Latent heat flux is the amount of heat which must be supplied to a system to convert a unit mass of water from one state (solid, liquid, or gas) to another without changing its temperature (Monteith and Unsworth, 2008). Sensible heat flux is the amount of heat needed to change temperature of a system through convection or conduction (Campbell and Norman, 1998). Sensible and latent heat flux are related through the energy balance equation in which the amount of energy entering a system (such as the atmosphere) must equal the energy leaving the system. Equation 2.1 illustrates the major components of the energy balance equation (adapted from Gates, 1980):

$$Q_a = R + C + \lambda E \tag{2.1}$$

where Q_a is the energy absorbed by the system, R is the radiation emitted by the system, C is sensible heat flux, and λE is latent heat flux.

To make a determination on a model's ability to maintain water balance at the surface, a comparison between monthly potential evapotranspiration (PET) and monthly mean precipitation (P) was performed by subtracting P from PET. PET is defined as the amount of water that can be evaporated from land, water, and plant surfaces if soil water were in unlimited supply. Positive values of P-PET indicate moisture surplus while negative values indicate moisture shortfall. PET was estimated empirically, using Thornthwaite's method (Thornthwaite, 1948) that requires only mean monthly temperature and day length as input. Although Thornthwaite's methodology does not account for advection of moist or dry air, but is suitable for estimating potential evaporation outside of arid and semi-arid climates (Mintz and Walker, 1993), providing a reasonably accurate estimate of PET (Palmer and Havens, 1958). Calculation of PET (in mm day^{-1}) utilizing Thornthwaite's methodology follows in Equations 2.2 through 2.4:

$$I = \sum_{i=1}^{n} \left(\frac{T_i}{5}\right)^{1.514} \tag{2.2}$$

$$a = (6.7E-7 * I^3) - (7.71E-5 * I^2) + (1.49E-2 * I) + 0.49 \tag{2.3}$$

$$PET = h\left[16\left(\frac{10T_i}{I}\right)^{a}\right] \tag{2.4}$$

where T_i is the montly mean surface air temperature (°C), I is the montly heat index, a is an empirical exponent based on I, and h is a constant varying by month to account for days per month and duration of sunlight hours. Values of h are found in Table 2.3 for 34°N latitude, which was assumed to be the central latitude for the Southeast U.S. domain as defined in this dissertation.

Table 2.3. Mean possible duration of sunlight at 34°N latitude expressed in units of 30 days of 12 hours each (Thornthwaite, 1948).

Month	*h*
January	0.88
February	0.85
March	1.03
April	1.09
May	1.20
June	1.20
July	1.22
August	1.16
September	1.03
October	0.97
November	0.87
December	0.86

NARR has a temporal resolution from 1979 to the present, available every 3 hours, with a spatial resolution of 32 kilometers (Mesinger et al., 2006). NARR assimilates a vast amount of observational data from ground-based platforms such as the Automated Surface Observing System (ASOS) and ships and buoys, upper-air platforms such as rawinsondes, piballs, dropsondes, and fixed-wing aircraft, and geostationary satellites (Mesinger et al., 2006). The dataset covers a general domain from 12.2°N to 57.3°N latitude and -152.9°E to -49.4E longitude.

2.2 METHODS

To answer the first research question, pertaining to model proficiency and bias, model skill was measured against the Maurer dataset for the Southeast U.S. for monthly minimum and maximum temperature and mean precipitation during the reference period,

1970-1999. It is hypothesized that most NARCCAP ensemble members will prove skillful in reconstructing monthly reference period temperature; however, hindcasts of precipitation will not be a skillful as temperature due mostly to the prescribed nature in which models form precipitation. Skill will be determined through calculation of four metrics: probability density function overlap (Perkins et al., 2007), an index of agreement (Willmott et al., 2011), root mean square error, and mean absolute error, all described fully in this section.

Sobolowski and Pavelsky utilize Perkins et al. (2007)'s method for determining model skill in their calculation of reliable ensemble averaging (REA), however, several differences are noted between their methodology and this dissertation's methodology and include:

- Sobolowski and Pavelsky's use of monthly mean values of temperature and precipitation, arguing monthly mean values illustrate a model's ability to replicate large-scale circulation and low-frequency variability. This dissertation utilizes daily minimum and maximum temperature and mean precipitation and argues daily data values provide insight into a model's ability to replicate conditions and patterns from the micro-scale (10's of kilometers) to the synoptic-scale (1000's of kilometers). Additionally, Sobolowski and Pavelsky's definition of "large-scale" is much too vague and can easily be taken to mean the same thing as the "synoptic-scale", making the distinction between the two fuzzy.
- Sobolowski and Pavelsky "bin" temperature every 2°C while this dissertation bins temperature every 0.5°C, following the methodology outlined by Perkins

et al. (2007). Smaller bin sizes allow for the determination of skill with increased precision while larger bin sizes not only reduce precision but leads to slightly higher skill scores due to smoothing of the probability density function (PDF).

- Sobolowski and Pavelsky chose to assess skill, bias, and present future projections from only six NARCCAP ensemble members while this dissertation utilizes nine members. Assessing a larger number of ensemble members enables users of NARCCAP data a larger pool from which to choose better performing models.
- Lastly, this dissertation utilizes four metrics to assess model skill, arguing that no one skill method provides "the" answer. Conversely, Sobolowski and Pavelsky use only Perkins' method for assessing skill.

To delve further into a model's short-comings, users of climate models must perform detailed analysis beyond looking at the variables of interest such as temperature and precipitation. There is an inherent need to find the systematic biases found in the small and large-scale model processes with particular emphasis on the land-atmosphere interchange (Ma et al., 2011). Here, I examine soil moisture content, which has been shown to impact temperature more so than precipitation (Giorgi et al., 1996) yet has importance in the formation of warm-season convective rainfall (Pielke, 2001; Koster et al., 2003), and cloud cover. Cloud cover is of particular interest because of its broad reaching impacts to not only temperature and precipitation, but more importantly to surface fluxes (latent and sensible) and well as evapotranspiration and atmospheric albedo (Lawrence and Chase, 2012). Additionally, the large-scale processes passed from

the parent GCM to the regional climate model have as much of an impact on the model's skill as micro-scale processes (Ray et al., 2010), necessitating exploration of variables such as 500-mb height and sea-level pressure. Lastly, to aid in determining model bias, percentile plots were created for minimum and maximum temperature and mean precipitation for each sub-region and month to determine where, within each variable's data distribution, the model has the most bias.

With respect to the second research question, pertaining to future temperature and precipitation projections, ensemble model mean change is calculated for each variable and sub-region. Results are presented as an ensemble mean for each sub-region with spread illustrated by box and whisker plots as recommended by Warner (2011). To provide a different perspective and utilize individual model Perkins' skill scores and RMSE values obtained in the first research question, weighted ensemble mean change for minimum and maximum temperature and mean precipitation for the Southeast U.S. were calculated, placing more weight in the ensemble mean for those models which prove skillful and less weight to those deemed less skillful. Change in temperature is expressed as the difference between the future climate (average period 2040-2069) and the reference climate (1970-1999). Precipitation change is expressed as a percent change from the reference period to the future. Sub-region domain-wide ensemble mean is calculated to gauge change on a more meaningful scale. Additionally, change at each grid location will be computed to determine change locally.

Within the following subsections, the step-by-step process for modifying raw NARCCAP files for analysis is explained. Further, the remaining six subsections detail the processes and procedures for calculating model skill, determining the inherent biases

within the RCMs, outlining how to determine if dynamically downscaling GCM data provides value over GCM projections alone, the method for exploring the effective number of models needed within an ensemble to provide meaningful information while maintaining model independence, and finally the last subsection details how future climate projections were calculated and how they will be displayed in Chapter 4.

2.2.1 RE-GRIDDING AND EXTRACTING DATA

Each of the NARCCAP ensemble members contained geospatial referencing native to each model and institution running the model. Yet, output from each model must be regridded to the same geospatial representation in order to perform robust analysis, assessing the NARCCAP ensemble members against the two observed datasets. This subsection outlines the procedure to re-grid model and observation data efficiently with commercial-off-the-shelf (COTS) software developed for meteorological and climatological purposes.

All datasets used in the dissertation were in the network Common Data Form (netCDF) format, preferred because it is a self-describing file (i.e., metadata is contained within the file), is portable (accessed by computers with different ways of storing integers, characters, and floating-point numbers), and is scalable by allowing a user to easily subset a large dataset (Rew et al., 2012). Analysis of netCDF data was performed with Climate Data Operators (CDO, Mueller and Schulzweida, 2010), a collection of more than 400 command line operators to manipulate and analyze climate and weather forecast model data. CDO can be run on any Unix/Linux platform as well as in Windows using either the Cygwin Unix (Cygwin, 2012) emulator or the binary DOS-prompt

executable. The Unix/Linux and Cygwin platforms require the installation of a netCDF library to properly read and manipulate netCDF files.

The first task before re-gridding could be achieved was to combine multiple netCDF files for each NARCCAP ensemble member and the observed datasets into one file for each dataset and variable. From the NARCCAP perspective, model output is saved in five year incremented netCDF files, resulting in seven netCDF files for one variable in the reference period and seven more files in the future period. Additionally, data files from the Maurer dataset were saved as annually compressed netCDF files (gzipped), resulting in 30 total files for one variable. The CDO command "cat" concatenates multiple files into one larger file with command line prompts like the example shown below:

```
> cdo cat infile1.nc infile 2.nc infile3.nc outfile.nc
```

The process to concatenate a file using CDO runs to completion in approximately 15 minutes using a 2 GHz dual-core processor with 4 GB of RAM.

Re-gridding and performing calculations on the netCDF files takes place within CDO. To improve computer processing and reduce the need for large quantities of disk storage space, CDO allows users to place multiple operators within one command line call if only one input file is used and one output file is created. This methodology is not applicable to multiple input files and one output file. An example of the multi-operator call is illustrated below:

```
> cdo –sellonlatbox,-94,-73,28,38 -remapnn,
"grid_description" –selyear 1970/1999 –daymax –subc,273.15
infile.nc outfile.nc
```

The CDO software breaks down the multiple commands by beginning with the inner- most command to the left of the input file, in this case performing a subtraction of 273.15 to convert from Kelvin to degrees Celsius for all grid points within the input file. The next command to the left of "-subc" takes the 3-hourly data from within the input file which has been converted from Kelvin to degrees Celsius in the step prior, and determines the daily maximum temperature at each grid point and each day. The third command selects only those data points which fall between the years of 1970 and 1999 (this step is not necessary for the two observed gridded datasets and only applies to NARCCAP data since the concatenate step produced a data file ranging from 1968 to 2000).

The fourth step builds on the three previous commands and re-grids the input file using a nearest-neighbors averaging (distance-weighted average; Jones, 2001) approach to map the data onto a regular latitude-longitude projection centered over the Southeast U.S. domain utilizing a text file named "grid_description.txt" to provide the new grid definition. The contents of "grid_description.txt" can be found in Appendix A. The nearest-neighbors algorithm was preferred over other available interpolation algorithms within CDO because it has been shown to reduce error inherent in the interpolation process relative to other interpolation methods such as bilinear interpolation and inverse distance weighting (McGinnis et al., 2010). Figure 2.4 illustrates the result of interpolation using the nearest-neighbors approach for one NARCCAP ensemble member from its native geospatial grid (Figure 2.4a) to the simple latitude-longitude grid (Figure 2.4b) defined in the "grid_description.txt" file. The final command in the

sequenceextracts data values within the box specified from -94°E to -73°E longitude and 28°N to 38°N latitude.

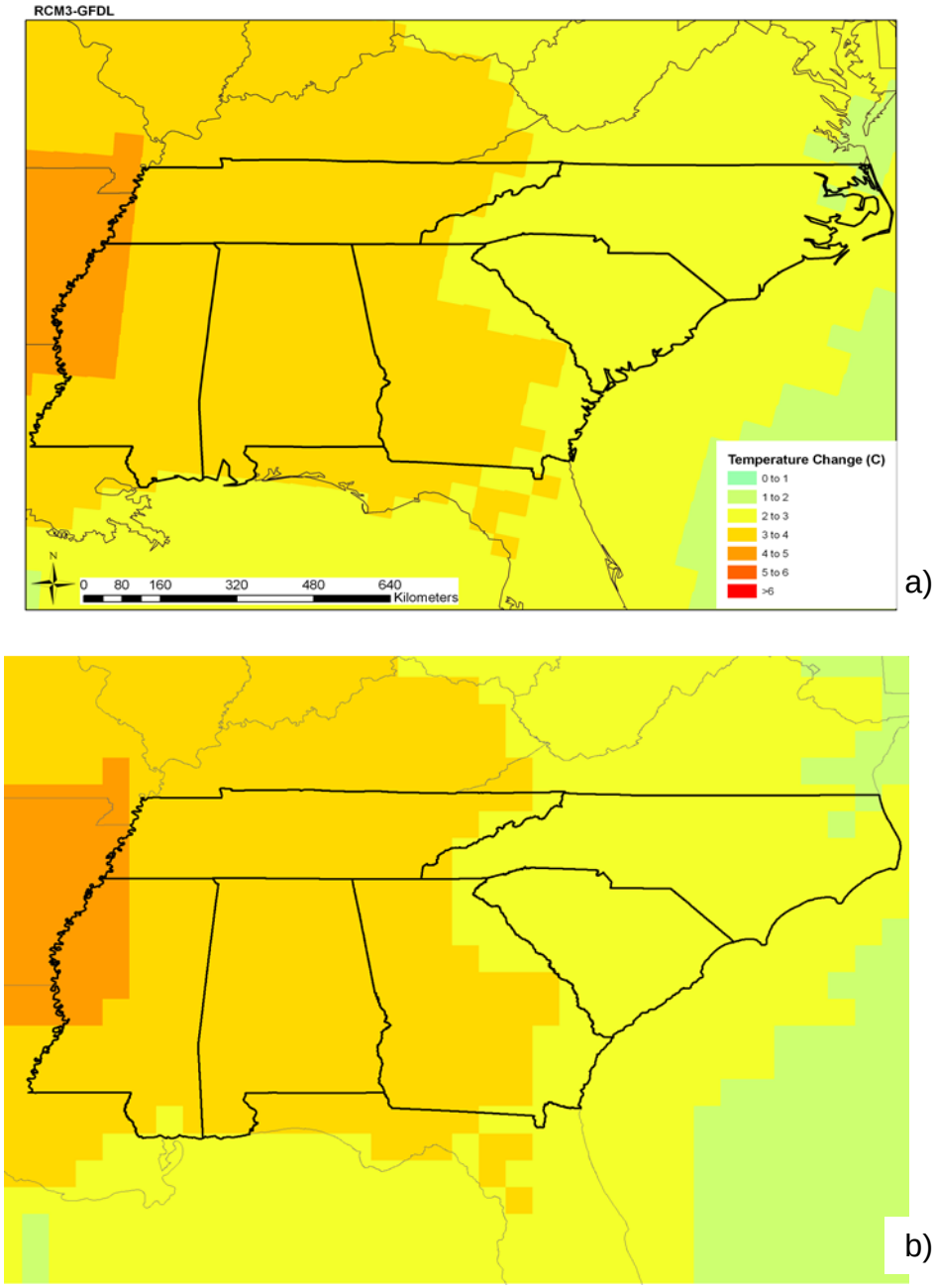

Figure 2.4. Illustration of a NARCCAP RCM in its native geospatial projection (a) and the geospatial projection after undergoing a nearest-neighbors transformation in CDO (b).

To maintain methodological consistency with Perkins' skill score calculation described in the next subsection and adapted from Perkins et al. (2007), daily values of

minimum and maximum temperature and mean precipitation from the dynamically downscaled results and observed data were extracted for the period 1970-1999 from grid points located inside and within a half-degree of the boundaries of the two Southeast U.S. sub-regions (Figure 2.5). The same daily data values extracted for the Perkins method were also used for calculation of Willmott's index of agreement, RMSE, and MAE. For comparsion of the NARCCAP ensemble members to the NARR and NCEP-driven RCM hindcasts, daily data from 1979-1999 were extracted from the same grid points. A half-degree buffer was chosen due to the spatial resolution of the data and that the data points may not completely lie on or within state boundaries, yet are representative of some portion of the region and sub-region. By extracting daily values at each grid point, it is possible to gauge a model's ability to simulate day-to-day variability rather than long-term averages, giving a proper gauge for testing a model's worth.

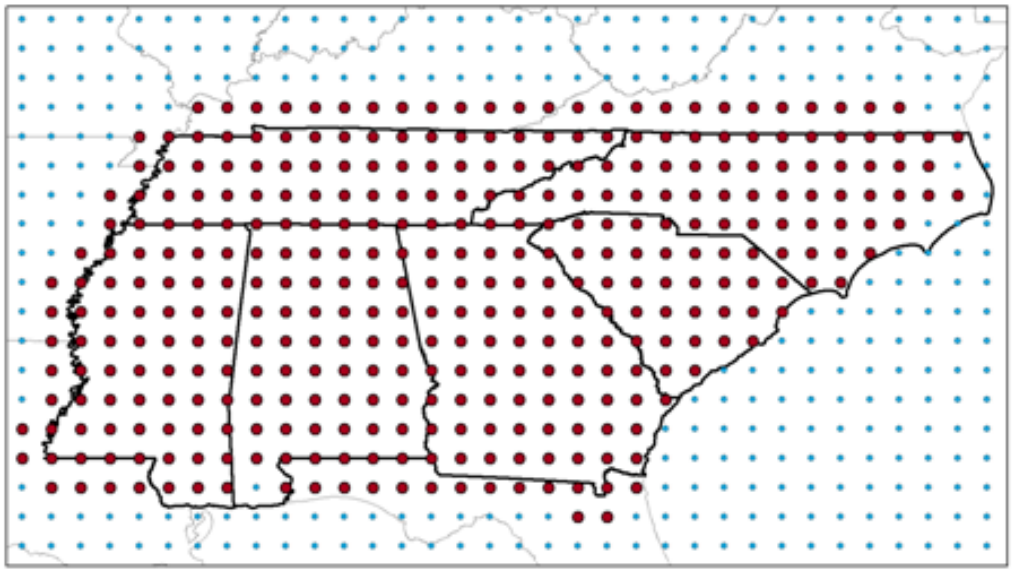

Figure 2.5. Southeast U.S. study area with emphasis on the grid points which were similar between all NARCCAP ensemble members, the Maurer dataset, and the NARR dataset (large red dots).

Data extraction was performed using the R Project for Statistical Computing software (available on the Comprehensive R Archive Network [CRAN] at http://www.r-project.org). R is described in detail in Ihaka and Gentleman (1996). The R library extension "ncdf" was utilized to read the netCDF files created using CDO. Appendix B.1 provides an example R script which calls a netCDF file and extracts the data points within the eastern sub-region for the month of December and saves the result in comma-delimited format with an appropriately detailed name of the contents within the file. A similar procedure was followed using R and the aforementioned R script to extract observation data from the Maurer, NARR, and GCM datasets. Upon the completion of re-gridding, performing calculations, and extracting variables from the multiple datasets, the processes described in the next subsections could be performed.

Although individual grid points were extracted within the six states classified as the Southeast U.S., all analysis was conducted by aggregating data to the sub-regional scale (rather than grid point by grid point) for several reasons. First, the PDF skill score metric was designed by Perkins et al. (2007) for determination of GCM skill across all of Austrailia (for the entire country rather than at individual grid locations) and is used in the same maner for regional climate model skill assessments (e.g., Boberg et al., 2010; Kjellstrom et al., 2010). To maintain methodological consistency with others studies using Perkin's method, aggregation was necessary. Additionally, although Kjellstrom et al. (2010) display skill scores spatially throughout Europe, they average individual grid skill scores to obtain a single skill score for each of their defined sub-regions. Second, aggregating data into sub-regions allows for meso- and synoptic-scale pattern recognition which may not be evident when analyzing at each grid location. To further this point,

GCMs were not meant to represent conditions at a single grid point but are more representative of the synoptic-scale (100s to 1000s of kilomters). Although RCMs are still not representative of a single grid location they are representative of the meso-scale (10s to 100s of kilometers). Third, most crop and hydrological assessments aggregate information from the single grid point scale to a field (or multi-field) or watershed-scale (e.g., Easterling et al., 1998; Jha et al., 2004) and assessing skill and bias on a sub-regional level is adequate. Lastly, although the information contained within an individual RCM grid better represents condictions within the grid point, models run at 50 km resolution will still have issues with pinpointing information at a specific location (e.g., town, city, weather station, etc.).

2.2.2 SKILL SCORE

Once the data was extracted and saved in a comma-delimited file, probability density functions (PDFs) were generated for monthly minimum and maximum temperature and mean precipitation from each of the downscaling approaches as well as gridded observations for the Southeast U.S. PDFs can be a convenient way of condensing a vast amount of data to find probability of occurrence of an event (Brankovic and Palmer, 1997; Koo et al., 2009; Jupp et al., 2010). Once the PDFs were created using code developed in R, a method developed by Perkins et al. (2007) was used to calculate the cumulative minimum value of two distributions of a binned value (defined by the user), measuring the common area between two PDFs (Equation 2.5):

$$S_{\text{score}} = \sum_{1}^{n} minimum(Z_m, Z_o) \tag{2.5}$$

where n is the number of bins used to calculate the PDF, Z_m is the frequency of values in a given bin from the model, and Z_o is the frequency of values in a given bin from the observed data. Temperature minimum and maximum bins were chosen as the minimum and maximum found in each month's observations, respectively, with a bin size of 0.5°C, while precipitation ranged from 1 mm/day to the maximum monthly value from observations, respectively, with a bin size of 1 mm/day (Perkins et al., 2007). Precipitation values below 1 mm/day were not included in the analysis as part of the dataset to create the PDFs because it contributes little to daily precipitation (Dai, 2001; Sun et al., 2006).

The following R code is a sample of how the PDFs were created and the Perkins' skill scores computed after opening the respective dataset and saved in R as a data frame (see the complete R script in Appendix B.2):

```
z1<-sort(gg$Obs)
z2<-sort(gg$MM5I_CCSM)

fff<-cbind(z1,z2)

a1<-z1[which(z1>=-12 & z1<=25)]
b1<-z2[which(z2>=-12 & z2<=25)]

#define the bins to use to create a histogram
bins<-seq(-12,25,by=0.5)

#create a histogram based on the bins defined above for both the
#observed data and model data
a2<-hist(a1, breaks=bins, freq=FALSE)
b2<-hist(b1, breaks=bins, freq=FALSE)

#extract the density value from the histogram - this is the height of
#each bin in the histogram
a3<-a2$density
b3<-b2$density

#combine the two density vectors into a data frame
b4<-cbind(a3,b3)

#find the minimum value at each row between the observations and the
#model
b5<-apply(b4,1,min)
```

```
#sum each of the minimum values found above and divide by 2 because the
#bins were spaced every 0.5 degrees C. If the bin size had been 1,
#there is no need to divide by anything. If the bin size was 0.25, the
#user needs to divide the sum by 4, etc. The value found in this step
#is the model's Perkins' skill score.
b6<-(sum(b5))/2
```

Perkins sorted each of the values within her domain from smallest to largest in order to compare the distribution of data values over the entire climatological period rather than specific dates or times.

Figure 2.6 illustrates the histogram/probability density functions created for observations and one NARCCAP ensemble member. As an example of how the algorithm calculates Perkins' skill score, the 20°C bin for observations has a PDF value of 0.1 while the model has a PDF value of 0.12. The minimum value between observation and model is 0.1 and would be added into the Perkins' skill score calculation for that respective bin.

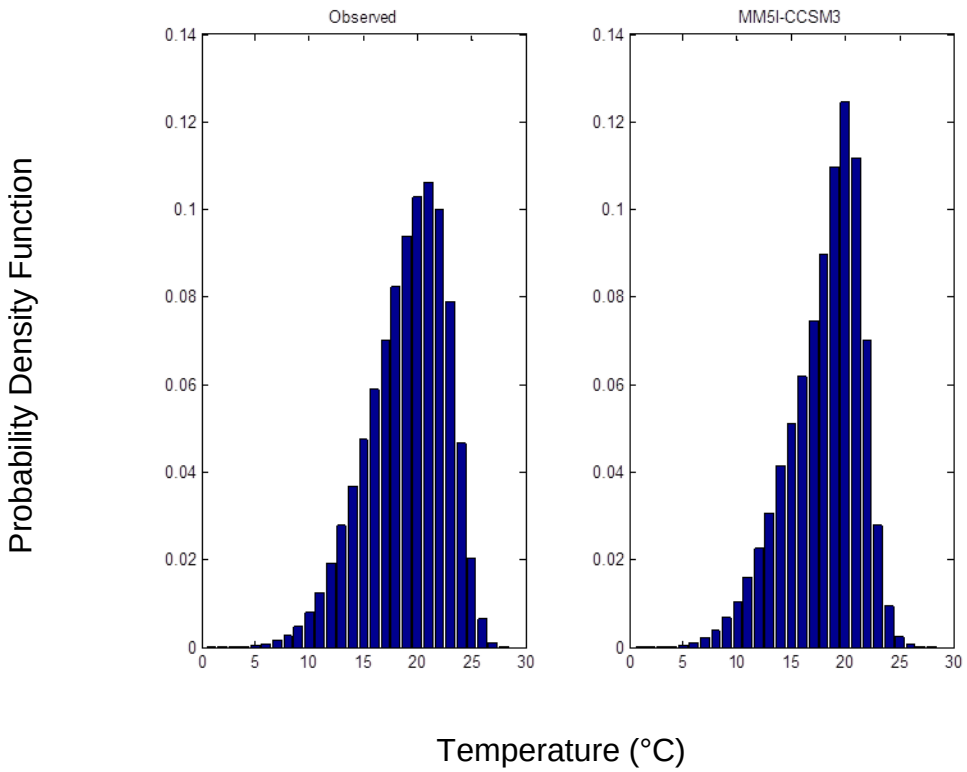

Figure 2.6. Example temperature probability density functions from observations (left) and from one NARCCAP ensemble member (right).

This method of determining model skill is described by Perkins as highly robust (Perkins, 2010) because its calculation does not rely on the underlying data distribution. Perkins' skill scores are based on a scale from zero to one. If the model is able to simulate the reference climate (represented by observed gridded data) adequately, model Perkins' skill score will be high. Conversely, if the model is unable to simulate the day-to-day variability found in the reference climate adequately, model Perkins' skill score will be low. Perkins' method has been used to determine model skill with coarse GCM data (Perkins et al., 2007; Maxino et al., 2008; Pitman and Perkins, 2009; Perkins, 2009, and Perkins et al., 2012) and more recently with RCM output from ENSEMBLES

(Boberg et al., 2010; Kjellstrom et al., 2010). The method has yet to be applied to RCM output from NARCCAP, a gap that this dissertation has filled. This simple method gives decision makers insight into model skill in the historical reference period and how much confidence they can place in its projections for future climate, as well as provide information on individual model bias. A weight in calculating ensemble model mean for each sub-region will be applied based on model Perkins' skill score, allowing for more meaningful results and is considered a good practice by IPCC Working Group I (Knutti et al., 2010).

2.2.3 INDEX OF AGREEMENT

Willmott et al. (2011) provide another method used to validate model performance. Their dimensionless index of agreement (d_r) is computed by finding the magnitudes of the differences between the model-predicted and observed deviations about the observed mean relative to the sum of the magnitudes of the perfect model and observed deviations about the observed mean (Willmott et al., 2011). The modified index of agreement is based on the original form of Willmott's index of agreement (Willmott and Wicks, 1980; Willmott, 1981). Equation 2.6 illustrates the revised index of agreement presented in Willmott et al. (2011), of which d_r is based:

$$d_l' = 1 - \frac{\sum_{i=1}^{n}|(P_i - \bar{O}) - (O_i - \bar{O})|}{\sum_{i=1}^{n}(|O_i - \bar{O}| + |O_i - \bar{O}|)} \tag{2.6}$$

where n is the number of values, P_i are the predicted values (model), O_i are the observed values, $\bar{O}$ is the observed mean. Equation 2.6 is unbounded at the lower values, thus Willmott et al. (2011) chose to refine the index of agreement such that the metric was

bounded between -1 and 1. The refined index of agreement is reduced from Equation 2.6 and written in the form illustrated in Equation 2.7:

$$d_r = \begin{cases} 1 - \dfrac{\sum_{i=1}^{n}|P_i - O_i|}{c\sum_{i=1}^{n}|O_i - \overline{O}|}, when \\ \quad \sum_{i=1}^{n}|P_i - O_i| \le c\sum_{i=1}^{n}|O_i - \bar{O}| \\ \dfrac{c\sum_{i=1}^{n}|O_i - \bar{O}|}{\sum_{i=1}^{n}|P_i - O_i|} - 1, when \\ \quad \sum_{i=1}^{n}|P_i - O_i| > c\sum_{i=1}^{n}|O_i - \bar{O}| \end{cases} \tag{2.7}$$

where *c*=2, representing the two mean absolute deviation terms in the numerator of Equation 2.6. Appendix B.3 provides an example R script for computing Willmott's index of agreement. Table 2.4 breaks down Equation 2.7, using Equation 2.6 to aid in interpreting Willmott's index of agreement values.

Table 2.4. Explanation and interpretation of the meaning behind values for Willmott's index of agreement.

Willmott's Index of Agreement Value (d_r)	Condition	Equation-based Form (from Equation 2.6)	Interpretation
1.0	$\sum_{i=1}^{n}\|P_i - O_i\| \leq c\sum_{i=1}^{n}\|O_i - \bar{O}\|$	$1 - \frac{1-1}{1+1}$ ↓ 1 - 0 = **1**	Perfect model agreement with observations.
0.5	$\sum_{i=1}^{n}\|P_i - O_i\| \leq c\sum_{i=1}^{n}\|O_i - \bar{O}\|$	$1 - \frac{2-1}{1+1}$ ↓ 1 – 0.5 = **0.5**	Sum of the error magnitudes (denominator) is half the perfect model deviation and observed deviation magnitudes (numerator).
-0.5	$\sum_{i=1}^{n}\|P_i - O_i\| > c\sum_{i=1}^{n}\|O_i - \bar{O}\|$	$\frac{1+1}{5-1} - 1$ ↓ 0.5 - 1 = **-0.5**	Sum of the error magnitudes (numerator) is twice the perfect model and observed deviation magnitudes (denominator).
Approaching -1.0	$\sum_{i=1}^{n}\|P_i - O_i\| > c\sum_{i=1}^{n}\|O_i - \bar{O}\|$	As $\sum_{i=1}^{n}\|P_i - O_i\|$ increases, d_r will approach -1 ***OR*** $\frac{0+0}{5-1} - 1$ ↓ 0 - 1 = **-1**	Model-estimated deviations about the observed mean are poor esimates of the observed deviation OR there is little observed variability.

Willmott et al. (2011) argue their modified index is an improvement over other non-dimensional techniques described in Nash and Sutcliffe (1970), Watterson (1996), Legates and McCabe (1999), and Mielke and Berry (2001) because of its flexibility, its well behaved nature, and because it can be used in a multitude of model-performance applications. While Willmott et al.'s index provides an intuitive and understandable metric, its performance and flexibility is very similar to Perkins' method as illustrated in Figures 2.8 through 2.10 of the next sub-section. Minimum temperature has a correlation coefficient between the two metrics of 0.94 and 0.95, respectively, for the east and west sub-regions; maximum temperature has a 0.97 and 0.94 correlation coefficient, respectively, for each sub-region; and mean precipitation has a weaker, but still high, correlation coefficient of 0.58 and 0.65, respectively, for each sub-region. Due to the strong relationship between Perkins' skill score and Willmott's index of agreement, only values obtained from Perkins' method are used to calculate the ensemble weighted mean.

2.2.4 SKILL DETERMINATION USING ROOT MEAN SQUARE ERROR AND MEAN ABSOLUTE ERROR

The last two methods to aid in the validation of RCM data are root mean square error (RMSE) and mean absolute error (MAE) for temperature and precipitation. Equation 2.8 illustrates the computation of RMSE:

$$\mathrm{RMSE} = \sqrt{\frac{1}{n}\sum_{j=1}^{n}(y_j - \hat{y}_j)^2} \tag{2.8}$$

where n is the number of values, y_j are the observed values, and $\hat{y}_j$ are the modeled values. Appendix B.4 provides an example R script used to calculate RMSE. Equation 2.9 illustrates the computation of MAE, following the same notation as RMSE:

$$\mathrm{MAE} = \frac{1}{n}\sum_{j=1}^{n}\left|y_j - \hat{y}_j\right| \tag{2.9}$$

Direct comparison of specific daily values from GCM-driven RCM runs were not compared to specific observational values (i.e., January 1, 1979 in the GCM-driven runs were not compared to January 1, 1979 in the observational record) to compute RMSE and MAE because although GCM-based runs have a date and time associated with the output, the output is simply a general time keeping measure. However, over the course of a lengthy climatology (20-30 years) the intra- and inter-annual variability shown in observations is also illustrated in the GCM-based climatology. For this reason, daily data values for each month within both sub-regions were sorted from lowest to highest with the assumption that general values found in the GCM-driven RCMs are found at some instance in the observational record of the same period.

RMSE is commonly reported in the climatological/meteorological peer-reviewed literature to express model error and aid in quantifying model skill compared to observations. (Murphy and Epstein, 1989; Huffman, 1997; Yang and Arritt, 2002; Wu et al., 2005; Wilks, 2006; Seiler, 2009; Liu et al., 2012). Additionally, RMSE is a preferred method of expressing model accuracy because it not only includes contributions from each individual data point, but also includes any mean bias error (von Storch and Zwiers, 1999; Stull, 2000; Wilks, 2006). However, Willmott and Matsuura (2005) argue mean

absolute error (MAE) should be reported because it represents a more natural measure of average error with a clearly defined meaning, something RMSE lacks. Both values indicate dimensional (i.e., °C for temperature and either percent or mm/day for precipitation) mean model error compared to observations; however, large errors have a relatively greater influence on RMSE than MAE. Both methods were chosen to represent mean model error/skill because a suite of measures is appropriate to gain a well-rounded assessment of skill (Willmott, 1981). Figure 2.7 provides an example of poor RMSE (Figure 2.7a) and excellent RMSE (Figure 2.7b). Additionally, examples of poor and excellent MAE would appear similar to RMSE.

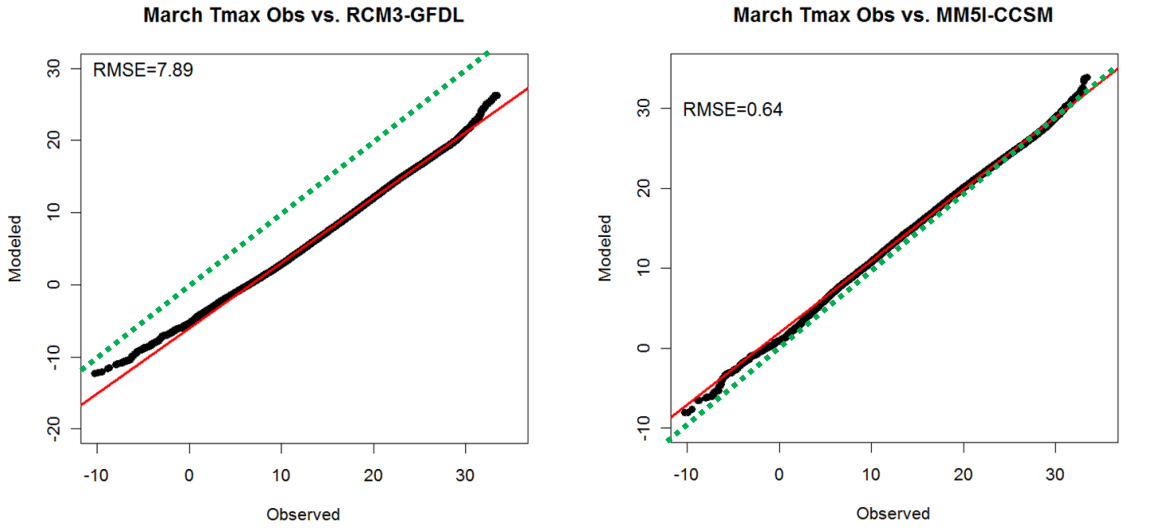

a) b)

Figure 2.7. Example of poor RMSE (a) and excellent RMSE (b) for March maximum temperature from two NARCCAP ensemble members. Temperature on the x- and y-axis for both plots are in degrees Celsius. If model data matched observations exactly, the scatter plot will lie directly on the green dotted line. The solid red line represents linear regression trend line.

If a model is able to simulate the exact trend found in observations, the scatterplots found in Figure 2.7 will demonstrate a straight line consistent with the dotted green line plotted in Figures 2.7a and 2.7b. The model with a high RMSE (Figure 2.7a) shows that it, in this case, under predicts maximum temperature at every step in the distribution while the model with low RMSE follows extremely closely to the dotted green line.

Comparison of Perkins' skill score and Willmott's index of agreement provide similar measures of skill to RMSE-based skill for temperature (Figure 2.8 and 2.9). However, with respect to precipitation, Perkins' and Willmott versus RMSE-based skill scores present virtually no correlation (Figure 2.10). Although not shown, comparison of Perkins and Willmott skill scores to MAE would be virtually identical to those found with RMSE since a strong relationship between RMSE and MAE exists (Willmott and Matsurra, 2005). This dichotomy is rooted in what each method is measuring. Perkins' and Willmott's skill computations compare how the distribution of the model and observations overlap, giving less weight to individual numbers and more weight to the overall distribution, while RMSE-based skill is the opposite in that individual numbers are less important than the data distribution. For non-Gaussian distributions (like the gamma distribution of precipitation), the correlation between Perkins' and Willmott's methods are low, illustrating how different metrics measure non-Gaussian distributions.

For use in weighting future projections, RMSE was normalized to unit length using the R operator "normalize.vector" found within the "ppls" package (Kramer et al., 2008). The normalized RMSE is used as the weight when calculating weighted ensemble means described in Sub-section 2.2.8. The normalized RMSE is expressed as one minus

the normalized RMSE so that low RMSE will be close to one after normalization (good skill) and high RMSE will be close to zero after normalization (poor skill). The relationship between RMSE and normalized RMSE (before taking one minus normalized RMSE) has a correlation of one and is illustrated in Appendix E along with the R script used to normalize RMSE.

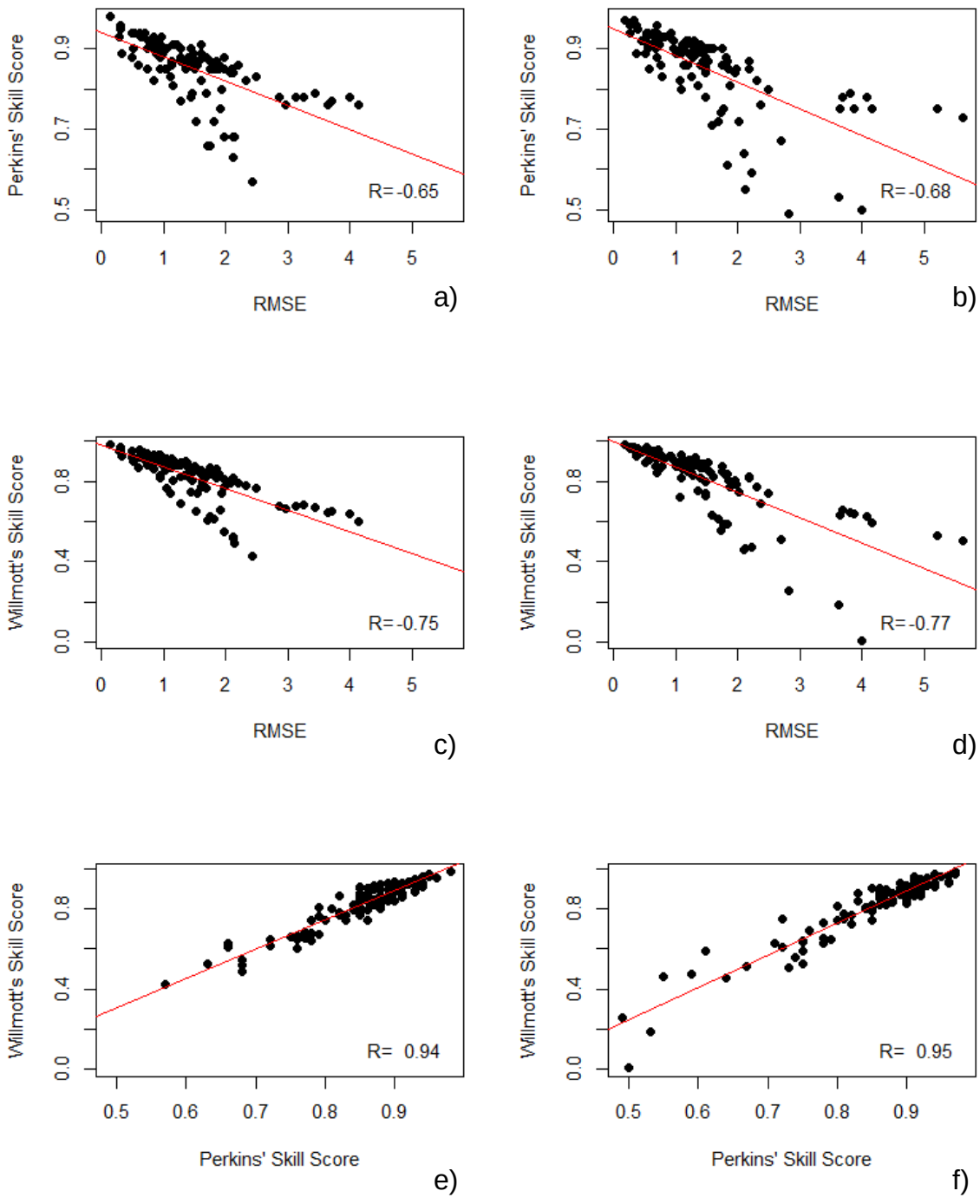

Figure 2.8. Scatterplot of minimum temperature Perkins' skill score, Willmott's index of agreement, and RMSE for the east (a, c, and e) and west (b, d, and f) sub-regions. The straight red line indicates the linear regression line fit to the data. "R" values in the upper-left of each figure represents the correlation between the skill metrics.

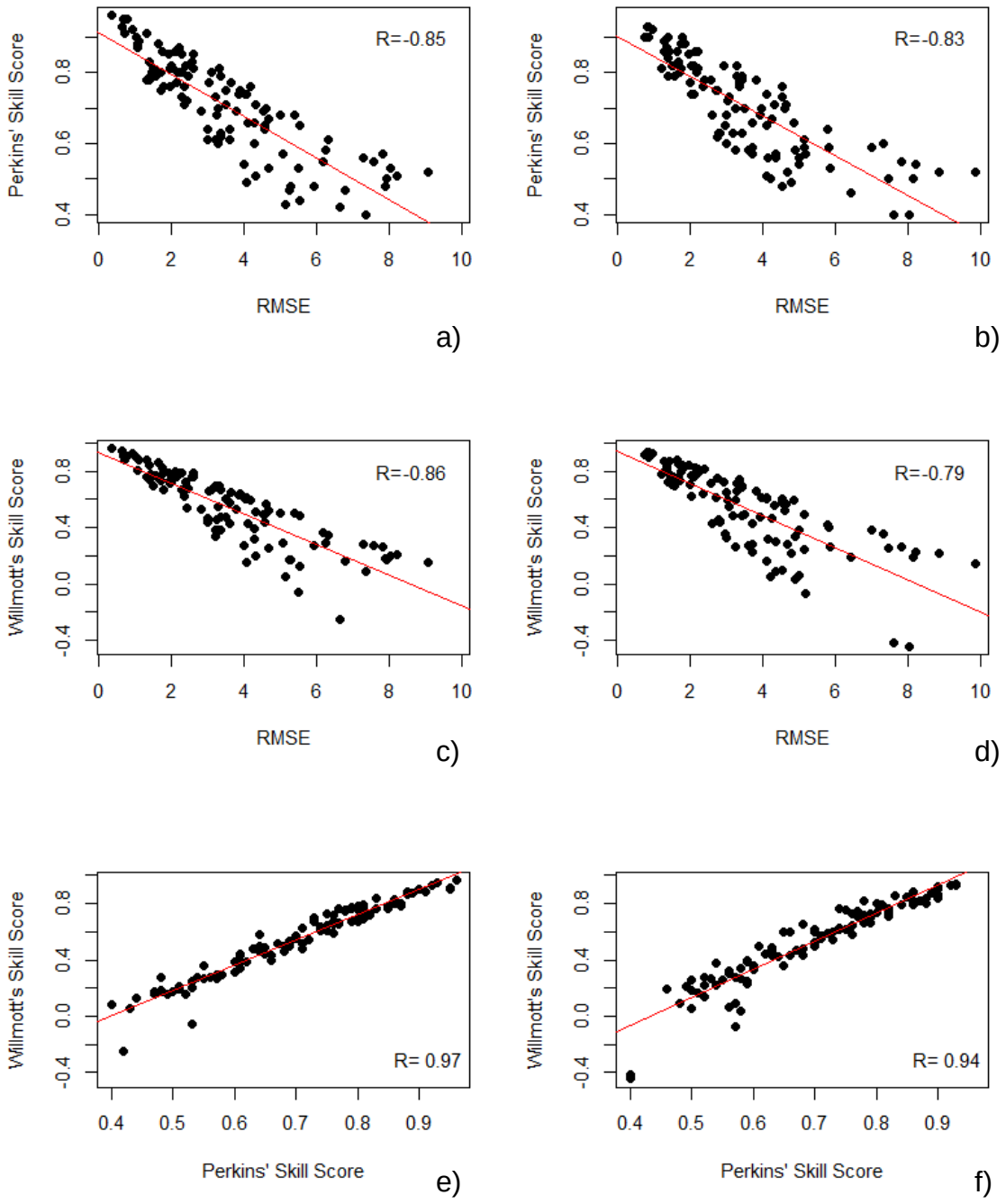

Figure 2.9. Scatterplot of maximum temperature Perkins' skill score, Willmott's index of agreement, and RMSE for the east (a, c, and e) and west (b, d, and f) sub-regions. The straight red line indicates the linear regression line fit to the data. "R" values in the upper-left of each figure represents the correlation between the skill metrics.

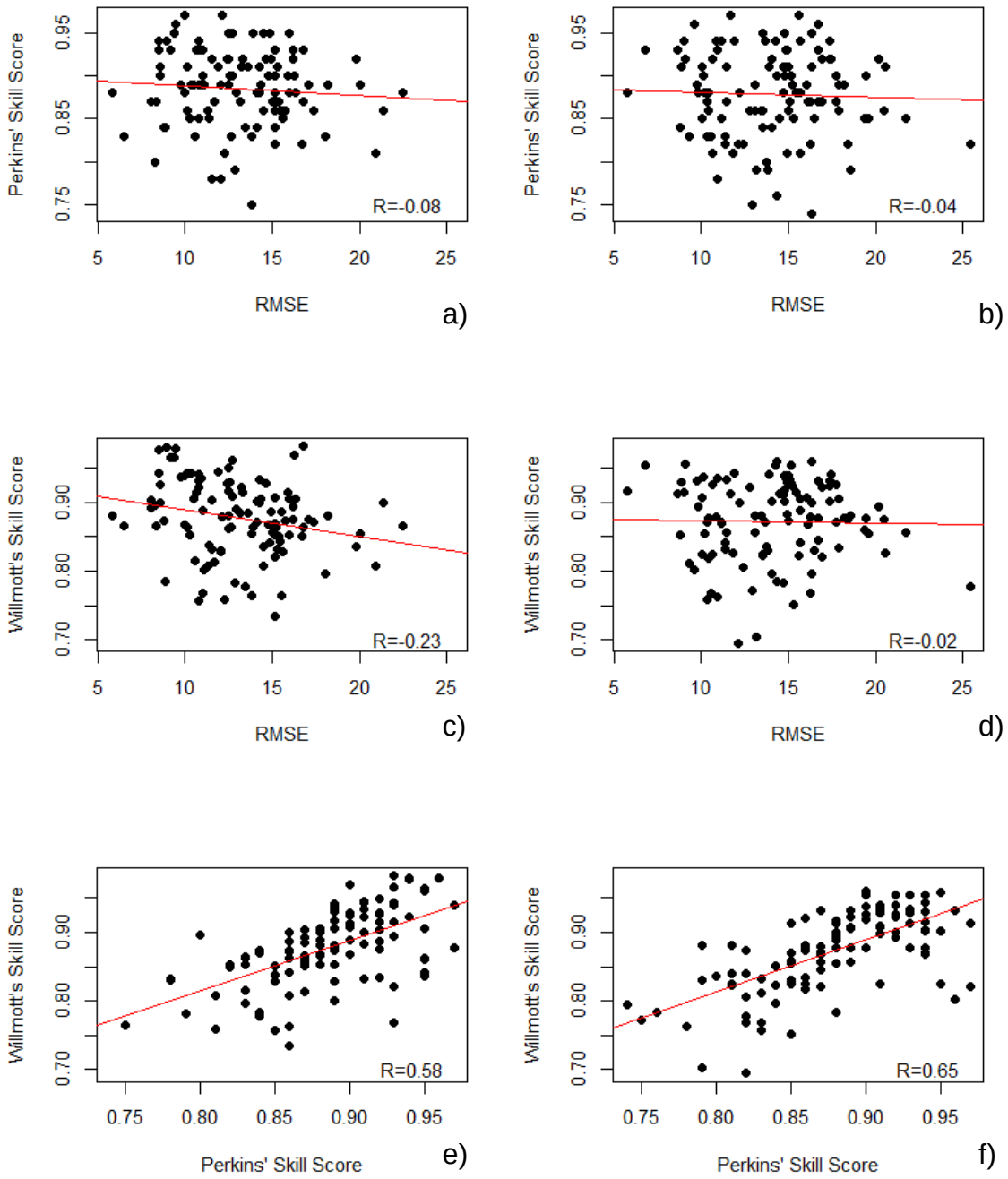

Figure 2.10. Scatterplot of mean precipitation Perkins' skill score, Willmott's index of agreement, and RMSE for the east (a, c, and e) and west (b, d, and f) sub-regions. The straight red line indicates the linear regression line fit to the data. "R" values in the upper-left of each figure represents the correlation between the skill metrics.

Perkins skill score, Willmott's index of agreement, RMSE, and MAE values are plotted in a modified Hovmöller diagram (Hovmöller, 1949) in Chapter 3 in which the x-axis consists of the nine NARCCAP ensemble members for whom these values were calculated and the y-axis represents each month. Although the Hovmöller plot is commonly used to plot atmospheric waves moving longitudinally, latitudinally, or vertically over time, it can also be a convenient way to plot and display large quantities of data within a single diagram. The plots should be read beginning with from the upper-left corner and working toward the bottom. The y-axis begins with the month of December (rather than the first calendar month of January) so that each season is grouped together for easy diagnosis of low and high skill by month as well as season. Appendix B.5 provides an example R script used to create a modified Hovmöller diagram.

Perkins skill score, Willmott's index of agreement, RMSE, and MAE were the four preferred methods because the results of each calculation had the potential to provide either similar or completely opposing assessments of skill. Additionally, it was important to illustrate the short-comings of relying solely on one method for model skill determination, as each measure provides unique insight into model performance.

2.2.5 MODEL BIAS VERSUS OBSERVATIONS

Another important aspect of this research was to determine not only model skill, but also to evaluate why a model may lack skill. Kjellstrom et al. (2010) computed area-average model bias at the 1^{st}, 5^{th}, 10^{th}, 25^{th}, 50^{th}, 75^{th}, 90^{th}, 95^{th}, and 99^{th} percentiles for each of their sub-regions, variables, and models. This method allows for determination of where, within the probability density function (or distribution), a model under or over

predicts a given variable, leading to degradation in skill. For example, a model with a warm temperature bias in the lower percentiles (the coldest days) may decrease the number of cold air outbreaks and potential decrease snow cover in the region during winter. A model with a warm summer bias in the upper percentiles could cause over prediction of heat waves and drought. Figure 2.11 illustrates January Southeast U.S. mean model bias for three NARCCAP RCMs. Perkins' skill scores for the RCM3-GFDL and WRFG-CCSM3 models are reduced because of cold temperature bias at each percentile while the MM5I-CCSM3 model has a slight warm bias in the lower percentiles, while showing virtually no other bias in the rest of the PDF, leading to higher skill than the other RCMs. Appendix B.6 provides an example R script used to calculate and create the percentile plots for this dissertation work.

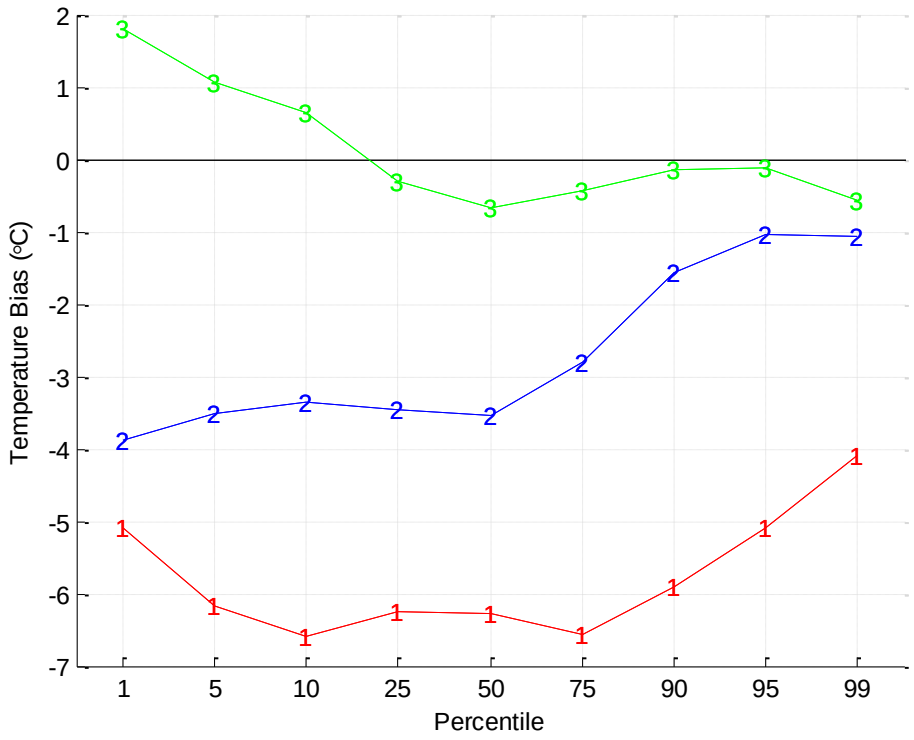

Figure 2.11. January Southeast U.S. mean model temperature bias during the reference period for the RCM3-GFDL (1), WRFG-CCSM (2), and the MM5I-CCSM (3) NARCCAP RCMs.

In addition to investigating temperature and precipitation biases using percentile plots, several variables in the NARR dataset were compared against corresponding variables output by the NARCCAP RCMs, which included soil moisture content, latent heat flux, sensible heat flux, total cloud cover, 500-mb height, and sea-level pressure. Each variable was averaged monthly for each sub-region and a time series from January 1979 to December 1999 was plotted to calculate the overall bias in each of the variables in comparison to NARR, and to see if the model was able to simulate the month-to-month variability found in observations. Additionally, these plots allowed for the determination of whether extreme conditions (droughts or floods) observed in a particular month were translated into the models.

2.2.6 DETERMINATION OF VALUE ADDED THROUGH DOWNSCALING

This work determines if downscaling provides a positive impact a slightly different way from the two Di Luca pieces cited above. Di Luca's methodology is similar to this dissertation in that value added is determined by calculating the difference between RCM skill and GCM skill used for LBCs. This dissertation, however, utilizes daily observations and calculates value added on a month-by-month basis, while Di Luca utilizes monthly mean observations and calculates value added on a season-by-season basis. Another major short-coming of the Di Luca studies are they determine value added by finding the difference between the squared error of the GCM providing LBCs to the RCM, wherein if the squared error of the RCM was smaller than the squared error of the GCM, value was added.

The three GCMs were re-gridded using a nearest-neighbors algorithm in CDO and the same grid points displayed in Figure 2.5 were extracted. Then, Perkins skill scores, Willmott's index of agreement, root mean square and mean absolute errors were computed. In the final step, monthly Perkins skill scores, Willmott's index of agreement, RMSE, and MAE values from each GCM were subtracted from each NARCCAP RCM simulation. If the skill values from any of the three metrics from the NARCCAP members were greater than the GCM values, it was determined that downscaling provided value; however, if the GCM proved superior, value was not added through the downscaling process. Obviously, there will be cases where downscaling does not provide value. It was hypothesized that downscaling precipitation would add more value than downscaling temperature because precipitation initialization and formation takes place on scales not resolved by GCMs; however, GCMs are able to skillfully replicate meso- and synoptic-scale processes which primarily drive temperature.

2.2.7 DETERMINING THE EFFECTIVE NUMBER OF ENSEMBLE MEMBERS

A common and often violated rule of model independence between ensemble members plagues the meteorological and climatological fields (Masson and Knutti, 2011). Typically, the purpose of creating an ensemble is to gain as much information as possible while hoping to reduce errors associated with individual member models and creating a consensus which can then be conveyed to users to make more informed decisions. Often there is an overlap in RCMs and/or GCMs used within an ensemble violating the notion of model independence. While RCMs might have different physics packages, they could be driven by the same GCM. There is a point in which the effective

number of models is reached (Pennell and Reichler, 2010), ensemble model independence is not met, and the resulting predictions are more likely than not to be biased toward a false ensemble mean. Since reducing the effective number of ensemble members to a bare minimum will not provide a realistic understanding of the range of potential climate outcomes (Knutti, 2008), a common ground should be sought to incorporate as many models as possible without violating independence. Although the NARCCAP team intends for users to utilize a subset of the members available in the ensemble, the hierarchical cluster analysis allows users to make an educated decision on how many and which members to include from the NARCCAP ensemble in their assessment.

To determine the effective number of models within this work, a hierarchical clustering analysis was performed in which models that have strong similarities will cluster together. Daily data extracted for all months from the NARCCAP ensemble members, Maurer's observed dataset, and the three GCMs providing LBCs were merged together to create a single data frame. This was done for three reasons: 1) To determine which RCMs exhibited strong similarities, 2) Determine if RCMs clustered with GCMs providing LBCs, and 3) Determine if observations tended to cluster around certain RCMs and/or GCMs. To perform the clustering analysis, the R package "pvclust" (Suzuki and Shimodaira, 2006) was utilized (see Appendix B.7 for sample R script). Suzuki and Shimodaira's R package uses a distance and clustering method specified by the user to cluster columns of data from within a data frame. Additionally, the package calculates p-values for each clustered pair via multi-scale bootstrap resampling on each of the columns within a user's dataset, giving an indication of the strength of the cluster

supported by raw data. In this work, Ward's hierarchical clustering method (Ward, 1963) was utilized. Ward's method begins with 13 one-member clusters (nine NARCCAP members, one observed dataset, and three GCMs) and stepwise merges two clusters until all metrics belong to a single cluster. Clusters are formed using the Euclidean distance metric between two points of data, which takes a similar form to RMSE when calculated in a two-dimensional space (Equation 2.10; adapted from Wilks, 2006):

$$\left|\left|x - y\right|\right| = \sqrt{\sum_{k=1}^{K} (x_k - y_k)^2} \tag{2.10}$$

where x is one NARCCAP ensemble member (for instance), y is another NARCCAP ensemble member (for instance), x_k is the raw data contained within x, y_k is the raw data contained within y, and K is the number of geometric dimensions (K=2 in this work because both time and the variable of interest [temperature or precipitation] make up the geometric dimensions). Ward's linkage and Euclidean distance are standard methods of utilizing hierarchical clustering in meteorology and climatology (Pennell and Reichler, 2010; Masson and Knutti, 2011).

A dendrogram is created to illustrate the relationship between each of the regional climate models and driving GCMs (and/or observations), in which clusters with high similarity are coupled toward the bottom of the diagram (lowest height) and the least similar clusters are attached within the dendrogram as height increases in the positive y-direction. Suzuki and Shimodaira's R package (pvlust) provides not only the dendrogram plot, but also plots the approximately unbiased (AU) p-value, bootstrap probability (BP), and the order in which the clusters were made. AU and BP are discussed at length in

Shimodaira (2002), Shimodaira (2004), and Suzuki and Shimodaira (2006). The "pvclust" package assesses the uncertainty in hierarchical cluster analysis. For each cluster in the hierarchical clustering, quantities called p-values are calculated via multiscale bootstrap resampling. The p-value of a cluster has a value between 0 and 1, which indicates how strong the cluster is supported by data. The approximately unbiased p-value, computed by multiscale bootstrap resampling, is a better approximation to the unbiased p-value than the bootstrap probability value computed by normal bootstrap resampling. (Suzuki and Shimodaira (2006). The "pvclust" package performs hierarchical cluster analysis via the "hclust" R statistical function and automatically computes p-values for all clusters contained in the clustering of original data. The "hclust" function (and thus the "pvclust" package) performs a hierarchical cluster analysis using a set of dissimilarities for the *n* objects being clustered. Initially, each object is assigned to its own cluster and then the algorithm proceeds iteratively, at each stage joining the two most similar clusters, continuing until there is just a single cluster. At each stage distances between clusters are recomputed by the Lance–Williams dissimilarity update formula according to the particular clustering method being used (in this dissertation Ward's method utilizing Euclidean distance). The Lance-Williams dissimilarity update formula calculates the dissimilarities between a new cluster and existing points, based on the dissimilarities prior to forming new clusters.

To validate clusters formed in the hierarchical cluster analysis, a non-metric multidimensional scaling technique was utilized (Venables and Ripley, 2002). The non-metric multidimensional scaling technique utilized the "isoMDS" package in R which uses Kruskal's non-metric multidimensional scaling (Kruskal, 1964) to find similarities

(and dissimilarities) between data. Multidimensional scaling (MDS) assigns Euclidean coordinates to a dataset such that given a set of dissimilarity, similarity, or ordinal relations between data points, the relations are obeyed as closely as possible by each model member while making few assumptions about the nature of the data. Non-metric multidimensional scaling (NMDS) is an ordination technique in which the MDS algorithm finds a configuration of points whose distances reflect as closely as possible the rank order of the data (Agarwal et al., 2009). In order words, the NMDS will ordinally rank data points according to their similarity and will distance (and rank further away) data points which show higher dissimilarity.

Based on information obtained on model skill and the effective number of models, a smaller ensemble was created and new ensemble mean, median, 25^{th} percentile, and 75^{th} percentile values were computed. Models from the greater NARCCAP ensemble were chosen by month based on their skill. In other words, if the hierarchical cluster analysis shows RCMs clustering around similar GCMs, the RCM with the highest skill in a given month would be the model chosen for the smaller ensemble. This allowed for the fulfillment of inter-ensemble independence while still providing relevant and useful information on ensemble central tendency and spread.

The use of hierarchical clustering in the meteorological and climatological community is relatively new (e.g., Pennell and Reichler, 2010; Johnson et al., 2011a; Johnson et al., 2011b; Masson and Knutti, 2011; Yokoi et al., 2011; Riccio et al., 2012); however it is being embraced as a simple, yet effective way, of finding similarities between models and reducing the number ensemble members used for providing

ensemble-based projections. With ensemble modeling becoming the "norm" in meteorology and climatology, the use of hierarchical clustering will surely increase.

2.2.8 FUTURE CLIMATE CHANGE PROJECTIONS

Research question two – to determine future changes of minimum and maximum temperature and mean precipitation for the Southeast U.S – involved computing differences in temperature for reference climate simulations from future projections, while precipitation is expressed as percent of change from the reference to the future period. Equations 2.11 and 2.12 illustrate how temperature and precipitation change were computed,

$$\Delta T = T_{fut} - T_{ref} \tag{2.11}$$

$$\Delta P = \left(\frac{P_{fut} - P_{ref}}{P_{ref}}\right) * 100 \tag{2.12}$$

where T_{fut} and P_{fut} represent future temperature and precipitation, respectively, and T_{ref} and P_{ref} represent reference period temperature and precipitation, respectively. Expressing precipitation change as a percentage is common practice in meteorology and climatology (IPCC, 2007) as absolute values of precipitation change do not adequately allow for comparison between regions with differing climate classifications.

Table 2.5. Calculations performed, the data frequency used for each computation, and the equation number used in computing each calculation.

Computation	Data Frequency	Equation Number
Potential Evapotranspiration	Monthly	Equations 2.2 through 2.4
Perkin's skill score	Daily	Equation 2.5
Willmott's index of agreement	Daily	Equation 2.7
RMSE	Daily	Equation 2.8
MAE	Daily	Equation 2.9
Bias/Percentile – Temperature	Daily	Same form as Equation 2.11
Bias/Percentile - Precipitaiton	Daily	Same form as Equation 2.12
Future Temperature Change	Monthly	Equation 2.11
Future Precipitation Change	Monthly	Equation 2.12

To test if modeled change from the reference period to the future period was statistically significant, a nonparametric bootstrap was employed. The bootstrap is an approach to statistical inference that makes few assumptions about the underlying probability distribution that describes the data (Wilks, 2006) and is commonly used in both the meteorology (e.g., Livezey and Chen, 1983; Hamill, 1999; and Xu, 2006) and climatology climatology (e.g., Zwiers, 1990; Beersma and Buishand, 1999; von Storch and Zwiers, 1999; Huntingford et al., 2003; and Wilks, 2006) fields. This approach assumes the sample distribution is a good estimate of the population distribution and does not depend on the sample and population distributions being normally distributed. Using the data as an approximation to the population's distribution, data are resampled

randomly with replacement from the modeled dataset to create an estimate to the population distribution.

A sample R script used to perform the bootstrap significance testing is provided in Appendix B.8. Data passed to the R script included monthly sub-region-based means for the historical reference and future periods (for each grid point) and 30-year mean change values aggregated over each sub-region (as described above). The script performed the nonparametric bootstrap in the following order:

1) Generate a sample dataset for minimum and maximum temperature and mean precipitation by sampling with replacement n=162 for the east sub-region (number of grid points in the east sub-region) and n=168 times for the west sub-region (number of grid points in the west sub-region). This was done for the historical reference and future periods.
2) Calculate the aggregated mean for both time periods for each sub-region.
3) Use Equation 2.8 to calculate temperature change and Equation 2.9 to calculate precipition change for both time periods.
4) Perform steps 1) through 3) 10,000 times to generate a sample PDF of changes projected through the bootstrapping process.

To find if the aggregated mean change from the models for each sub-region were statistically significant, percentiles were computed based on the bootstrapped-based "change" distributions at the 0.5^{th}, 2.5^{th}, 5^{th}, 95^{th}, 97.5^{th}, and 99.5^{th} percentiles (providing the equivalent to a two-tailed t-test). From these percentiles, where the modeled change fell within the bootstrap-generated sample distribution determined how statistically

significant the change was, if any (i.e., if the aggregated 30-year change reported in Chapter 4 was less than the 2.5th percentile but greater than 0.5st percentile of the bootstrap-generated distribution, change was considered statistically significant at the α=0.05 level).

The null hypothesis with this type of testing states, the difference between historical temperature and precipitation values are similar to future values expressed in the models. The levels of significance, called α, are chosen in this dissertation to be 0.1, 0.05, and 0.01. The α-value is the probability of rejecting the null hypothesis when it is true, which is called a "type I error". As the α-level decreases, the probability of committing a type I error decreases. If one fails to reject the null hypothesis when the null hypothesis is not true, this is called a "type II error" (Ott and Longnecker, 2010). The probability of making a type II error (called β) decreases as the sample size increases (Xu, 2006).

Weighted ensemble mean change was computed for each sub-region by utilizing the monthly model Perkins' skill scores and RMSE values computed based on the procedures found in subsections 2.2.2 and 2.2.3. Equation 2.13 illustrates the computation of weighted mean ensemble change,

$$mean_w = \frac{[mean_1 * w_1] + [mean_2 * w_2] + \ldots + [mean_n * w_n]}{w_1 + w_2 + \ldots + w_n} \qquad (2.13)$$

where $mean_n$ represents the unweighted mean change from the n^{th} ensemble member and w_n represents the weight garnered from either Perkins' skill score or RMSE.

Weighting allowed models that accurately simulated the reference period to have more weight in the ensemble mean than those models lacking skill (Perkins et al., 2012). Additionally, weighted ensemble mean change was applied at each grid point to allow for investigation of changes at a finer scale across the entire Southeast U.S. Both weighted and unweighted projections are presented because there continues to be contentious debate on the proper use of weighting models from an ensemble (Weigel et al., 2010); however, if much is known about the individual models, such as the relative contribution of individual model errors and model noise, generating biased weights can be avoided (Christensen et al., 2010).

A series of maps were generated for monthly temperature and precipitation to illustrate the spatial distribution of weighted and unweighted mean change using the Grid Analysis and Display System (GrADS) (Doty and Kinter, 1992; Doty and Kinter 1993). Lastly, box and whisker plots for each month, sub-region, and variable were generated to illustrate weighted and unweighted mean change for the two sub-regions as well as the associated spread between the models (Warner, 2011), with the lowest and highest projected mean change represented by the whiskers of the boxplot. Each model's grid points (for each sub-region) contributed to the box and whisker plots.

In summary, data used this work and described in this chapter included the NARCCAP dynamically downscaled ensemble, the Maurer gridded observed dataset, and the NARR dataset. The Maurer dataset is used to assess the skill of individual NARCCAP members in reproducing daily minimum and maximum temperature and mean precipitation, by month, utilizing four statistically-based skill metrics including Perkin's overlapping PDF method, Willmott's index of agreement, root mean square

error, and mean absolute error. Additionally, model bias was assessed by observing differences in various percentiles (1^{st}, 5^{th}, 10^{th}, 25^{th}, 50^{th}, 75^{th}, 90^{th}, 95^{th}, and 99^{th}) within the modeled and observed distributions. The NARR dataset is used to gain insights into the atmospheric system issues within each model at differing scales from the micro- to the synoptic-scale. The methodology for determining "value added" in the downscaling process was also described. Finally, calculation procedures of future model proejctions of minimum and maximum temperature and mean precipitation were outlined. The results of each of these metrics and methods are presented in the ensuing two chapters.

CHAPTER 3

NARCCAP MODEL VALIDATION

3.1 VALIDATION AND MODEL SKILL IN A HISTORICAL REFERENCE PERIOD

In this chapter, I evaluate NARCCAP model performance during the historical reference period. Perkins skill scores, Willmott's index of agreement, RMSE, and MAE values are presented for each month and model along with percentile plots to aid in determining degradation in model skill based on biases within their respective distributions. Values considered owning to high model skill for each metric and climate variable are defined in Table 3.1.

Table 3.1. Values considered owning to high skill for each of the four skill metrics.

Skill Metric	High Skill Threshold
Perkins skill score	0.7 – 1.0 (temperature and precipitation)
Willmott's index of agreement	0.5 – 1.0 (temperature and precipitation)
RMSE	0.0 – 2.0°C (temperature) 0.0 – 2.0 mm day^{-1} (precipitation)
MAE	0.0 – 2.0°C (temperature) 0.0 – 2.0 mm day^{-1} (precipitation)

3.1.1 MINIMUM TEMPERATURE

Validation of NARCCAP ensemble members for minimum temperature reveal that, overall, each member performs well in replicating observed conditions. Perkins skill scores for most RCMs (with the exception of theWRFG models, and RCM3-GFDL and ECP2-GFDL) remain above 0.7 for each month with Willmott values mostly above 0.5 for each NARCCAP ensemble member and month in the east (Figure 3.1 and 3.2; Table C.1 and C.2 in Appendix C) and west (Figure 3.4 and 3.5; Table C.3 and C.4 in Appendix C) sub-regions. RMSE and MAE values typically fall below 3°C for most models. For the WRFG RCMs, ECP2-GFDL, and GFDL-timeslice, July and August shows the worst skill. The degradation in skill for the WRFG RCMs and ECP2-GFDL are attributed to a cold bias between 1° to 3°C (Figure 3.3h and 3.3i). Additionally, the WRFG model illustrates a slight cold bias in the same months for the NCEP-driven runs found in Figure H.1 (Appendix H). The ECP2-GFDL's cold bias in July and August must be a function of the GFDL LBCs, as the NCEP-driven runs of the ECP2 model illustrate a warm bias in all months between 1° and 4°C (Figure H.1). The GFDL-timeslice, on the other hand, exhibits a warm bias of 2° to 5°C from the 50^{th} through 99^{th} percentiles. The best performing models are the RCM3-CGCM3 and CRCM-CGCM3 which show very little warm or cold bias, remaining within ±2°C of observations across all percentiles and months, and only a 1° to 2°C warm bias in the NCEP-driven runs. Although a bias of 1° to 2°C may seem rather large, it falls within a commonly known and accepted threshold in climate models (e.g., Randall et al., 2007; John and Soden, 2007).

Interestingly, the two models driven by GFDL exhibit degradation in skill in the winter and early spring, an observation not found in the other ensemble members.

Percentile plots reveal these RCMs suffer from significant cold bias between 4° and 8°C. This strong cold bias is passed from the GFDL model to each RCM, and is portrayed in Figure F.1. Conversely, the CCSM GCM exhibits a warm bias in most months between 1° and 5°C which is tempered slightly in the downscaling process by both the MM5I and CRCM, resulting in a slight warm bias of not more than 2°C in any given.

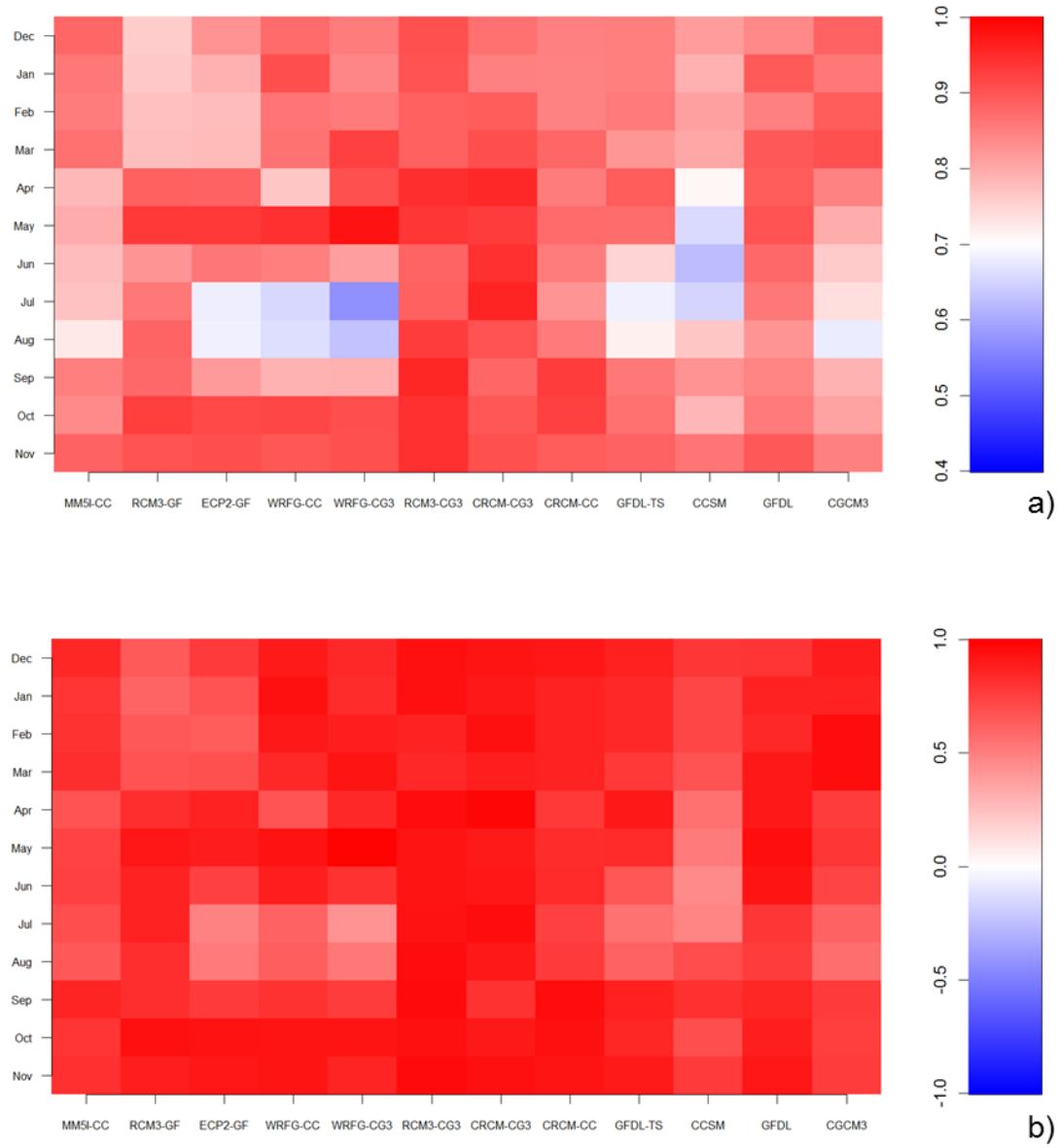

Figure 3.1. Hovmöller diagram of minimum temperature Perkins skill score (a) and Willmott's index of agreement (b) for the east sub-region. Abbreviations for NARCCAP ensemble members and GCMs: "MM5I-CC"=MM5I-CCSM, "RCM3-GF"=RCM3-GFDL, "ECP2-GF"=ECP2-GFDL, "WRFG-CC"=WRFG-CCSM, "WRFG-CG3"=WRFG-CGCM3, "RCM3-CG3"=RCM3-CGCM3, "CRCM-CG3"=CRCM-CGCM3, "CRCM-CC"=CRCM-CCSM", "GFDL-TS"=GFDL-Timeslice, "CCSM"=CCSM GCM, "GFDL"=GFDL GCM, and "CGCM3"=CGCM3 GCM.

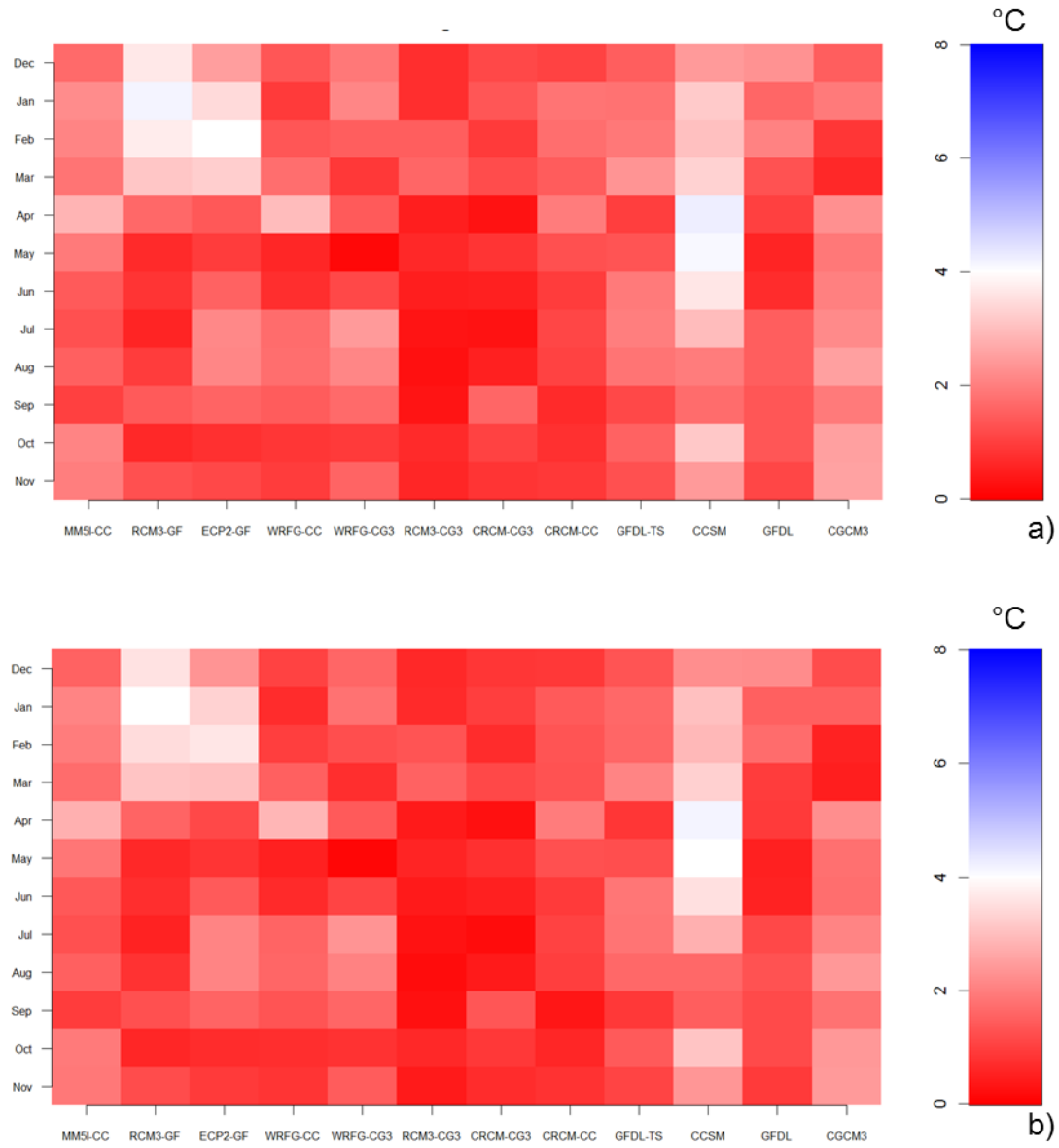

Figure 3.2. Hovmöller diagram of minimum temperature RMSE (a) and MAE (b) for the east sub-region. Abbreviations for NARCCAP ensemble members and GCMs: "MM5I-CC"=MM5I-CCSM, "RCM3-GF"=RCM3-GFDL, "ECP2-GF"=ECP2-GFDL, "WRFG-CC"=WRFG-CCSM, "WRFG-CG3"=WRFG-CGCM3, "RCM3-CG3"=RCM3-CGCM3, "CRCM-CG3"=CRCM-CGCM3, "CRCM-CC"=CRCM-CCSM", "GFDL-TS"=GFDL-Timeslice, "CCSM"=CCSM GCM, "GFDL"=GFDL GCM, and "CGCM3"=CGCM3 GCM.

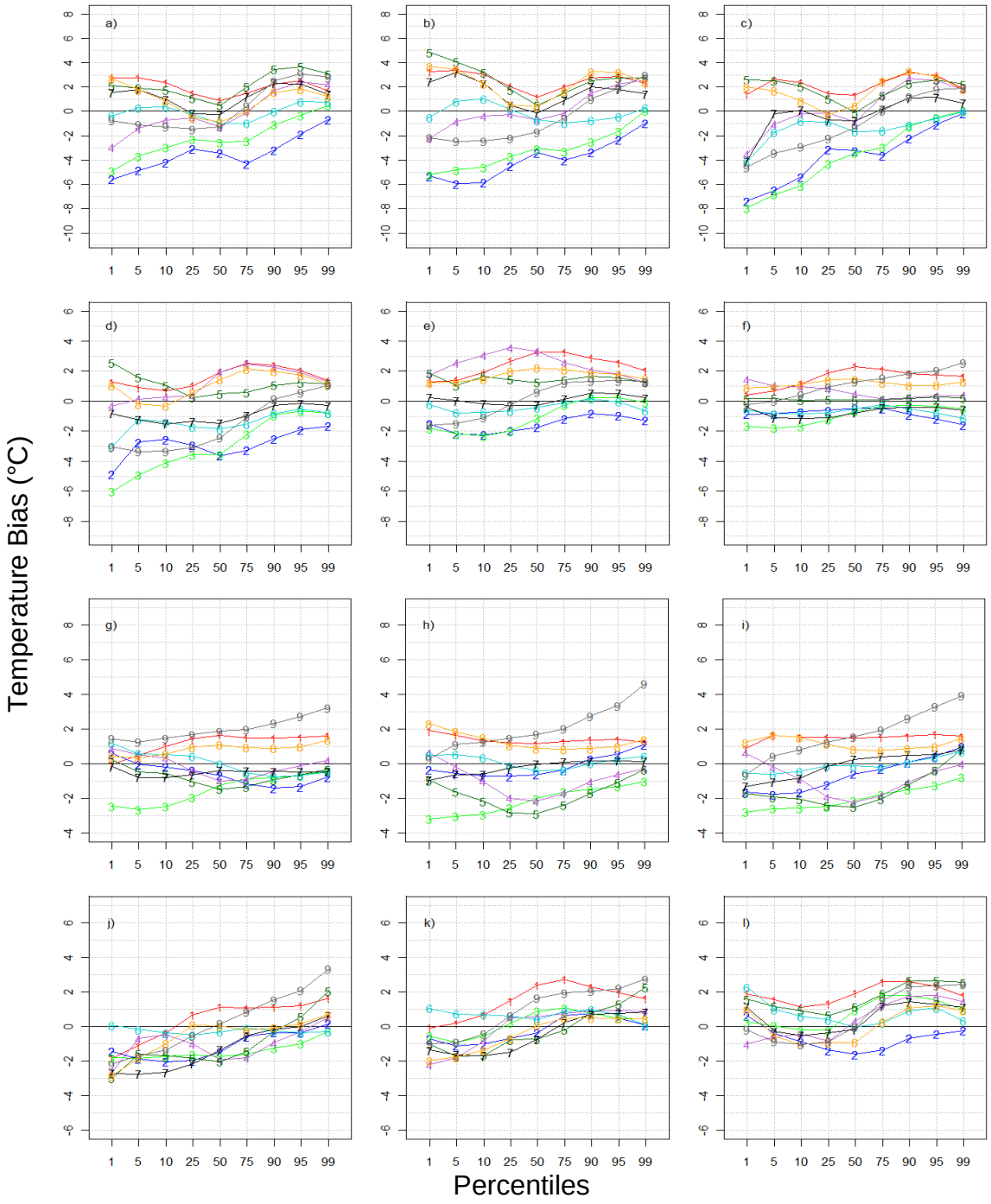

Figure 3.3. Percentile plots of minimum temperature bias for the east sub-region from nine NARCCAP members for December (a), January (b), February (c), March (d), April (e), May (f), June (g), July (h), August (i), September (j), October (k), and November (l). Labels for the NARCCAP ensemble members: “1”=MM5I-CCSM, “2”=RCM3-GFDL, “3”=ECP2-GFDL, “4”=WRFG-CCSM, “5”=WRFG-CGCM3, “6”=RCM3-CGCM3, “7”=CRCM-CGCM3, “8”=CRCM-CCSM, and “9”=GFDL-timeslice.

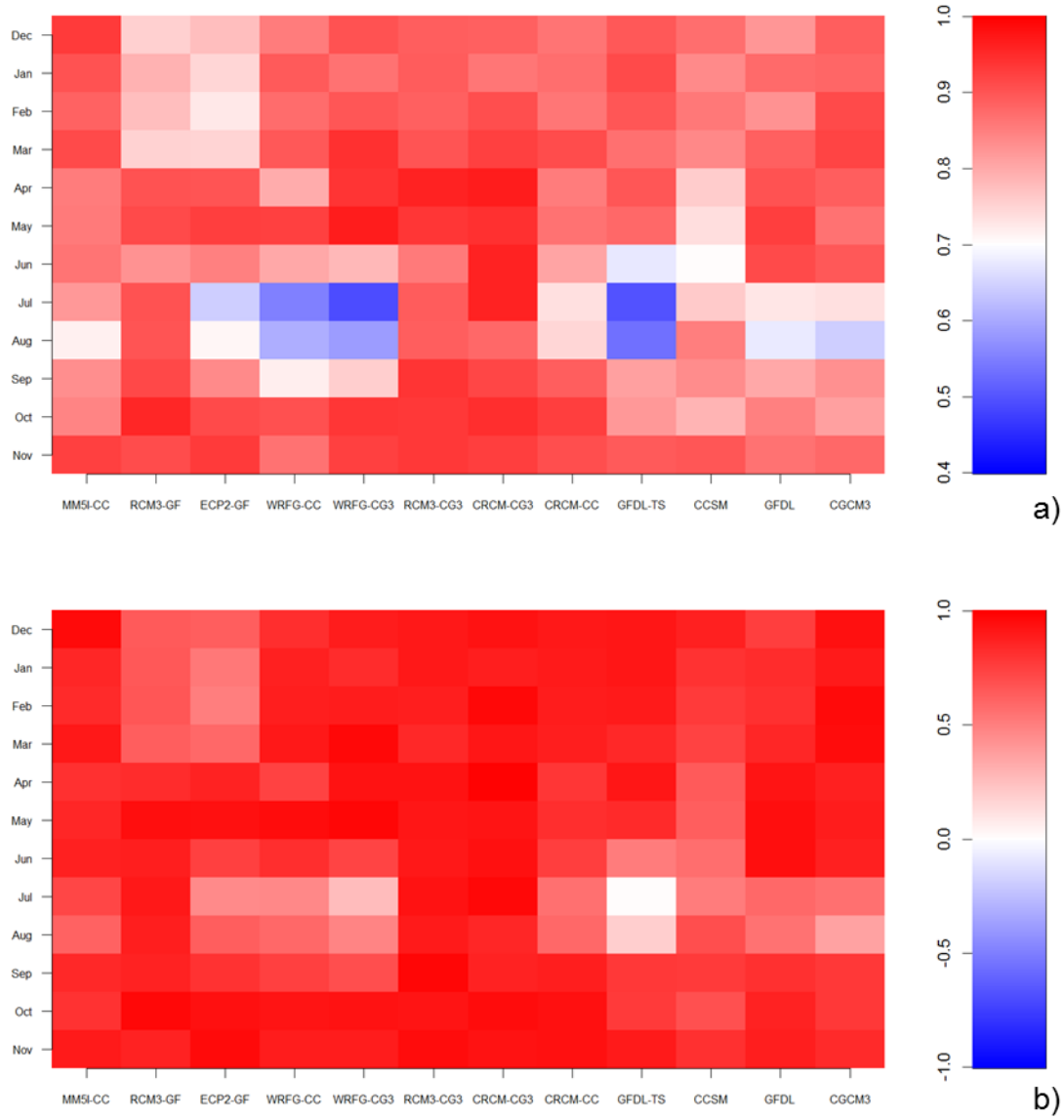

Figure 3.4. Hovmöller diagram of minimum temperature Perkins skill score (a) and Willmott's index of agreement (b) for the west sub-region. Abbreviations for NARCCAP ensemble members and GCMs: "MM5I-CC"=MM5I-CCSM, "RCM3-GF"=RCM3-GFDL, "ECP2-GF"=ECP2-GFDL, "WRFG-CC"=WRFG-CCSM, "WRFG-CG3"=WRFG-CGCM3, "RCM3-CG3"=RCM3-CGCM3, "CRCM-CG3"=CRCM-CGCM3, "CRCM-CC"=CRCM-CCSM", "GFDL-TS"=GFDL-Timeslice, "CCSM"=CCSM GCM, "GFDL"=GFDL GCM, and "CGCM3"=CGCM3 GCM.

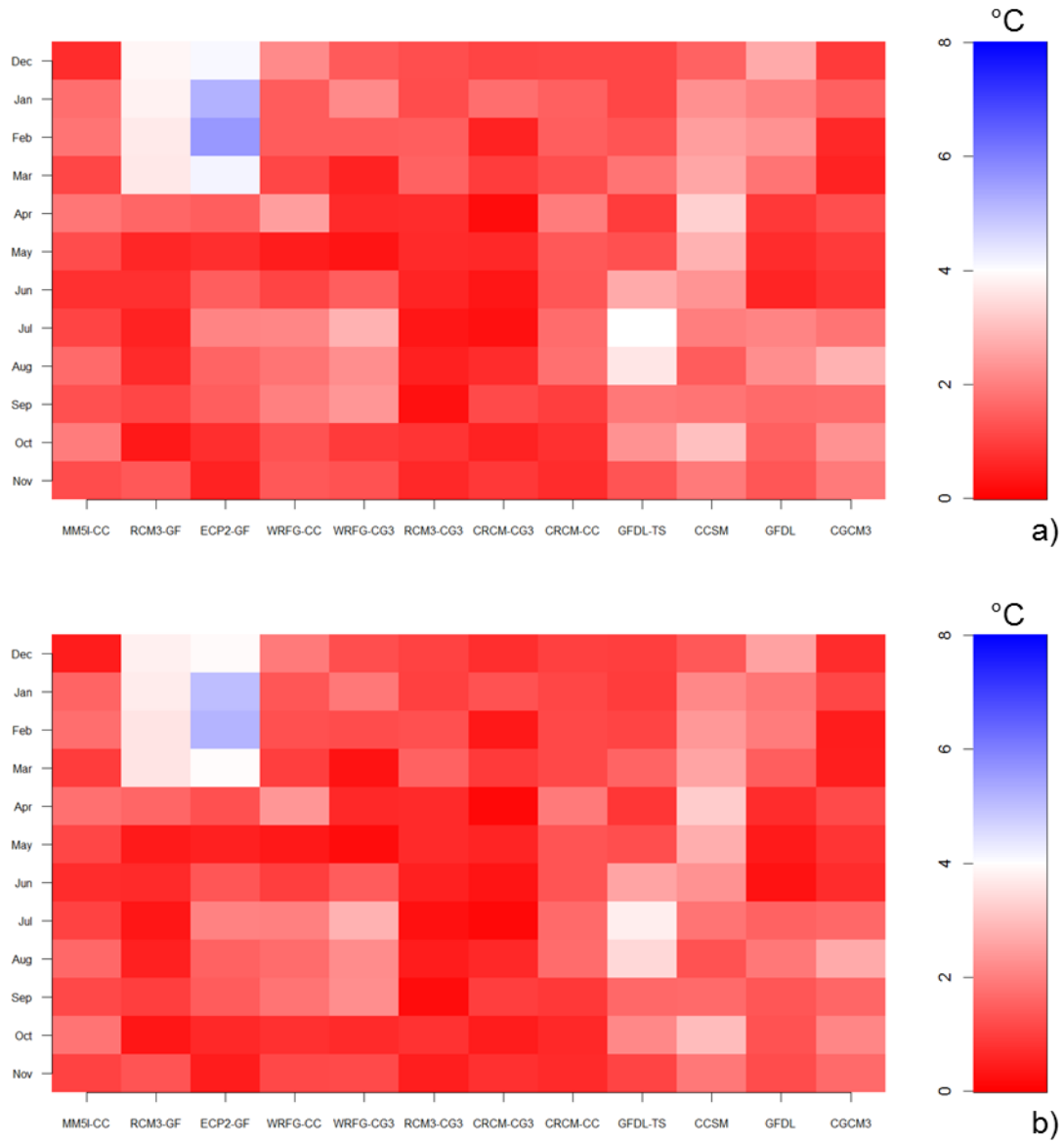

Figure 3.5. Hovmöller diagram of minimum temperature RMSE (a) and MAE (b) for the west sub-region. Abbreviations for NARCCAP ensemble members and GCMs: "MM5I-CC"=MM5I-CCSM, "RCM3-GF"=RCM3-GFDL, "ECP2-GF"=ECP2-GFDL, "WRFG-CC"=WRFG-CCSM, "WRFG-CG3"=WRFG-CGCM3, "RCM3-CG3"=RCM3-CGCM3, "CRCM-CG3"=CRCM-CGCM3, "CRCM-CC"=CRCM-CCSM", "GFDL-TS"=GFDL-Timeslice, "CCSM"=CCSM GCM, "GFDL"=GFDL GCM, and "CGCM3"=CGCM3 GCM.

Percentile plots for the west sub-region (Figure 3.6) reveal the RCM3-GFDL and ECP2-GFDL models have a more pronounced cold bias than the eastern sub-region, with cold biases from December through March on the order of 4° to 10.5°C for the lower 50th percentiles. The cold bias must be a function of the GFDL LBCs as both the ECP2 and RCM3 RCMs have a warm bias of 1° to 3°C from December through March with the NCEP-driven runs (Figure H.2). Conversely, the GFDL-timeslice's warm bias observed in the east sub-region is enhanced in the west sub-region. What was a 2° to 5°C warm bias in above-median temperatures in the east becomes a 3° to 8°C warm bias in the west, the result of a strong warm bias in the same percentiles with the driving GCM (Figure F.2). This bias during the warmest months of the year, especially in the upper percentiles, leads to an increase in nocturnal evaporation from the soil (Novick, et al., 2009). Enhanced nocturnal evaporation aids rapid daytime temperature increases and contribute to an increased number of heat waves, leading to a positive feedback wherein evaporation is increased leading to drier soil (assuming little to no replenishment) which perpetuates the warm cycle (Trenberth, 2008).

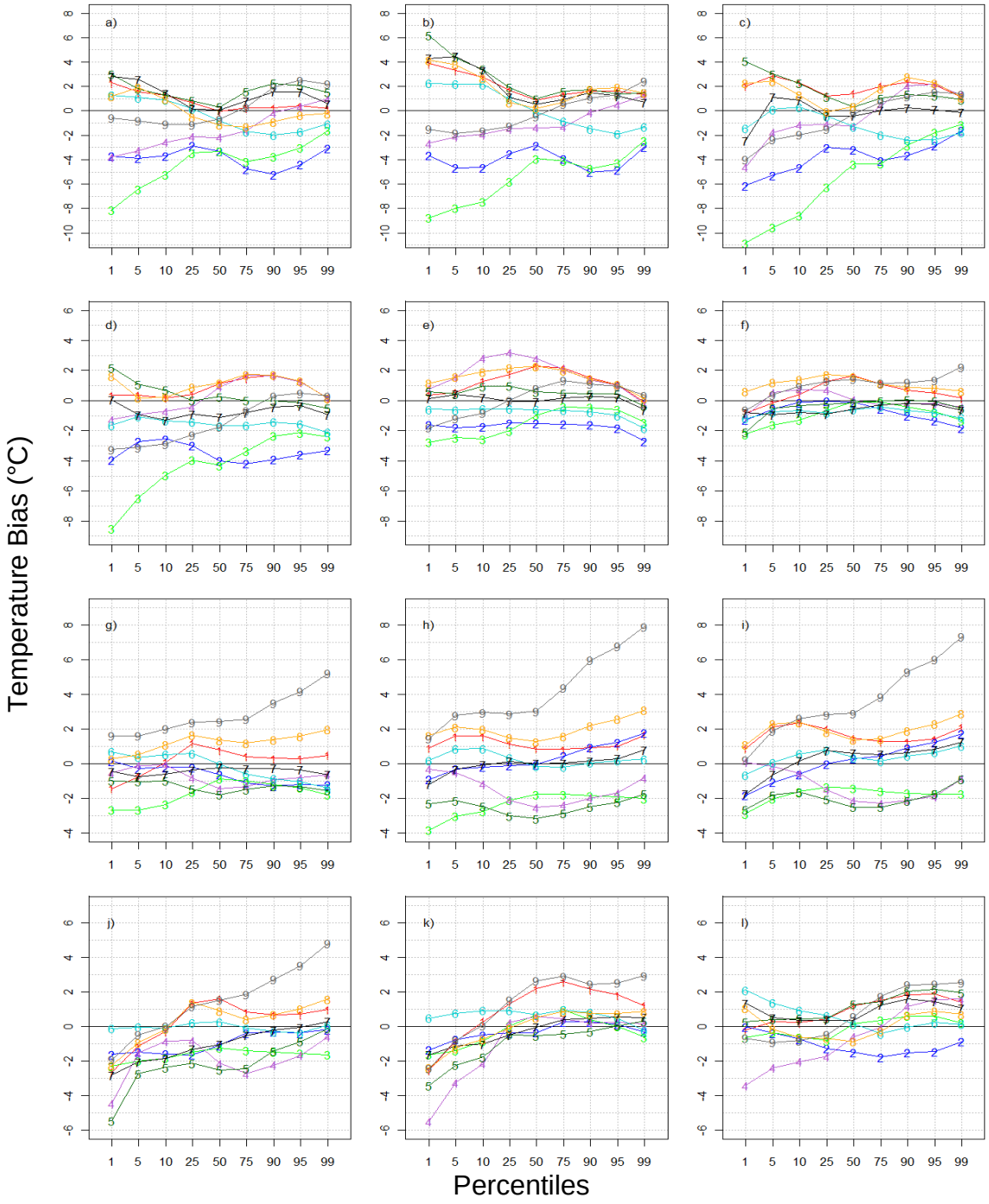

Figure 3.6. Percentile plots of minimum temperature bias for the west sub-region from nine NARCCAP members for December (a), January (b), February (c), March (d), April (e), May (f), June (g), July (h), August (i), September (j), October (k), and November (l). Labels for the NARCCAP ensemble members: “1”=MM5I-CCSM, “2”=RCM3-GFDL, “3”=ECP2-GFDL, “4”=WRFG-CCSM, “5”=WRFG-CGCM3, “6”=RCM3-CGCM3, “7”=CRCM-CGCM3, “8”=CRCM-CCSM, and “9”=GFDL-timeslice.

3.1.2 MAXIMUM TEMPERATURE

Unlike minimum temperature which proves relatively skillful for almost all NARCCAP members, maximum temperature is less skillful with higher errors/bias in both sub-regions. The most glaring short-comings are the lack of skill and high RMSE and MAE values shown by the RCM3-GFDL and ECP2-GFDL (Figures 3.7, 3.8, 3.10, and 3.11; Tables C.5 through C.8). The low skill values are attributed to a cold bias in the GFDL GCM (Figure F.3 and F.4) from winter through mid spring between 3°C and 7°C. Although two models with the same LBCs show relatively little skill in replicating daily maximum temperature and have high RMSE and MAE values, the fact the RCM3-CGCM3 illustrates relatively little skill points to a systematic error within the RCM3 itself, and is not simply an issue of the GCM providing biased LBCs. This point will be discussed further in Section 3.2. Conversely, the CRCM-CCSM suffers a reduction in skill from July through September, a direct result of the model exhibiting a strong warm bias from the 50^{th} percentile to the 99^{th} percentile and a lesser warm bias in the 1^{st} through 50^{th} percentiles. Part of the warm bias can be attributed to the CCSM GCM (Figure F.4) which shows a warm bias from the 50^{th} through the 99^{th} percentiles and a slight warm bias of less than 2°C from the 1^{st} through 50^{th} percentiles while the other part is attributed to the strong warm bias observed with the NCEP-driven runs of the CRCM observed over the same period.

Percentile plots (Figure 3.9 and 3.12) highlight the significant cold bias found within the GFDL-based NARCCAP ensemble members, leading to low skill scores and high RMSE and MAE values. Most months exhibit a cold bias on the order of 4°C with values as low as 9° and 10°C in winter. Four of the nine NARCCAP members have a

cold bias greater than 4°C during the months encompassing boreal winter, spring, and mid to late fall. The cold bias observed with the GCM-driven runs is partially attributed to the persistent cold bias observed in most months (and percentiles) for each RCM driven with NCEP LBCs (Figure H.3). Percentile plots also reveal the CRCM-CCSM suffers from a warm bias, most pronounced from June through September with the largest warm bias occurring from the 50^{th} to 99^{th} percentiles.

An interesting comparison between the GFDL-driven (RCM-based runs) and the GFDL-timeslice reveals the GFDL-timeslice typically outperforms the RCM-driven GFDL runs, with higher skill-based values and lower error/bias values. This can be attributed to the timeslice experiment utilizing observed sea-surface conditions rather than GCM-based sea-surface conditions. By applying observations into the model, the model is "nudged" closer to solution found in observations rather than allowing the GCM to completely control the simulation. Additionally, it should be noted that the separation of skill and bias metrics of the GFDL-driven models are not widely separated with respect to minimum temperature, potentially revealing that the inclusion of observed sea-surface conditions impacts maximum temperatures more than minimum temperatures.

The most consistent and least bias model in both sub-regions is the MM5I-CCSM with Perkins skill scores and Willmott values exceeding 0.75, and low RMSE and MAE values between 0.5° and 2°C. Percentile plots concur with the MM5I-CCSM's skillfulness by showing the model rarely deviates beyond ±2°C from observations across all percentiles. The only months in which the MM5I-CCSM observes a small deviation in skill are December, August, and November when the model exhibits a consistent bias throughout all percentiles (slight cold bias in December and November; slight warm bias

in August). The MM5I-CCSM is the only model (with respect to temperature) to attain Perkins skill scores of greater than 0.9 for at least eight months, Willmott values of 0.85 for at least eight months, and RMSE and MAE values less than 1.5°C for 10 months.

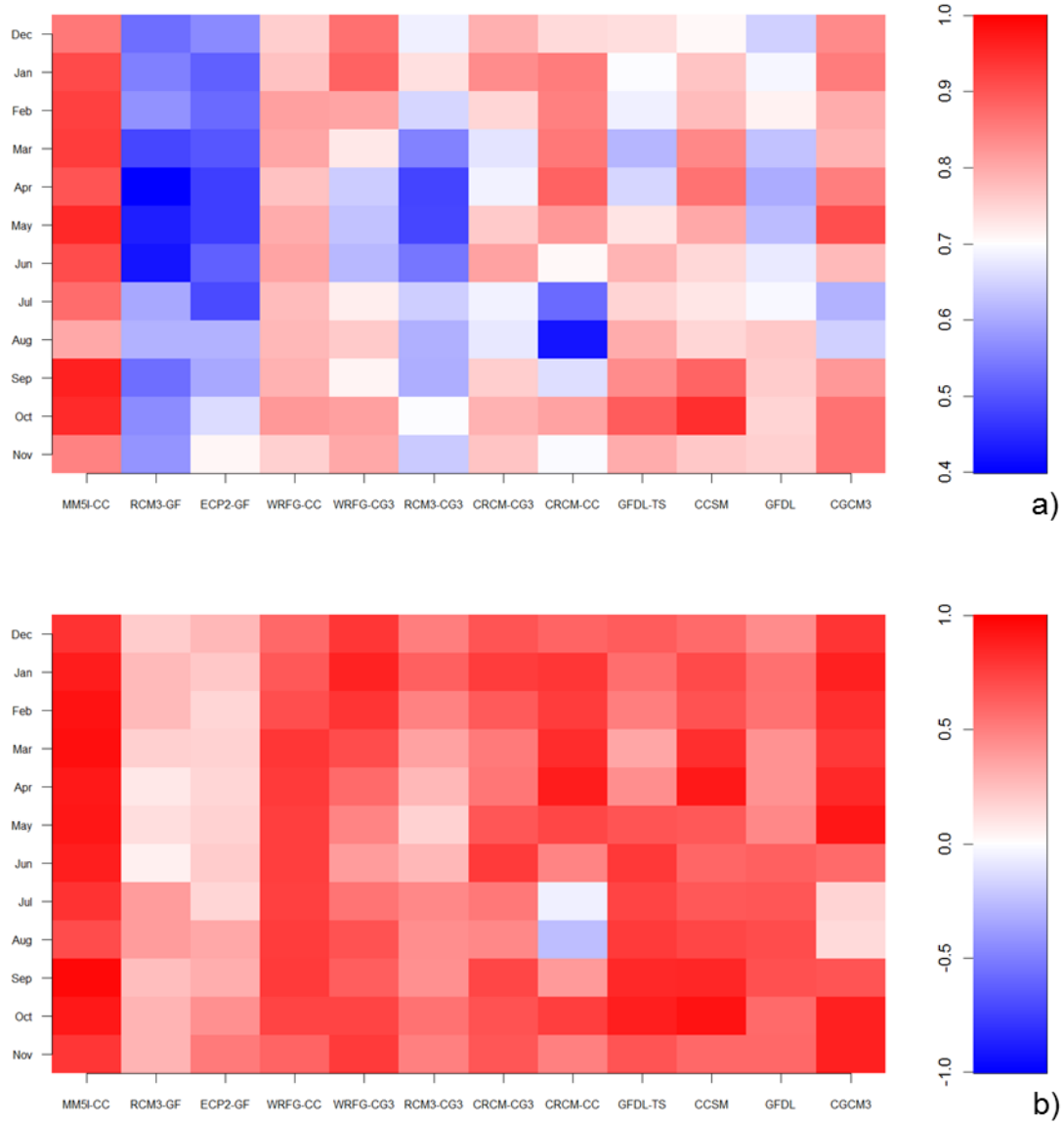

Figure 3.7. Hovmöller diagram of maximum temperature Perkins skill score (a) and Willmott's index of agreement (b) for the east sub-region. Abbreviations for NARCCAP ensemble members and GCMs: "MM5I-CC"=MM5I-CCSM, "RCM3-GF"=RCM3-GFDL, "ECP2-GF"=ECP2-GFDL, "WRFG-CC"=WRFG-CCSM, "WRFG-CG3"=WRFG-CGCM3, "RCM3-CG3"=RCM3-CGCM3, "CRCM-CG3"=CRCM-CGCM3, "CRCM-CC"=CRCM-CCSM", "GFDL-TS"=GFDL-timeslice, "CCSM"=CCSM GCM, "GFDL"=GFDL GCM, and "CGCM3"=CGCM3 GCM.

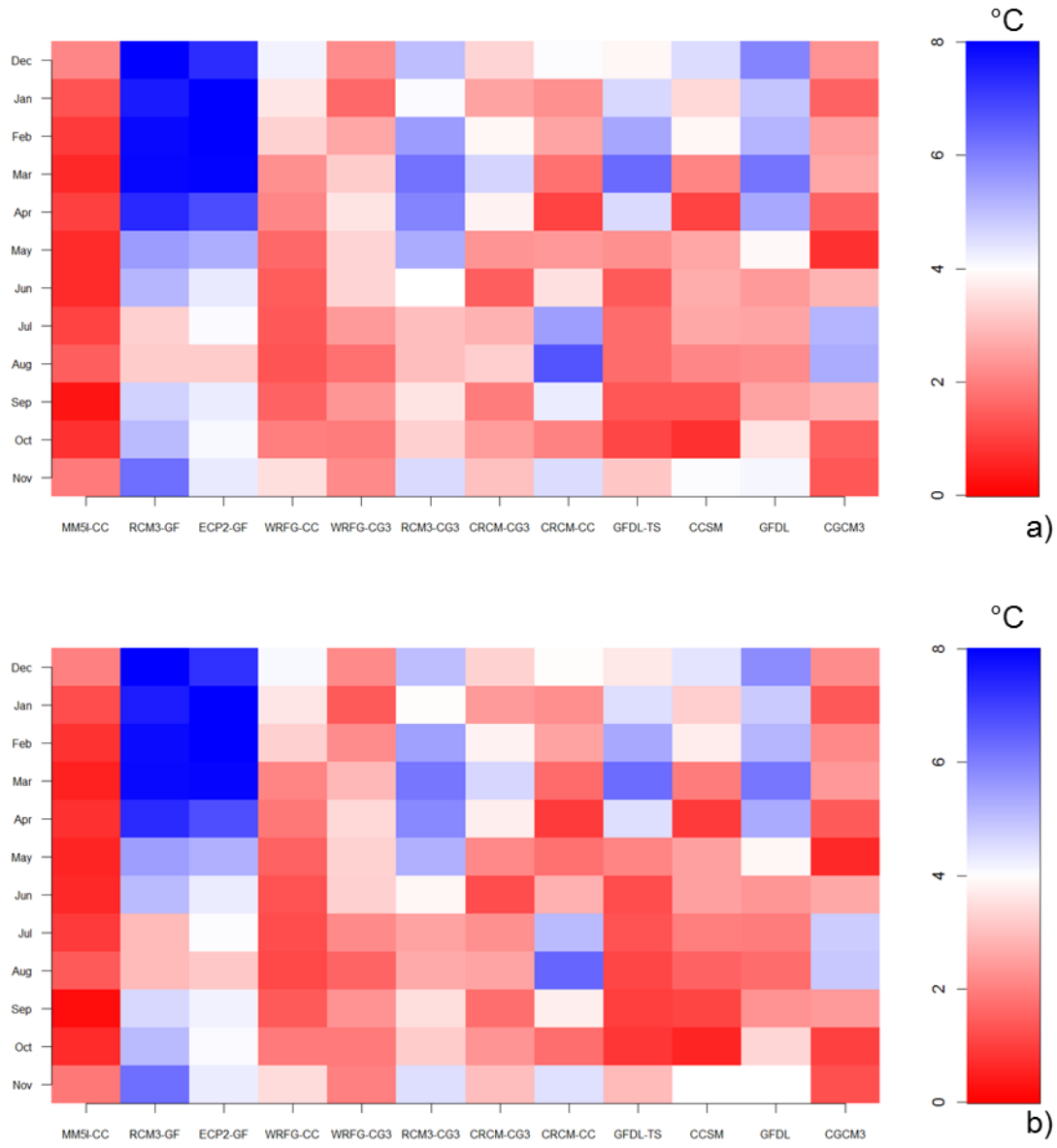

Figure 3.8. Hovmöller diagram of maximum temperature RMSE (a) and MAE (b) for the east sub-region. Abbreviations for NARCCAP ensemble members and GCMs: "MM5I-CC"=MM5I-CCSM, "RCM3-GF"=RCM3-GFDL, "ECP2-GF"=ECP2-GFDL, "WRFG-CC"=WRFG-CCSM, "WRFG-CG3"=WRFG-CGCM3, "RCM3-CG3"=RCM3-CGCM3, "CRCM-CG3"=CRCM-CGCM3, "CRCM-CC"=CRCM-CCSM", "GFDL-TS"=GFDL-timeslice, "CCSM"=CCSM GCM, "GFDL"=GFDL GCM, and "CGCM3"=CGCM3 GCM.

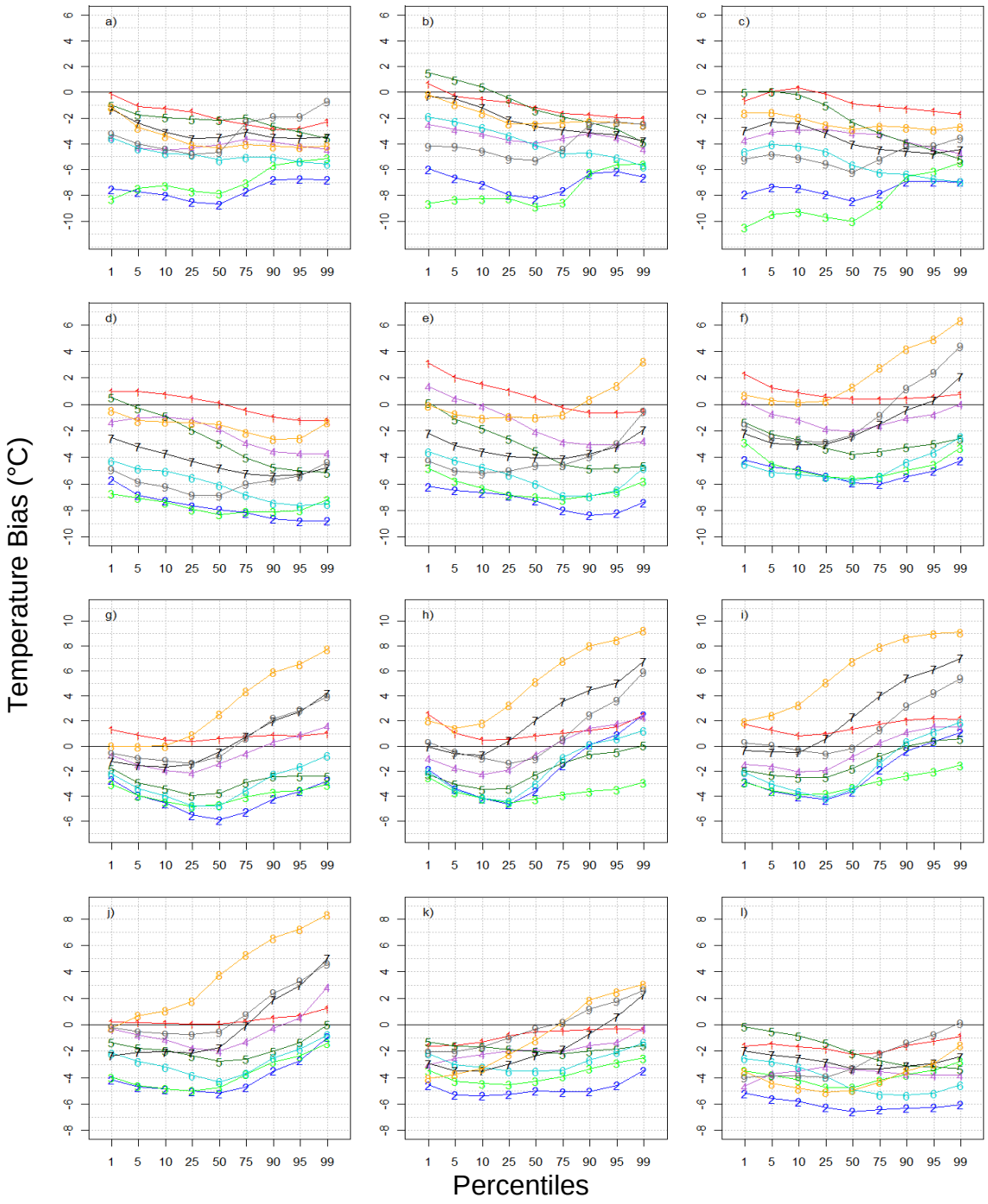

Figure 3.9. Percentile plots of minimum temperature bias for the east sub-region from nine NARCCAP ensemble members for December (a), January (b), February (c), March (d), April (e), May (f), June (g), July (h), August (i), September (j), October (k), and November (l). Labels for the NARCCAP ensemble members: "1"=MM5I-CCSM, "2"=RCM3-GFDL, "3"=ECP2-GFDL, "4"=WRFG-CCSM, "5"=WRFG-CGCM3, "6"=RCM3-CGCM3, "7"=CRCM-CGCM3, "8"=CRCM-CCSM, and "9"=GFDL-Timeslice.

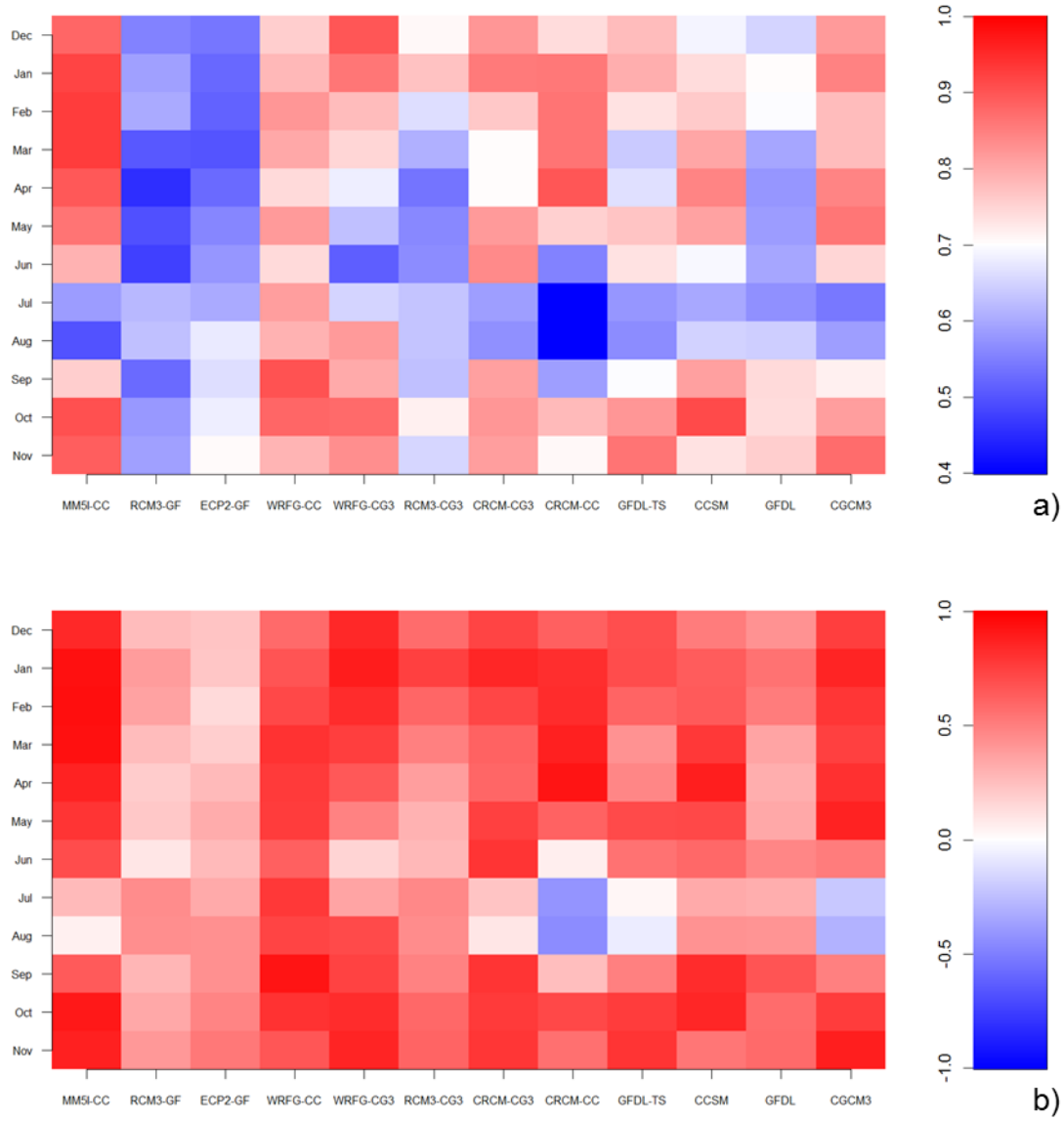

Figure 3.10. Hovmöller diagram of maximum temperature Perkins skill score (a) and Willmott's index of agreement (b) for the west sub-region. Abbreviations for NARCCAP ensemble members and GCMs: "MM5I-CC"=MM5I-CCSM, "RCM3-GF"=RCM3-GFDL, "ECP2-GF"=ECP2-GFDL, "WRFG-CC"=WRFG-CCSM, "WRFG-CG3"=WRFG-CGCM3, "RCM3-CG3"=RCM3-CGCM3, "CRCM-CG3"=CRCM-CGCM3, "CRCM-CC"=CRCM-CCSM", "GFDL-TS"=GFDL-timeslice, "CCSM"=CCSM GCM, "GFDL"=GFDL GCM, and "CGCM3"=CGCM3 GCM.

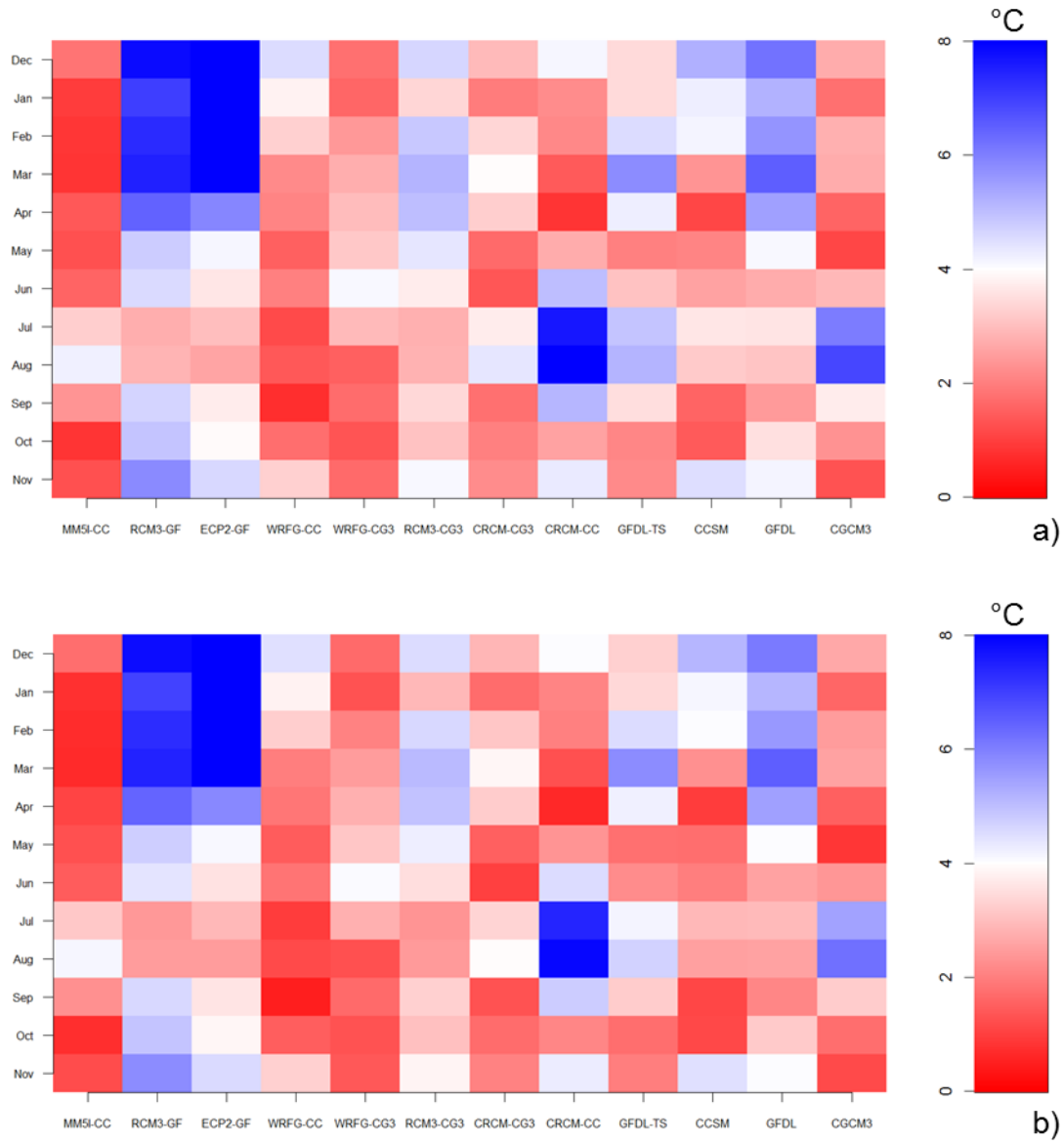

Figure 3.11. Hovmöller diagram of maximum temperature RMSE (a) and MAE (b) for the west sub-region. Abbreviations for NARCCAP ensemble members and GCMs: "MM5I-CC"=MM5I-CCSM, "RCM3-GF"=RCM3-GFDL, "ECP2-GF"=ECP2-GFDL, "WRFG-CC"=WRFG-CCSM, "WRFG-CG3"=WRFG-CGCM3, "RCM3-CG3"=RCM3-CGCM3, "CRCM-CG3"=CRCM-CGCM3, "CRCM-CC"=CRCM-CCSM", "GFDL-TS"=GFDL-timeslice, "CCSM"=CCSM GCM, "GFDL"=GFDL GCM, and "CGCM3"=CGCM3 GCM.

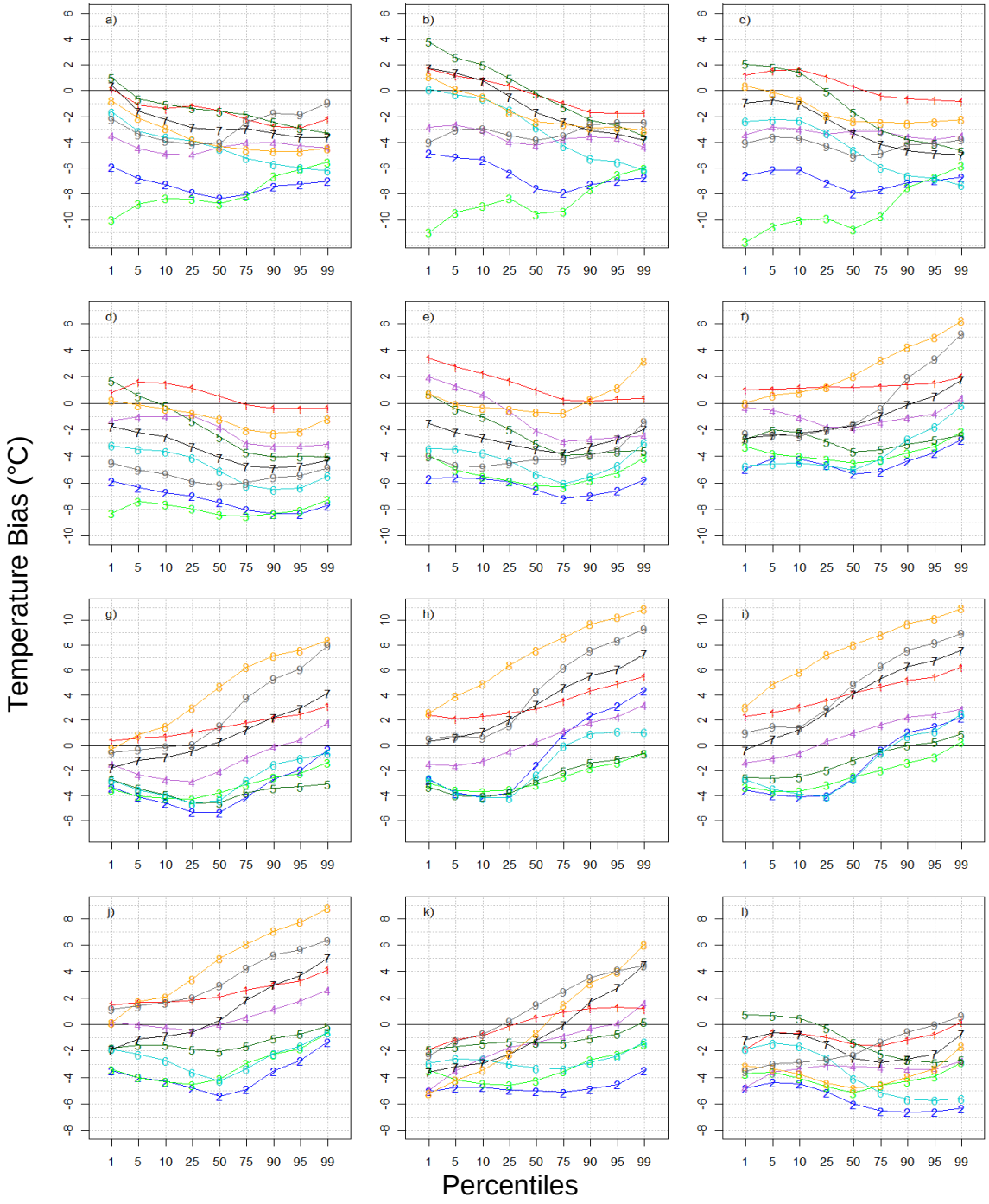

Figure 3.12. Percentile plots of minimum temperature bias for the west sub-region from nine NARCCAP ensemble members for December (a), January (b), February (c), March (d), April (e), May (f), June (g), July (h), August (i), September (j), October (k), and November (l). Labels for the NARCCAP ensemble members: "1"=MM5I-CCSM, "2"=RCM3-GFDL, "3"=ECP2-GFDL, "4"=WRFG-CCSM, "5"=WRFG-CGCM3, "6"=RCM3-CGCM3, "7"=CRCM-CGCM3, "8"=CRCM-CCSM, and "9"=GFDL-Timeslice.

3.1.3 MEAN PRECIPITITATION

Results of skill associated with mean precipitation for the NARCCAP RCMs greatly depend on the metrics used to quantify skill. As discussed in Sub-section 2.2.4, no discernible relationship between Perkins/Willmott scores and RMSE/MAE for precipitation can be found, indicating the metrics quantitatively measure non-Gaussian, with outliers having a much larger impact in the calculation of RMSE and MAE than in Perkins or Willmotts' methods. Very rarely is a models' Perkins or Willmott skill score below 0.8, indicating the models are able to adequately reproduce the daily data distribution found in observations, especially considering most data points are contained within the left tail of the distribution, with a very small number comprising the right tail of the distribution. However, a high RMSE and MAE, coupled with high Perkins skill score, indicates the model either under- or over-predicts the quantity and/or frequency of precipitation events in the upper percentiles (from 75^{th} through 99^{th}-percentile). Although the upper percentiles account for an extremely small portion of the data distribution (while still having a large impact on daily total rainfall), their impact on RMSE and MAE is significant because these values are large outliers from the mean. Save for a few exceptions, most of the models have Perkins skill scores which exceed 0.8, with several in the 0.85 to 0.95 range for both sub-regions (Figure 3.13 and Table C.9). Additionally, Willmott index of agreement values (Table C.10) are mostly contained within the 0.82 to 0.96 range.

The only models to exhibit degradation in Perkins and Willmott skill scores in the east sub-region are the CRCM-CGCM3 and CRCM-CCSM in September and October, with Perkins skill scores between 0.7 and 0.8 (save for CRCM-CGCM3's September

Perkins skill score between 0.8 and 0.85) and Willmott values between 0.75 and 0.85. Percentile plots (Figure 3.15) reveal the CRCM RCMs exhibit a dry bias across all percentiles, but is most pronounced from the 50th through 99th percentiles and ranges between 30 and 60% below observations. A similar dry bias is observed from the winter through mid spring and fall for the NCEP-driven runs of the CRCM (Figure H.5). In terms of real numbers, assume the 75th percentile value from observations was 100 mm/day, a 30 to 60% dry bias would mean the model predicts the 75th percentile value to fall between 40 and 70 mm/day. RMSE and MAE values are hurt not only by the quantity of model bias, but also the number of percentiles in which the model exhibits said bias.

The west sub-region performs slightly worse than the east sub-region with regards to Perkins and Willmott scores, however, RMSE and MAE values are higher for most models, particularly in the winter and spring months (Figure 3.16 and 3.17; Table C.11 and C.12). Percentile plots (Figure 3.18) reveal from December through May, most all models have a dry bias in the lower 50th percentiles between 5 and 30%. Although Perkins and Willmott scores are respectable during this period (between 0.8 and 0.9 for both, respectively), indicating the models are able to replicate the daily precipitation pattern, they fail to generate lighter precipitation found in the bottom half of the distribution. This under-estimation can lead to sustained water issues because precipitation values found within the first half of the PDF are responsible for the majority over observed precipitation.

GCM-based percentile plots (Figure F.5) illustrate all three models stay within a bias of ±15% below the 50th percentile, steadily increasing to a dry bias between 20 and 65% at the 99th percentile. Most RCMs, save for those run by the CCSM GCM, are able

to take input from their GCM and curb the dry bias at the higher percentiles, however, some models over compensate and what was once a dry bias within the GCM becomes a wet bias of the same magnitude in the RCM. This finding is attributed to the wet bias observed consistently in the ECP2, MM5I, and WRFG NCEP-driven models (Figure H.5) for all months. Additionally, the RCM3-NCEP model illustrates a pronounced wet bias in the highest percentiles from spring through mid summer. Given the findings from this sub-section, future work should consider if precipitation should be subjected to different evaluation criteria (from those used in assessing temperature) such as the number of rain days or precipitation intensity return intervals.

Although more than half of the models have a wet bias in the 50th through 99th percentiles and is a function of a wet bias in the same percentiles for each RCM driven by NCEP boundary conditions (Figure H.6). These precipitation amounts do not adequately replenish water supplies and sub-surface moisture due to high runoff rates. Even more troubling is the dry bias observed from most models during the summer across all percentiles. The dry bias within the GCMs noted for the east sub-region is slightly greater in the west sub-region (Figure F.6) which is maintained, and in some cases enhanced, within the RCMs. The dry bias must be attributed to the GCMs because each RCM run with NCEP LBCs illustrates a wet bias during the summer, with the exception of the WRFG from the 5th through 50th percentiles and the CRCM from the 90th to 99th percentiles. Although observations show extreme precipitation (both high and low) is increasing across the Northern Hemisphere (Min et al., 2011) and U.S. (Samenow, 2012), the models exhibit a propencity to high-end exaggeration.

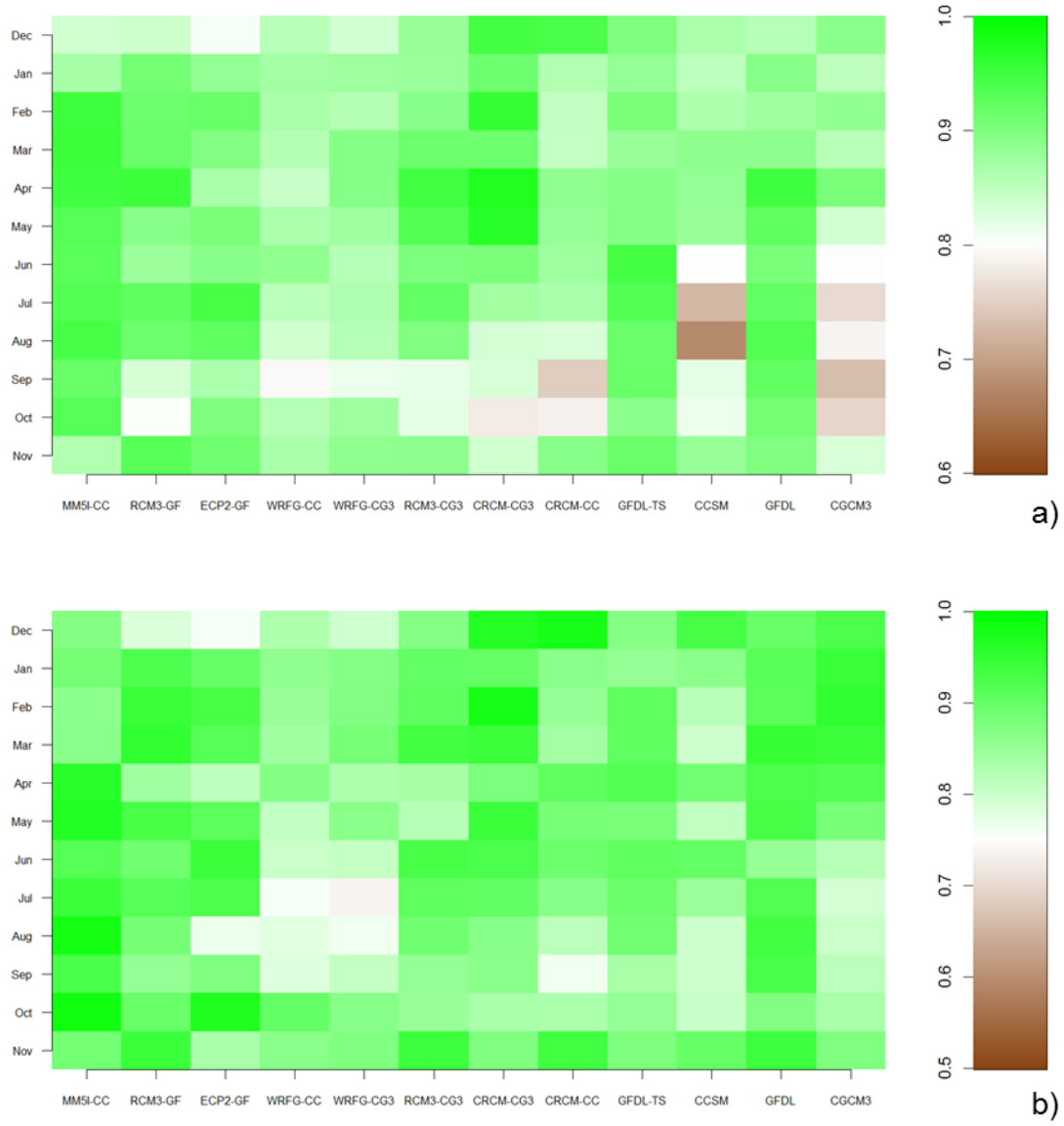

Figure 3.13. Hovmöller diagram of mean precipitation Perkins skill score (a) and Willmott's index of agreement (b) for the east sub-region. Abbreviations for NARCCAP ensemble members and GCMs: "MM5I-CC"=MM5I-CCSM, "RCM3-GF"=RCM3-GFDL, "ECP2-GF"=ECP2-GFDL, "WRFG-CC"=WRFG-CCSM, "WRFG-CG3"=WRFG-CGCM3, "RCM3-CG3"=RCM3-CGCM3, "CRCM-CG3"=CRCM-CGCM3, "CRCM-CC"=CRCM-CCSM", "GFDL-TS"=GFDL-Timeslice, "CCSM"=CCSM GCM, "GFDL"=GFDL GCM, and "CGCM3"=CGCM3 GCM.

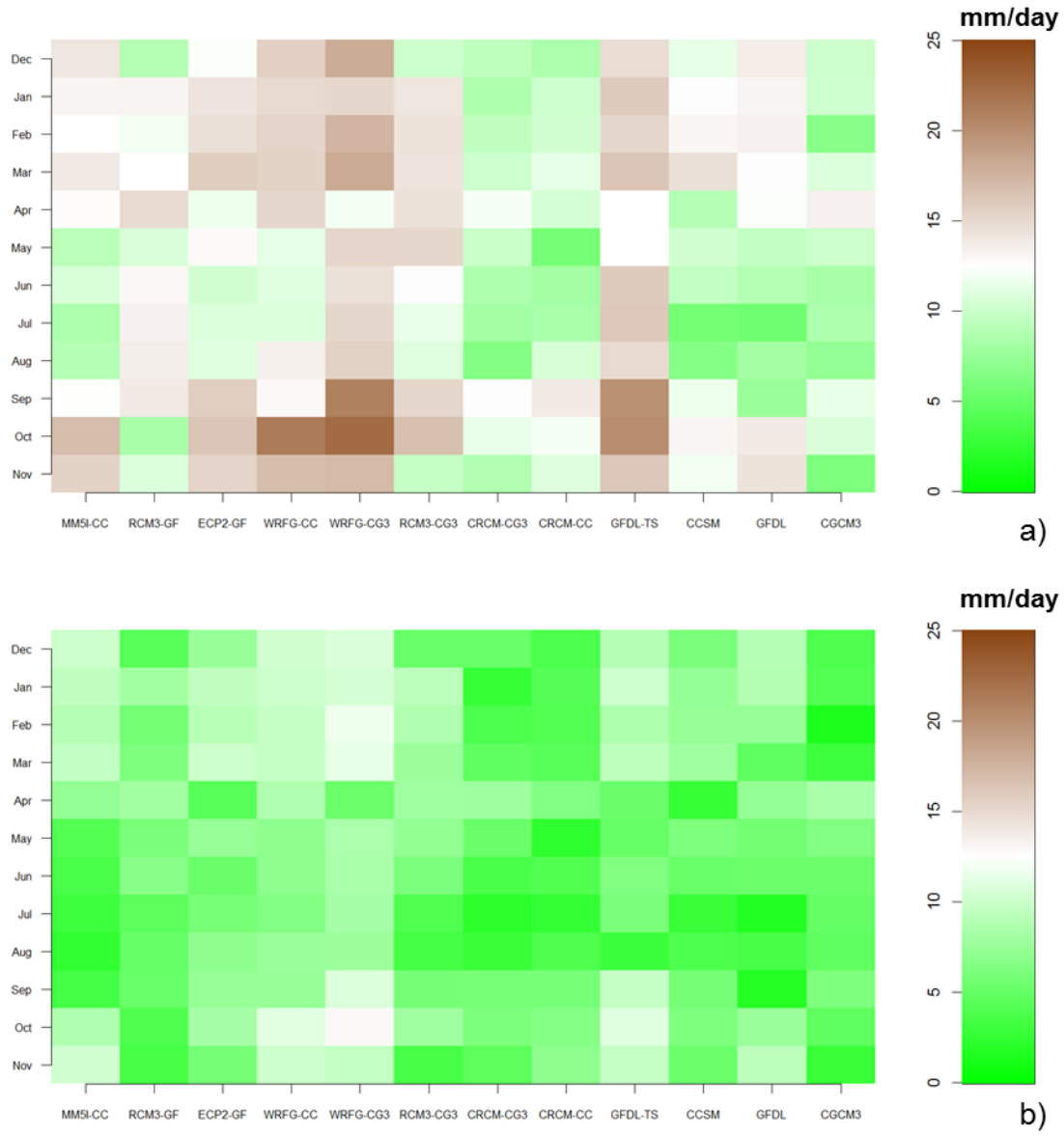

Figure 3.14. Hovmöller diagram of mean precipitation RMSE (a) and MAE (b) for the east sub-region. Abbreviations for NARCCAP ensemble members and GCMs: "MM5I-CC"=MM5I-CCSM, "RCM3-GF"=RCM3-GFDL, "ECP2-GF"=ECP2-GFDL, "WRFG-CC"=WRFG-CCSM, "WRFG-CG3"=WRFG-CGCM3, "RCM3-CG3"=RCM3-CGCM3, "CRCM-CG3"=CRCM-CGCM3, "CRCM-CC"=CRCM-CCSM", "GFDL-TS"=GFDL-Timeslice, "CCSM"=CCSM GCM, "GFDL"=GFDL GCM, and "CGCM3"=CGCM3 GCM.

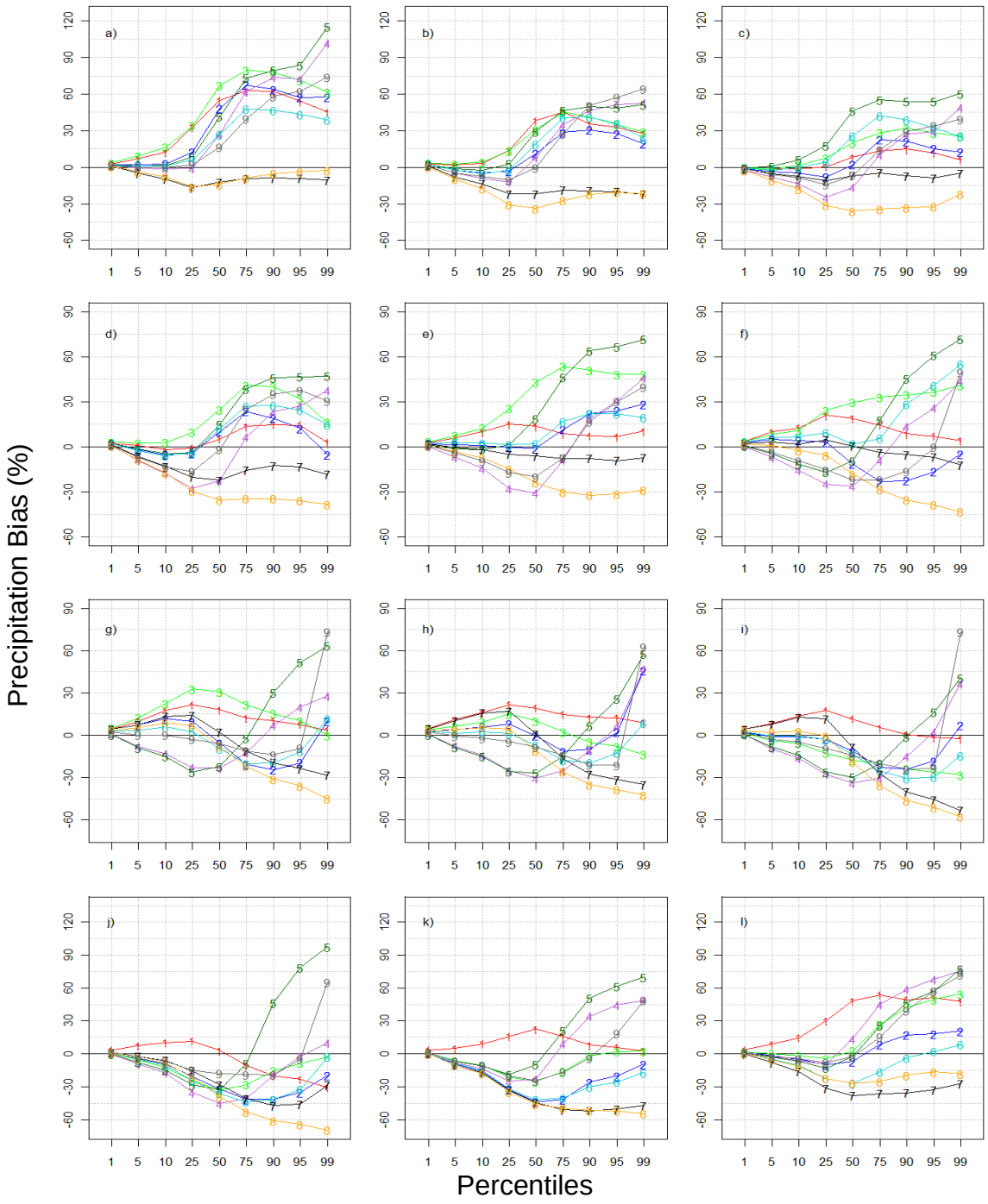

Figure 3.15. Percentile plots of mean precipitation bias for the east sub-region from nine NARCCAP ensemble members for December (a), January (b), February (c), March (d), April (e), May (f), June (g), July (h), August (i), September (j), October (k), and November (l). Labels for the NARCCAP ensemble members: "1"=MM5I-CCSM, "2"=RCM3-GFDL, "3"=ECP2-GFDL, "4"=WRFG-CCSM, "5"=WRFG-CGCM3, "6"=RCM3-CGCM3, "7"=CRCM-CGCM3, "8"=CRCM-CCSM, and "9"=GFDL-Timeslice.

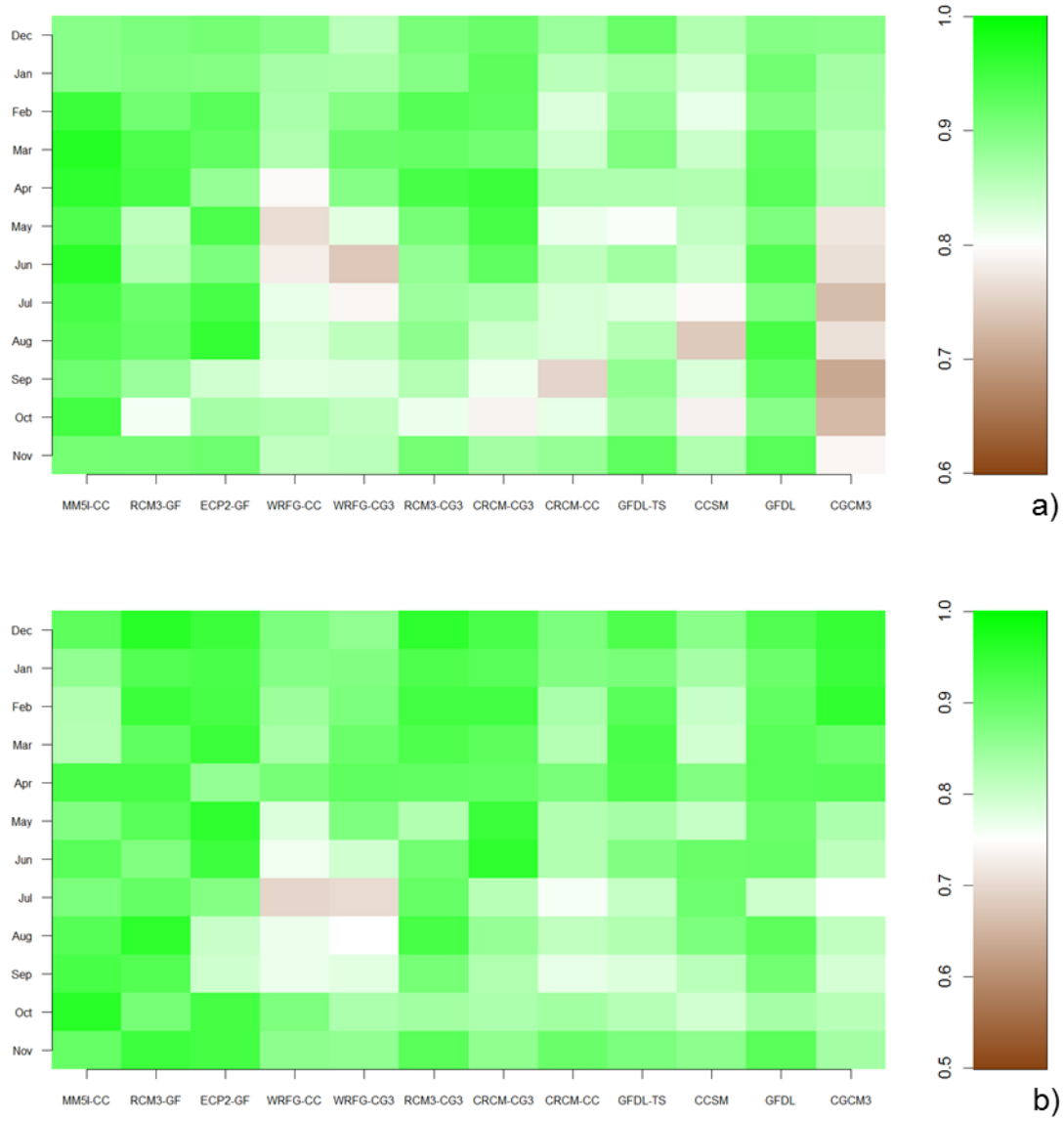

Figure 3.16. Hovmöller diagram of mean precipitation Perkins skill score (a) and Willmott's index of agreement (b) for the west sub-region. Abbreviations for NARCCAP ensemble members and GCMs: "MM5I-CC"=MM5I-CCSM, "RCM3-GF"=RCM3-GFDL, "ECP2-GF"=ECP2-GFDL, "WRFG-CC"=WRFG-CCSM, "WRFG-CG3"=WRFG-CGCM3, "RCM3-CG3"=RCM3-CGCM3, "CRCM-CG3"=CRCM-CGCM3, "CRCM-CC"=CRCM-CCSM", "GFDL-TS"=GFDL-Timeslice, "CCSM"=CCSM GCM, "GFDL"=GFDL GCM, and "CGCM3"=CGCM3 GCM.

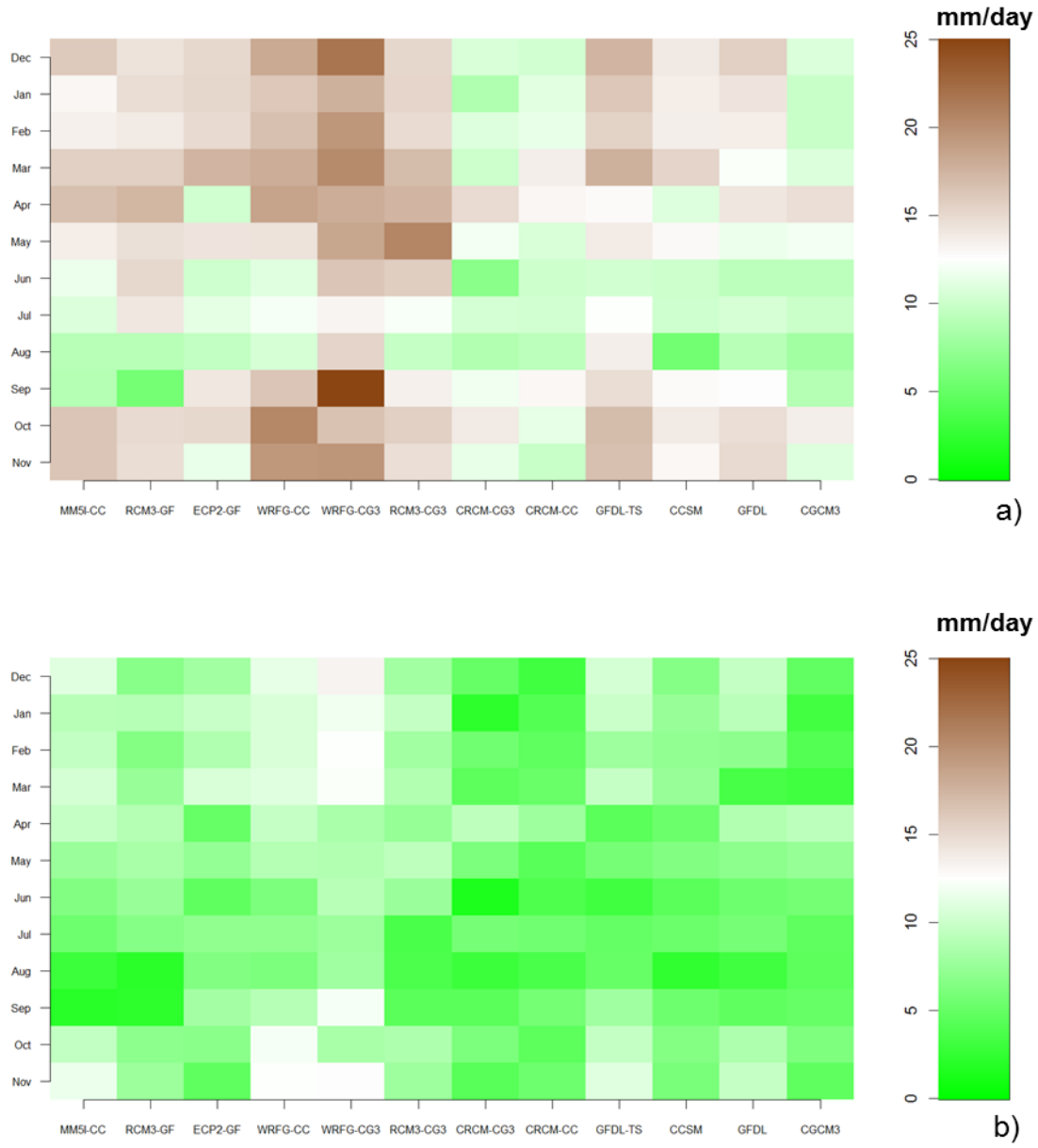

Figure 3.17. Hovmöller diagram of mean precipitation RMSE (a) and MAE (b) for the west sub-region. Abbreviations for NARCCAP ensemble members and GCMs: "MM5I-CC"=MM5I-CCSM, "RCM3-GF"=RCM3-GFDL, "ECP2-GF"=ECP2-GFDL, "WRFG-CC"=WRFG-CCSM, "WRFG-CG3"=WRFG-CGCM3, "RCM3-CG3"=RCM3-CGCM3, "CRCM-CG3"=CRCM-CGCM3, "CRCM-CC"=CRCM-CCSM", "GFDL-TS"=GFDL-Timeslice, "CCSM"=CCSM GCM, "GFDL"=GFDL GCM, and "CGCM3"=CGCM3 GCM.

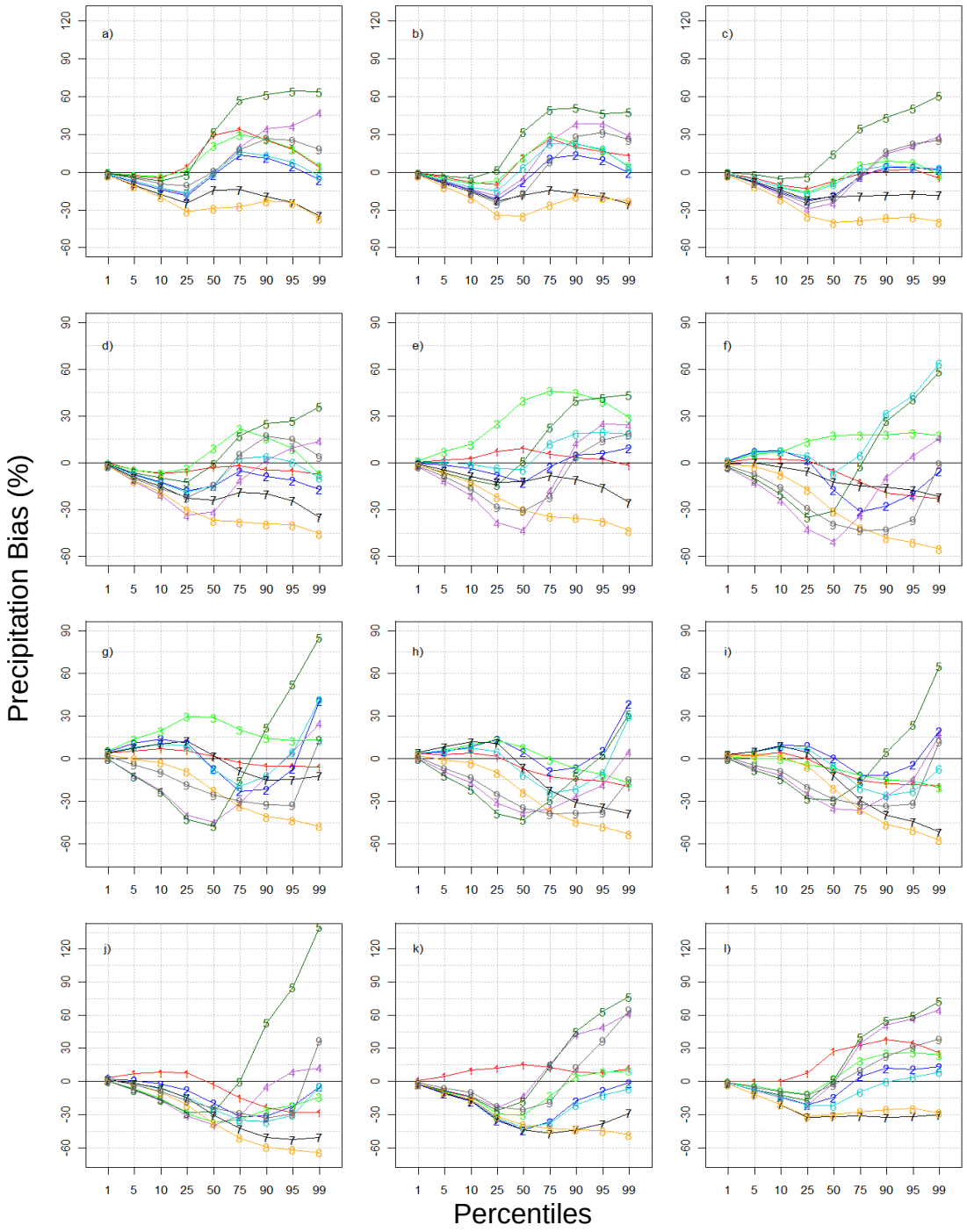

Figure 3.18. Percentile plots of mean precipitation bias for the west sub-region from nine NARCCAP ensemble members for December (a), January (b), February (c), March (d), April (e), May (f), June (g), July (h), August (i), September (j), October (k), and November (l). Labels for the NARCCAP ensemble members: "1"=MM5I-CCSM, "2"=RCM3-GFDL, "3"=ECP2-GFDL, "4"=WRFG-CCSM, "5"=WRFG-CGCM3, "6"=RCM3-CGCM3, "7"=CRCM-CGCM3, "8"=CRCM-CCSM, and "9"=GFDL-Timeslice.

3.2 NARCCAP VERSUS NARR VARIABLES

Six variables from the NARR were analyzed to determine how each model was handling other variables within their individual climate systems. Variables chosen give insight into micro-, meso-, and synoptic-scale processes that are vitally important to temperature and precipitation and the feedbacks within the climate system. Of note, not all models output or reported the variables presented below. The incorporation of latent and sensible heat flux, for example, was necessitated by two models not producing soil moisture content results, thus to gain perspective on other thermodynamic properties associated with surface and atmospheric moisture, heat fluxes were included. Caution should be exercised with regard to direct comparison of specific GCM-driven RCM values to NARR values because GCM-driven runs are not meant to compare with a specific moment in time like the NCEP-driven RCM runs. Rather, GCM-driven runs, when considered over a lengthy climatological period (20-30 years), are meant to represent intra- and inter-annual variability found over the same climate period. The findings below are general with respect to the 21-year climate period chosen (1979-1999).

3.2.1 SOIL MOISTURE CONTENT, LATENT HEAT FLUX, AND SENSIBLE HEAT FLUX

Soil moisture content, latent heat flux, and sensible heat flux were chosen to represent the micro-scale meteorological/climatological phenomenon near the surface of the earth. As discussed previously, soil moisture has a large influence on temperature by impacting the surface energy budget and on precipitation by impacting localized warm-

season convection. Figures 3.19 and 3.20 illustrate the monthly soil moisture content for seven of the nine NARCCAP ensemble members from 1979-1999. The RCM3-GFDL and RCM3-CGCM3 models exhibit erroneously high soil moisture compared to reanalysis. This may point to a systematic flaw within the RCM3 model in terms of its representation of surface and sub-surface processes; however, soil moisture content was not available for RCM3-NCEP runs and cannot be fully verified. Additionally, high soil moisture content is a likely cause to the degradation in skill and cold temperature bias observed in the RCM3-GFDL model. Conversely, the GFDL-timeslice exhibits a substantial dry soil moisture bias; however, no clear evidence exists to link the dry soil moisture bias in this model to its temperature or precipitation biases.

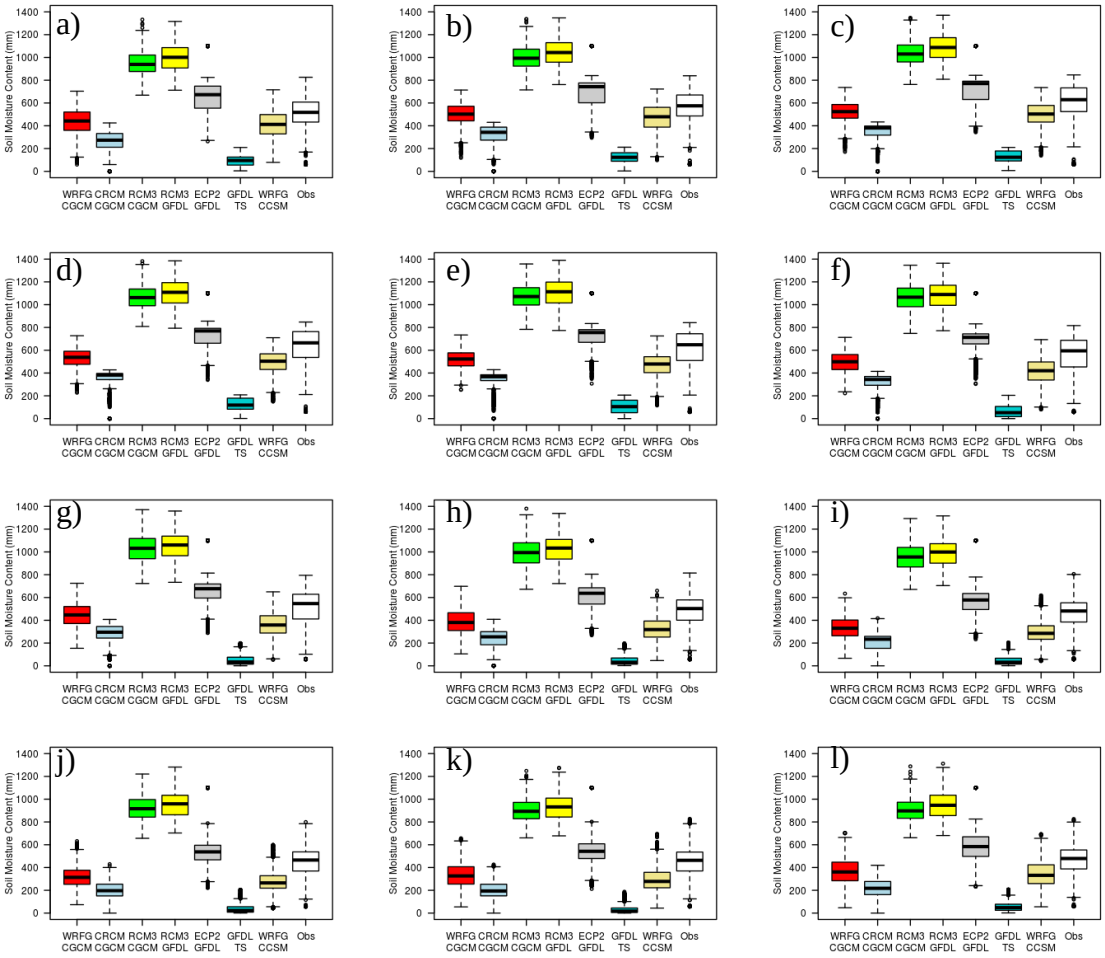

Figure 3.19. Box and whisker plots of RCM-GCM model results and observations of soil moisture for the period 1979-1999 for December (a), January (b), February (c), March (d), April (e), May (f), June (g), July (h), August (i), September (j), October (k), and November (l) for the east sub-region.

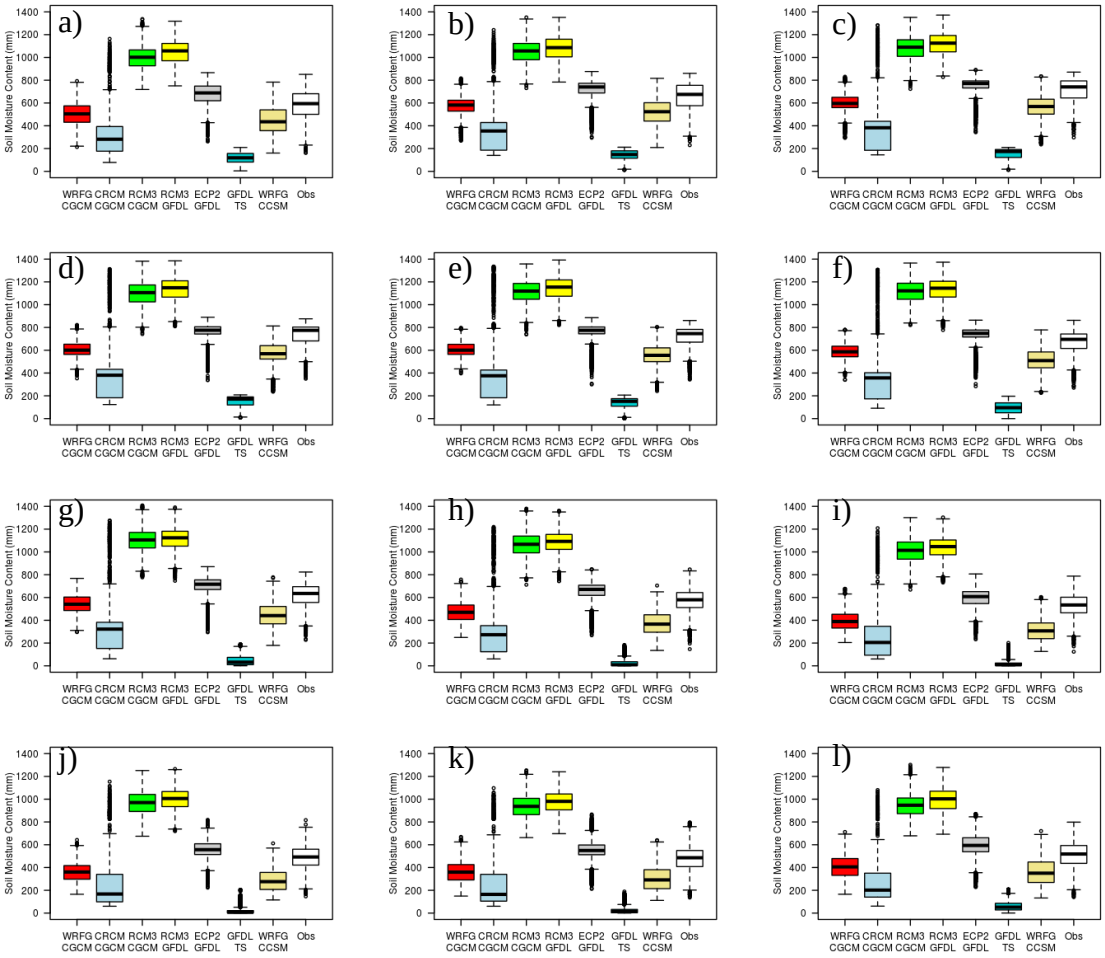

Figure 3.20. Box and whisker plots of RCM-GCM model results and observations of soil moisture for the period 1979-1999 for December (a), January (b), February (c), March (d), April (e), May (f), June (g), July (h), August (i), September (j), October (k), and November (l) for the west sub-region.

The CRCM-CGCM3 model, like the GFDL-timeslice, exhibits a dry soil moisture bias throughout each month and is also observed in the CRCM-NCEP runs (Figures H.7 and H.8). The greatest impact this appears to make is associated with summer maximum temperatures in which a warm bias of 2 to 6°C exists, especially beyond the 50th percentile. Additionally, the dry soil moisture bias may be a leading factor in the dry precipitation bias noted for the CRCM-CGCM3 in each season, with particularly dry bias

from late spring (April) through mid-fall (October) (Figures I.1 and I.2). The ECP2-GFDL exhibits the closest match to both the quantity and periodicity of soil moisture found in the reanalysis data, indicating the ECP2-GFDL model's bias is associated with another atmospheric process.

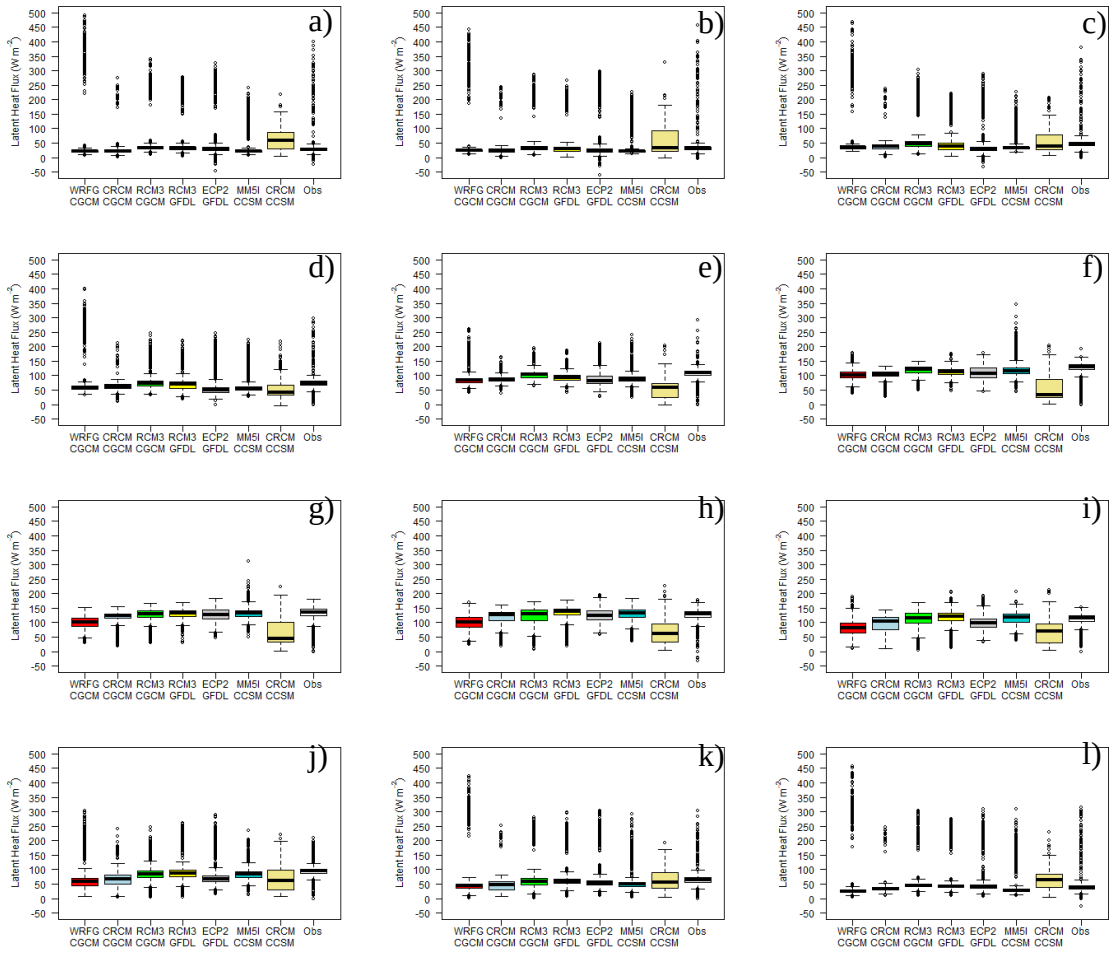

Figure 3.21. Box and whisker plots of RCM-GCM model results and observations of latent heat flux for the period 1979-1999 for December (a), January (b), February (c), March (d), April (e), May (f), June (g), July (h), August (i), September (j), October (k), and November (l) for the east sub-region.

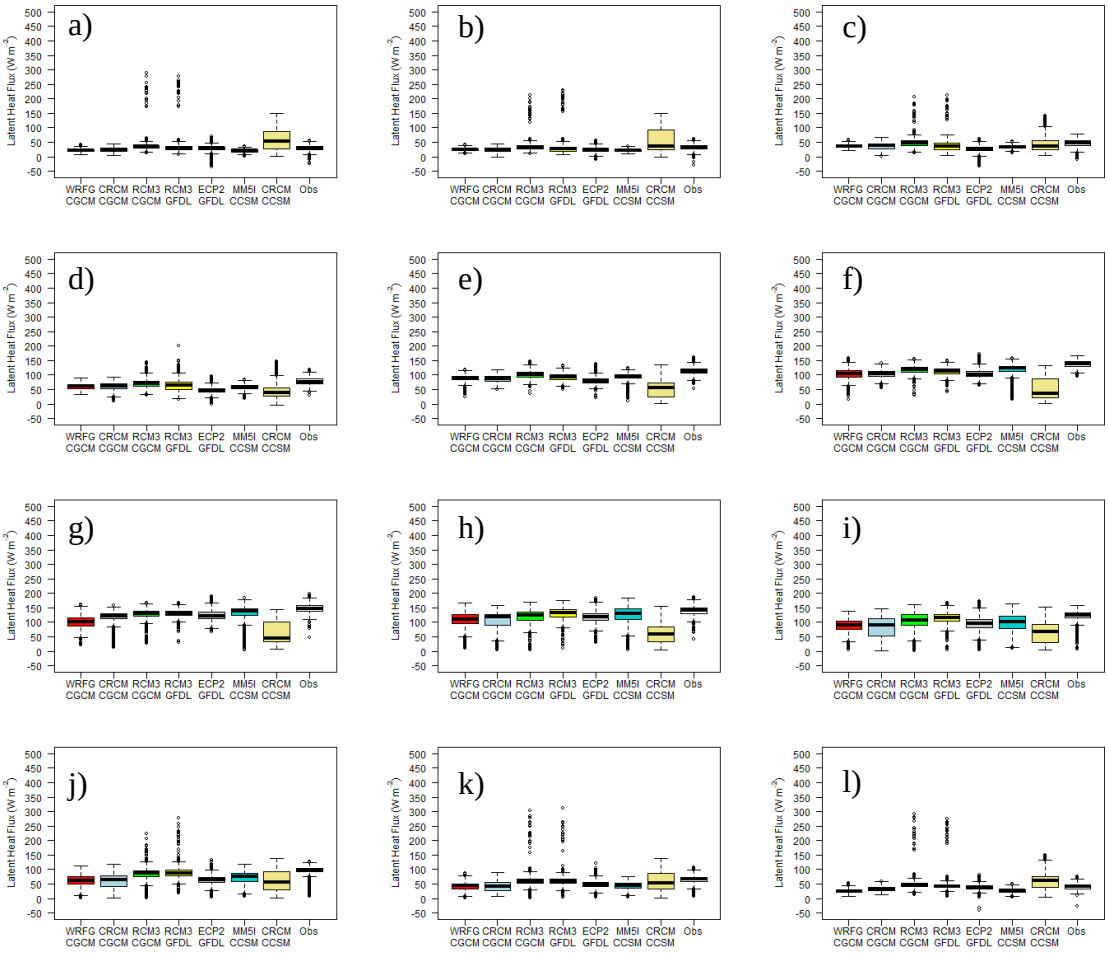

Figure 3.22. Box and whisker plots of RCM-GCM model results and observations of latent heat flux for the period 1979-1999 for December (a), January (b), February (c), March (d), April (e), May (f), June (g), July (h), August (i), September (j), October (k), and November (l) for the west sub-region.

Monthly latent (Figures 3.21 and 3.22) and sensible (Figures 3.23 and 3.24) heat flux plots reveal potential issues related to balancing the surface energy budget, wherein the amount of energy put into a system (atmosphere) must balance with energy out of the system. Latent and sensible heat fluxes are two methods in which the majority of energy is released out of the atmosphere. To maintain energy balance, if the latent heat flux is too low more energy is put into the sensible heat flux which leads to increased

temperature and can be an indication of dry soil bias. Conversely, if latent heat flux is too high, more energy is put into the process of evaporation and can be an indication of erroneously wet soil, which in turn reduces the amount of energy put into increasing temperature, resulting in cold temperature bias.

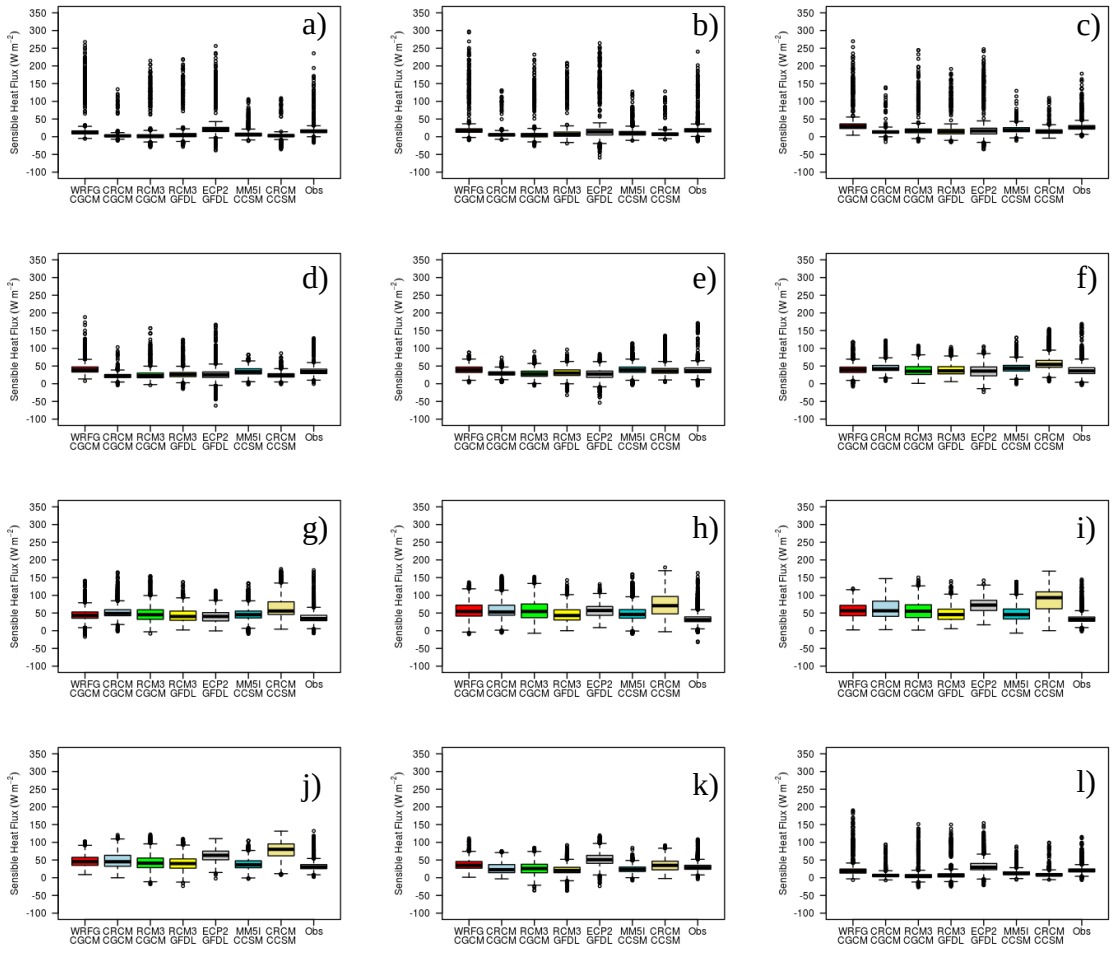

Figure 3.23. Box and whisker plots of RCM-GCM model results and observations of sensible heat flux for the period 1979-1999 for December (a), January (b), February (c), March (d), April (e), May (f), June (g), July (h), August (i), September (j), October (k), and November (l) for the east sub-region.

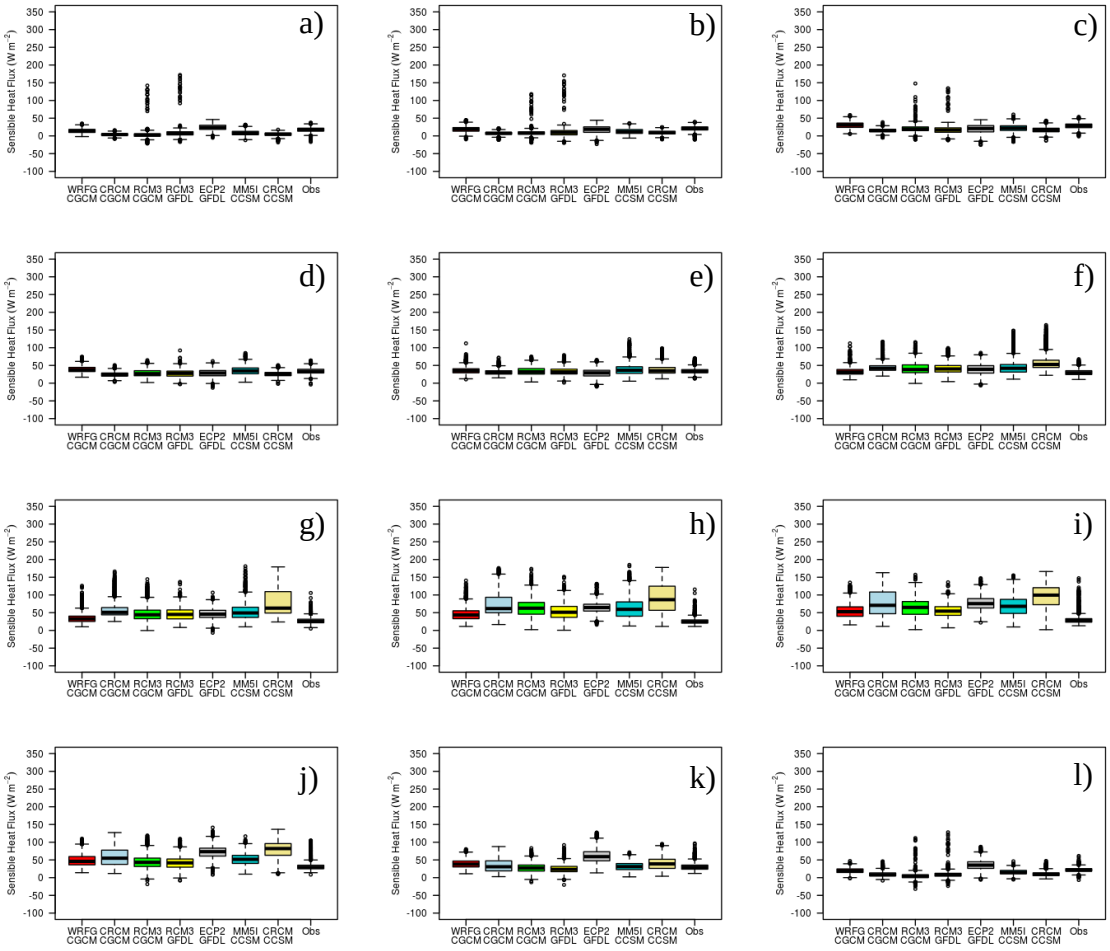

Figure 3.24. Box and whisker plots of RCM-GCM model results and observations of sensible heat flux for the period 1979-1999 for December (a), January (b), February (c), March (d), April (e), May (f), June (g), July (h), August (i), September (j), October (k), and November (l) for the west sub-region.

Latent heat flux plots for both sub-regions reveal a situation in which all models tend to under-predict latent heat flux in all months in the east sub-region, while under-predicting for most months in the west sub-region (Figures I.1 and I.2). Additionally, the RCM3-GFDL exhibits periods of higher latent heat flux in a few summers compared to reanalysis. Based on soil moisture plots above, the two RCM3 models should have higher than observed latent heat flux in most months as excessive soil moisture would need to be

evaporated back into the atmosphere to maintain energy balance. This very factor is a distinct possibility as precipitation minus potential evapotranspiration anomaly plots (Figures I.1 and I.2) indicate a moisture deficit, however, the P-PE rate does not appear to be high enough to allow for complete balance in the water and energy budgets. One troubling observation is the CRCM-CCSM's inability to replicate inter-annual variability found in the reanalysis data and a readily available diagnosis as to the cause of such an odd behavior is not available, especially since the CRCM behaves relatively well when driven with the NCEP data (Figures H.9 and H.10).

Sensible heat flux for both regions are below observations from late fall through early spring, while late spring through early fall values are well above observations (Figures 3.23 and 3.24). The same trend is found with each RCM run with NCEP LBCs (Figures H.11 and H.12). From an energy balance perspective, if the sensible and latent heat fluxes are low, more energy is going into other processes such as energy absorbed or reflected by the atmosphere. There is some merit to this thought. Maximum temperature is greatly influenced by sensible heat flux (as well as cloud cover). The percentile plots for maximum temperature show that all models have some form of cold bias from December through April and again in October and November, corresponding to sensible heat flux values below observations during the same period. Conversely, sensible heat flux values above observations, such as those during the summer, are more likely than not a contributing factor to the exceptional warm bias observed in the summer for the CRCM RCMs.

3.2.2 500-MB HEIGHT

Mean 500-mb height plots allow for the determination of "troughiness" and "ridgeiness" in the mid-troposphere. Troughs and ridges are the primary synoptic-scale features which drive weather patterns. Troughs are associated with stormy weather and cooler temperatures while ridges lead to fair weather and warmer temperatures. If mean 500-mb heights from a model are below observations, the model presents too much of a trough, which can result in the model over-predicting the passage frequency of mid-latitude waves and/or cold air intrusion into a region. Conversely, if mean 500-mb heights from a model are above observations, the model presents too much of a ridge which typically leads to reduced frequency of mid-latitude cyclones and potential increase in heat waves. Figures 3.25 and 3.26 illustrate mean monthly 500-mb heights for the east and west sub-regions for eight of the nine NARCCAP ensemble members while Figures I.1 and I.2 illustrate monthly 500-mb anomolies. Additionally, Figures I.3 through I.14 illustrate 500-mb anomalies (by month) spatially across the Southeast U.S. The two RCM3 models greatly under-predict 500-mb height for all months in both regions. The RCM3-NCEP run (Figures H.13 and H.14) illustrates the RCM3 under-predicts monthly mean 500-mb height for both sub-regions, however, the low height bias is not nearly as pronounced as RCM3 runs with GCM LBCs. Coupling these findings with that of soil moisture, it can be concluded the RCM3 model has a systematic issue of being too cold and wet which impact the rest of the modeled climate system. The item which separates the two RCM3 runs is their differing LBCs; of which the GFDL has a known cold bias, coupled with the cold and wet bias of the RCM3, leads to the observed reduction in all skill metrics, more notably with respect to maximum temperature.

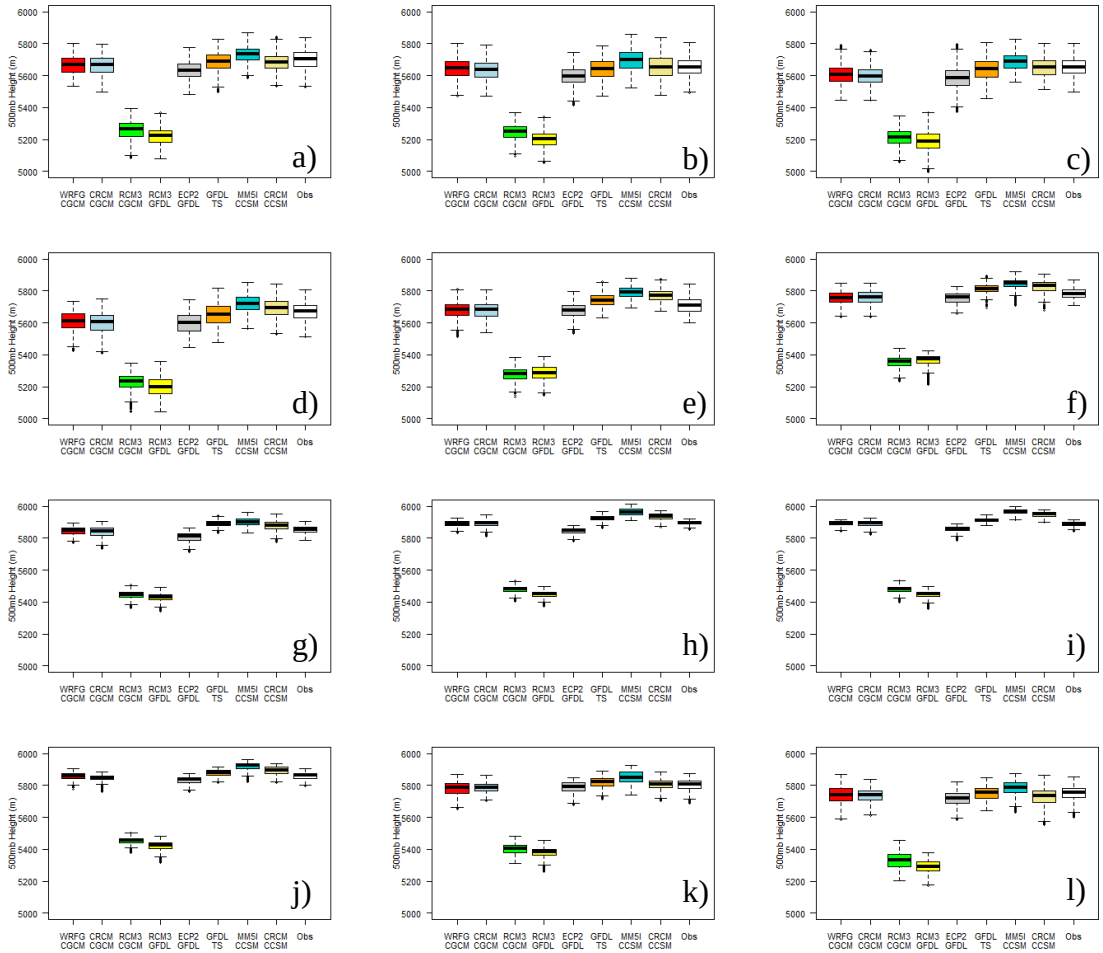

Figure 3.25. Box and whisker plots of RCM-GCM model results and observations of 500-mb heights for the period 1979-1999 for December (a), January (b), February (c), March (d), April (e), May (f), June (g), July (h), August (i), September (j), October (k), and November (l) for the east sub-region.

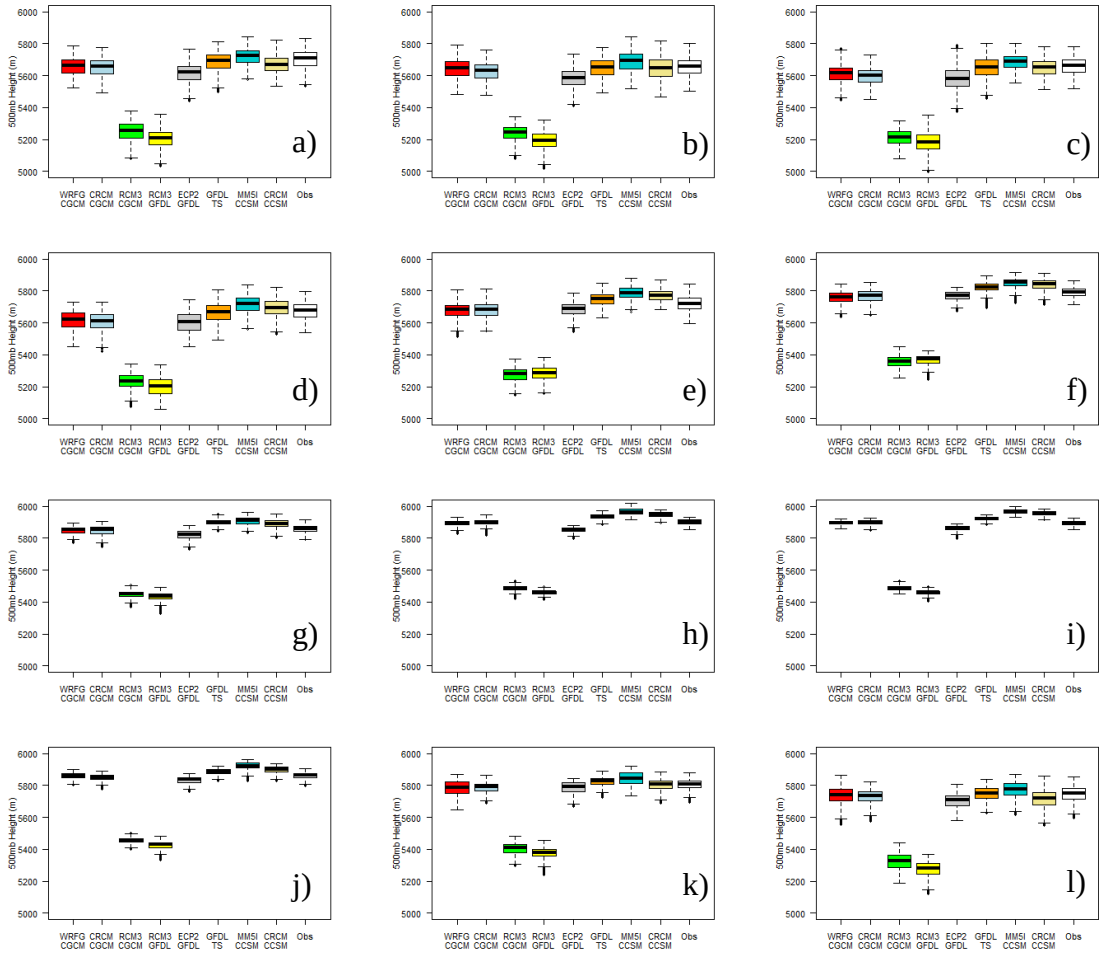

Figure 3.26. Box and whisker plots of RCM-GCM model results and observations of 500-mb heights for the period 1979-1999 for December (a), January (b), February (c), March (d), April (e), May (f), June (g), July (h), August (i), September (j), October (k), and November (l) for the west sub-region.

For the RCMs other than the RCM3 models, there is tendency in both sub-regions for enhanced troughs during the winter months (centered mostly to the west of the Mississippi River Basin) and enhanced ridges in the summer months (centered mostly over the Ohio River Valley), a pattern that is not evident in the NCEP-driven runs, indicating this pattern is most likely due to GCM LBCs. Enhanced troughs in the winter will result in the increased frequency of mid-latitude cyclones, which during this

particular season can result in increased snowfall for the mid and upper latitudes, increased rain in the lower latitudes, and increased cold air out breaks for all locations. The percentile plots for both sub-regions in winter reveal this exact scenario. Most models have a wet bias in the winter, with particular emphasis in the upper percentiles while maximum temperatures exhibit cold winter bias for virtually all models. Conversely, enhanced ridges during the summer typically result in the decreased frequency of mid-latitude cyclones, leading to decreased synoptic-scale driven precipitation (leaving small-scale driven convective precipitation as the main form of precipitation) and warmer surface temperatures. This exact trend is shown in the summer precipitation and maximum temperature percentile plots for the majority of the models for both sub-regions.

One final and interesting observation about mean 500-mb heights is made between the two RCMs driven by the GFDL. The influence of the GFDL can be seen in the periodic spikes in monthly 500-mb heights (e.g., January/February 1982). Similar observations can be made for RCMs utilizing the CGCM3 for LBCs (e.g., January/February 1991). The relationship between the CCSM model and its two RCMs is much less obvious.

3.2.3 SEA-LEVEL PRESSURE

Sea-level pressure is an important aspect of diagnosing systematic errors found within climate models. Sea-level pressure is closely tied to 500-mb height in that lower 500-mb heights are highly correlated with lower sea-level pressure; while higher 500-mb heights couple with higher sea-level pressure. To this end, high sea-level pressure

corresponds to warm/dry conditions while low sea-level pressure corresponds to cool/wet conditions. Figures 3.27 and 3.28 illustrate the monthly mean sea-level pressure for both sub-regions while Figures I.1 and I.2 illustrate the monthly sea-level pressure anomolies. Additionally, Figures I.15 through I.26 illustrate sea-level pressure anomalies spatially across the Southeast U.S. With a few notable exceptions, most models over-estimate sea-level pressure, regardless of month, with higher sea-level pressure anomalies over the Atlantic Ocean and smaller anomolies inland. Additionally, unlike the 500-mb and soil moisture plots, the models fail to separate themselves pattern or bias-wise, which may indicate sea-level pressure is not an adequate metric to determine deeper systematic biases within the RCMs. Although not a perfect representation, it appears most models attempt to replicate the periodicity found in the reanalysis data; however, the contribution of sea-level pressure to temperature and precipitation bias is not obvious.

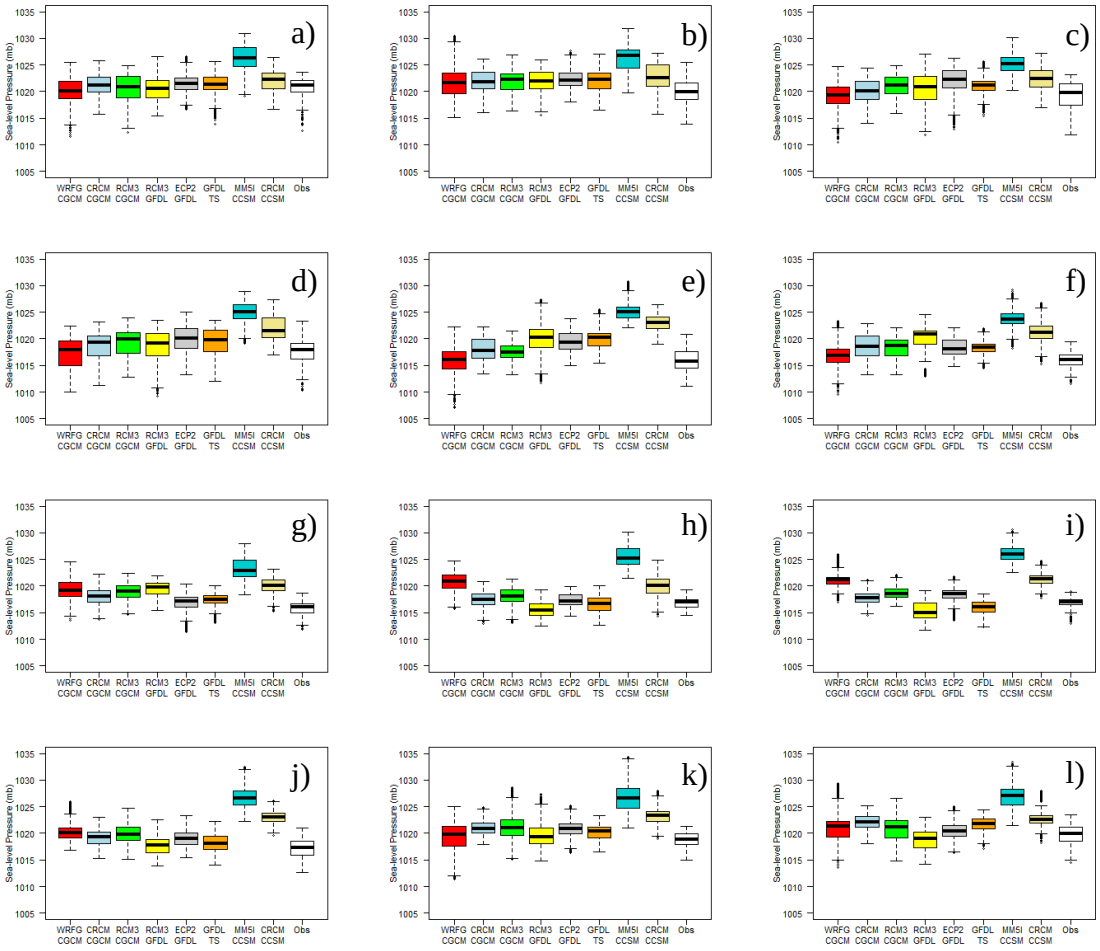

Figure 3.27. Box and whisker plots of RCM-GCM model results and observations of sea-level pressure for the period 1979-1999 for December (a), January (b), February (c), March (d), April (e), May (f), June (g), July (h), August (i), September (j), October (k), and November (l) for the east sub-region.

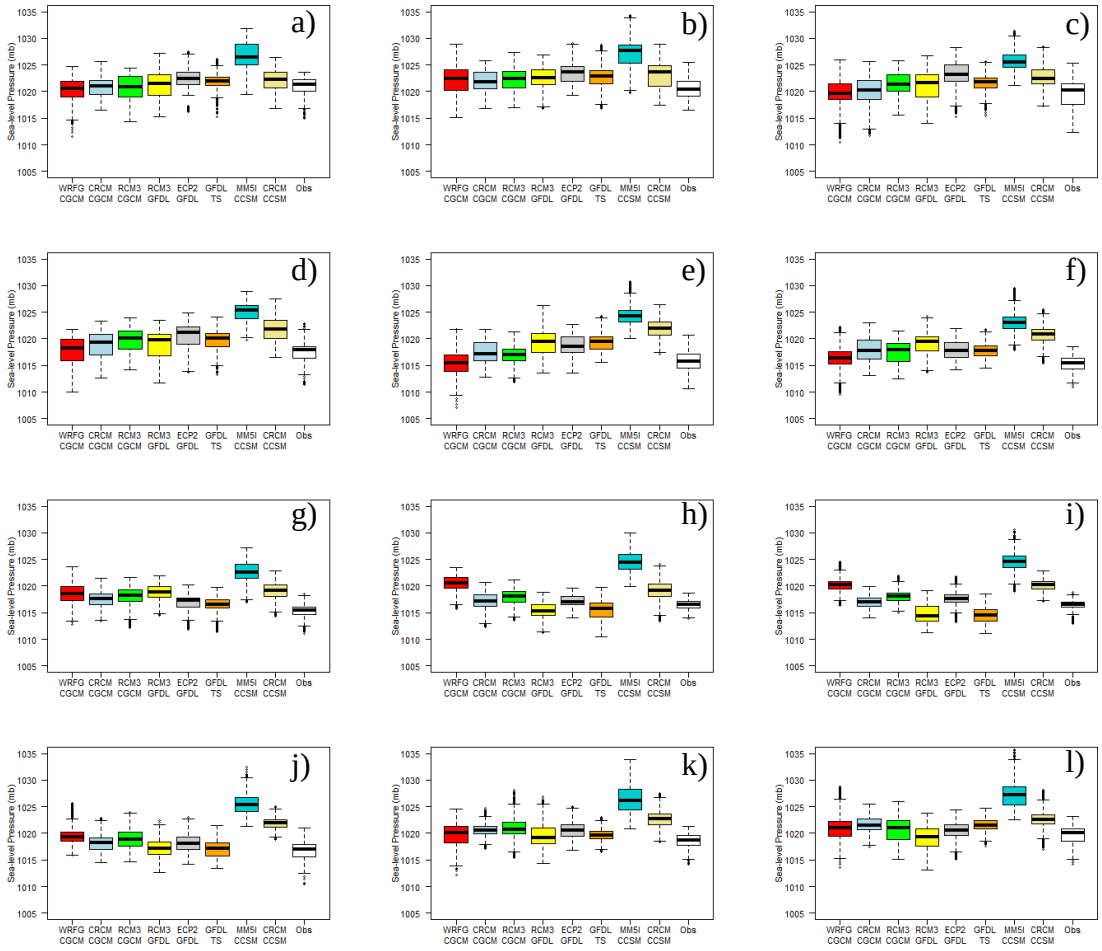

Figure 3.28. Box and whisker plots of RCM-GCM model results and observations of sea-level pressure for the period 1979-1999 for December (a), January (b), February (c), March (d), April (e), May (f), June (g), July (h), August (i), September (j), October (k), and November (l) for the west sub-region.

3.2.4 TOTAL CLOUD COVER

Total cloud cover assists in determining systematic issues inherent within individual models. High cloud cover modifies the energy balance equation by reducing the amount of solar radiation infused into the atmosphere and increasing the amount of radiation reflected back to space. Enhanced cloud cover is typically associated with cooler temperatures due to reflected radiation to space and less energy used in the

sensible heat flux portion of the energy balance equation. Cloudy conditions have less of an impact on precipitation than, for instance, 500-mb height; however, increased cloudiness in the summer leads to a less buoyant atmosphere which reduces the potential for convective precipitation formation. Less impact on precipitation relative to total cloud cover is felt in the winter because winter precipitation is driven by the synoptic-scale weather pattern (i.e., 500-mb height).

Figures 3.29, 3.30, I.1, and I.2 illustrate the monthly total cloud cover for the east and west sub-regions and a few patterns emerge. First, the models driven by the CRCM RCM exhibit low total cloud cover in the summer months which aids in explaining this RCM's warm maximum temperature and dry precipitation biases, however, this pattern is not evident in the CRCM-NCEP results (Figures H.15 and H.16) indicating GCM LBCs push the CRCM into the noted bias. Additionally, the CRCM RCM's negative cloud cover anomalies (not enough clouds) in summer coincide with anomalously high sensible heat flux, anomalously low latent heat flux, low soil moisture (from the CRCM-CGCM3 only), high maximum temperatures, low precipitation, and low precipitation minus potential evapotranspiration (Figures I.1 and I.2). The MM5I-CCSM model exhibits higher-than-observation total cloud cover values in both sub-regions, across all months; however, due to the MM5I-CCSM's high skill and low bias for temperature and precipitation, it is difficult to make conjectures about cause and effect as it relates to the temperature/precipitation/total cloud cover relationship in this case.

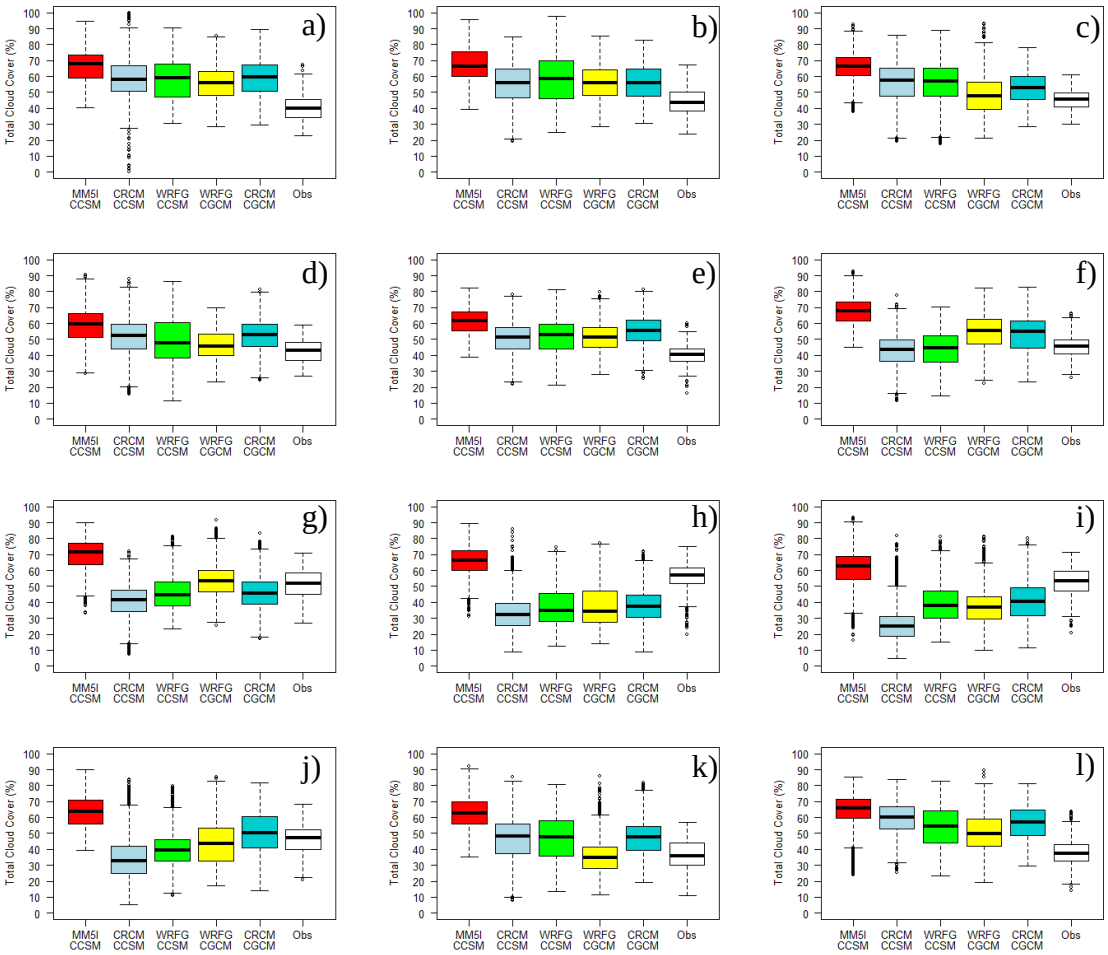

Figure 3.29. Box and whisker plots of RCM-GCM model results and observations of total cloud cover for the period 1979-1999 for December (a), January (b), February (c), March (d), April (e), May (f), June (g), July (h), August (i), September (j), October (k), and November (l) for the east sub-region.

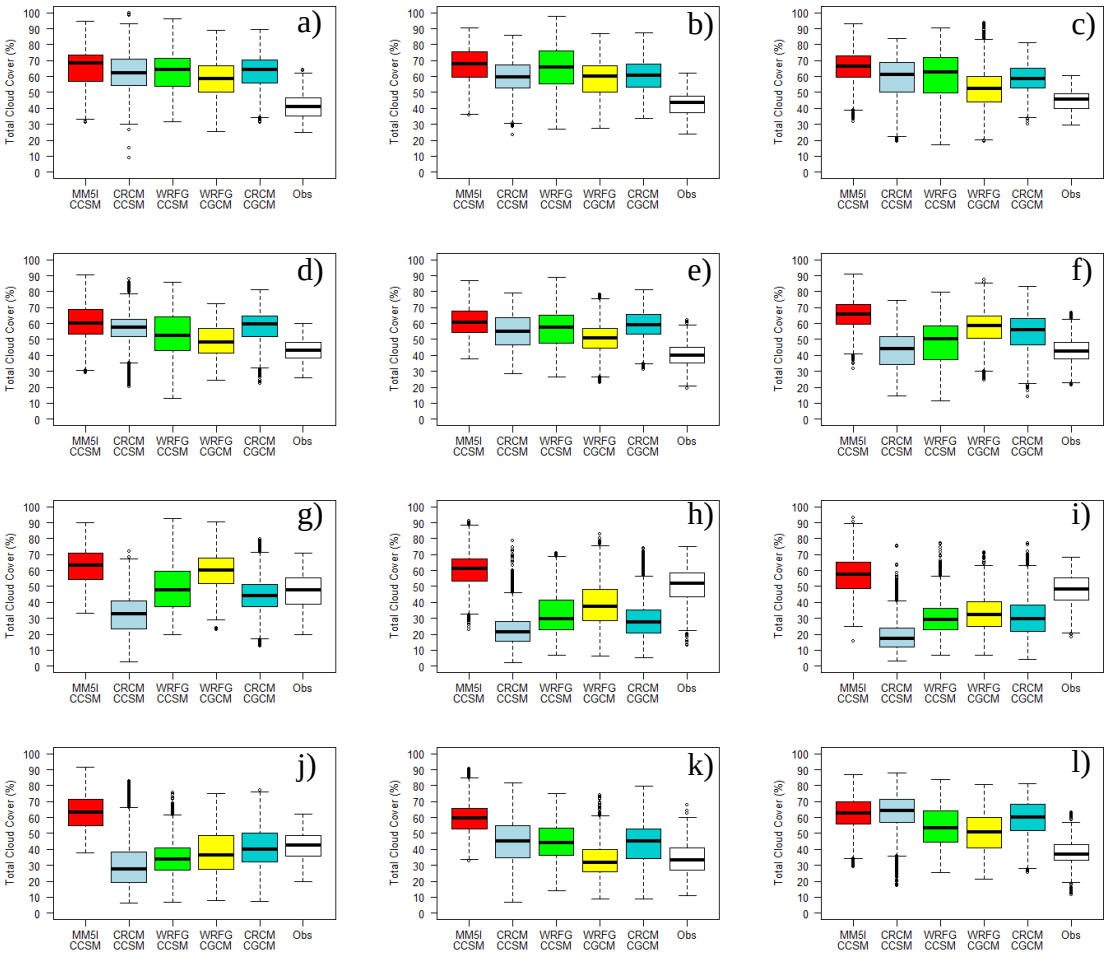

Figure 3.30. Box and whisker plots of RCM-GCM model results and observations of total cloud cover for the period 1979-1999 for December (a), January (b), February (c), March (d), April (e), May (f), June (g), July (h), August (i), September (j), October (k), and November (l) for the west sub-region.

Overall, the variables chosen to further investigate individual model short-comings from the NARCCAP ensemble do provide insight into the question of "why" the models perform the way they do. Although no one variable directly causes change in another, the sum of all climate variables feedback into the climate system, leading to the skill values and biases observed in the previous sub-section. The warm and dry bias of the CRCM model coincides with low soil moisture, lack of clouds, high sensible heat

flux, and high 500-mb heights creating a positive feedback wherein soil moisture is further decreased, sensible heat flux increased, temperature is raised, precipitation is potentially suppressed, and water deficits ensue. By contrast, the cool and wet bias of RCM3 simulations coincide with a negative feedback involving high soil moisture, cloudy skies, high latent heat flux, and low 500-mb heights. In the case of the RCM3 model, most of the energy balance issues are associated with the RCM3 itself and not the boundary conditions passed to the model. RCM3 results driven with NCEP LBCs illustrate the same low 500-mb height bias and high cloud cover bias noted with the GCM-driven runs. The only solutions to rectifying the energy balance issues within these models is to change either the physics package or land-atmosphere module to one in which the RCM performed well (such as the MM5I).

3.3 NARCCAP VALUE ADDED

The concept of value added in the context of climate model downscaling revolves around the argument that the effort of downscaling should provide additional knowledge that the GCM cannot or does not provide. Although sophisticated statistical measures of "value added" exist in the peer-reviewed literature, the overall topic is not well explored and studies determining value added are rare (Feser et al., 2011). The next three sub-sections present results that measure the value added by regional-model for minimum and maximum temperature, and mean precipitation. Downscaling is deemed to add value when a regional model has better skill scores than the GCM providing its boundary conditions; it is deemed not to add value if skill scores for the GCM output are better than regional models they drive.

3.3.1 MINIMUM TEMPERATURE

Hovmöller plots for the east (Figures 3.31 and 3.32) and west (Figures 3.33 and 3.34) sub-regions illustrate value added for minimum temperature. The notion of value added is not clear cut in that a model adding value in one month is not necessarily an indication it will add value in others and is a function of the RCM, GCM, and metric used for the comparison. For instance, all three RCMs utilizing CCSM LBCs typically add value in each month for all four metrics, mainly because the CCSM exhibits marginal skill. Conversely, the three RCMs running CGCM3 LBCs add little, if any, value from the winter through early spring, but typically add significant value the rest of the year. Interestingly, the notion of value added appears to have as much to do with the regional climate model as it does the driving CGM. For example, the RCM3 model fails to add value to the GFDL GCM from December through March, with relatively similar findings when run with CGCM3 boundary conditions. Another example can be found with the WRFG RCMs for July through September, in which both RCMs fail to add value.

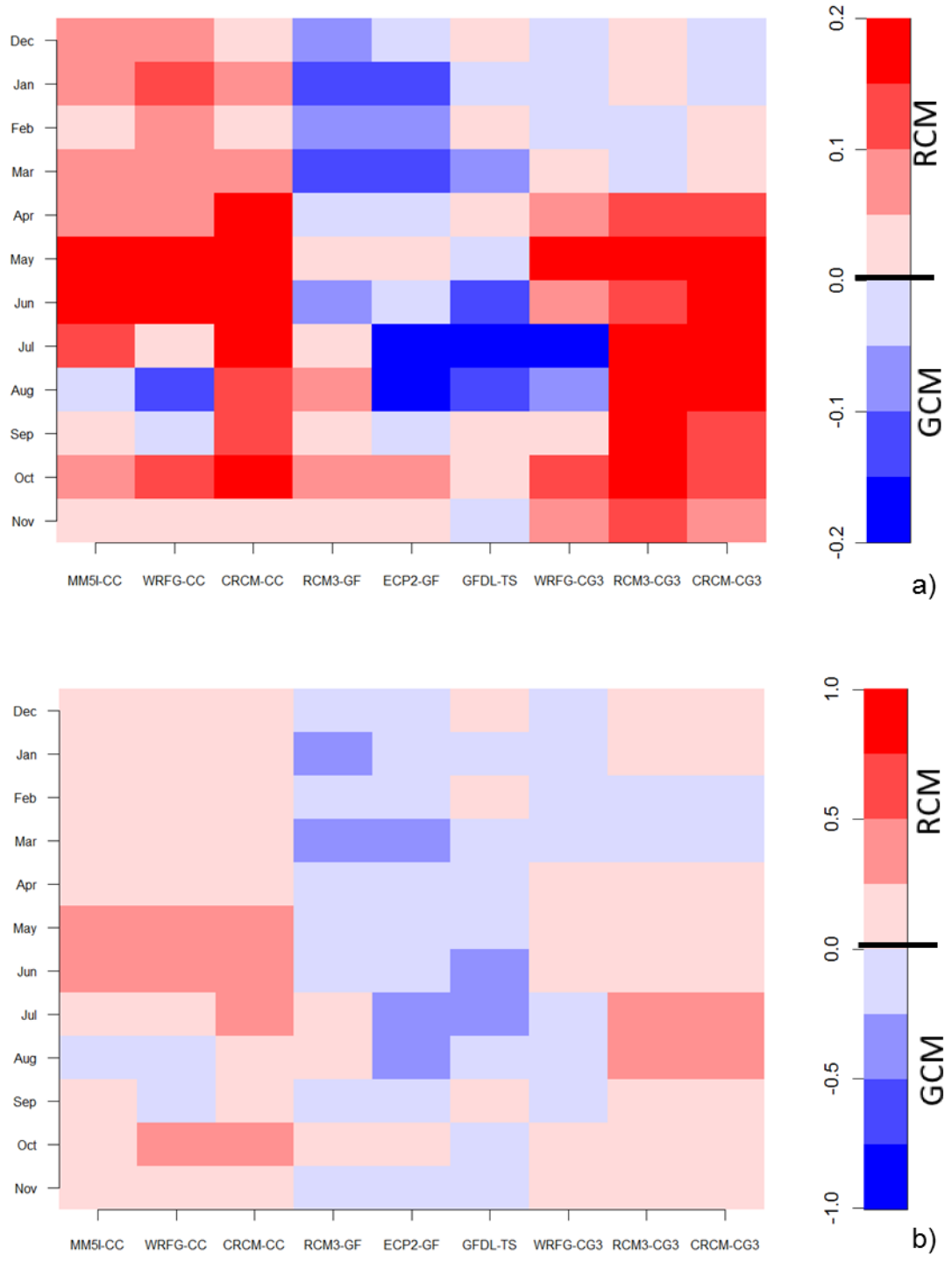

Figure 3.31. Value added for minimum temperature for Perkins skill score (a) and Willmott's index of agreement (b) for the east sub-region.

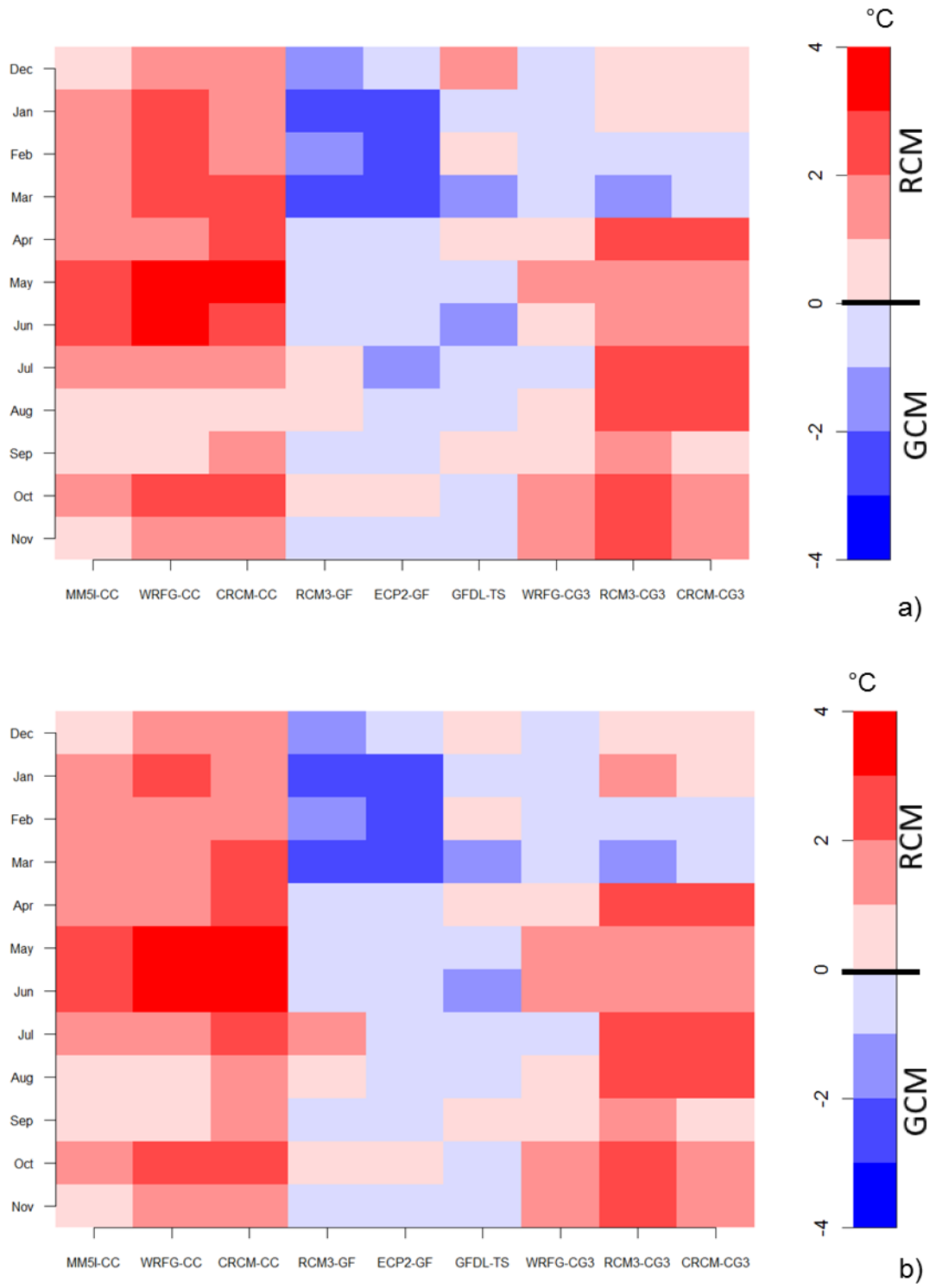

Figure 3.32. Value added for minimum temperature for MAE (a) and RMSE (b) for the east sub-region.

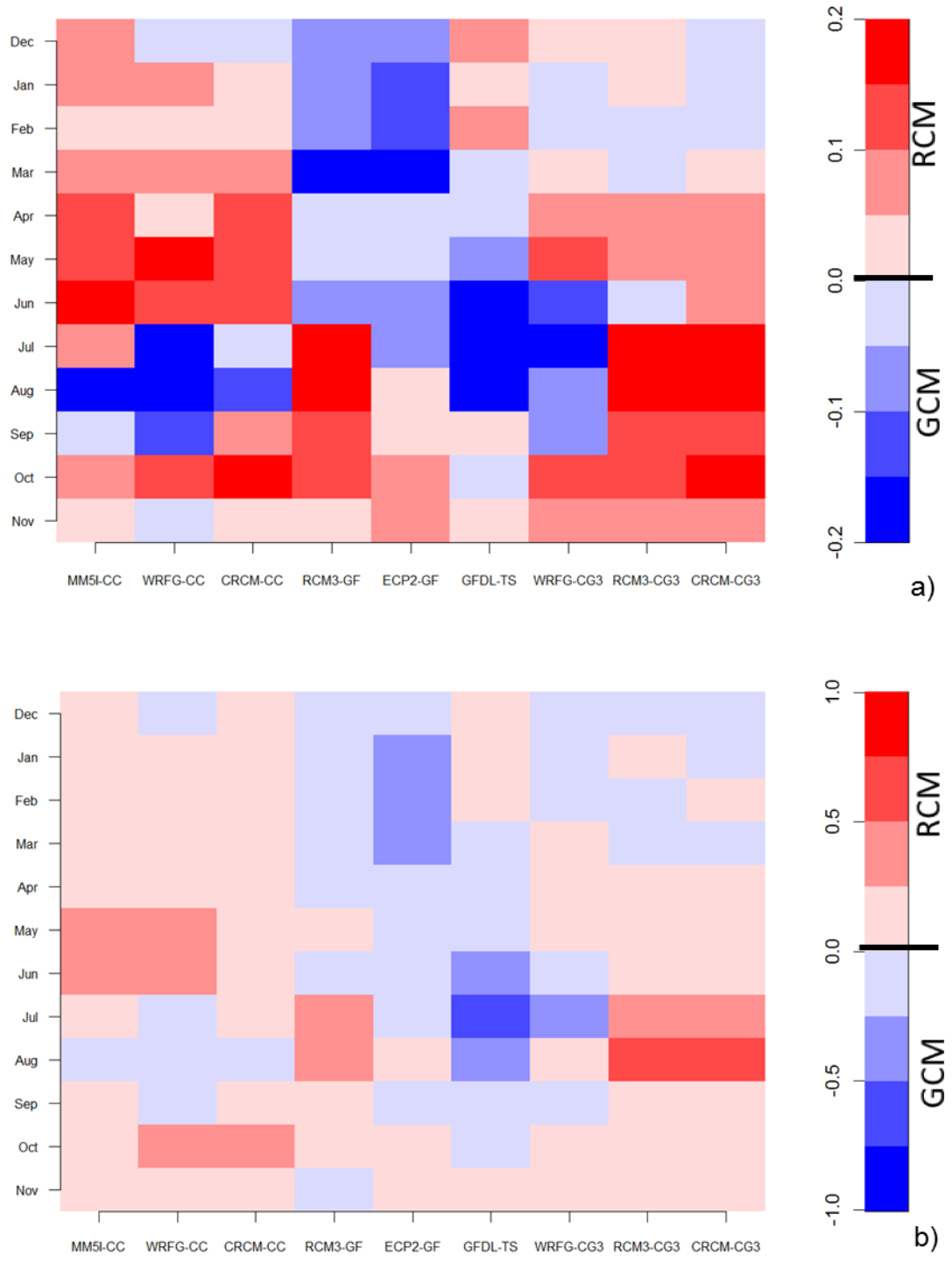

Figure 3.33. Value added for minimum temperature for Perkins skill score (a) and Willmott's index of agreement (b) for the west sub-region.

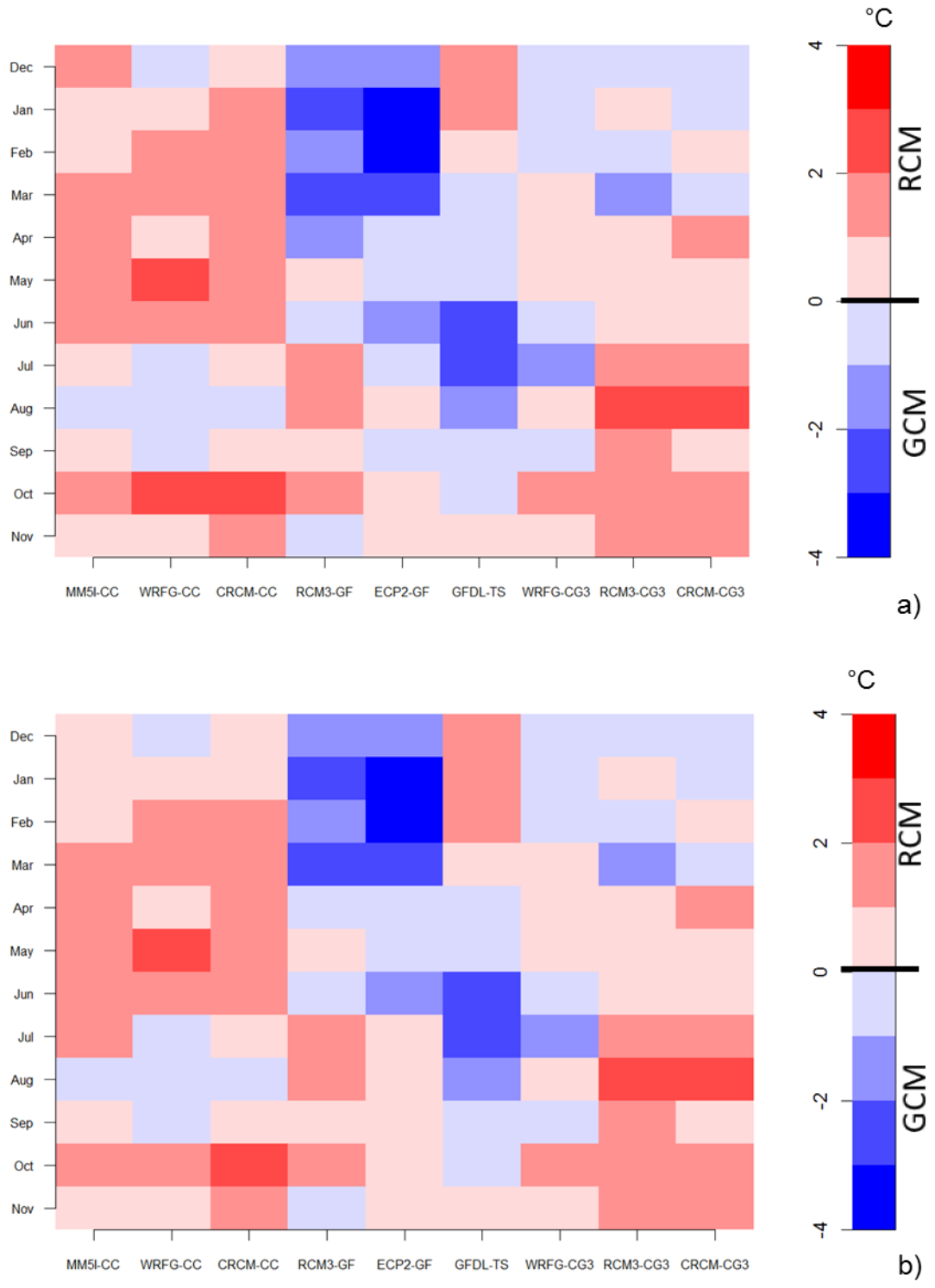

Figure 3.34. Value added for minimum temperature for MAE (a) and RMSE (b) for the west sub-region.

With regards to the GFDL GCM, minimal value is added through the downscaling process, regardless of season. The RCM3- and ECP2-GFDL models provided some added benefit from mid summer through late fall, while the GFDL-timeslice adds a small amount of value in winter and the transition seasons. This gives the indication that bounding a regional climate model with observed sea-surface conditions is beneficial for minimum temperature when synoptic-scale forces (e.g., mid-latitude cyclones, and troughs and ridges) drive local climate. Conversely, months when localized forcings provide a larger impact to the regional climate, regional climate models (i.e., RCM3- and ECP2-GFDL) are more beneficial. It would be interesting to observe value added for regional climate models if observed sea-surface conditions were incorporated in a timeslice-like manner.

Overall, there are several instances in which downscaling minimum temperature does provide added value. The MM5I-CCSM adds value in the most months (10 out of 12) for both sub-regions. Conversely, the ECP2-GFDL model provides the least amount of value added in the east sub-region with only one month superior to the driving GCM, while both the ECP2-GFDL and GFDL-timeslice add a small amount of value for 5 out of 12 months in the west sub-region. In terms of the magnitude of value added, the CRCM-CCSM and RCM3-CGCM3 models provide the greatest amount of value added for their respective GCMs in the east sub-region, while the RCM3-GFDL and CRCM-CGCM3 provide the greatest amount of value added in the west sub-region.

3.3.2 MAXIMUM TEMPERATURE

Maximum temperature results for value added differ greatly from minimum temperature with respect to the magnitude of the value added. With respect to minimum temperature, Perkins skill score differential between RCM and GCM typically fell within the ±0.1 range, RMSE and MAE within ±2°C, and Willmott values within ±0.5 for both sub-regions. With respect to maximum temperature, Figures 3.35 through 3.38 illustrate Perkins values typically falling in the ±0.2 range, RMSE and MAE within ±4°C, and Willmott values within ±0.75. The lone explanation for this behavior is the persistent cold bias expressed by several RCMs (specifically those run with the GFDL LBCs) across all months. Although each of the GCMs exhibit some magnitude of cold bias throughout each month, the magnitude of the bias in the RCM3 RCMs is greatest in several instances.

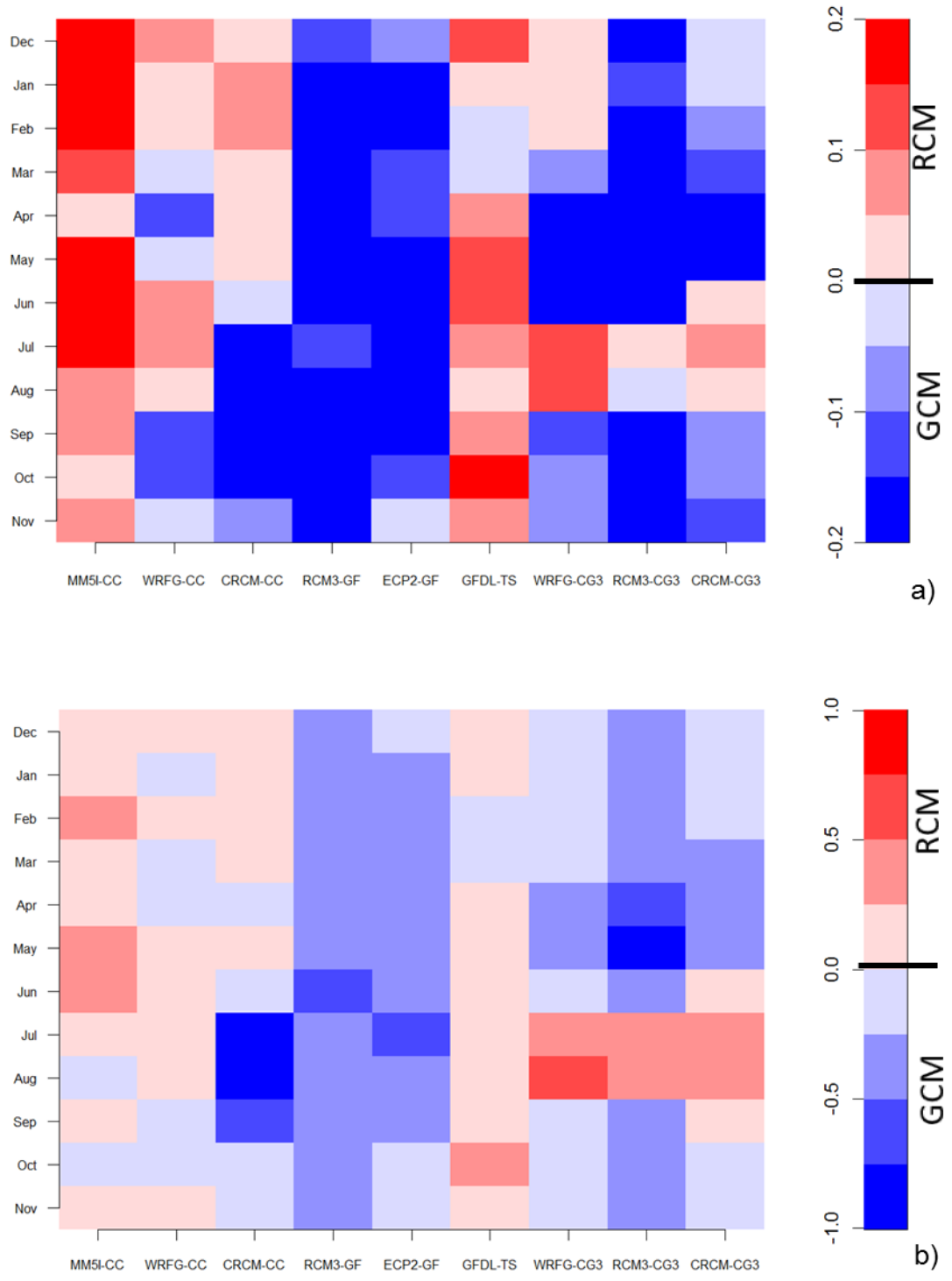

Figure 3.35. Value added for maximum temperature for Perkins skill score (a) and Willmott's index of agreement (b) for the east sub-region.

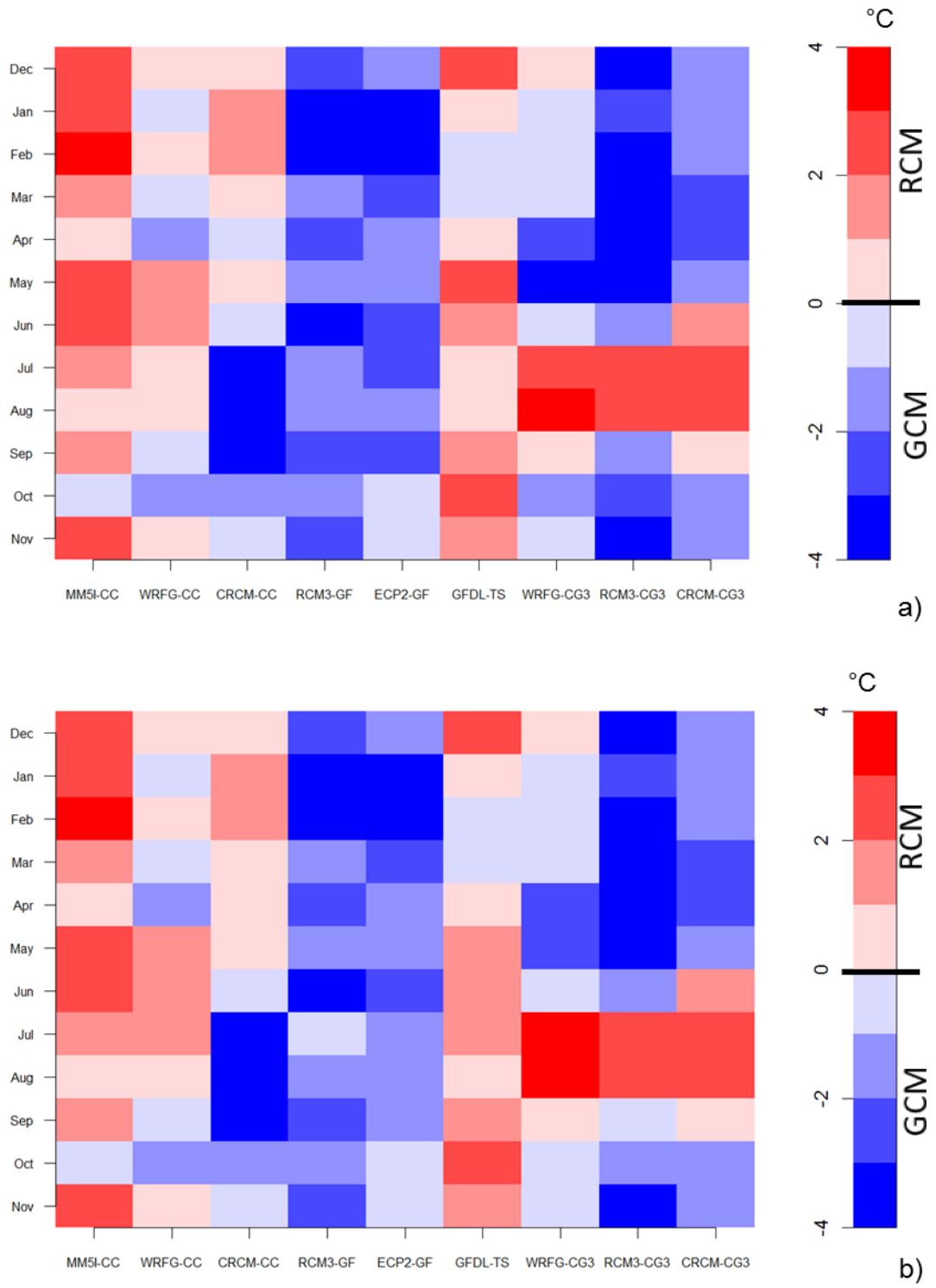

Figure 3.36. Value added for maximum temperature for MAE (a) and RMSE (b) for the east sub-region.

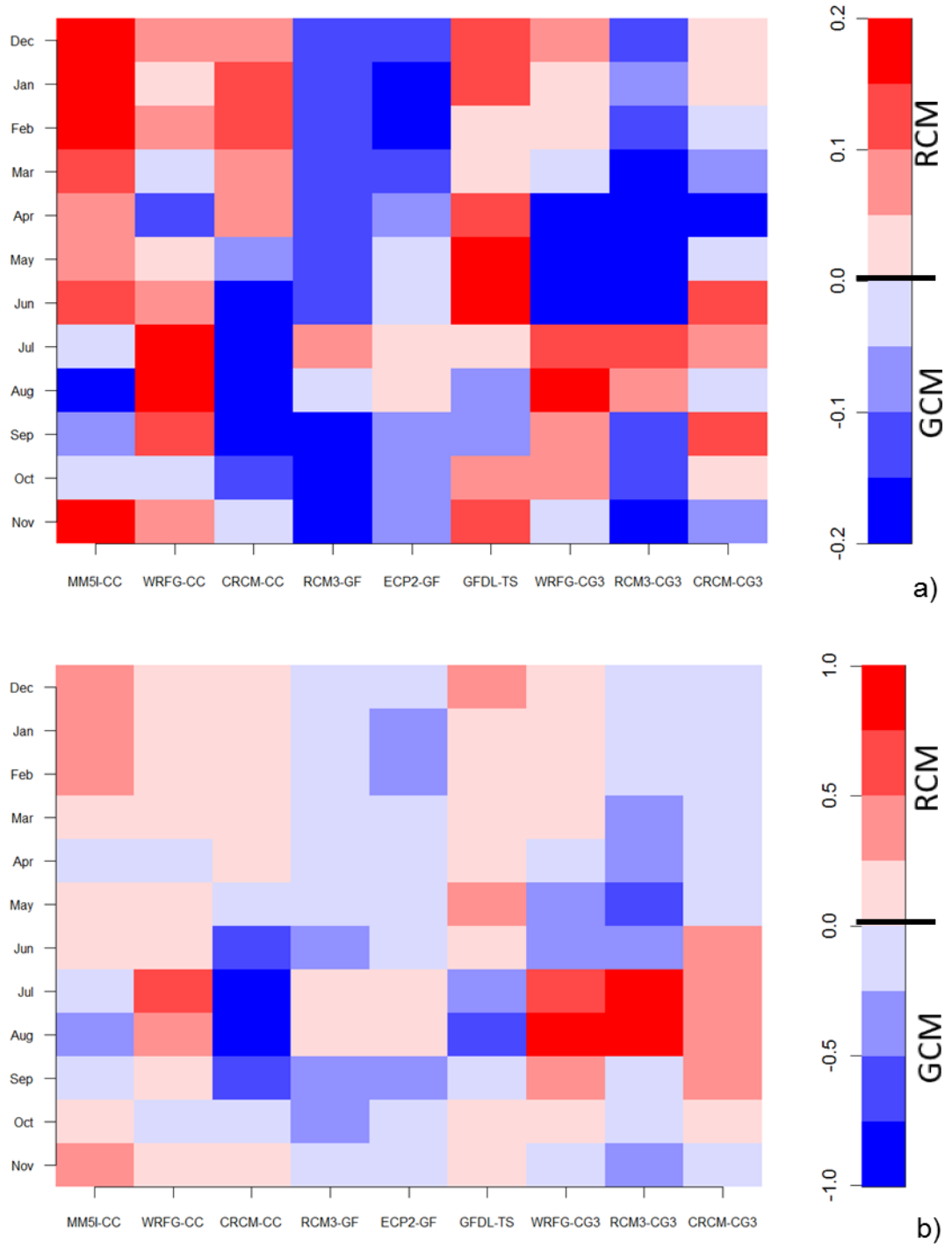

Figure 3.37. Value added for maximum temperature for Perkins skill score (a) and Willmott's index of agreement (b) for the west sub-region.

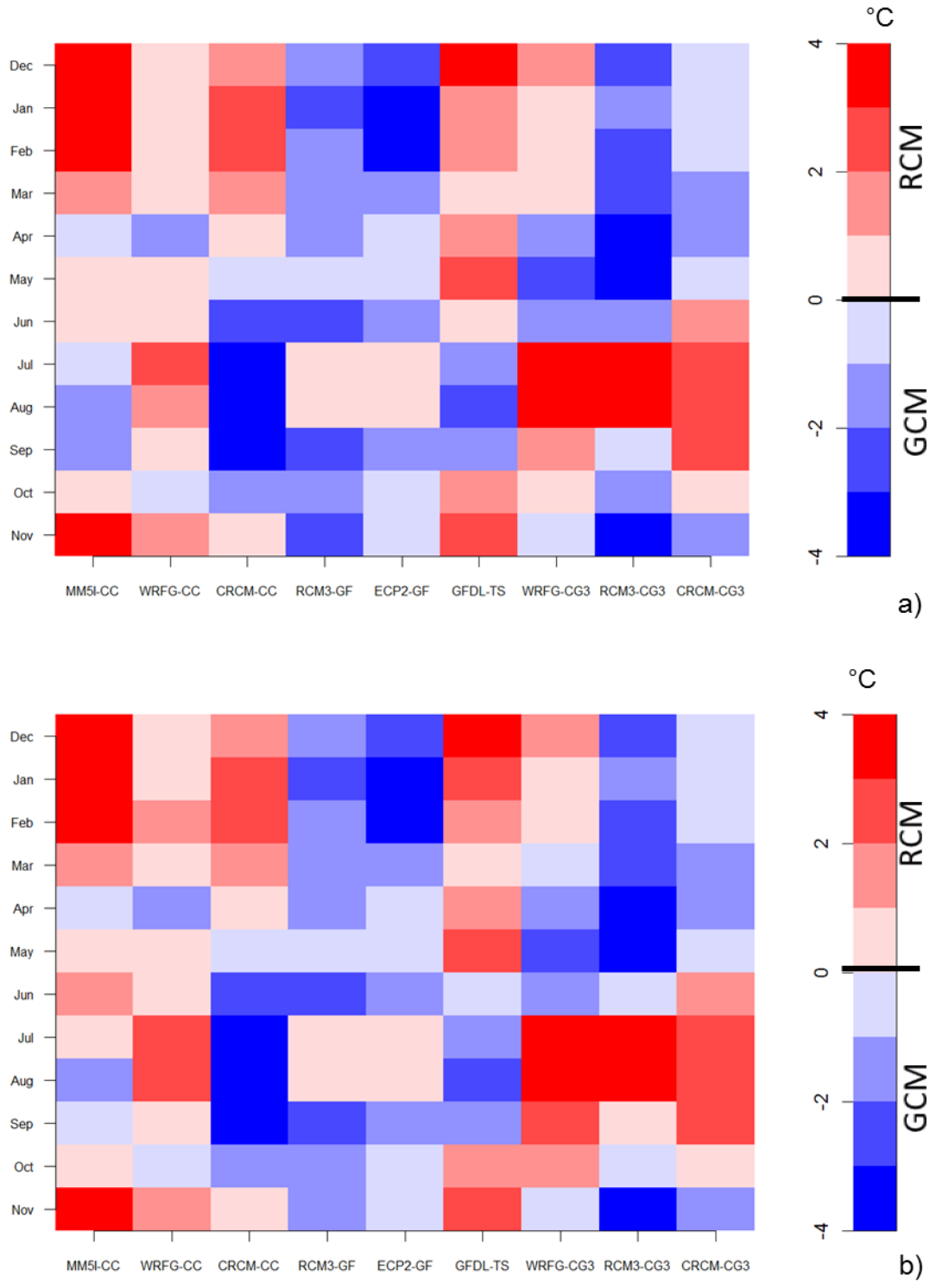

Figure 3.38. Value added for maximum temperature for MAE (a) and RMSE (b) for the west sub-region.

The RCM3 and ECP2 models fail to add value in downscaling for any month, a slight contrast with results from minimum temperature in which a small order of value is added for a few months. Further, these models substantially degrade any skill the GFDL GCM may have provided. The GFDL-timeslice, on the other hand, adds value for most months out of the year, indicating including observed sea-surface conditions plays a factor in bounding maximum temperatures (more so than with minimum temperatures), overcoming any bias the regional climate models could not overcome. This observation provides merit to performing timeslice experiments where maximum temperature predictions are concerned by bringing the model back toward realism rather than blindly following GCM conditions. Interestingly, plots of value added for the GFDL-driven models in the west sub-region look similar to the east sub-region, save for the summer months, in which the RCMs add a minimal amount of value over the GFDL. Conversely, the GFDL-timeslice fails to add value during the same season. This dichodomy may reflect that the direct influence of sea-surface conditions are more important in the east sub-region and illustrate that they are less important to maximum temperature in the west sub-region. Although the entire Southeast U.S. is under the influence of the maritime tropical air mass in the summer, the inclusion of Tenessee and its "land-locked" nature may allow influence of the continential tropical air mass found in the Upper and Mid-Mississippi River Valley and Ohio River Valley to lessen the impact of sea-surface conditions for the west sub-region.

Overall, the MM5I-CCSM and GFDL-timeslice provide the most value added (at least 10 months with positive contribution) when compared to all other ensemble members. To determine if the MM5I proves superior with other LBCs, future work

should investigate the MM5I's worth with other LBCs and perform similar analysis to that presented in this dissertation. The CRCM-CCSM provides some value added in winter and spring while the WRFG-CCSM provides minimal value added in summer. The three RCMs driven by the CGCM3 GCM provide value added contained within the summer, a result of the RCMs mitigating a large warm bias found within the CGCM3 (compare Figures 3.9 and 3.12 to Figures F.4 and F.5).

3.3.3 MEAN PRECIPITATION

Figures 3.39 through 3.42 illustrate the value added with respect to Perkins skill score, Willmott's index of agreement, RMSE and MAE for the both sub-regions. Value added for precipitation is perhaps the most important aspect in the downscaling process. GCMs lack the optimal horizontal resolution to resolve micro- and meso-scale processes related to warm season convective precipitation and are unable to resolve complex terrain influences such as mountains and coastlines. RCMs potentially could overcome these short-comings. With respect to Perkins skill score and Willmott's index of agreement, most RCMs add some value from March through September, coinciding with the convective season, indicating intra- and inter-annual variability replication is improved through downscaling. RMSE and MAE values show improvement in several instances over their driving GCMs, indicating errors and bias are also reducted in the downscaling process.

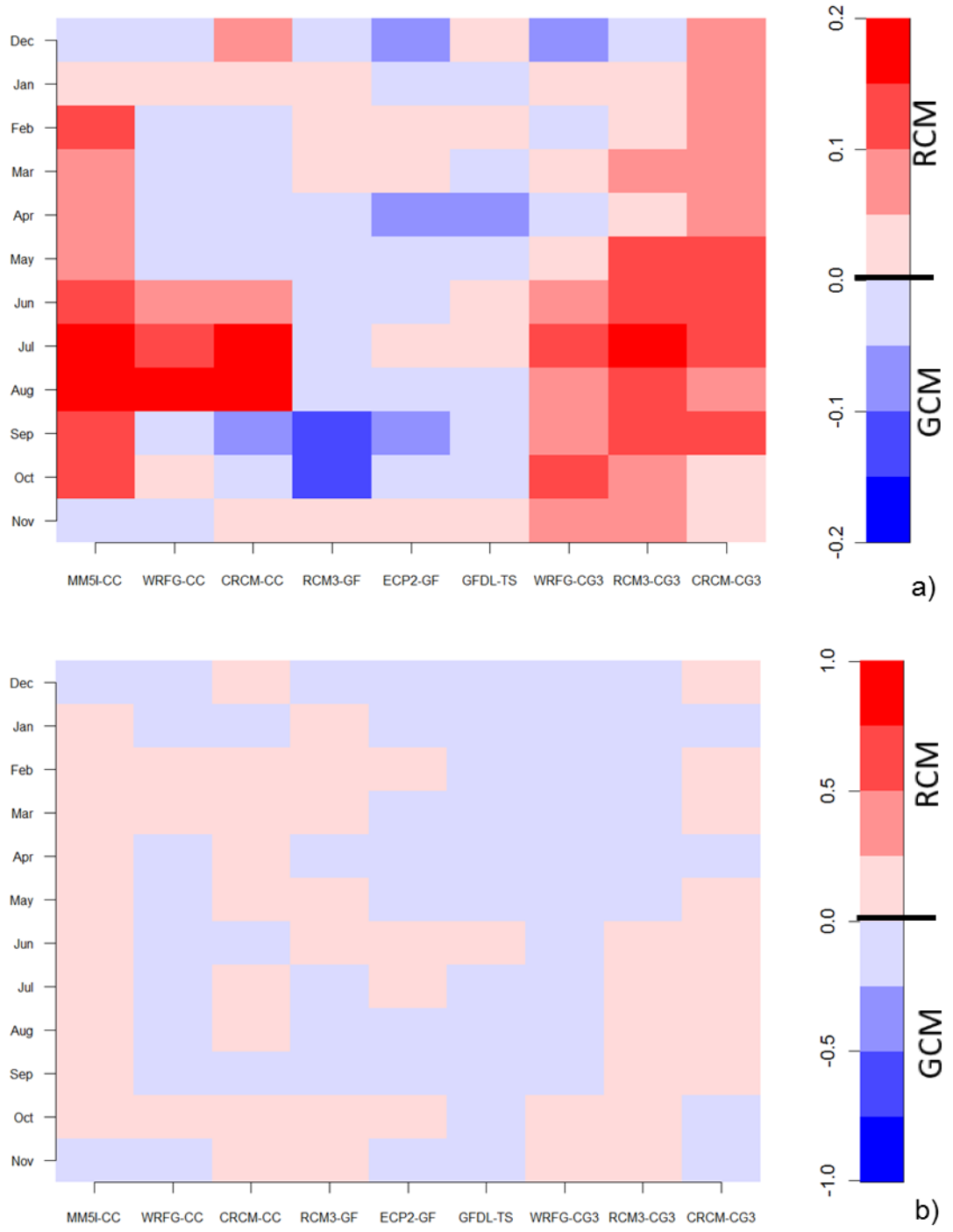

Figure 3.39. Value added for mean precipitation for Perkins skill score (a) and Willmott's index of agreement (b) for the east sub-region.

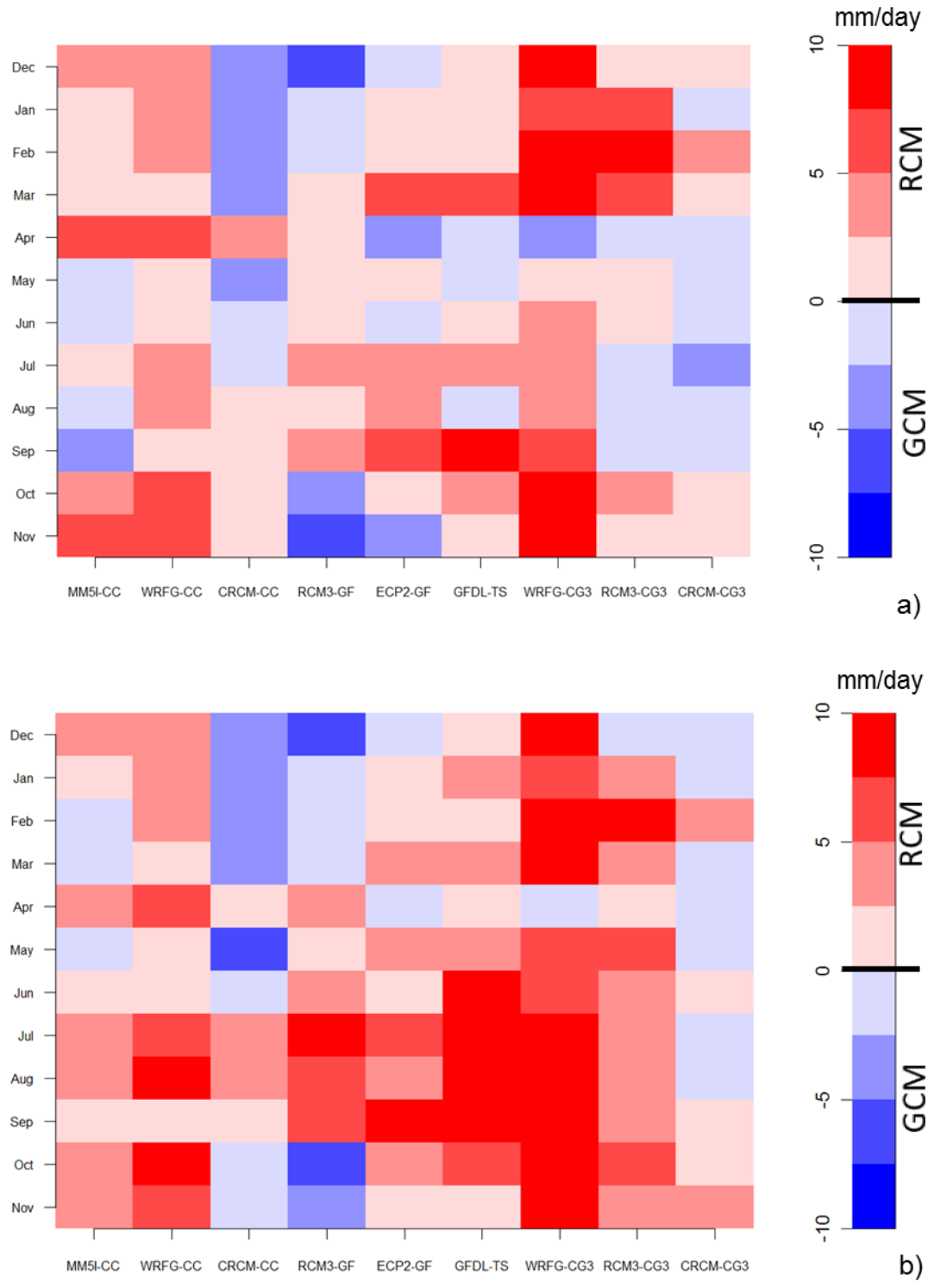

Figure 3.40. Value added for mean precipitation for MAE (a) and RMSE (b) for the east sub-region.

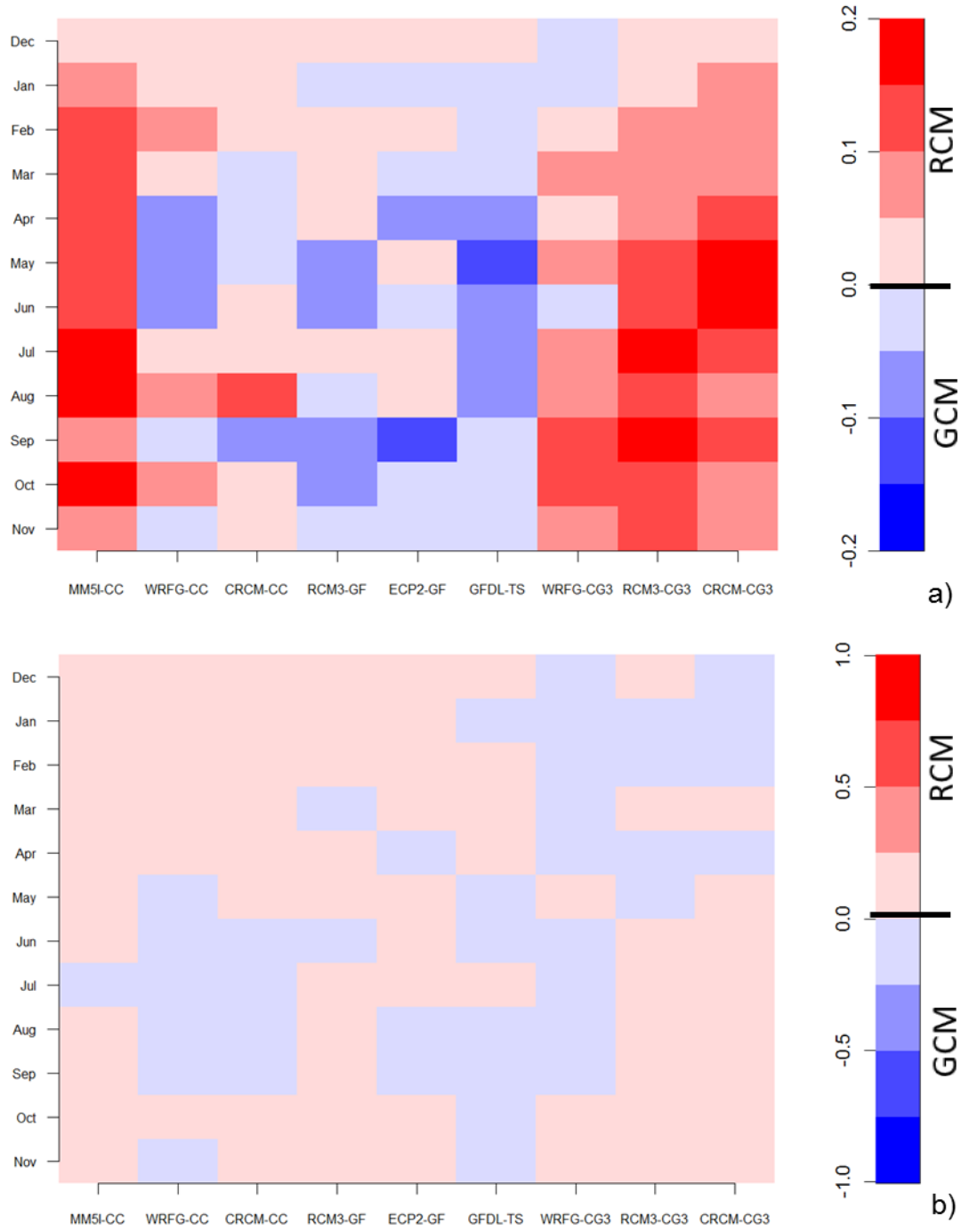

Figure 3.41. Value added for mean precipitation for Perkins skill score (a) and Willmott's index of agreement (b) for the west sub-region.

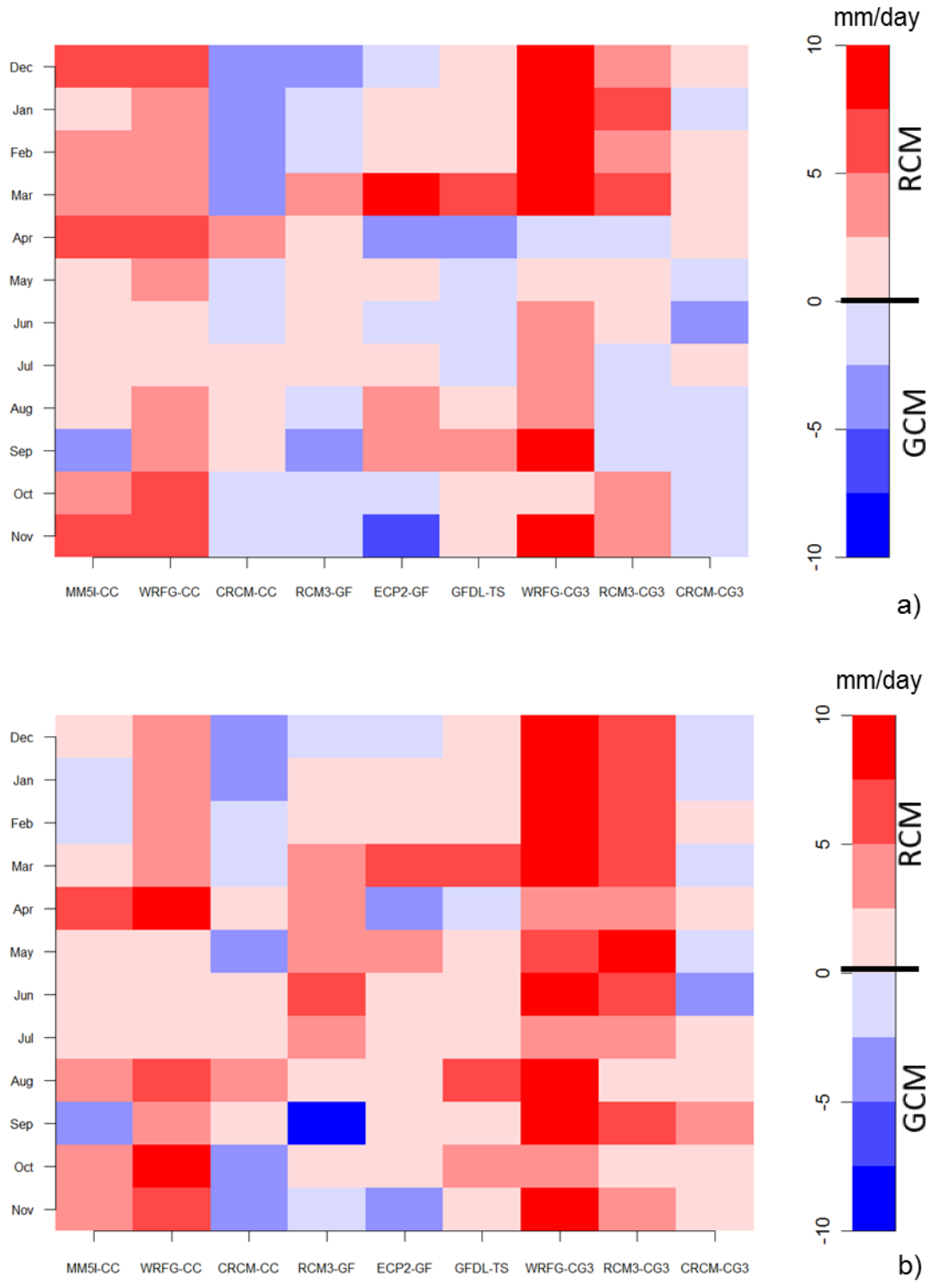

Figure 3.42. Value added for mean precipitation for MAE (a) and RMSE (b) for the west sub-region.

In general, the CGCM3-driven runs add little value in the winter months while the CCSM-driven runs each add value from winter through mid spring. Conversely, the CCSM-driven runs add the least value during the summer months (with the exception of the MM5I model which does not add value in July only). The GFDL-driven RCMs, overall, tend to exhibit the least amount of improvement in Perkins skill scores and only illustrate marginal improvement with respect to the index of agreement, RMSE, and MAE. The WRFG-CGCM3 and MM5I-CCSM models exhibit the most value added (regardless or metric) for their repective LBCs with significant improvement (relative to the maginitude of value added) noted in the convective season.

A few instanstances exist in which skill metrics (Perkins or Willmott) favor the GCM, however, RMSE and MAE favor the RCM. One instance involves the WRFG-CCSM model, particularly from mid spring through late fall. Another more notable instance occurs with the GFDL-timeslice in which value is rarely added with respect to the Perkins and Willmott values yet significant improvement is found for RMSE and MAE values. This indicates that although the intra- and inter-annual variability pattern is not improved with the timeslice experiement, the process does reduce error and bias found within the GCM. Conversely, the CRCM-CGCM3 illustrates an instance in which Perkins and Willmott values are increased in the downscaling process but at the cost of slightly increasing error and bias (particularly in the late spring and summer months).

In the end, the notion of "value added" is relative to the metric being used. A blanket statement about value added for precipitation (and temperature for that matter) cannot be made, as value added can only be evaluated on a month-by-month and model-by-model basis. Future work on this subject needs to evaluate value added with each

metric on a grid point by grid point basis rather than at the sub-regional scale to pinpoint locations of added value, particularly in locations poorly resolved by GCMs.

3.4 EFFECTIVE NUMBER OF ENSEMBLE MEMBERS

The effective number of models needed from an ensemble should be seriously considered by users of climate model output because: 1) maximizing the number of models used from an ensemble for an assessment has the potential to bias the assessed change in a variable (temperature, precipitation, etc.) toward an artificial mean because independence is assumed but not necessarily met; and 2) most users of climate model data do not want to gather information from nine ensemble members when they can glean the same amount of information from three or four ensemble members with high fidelity. The dendrograms and scatterplots in this section illustrate the similarities between RCMs, GCMs, and observations from a historical reference period by clustering models according to the strength of their relationship. Models which exhibit strong similarities are clustered low on the dendrogram while models with less similarity are clustered higher on the dendrogram. By incorporating observations and the driving GCMs into the cluster analysis, the goal is to determine if RCMs cluster with their driving GCM and determine which, if any, models cluster with observations.

Dendrograms generated for minimum and maximum temperature and mean precipitation based on hierarchical clustering for the east and west sub-regions (Figures 3.43, 3.45, and 3.47) show strong clustering between RCM and the GCM used for LBCs. This indicates RCMs run with the same LBCs are not independent of each other. The clusters generated by the hierarchical analysis show similar patterns revealed in the

percentile plots (bias plots), the four skill metric Hovmoller plots, and value added Hovmoller plots in that RCMs run with similar LBCs tend to exhibit relatively similar bias, skill scores, and add (or detract) similarly with regard to value added. Interestingly, none of the RCMs (regardless of LBCs) tended to cluster with each other (e.g., RCM3-GFDL does not cluster with RCM3-CGCM3), an indication that in general, RCMs are unable to distance themselves from their underlying boundary conditions. The sentiment of RCMs clustering based on similar LBCs is verified through the non-metric multidimensional scaling technique and illustrated in Figures 3.44 (minimum temperature), 3.46 (maximum temperature), and 3.48. The proximity of each point represents the strength of the relationship between observations, RCMs, and GCMs. Those which are closer together have higher similarity while those further from each other illustrate higher dissimilarity.

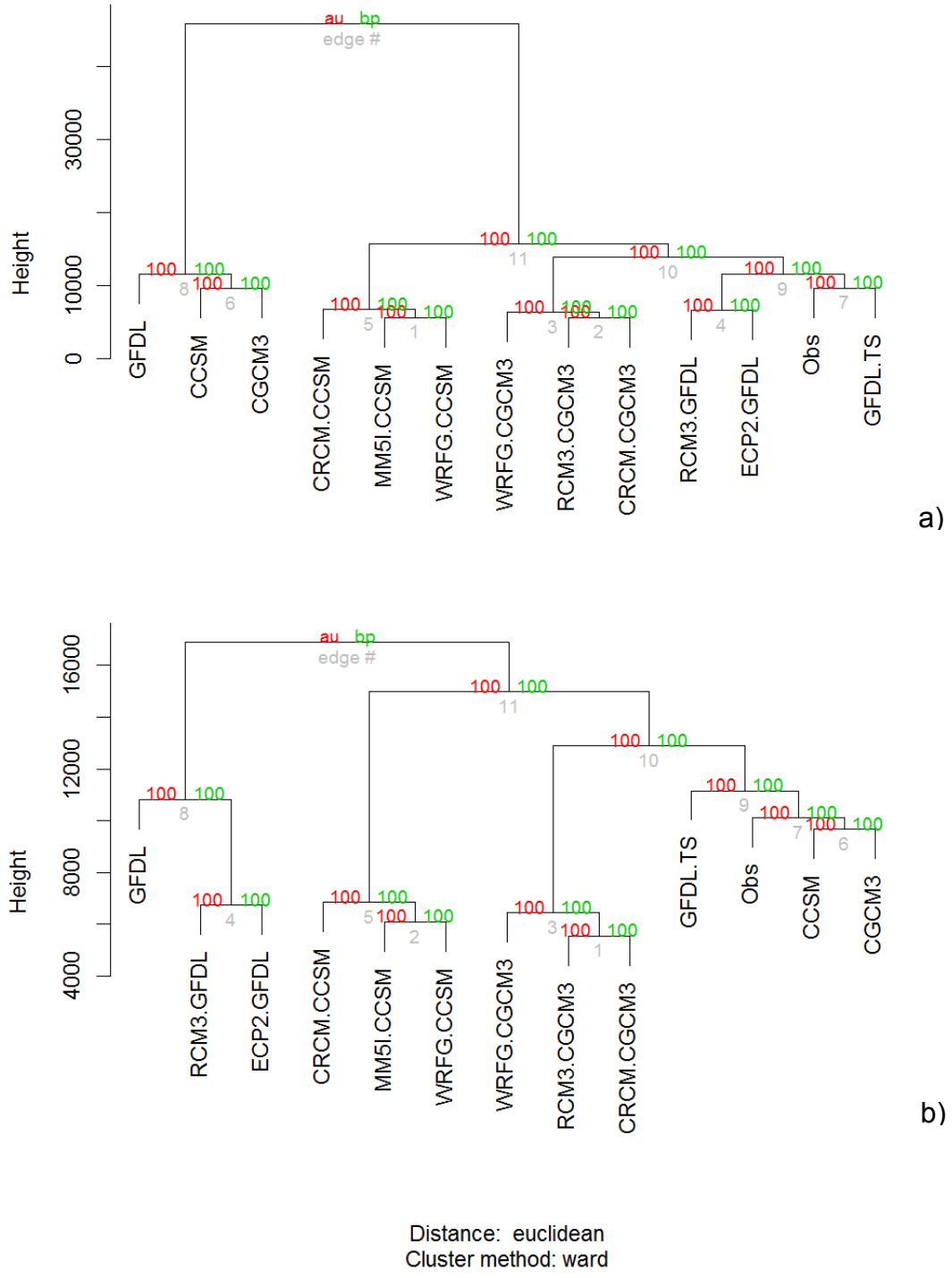

Figure 3.43. Dendrograms generated from hierarchical cluster analysis for minimum temperature for the east (a) and west (b) sub-regions.

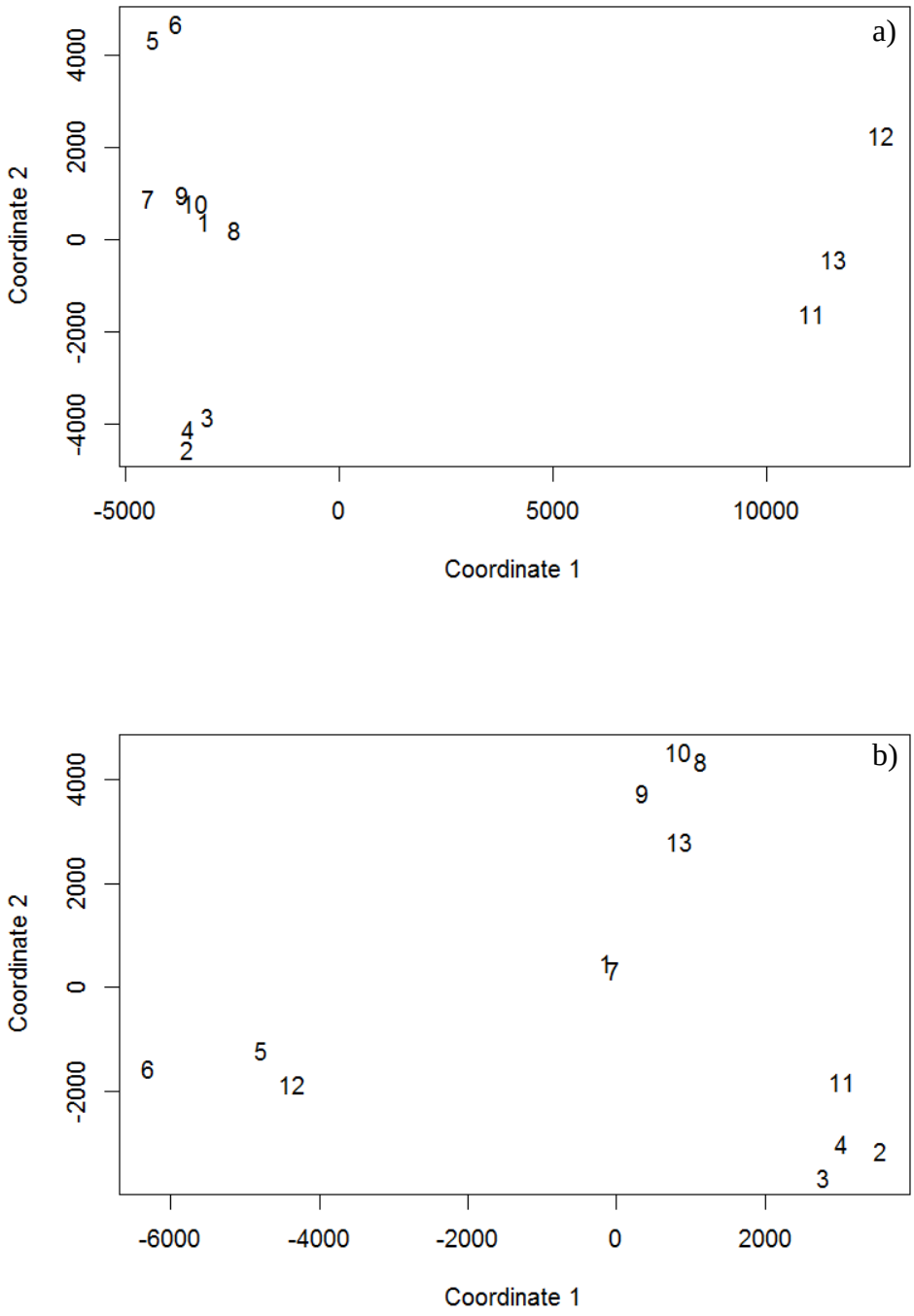

Figure 3.44. Scatterplot of results from the non-metric multidimensional scaling minimum temperature for the east (a) and west (b) sub-regions. Numbers coorespond to observations and models as follows: “1”=observations, “2”=MM5I-CCSM, “3”=WRFG-CCSM, “4”=CRCM-CCSM, “5”=RCM3-GFDL, “6”=ECP2-GFDL, “7”=GFDL-Timeslice, “8”=WRFG-CGCM3, “9”=RCM3-CGCM3, “10”=CRCM-CGCM3, “11”=CCSM GCM, “12”=GFDL GCM, and “13”=CGCM3 GCM.

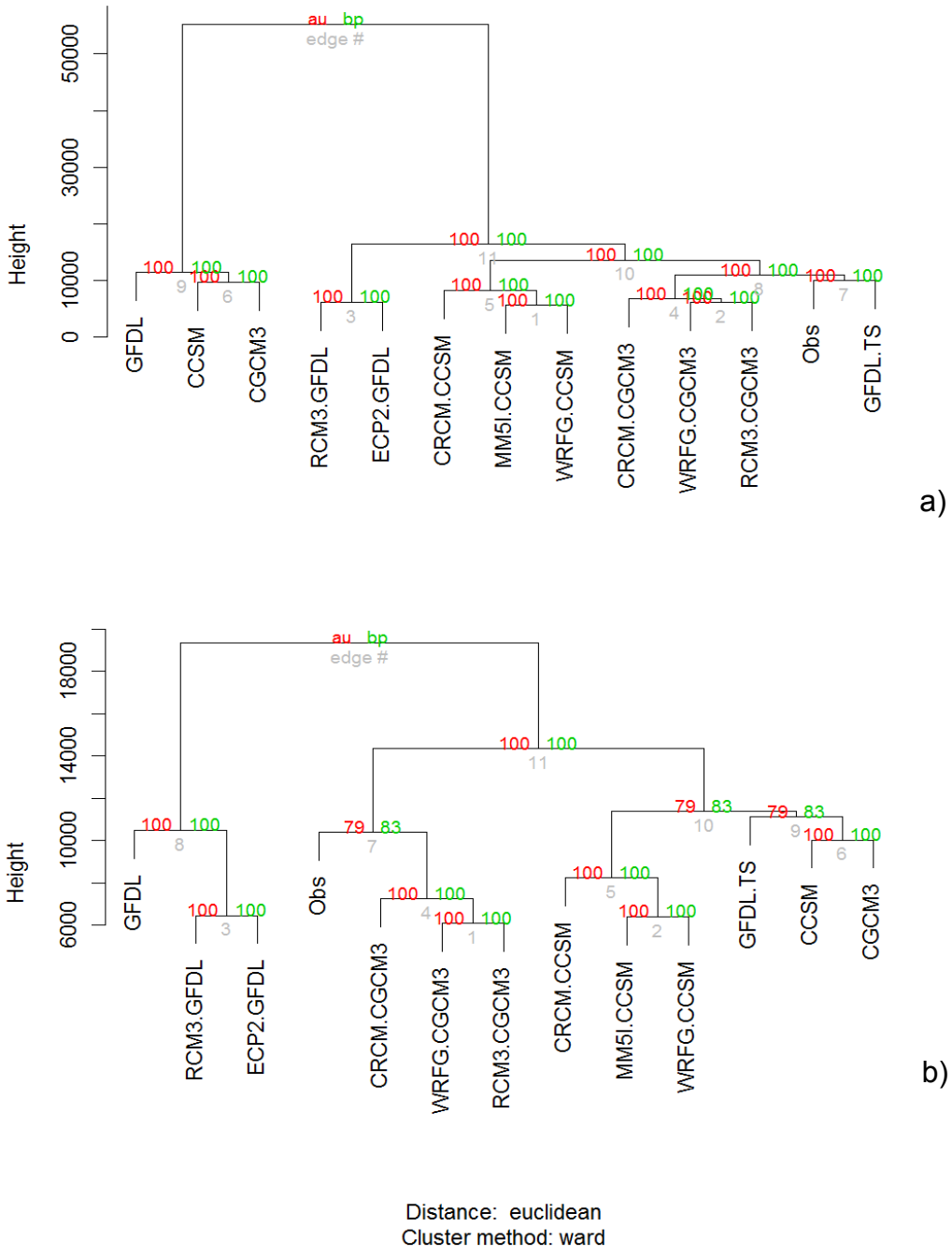

Figure 3.45. Dendrograms generated from hierarchical cluster analysis for maximum temperature for the east (a) and west (b) sub-regions.

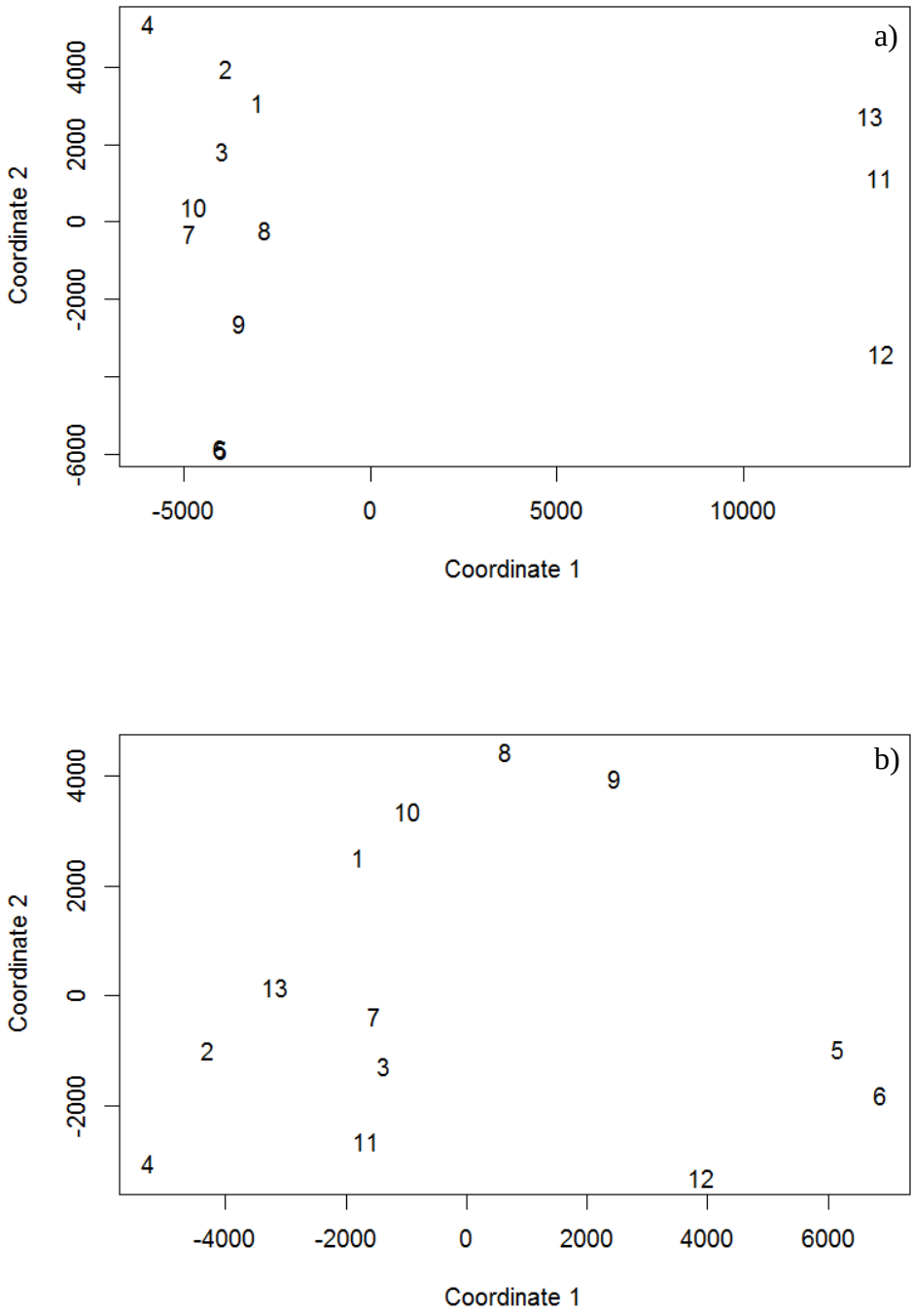

Figure 3.46. Scatterplot of results from the non-metric multidimensional scaling maximum temperature for the east (a) and west (b) sub-regions. Numbers coorespond to observations and models as follows: “1”=observations, “2”=MM5I-CCSM, “3”=WRFG-CCSM, “4”=CRCM-CCSM, “5”=RCM3-GFDL, “6”=ECP2-GFDL, “7”=GFDL-Timeslice, “8”=WRFG-CGCM3, “9”=RCM3-CGCM3, “10”=CRCM-CGCM3, “11”=CCSM GCM, “12”=GFDL GCM, and “13”=CGCM3 GCM.

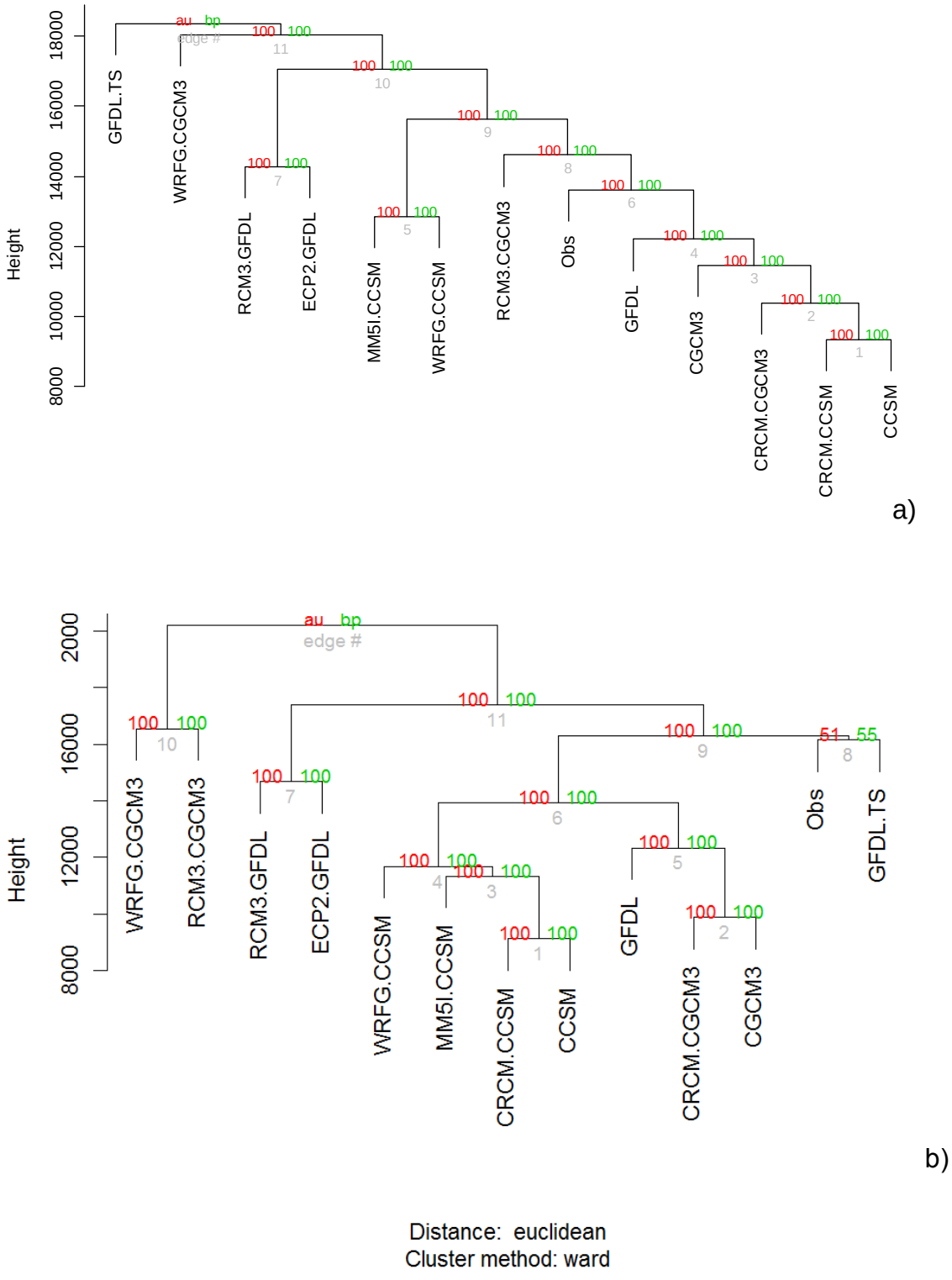

Figure 3.47. Dendrograms generated from hierarchical cluster analysis for mean precipitation for the east (a) and west (b) sub-regions.

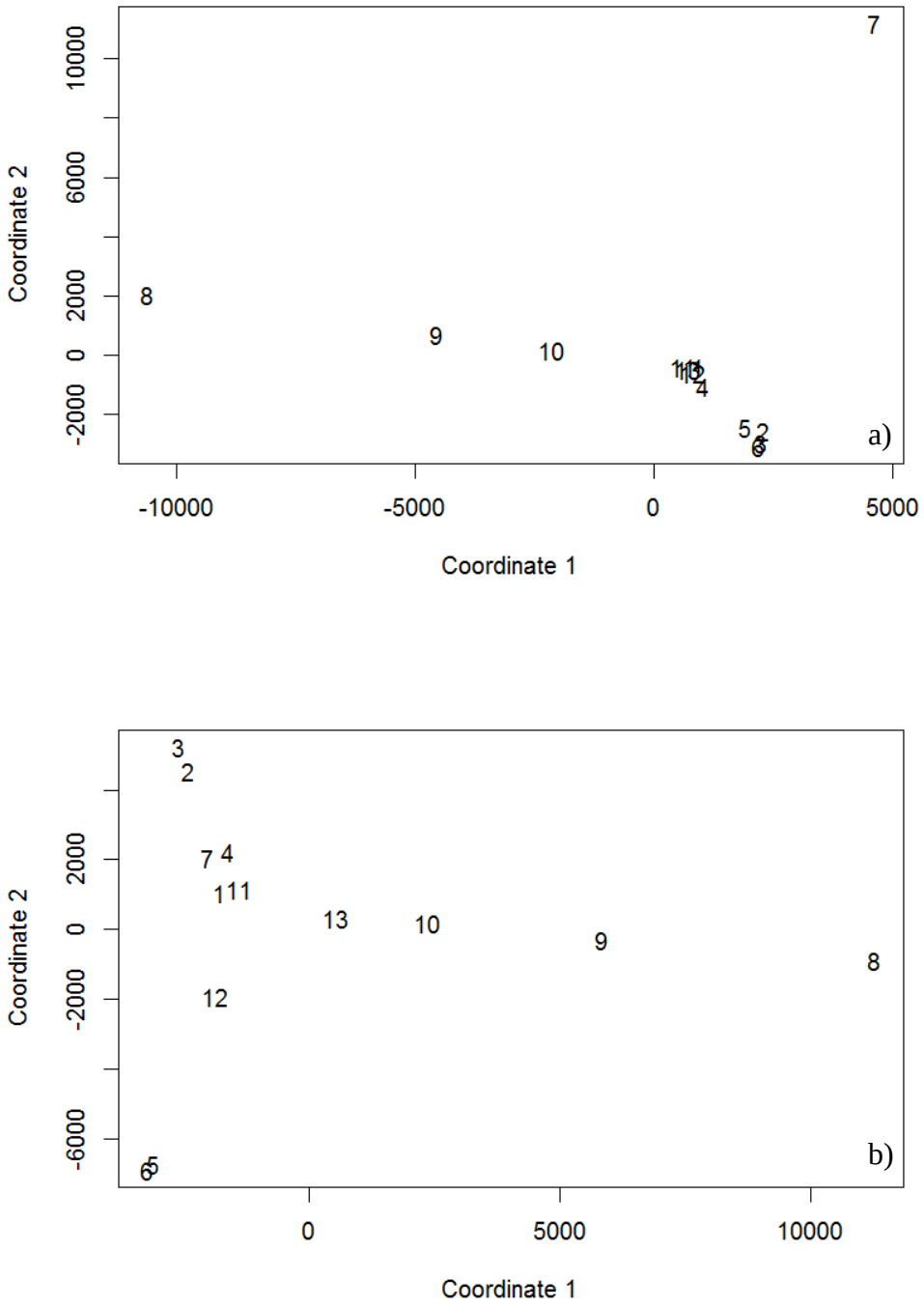

Figure 3.48. Scatterplot of results from the non-metric multidimensional scaling mean precipitation for the east (a) and west (b) sub-regions. Numbers coorespond to observations and models as follows: “1”=observations, “2”=MM5I-CCSM, “3”=WRFG-CCSM, “4”=CRCM-CCSM, “5”=RCM3-GFDL, “6”=ECP2-GFDL, “7”=GFDL-Timeslice, “8”=WRFG-CGCM3, “9”=RCM3-CGCM3, “10”=CRCM-CGCM3, “11”=CCSM GCM, “12”=GFDL GCM, and “13”=CGCM3 GCM.

Observations typically cluster with the GFDL-timeslice in both sub-regions for all variables (with the exception of maximum temperature in the west sub-region and mean precipitation for the east sub-region). This indicates the GFDL-timeslice best captures the intra- and inter-annual variability found in observations; however, inspection of the skill metrics does not reveal the GFDL-timeslice owning superior skill in reproducing observations relative to other RCMs in NARCCAP on a month-by-month comparison. GFDL-timeslice and observations clustering together appears to be a function of the timeslice experiment using observed sea surface and ice boundary conditions rather than utilizing boundary conditions from a GCM with fully coupled atmosphere and ocean components. The timeslice results illustrate the degree to which incorporating (or assimilating) observations into the model provide realistic "bounds", keeping the model closely coupled to observed conditions.

Mean precipitation dendrograms (Figure 3.45) illustrate the CRCM RCM clusters with its driving GCM (CRCM-CCSM with the CCSM GCM and the CRCM-CGCM3 with the CGCM3 GCM), something not found in any of the other clusters produced for temperature. One explanation of this behavior may be extracted from the value added Hovmöller plots in Figures 3.33 through 3.36 in which the CRCM RCMs add little if any value to the downscaling process (with respect to the magnitude of the value added), giving an indication that, in this case, the RCMs perform similarly to the GCMs driving them. Although RCMs should matter most with respect to precipitation, this is one instance in which the RCM cannot disengage from the influence of the driving GCM. Conversely, neither the RCM3 nor WRFG RCMs find themselves in clusters in close proximity to one another.

Based on the hierarchical clustering and NMDS procedures and findings from Pennell and Reichler (2010) and Masson and Knutti (2011), the effective number of models recommended from NARCCAP to provide an adequate ensemble would be one RCM for each GCM (three) plus the GFDL-timeslice (as the GFDL-timeslice does not cluster with either the GFDL GCM or the RCMs run with GFDL LBCs). The choice of RCM should be based on performance metrics by either month, season, or over the entire year, depending on the assessment being conducted. The hierarchical clustering analysis provides additional quantitative analysis that RCMs run with similar LBCs tend to provide similar results to those found in the previous three sections. The added bonus is found with respect to the explicit grouping of models by semblance rather than making qualitative assumptions about RCM-GCM similarity. Lastly, incorporating observations allowed for the finding that the GFDL-timeslice, driven with observed sea-surface conditions, tended to follow the daily-, monthly-, and inter-annual variability found in observations, a conclusion not found in the bias or skill metrics. Skill for the GFDL-timeslice is degraded by persistent bias; however, the cluster analysis reveals observed weather pattern replication in the timeslice experiment regardless of bias.

All apsects of the work presented in Chapter 3 were used to provide stakeholders with recommendations of models to use for their specific applications. Table 3.2 provides a comprehensive view of example model output uses (e.g., further modeling studies, extreme precipitation applications, etc.), the variables typically used for those activities, the recommended ensemble, as well as the overall "best" model as found in this dissertation. The recommended ensemble was constructed based on one RCM per GCM, included the GFDL-Timeslice, and was ultimately formed based on superiority on a

monthly basis for each respective variable (a tally which is illustrated in the next chapter). Additionally, a grade according to efficacy of the model is shown from low efficacy to high efficacy. It should be noted that although the GFDL-based models tended showed several shortcomings, their inclusion in an ensemble is important because although they may not satisfactorally replicate observations their future projects may still prove valid and thus provide decision makers with a broader range of future uncertainties in which they can base their assessments (Stainforth et al., 2007).

Table 3.2. Examples of uses for climate model output, variables utilized, the recommended ensemble based on results from this dissertation, and the recommended single model (if output from a single model is desired for any given application).[2]

Use of Model Output	Daily Variables Utilized	Recommended Ensemble (Efficacy)	Recommended Single Model (Efficacy)
Hydrologic and Crop Modeling	T_{min}, T_{max}, P_{mean}	MM5I-CCSM (H) RCM3-GFDL (L) GFDL-Timeslice (M) CRCM-CGCM3 (M)	MM5I-CCSM (H)
Growing Degree Days and Potential Evapotranspirtation Modeling	T_{min}, T_{max}	MM5I-CCSM (H) RCM3-GFDL (L) GFDL-Timeslice (M) CRCM-CGCM3 (M)	MM5I-CCSM (H)
Extreme Precipitation and Precipitation Return Intervals	P_{mean}	MM5I-CCSM (H) RCM3-GFDL (L) GFDL-Timeslice (M) CRCM-CGCM3 (M)	MM5I-CCSM (H)
Minimum Temperature Applications	T_{min}	MM5I-CCSM (H) ECP2-GFDL (L) GFDL-Timeslice (M) WRFG-CGCM3 (M)	MM5I-CCSM (H)
Maximum Temperature Applications	T_{max}	MM5I-CCSM (H) RCM3-GFDL (L) GFDL-Timeslice (M) RCM3-CGCM3 (M)	MM5I-CCSM (H)

[2] Letters in parenthesis represent the efficacy of the model with respect to all metrics (Perkin's skill score, Willmott's index of agreement, RMSE, and MAE) and variables (T_{min}, T_{max}, P_{mean}, sea-level pressure, 500-mb height, soil moisture, latent and sensible heat flux, and total cloud cover). "H" represents high efficacy (most aspects replicated well compared to observations), "M" represents moderate efficacy (some aspects replicated well compared to observations), and "L" represents low efficacy (few aspects replicated well compared to observations).

CHAPTER 4

NARCCAP-BASED FUTURE CLIMATE PROJECTIONS

Chapter 4 includes projected future changes in minimum temperature, maximum temperature, and mean precipitation from a 30-year historical reference period (1970-1999) to a 30-year future period (2040-2069) for the east and west sub-regions within the Southeast U.S.

4.1 MINIMUM TEMPERATURE

Projections of change in future minimum temperature with respect to a 30-year historical reference period (1970-1999) illustrate a strong consensus among all NARCCAP ensemble members in that all locations, regardless of month, will warm by at least 1°C. Figure 4.1 illustrates the spatial distribution of ensemble mean change and standard deviation in minimum temperature for each month. Plotting the spatial pattern of ensemble standard deviation illustrates agreement between ensemble members relative to each other. Additionally, the box and whisker plots illustrated in Figure 4.2 provide a similar assessment but is only representative of the entire sub-region rather than a grid point by grid point basis. Lastly, Figures G.1 through G.12 illustrate change in minimum temperature by month from each ensemble members.

In both sub-regions, months with the lowest projected change occurred from December through March while months exhibiting the highest minimum temperature increase included July through September (Tables 4.1 and 4.3), respectively. The month

with the least spread among the ensemble members (indicating the highest level of agreement between models) was October with mean warming values of approximately 2°C and IQ values between 1.7°C and 2.1°C, respectively. From a statistical significance stand point, between 1 and 3 models indicate projected change (for that particular ensemble member) to be significant at any α-level in the east sub-region, while only 1 to 2 models indicate statistical significance at any α-level in the west sub-region. Both sub-regions exhibit little skewness with respect to ensemble change distributions (Figure 4.2), with the months of March, July, August, and November exhibiting a slightly right skewness and September illustrating a slight skew to the left. A right skewed distribution indicates half the data points from the ensemble are less than the mean while a left skewed distribution indicates half the points are greater than the mean.

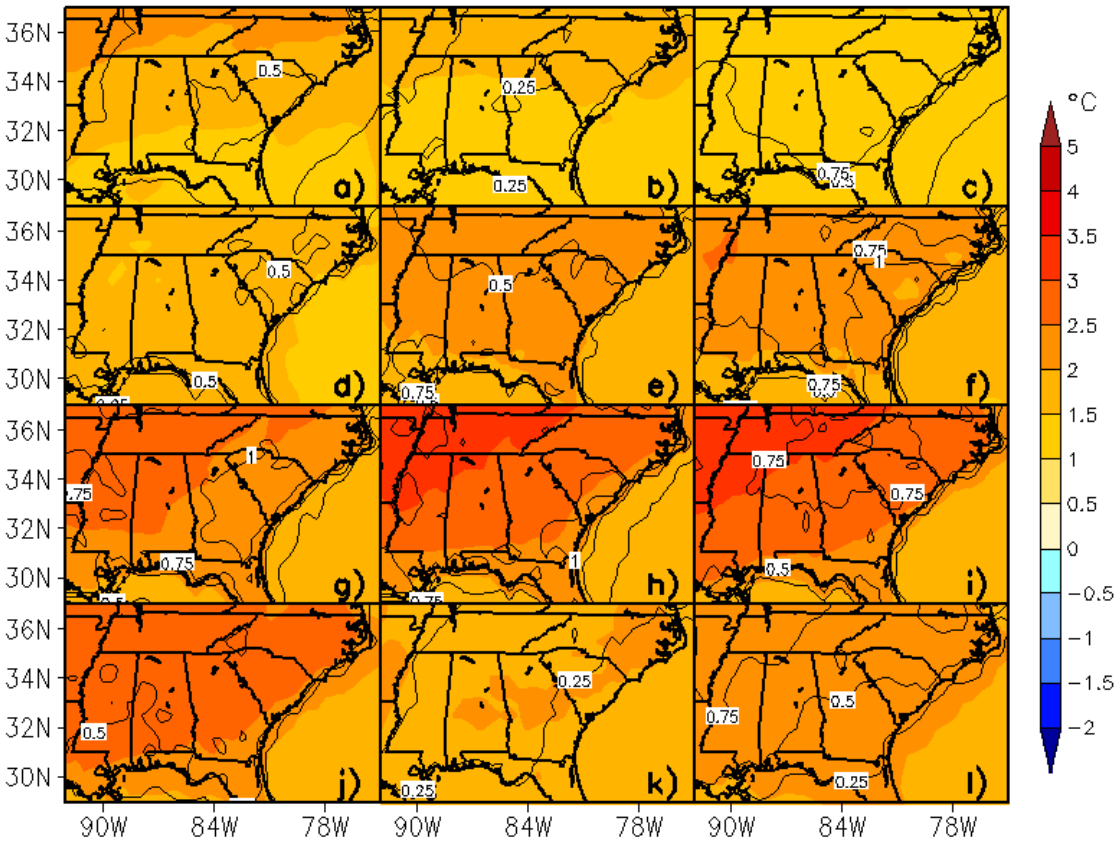

Figure 4.1. Ensemble mean change (shaded) and standard deviation (contoured) for minimum temperature for December (a), January (b), February (c), March (d), April (e), May (f), June (g), July (h), August (i), September (j), October (k), and November (l).

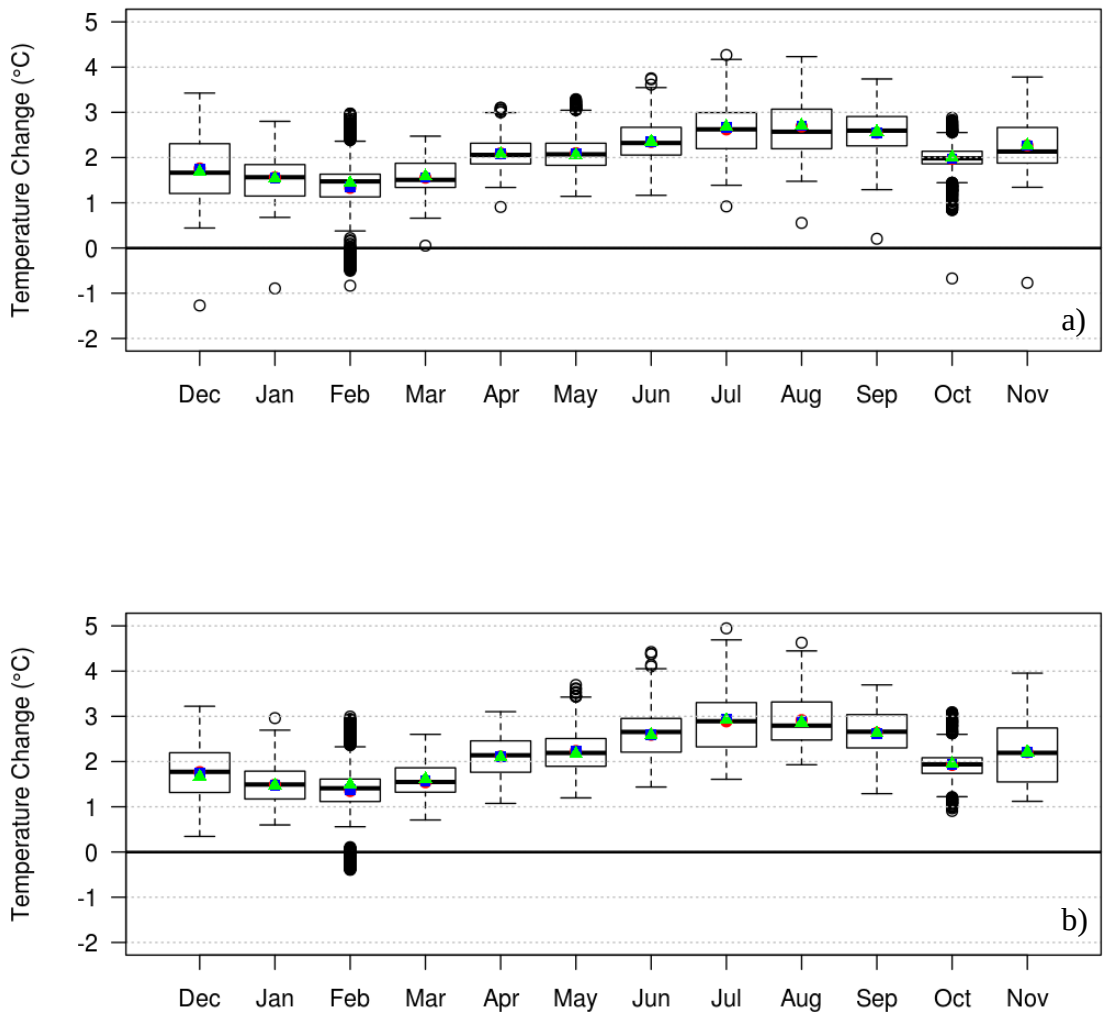

Figure 4.2. Box and whisker plots of change in minimum temperature from all ensemble members in the east (a) and west (b) sub-regions. Blue squares represent unweighted ensemble mean change, red circless represent weighted ensemble mean with Perkins skill score, and green triangles represent weighted ensemble mean with RMSE.

Weighting the ensemble mean for each sub-region provided little difference from unweighted ensemble mean values. However, Figures 4.3 and 4.4 reveal the impact weighting can have spatially. Weighting (regardless of the metric used) slightly raised the

ensemble mean in half the months while slightly reducing or leaving unchanged for the remaining six months in the east sub-region. The west sub-region, conversely, observes weighted means less than or equal to the unweighted mean in eight months, while only three months observe a uniform warming between the weighting schemes (and one month in which Perkins skill score resulted in an unchanged mean while the RMSE weight raised the mean).

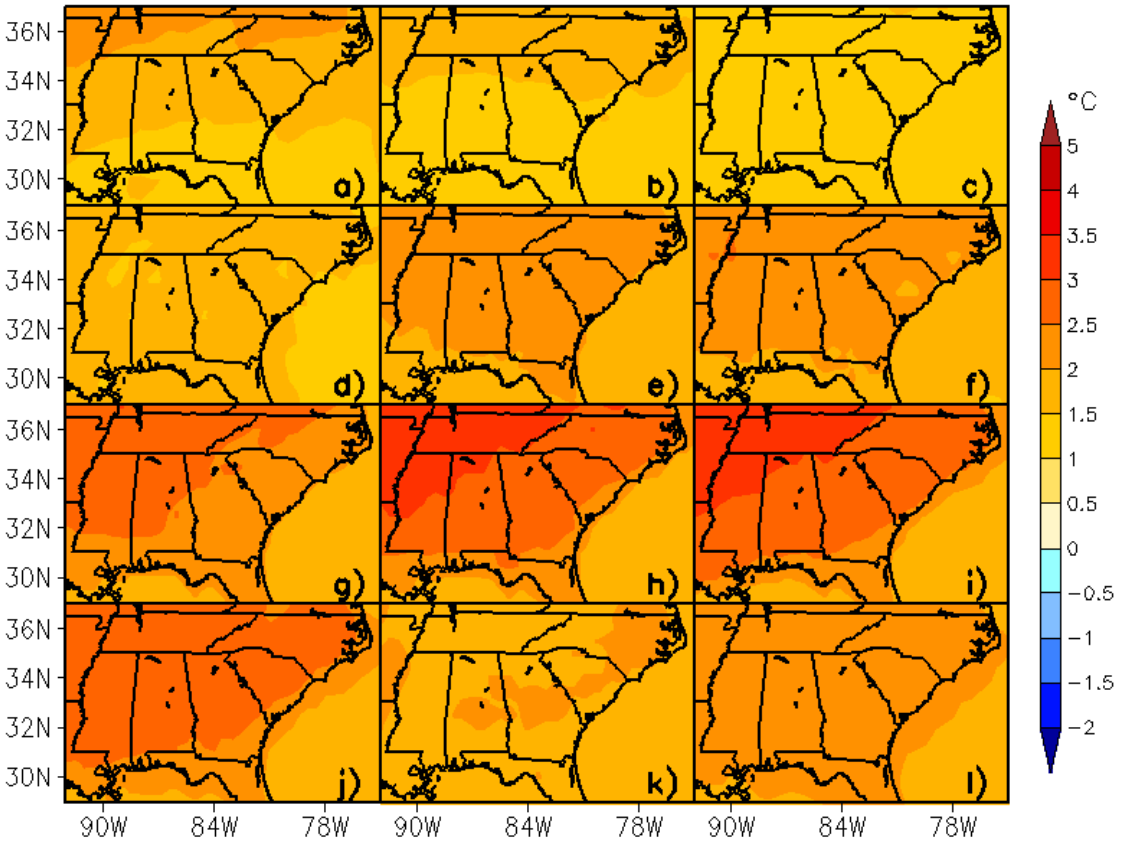

Figure 4.3. Weighted ensemble mean using Perkins skill scores for minimum temperature for December (a), January (b), February (c), March (d), April (e), May (f), June (g), July (h), August (i), September (j), October (k), and November (l).

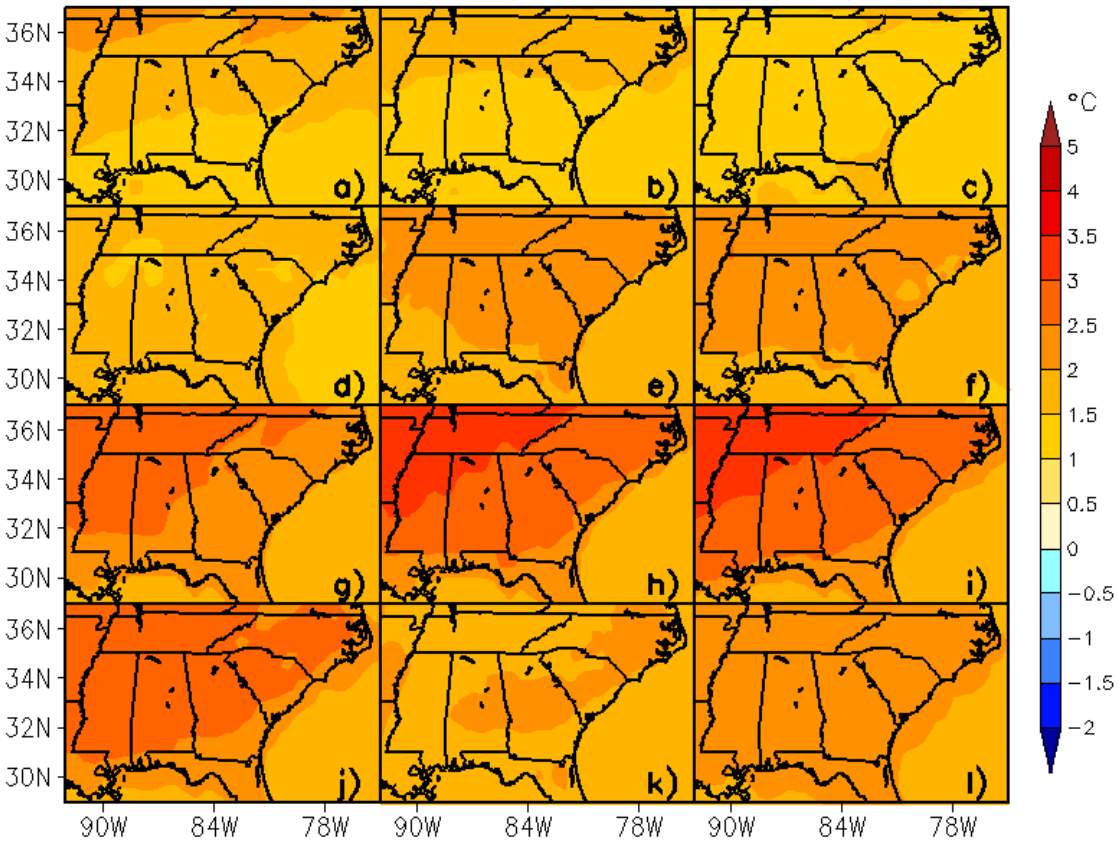

Figure 4.4. Weighted ensemble mean using RMSE for minimum temperature for December (a), January (b), February (c), March (d), April (e), May (f), June (g), July (h), August (i), September (j), October (k), and November (l).

Tables 4.1 and 4.3 illustrates ensemble mean, median, and IQ values for one RCM from each GCM plus the GFDL-timeslice. RCMs were chosen based on superiority with respect to Perkins' skill score, Willmott's index of agreement, and RMSE by month (Tables 4.2 and 4.4). With respect to the nine member NARCCAP ensemble, the east sub-region exhibits increased warming for selected ensemble mean and median (relative to the greater NARCCAP ensemble) for 10 months, while the west sub-region exhibits increased warming for the selected ensemble mean in 11 months and ensemble median

for 9 months, respectively. Compared to the nine member ensemble, the selected ensemble mean and median rose anywhere from 0.1 to 0.5°C.

Table 4.1. Change in 30 year minimum temperature for the west sub-region based on unweighted ensemble mean, weighted mean utilizing Perkins skill scores (SS), and weighted mean utilizing RMSE for the entire nine-member NARCCAP ensemble. [3]

	NARCCAP 9-Member Ensemble – East						4-Member Select Ensemble – East			
	Unweighted Ensemble Mean Change (°C)	SS Weight Mean Change (°C)	RMSE Weight Mean Change (°C)	Ensemble Median Change (°C)	25th Percentile (°C)	75th Percentile (°C)	Ensemble Mean Change (°C)	Ensemble Median Change (°C)	25th Percentile (°C)	75th Percentile (°C)
Dec	1.76*3	1.74	1.68	1.66	1.21	2.31	1.94	2.10	1.43	2.46
Jan	1.56*2	1.55	1.54	1.57	1.15	1.84	1.75	1.73	1.56	1.92
Feb	1.33*2	1.36	1.44	1.47	1.13	1.63	1.62	1.55	1.23	1.89
Mar	1.55*2	1.56	1.58	1.51	1.34	1.87	1.55	1.52	1.39	1.67
Apr	2.09*2	2.09	2.07	2.06	1.86	2.32	2.27	2.22	2.03	2.52
May	2.10*2	2.09	2.05	2.07	1.83	2.32	1.94	2.01	1.66	2.20
Jun	2.34*2	2.35	2.35	2.32	2.06	2.67	2.58	2.59	2.39	2.80
Jul	2.62*2	2.66	2.68	2.62	2.20	2.99	3.01	2.97	2.82	3.18
Aug	2.69*1	2.70	2.71	2.57	2.20	3.07	3.09	3.01	2.67	3.53
Sep	2.55*2	2.55	2.58	2.59	2.26	2.91	2.62	2.84	2.08	3.17
Oct	1.97*2	1.98	2.01	1.98	1.86	2.14	2.11	2.07	1.91	2.30
Nov	2.27*2	2.27	2.27	2.13	1.88	2.66	2.21	2.09	1.78	2.53

[3] Ensemble median, 25th percentile, and 75th percentile change are also presented. Weighted mean numbers in red represent cases in which weighting results in higher mean change, blue represent cases in which weighting results in lower mean change and black are values which resulted in zero change. Superscripts for the unweighted ensemble mean change indicate change considered statistically significant at the α=0.1 (#), α=0.05 (@), and α=0.01 (*) levels for each individual ensemble member. The number following the superscript indicates the number of models from the NARCCAP ensemble considering change statistically significant at each α-level. The four-member select ensemble is comprised of models illustrated in Table 4.2. Red indicates cases were the select ensemble is warmer than the 9-member ensemble, blue is colder, and black unchanged.

Table 4.2. Models chosen, by month and GCM LBCs, for the four-member ensemble based on findings from the hierarchical cluster analysis and superiority in the four skill metrics for minimum temperature in the east sub-region.

	MM5I-CCSM	WRFG-CCSM	CRCM-CCSM	RCM3-GFDL	ECP2-GFDL	GFDL-Timeslice	WRFG-CGCM3	RCM3-CGCM3	CRCM-CGCM3
Dec	X				X	X		X	
Jan		X			X	X		X	
Feb		X		X		X			X
Mar			X	X		X	X		
Apr			X		X	X			X
May		X		X		X	X		
Jun		X		X		X			X
Jul			X	X		X			X
Aug			X	X		X		X	
Sep			X	X		X		X	
Oct			X	X		X		X	
Nov			X		X	X		X	
Total	**1**	**4**	**7**	**8**	**4**	**12**	**2**	**6**	**4**

Table 4.3. Change in 30 year minimum temperature for the west sub-region based on unweighted ensemble mean, weighted mean utilizing Perkins skill scores (SS), and weighted mean utilizing RMSE for the entire nine-member NARCCAP ensemble. [4]

	NARCCAP 9-Member Ensemble – West						4-Member Select Ensemble – West			
	Unweighted Ensemble Mean Change (°C)	SS Weight Mean Change (°C)	RMSE Weight Mean Change (°C)	Ensemble Median Change (°C)	25th Percentile (°C)	75th Percentile (°C)	Ensemble Mean Change (°C)	Ensemble Median Change (°C)	25th Percentile (°C)	75th Percentile (°C)
Dec	1.49*1	1.48	1.48	1.49	1.17	1.79	1.75	1.73	1.32	2.15
Jan	1.35*1	1.39	1.49	1.41	1.12	1.61	1.53	1.58	1.14	1.89
Feb	1.54*1	1.56	1.61	1.55	1.32	1.86	1.70	1.58	1.27	1.91
Mar	2.11*1	2.10	2.09	2.14	1.76	2.46	1.55	1.49	1.25	1.91
Apr	2.23*1	2.22	2.17	2.19	1.90	2.51	2.35	2.38	2.13	2.67
May	2.59*1	2.59	2.58	2.65	2.21	2.95	2.31	2.34	2.09	2.49
Jun	2.89*1	2.95	2.92	2.89	2.33	3.30	2.86	2.83	2.60	3.11
Jul	2.92*1	2.90	2.86	2.79	2.48	3.32	3.27	3.21	2.89	3.64
Aug	2.63*1	2.62	2.63	2.66	2.30	3.04	2.97	2.79	2.54	3.29
Sep	1.93*1	1.93	1.95	1.94	1.74	2.08	2.66	2.71	2.08	3.29
Oct	2.21*1	2.20	2.21	2.19	1.55	2.74	1.92	1.93	1.76	2.08
Nov	1.77*2	1.74	1.67	1.77	1.32	2.20	2.22	2.21	1.56	2.71

[4] Ensemble median, 25th percentile, and 75th percentile change are also presented. Weighted mean numbers in red represent cases in which weighting results in higher mean change, blue represent cases in which weighting results in lower mean change and black are values which resulted in zero change. Superscripts for the unweighted ensemble mean change indicate change considered statistically significant at the α=0.1 (#), α=0.05 (@), and α=0.01 (*) levels for each individual ensemble member. The number following the superscript indicates the number of models from the NARCCAP ensemble considering change statistically significant at each α-level. The four-member select ensemble is comprised of models illustrated in Table 4.2. Red indicates cases were the select ensemble is warmer than the 9-member ensemble, blue is colder, and black unchanged.

Table 4.4. Models chosen, by month and GCM LBCs, for the four-member ensemble based on findings from the hierarchical cluster analysis and superiority in the four skill metrics for minimum temperature in the west sub-region.

	MM5I-CCSM	WRFG-CCSM	CRCM-CCSM	RCM3-GFDL	ECP2-GFDL	GFDL-Timeslice	WRFG-CGCM3	RCM3-CGCM3	CRCM-CGCM3
Dec	X			X		X			X
Jan	X			X		X		X	
Feb		X		X		X			X
Mar	X			X		X	X		
Apr	X				X	X			X
May		X		X		X	X		
Jun	X			X		X			X
Jul	X			X		X			X
Aug	X			X		X		X	
Sep			X	X		X		X	
Oct			X	X		X			
Nov			X		X	X		X	
Total	**7**	**2**	**3**	**10**	**2**	**12**	**2**	**5**	**5**

In terms of individual models, the GFDL-timeslice consistently exhibits greatest warming from month-to-month out of any of the models, typically 1°C warmer. The CRCM-CCSM also exhibits among the highest increases in minimum temperature with 6 of 12 months among the highest increases. The ECP2-GFDL shows the smallest increases from month-to-month, consistently 0.5°C below a majority of the models. Additionally, the ECP2-GFDL is the only model to exhibit a decrease in minimum temperature (0.5°C for 90% of the Southeast U.S. in March). Lastly, the MM5I-CCSM consistently exhibits change that establishes its place the middle of the ensemble.

Increased nocturnal temperatures would result in increased nocturnal evaporation. Assuming unchanged dew point temperatures and annual mean precipitation, increased nocturnal evaporation will strain the water supply through enhanced water loss at both the surface and sub-surface. This would reduce flow in rivers and streams available for power plants and irrigation, and decrease the amount of available drinking water from reservoirs and lakes for municipalities. From an energy balance perspective, decreased surface and sub-surface moisture allows more heat to be stored in the soil and released as sensible heat, leading to potentially warmer daytime temperatures and a positive climate feedback. Additionally, crops such as corn (*Zea mays L.*) whose growth and development is determined by temperature (rather than calendar days like soybeans (*Glycine max*)) would be at increased risk for reduced yields due to rapid accumulation of growing degree days.

4.2 MAXIMUM TEMPERATURE

Maximum temperature change, like minimum temperature change, exhibits a warming trend of at least 1°C for all months, with seven months exhibiting weighted and unweighted change of at least 2°C (Figure 4.5, Figure 4.6, and Tables 4.5 and 4.7). In both sub-regions, February exhibits the smallest warming while July exhibits the greatest warming. October presents the greatest agreement between ensemble members with mean change of 1.7°C and an inter-quartile range of 0.46°C while the months of May through August exhibit the highest inter-quartile ranges of at least 1°C, escalating to 1.5°C in July, respectively. Only the CRCM-CGCM3 indicates change is statistically significant at any α-level (α=0.01 level for both sub-regions). Spatially, the greatest disagreement between models is mostly contained to South Carolina and eastern Georgia from May through August. In the east sub-region, weighting the ensemble mean resulted in an increase in mean change from February through July and September, and a decrease in January, November, and December, while in the west sub-region weighting resulted in increased mean change from December through May, July, September, and October, with decreases in August and November.

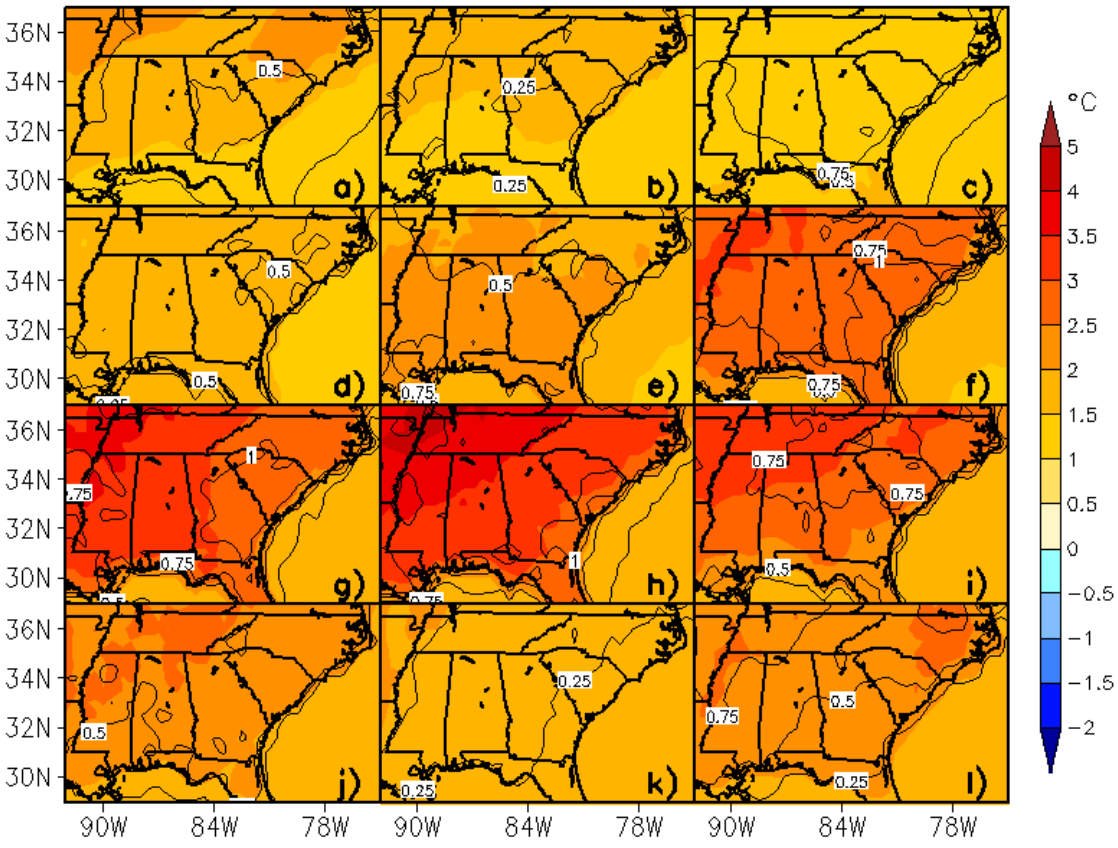

Figure 4.5. Ensemble mean change (shaded) and standard deviation (contoured) for maximum temperature for December (a), January (b), February (c), March (d), April (e), May (f), June (g), July (h), August (i), September (j), October (k), and November (l).

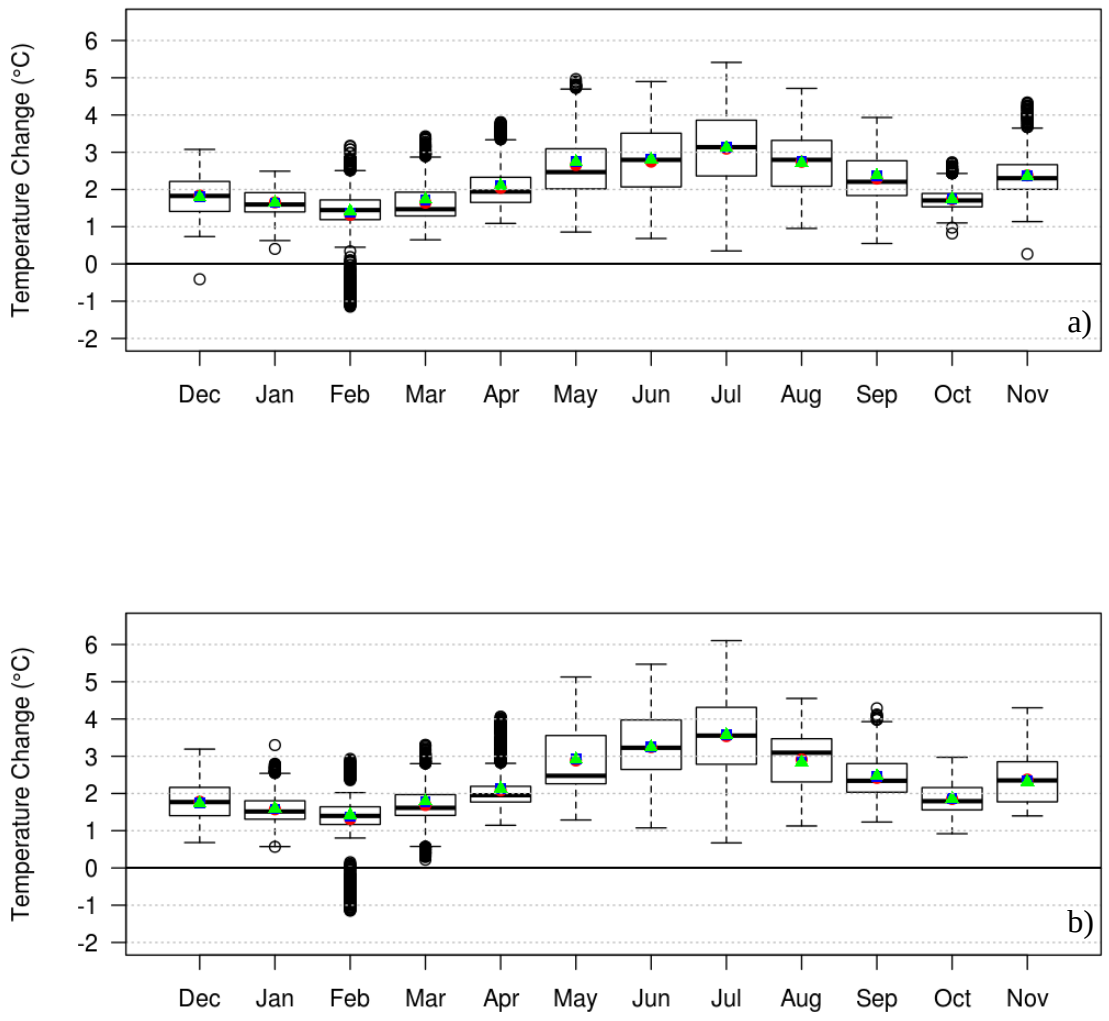

Figure 4.6. Box and whisker plots of change in maximum temperature from all ensemble members in the east (a) and west (b) sub-regions. Blue squares represent unweighted ensemble mean change, red circless represent weighted ensemble mean with Perkins skill score, and green triangles represent weighted ensemble mean with RMSE.

Table 4.5. Change in 30 year maximum temperature for the east sub-region based on unweighted ensemble mean, weighted mean utilizing Perkins skill scores (SS), and weighted mean utilizing RMSE for the entire nine-member NARCCAP ensemble. [5]

	NARCCAP 9-Member Ensemble – East						4-Member Select Ensemble – East			
	Unweighted Ensemble Mean Change (°C)	SS Weight Mean Change (°C)	RMSE Weight Mean Change (°C)	Ensemble Median Change (°C)	25th Percentile (°C)	75th Percentile (°C)	Ensemble Mean Change (°C)	Ensemble Median Change (°C)	25th Percentile (°C)	75th Percentile (°C)
Dec	1.84*1	1.80	1.80	1.83	1.41	2.22	2.04	2.08	1.68	2.39
Jan	1.65*1	1.64	1.64	1.60	1.40	1.91	1.64	1.53	1.37	1.91
Feb	1.32*1	1.38	1.42	1.45	1.19	1.72	1.50	1.34	1.16	1.56
Mar	1.65*1	1.73	1.73	1.47	1.29	1.93	1.56	1.43	1.28	1.85
Apr	2.04*1	2.12	2.10	1.94	1.65	2.33	2.29	2.18	1.81	2.67
May	2.66*1	2.76	2.74	2.47	2.02	3.09	1.98	1.95	1.63	2.29
Jun	2.75*1	2.82	2.80	2.80	2.07	3.51	2.49	2.68	1.93	2.96
Jul	3.10*1	3.13	3.12	3.14	2.36	3.86	2.89	2.83	2.26	3.46
Aug	2.74*1	2.74	2.71	2.80	2.09	3.32	2.65	2.67	1.96	3.23
Sep	2.29*1	2.36	2.38	2.21	1.84	2.77	2.54	2.63	1.99	2.99
Oct	1.74*1	1.74	1.74	1.71	1.53	1.89	1.69	1.64	1.51	1.83
Nov	2.38*1	2.36	2.35	2.30	2.00	2.67	2.40	2.27	2.00	2.54

[5] Ensemble median, 25th percentile, and 75th percentile change are also presented. Weighted mean numbers in red represent cases in which weighting results in higher mean change, blue represent cases in which weighting results in lower mean change and black are values which resulted in zero change. Superscripts for the unweighted ensemble mean change indicate change considered statistically significant at the α=0.1 (#), α=0.05 (@), and α=0.01 (*) levels for each individual ensemble member. The number following the superscript indicates the number of models from the NARCCAP ensemble considering change statistically significant at each α-level. The four-member select ensemble is comprised of models illustrated in Table 4.6. Red indicates cases were the select ensemble is warmer than the 9-member ensemble, blue is colder, and black unchanged.

Table 4.6. Models chosen, by month and GCM LBCs, for the four-member ensemble based on findings from the hierarchical cluster analysis and superiority in the four skill metrics for maximum temperature in the east sub-region.

	MM5I-CCSM	WRFG-CCSM	CRCM-CCSM	RCM3-GFDL	ECP2-GFDL	GFDL-Timeslice	WRFG-CGCM3	RCM3-CGCM3	CRCM-CGCM3
Dec	X				X	X	X		
Jan	X			X		X	X		
Feb	X			X		X	X		
Mar	X			X		X	X		
Apr	X				X	X	X		
May	X				X	X			X
Jun	X				X	X			X
Jul	X			X		X	X		
Aug		X		X		X	X		
Sep	X				X	X			X
Oct	X				X	X	X		
Nov	X				X	X	X		
Total	**11**	**1**	**0**	**5**	**7**	**12**	**9**	**0**	**3**

Table 4.7. Change in 30 year maximum temperature for the west sub-region based on unweighted ensemble mean, weighted mean utilizing Perkins skill scores (SS), and weighted mean utilizing RMSE for the entire nine-member NARCCAP ensemble. [6]

	NARCCAP 9-Member Ensemble – West						4-Member Select Ensemble – West			
	Unweighted Ensemble Mean Change (°C)	SS Weight Mean Change (°C)	RMSE Weight Mean Change (°C)	Ensemble Median Change (°C)	25th Percentile (°C)	75th Percentile (°C)	Ensemble Mean Change (°C)	Ensemble Median Change (°C)	25th Percentile (°C)	75th Percentile (°C)
Dec	1.78*1	1.75	1.73	1.77	1.40	2.16	1.67	1.77	1.50	1.91
Jan	1.58*1	1.59	1.59	1.52	1.31	1.80	1.44	1.41	1.26	1.64
Feb	1.32*1	1.38	1.43	1.40	1.17	1.64	1.59	1.33	1.22	1.71
Mar	1.69*1	1.78	1.79	1.61	1.41	1.97	1.63	1.52	1.40	1.92
Apr	2.08*1	2.14	2.14	1.95	1.77	2.19	2.13	2.04	1.91	2.25
May	2.89*1	2.92	2.92	2.48	2.26	3.56	2.33	2.33	2.20	2.45
Jun	3.25*1	3.26	3.24	3.23	2.64	3.97	2.85	2.90	2.40	3.28
Jul	3.54*1	3.58	3.58	3.55	2.78	4.31	4.20	4.28	3.81	4.64
Aug	2.91*1	2.85	2.84	3.09	2.31	3.47	2.82	2.62	2.14	3.50
Sep	2.42*1	2.47	2.47	2.34	2.03	2.80	2.63	2.67	2.10	3.14
Oct	1.85*1	1.86	1.86	1.79	1.56	2.16	1.88	1.81	1.64	2.11
Nov	2.37*1	2.35	2.31	2.35	1.78	2.85	2.41	2.27	1.75	2.83

[6] Ensemble median, 25th percentile, and 75th percentile change are also presented. Weighted mean numbers in red represent cases in which weighting results in higher mean change, blue represent cases in which weighting results in lower mean change and black are values which resulted in zero change. Superscripts for the unweighted ensemble mean change indicate change considered statistically significant at the α=0.1 (#), α=0.05 (@), and α=0.01 (*) levels for each individual ensemble member. The number following the superscript indicates the number of models from the NARCCAP ensemble considering change statistically significant at each α-level. The four-member select ensemble is comprised of models illustrated in Table 4.8. Red indicates cases were the select ensemble is warmer than the 9-member ensemble, blue is colder, and black unchanged.

Table 4.8. Models chosen, by month and GCM LBCs, for the four-member ensemble based on findings from the hierarchical cluster analysis and superiority in the four skill metrics for maximum temperature in the west sub-region.

	MM5I-CCSM	WRFG-CCSM	CRCM-CCSM	RCM3-GFDL	ECP2-GFDL	GFDL-Timeslice	WRFG-CGCM3	RCM3-CGCM3	CRCM-CGCM3
Dec	X			X		X	X		
Jan	X			X		X	X		
Feb	X			X		X	X		
Mar	X			X		X	X		
Apr			X		X	X	X		
May	X				X	X	X		
Jun	X				X	X			X
Jul		X		X		X		X	
Aug		X			X	X	X		
Sep		X			X	X			X
Oct	X				X	X	X		
Nov	X				X	X	X		
Total	**8**	**3**	**1**	**5**	**7**	**12**	**9**	**1**	**2**

The increase in mean change is attributed to the decreased weight of the two RCMs utilizing GFDL LBCs, specifically the ECP2-GFDL which consistently showed the least amount of change regardless of month (Figures G.13 through G.24). Additionally, the ECP2-GFDL is the only ensemble member to project a decrease in maximum temperature in any month, illustrating a 1°C decrease in March (Figure G.15). The WRFG-CCSM and CRCM-CCSM are the warmest models from January through July, while the CRCM-CGCM3 is the warmest model in August through October. The CRCM RCMs and WRFG-CCSM were among the most skillful models during these months, lending credence to a potentially warmer solution.

Tables 4.5 and 4.7 illustrate the ensemble mean, median, and IQ values for the selected ensemble comprised of one RCM per GCM with the addition of the GFDL-timeslice (with Tables 4.6 and 4.8 illustrating which model was used for each month). The east sub-region exhibits a warmer central tendency (compared to the larger ensemble) from the fall through mid-spring with cooler central tendency from late spring through summer. The west sub-region does not exhibit a consistent pattern of warmer/cooler than the larger ensemble. Interestingly, the July selected ensemble mean and median are 0.7°C warmer than the greater ensemble, while the greatest increase or decrease from the greater ensemble was not more than 0.4°C for any month in either sub-region.

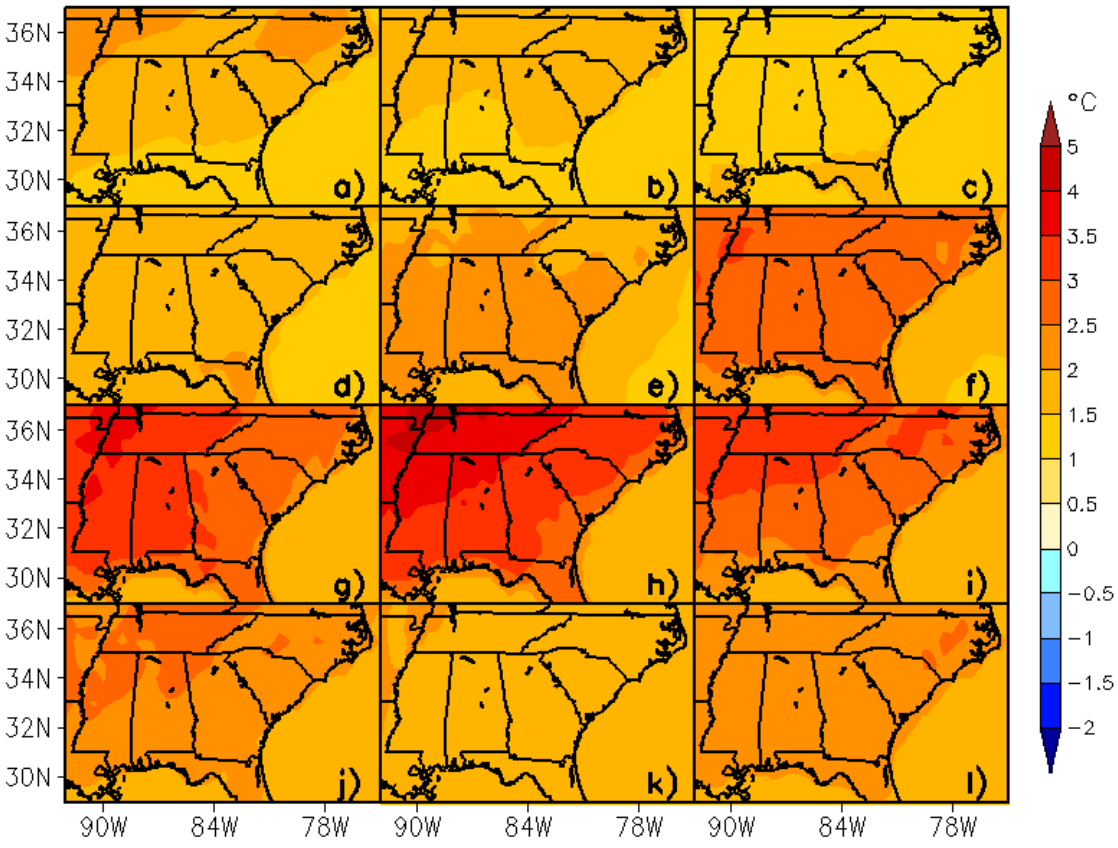

Figure 4.7. Weighted ensemble mean using Perkins skill scores for maximum temperature for December (a), January (b), February (c), March (d), April (e), May (f), June (g), July (h), August (i), September (j), October (k), and November (l).

The potential impacts from increased maximum temperature are similar to those outlined for minimum temperature with respect to crop growth and development and stream flow/water availability. Assuming all other atmospheric factors remain similar to the historical climate (including precipitation), increased maximum temperatures will result in an increased potential for stress and mortality in plants and livestock. Additionally, power demand will increase due to additional cooling requirements for homes and businesses.

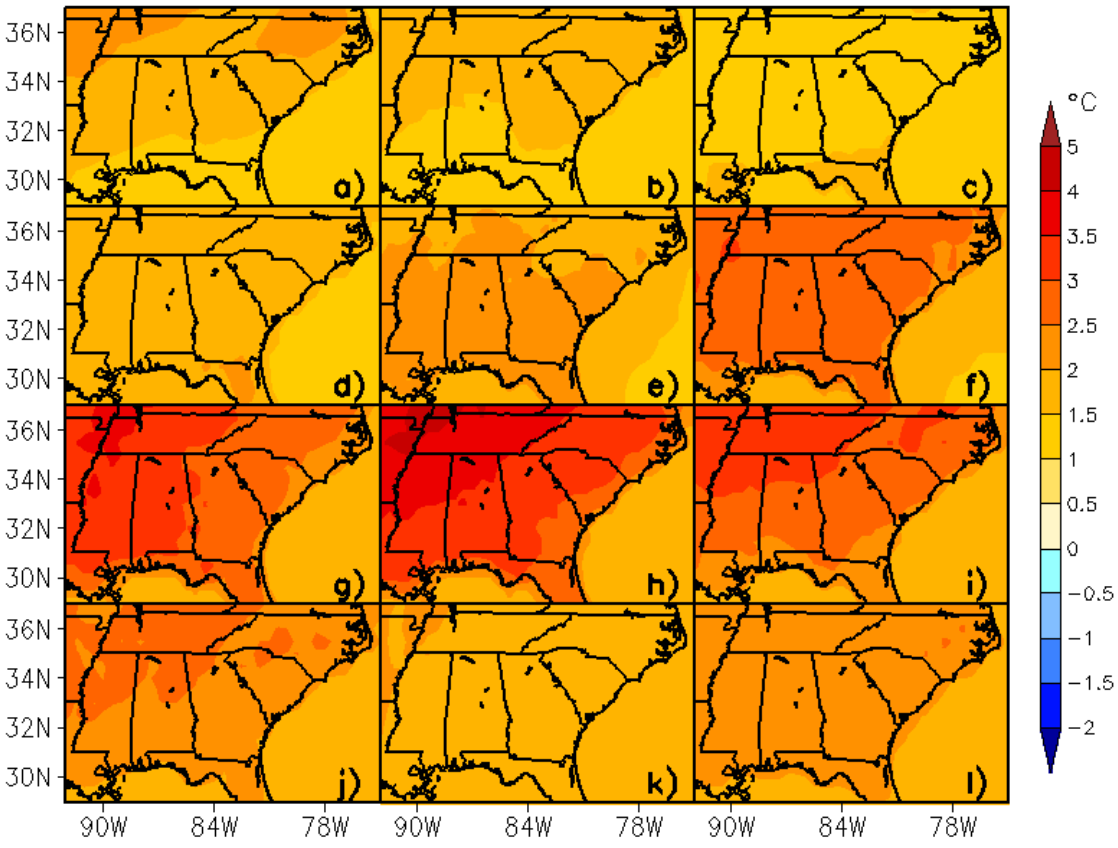

Figure 4.8. Weighted ensemble mean using RMSE for maximum temperature for December (a), January (b), February (c), March (d), April (e), May (f), June (g), July (h), August (i), September (j), October (k), and November (l).

4.3 MEAN PRECIPITATION

Changes in mean precipitation for the Southeast U.S. could create greater impacts to the region than changes in temperature, as all forms of industry and society depend on water supply. Unlike temperature, changes in precipitation are highly dependent on location within the Southeast U.S. rather than strictly at the sub-region level. The highest spatial variability with respect to the Southeast U.S. occurs from April through September when localized convective activity provides more precipitation than large/synoptic-scale-driven precipitation. Conversely, December through March, October, and November illustrate the least amount of spatial variability due to synoptic-scale driven precipitation, consisting of frequent cold frontal passage, which dominates over localized convection.

In the east sub-region, ensemble mean change is within ±10% of the historical reference period with nine months illustrating less than ±5% change (Figure 4.9 and 4.10; Tables 4.9 and 4.11). February exhibits the highest increase in ensemble mean (weighted and unweighted) change of 8.6% and IQ values of -0.83 and 18.38%, respectively. Conversely, May exhibits the highest decrease in ensemble unweighted and Perkins-based skill weighted change of -4.1% (and -4.6% for RMSE-based weight) with IQ values of -15.62 and 4.6%, respectively. The smallest inter-quartile range is observed in February at 14.9% while the highest inter-quartile range is observed in August at 26.2%.

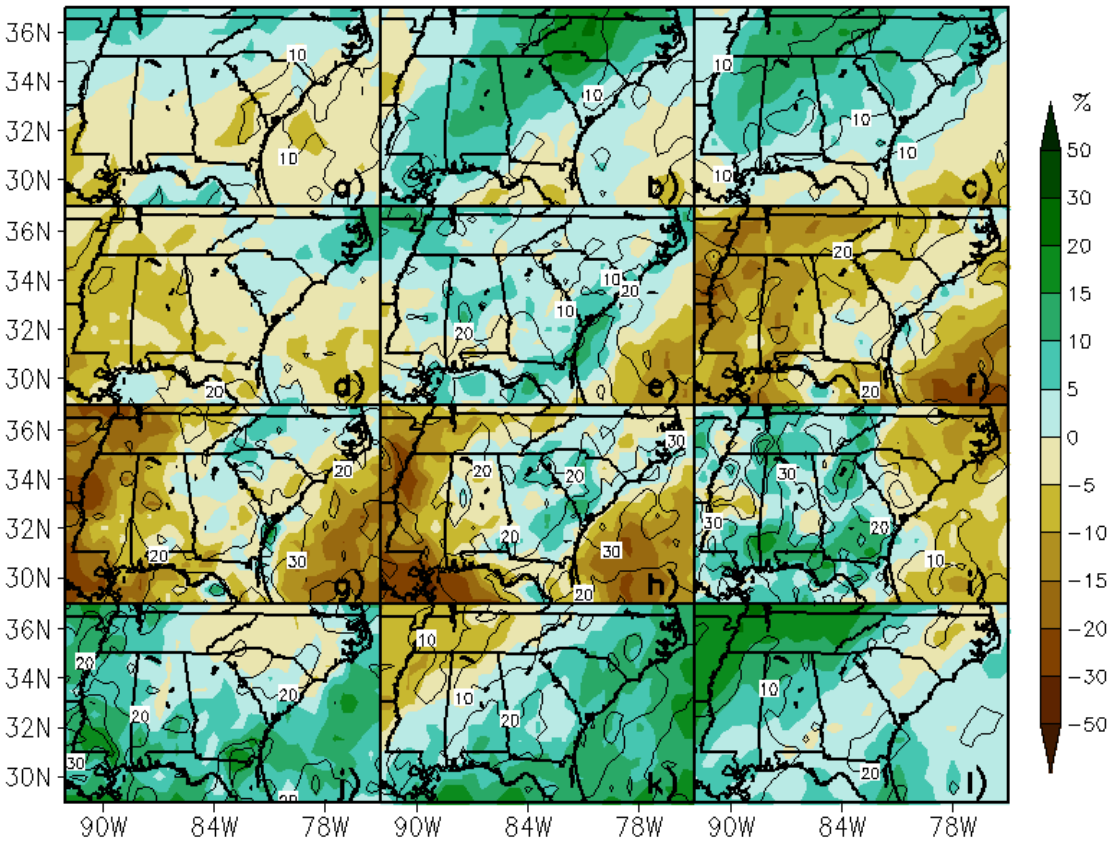

Figure 4.9. Ensemble mean change (shaded) and standard deviation (contoured) for mean precipitation for December (a), January (b), February (c), March (d), April (e), May (f), June (g), July (h), August (i), September (j), October (k), and November (l).

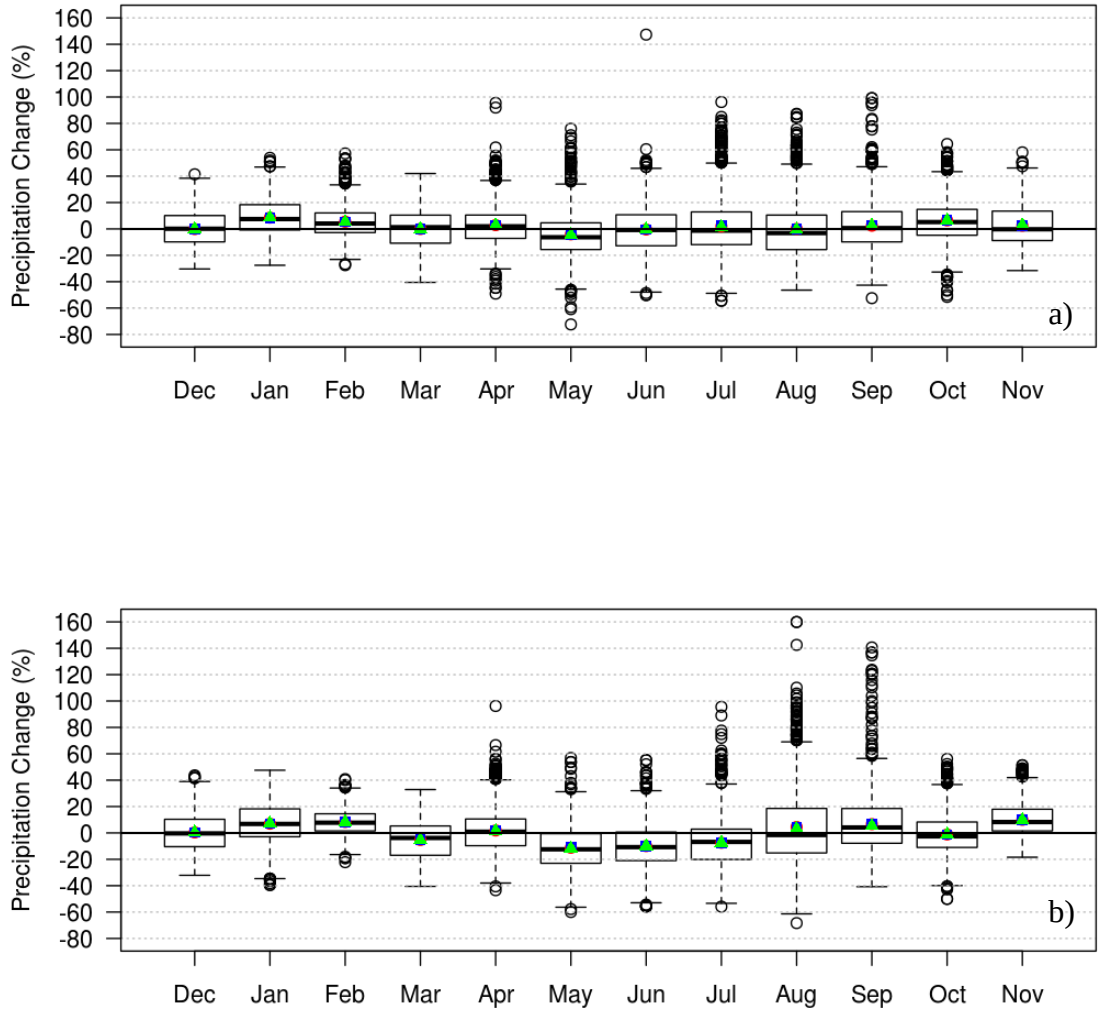

Figure 4.10. Box and whisker plots of change in mean precipitation from all ensemble members in the east (a) and west (b) sub-regions. Blue squares represent unweighted ensemble mean change, red circless represent weighted ensemble mean with Perkins skill score, and green triangles represent weighted ensemble mean with RMSE.

Table 4.9. Change in 30 year mean precipitation for the east sub-region based on unweighted ensemble mean, weighted mean utilizing Perkins skill scores (SS), and weighted mean utilizing RMSE for the entire nine-member NARCCAP ensemble. [7]

	NARCCAP 9-Member Ensemble – East						4-Member Select Ensemble – East			
	Unweighted Ensemble Mean Change	SS Weight Mean Change	RMSE Weight Mean Change	Ensemble Median Change	25th Percentile	75th Percentile	Ensemble Mean Change	Ensemble Median Change	25th Percentile	75th Percentile
	(%)	(%)	(%)	(%)	(%)	(%)	(%)	(%)	(%)	(%)
Dec	-0.11*3	-0.04	-0.05	0.14	-9.84	10.15	0.19	-0.48	-9.37	7.99
Jan	8.58*2	8.55	8.58	7.47	-0.83	18.38	7.63	6.25	-3.10	19.12
Feb	5.51*2	5.42	5.34	4.09	-2.76	12.11	0.94	-1.12	-6.31	7.90
Mar	-0.05*2	0.22	-0.22	1.30	-10.82	10.47	5.10	4.94	-0.74	10.82
Apr	2.88*1	2.88	2.80	1.97	-7.19	10.48	4.69	2.87	-6.11	11.00
May	-4.08*2	-4.05	-4.63	-6.30	-15.62	4.60	-3.67	-7.20	-17.16	4.08
Jun	-0.43*2	-0.50	-0.50	-0.81	-12.80	10.72	-0.31	-1.90	-11.23	8.94
Jul	1.96#1, *1	2.28	1.59	-1.29	-11.89	12.88	5.05	0.89	-9.45	14.55
Aug	0.02*2	0.08	-0.54	-2.17	-15.69	10.48	2.47	-1.49	-12.82	12.92
Sep	2.47*2	2.85	2.34	0.62	-9.86	13.13	11.93	8.90	-0.92	21.12
Oct	6.45*2	6.42	6.33	5.19	-4.79	14.84	6.71	5.28	-5.97	18.12
Nov	2.48*3	2.38	2.84	-0.24	-8.81	13.52	4.25	2.64	-6.00	13.99

[7] Ensemble median, 25th percentile, and 75th percentile change are also presented. Weighted mean numbers in red represent cases in which weighting results in higher mean change, blue represent cases in which weighting results in lower mean change and black are values which resulted in zero change. Superscripts for the unweighted ensemble mean change indicate change considered statistically significant at the α=0.1 (#), α=0.05 (@), and α=0.01 (*) levels for each individual ensemble member. The number following the superscript indicates the number of models from the NARCCAP ensemble considering change statistically significant at each α-level. The four-member select ensemble is comprised of models illustrated in Table 4.10. Brown indicates cases were the select ensemble is drier than the 9-member ensemble, green wetter, and black unchanged.

Table 4.10. Models chosen, by month and GCM LBCs, for the four-member ensemble based on findings from the hierarchical cluster analysis and superiority in the four skill metrics for mean precipitation in the east sub-region.

	MM5I-CCSM	WRFG-CCSM	CRCM-CCSM	RCM3-GFDL	ECP2-GFDL	GFDL-Timeslice	WRFG-CGCM3	RCM3-CGCM3	CRCM-CGCM3
Dec			X	X		X		X	
Jan	X			X		X			X
Feb	X			X		X			X
Mar	X			X		X			X
Apr	X			X		X			X
May	X			X		X			X
Jun	X				X	X			X
Jul	X				X	X		X	
Aug	X				X	X		X	
Sep	X				X	X			X
Oct	X				X	X	X		
Nov	X			X		X		X	
Total	**11**	**0**	**1**	**7**	**5**	**12**	**1**	**4**	**7**

Table 4.11. Change in 30 year mean precipitation for the west sub-region based on unweighted ensemble mean, weighted mean utilizing Perkins skill scores (SS), and weighted mean utilizing RMSE for the entire nine-member NARCCAP ensemble. [8]

	NARCCAP 9-Member Ensemble – West						4-Member Select Ensemble – West			
	Unweighted Ensemble Mean Change	SS Weight Mean Change	RMSE Weight Mean Change	Ensemble Median Change	25th Percentile	75th Percentile	Ensemble Mean Change	Ensemble Median Change	25th Percentile	75th Percentile
	(%)	(%)	(%)	(%)	(%)	(%)	(%)	(%)	(%)	(%)
Dec	0.38^{*1}	0.48	0.38	-0.36	-10.43	10.33	2.73	3.91	-8.90	14.17
Jan	6.98^{*2}	7.06	7.24	6.80	-2.90	18.25	6.95	5.60	-1.62	15.47
Feb	8.35^{*1}	8.34	8.31	7.77	1.50	14.52	6.15	6.23	0.71	11.78
Mar	-5.33^{*1}	-5.12	-5.27	-3.82	-16.94	5.28	0.44	0.92	-6.08	8.84
Apr	1.88^{*1}	2.13	1.53	0.94	-9.67	10.56	10.88	8.18	0.40	17.75
May	-11.22$^{@1, *1}$	-11.09	-11.72	-12.42	-23.04	-0.58	-9.40	-11.84	-19.15	-2.54
Jun	-9.95$^{\#1, *1}$	-10.05	-9.82	-10.78	-21.02	0.64	-11.08	-13.00	-21.14	-2.00
Jul	-7.42$^{\#1, *1}$	-7.43	-7.38	-6.82	-20.10	2.86	-7.44	-5.82	-19.03	3.20
Aug	4.51$^{@1, *1}$	4.35	3.05	-1.60	-15.19	18.56	9.60	3.67	-9.90	25.03
Sep	6.65^{*1}	6.42	5.24	4.13	-7.86	18.50	1.31	0.47	-9.12	13.59
Oct	-1.15^{*1}	-1.38	-1.14	-2.58	-11.02	8.29	-4.27	-4.43	-12.86	4.94
Nov	9.95$^{\#1, @1, *1}$	9.78	9.70	8.27	1.48	17.98	4.78	4.39	-0.45	9.83

[8] Ensemble median, 25th percentile, and 75th percentile change are also presented. Weighted mean numbers in red represent cases in which weighting results in higher mean change, blue represent cases in which weighting results in lower mean change and black are values which resulted in zero change. Superscripts for the unweighted ensemble mean change indicate change considered statistically significant at the α=0.1 (#), α=0.05 (@), and α=0.01 (*) levels for each individual ensemble member. The number following the superscript indicates the number of models from the NARCCAP ensemble considering change statistically significant at each α-level. The four-member select ensemble is comprised of models illustrated in Table 4.12. Brown indicates cases were the select ensemble is drier than the 9-member ensemble, green wetter, and black unchanged.

Table 4.12. Models chosen, by month and GCM LBCs, for the four-member ensemble based on findings from the hierarchical cluster analysis and superiority in the four skill metrics for mean precipitation in the west sub-region.

	MM5I-CCSM	WRFG-CCSM	CRCM-CCSM	RCM3-GFDL	ECP2-GFDL	GFDL-Timeslice	WRFG-CGCM3	RCM3-CGCM3	CRCM-CGCM3
Dec	X			X		X			X
Jan			X		X	X			X
Feb	X			X		X			X
Mar	X			X		X		X	
Apr	X			X		X			X
May	X				X	X			X
Jun	X				X	X			X
Jul	X				X	X		X	
Aug	X			X		X		X	
Sep	X			X		X		X	
Oct	X				X	X		X	
Nov	X			X		X		X	
Total	**11**	**0**	**1**	**7**	**5**	**12**	**0**	**6**	**6**

Spatially, the highest amount of variability in August is observed in the complex terrain regions covering northern Georgia, western North Carolina, and northwestern South Carolina with standard deviation values in the 20-30% range. The WRFG-CGCM3 and RCM3-CGCM3 exhibit increased August precipitation in these regions of 30-50% while the WRFG-CCSM dries the region by 20-50% (Figure G.32). Based on the three skill metrics, the RCM3-CGCM3 is the most skillful of the three models with the WRFG-CGCM3 the least skillful in August, indicating more weight is applied to the RCM3-CGCM3 solution illustrated in Figures 4.11 and 4.12.

Increases in mean precipitation change are noted for eight months of the year for unweighted ensemble change, seven months for Perkins skill score-based weights and ensemble median change, and six months for RMSE-based weighted mean change. Additionally, with the exception of December and March, all other months illustrate an ensemble median change less than any of the means (weighted and unweighted), indicating the ensemble distribution is right skewed. Spatially, eastern North Carolina illustrates the most consistent drying pattern from May through September while central and northern Georgia and all South Carolina illustrate slightly wetter conditions in January, February, April, July, and October. Of particular note, changes in precipitation over the Atlantic Ocean indicate drier conditions during most of the Atlantic hurricane season from June through August. Future work should explore the frequency of tropical activity in this region, first determining model skill in replicating historical tropical activity and then exploring changes in future tropical activity.

The west sub-region exhibits higher variability in projected mean change than the east sub-region with mean change (weighted and unweighted) falling within ±12% for all

months while only within ±5% for three months. November exhibits the wettest mean change between 9.7 and 10% while May exhibits the driest mean change between 11.1 and 11.7%, respectively. The smallest inter-quartile range occurs in February (13%), indicating relatively high model consensus, while the highest inter-quartile range occurs in August (33.8%), indicating a relatively large amount of model disagreement with respect to the magnitude and direction of projected change. Locations projecting the largest decreases in mean precipitation occur in Mississippi and most of Tennessee in March, May through July, and October between 10 and 30% (5 to 15% in Alabama) while showing strong increases in precipitation in March, September, and November between 10 and 20% (0 to 15% in Alabama).

Figures G.25 through G.36 exhibit individual model contributions to mean ensemble change by month. The WRFG-CGCM3, RCM3-CGCM3, ECP2-GFDL, and RCM3-GFDL illustrate consistently high increase in mean precipitation in the east sub-region while the RCM3-CGCM3 is the only ensemble member to consistently show high increases in the west sub-region across all months. All three RCMs driven with CCSM LBCs exhibit consistently high drying conditions in both sub-regions, most pronounced from April through September. Lastly, the two RCMs run with GFDL LBCs illustrate consistent drying in the west sub-region, contained to late spring through early fall, a direct contrast to their projections for the east sub-region during the same time period.

Tables 4.9 and 4.11 illustrate the selected ensemble mean, median, and IQ values for the three best performing RCMs from each GCM plus the GFDL-timeslice (with Tables 4.12 and 4.14 illustrating the models used by month). The east sub-region exhibits a wetter mean change than the greater ensemble in all months except for January and

February, when mean change is slightly drier than the full ensemble. The most significant increase in mean ensemble change is found in September (approximately 7% wetter) while the most significant decrease was observed in February (approximately 4.5% drier). The select ensemble mean exhibits wetter conditions for all months with the exception of May and June, however, May and June exhibit only slight decreases in mean precipitation of 3.7 and 0.3%, respectively. Additionally, the increase in mean precipitation during the summer and fall would be mostly timely as these months are typically the driest for this sub-region. In the west sub-region, only half of the months observed an increase in mean precipitation, mostly contained to the winter and spring, while the summer and fall observed a decrease in mean precipitation. Relatively substantial mean decreases in precipitation occur from May through July, which is a crucial time period for the growth and development of crops in this sub-region. Drier conditions during the most important points in development of such crops as corn have the potential to substantially reduce yield (assuming precipitation is the most limiting factor for yield), which impacts livestock producers and consumers through increased prices (assuming demand for the crop remains steady).

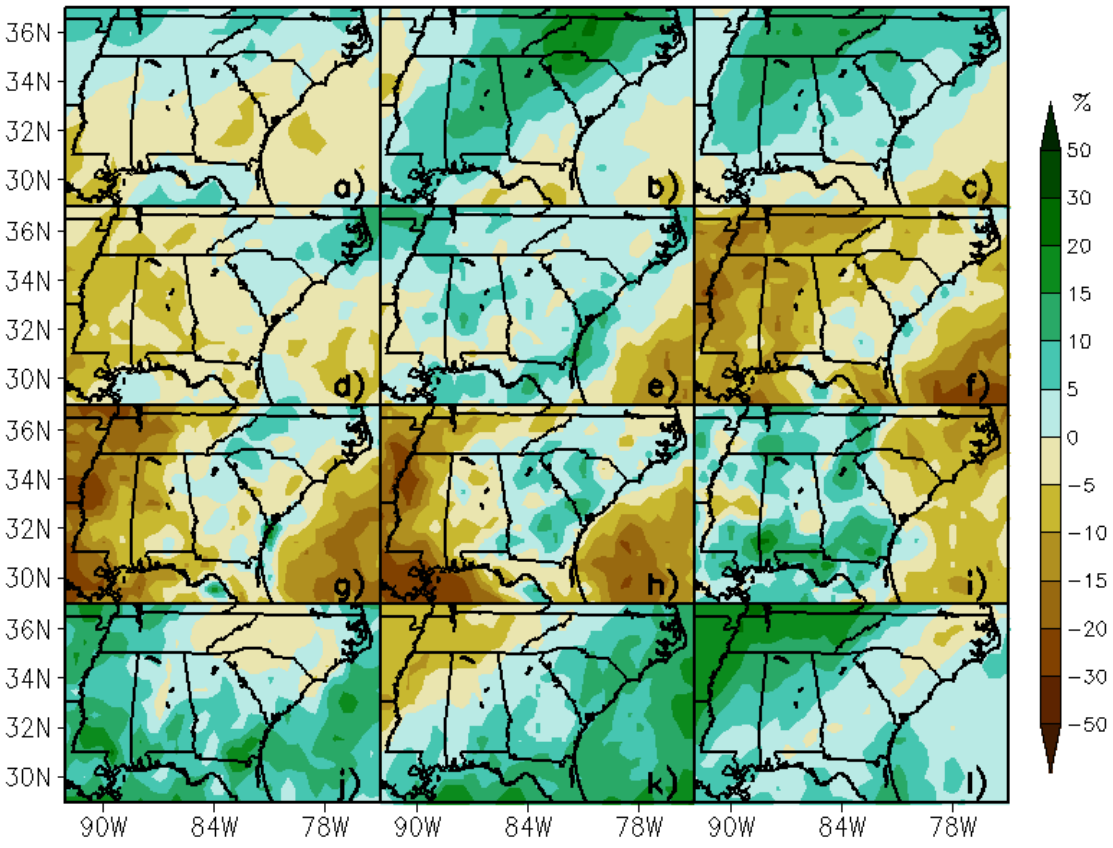

Figure 4.11. Weighted ensemble mean using Perkins skill scores for mean precipitation for December (a), January (b), February (c), March (d), April (e), May (f), June (g), July (h), August (i), September (j), October (k), and November (l).

For both sub-regions, wetter projections in mean precipitation generally occur in the winter and fall while drier projections occur in the spring and summer months. During the growing season (spring and summer), decreases in mean precipitation coupled with increased minimum and maximum temperature will increase the potential for additional water issues for agriculture by decreasing sub-soil moisture availability and decreasing water supplies used for irrigation. Due to the sandy soils typical of the east sub-region, decreased sub-soil moisture exacerbates the projected increase in temperature

and decrease in precipitation during the growing season. Although increased mean precipitation is projected for the fall and winter months which would allow water supplies the opportunity to recharge, physical properties of the soils (sandy and clay) in both sub-regions will be the limiting factor with respect to recharge of water supplies. Sandy and clay soils are among the most porous and their ability to "hold" moisture is much less than the soils of the Ohio and Mississippi River Valleys (Campbell and Norman, 1998), potentially prolonging water scarcity issues already observed in the Southeast U.S.

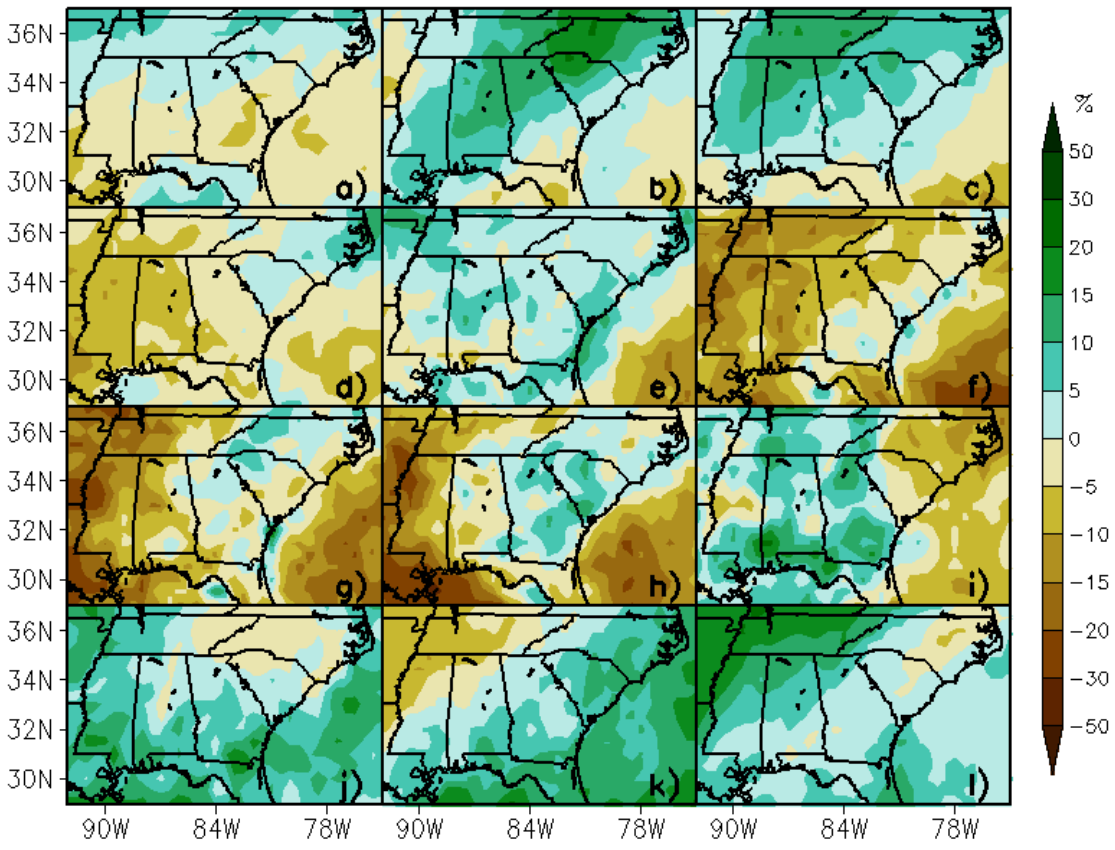

Figure 4.12. Weighted ensemble mean using RMSE for mean precipitation for December (a), January (b), February (c), March (d), April (e), May (f), June (g), July (h), August (i), September (j), October (k), and November (l).

CHAPTER 5

SUMMARY, KEY FINDINGS, SCIENTIFIC MERIT, AND FUTURE WORK

5.1 SUMMARY

Two general research questions structure the dissertation:

- How skillful are the NARCCAP ensemble members in simulating minimum and maximum temperature and mean precipitation in the reference period (1970-1999) for the Southeast United States? What are their biases? Does downscaling provide "value added" at local scales?
- What are future projections (2040-2069) of minimum and maximum temperature and mean precipitation change for the Southeast United States?

This dissertation used four statistically-based metrics to assess monthly temperature and precipitation output from nine NARCCAP ensemble members in the Southeast United States for the historical reference period. Most models demonstrated high skill for temperature during the historical period. The outlier models included two RCMs run with the Geophysical Fluids Dynamics Lab (GFDL) as their lateral boundary conditions; these models suffered from a cold maximum temperature bias, attributed to erroneously high soil moisture. Precipitation skill showed mixed skill – relatively high when measured using a probability density function overlap measure or the index of agreement, but relatively low when measured with root-mean square error or mean absolute error, because several models overestimate the frequency of extreme

precipitation events. Downscaling generally improves projections of minimum temperature and mean precipitation at local scales for RCMs run with the Community Climate Model (CCSM) and Candian Global Climate Model version 3 (CGCM3), while only adding value for CCSM-based runs with respect to maximum temperatures. Additionally, hierarchical cluster analysis and non-metric multipdimensional scaling provided recommendations into the maximum number models from the ensemble required to maintain model independence.

Projected minimum temperatures show an ensemble mean increase between 1° and 2°C in the winter and early spring, and an increase between 2° and 3°C for all other months. Maximum temperatures show an ensemble mean increase between 1° and 2°C in winter and early spring with increases between 2° and 4°C from mid spring through fall. Precipitation increases up to 10% in the eastern part of the region from late summer through early spring. Ensemble mean decreases of up to 10% occurred in January, April, June, and July. In western portions, precipitation increases up to 10% in January through March, May, August, September, and November with an up to 12% decrease in precipitation in March, May through July, and October.

5.2 KEY FINDINGS

The first key finding is that all models are relatively skillful (with respect to all four metrics) in reproducing daily minimum temperature trends for both sub-regions. The WRFG RCMs (run with CCSM and CGCM3 LBCs), the ECP2-GFDL, and GFDL-timeslice show degradation in skill during the summer months (June, July, and August) while the RCM3-GFDL and ECP2-GFDL exhibit slight degradation from December

through March. The most consistently skillful models across all months are the RCM3- and CRCM-CGCM3. Additionally, the WRFG RCMs and ECP2-GFDL exhibit a minimum temperature cold bias of 2-4°C across all percentiles during the summer while the GFDL-timeslice exhibits a warm bias between 2° and 4°C below the 50th percentile and 4° to 8°C above the 50th percentile. December through March cold bias between 4° and 10°C plagues the RCM3- and ECP2-GFDL models. Less overall skill is observed for all models with respect to maximum temperature. The worst performing models are the RCM3- and ECP2-GFDL with strong cold biases between 2° and 10°C for several months. Degradation in skill is caused by a cold bias exhibited in the GFDL GCM that is transmitted and enhanced thought the downscaling process. The most skillful model across all months is the MM5I-CCSM in both sub-regions.

With respect to mean precipitation (regardless of sub-region), is highly dependent on skill metric. With the Perkins' and Willmott's methodologies, the MM5I-CCSM is the most consistently skillful in all months, and the WRFG RCMs and CRCM-CCSM are the least skillful. By contrast, using RMSE suggests the CRCM RCMs are the most consistently skillful while the WRFG-CGCM3 and GFDL-timeslice are the least skillful. These differences demonstrate that complexity of assessing precipitation skill and the need to incorporate several skill metrics. Additionally, the WRFG RCMs overestimate either the frequency or magnitude of daily mean precipitation as they consistently exhibit wet bias of 15 to 30% (sometimes higher) above the 50th percentile. The CRCM RCMs illustrate a consistent dry bias between 10 and 40% for most percentiles and months, indicating they underestimate either the frequency or magnitude of daily mean precipitation.

The next major finding from this dissertation is Perkins' skill score, Willmott's index of agreement, RMSE, and MAE are strongly correlated relative to minimum and maximum temperature because the temperature values are constrained within the Gaussian distribution such that large outliers are rarely observed (as 99.5% of the data values are contained within three standard deviations of the mean). However, little correlation is found between RMSE and either Willmott's or Perkins' methods relative to mean precipitation. Large outliers from the mean are inherent in the gamma distribution (precipitation) and are enhanced in the calculation of RMSE and MAE because of its value-by-value comparison but not the other two metrics, which evaluate on value-by-value basis relative to the underlying data distribution. Willmott's and Perkins' methods exhibit marginal correlations of 0.58 and 0.65 for the east and west sub-regions, respectively. This finding indicates multiple statistical metrics should be used to assess rather than one, which is the common approach to model validation in climate research.

The third important finding from this work found the comparison of climatological variables at the micro-, meso-, and synoptic-scale revealed systematic biases for those models which exhibited less skill. The RCM3 RCM illustrates excessive soil moisture content, lower-than-observed 500-mb heights and latent heat flux, and low sensible heat flux from late fall through early spring. Additionally, the dry bias observed in the CRCM RCMs is attributed to excessively high sensible heat flux and low cloud cover, particularly during the summer. This finding implies that much work still needs to be done within climate models to better represent the surface and sub-surface processes and feedbacks which are vital to local climate and crutial for stakeholders utilizing

climate model data as input to other modelings studies (e.g., hydrological modeling, crop modeling, etc.).

The fourth important finding from this dissertation is the value added by individual ensemble members was highly dependent on skill metric and month. Overall for both minimum and maximum temperature, the RCMs driven by the CCSM GCM added the most value mainly because the CCSM illustrated a relative lack of skill from mid-spring through mid-fall. Conversely, models driven by the GFDL added the least value because these models tended to enhance bias inherent in the GFDL GCM. The lone exception is the high value added by the GFDL-timeslice with respect to maximum temperature, indicating using observed ocean temperatures aid in predicting maximum temperatures for the Southeast United States. This point is illustrated by the GFDL-timeslice and observations closely clustering in the hierarchical cluster analysis and non-metric multidimensional scaling cluster analysis. Value added for precipitation, like temperature, was highly dependent on skill metric. The WRFG- and RCM3-CGCM3 most consistently added value across all months with the MM5I-CCSM adding positive value at least nine months out of the year. The models adding the least value were the CRCM-CCSM and GFDL-timeslice. Hierarchical cluster and non-metric multidimensional scaling analysis for minimum and maximum temperature revealed models with similar LBCs tended to cluster together. The only exception was the GFDL-timeslice which did not trend with either the GFDL-driven RCMs or other RCM-GCM combinations. This indicates that to achieve model independence, the effective number of is equal to one RCM per GCM plus the GFDL-timeslice; a total of four models from the nine member ensemble. Model clustering with respect to mean precipitation is less clear

than for clusters for temperature, particularly in the east sub-region; however, the effective number of models for precipitation, like temperature, is one RCM per GCM plus the GFDL-timeslice.This finding highlights the utility of downscaling to obtain information at local scales of interest while providing stakeholders with guidance on how to choose climate models and climate model-based data for their assessments to obtain reasonable uncertainty bounds (with respect to future climate) while building confidence in the fidelity of their projections. Additionally, this finding illustrates the nature to which RCMs are unable to separate themselves from their driving GCMs.

With respect to future projections, findings from this work show minimum temperature warming by at least 1°C for all months. The highest minimum temperature increases in both sub-regions are shown in the summer (2-3°C, respectively) while the smallest increases occur in the winter (1-2°C, respectively). Maximum temperature increases the most in the summer in both sub-regions (2-3°C in the east and 3-4°C in the west, respectively). The smallest increase in maximum temperature is observed in the winter (1-2°C for both sub-regions, respectively). Overall, change in mean precipitation is within ±10% in the east sub-region and ±12% in the west sub-region. Late fall through early spring exhibit slight increases in mean precipitation for both sub-regions while late spring through early fall exhibit no change to as much as a 12% decrease. Changes in precipitation are highly dependent on a location as not all locations within each sub-region exhibit the same magnitude or directional change observed for their respective sub-region. Weighting the ensemble mean (regardless of metric) had little impact on mean temperature change, with the weighted mean always within ±0.1°C of the weighted mean. Additionally, weighted mean precipitation was always within ±1% of the

unweighted ensemble mean. These findings indicate the Southeast U.S., as a whole, will experience generally warmer and drier conditions from late spring through early fall by the 2040-2069 timeframe, placing potentially serious strain on the hydrologic and agricultural realms of the region. Although slight increases in precipitation are projected for late fall through early spring and projected temperatures are anticipated to increase less compared to late spring through early fall, it may not be enough to off-set warm season water losses, causing decision makers to heavily factor these findings into their risk assessments and adaptation proposals.

The last finding from this work showed that through utilization of the recommendations on the effective number of models, a smaller selective ensemble was created with the most skillful RCM from each GCM plus the GFDL-timeslice for each month. The new, smaller ensemble exhibited a slightly warmer mean in all months with respect to projected minimum temperature change. Maximum temperature change exhibited a slightly warmer mean in the winter, spring and fall while ensemble mean change decreased in the summer. Mean precipitation change in the east sub-region is wetter than the larger ensemble with only two months exhibiting a decrease in mean precipitation. The west sub-region saw enhanced drying in May through July and October with a wetter mean in January, April, and August. This finding illustrates the implications of climate model choice when constructing an ensemble to provide wide-ranging and realistic uncertainty bounds and central tendency of future climate projections. Selection of more than one RCM for each lateral boundary condition will bias ensemble-based projections toward an artificial result.

5.3 SCIENTIFIC MERIT AND RELEVANCE

The Intergovernmental Panel on Climate Change's 2007 report (AR4) calls for reliable estimates of the impacts to be expected under projected climate change and to gain trust and improve decisions, build awareness, and increase dialog necessary between stakeholders with knowledge to share (such as researchers) and with the wider public. Additionally, Cutter et al. (2012) and Seneviratne et al. (2012) highlight assessment of climate model skill as a barrier in confidently using model projections for managing risks associated with climate extremes. The findings from this work answer the call from the IPCC reports for the Southeast U.S. by not only providing reliable estimates of future climate change but also heavily assessing multiple variables from several dynamically downscaled climate models to enhance trust and confidence in their findings. Data from the assessed NARCCAP models are currently being used or will be used as input to hydrologic and crop models. This dissertation provides these users with an assessment of each models' fidelity while providing specific shortcomings. This work serves as a template for the type of analysis that needs to be conducted for users of single or ensemble climate models to provide confidence in the data being used to conduct assessments of future climate.

Biases related to small-scale phenomenon such as the surface energy and water budgets are shown to feedback into the climate system in a negative way, impacting regional hindcasts of temperature and precipitation. The parameterization of land-atmosphere processes such as latent and sensible heat flux must be further developed to close loopholes in this important process. Additionally, cloud physics must continue to be addressed as current parameterizations continue to lack in the representation of this

complex process which has major implications on the energy budget and precipitation. Lastly, large biases in soil moisture (low and high) illustrate the need for further modification and better representation of sub-surface processes.

5.4 FUTURE WORK

- At the time of performing the analysis for this dissertation, only nine NARCCAP members were available. Future work should incorporate other NARCCAP members, as they become available, to assess model skill and provide projections of future climate change.
- Model skill focused on two sub-regions within the Southeast U.S. Future work should determine skill at individual grid locations. It is hypothesized that locations within the complex terrain of the Appalachian Mountains and along the Atlantic and Gulf Coasts will observe the greatest degradation in skill while other locations should prove relatively skillful. Additionally, it is hypothesized that temperature skill by grid point will be higher than precipitation, as the chaotic and prescribed nature of precipitation within the models lends itself to higher spatial variability than temperature.
- To determine locations in which downscaling adds value, one should assess the spatial extent to which skill is added. It is hypothesized that locations within the Appalachian Mountains and along the Atlantic and Gulf Coasts will exhibit more value added for temperature than other locations. Precipitation may also exhibit more value added in the complex environments, however, the chaotic nature of precipitation makes a firm hypothesis weak at best. This future work will go beyond Di Luca et al. (2012a; 2012b) who used 300 km by 300 km grid blocks to calculate

value added. Future work will calculate value added at the native 50 km resolution of the RCMs.

- Utilize differenet metrics to analyze modeled precipitation skill and future change such as the number of rain days and return intervals. As Trenberth et al. (2003) point out, as climate continues to change, the most probable changes in precipitation will mostly likely be in the intensity, frequency, and duration of precipitation events rather than mean precipitation.
- Assess NARCCAP members' ability to model the frequency of tropical cyclone activity for a historical reference period and explore changes in future tropical activity. Information from this assessment will be useful is coastal hazard and adaptation analysis.
- Determine the role of the El Niño-Southern Oscillation (ENSO) within each of the NARCCAP models with particular emphasis on determining if the timeslice experiments (run with observed sea-surface conditions) are able to properly replicate this important process.

REFERENCES

Adger, W. N., S. Dessai, M. Goulden, M. Hulme, I. Lorenzoni, D. R. Nelson, L. O. Naess, J. Wolfe, and A. Wreford, 2009: Are there social limits to adaptation to climate change? *Clim. Change*, 93, 335-354, doi: 10.1007/s10584-008-9520-z.

Agarwal, S. J. Wills, L. Cayton, G. Lanckriet, D. Kriegman, and S. Belongie, 2009: Generalized non-metric multi-dimensional scaling. In: Proceedings of the Twelfth International Conference on Artificial Intelligence and Statistics, Clearwater Beach, FL, 16-18 April 2009.

Beersma, J. L. and T. Adri Buishand, 1999: A simple test for equality of variances in monthly climate data. *J. Climate*, 12, 1770-1779.

Brankovic, C. and T. N. Palmer, 1997: Atmospheric seasonal predictability and estimates of ensemble site. *Mon. Weather Rev.*, 125, 859-874.

Boberg, F., P. Berg, P. Thejill, W. J. Gutowski, and J. H. Christensen, 2010: Improved confidence in climate change projections of precipitation further evaluated using daily statistics from ENSEMBLES models. *Clim. Dyn.*, 35, 1509-1520, doi: 10.1007/s00382-009-0683-8.

Brooks, N., W. N. Adger, and P. M. Kelly, 2005: The determinants of vulnerability and adaptive capacity at the national level and the implications for adaptation. *Global Environ. Chang.*, 15(2), 151-163.

Bukovsky, M. S., 2011: *Masks for the Bukovsky regionalization of North America*, Regional Integrated Sciences Collective, Intitute for Mathematics Applied to Geosciences, National Center for Atmospheric Research, Boulder, CO, http://www.narccap.ucar.edu/contrib/bukovsky/.

Campbell, G. S. and J. M. Norman, 1996: *An Introduction to Environmental Biophysics*. Second ed. New York: Springer-Verlag.

Castro, C. L., R. A. Pielke Sr., and G. Leoncini, 2005: Dynamical downscaling: Assessment of value retained and added using the Regional Atmospheric Modeling System (RAMS). *J. Geophys. Res.*, 110, D05108, doi: 10.1029/2004/JD004721.

Caya, D. and R. Laprise, 1999: A semi-implicit semi-Lagrangian regional climate model: the Canadian RCM. *Mon. Wea. Rev.*, 127(3), 341-362.

Christensen, J. H, and O. B. Christensen, 2007: A summary of the PRUDENCE model projections of changes in the European climate by the end of this century. *Clim. Change*, 81, 7-30, doi: 10.1007/s10584-006-9210-7.

Christensen, J. H., E. Kjellstrom, F. Giorgi, G. Lenderink, M. Rummukainen, 2010: Weight assignment in regional climate models. *Clim. Res.*, 44, 179-194, doi: 10.3354/cr00916.

Collins, W. D. et al., 2006: The Community Climate System Model: CCSM3. *J. Climate*, 19, 2122-2143.

Cutter, S., B. Osman-Elasha, J. Campbell, S.-M. Cheong, S. McCormick, R. Pulwarty, and G. Ziervogel, 2012: Managing the risks from climate extremes at the local level. In: *Managing the Risks of Extreme Events and Distasters to Advance Climate Change Adaptation* [Field, C. B., V. Barros, T. F. Stocker, D. Qin, D. J. Dokken, K. L. Ebi, M. D. Mastrandrea, K. J. Mach, G.-K. Plattner, S. K. Allen, M. Tignor, and P. M. Midgley (eds.)]. A Special Report of Working Groups I and II of the Intergovernmental Panel on Climate Change (IPCC). Cambridge, U.K. and New York, NY: Cambridge University Press, pp. 291-338.

Cygwin, 2012: Cygwin Users Guide. retrieved from http://cygwin.com/cygwin-ug-net/cygwin-ug-net.pdf.

Dai, A., 2001: Global precipitation and thunderstorm frequencies. Part I: Seasonal and interannual variations. *J. Climate*, 14, 1092-1111.

Deque, M., D. P. Rowell, D. Luthi, F. Giorgi, J. H. Christensen, B. Rockel, D. Jacob, E. Kjellstrom, M. de Castro, and B. van den Hurk, 2007: An Intercomparison of regional climate simulations for Europe: Assessing uncertainties in model projections. *Clim. Change*, 81, 53-70, doi: 10.1007/s10584-006-9228-x.

Di Luca, A., R. de Elia, and R. Laprise, 2012a: Potential for added value in temperature simulated by high-resolution nested RCMs in present climate and in the climate change signal. *Clim. Dyn.*, pp. 22, doi: 10.1007/s00382-012-1384-2.

Di Luca, A., R. de Elia, and R. Laprise, 2012b: Potential for small scale added value of RCMs downscaled climate change. *Clim. Dyn.*, pp. 18, doi: 10.1007/s00382-012-1415-z.

Doty, B. and J. L. Kinter III, 1992: The Grid Analysis and Display System (GrADS): A practical tool for earth science visualization. *Eigth International Conference on Interactive Information and Procession Systems*, Atlanta, GA, 5-10 January 1992.

Doty, B. and J. L. Kinter III, 1993: The Grid Analysis and Display System (GrADS) and update. *Ninth International Conference on Interactive Information and Processing Systems*, Anaheim, CA, 17-22 January 1993.

Easterling, W. E., A. Weiss, C. J. Hays, and L. O. Mearns, 1998: Spatial scales of climate information for simulating wheat and maize productivity: the case of the US Great Plains. *Ag. For. Met.*, 90, 51-63.

Eum, H.-L., P. Gachon, R. Laprise, and T. Ouarda, 2012: Evaluation of regional climate model simulations versus gridded observed and regional reanalysis products using a combined weighted scheme. *Clim. Dyn.*, 38(7-8), 1433-1457, doi: 10.1007/s00382-011-1149-3.

Feser, F., B. Rockel, H. von Storch, J. Winterfeldt, and M. Zahn, 2011: Regional climate models add value to global model data. *Bull. Am. Meteorol. Soc.*, 9, 1181-1192.

Flato, G. M., 2005: The third generation coupled global climate model (CGCM3). retrieved from http://www.cccma.bc.ec.gc.ca/models/cgcm3.shtml.

Gangopadhyay, S., M. Clark, B. Rajagopalan, 2005: Statistical downscaling using K-nearest neighbors. *Water Resour. Res.*, 41, W02024, doi: 10.1029/2004WR003444.

Gao, Y., J. A. Vano, C. Zhu, and D. P. Lettenmaier, 2011: Evaluating climate change over the Colorado River basin using regional climate models. *J. Geophys. Res.*, doi: 10.1029/2010JD015278, in press., 5 Apr 2011.

Gao, Y, Y. Xue, W. Peng, H.-S. Kang, and D. Waliser, 2011: Assessment of dynamic downscaling of the extreme rainfall over East Asia using a regional climate model. *Adv. Atmos. Sci.*, 28 (5), 1077-1098, doi: 10.1007/s00376-010-0039-7.

Gates, D. M., 1980: *Biophysical Ecology*, 1st Edition, NewYork: Springer-Verlag.

Gavrilles, B., 2010: Southeastern U.S., with exception of Florida, likely to have serious water scarcity issues. *Science Daily*. December 13, 2010, http://www.sciencedaily.com/releases/2010/12/101213184436.htm.

GFDL GAMDT (The GFDL Global Model Development Team), 2004: The new GFDL global atmospheric and land model AM2-LM2: Evaluation with prescribed SST simulations. *J. Climate*, 17, 4641-4673.

Giorgi, F., M. Marinucci, and G. Bates, 1993: Development of a second generation regional climate model (regcm2) I: Boundary layer and radiative transfer processes. *Mon. Wea. Rev.*, 121, 2794-2813.

Giorgi, F., L. O. Mearns, C. Shields, and L. Mayer, 1996: A regional model study of the importance of local versus remote controls of the 1988 drought and the 1993 flood over the Central United States. *J. Climate*, 9 (5), 1150-1162.

Giorgi, F., 2006: Regional climate modeling: Status and perspectives. *J. Phys. IV France*, 139, 101-118, doi: 10.1051/jp4:2006139008.

Gordon, C., C. Cooper, C. Senior, H. Banks, J. Gregory, T. Johns, J. Mitchell, and R. Wood, 2000: The simulation of SST, sea ice extents and ocean heat transports in a version of the Hadley Centre coupled model without flux adjustments. *Clim. Dyn.*, 16, 147-168.

Grell, J.D. and D. R. Stauffer, 1993: A description of the fifth-generation Penn State/NCAR mesoscale model (MM5). National Center for Atmospheric Research, ncar/tn-398 1 ia edn.

Hambly, D., J. Audrey, B. Mills, and C. Fletcher, 2012: Projected implications of climate change for road safety in Greater Vancouver, Canada. *Clim. Change*, doi: 10.1007/s10584-012-0499-0, in press, 23 May 2012.

Hamill, T. M., 1999: Hypothesis test for evaluating numerical precipitation forecasts. *Wea. Forecasting*, 14, 155-167.

Hewitt, C. D. and D. J. Griggs, 2004: Ensembles-based predictions of climate changes and their impacts. *EOS Trans. AGU*, 85, pg 566.

Hewitson, B. C. and R. G. Crane, 1996: Climate downscaling: Techniques and application. *Clim. Res.*, 7, 85-95.

Hovmoller, E. A., 1949: The trough-and-ridge diagram. *Tellus*, 1(2), 62-66.

Huffman, G. J., 1997: Estimates of root-mean-square random error for finite samples of estimated precipitation. *J. Appl. Meteorol.*, 36, 1191-1201.

Huntingford, C., R. G. Jones, C. Prudhomme, R. Lamb, J. H. Gash, and D. A. Jones, 2003: Regional climate-model predictions of extreme rainfall for a changing climate. *Q. J. R. Meteorol. Soc.*, 129, 1607-1621, doi: 10.1256/gj.02.97.

Ihaka, R. and R. Gentleman, 1996: R: A language for data analysis. *J. Comput. Graph. Stat.*, 5(3), 299-314.

IPCC, 2001: IPCC Special Report on Emissions Scenarios. http://www.grida.no/publications/other/ipcc_sr/?src=/climate/ipcc/emission/094.htm, visited 11/9/2010.

IPCC, 2007: *Climate Change 2007: The Physical Basis.* (Solomon et al. (eds)), Cambridge: Cambridge University Press.

Jacob, D., L. Barring, O. B. Christensen, J. H. Christensen, M. de Castro, M. Deque, F. Giorgi, S. Hagemann, M. Hirschi, R. Jones, E. Kjellstrom, G. Lenderink, B. Rockel, E. Sanchez, C. Schar, S. I. Seneviratne, S. Somot, A. van Ulden, and B. van den Hurk, 2007: An inter-comparison of regional climate models for Europe: Model performance in present-day climate. *Clim. Change*, 81, 31-52, doi: 10.1007/s10584-006-9213-4.

Jha, M., Z. Pan, E. S. Takle, and R. Gu, 2004: Impacts of climate change on streamflow in the Upper Mississippi River Basin: A regional climate model perspective. *J. Geophys. Res.*, 109, D09105, doi: 10.1029/2003JD003686.

John, V. O. and B. J. Soden, 2007: Temperature and humidity biases in global climate models and their impact on climate feedbacks. *Geophys. Res. Lett.*, 34, doi: 10.1029/2007GL030429.

Johns, T. C., J.-F. Royer, I. Hoschel, H. Huebener, E. Roeckner, E. Manzini, W. May, J.-L. Dufresne, O. H. Ottera, D. P. van Vuuren, D. Salas y Melia, M. A. Giorgetta, S. Denvil, S. Yang, P. G. Fogli, J. Korper, J. F. Tjiputra, E. Stehfest, and C. D. Hewitt, 2011: Climate change under aggressive mitigation: the ENSEMBLES multi-model experiment. *Clim. Dyn.*, 37, 1975-2003, doi: 10.1007/s00382-011-1005-5.

Johnson, A., X. Wang, F. Fong, and M. Xue, 2011a: Hierarchical cluster analysis of a convection-allowing ensemble during the Hazardous Weather Testbed 2009 Spring Experiment. Part I: Development of the object-oriented cluster analysis method for precipitation fields. *Mon. Wea. Rev.*, 139(12), 3673-3693, doi: 10.1175/MWR-D-11-00015.1.

Johnson, A., X. Wang, M. Xue, and F. Kong, 2011b: Hierarchical cluster analysis of a convection-allowing ensemble during the Hazardous Weather Testbed 2009 Spring Experiment. Part II: Ensemble clustering over the whole experiment period. *Mon. Wea. Rev.*, 139(12), 3694-3710, doi: 10.1175/MWR-D-11-00016.1.

Juang, H. M. H., S. Y. Hong, and M. Kanamitsu, 1997: The NCEP regional spectral model: an update. *Bull. Am. Meteorol. Soc.*, 78, 2125-2143.

Jupp, T. E., P. M. Cox, A. Ramming, K. Thonicke, W. Lucht, and W. Cramer, 2010: Development of probability density functions for future South America rainfall. *New Phytol.*, 187, 682-693, doi: 10.1111/j.1469-8137.2010.03368.x.

Kabela, E. D., 2006: Dew duration and amount on corn leaves as determined from measurements during SMEX05 and simulation using the ALEX model. MS thesis Iowa State University, 54 pp.

Kanamitsu, M., W. Ebisuzaki, J. Woollen, S.-K. Yang, J. J. Hnilo, M. Fiorino, and G. L. Potter, 2002: NCEP-DOE AMIP-II Reanalysis (R-2), *Bull. Am. Meteorol. Soc.*, November, 1631-1643.

Kidson, J. W. and C. S. Thompson, 1998. A comparison of statistical and model-based downscaling techniques for estimating local climate variations. *J. Climate*, 11, 735-753.

Kjellstrom, E., F. Boberg, M. Castro, J. H. Christensen, G. Nikulin, and E. Sanchez, 2010: Daily and monthly temperature and precipitation statistics as performance indicators for regional climate models. *Clim. Res.*, 44, 135-150, doi: 10.3354/cr00932.

Knutti, R. G., 2008: Should we believe model predictions of future climate change? *Philos. Trans. R. Soc. A.*, 366 (1885), 4647-4664.

Knutti, R., G. Abromowitz, M. Collins, V. Eyring, P. J. Gleckler, B. Hewitson, and L. Mearns, 2010: Good practice guidance paper on assessing and combining multi model climate projections. In: *Meeting Report of the Intergovernmental Panel on Climate Change Expert Meeting on Assessing and Combining Multi Model Climate Projections* [Stocker, T. F., D. Quin, G-K. Plattner, M. Tignor, and P. M. Midgley (eds.)]. IPCC Working Group I Technical Support Unit, University of Bern, Bern, Switzerland.

Koo, G-S., K-O. Boo, and W-T. Kwon, 2009: Projections of temperature over Korea using an MM5 regional climate simulation. *Clim. Res.*, 40, 241-248, doi: 10.3354/cr00825.

Koster, R. D., M. J. Suarez, R. W. Higgins, and H. van den Dool, 2003: Observational evidence that soil moisture variations affect precipitation. *Geophys. Res. Lett.*, 30, 1241, doi: 10.1029/2002GL016571.

Kramer, N., A.-L. Boulesteix, and G. Tutz, 2008: Penalized partial least squares with applications to B-spline transformations and functional data. *Chemometr. Intell. Lab.*, 94 (1), 60-69, doi: 10.1016/j.chemolab.2008.06.009.

Kruijt, B., J-P. M. Witte, C. M. J. Jacobs, and T. Kroon, 2008: Effects of rising atmospheric CO2 on evapotranspiration and soil moisture: A practical approach for the Netherlands. *J. Hydrol.*, 349, 257-267.

Kruskal, J. B., 1964: Nonmetric multidimensional scaling: A numerical method. *Psychometrika*, 29 (2), 115-129, doi: 10.1007/BF02289694.

Lawrence, P. J. and T. N. Chase, 2012: Investigating the climate impacts of global land cover change in the Community Climate System Model (CCSM 3.0). *Int. J. Climatol.*, in press, 30 pp.

Legates, D. R. and G. J. McCabe Jr., 1999: Evaluating the use of "goodness-of-fit" measures in hydrologic and hydroclimatic model validation. *Water Resour. Res.*, 35(1), 233-241.

Leung, L., J. Done, J. Dudhia, T. Henderson, M. Vertenstein, and B. Kuo, 2005: Preliminary results of WRF for regional climate simulations. In: Workshop research needs and directions of regional climate modeling using WRF and CCSM, Boulder, CO, 6, pp 833-854. Available from http://www.cs.berkeley.edu/~luca/cs278/notes/lecture09.pdf.

Lim, Y.-K., D. W. Shin, S. Cocke, T. E. LaRow, J. T. Schoof, J. J. O'Brien, and E. P. Cassignet, 2007: Dynamically and statistically downscaled seasonal simulations of maximum surface air temperature over the southeastern United States. *J. Geophys. Res.*, 112, D24102, doi: 10.1029/2007JD008764.

Liu, M., Y.-J. Kim, and Q. Zhao, 2012: Numerical experiments of an advanced radiative transfer model in the U.S. navy operational global atmospheric prediction system. *J. Appl. Meteorol. Clim.*, 51, 554-570, doi: 10.1175/JAMC-D-11-018.1.

Livezey, R. E. and W. Y. Chen, 1983: Statistical field significance and its determination by Monte Carlo techniques. *Mon. Wea. Rev.*, 109, 120-126.

Ma, H.-Y., C. R. Mechoso, Y. Xue, H. Xaio, C.-M. Wu, J.-L. Li, and F. De Sales, 2011: Impact of land surface processes on the South American warm season climate. *Clim. Dyn.* 37, 187-203, doi: 10.1007/s00382-010-0813-3.

Masson, D. and R. Knutti, 2011: Climate model genealogy. *Geophys. Res. Lett.*, 38, L08703, doi: 10.1029/2011GL046864.

Maurer, E. P., B. Nijssen, and D. P. Lattenmaier, 2000: Use of the reanalysis land surface water budget variables in hydrolic studies. *GEWEX News*, 10(4), 6-8.

Maurer, E. P., A. W. Wood, J. C. Adam, D. P. Lattenmaier, and B. Nijssen, 2002: A long-term hydrologically-based dataset of land surface fluxes and states for the conterminous United States. *J. Climate*, 15, 3237-3251.

Maurer, E. P., G. M. O'Donnell, D. P. Lettenmaier, and J. O. Roads, 2001: Evaluation of the land surface water budget in NCEP/NCAR and NCEP/DOE reanalyses using an off-line hydrologic model. *J. Geophys. Res.*, 106 (D16), 17 841-17 862.

Maurer, E. P., L. Brekke, T. Pruitt, and P. B. Duffy, 2007: Fine-resolution climate projections enhance regional climate change impact studies, *EOS Trans. AGU*, 88 (47), 504.

Maxino, C. C., B. J. McAvaney, A. J. Pitman, and S. E. Perkins, 2008: Ranking the AR4 climate models over the Murray-Darling Basin using simulated maximum temperature, minimum temperature and precipitation. *Int. J. Climatol.*, 28, 1097-1112, doi: 10.1002/joc.1612.

McGinnis, S., L. Mearns, and L. McDaniel, 2010: Effects of spatial interpolation algorithm choice on regional climate model analysis. Fall Meeting, American Geophysical Union, San Francisco, 13-17 Dec. 2010.

Mearns, L. O., W. Gutowski, R. Jones, R. Leung, S. McGuinnis, A. Nunes, and Y. Qian, 2009: A regional climate change assessment program for North America, *EOS Trans. AGU*, 90(36), 311-312.

Mesinger, F., G. DiMego, E. Kalnay, K. Mitchell, P. C. Shafran, W. Ebisuzaki, D. Jovic, J. Woollen, E. Rogers, E. H. Berbery, M. B. Ek, Y. Fan, R. Grumbine, W. Higgins, H. Li, Y. Lin, G. Manikin, D. Parrish, and W. Shi, 2006: North American regional reanalysis. *Bull. Am. Meteorol. Soc.*, 3, 343-360, doi: 10.1175/BAMS-87-3-343.

Mielke, P. W. and K. J. Berry, 2001: *Permutation Methods: A Distance Function Approach*. New York: Springer-Verlag.

Min, S.-K., X. Zhang, F. W. Zwiers, and G. C. Hegerl, 2011: Human contribution to more-intense precipitation extremes. *Nature*, 470, 378-381, 10.1038/nature09763.

Monteith, J. L. and M. H. Unsworth, 2008: *Principles of Environmental Physics*. Third ed. London: Academic Press.

Mueller, R. and U. Schulzweida, 2010: Max-Planck-Institute for Meteorology: Climate Data Operators (CDO), https://code.zmaw.de/projects/cdo.

Murphy, A. H. and E. S. Epstein, 1989: Skill scores and correlation coefficients in model verification. *Mon. Wea. Rev.*, 117(3), 572-581.

Murphy, J., 1999: An evaluation of statistical and dynamical techniques for downscaling local climate. *J. Climate*, 12(8), 2256-2284.

Nakicenvoic et al., 2000: *Special Report on Emissions Scenarios*. *A Special Report of Working Group III of the Intergovernmental Panel on Climate Change*. Cambridge: Cambridge University Press. 599 pp.

Nash, J. E. and J. V. Sutcliffe, 1970: River flow forecasting through conceptual models part I: A discussion of prinicples. *J. Hydrol.*, 10(3), 282-290.

Novick, K. A., R. Oren, P. C. Stoy, M. B. S. Siqueira, and G. G. Katul, 2009: Nocturnal evaportranspiration in eddy-covariance records from three co-located ecosystems in the Southeastern U.S.: Implications for annual fluxes. *Ag. For. Met.*, 149, 1491-1504, doi: 10.1016/j.agformet.2009.04.005.

Ott, R. L. and M. T. Longnecker, 2010: *Introduction to Statistical Methods and Data Analysis*. Sixth ed. London, U.K.: Academic Press.

Pan, L.-L., S.-H. Chen, D. Cayan, M.-Y. Lin, Q. Hart, M.-H. Zhang, Y. Liu, and J. Wang, 2011: Influences of climate change on California and Nevada regions revealed by a high-resolution dynamical downscaling study. *Clim. Dyn.*, 37, 2005-2020, doi: 10.1007/s00382-010-0961-5.

Parry, M. L., O. F. Canziani, J. P. Palutikof, P. G. van der Linden, and C. E. Hanson (eds), 2007: *Contribution of Working Group II to the Fourth Assessment Report of the Intergovernmental Panel on Climate Change*. Cambridge and New York: Cambridge University Press.

PCMDI, 2010: Program for Climate Model Diagnosis and Intercomparison's IPCC AR4 models, http://www-pcmdi.llnl.gov/ipcc/about_ipcc.php, visited 11/9/10.

Pielke, R. A., 2001: Influence of the spatial distribution of vegetation and soils on the prediction of cumulus convective rainfall. *Rev. Geophys.*, 39, 151-177.

Pielke, R. A., G. Prins, S. Rayner, and D. Sarewitz, 2007: Climate change 2007: Lifting the taboo on adaptation. *Nature*, 445, 597-598, doi: 10.1038/445597a.

Pierce, D. W., T. P. Barnett, B. D. Santer, and P. J. Gleckler, 2009: Selecting global climate models for regional climate change studies. *P. Natl. Acad. Sci.*, 106(21), 8441-8446.

Pitman, A. J. and S. E. Perkins, 2009: Global and regional comparison of daily 2-m and 1000-hPa maximum and minimum temperatures in three global reanalyses. *J. Climate*, 22, 4667-4681, doi: 10.1175/2009JCLI2799.1.

Pennell, C. and T. Reichler, 2010: On the effective number of climate models. *J. Climate*, 24(5), 2358-2367, doi: 10.1175/2010JCLI3814.1.

Perkins, S. E., A. J. Pitman, N. J. Holbrook, and J. McAneney, 2007: Evaluation of the AR4 climate model's simulated daily maximum temperature, minimum temperature, and precipitation over Australia using probability density functions, *J. Climate*, 20, 4356-4376, doi: 10.1175/JCLI4253.1.

Perkins, S. E., 2009: Smaller projected increases in 20-year temperature returns over Australia in skill-selected climate models. *Geophys. Res. Lett.*, 36, L06710, doi: 10.1029/2009GL037293.

Perkins, S. E., 2010. Personal communication.

Perkins, S. E., D. B. Irving, J. R. Brown, S. B. Power, A. F. Moise, R. A. Colman, and I. Smith, 2012: CMIP3 ensemble climate projections over the western tropical Pacific based on model skill. *Clim. Res.*, 51, 35-58, doi: 10.3354/cr01046.

Randall, D. A., R. A. Wood, S. Bony, R. Colman, T. Fichefet, J. Fyfe, V. Kattsov, A. Pitman, J. Shukla, J. Srinvasan, R. J. Stouffer, A. Sumi, and K. E. Taylor, 2007: Climate models and their evaluation: In: *Climate Change 2007: The Physical Science Basis. Contribution of Working Group I to the Fourth Assessment Report of the Intergovernmental Panel on Climate Change* [Solomon, S., D. Qin, M. Manning, Z. Chen, M. Marquis, K. B. Averyt, M. Tignor, and H. L. Miller (eds.)]. Cambridge University Press, Cambridge, United Kingdom and New York, NY, USA.

Rangwala, I., B. Joseph, C. Karen, N. Jason, and P. James, 2012: Mid-21st century projections in temperature extremes in the southern Colorado Rocky Mountains from regional climate models. *Clim. Dyn.*, doi: 10.1007/s00382-011-1282-z.

Ray, D. K., R. A. Pielke Sr., U. S. Nair, and D. Niyogi, 2010: Roles of atmospheric and land surface data in dynamic regional downscaling. *J. Geophys. Res.*, 115, D05102, doi: 10.1029/2009JD012218.

Rew, R., G. Davis, S. Emmerson, H. Davies, E. Hartnett, D. Heimbigner, and W. Fisher, 2012: The NetCDF Users Guide. retrieved from http://www.unidata.ucar.edu/software/netcdf/docs/.

Riccio, A., A. Ciaramella, G. Giunta, S. Galmarini, E. Solazzo, and S. Potempski, 2012: On the systematic reduction of data complexity in multimodel atmospheric dispersion ensemble modeling. *J. Geophys. Res.*, 117, D05314, doi: 10.1029/2011JD016503.

Samenow, J., 2012: U.S. had most extreme precipitation on record in 2011. *The Washington Post*. January 12, 2012, http://www.washingtonpost.com/blogs/capital-weather-gang/post/us-had-most-extreme-precipitation-on-record-in-2011/2012/01/11/gIQA7oJXrP_blog.html.

Schliep, E. M., D. Cooley, S. R. Sain, and J. A. Hoeting, 2010: A comparison study of extreme precipitation from six different regional climate models via spatial hierarchical modeling. *Extremes*, 13, 219-239, doi: 10.1007/s10687-009-0098-2.

Schoof, J. T., D. W. Shin, S. Cocke, T. E. LaRow, Y-K. Lim, and J. J. O'Brien, 2009: Dynamically and statistically downscaled seasonal temperature and precipitation hindcast ensembles for the southeastern USA. *Int. J. Climatol.*, 29, 243-257, doi: 10.1002/joc.1717.

Semenov, M. A. and P. Stratonovitch, 2010: Use of multi-model ensembles from global climate models for assessment of climate change impacts. *Clim. Res.*, 41, 1-14, doi: 10.3354/cr00836.

Seneviratne, S. I., N. Nicholls, D. Easterling, C. M. Goodess, S. Kanae, J. Kossin, Y. Luo, J. Marengo, K. McInnes, M. Rahimi, M. Reichstein, A. Sorteberg, C. Vera, and X. Zhang, 2012: Changes in climate extremes and their impacts on the natural physical environment. In: *Managing the Risks of Extreme Events and Distasters to Advance Climate Change Adaptation* [Field, C. B., V. Barros, T. F. Stocker, D. Qin, D. J. Dokken, K. L. Ebi, M. D. Mastrandrea, K. J. Mach, G.-K. Plattner, S. K. Allen, M. Tignor, and P. M. Midgley (eds.)]. A Special Report of Working Groups I and II of the Intergovernmental Panel on Climate Change (IPCC). Cambridge, U.K. and New York, NY: Cambridge University Press, pp. 109-230.

Shem, W. O., T. L. Mote, and J. M. Shepard, 2010: Validation of NARCCAP climate products for forest resource applications in the southeast United States. In: *18th Conference on Applied Climatology, Session 10*, American Meteorological Society.

Shrestha, R., Y. Dibike, and T. Prowse, 2011: Modelling of climate-induced hydrologic changes in the Lake Winnipeg watershed. *J. Great Lakes Res.*, doi: 10.1016/j.jglr.2011.02.004.

Smith, J. B., J. M. Vogel, and J. E. Cromwell III, 2009: An architecture for government action on adaptation to climate change. An editorial comment, *Clim. Change*, 95, 53-61, doi: 10.1007/s10584-009-9623-1.

Sobolowski, S. and T. Pavelsky, 2012: Evaluation of present and future North American Regional Climate Change Assessment Program (NARCCAP) regional climate simulations over the southeast United States. *J. Geophys. Res.*, 117, D01101, doi: 10.1029/2011/JD016430.

Stainforth, D. A., T. E. Downing, R. Washington, A. Lopez, and M. New, 2007: Issues in the interpretation of climate model ensembles to inform decisions. *Philos. Trans. R. Soc. A.*, 365, 2163-2177, doi: 10.1098/rsta.2007.2073

Stull, R. B., 2000: *Meteorology for Scientists and Engineers*. Second ed. Pacific Grove, CA: Brooks/Cole Thomson Learning.

Sun, Y., S. Solomon, A. Dai, and R. W. Portmann, 2006: How often does it rain? *J. Climate*, 19, 916-934.

Suzuki, R. and H. Shimodaira, 2006: Pvclust: an R package for assessing the uncertainty in hierarchical clustering. *Bioinformatics*, 22(12), 1540-1542, doi: 10.1093/bioinformatics/btl117.

Takle, E. S., M. Jha, E. Lu, R. W. Arritt, and W. J. Gutowski, 2010: Streamflow in the upper Mississippi river basin as simulated by SWAT driven by 20th Century contemporary results of global climate models and NARCCAP regional climate models. *Meteorol. Z.*, 19(4), 341-346, doi: 10.1127/0941-2948/2010/0464.

Thornthwaite, C. W., 1948: An approach toward a rational classification of climate. *Geogr. Rev.*, 38 (1), 55-94, doi: 10.2307/210739.

Trenberth, K. E., A. Dai, R. M. Rasmussen, and D. B. Parsons, 2003: The changing character of precipitation. *Bull. Am. Meteorol. Soc.*, 9, 1205-1217, doi: 10.1175/BAMS-84-9-1205.

Trenberth, K. E., 2008: The Impact of Climate Change and Variablility on Heavy Precipitation, Floods, and Droughts, *The Encycolpedia of Hydrological Sciences*. John Wiley & Sons, Ltd., Chichester, UK, doi: 10.1002/0470848944.hsa211.

Tubiello, F. N., J-F. Soussana, and S. M. Howden, 2007: Crop and pasture response to climate change. *P. Natl. Acad. Sci.*, 104(50), 19686-19690.

Venables, W. N. and B. D. Ripley, 2002: Modern Applied Statistics with S. Fourth ed., Springer: New York, NY. ISBN: 0-387-95457-0.

von Storch, H. and F. W. Zwiers, 1999: *Statistical Analysis in Climate Research*. New York: Cambridge University Press.

Vorosmarty, C. J., P. Green, J. Salisbury, and R. B. Lammers, 2000: Global water resources: Vulnerability from climate change and population growth. *Science*, 289(5477), 284-288, doi: 10.1126/science.289.5477.284.

Wang, S-Y. R. R. Gillies, E. S. Takle, and W. J. Gutowski, 2009: Evaluation of precipitation in the intermountain region as simulated by the NARCCAP regional climate models. *Geophys. Res. Lett.*, 36, L11704, doi: 10.1029/2009GL037930.

Ward, J. H., 1963: Hierarchical grouping to optimize an objective function. *J. Am. Stat. Assoc.*, 58(301), 236-244.

Warner, T. T, 2011: *Numerical Weather and Climate Prediction*. New York: Cambridge University Press.

Watterson, I.G., 1996: Non-dimensional measures of climate model performance. *Int. J. Climatol.*, 16, 379-391.

Weigel, A. P., R. Knutti, M. A. Liniger, and C. Appenzeller, 2010: Risks of model weighting in multimodel climate projections. *J. Climate*, 23(15), 4175-4191, doi: 10.1175/2010JCLI3594.1.

Wilks, D. S., 2006: *Statistical Methods in the Atmospheric Sciences*. Second ed. London: Academic Press.

Willmott, C. J. and D. E. Wicks, 1980: An empirical method for the spatial interpolation of monthly precipitation within California. *Phys. Geogr.*, 1, 59-73.

Willmott, C. J., 1981: On the validation of models. *Phys. Geogr.*, 2, 184-194.

Willmott, C. J. and K. Matsuura, 2005: Advantages of the mean absolute error (MAE) over the root mean square error (RMSE) in assessing average model performance. *Clim. Res.*, 30, 79-82.

Willmott, C. J., S. M. Robeson, and K. Matsuura, 2011: Short communication: A refined index of model performance. *Int. J. Climatol.*, doi: 10.1002/joc.2419.

Wood, A. W., E. P. Maurer, A. Kumar, and D. P. Lettenmaier, 2002: Long-range experimental hydrologic forecasting for the eastern United States. *J. Geophys. Res-Atmos.*, 107(D20), 4429.

Wood, A. W., L. R. Leung, V. Sridhar, and D. P. Lettenmaier, 2004: Hydrologic implications of dynamical and statistical approaches to downscaling climate model outputs. *Clim. Change*, 15(62), 189-216.

World Resources Institute, 2009: Energy demands drain water resources in Southeast U.S., policies needed. *World Resources Institute – Climate, Energy & Transport*, May 13, 2009, http://www.wri.org/press/2009/05/energy-demands-drain-water-resources-southeast-us-policies-needed.

Wu, H., K. G. Hubbard, and J. You, 2005: Some concerns when using data from the cooperative weather station networks: A Nebraska case study. *J. Atmos. Oceanic Technol.*, 22, 592-602, doi: 10.1175/JTECH1733.1.

Yang, Z. and R. W. Arritt, 2002: Test of perturbed physics ensemble approach for regional climate modeling. *J. Clim.*, 15, 2881-2896.

Yokoi, S., Y. N. Takayabu, K. Nishii, H. Nakamura, H. Endo, H. Ichikawa, T. Inoue, M. Kimoto, Y. Kosaka, T. Mitasaka, K. Oshima, N. Sato, Y. Tsushima, and M. Watanabe, 2011: Application of cluster analysis to climate model performance metrics. *J. Appl. Meteorol. Clim.*, 50, 1666-1675, doi: 10.1175/2011JAMC2643.1.

Zhang, X. C., 2005: Spatial downscaling of global climate output for site-specific assessment of crop production and soil erosion. *Ag. For. Met.*, 135, 215-229.

Zorita, E. and H. von Storch, 1999: The analog method as a simple statistical downscaling technique: comparison with more complicated methods. *J. Climate*, 12, 2474-2489.

Zwiers, F. W., 1990: The effect of serial correlation on statistical inferences made with the resampling procedures. *J. Climate*, 3, 14521461.

APPENDIX A – "GRID_DESCRIPTION.TXT"

The following seven lines of code were saved in a text file called "grid_description.txt" and were used as the re-gridding descriptor file in CDO in conjunction with the nearest-neighbors algorithm. The first line in the code passes to CDO what the grid type/projection will be after re-gridding, in this case the grid type will simply be a longitude/latitude grid. The next two lines tell CDO the number of grid points in the x- and y-directions. Line four informs CDO that the first grid points in the x-direction (longitude) begin at -126°W with line five indicating the grid points will be spaced at 0.5° longitude increments. Line six informs CDO that the first grid points in the y-direction (latitude) begin at 20°N with line seven indicating the grid points will be spaced at 0.5° latitude increments.

```
gridtype = lonlat
xsize = 134
ysize = 104
xfirst = -126
xinc = 0.5
yfirst = 20
yinc = 0.5
```

APPENDIX B – R SCRIPTS

B.1 EXAMPLE CODE TO EXTRACT EAST SUB-REGION DATA POINTS

This code extracts only the data points I want for the east sub-region after I have re-mapped the data from the native coordinates run by the model executors.

```
#open up the R library to read in and manipulate netCDF files
library(ncdf)

#open the netCDF file and define latitude, longitude, and the variable
#of interest
ex.nc = open.ncdf("C://Dissertation//tasmin_RCM3_gfdl_1970-
1999_C_remap_sel_dec.nc")
y = get.var.ncdf( ex.nc, "lat")      # coordinate variable
x = get.var.ncdf( ex.nc, "lon")      # coordinate variable
z = get.var.ncdf( ex.nc, "tasmin")   # variable

#tf = 30.5  to = 31           to_f = 31.5 tt = 32
#tt_f = 32.5      tth = 33    tth_f = 33.5      tfo = 34
#tfo_f = 34.5
#tfi = 35   tfi_f = 35.5      ts = 36           ts_f = 36.5
#nt = -90   no_f = -91.5      efo_f = -84.5     efo = -84
#en_f = -89.5     no = -91    et_f = -83.5      et = -83
#en = -89   nt_f = -90.5      etw_f = -82.5     etw = -82
#ee_f = -88.5     es = -87    eo_f = -81.5
#ee = -88   esi_f = -86.5
#es_f = -87.5     esi = -86
#ef_f = -85.5     ef = 85

#eo = -81   e_f = -80.5 e = -80  sn_f = -79.5   sn = -79
#se_f = -78.5     se = -78
#ss_f = -77.5     ss = -77    ssi_f = -76.5     ssi = -76

#extract the data points of interest from the netCDF file
```

```
tf_efo_f<-z[20,6,]
tf_efo<-z[21,6,]
tf_et_f<-z[22,6,]
tf_et<-z[23,6,]
tf_etw_f<-z[24,6,]
tf_etw<-z[25,6,]

to_ef<-z[19,7,]
to_efo_f<-z[20,7,]
to_efo<-z[21,7,]
to_et_f<-z[22,7,]
to_et<-z[23,7,]
to_etw_f<-z[24,7,]
to_etw<-z[25,7,]
to_eo_f<-z[26,7,]

to_f_ef<-z[19,8,]
to_f_efo_f<-z[20,8,]
to_f_efo<-z[21,8,]
to_f_et_f<-z[22,8,]
to_f_et<-z[23,8,]
to_f_etw_f<-z[24,8,]
to_f_etw<-z[25,8,]
to_f_eo_f<-z[26,8,]

tt_ef<-z[19,9,]
tt_efo_f<-z[20,9,]
tt_efo<-z[21,9,]
tt_et_f<-z[22,9,]
tt_et<-z[23,9,]
tt_etw_f<-z[24,9,]
tt_etw<-z[25,9,]
tt_eo_f<-z[26,9,]
tt_eo<-z[27,9,]

tt_f_ef<-z[19,10,]
tt_f_efo_f<-z[20,10,]
tt_f_efo<-z[21,10,]
tt_f_et_f<-z[22,10,]
tt_f_et<-z[23,10,]
tt_f_etw_f<-z[24,10,]
tt_f_etw<-z[25,10,]
tt_f_eo_f<-z[26,10,]
tt_f_eo<-z[27,10,]
tt_f_e_f<-z[28,10,]

tth_ef<-z[19,11,]
tth_efo_f<-z[20,11,]
tth_efo<-z[21,11,]
tth_et_f<-z[22,11,]
tth_et<-z[23,11,]
tth_etw_f<-z[24,11,]
tth_etw<-z[25,11,]
tth_eo_f<-z[26,11,]
tth_eo<-z[27,11,]
tth_e_f<-z[28,11,]
tth_e<-z[29,11,]
```

```
tth_sn_f<-z[30,11,]

tth_f_ef_f<-z[18,12,]
tth_f_ef<-z[19,12,]
tth_f_efo_f<-z[20,12,]
tth_f_efo<-z[21,12,]
tth_f_et_f<-z[22,12,]
tth_f_et<-z[23,12,]
tth_f_etw_f<-z[24,12,]
tth_f_etw<-z[25,12,]
tth_f_eo_f<-z[26,12,]
tth_f_eo<-z[27,12,]
tth_f_e_f<-z[28,12,]
tth_f_e<-z[29,12,]
tth_f_sn_f<-z[30,12,]
tth_f_sn<-z[31,12,]

tfo_ef_f<-z[18,13,]
tfo_ef<-z[19,13,]
tfo_efo_f<-z[20,13,]
tfo_efo<-z[21,13,]
tfo_et_f<-z[22,13,]
tfo_et<-z[23,13,]
tfo_etw_f<-z[24,13,]
tfo_etw<-z[25,13,]
tfo_eo_f<-z[26,13,]
tfo_eo<-z[27,13,]
tfo_e_f<-z[28,13,]
tfo_e<-z[29,13,]
tfo_sn_f<-z[30,13,]
tfo_sn<-z[31,13,]
tfo_se_f<-z[32,13,]
tfo_se<-z[33,13,]

tfo_f_ef_f<-z[18,14,]
tfo_f_ef<-z[19,14,]
tfo_f_efo_f<-z[20,14,]
tfo_f_efo<-z[21,14,]
tfo_f_et_f<-z[22,14,]
tfo_f_et<-z[23,14,]
tfo_f_etw_f<-z[24,14,]
tfo_f_etw<-z[25,14,]
tfo_f_eo_f<-z[26,14,]
tfo_f_eo<-z[27,14,]
tfo_f_e_f<-z[28,14,]
tfo_f_e<-z[29,14,]
tfo_f_sn_f<-z[30,14,]
tfo_f_sn<-z[31,14,]
tfo_f_se_f<-z[32,14,]
tfo_f_se<-z[33,14,]
tfo_f_ss_f<-z[34,14,]

tfi_ef_f<-z[18,15,]
tfi_ef<-z[19,15,]
tfi_efo_f<-z[20,15,]
tfi_efo<-z[21,15,]
tfi_et_f<-z[22,15,]
```

```
tfi_et<-z[23,15,]
tfi_etw_f<-z[24,15,]
tfi_etw<-z[25,15,]
tfi_eo_f<-z[26,15,]
tfi_eo<-z[27,15,]
tfi_e_f<-z[28,15,]
tfi_e<-z[29,15,]
tfi_sn_f<-z[30,15,]
tfi_sn<-z[31,15,]
tfi_se_f<-z[32,15,]
tfi_se<-z[33,15,]
tfi_ss_f<-z[34,15,]
tfi_ss<-z[35,15,]

tfi_f_efo<-z[21,16,]
tfi_f_et_f<-z[22,16,]
tfi_f_et<-z[23,16,]
tfi_f_etw_f<-z[24,16,]
tfi_f_etw<-z[25,16,]
tfi_f_eo_f<-z[26,16,]
tfi_f_eo<-z[27,16,]
tfi_f_e_f<-z[28,16,]
tfi_f_e<-z[29,16,]
tfi_f_sn_f<-z[30,16,]
tfi_f_sn<-z[31,16,]
tfi_f_se_f<-z[32,16,]
tfi_f_se<-z[33,16,]
tfi_f_ss_f<-z[34,16,]
tfi_f_ss<-z[35,16,]
tfi_f_ssi_f<-z[36,16,]
tfi_f_ssi<-z[37,16,]

ts_et<-z[23,17,]
ts_etw_f<-z[24,17,]
ts_etw<-z[25,17,]
ts_eo_f<-z[26,17,]
ts_eo<-z[27,17,]
ts_e_f<-z[28,17,]
ts_e<-z[29,17,]
ts_sn_f<-z[30,17,]
ts_sn<-z[31,17,]
ts_se_f<-z[32,17,]
ts_se<-z[33,17,]
ts_ss_f<-z[34,17,]
ts_ss<-z[35,17,]
ts_ssi_f<-z[36,17,]

ts_f_etw<-z[25,18,]
ts_f_eo_f<-z[26,18,]
ts_f_eo<-z[27,18,]
ts_f_e_f<-z[28,18,]
ts_f_e<-z[29,18,]
ts_f_sn_f<-z[30,18,]
ts_f_sn<-z[31,18,]
ts_f_se_f<-z[32,18,]
ts_f_se<-z[33,18,]
ts_f_ss_f<-z[34,18,]
```

```
ts_f_ss<-z[35,18,]
ts_f_ssi_f<-z[36,18,]
ts_f_ssi<-z[37,18,]


#combine and make a data frame out of each of the extracted data points


data<-cbind(tf_efo_f,tf_efo,tf_et_f,tf_et,tf_etw_f,tf_etw,to_ef,
to_efo_f,to_efo,to_et_f,to_et,to_etw_f,to_etw,to_eo_f,to_f_ef,
to_f_efo_f,to_f_efo,to_f_et_f,to_f_et,to_f_etw_f,to_f_etw,to_f_eo_f,
tt_ef,tt_efo_f,tt_efo,tt_et_f,tt_et,tt_etw_f,tt_etw,tt_eo_f,tt_eo,
tt_f_ef,tt_f_efo_f,tt_f_efo,tt_f_et_f,tt_f_et,tt_f_etw_f,tt_f_etw,
tt_f_eo_f,tt_f_eo,tt_f_e_f,tth_ef,tth_efo_f,tth_efo,tth_et_f,tth_et,
tth_etw_f,tth_etw,tth_eo_f,tth_eo,tth_e_f,tth_e,tth_sn_f,tth_f_ef_f,
tth_f_ef,tth_f_efo_f,tth_f_efo,tth_f_et_f,tth_f_et,tth_f_etw_f,
tth_f_etw,tth_f_eo_f,tth_f_eo,tth_f_e_f,tth_f_e,tth_f_sn_f,tth_f_sn,
tfo_ef_f,tfo_ef,tfo_efo_f,tfo_efo,tfo_et_f,tfo_et,tfo_etw_f,tfo_etw,
tfo_eo_f,tfo_eo,tfo_e_f,tfo_e,tfo_sn_f,tfo_sn,tfo_se_f,tfo_se,
tfo_f_ef_f,tfo_f_ef,tfo_f_efo_f,tfo_f_efo,tfo_f_et_f,tfo_f_et,
tfo_f_etw_f,tfo_f_etw,tfo_f_eo_f,tfo_f_eo,tfo_f_e_f,tfo_f_e,tfo_f_sn_f,
tfo_f_sn,tfo_f_se_f,tfo_f_se,tfo_f_ss_f,tfi_ef_f,tfi_ef,tfi_efo_f,
tfi_efo,tfi_et_f,tfi_et,tfi_etw_f,tfi_etw,tfi_eo_f,tfi_eo,tfi_e_f,
tfi_e,tfi_sn_f,tfi_sn,tfi_se_f,tfi_se,tfi_ss_f,tfi_ss,tfi_f_efo,tfi_f_e
t_f,tfi_f_et,tfi_f_etw_f,tfi_f_etw,tfi_f_eo_f,tfi_f_eo,tfi_f_e_f,
tfi_f_e,tfi_f_sn_f,tfi_f_sn,tfi_f_se_f,tfi_f_se,tfi_f_ss_f,tfi_f_ss,
tfi_f_ssi_f,tfi_f_ssi,ts_et,ts_etw_f,ts_etw,ts_eo_f,ts_eo,ts_e_f,ts_e,
ts_sn_f,ts_sn,ts_se_f,ts_se,ts_ss_f,ts_ss,ts_ssi_f,ts_f_etw,ts_f_eo_f,
ts_f_eo,ts_f_e_f,ts_f_e,ts_f_sn_f,ts_f_sn,ts_f_se_f,ts_f_se,ts_f_ss_f,
ts_f_ss,ts_f_ssi_f,ts_f_ssi)

#write the data frame to a .csv file
write.table(data,file="C:\\Dissertation\\tasmin_RCM3_gfdl_extract_east_
dec.csv",sep=",",row.names=F,quote=F,col.names=c("305_845","305_84",
"305_835","305_83","305_825","305_82","31_85","31_845","31_84",
"31_835","31_83","31_825","31_82","31_815","315_85","315_845","315_84",
"315_835","315_83","315_825","315_82","315_815","32_85","32_845",
"32_84","32_835","32_83","32_825","32_82","32_815","32_81","325_85",
"325_845","325_84","325_835","325_83","325_825","325_82","325_815",
"325_81","325_805","33_85","33_845","33_84","33_835","33_83","33_825",
"33_82","33_815","33_81","33_805","33_80","33_795","335_855","335_85",
"335_845","335_84","335_835","335_83","335_825","335_82","335_815",
"335_81","335_805","335_80","335_795","335_79","34_855","34_85",
"34_845","34_84","34_835","34_83","34_825","34_82","34_815","34_81",
"34_805","34_80","34_795","34_79","34_785","34_78","345_855","345_85",
"345_845","345_84","345_835","345_83","345_825","345_82","345_815",
"345_81","345_805","345_80","345_795","345_79","345_785","345_78",
"345_775","35_855","35_85","35_845","35_84","35_835","35_83","35_825",
"35_82","35_815","35_81","35_805","35_80","35_795","35_79","35_785",
"35_78","35_775","35_77","355_84","355_835","355_83","355_825",
"355_82","355_815","355_81","355_805","355_80","355_795","355_79",
"355_785","355_78","355_775","355_77","355_765","355_76","36_83",
"36_825","36_82","36_815","36_81","36_805","36_80","36_795","36_79",
"36_785","36_78","36_775","36_77","36_765","365_82","365_815","365_81",
"365_805","365_80","365_795","365_79","365_785","365_78","365_775",
"365_77","365_765","365_76"))
```

B.2 PERKINS' SKILL SCORE COMPUTATION

The next code computes Perkins' skill score for a given model:

```
#open the observations table and the MM5I-CCSM model output
l<-read.csv(file="C:\\Dissertation\\Tmin_obs_apr_extract_east_sub.csv",
sep=",", header=TRUE)
ll<-read.csv(file="C:\\Dissertation\\
tas_MM5I_ccsm_daymin_apr_extract_east_sub.csv",sep=",", header=TRUE)

#make the observations and model data into two separate vectors
obs<-c(l$X305_845,l$X305_84,l$X305_835,l$X305_83,l$X305_825,l$X305_82,
l$X31_85,l$X31_845,l$X31_84,l$X31_835,l$X31_83,l$X31_825,l$X31_82,
l$X31_815,l$X315_85,l$X315_845,l$X315_84,l$X315_835,l$X315_83,
l$X315_825,l$X315_82,l$X315_815,l$X32_85,l$X32_845,l$X32_84,l$X32_835,
l$X32_83,l$X32_825,l$X32_82,l$X32_815,l$X32_81,l$X325_85,l$X325_845,
l$X325_84,l$X325_835,l$X325_83,l$X325_825,l$X325_82,l$X325_815,
l$X325_81,l$X325_805,l$X33_85,l$X33_845,l$X33_84,l$X33_835,l$X33_83,
l$X33_825,l$X33_82,l$X33_815,l$X33_81,l$X33_805,l$X33_80,l$X33_795,
l$X335_855,l$X335_85,l$X335_845,l$X335_84,l$X335_835,l$X335_83,
l$X335_825,l$X335_82,l$X335_815,l$X335_81,l$X335_805,l$X335_80,
l$X335_795,l$X335_79,l$X34_855,l$X34_85,l$X34_845,l$X34_84,l$X34_835,
l$X34_83,l$X34_825,l$X34_82,l$X34_815,l$X34_81,l$X34_805,l$X34_80,
l$X34_795,l$X34_79,l$X34_785,l$X34_78,l$X345_855,l$X345_85,l$X345_845,
l$X345_84,l$X345_835,l$X345_83,l$X345_825,l$X345_82,l$X345_815,
l$X345_81,l$X345_805,l$X345_80,l$X345_795,l$X345_79,l$X345_785,
l$X345_78,l$X345_775,l$X35_855,l$X35_85,l$X35_845,l$X35_84,l$X35_835,
l$X35_83,l$X35_825,l$X35_82,l$X35_815,l$X35_81,l$X35_805,l$X35_80,
l$X35_795,l$X35_79,l$X35_785,l$X35_78,l$X35_775,l$X35_77,l$X355_84,
l$X355_835,l$X355_83,l$X355_825,l$X355_82,l$X355_815,l$X355_81,
l$X355_805,l$X355_80,l$X355_795,l$X355_79,l$X355_785,l$X355_78,
l$X355_775,l$X355_77,l$X355_765,l$X355_76,l$X36_83,l$X36_825,l$X36_82,
l$X36_815,l$X36_81,l$X36_805,l$X36_80,l$X36_795,l$X36_79,l$X36_785,
l$X36_78,l$X36_775,l$X36_77,l$X36_765,l$X365_82,l$X365_815,l$X365_81,
l$X365_805,l$X365_80,l$X365_795,l$X365_79,l$X365_785,l$X365_78,
l$X365_775,l$X365_77,l$X365_765,l$X365_76)

mm<-c(ll$X305_845,ll$X305_84,ll$X305_835,ll$X305_83,ll$X305_825,
ll$X305_82,ll$X31_85,ll$X31_845,ll$X31_84,ll$X31_835,ll$X31_83ll$X31_82
5,ll$X31_82,ll$X31_815,ll$X315_85,ll$X315_845,ll$X315_84,ll$X315_835,
ll$X315_83,ll$X315_825,ll$X315_82,ll$X315_815,ll$X32_85,ll$X32_845,
ll$X32_84,ll$X32_835,ll$X32_83,ll$X32_825,ll$X32_82,ll$X32_815,
ll$X32_81,ll$X325_85,ll$X325_845,ll$X325_84,ll$X325_835,ll$X325_83,
ll$X325_825,ll$X325_82,ll$X325_815,ll$X325_81,ll$X325_805,ll$X33_85,
ll$X33_845,ll$X33_84,ll$X33_835,ll$X33_83,ll$X33_825,ll$X33_82,
ll$X33_815,ll$X33_81,ll$X33_805,ll$X33_80,ll$X33_795,ll$X335_855,
ll$X335_85,ll$X335_845,ll$X335_84,ll$X335_835,ll$X335_83,ll$X335_825,
ll$X335_82,ll$X335_815,ll$X335_81,ll$X335_805,ll$X335_80,ll$X335_795,
ll$X335_79,ll$X34_855,ll$X34_85,ll$X34_845,ll$X34_84,ll$X34_835,
ll$X34_83,ll$X34_825,ll$X34_82,ll$X34_815,ll$X34_81,ll$X34_805,
ll$X34_80,ll$X34_795,ll$X34_79,ll$X34_785,ll$X34_78,ll$X345_855,
ll$X345_85,ll$X345_845,ll$X345_84,ll$X345_835,ll$X345_83,ll$X345_825,
ll$X345_82,ll$X345_815,ll$X345_81,ll$X345_805,ll$X345_80,ll$X345_795,
ll$X345_79,ll$X345_785,ll$X345_78,ll$X345_775,ll$X35_855,ll$X35_85,
ll$X35_845,ll$X35_84,ll$X35_835,ll$X35_83,ll$X35_825,ll$X35_82,
ll$X35_815,ll$X35_81,ll$X35_805,ll$X35_80,ll$X35_795,ll$X35_79,
```

```
ll$X35_785,ll$X35_78,ll$X35_775,ll$X35_77,ll$X355_84,ll$X355_835,
ll$X355_83,ll$X355_825,ll$X355_82,ll$X355_815,ll$X355_81,ll$X355_805,
ll$X355_80,ll$X355_795,ll$X355_79,ll$X355_785,ll$X355_78,ll$X355_775,
ll$X355_77,ll$X355_765,ll$X355_76,ll$X36_83,ll$X36_825,ll$X36_82,
ll$X36_815,ll$X36_81,ll$X36_805,ll$X36_80,ll$X36_795,ll$X36_79,
ll$X36_785,ll$X36_78,ll$X36_775,ll$X36_77,ll$X36_765,ll$X365_82,l
l$X365_815,ll$X365_81,ll$X365_805,ll$X365_80,ll$X365_795,ll$X365_79,
ll$X365_785,ll$X365_78,ll$X365_775,ll$X365_77,ll$X365_765,ll$X365_76)

#combine the two vectors into a data frame by columns
ff<-cbind(obs,mm)

#write the data frame to a .csv file
bb<-write.table(ff,file="C://Dissertation//tasmin_east_apr.csv",
sep=",",row.names=F, quote=F,col.names=c("Obs","MM5I_CCSM"))

#read the .csv file back into R
gg<-read.csv(file="C:\\Dissertation\\tasmin_east_apr.csv",sep=",",
header=TRUE)

#sort each of the columns from smallest value to largest value
z1<-sort(gg$Obs)
z2<-sort(gg$MM5I_CCSM)

#combine the sorted vectors back into a data frame
fff<-cbind(z1,z2)

#use only those values which fall between the minimum and maximum
#values found in observations
a1<-z1[which(z1>=-12 & z1<=25)]
b1<-z2[which(z2>=-12 & z2<=25)]

#define the bins to use to create a histogram
bins<-seq(-12,25,by=0.5)

#create a histogram based on the bins defined above for both the
#observed data and model data
a2<-hist(a1, breaks=bins, freq=FALSE)
b2<-hist(b1, breaks=bins, freq=FALSE)

#extract the density value from the histogram - this is the height of
#each bin in the histogram
a3<-a2$density
b3<-b2$density

#combine the two density vectors into a data frame
b4<-cbind(a3,b3)

#find the minimum value at each row between the observations and the
#model
b5<-apply(b4,1,min)

#sum each of the minimum values found above and divide by 2 because the
#bins were spaced every 0.5 degrees C. If the bin size had been 1,
#there is no need to divide by anything. If the bin size was 0.25, the
#user needs to divide the sum by 4, etc. The value found in this step
#is the model's Perkins' skill score.
```

```
b6<-(sum(b5))/2

#save the Perkins' skill score as a new variable
data<-b6

#write the Perkins' skill score to a table
write.table(data,file="C:\\Dissertation\\tasmin_east_skill_apr.csv",
sep=",",row.names=c("Apr"),quote=F, col.names=c("MM5I_CCSM"))
```

B.3 WILLMOTT'S INDEX OF AGREEMENT COMPUTATION

```
#Define the function for 2 times the sum of the magnitude of the
#difference between individual observations about the observed mean
right1<-function(obs) c*sum(abs(obs-mean_ob))

#Define the function for the sum of the magnitude of the difference
#between individual observations and model results
left1<-function(pred1,obs) sum(abs(pred1-obs))

#Function to define Equation 2 from Section 2.1
will<-function(right1,left1,pred1,obs) if (left1<=right1){
d_r<-1-((sum(abs(pred1-obs)))/(c*sum(abs(obs-mean_ob))))
} else {
d_r<-((c*sum(abs(obs-mean_ob)))/(sum(abs(pred1-obs))))-1
}

#Read in a dataset
gg<-read.csv(file="H:\\Dissertation\\tasmin_west_dec.csv",
sep=",", header=TRUE)

#Extract each column corresponding to individual models
y1<-sort(gg$Obs)
y2<-sort(gg$MM5I_CCSM)
y3<-sort(gg$RCM3_GFDL)
y4<-sort(gg$ECP2_GFDL)
y5<-sort(gg$WRFG_CCSM)
y6<-sort(gg$WRFG_CGCM3)
y7<-sort(gg$RCM3_CGCM3)
y8<-sort(gg$CRCM_CGCM3)
y9<-sort(gg$CRCM_CCSM)
y10<-sort(gg$HRM3_HADCM3)
y11<-sort(gg$GFDL_TS)

#Give the variables defined above a different variable name
a1<-y1
b1<-y2
c1<-y3
d1<-y4
e1<-y5
f1<-y6
g1<-y7
h1<-y8
i1<-y9
j1<-y10
```

```
k1<-y11

#Define c=2 based on Willmott et al (2011)
c=2

#Find the mean of the observations (O-bar)
mean_ob<-mean(a1)
#Use the functions defined above to calculate Willmott's index of
#agreement for each individual model
aa<-right1(a1)
ab<-left1(b1,a1)
will1a<-will(aa,ab,b1,a1)

aa<-right1(a1)
ab<-left1(c1,a1)
will2a<-will(aa,ab,c1,a1)

aa<-right1(a1)
ab<-left1(d1,a1)
will3a<-will(aa,ab,d1,a1)

aa<-right1(a1)
ab<-left1(e1,a1)
will4a<-will(aa,ab,e1,a1)

aa<-right1(a1)
ab<-left1(f1,a1)
will5a<-will(aa,ab,f1,a1)

aa<-right1(a1)
ab<-left1(g1,a1)
will6a<-will(aa,ab,g1,a1)

aa<-right1(a1)
ab<-left1(h1,a1)
will7a<-will(aa,ab,h1,a1)

aa<-right1(a1)
ab<-left1(i1,a1)
will8a<-will(aa,ab,i1,a1)

aa<-right1(a1)
ab<-left1(k1,a1)
will9a<-will(aa,ab,k1,a1)
```

B.4 ROOT MEAN SQUARE ERROR COMPUTATION

This code computes the root mean square error for a model:

```
#read in the data values
gg<-read.csv(file="C:\\Dissertation\\tasmin_east_dec.csv",sep=",",
header=TRUE)
```

```
#create a vector and sort from smallest to largest value from
#observations and model
y1<-sort(gg$Obs)
y2<-sort(gg$MM5I_CCSM)

#combine the sorted vectors into a data frame
fff<-cbind(y1,y2)

#function to define root mean square error
rmse <- function(obs, pred) sqrt(mean((obs-pred)^2))

#calculate the root mean square error between observations and model
b6<-rmse(a1,b1)

#save the root mean square error to a different variable
data<-b6

#write the root mean square error to a .csv file
write.table(data,file="C:\\Dissertation\\tasmin_east_rmse_dec.csv",
sep=",",row.names=c("dec"),quote=F, col.names=c("MM5I-CCSM"))
```

B.5 HOVMOLLER PLOT SCRIPT

This code creates a hovmoller plot from the Perkins' skill score values.

Additionally, code is included to make the color palate.

```
#open each of the libraries that either will or potentially could be
#used to create the hovmoller plots
library(reshape)
library(fields)
library(colorRamps)
library(RColorBrewer)
library(maps)
library(fields)
library(grid)
library(lattice)
library(graphics)
library(grDevices)
library(utils)
library(zoo)
library(tools)
library(ade4)

#open the R script which will plot the hovmoller plots
source("C://Dissertation//myImagePlot.R")

#read in the data from all months
gg<-read.csv(file="C:\\Dissertation\\tasmin_east_skill_dec.csv",
sep=",",header=T)
hh<-read.csv(file="C:\\Dissertation\\tasmin_east_skill_jan.csv",
sep=",",header=T)
```

```
ii<-read.csv(file="C:\\Dissertation\\tasmin_east_skill_feb.csv",
sep=",",header=T)
gg2<-read.csv(file="C:\\Dissertation\\tasmin_east_skill_mar.csv",
sep=",",header=T)
hh2<-read.csv(file="C:\\Dissertation\\tasmin_east_skill_apr.csv",
sep=",",header=T)
ii2<-read.csv(file="C:\\Dissertation\\tasmin_east_skill_may.csv",
sep=",",header=T)
gg3<-read.csv(file="C:\\Dissertation\\tasmin_east_skill_jun.csv",
sep=",",header=T)
hh3<-read.csv(file="C:\\Dissertation\\tasmin_east_skill_jul.csv",
sep=",",header=T)
ii3<-read.csv(file="C:\\Dissertation\\tasmin_east_skill_aug.csv",
sep=",",header=T)
gg4<-read.csv(file="C:\\Dissertation\\tasmin_east_skill_sep.csv",
sep=",",header=T)
hh4<-read.csv(file="C:\\Dissertation\\tasmin_east_skill_oct.csv",
sep=",",header=T)
ii4<-read.csv(file="C:\\Dissertation\\tasmin_east_skill_nov.csv",
sep=",",header=T)

#make data frames for each of the ensemble model members
data1<-rbind(gg$MM5I_CCSM,hh$MM5I_CCSM,ii$MM5I_CCSM,gg2$MM5I_CCSM,
hh2$MM5I_CCSM,ii2$MM5I_CCSM,gg3$MM5I_CCSM,hh3$MM5I_CCSM,ii3$MM5I_CCSM,
gg4$MM5I_CCSM,hh4$MM5I_CCSM,ii4$MM5I_CCSM)

data2<-rbind(gg$RCM3_GFDL,hh$RCM3_GFDL,ii$RCM3_GFDL,gg2$RCM3_GFDL,
hh2$RCM3_GFDL,ii2$RCM3_GFDL,gg3$RCM3_GFDL,hh3$RCM3_GFDL,ii3$RCM3_GFDL,
gg4$RCM3_GFDL,hh4$RCM3_GFDL,ii4$RCM3_GFDL)

data3<-rbind(gg$ECP2_GFDL,hh$ECP2_GFDL,ii$ECP2_GFDL,gg2$ECP2_GFDL,
hh2$ECP2_GFDL,ii2$ECP2_GFDL,gg3$ECP2_GFDL,hh3$ECP2_GFDL,ii3$ECP2_GFDL,
gg4$ECP2_GFDL,hh4$ECP2_GFDL,ii4$ECP2_GFDL)

data4<-rbind(gg$WRFG_CCSM,hh$WRFG_CCSM,ii$WRFG_CCSM,gg2$WRFG_CCSM,
hh2$WRFG_CCSM,ii2$WRFG_CCSM,gg3$WRFG_CCSM,hh3$WRFG_CCSM,ii3$WRFG_CCSM,
gg4$WRFG_CCSM,hh4$WRFG_CCSM,ii4$WRFG_CCSM)

data5<-rbind(gg$WRFG_CGCM3,hh$WRFG_CGCM3,ii$WRFG_CGCM3,gg2$WRFG_CGCM3,
hh2$WRFG_CGCM3,ii2$WRFG_CGCM3,gg3$WRFG_CGCM3,hh3$WRFG_CGCM3,
ii3$WRFG_CGCM3,gg4$WRFG_CGCM3,hh4$WRFG_CGCM3,ii4$WRFG_CGCM3)

data6<-rbind(gg$RCM3_CGCM3,hh$RCM3_CGCM3,ii$RCM3_CGCM3,gg2$RCM3_CGCM3,
hh2$RCM3_CGCM3,ii2$RCM3_CGCM3,gg3$RCM3_CGCM3,hh3$RCM3_CGCM3,
ii3$RCM3_CGCM3,gg4$RCM3_CGCM3,hh4$RCM3_CGCM3,ii4$RCM3_CGCM3)
data7<-rbind(gg$CRCM_CGCM3,hh$CRCM_CGCM3,ii$CRCM_CGCM3,gg2$CRCM_CGCM3,
hh2$CRCM_CGCM3,ii2$CRCM_CGCM3,gg3$CRCM_CGCM3,hh3$CRCM_CGCM3,
ii3$CRCM_CGCM3,gg4$CRCM_CGCM3,hh4$CRCM_CGCM3,ii4$CRCM_CGCM3)

data8<-rbind(gg$CRCM_CCSM,hh$CRCM_CCSM,ii$CRCM_CCSM,gg2$CRCM_CCSM,
hh2$CRCM_CCSM,ii2$CRCM_CCSM,gg3$CRCM_CCSM,hh3$CRCM_CCSM,ii3$CRCM_CCSM,
gg4$CRCM_CCSM,hh4$CRCM_CCSM,ii4$CRCM_CCSM)

data10<-rbind(gg$GFDL_TS,hh$GFDL_TS,ii$GFDL_TS,gg2$GFDL_TS,hh2$GFDL_TS,
ii2$GFDL_TS,gg3$GFDL_TS,hh3$GFDL_TS,ii3$GFDL_TS,gg4$GFDL_TS,
hh4$GFDL_TS,ii4$GFDL_TS)
```

```
#combine each of the data frames into a larger data frame and put each
#into their own column
data<-cbind(data1,data2,data3,data4,data5,data6,data7,data8,data10)

#open a new blank window for plotting
windows()

#this is a call to say where the hovmoller plot will be saved, what it
#will be called and its dimensions
png(filename = "C://Dissertation//east_tmin_hovmoller.png", width =
1250, height = 800,units = "px", pointsize = 13.5, bg = "white",
res = 130,restoreConsole = TRUE)

#create the hovmoller plot using the R script "myImagePlot.R"
myImagePlot(data,zlim=c(0.4,1),title=c("East Subregion Tmin Perkins'
skill scores"),xLabels=c("MM5I-CC","RCM3-GF","ECP2-GF","WRFG-CC",
"WRFG-CG3","RCM3-CG3","CRCM-CG3","CRCM-CC","GFDL-TS"),yLabels=c("Dec",
"Jan","Feb","Mar","Apr","May","Jun","Jul","Aug","Sep","Oct","Nov"))

#turn off the graphics driver
dev.off()

##########################################################################
#Code for myImagePlot.R
##########################################################################
# ----- Define a function for plotting a matrix ----- #
myImagePlot <- function(x, ...){
     min <- min(x)
     max <- max(x)
     yLabels <- rownames(x)
     xLabels <- colnames(x)
     title <-c()
  # check for additional function arguments
  if( length(list(...)) ){
    Lst <- list(...)
    if( !is.null(Lst$zlim) ){
       min <- Lst$zlim[1]
       max <- Lst$zlim[2]
    }
    if( !is.null(Lst$yLabels) ){
       yLabels <- c(Lst$yLabels)
    }
    if( !is.null(Lst$xLabels) ){
       xLabels <- c(Lst$xLabels)
    }
    if( !is.null(Lst$title) ){
       title <- Lst$title
    }
  }
# check for null values
if( is.null(xLabels) ){
   xLabels <- c(1:ncol(x))
}
if( is.null(yLabels) ){
   yLabels <- c(1:nrow(x))
}
```

```
layout(matrix(data=c(1,2), nrow=1, ncol=2), widths=c(6,1),
heights=c(1,1))

 # Red and green range from 0 to 1 while Blue ranges from 1 to 0
 ColorRamp <- rgb( seq(0,1,length=255),  # Red
                   seq(0,1,length=255),  # Green
                   seq(0,1,length=255))  # Blue

ramp=colorRamp(c("blue","white","red"),space ="rgb")
kleur <- rgb( ramp(seq(0,1,length=255)),max = 255)

ColorLevels <- seq(min, max, length=length(kleur))

# Reverse Y axis
 reverse <- nrow(x) : 1
 yLabels <- yLabels[reverse]
 x <- x[reverse,]

 # Data Map
 par(mar = c(3,5,2.5,2))
 image(1:length(xLabels), 1:length(yLabels), t(x), col=kleur, xlab="",
 ylab="", axes=FALSE, zlim=c(min,max))
 if( !is.null(title) ){
    title(main=title)
 }
axis(BELOW<-1, at=1:length(xLabels), labels=xLabels, cex.axis=0.7)
 axis(LEFT <-2, at=1:length(yLabels), labels=yLabels, las= HORIZONTAL<-
1,
 cex.axis=0.7)

 # Color Scale
 par(mar = c(3,2.5,2.5,2))
 image(1, ColorLevels,
      matrix(data=ColorLevels, ncol=length(ColorLevels),nrow=1),
      col=kleur,
      xlab="",ylab="",
      xaxt="n")

 layout(1)
}
# ----- END plot function ----- #
```

B.6 PERCENTILE CALCULATION AND PLOT SCRIPT

This code creates the percentile plots:

```
#read in the data from one month
gg<-read.csv(file="C:\\Dissertation\\tasmin_east_dec.csv",
sep=",",header=T)

#sort extract observation and model data from the data file then sort
#each of their values from smallest to largest
a1<-sort(gg$Obs)
```

```
b1<-sort(gg$MM5I_CCSM)
c1<-sort(gg$RCM3_GFDL)
d1<-sort(gg$ECP2_GFDL)
e1<-sort(gg$WRFG_CCSM)
f1<-sort(gg$WRFG_CGCM3)
g1<-sort(gg$RCM3_CGCM3)
h1<-sort(gg$CRCM_CGCM3)
i1<-sort(gg$CRCM_CCSM)
k1<-sort(gg$GFDL_TS)

#save the sorted values as new variables
aa1<-a1
bb1<-b1
cc1<-c1
dd1<-d1
ee1<-e1
ff1<-f1
gg1<-g1
hh1<-h1
ii1<-i1
kk1<-k1

#find the quantile values for observations and model data
aaa1<-quantile(aa1,c(0.01,0.05,0.1,0.25,0.5,0.75,0.9,0.95,0.99))
bbb1<-quantile(bb1,c(0.01,0.05,0.1,0.25,0.5,0.75,0.9,0.95,0.99))
ccc1<-quantile(cc1,c(0.01,0.05,0.1,0.25,0.5,0.75,0.9,0.95,0.99))
ddd1<-quantile(dd1,c(0.01,0.05,0.1,0.25,0.5,0.75,0.9,0.95,0.99))
eee1<-quantile(ee1,c(0.01,0.05,0.1,0.25,0.5,0.75,0.9,0.95,0.99))
fff1<-quantile(ff1,c(0.01,0.05,0.1,0.25,0.5,0.75,0.9,0.95,0.99))
ggg1<-quantile(gg1,c(0.01,0.05,0.1,0.25,0.5,0.75,0.9,0.95,0.99))
hhh1<-quantile(hh1,c(0.01,0.05,0.1,0.25,0.5,0.75,0.9,0.95,0.99))
iii1<-quantile(ii1,c(0.01,0.05,0.1,0.25,0.5,0.75,0.9,0.95,0.99))
kkk1<-quantile(kk1,c(0.01,0.05,0.1,0.25,0.5,0.75,0.9,0.95,0.99))

#subtract each of the model's quantile values from observations to
#determine the bias at each quantile
l1<-(bbb1-aaa1)
m1<-(ccc1-aaa1)
n1<-(ddd1-aaa1)
o1<-(eee1-aaa1)
p1<-(fff1-aaa1)
q1<-(ggg1-aaa1)
r1<-(hhh1-aaa1)
s1<-(iii1-aaa1)
v1<-(kkk1-aaa1)
#define some values which will be used to create plots
tt1<-seq(1,9,by=1)
ys<-seq(-14,9, by=1)

tt2<-seq(0,10,by=1)
xs<-rep(0,11)

#open a new, blank window
windows()

#define where and what the image will be saved as well as dimensions
```

```
png(filename = "C://Dissertation//percentile_plots_tmin_east_djf.png",
width = 1250, height = 430,units = "px", pointsize = 15, bg = "white",
res = 120,restoreConsole = TRUE)

#creates the spacing needed to create a plot of 1x3 sub-figures
lvec = c(1:3)
layout(matrix(lvec,nrow=1,byrow=TRUE),
heights=c(rep(1.5,3)),widths=c(rep(1,3)))
par(mai=c(0.35,0.3,0.3,0.3))

#plots the first variable
plot(tt1,l1,xlim=c(0.5,9.5),axes=FALSE,ylim=c(-10.5,8),col="red",
pch=49,ylab="Temperature Bias (degrees C)",xlab="Percentiles")

#creates a solid line at 0 degree C bias
abline(h = ys, v = tt1, col = "gray", lty = "dotted")

#plots the lines and points of the remaining models
lines(tt2,xs,type="l",col="black", lwd=1)
lines(tt1,l1,type="l",col="red")
points(tt1,m1,pch=50,col="blue")
lines(tt1,m1,type="l",col="blue")
points(tt1,n1,pch=51,col="green")
lines(tt1,n1,type="l",col="green")
points(tt1,o1,pch=52,col="mediumorchid3")
lines(tt1,o1,type="l",col="mediumorchid3")
points(tt1,p1,pch=53,col="darkgreen")
lines(tt1,p1,type="l",col="darkgreen")
points(tt1,q1,pch=54,col="cyan3")
lines(tt1,q1,type="l",col="cyan3")
points(tt1,r1,pch=55,col="black")
lines(tt1,r1,type="l",col="black")
points(tt1,s1,pch=56,col="orange")
lines(tt1,s1,type="l",col="orange")
#points(tt1,u1,pch="i",col="gray40")
#lines(tt1,u1,type="l",col="gray40")
points(tt1,v1,pch=57,col="gray40")
lines(tt1,v1,type="l",col="gray40")
text(1,7.25,"a)")

#overwrites the default axis labels
axis(1,at=1:9,lab=c("1","5","10","25","50","75","90","95","99"))
axis(2, at=c(-10,-8,-6,-4,-2,0,2,4,6,8),lab=c("-10","-8","-6","-4",
"-2","0","2","4","6","8"))
box()

dev.off()
```

B.7 HIERARCHICAL CLUSTERING SCRIPT

```
library(pvclust)
library(plyr)
library(gtools)
```

```
gg<-read.csv(file="H:\\Dissertation\\tasmin_west_dec.csv",
sep=",",header=T)
hh<-read.csv(file="H:\\Dissertation\\tasmin_west_jan.csv",
sep=",",header=T)
ii<-read.csv(file="H:\\Dissertation\\tasmin_west_feb.csv",
sep=",",header=T)
gg2<-read.csv(file="H:\\Dissertation\\tasmin_west_mar.csv",
sep=",",header=T)
hh2<-read.csv(file="H:\\Dissertation\\tasmin_west_apr.csv",
sep=",",header=T)
ii2<-read.csv(file="H:\\Dissertation\\tasmin_west_may.csv",
sep=",",header=T)
gg3<-read.csv(file="H:\\Dissertation\\tasmin_west_jun.csv",
sep=",",header=T)
hh3<-read.csv(file="H:\\Dissertation\\tasmin_west_jul.csv",
sep=",",header=T)
ii3<-read.csv(file="H:\\Dissertation\\tasmin_west_aug.csv",
sep=",",header=T)
gg4<-read.csv(file="H:\\Dissertation\\tasmin_west_sep.csv",
sep=",",header=T)
hh4<-read.csv(file="H:\\Dissertation\\tasmin_west_oct.csv",
sep=",",header=T)
ii4<-read.csv(file="H:\\Dissertation\\tasmin_west_nov.csv",
sep=",",header=T)
gg5<-read.csv(file="H:\\Dissertation\\tasmin_GCM_west_dec.csv",
sep=",",header=T)
hh5<-read.csv(file="H:\\Dissertation\\tasmin_GCM_west_jan.csv",
sep=",",header=T)
ii5<-read.csv(file="H:\\Dissertation\\tasmin_GCM_west_feb.csv",
sep=",",header=T)
gg6<-read.csv(file="H:\\Dissertation\\tasmin_GCM_west_mar.csv",
sep=",",header=T)
hh6<-read.csv(file="H:\\Dissertation\\tasmin_GCM_west_apr.csv",
sep=",",header=T)
ii6<-read.csv(file="H:\\Dissertation\\tasmin_GCM_west_may.csv",
sep=",",header=T)
gg7<-read.csv(file="H:\\Dissertation\\tasmin_GCM_west_jun.csv",
sep=",",header=T)
hh7<-read.csv(file="H:\\Dissertation\\tasmin_GCM_west_jul.csv",
sep=",",header=T)
ii7<-read.csv(file="H:\\Dissertation\\tasmin_GCM_west_aug.csv",
sep=",",header=T)
gg8<-read.csv(file="H:\\Dissertation\\tasmin_GCM_west_sep.csv",
sep=",",header=T)
hh8<-read.csv(file="H:\\Dissertation\\tasmin_GCM_west_oct.csv",
sep=",",header=T)
ii8<-read.csv(file="H:\\Dissertation\\tasmin_GCM_west_nov.csv",
sep=",",header=T)

www<-rbind(gg,hh,ii,gg2,hh2,ii2,gg3,hh3,ii3,gg4,hh4,ii4)
wwwa<-rbind(gg5,hh5,ii5,gg6,hh6,ii6,gg7,hh7,ii7,gg8,hh8,ii8)

www1<-www$Obs
www2<-www$MM5I_CCSM
www3<-www$RCM3_GFDL
www4<-www$ECP2_GFDL
www5<-www$WRFG_CCSM
```

```
www6<-www$WRFG_CGCM3
www7<-www$RCM3_CGCM3
www8<-www$CRCM_CGCM3
www9<-www$CRCM_CCSM
www11<-www$GFDL_TS
www12<-wwwa$CCSM
www13<-wwwa$GFDL
www14<-wwwa$CGCM3

wwww<-cbind(www1,www2,www3,www4,www5,www6,www7,www8,www9,www11,
www12,www13,www14)

write.table(wwww,file="H:\\Dissertation\\tasmin_west_all_data.csv",sep=
",", quote=F, col.names=c("Obs","MM5I-CCSM","RCM3-GFDL","ECP2-GFDL",
"WRFG-CCSM","WRFG-CGCM3","RCM3-CGCM3","CRCM-CGCM3","CRCM-CCSM","GFDL-
TS","CCSM","GFDL","CGCM3"))

wtasmin<-read.csv(file="H:\\Dissertation\\tasmin_west_all_data.csv",
sep=",",header=T)

fit_wtmin <- pvclust(wtasmin, method.hclust="ward",
method.dist="euclidean")

windows()

png(filename = "H://Dissertation//tasmin_west_all_data_ward_euc.png",
width = 1000, height = 800,units = "px", pointsize = 13.5, bg =
"white", res = 130,restoreConsole = TRUE)
plot(fit_wtmin)


dev.off()
```

B.8 BOOTSTRAP AND SIGNIFICANCE TEST SCRIPT

```
library(plyr)

present<-
read.csv(file="H:\\Future_model_work\\tmax_CRCM_ccsm_extract_east_30yr_
mon_aves_present.csv",sep=",",header=T)
future<-
read.csv(file="H:\\Future_model_work\\tmax_CRCM_ccsm_extract_east_30yr_
mon_aves_future.csv",sep=",",header=T)
model<-read.csv(file="H:\\Future_model_work\\tas_CRCM_ccsm_fut-
ref_max_extract_east.csv",sep=",",header=T)

janf=data.frame(future[c(1,13,25,37,49,61,73,85,97,109,121,133,145,157,
169,181,193,205,217,229,241,253,265,277,289,301,313,325,337,349),])
janc=data.frame(present[c(1,13,25,37,49,61,73,85,97,109,121,133,145,157
,169,181,193,205,217,229,241,253,265,277,289,301,313,325,337,349),])
janm=model[1,]

jan_meanf=stack(janf)
jan_meanc=stack(janc)
```

```
janfu=c(jan_meanf$values)
jancu=c(jan_meanc$values)

func<- function(x) replicate(10000,sample(x, replace = T))

sampf<-func(janfu)
sampc<-func(jancu)

meanf<-colMeans(sampf)
meanc<-colMeans(sampc)

diff1<-meanf-meanc

sigj1<-quantile(diff1,  probs =
c(0.001,0.01,0.05,0.1,0.9,0.95,0.99,0.999),na.rm=T)
mod1<-rowMeans(janm)

test1<-0

test1[mod1<=sigj1[1]]<-0.01
test1[mod1<=sigj1[2] & mod1>sigj1[1]]<-0.01
test1[mod1<=sigj1[3] & mod1>sigj1[2]]<-0.05
test1[mod1<=sigj1[4] & mod1>sigj1[3]]<-0.1
test1[mod1>=sigj1[5] & mod1<sigj1[6] ]<-0.1
test1[mod1>=sigj1[6] & mod1<sigj1[7] ]<-0.05
test1[mod1>=sigj1[7] & mod1<sigj1[8] ]<-0.01
test1[mod1>=sigj1[8]]<-0.01
test1[mod1>sigj1[4] & mod1<sigj1[5] ]<-0

rm(present)
rm(future)
rm(janf)
rm(janc)
rm(janm)
rm(jan_meanf)
rm(jan_meanc)
rm(janfu)
rm(jancu)
rm(sampf)
rm(sampc)
rm(meanf)
rm(meanc)
gc()

present<-
read.csv(file="H:\\Future_model_work\\tmax_CRCM_cgcm3_extract_east_30yr
_mon_aves_present.csv",sep=",",header=T)
future<-
read.csv(file="H:\\Future_model_work\\tmax_CRCM_cgcm3_extract_east_30yr
_mon_aves_future.csv",sep=",",header=T)
model<-read.csv(file="H:\\Future_model_work\\tas_CRCM_cgcm3_fut-
ref_max_extract_east.csv",sep=",",header=T)

janf=data.frame(future[c(1,13,25,37,49,61,73,85,97,109,121,133,145,157,
169,181,193,205,217,229,241,253,265,277,289,301,313,325,337,349),])
```

```
janc=data.frame(present[c(1,13,25,37,49,61,73,85,97,109,121,133,145,157
,169,181,193,205,217,229,241,253,265,277,289,301,313,325,337,349),])
janm=model[1,]

jan_meanf=stack(janf)
jan_meanc=stack(janc)

janfu=c(jan_meanf$values)
jancu=c(jan_meanc$values)

func<- function(x) replicate(10000,sample(x, replace = T))

sampf<-func(janfu)
sampc<-func(jancu)

meanf<-colMeans(sampf)
meanc<-colMeans(sampc)

diff2<-meanf-meanc

sigj2<-quantile(diff2,  probs =
c(0.001,0.01,0.05,0.1,0.9,0.95,0.99,0.999),na.rm=T)
mod2<-rowMeans(janm)

test2<-0

test2[mod2<=sigj2[1]]<-0.01
test2[mod2<=sigj2[2] & mod2>sigj2[1]]<-0.01
test2[mod2<=sigj2[3] & mod2>sigj2[2]]<-0.05
test2[mod2<=sigj2[4] & mod2>sigj2[3]]<-0.1
test2[mod2>=sigj2[5] & mod2<sigj2[6] ]<-0.1
test2[mod2>=sigj2[6] & mod2<sigj2[7] ]<-0.05
test2[mod2>=sigj2[7] & mod2<sigj2[8] ]<-0.01
test2[mod2>=sigj2[8]]<-0.01
test2[mod2>sigj2[4] & mod2<sigj2[5] ]<-0

rm(present)
rm(future)
rm(janf)
rm(janc)
rm(janm)
rm(jan_meanf)
rm(jan_meanc)
rm(janfu)
rm(jancu)
rm(sampf)
rm(sampc)
rm(meanf)
rm(meanc)
gc()


present<-
read.csv(file="H:\\Future_model_work\\tmax_RCM3_cgcm3_extract_east_30yr
_mon_aves_present.csv",sep=",",header=T)
```

```
future<-
read.csv(file="H:\\Future_model_work\\tmax_RCM3_cgcm3_extract_east_30yr
_mon_aves_future.csv",sep=",",header=T)
model<-read.csv(file="H:\\Future_model_work\\tas_RCM3_cgcm3_fut-
ref_max_extract_east.csv",sep=",",header=T)

janf=data.frame(future[c(1,13,25,37,49,61,73,85,97,109,121,133,145,157,
169,181,193,205,217,229,241,253,265,277,289,301,313,325,337,349),])
janc=data.frame(present[c(1,13,25,37,49,61,73,85,97,109,121,133,145,157
,169,181,193,205,217,229,241,253,265,277,289,301,313,325,337,349),])
janm=model[1,]

janf=data.frame(future[c(1,13,25,37,49,61,73,85,97,109,121,133,145,157,
169,181,193,205,217,229,241,253,265,277,289,301,313,325,337,349),])
janc=data.frame(present[c(1,13,25,37,49,61,73,85,97,109,121,133,145,157
,169,181,193,205,217,229,241,253,265,277,289,301,313,325,337,349),])
janm=model[1,]

jan_meanf=stack(janf)
jan_meanc=stack(janc)

janfu=c(jan_meanf$values)
jancu=c(jan_meanc$values)

func<- function(x) replicate(10000,sample(x, replace = T))

sampf<-func(janfu)
sampc<-func(jancu)

meanf<-colMeans(sampf)
meanc<-colMeans(sampc)


diff3<-meanf-meanc

sigj3<-quantile(diff3,  probs =
c(0.001,0.01,0.05,0.1,0.9,0.95,0.99,0.999),na.rm=T)
mod3<-rowMeans(janm)

test3<-0

test3[mod3<=sigj3[1]]<-0.01
test3[mod3<=sigj3[2] & mod3>sigj3[1]]<-0.01
test3[mod3<=sigj3[3] & mod3>sigj3[2]]<-0.05
test3[mod3<=sigj3[4] & mod3>sigj3[3]]<-0.1
test3[mod3>=sigj3[5] & mod3<sigj3[6] ]<-0.1
test3[mod3>=sigj3[6] & mod3<sigj3[7] ]<-0.05
test3[mod3>=sigj3[7] & mod3<sigj3[8] ]<-0.01
test3[mod3>=sigj3[8]]<-0.01
test3[mod3>sigj3[4] & mod3<sigj3[5] ]<-0

rm(present)
rm(future)
rm(janf)
rm(janc)
rm(janm)
rm(jan_meanf)
```

```
rm(jan_meanc)
rm(janfu)
rm(jancu)
rm(sampf)
rm(sampc)
rm(meanf)
rm(meanc)
gc()


present<-
read.csv(file="H:\\Future_model_work\\tmax_RCM3_gfdl_extract_east_30yr_
mon_aves_present.csv",sep=",",header=T)
future<-
read.csv(file="H:\\Future_model_work\\tmax_RCM3_gfdl_extract_east_30yr_
mon_aves_future.csv",sep=",",header=T)
model<-read.csv(file="H:\\Future_model_work\\tas_RCM3_gfdl_fut-
ref_max_extract_east.csv",sep=",",header=T)

janf=data.frame(future[c(1,13,25,37,49,61,73,85,97,109,121,133,145,157,
169,181,193,205,217,229,241,253,265,277,289,301,313,325,337,349),])
janc=data.frame(present[c(1,13,25,37,49,61,73,85,97,109,121,133,145,157
,169,181,193,205,217,229,241,253,265,277,289,301,313,325,337,349),])
janm=model[1,]

jan_meanf=stack(janf)
jan_meanc=stack(janc)

janfu=c(jan_meanf$values)
jancu=c(jan_meanc$values)

func<- function(x) replicate(10000,sample(x, replace = T))

sampf<-func(janfu)
sampc<-func(jancu)

meanf<-colMeans(sampf)
meanc<-colMeans(sampc)

diff4<-meanf-meanc

sigj4<-quantile(diff4,  probs =
c(0.001,0.01,0.05,0.1,0.9,0.95,0.99,0.999),na.rm=T)
mod4<-rowMeans(janm)

test4<-0

test4[mod4<=sigj4[1]]<-0.01
test4[mod4<=sigj4[2] & mod4>sigj4[1]]<-0.01
test4[mod4<=sigj4[3] & mod4>sigj4[2]]<-0.05
test4[mod4<=sigj4[4] & mod4>sigj4[3]]<-0.1
test4[mod4>=sigj4[5] & mod4<sigj4[6] ]<-0.1
test4[mod4>=sigj4[6] & mod4<sigj4[7] ]<-0.05
test4[mod4>=sigj4[7] & mod4<sigj4[8] ]<-0.01
test4[mod4>=sigj4[8]]<-0.01
test4[mod4>sigj4[4] & mod4<sigj4[5] ]<-0
```

```
rm(present)
rm(future)
rm(janf)
rm(janc)
rm(janm)
rm(jan_meanf)
rm(jan_meanc)
rm(janfu)
rm(jancu)
rm(sampf)
rm(sampc)
rm(meanf)
rm(meanc)
gc()


present<-
read.csv(file="H:\\Future_model_work\\tmax_ECP2_gfdl_extract_east_30yr_
mon_aves_present.csv",sep=",",header=T)
future<-
read.csv(file="H:\\Future_model_work\\tmax_ECP2_gfdl_extract_east_30yr_
mon_aves_future.csv",sep=",",header=T)
model<-read.csv(file="H:\\Future_model_work\\tas_ECP2_gfdl_fut-
ref_max_extract_east.csv",sep=",",header=T)

janf=data.frame(future[c(1,13,25,37,49,61,73,85,97,109,121,133,145,157,
169,181,193,205,217,229,241,253,265,277,289,301,313,325,337,349),])
janc=data.frame(present[c(1,13,25,37,49,61,73,85,97,109,121,133,145,157
,169,181,193,205,217,229,241,253,265,277,289,301,313,325,337,349),])
janm=model[1,]

jan_meanf=stack(janf)
jan_meanc=stack(janc)

janfu=c(jan_meanf$values)
jancu=c(jan_meanc$values)

func<- function(x) replicate(10000,sample(x, replace = T))

sampf<-func(janfu)
sampc<-func(jancu)

meanf<-colMeans(sampf)
meanc<-colMeans(sampc)

diff5<-meanf-meanc

sigj5<-quantile(diff5,  probs =
c(0.001,0.01,0.05,0.1,0.9,0.95,0.99,0.999),na.rm=T)
mod5<-rowMeans(janm)

test5<-0

test5[mod5<=sigj5[1]]<-0.01
test5[mod5<=sigj5[2] & mod5>sigj5[1]]<-0.01
test5[mod5<=sigj5[3] & mod5>sigj5[2]]<-0.05
test5[mod5<=sigj5[4] & mod5>sigj5[3]]<-0.1
```

```
test5[mod5>=sigj5[5] & mod5<sigj5[6] ]<-0.1
test5[mod5>=sigj5[6] & mod5<sigj5[7] ]<-0.05
test5[mod5>=sigj5[7] & mod5<sigj5[8] ]<-0.01
test5[mod5>=sigj5[8]]<-0.01
test5[mod5>sigj5[4] & mod5<sigj5[5] ]<-0

rm(present)
rm(future)
rm(janf)
rm(janc)
rm(janm)
rm(jan_meanf)
rm(jan_meanc)
rm(janfu)
rm(jancu)
rm(sampf)
rm(sampc)
rm(meanf)
rm(meanc)
gc()

present<-
read.csv(file="H:\\Future_model_work\\tmax_MM5I_ccsm_extract_east_30yr_
mon_aves_present.csv",sep=",",header=T)
future<-
read.csv(file="H:\\Future_model_work\\tmax_MM5I_ccsm_extract_east_30yr_
mon_aves_future.csv",sep=",",header=T)
model<-read.csv(file="H:\\Future_model_work\\tas_MM5I_ccsm_fut-
ref_max_extract_east.csv",sep=",",header=T)

janf=data.frame(future[c(1,13,25,37,49,61,73,85,97,109,121,133,145,157,
169,181,193,205,217,229,241,253,265,277,289,301,313,325,337,349),])
janc=data.frame(present[c(1,13,25,37,49,61,73,85,97,109,121,133,145,157
,169,181,193,205,217,229,241,253,265,277,289,301,313,325,337,349),])
janm=model[1,]

jan_meanf=stack(janf)
jan_meanc=stack(janc)

janfu=c(jan_meanf$values)
jancu=c(jan_meanc$values)

func<- function(x) replicate(10000,sample(x, replace = T))

sampf<-func(janfu)
sampc<-func(jancu)

meanf<-colMeans(sampf)
meanc<-colMeans(sampc)

diff6<-meanf-meanc

sigj6<-quantile(diff6,  probs =
c(0.001,0.01,0.05,0.1,0.9,0.95,0.99,0.999),na.rm=T)
mod6<-rowMeans(janm)

test6<-0
```

```
test6[mod6<=sigj6[1]]<-0.01
test6[mod6<=sigj6[2] & mod6>sigj6[1]]<-0.01
test6[mod6<=sigj6[3] & mod6>sigj6[2]]<-0.05
test6[mod6<=sigj6[4] & mod6>sigj6[3]]<-0.1
test6[mod6>=sigj6[5] & mod6<sigj6[6] ]<-0.1
test6[mod6>=sigj6[6] & mod6<sigj6[7] ]<-0.05
test6[mod6>=sigj6[7] & mod6<sigj6[8] ]<-0.01
test6[mod6>=sigj6[8]]<-0.01
test6[mod6>sigj6[4] & mod6<sigj6[5] ]<-0

rm(present)
rm(future)
rm(janf)
rm(janc)
rm(janm)
rm(jan_meanf)
rm(jan_meanc)
rm(janfu)
rm(jancu)
rm(sampf)
rm(sampc)
rm(meanf)
rm(meanc)
gc()

present<-
read.csv(file="H:\\Future_model_work\\tmax_WRFG_ccsm_extract_east_30yr_
mon_aves_present.csv",sep=",",header=T)
future<-
read.csv(file="H:\\Future_model_work\\tmax_WRFG_ccsm_extract_east_30yr_
mon_aves_future.csv",sep=",",header=T)
model<-read.csv(file="H:\\Future_model_work\\tas_WRFG_ccsm_fut-
ref_max_extract_east.csv",sep=",",header=T)

janf=data.frame(future[c(1,13,25,37,49,61,73,85,97,109,121,133,145,157,
169,181,193,205,217,229,241,253,265,277,289,301,313,325,337,349),])
janc=data.frame(present[c(1,13,25,37,49,61,73,85,97,109,121,133,145,157
,169,181,193,205,217,229,241,253,265,277,289,301,313,325,337,349),])
janm=model[1,]

jan_meanf=stack(janf)
jan_meanc=stack(janc)

janfu=c(jan_meanf$values)
jancu=c(jan_meanc$values)

func<- function(x) replicate(10000,sample(x, replace = T))

sampf<-func(janfu)
sampc<-func(jancu)

meanf<-colMeans(sampf)
meanc<-colMeans(sampc)

diff7<-meanf-meanc
```

```
sigj7<-quantile(diff7,  probs =
c(0.001,0.01,0.05,0.1,0.9,0.95,0.99,0.999),na.rm=T)
mod7<-rowMeans(janm)

test7<-0

test7[mod7<=sigj7[1]]<-0.01
test7[mod7<=sigj7[2] & mod7>sigj7[1]]<-0.01
test7[mod7<=sigj7[3] & mod7>sigj7[2]]<-0.05
test7[mod7<=sigj7[4] & mod7>sigj7[3]]<-0.1
test7[mod7>=sigj7[5] & mod7<sigj7[6] ]<-0.1
test7[mod7>=sigj7[6] & mod7<sigj7[7] ]<-0.05
test7[mod7>=sigj7[7] & mod7<sigj7[8] ]<-0.01
test7[mod7>=sigj7[8]]<-0.01
test7[mod7>sigj7[4] & mod7<sigj7[5] ]<-0

rm(present)
rm(future)
rm(janf)
rm(janc)
rm(janm)
rm(jan_meanf)
rm(jan_meanc)
rm(janfu)
rm(jancu)
rm(sampf)
rm(sampc)
rm(meanf)
rm(meanc)
gc()

present<-
read.csv(file="H:\\Future_model_work\\tmax_WRFG_cgcm3_extract_east_30yr
_mon_aves_present.csv",sep=",",header=T)
future<-
read.csv(file="H:\\Future_model_work\\tmax_WRFG_cgcm3_extract_east_30yr
_mon_aves_future.csv",sep=",",header=T)
model<-read.csv(file="H:\\Future_model_work\\tas_WRFG_cgcm3_fut-
ref_max_extract_east.csv",sep=",",header=T)

janf=data.frame(future[c(1,13,25,37,49,61,73,85,97,109,121,133,145,157,
169,181,193,205,217,229,241,253,265,277,289,301,313,325,337,349),])
janc=data.frame(present[c(1,13,25,37,49,61,73,85,97,109,121,133,145,157
,169,181,193,205,217,229,241,253,265,277,289,301,313,325,337,349),])
janm=model[1,]

jan_meanf=stack(janf)
jan_meanc=stack(janc)

janfu=c(jan_meanf$values)
jancu=c(jan_meanc$values)

func<- function(x) replicate(10000,sample(x, replace = T))

sampf<-func(janfu)
sampc<-func(jancu)
```

```
meanf<-colMeans(sampf)
meanc<-colMeans(sampc)

diff8<-meanf-meanc

sigj8<-quantile(diff8,  probs =
c(0.001,0.01,0.05,0.1,0.9,0.95,0.99,0.999),na.rm=T)
mod8<-rowMeans(janm)

test8<-0

test8[mod8<=sigj8[1]]<-0.01
test8[mod8<=sigj8[2] & mod8>sigj8[1]]<-0.01
test8[mod8<=sigj8[3] & mod8>sigj8[2]]<-0.05
test8[mod8<=sigj8[4] & mod8>sigj8[3]]<-0.1
test8[mod8>=sigj8[5] & mod8<sigj8[6] ]<-0.1
test8[mod8>=sigj8[6] & mod8<sigj8[7] ]<-0.05
test8[mod8>=sigj8[7] & mod8<sigj8[8] ]<-0.01
test8[mod8>=sigj8[8]]<-0.01
test8[mod8>sigj8[4] & mod8<sigj8[5] ]<-0

rm(present)
rm(future)
rm(janf)
rm(janc)
rm(janm)
rm(jan_meanf)
rm(jan_meanc)
rm(janfu)
rm(jancu)
rm(sampf)
rm(sampc)
rm(meanf)
rm(meanc)
gc()

present<-
read.csv(file="H:\\Future_model_work\\tmax_gfdl_extract_east_30yr_mon_a
ves_present.csv",sep=",",header=T)
future<-
read.csv(file="H:\\Future_model_work\\tmax_gfdl_extract_east_30yr_mon_a
ves_future.csv",sep=",",header=T)
model<-read.csv(file="H:\\Future_model_work\\tas_GFDL_ts_fut-
ref_max_extract_east.csv",sep=",",header=T)

janf=data.frame(future[c(1,13,25,37,49,61,73,85,97,109,121,133,145,157,
169,181,193,205,217,229,241,253,265,277,289,301,313,325,337,349),])
janc=data.frame(present[c(1,13,25,37,49,61,73,85,97,109,121,133,145,157
,169,181,193,205,217,229,241,253,265,277,289,301,313,325,337,349),])
janm=model[1,]

jan_meanf=stack(janf)
jan_meanc=stack(janc)

janfu=c(jan_meanf$values)
jancu=c(jan_meanc$values)
```

```
func<- function(x) replicate(10000,sample(x, replace = T))

sampf<-func(janfu)
sampc<-func(jancu)

meanf<-colMeans(sampf)
meanc<-colMeans(sampc)

diff9<-meanf-meanc

sigj9<-quantile(diff9,  probs =
c(0.001,0.01,0.05,0.1,0.9,0.95,0.99,0.999),na.rm=T)
mod9<-rowMeans(janm)

test9<-0

test9[mod9<=sigj9[1]]<-0.01
test9[mod9<=sigj9[2] & mod9>sigj9[1]]<-0.01
test9[mod9<=sigj9[3] & mod9>sigj9[2]]<-0.05
test9[mod9<=sigj9[4] & mod9>sigj9[3]]<-0.1
test9[mod9>=sigj9[5] & mod9<sigj9[6] ]<-0.1
test9[mod9>=sigj9[6] & mod9<sigj9[7] ]<-0.05
test9[mod9>=sigj9[7] & mod9<sigj9[8] ]<-0.01
test9[mod9>=sigj9[8]]<-0.01
test9[mod9>sigj9[4] & mod9<sigj9[5] ]<-0

tests1<-table(c(test1,test2,test3,test4,test5,test6,test7,test8,test9))

rm(present)
rm(future)
rm(janf)
rm(janc)
rm(janm)
rm(jan_meanf)
rm(jan_meanc)
rm(janfu)
rm(jancu)
rm(sampf)
rm(sampc)
rm(meanf)
rm(meanc)
gc()

write.table(tests1,file="H:\\Dissertation\\tmax_east_stat_sig_jan.csv",
sep=",",col.names=F, quote=F,
row.names=F)
```

APPENDIX C – PERKINS SKILL SCORE, WILLMOTT'S INDEX OF AGREEMENT, RMSE, AND MAE TABLES

Table C.1. East sub-region minimum temperature values of Perkins skill score (SS) and Willmott's index of agreement (W).

	MM5I-CCSM		RCM3-GFDL		ECP2-GFDL		WRFG-CCSM		WRFG-CGCM3		RCM3-CGCM3		CRCM-CGCM3		CRCM-CCSM		GFDL-TIMESLICE	
	SS	W	SS	W	SS	W	SS	W	SS	W	SS	W	SS	W	SS	W	SS	W
Dec	0.88	0.96	0.76	0.64	0.83	0.63	0.87	0.82	0.85	0.88	0.90	0.90	0.87	0.93	0.85	0.90	0.85	0.91
Jan	0.86	0.85	0.76	0.65	0.79	0.53	0.91	0.87	0.84	0.82	0.90	0.90	0.85	0.88	0.85	0.90	0.85	0.91
Feb	0.85	0.83	0.77	0.66	0.78	0.50	0.86	0.88	0.86	0.88	0.89	0.88	0.89	0.96	0.85	0.89	0.86	0.90
Mar	0.87	0.90	0.78	0.63	0.78	0.59	0.87	0.90	0.92	0.97	0.89	0.84	0.91	0.91	0.88	0.88	0.82	0.84
Apr	0.78	0.81	0.88	0.82	0.88	0.86	0.76	0.74	0.90	0.93	0.94	0.93	0.95	0.99	0.85	0.79	0.89	0.91
May	0.80	0.85	0.93	0.94	0.93	0.93	0.94	0.95	0.98	0.97	0.93	0.91	0.93	0.92	0.87	0.82	0.87	0.83
Jun	0.78	0.87	0.82	0.88	0.86	0.74	0.85	0.81	0.81	0.73	0.88	0.90	0.94	0.94	0.85	0.75	0.75	0.51
Jul	0.77	0.72	0.86	0.90	0.68	0.46	0.66	0.46	0.57	0.26	0.89	0.93	0.96	0.97	0.83	0.56	0.68	0.01
Aug	0.72	0.61	0.88	0.88	0.68	0.63	0.66	0.59	0.63	0.48	0.93	0.89	0.90	0.85	0.85	0.59	0.72	0.19
Sept	0.85	0.84	0.88	0.86	0.82	0.80	0.79	0.75	0.79	0.69	0.95	0.97	0.88	0.86	0.93	0.88	0.86	0.77
Oct	0.84	0.80	0.93	0.96	0.92	0.93	0.92	0.92	0.91	0.93	0.94	0.91	0.90	0.95	0.92	0.93	0.87	0.77
Nov	0.88	0.90	0.90	0.87	0.91	0.95	0.90	0.88	0.91	0.88	0.94	0.95	0.90	0.92	0.89	0.93	0.88	0.89

Table C.2. East sub-region minimum temperature values of mean absolute error (MAE) and root mean square error (RMSE).

	MM5I-CCSM		RCM3-GFDL		ECP2-GFDL		WRFG-CCSM		WRFG-CGCM3		RCM3-CGCM3		CRCM-CGCM3		CRCM-CCSM		GFDL-TIMESLICE	
	MAE	RMSE	MAE	RMSE	MAE	RMSE	MAE	RMSE	MAE	RMSE	MAE	RMSE	MAE	RMSE	MAE	RMSE	MAE	RMSE
Dec	1.57	1.68	3.55	3.65	2.34	2.49	1.04	1.37	1.62	1.90	0.64	0.74	0.85	1.14	0.89	1.05	1.32	1.50
Jan	2.08	2.20	4.01	4.14	3.31	3.43	0.71	0.94	1.82	2.12	0.66	0.74	1.00	1.35	1.42	1.85	1.64	1.79
Feb	1.96	2.09	3.46	3.71	3.61	3.99	0.99	1.35	1.24	1.51	1.34	1.48	0.70	0.92	1.34	1.75	1.61	1.90
Mar	1.72	1.85	3.08	3.13	3.01	3.25	1.52	1.75	0.74	0.88	1.54	1.60	1.14	1.22	1.29	1.46	2.08	2.33
Apr	2.79	2.85	1.59	1.66	1.16	1.40	2.88	2.96	1.41	1.43	0.43	0.49	0.26	0.30	1.95	1.97	0.88	0.99
May	1.88	1.94	0.63	0.68	0.83	0.97	0.52	0.61	0.11	0.14	0.58	0.63	0.78	0.84	1.26	1.28	1.23	1.34
Jun	1.40	1.44	0.74	0.84	1.42	1.55	0.66	0.74	1.09	1.15	0.43	0.50	0.51	0.53	0.92	0.95	1.88	1.92
Jul	1.27	1.28	0.55	0.59	2.08	2.15	1.60	1.71	2.34	2.43	0.29	0.33	0.20	0.30	1.05	1.11	1.85	1.98
Aug	1.51	1.52	0.79	0.94	2.07	2.12	1.61	1.75	2.05	2.12	0.22	0.28	0.43	0.52	1.00	1.04	1.66	1.82
Sept	0.97	1.03	1.27	1.42	1.57	1.60	1.34	1.47	1.61	1.69	0.28	0.31	1.37	1.62	0.36	0.67	0.89	1.13
Oct	1.93	2.08	0.60	0.65	0.72	0.78	0.75	0.86	0.79	0.92	0.65	0.69	0.90	1.05	0.61	0.77	1.42	1.57
Nov	1.90	1.98	1.20	1.28	0.94	1.15	0.82	0.97	1.46	1.60	0.42	0.62	0.70	0.84	0.82	0.89	1.08	1.27

Table C.3. West sub-region minimum temperature values of Perkins' skill score (SS) and Willmott's index of agreement (W).

	MM5I-CCSM		RCM3-GFDL		ECP2-GFDL		WRFG-CCSM		WRFG-CGCM3		RCM3-CGCM3		CRCM-CGCM3		CRCM-CCSM		GFDL-TIMESLICE	
	SS	W	SS	W	SS	W	SS	W	SS	W	SS	W	SS	W	SS	W	SS	W
Dec	0.93	0.96	0.75	0.64	0.78	0.63	0.85	0.82	0.90	0.88	0.89	0.90	0.89	0.93	0.86	0.90	0.90	0.91
Jan	0.90	0.85	0.79	0.65	0.75	0.53	0.89	0.87	0.87	0.82	0.89	0.90	0.86	0.88	0.87	0.90	0.91	0.91
Feb	0.88	0.83	0.78	0.66	0.73	0.50	0.87	0.88	0.90	0.88	0.88	0.88	0.91	0.96	0.86	0.89	0.90	0.90
Mar	0.91	0.90	0.75	0.63	0.75	0.59	0.90	0.90	0.94	0.97	0.90	0.84	0.92	0.91	0.91	0.88	0.87	0.84
Apr	0.85	0.81	0.90	0.82	0.90	0.86	0.80	0.74	0.94	0.93	0.96	0.93	0.97	0.99	0.85	0.79	0.90	0.91
May	0.86	0.85	0.91	0.94	0.93	0.93	0.92	0.95	0.97	0.97	0.94	0.91	0.94	0.92	0.86	0.82	0.88	0.83
Jun	0.86	0.87	0.83	0.88	0.85	0.74	0.80	0.81	0.78	0.73	0.85	0.90	0.96	0.94	0.81	0.75	0.67	0.51
Jul	0.82	0.72	0.90	0.90	0.64	0.46	0.55	0.46	0.49	0.26	0.89	0.93	0.96	0.97	0.74	0.56	0.50	0.01
Aug	0.72	0.61	0.90	0.88	0.71	0.63	0.61	0.59	0.59	0.48	0.89	0.89	0.88	0.85	0.75	0.59	0.53	0.19
Sept	0.83	0.84	0.91	0.86	0.84	0.80	0.72	0.75	0.76	0.69	0.94	0.97	0.92	0.86	0.89	0.88	0.81	0.77
Oct	0.84	0.80	0.95	0.96	0.91	0.93	0.90	0.92	0.94	0.93	0.93	0.91	0.94	0.95	0.93	0.93	0.82	0.77
Nov	0.92	0.90	0.91	0.87	0.93	0.95	0.86	0.88	0.92	0.88	0.93	0.95	0.93	0.92	0.91	0.93	0.89	0.89

Table C.4. West sub-region minimum temperature values of mean absolute error (MAE) and root mean square error (RMSE).

	MM5I-CCSM		RCM3-GFDL		ECP2-GFDL		WRFG-CCSM		WRFG-CGCM3		RCM3-CGCM3		CRCM-CGCM3		CRCM-CCSM		GFDL-TIMESLICE	
	MAE	RMSE	MAE	RMSE	MAE	RMSE	MAE	RMSE	MAE	RMSE	MAE	RMSE	MAE	RMSE	MAE	RMSE	MAE	RMSE
Dec	0.46	0.72	3.79	3.87	3.93	4.08	1.94	2.19	1.23	1.42	1.06	1.22	0.75	1.09	1.02	1.13	0.97	1.13
Jan	1.59	1.75	3.73	3.81	5.00	5.20	1.36	1.45	1.90	2.19	1.01	1.21	1.32	1.74	1.10	1.53	0.95	1.11
Feb	1.74	1.82	3.59	3.68	5.17	5.61	1.26	1.45	1.21	1.45	1.28	1.48	0.40	0.56	1.15	1.49	1.09	1.34
Mar	0.97	1.11	3.60	3.64	3.98	4.16	0.99	1.11	0.31	0.54	1.54	1.56	0.91	0.96	1.16	1.25	1.59	1.84
Apr	1.77	1.86	1.60	1.61	1.27	1.50	2.36	2.48	0.65	0.69	0.66	0.70	0.13	0.19	1.93	1.98	0.85	0.96
May	1.11	1.20	0.41	0.61	0.52	0.75	0.39	0.46	0.20	0.33	0.66	0.69	0.58	0.64	1.35	1.39	1.23	1.27
Jun	0.69	0.77	0.66	0.78	1.37	1.48	0.99	1.09	1.45	1.48	0.51	0.58	0.34	0.37	1.33	1.36	2.60	2.69
Jul	1.04	1.08	0.36	0.55	2.04	2.10	2.02	2.11	2.80	2.82	0.27	0.36	0.13	0.26	1.67	1.72	3.75	3.99
Aug	1.63	1.68	0.52	0.67	1.55	1.58	1.72	1.84	2.20	2.23	0.46	0.52	0.65	0.70	1.72	1.77	3.41	3.63
Sept	1.15	1.26	0.99	1.12	1.47	1.49	1.83	2.01	2.25	2.36	0.20	0.26	1.00	1.17	0.89	1.00	1.64	1.88
Oct	1.84	1.96	0.35	0.40	0.66	0.75	0.77	1.31	0.67	0.93	0.81	0.83	0.45	0.56	0.65	0.76	2.15	2.31
Nov	1.05	1.21	1.34	1.40	0.46	0.54	1.16	1.41	1.18	1.30	0.48	0.65	0.76	0.91	0.66	0.71	1.09	1.33

Table C.5. East sub-region maximum temperature values of Perkins' skill score (SS) and Willmott's index of agreement (W).

	MM5I-CCSM		RCM3-GFDL		ECP2-GFDL		WRFG-CCSM		WRFG-CGCM3		RCM3-CGCM3		CRCM-CGCM3		CRCM-CCSM		GFDL-TIMESLICE	
	SS	W	SS	W	SS	W	SS	W	SS	W	SS	W	SS	W	SS	W	SS	W
Dec	0.86	0.80	0.53	0.20	0.56	0.28	0.76	0.59	0.87	0.78	0.68	0.50	0.79	0.67	0.74	0.60	0.74	0.63
Jan	0.91	0.88	0.55	0.27	0.51	0.21	0.77	0.65	0.88	0.86	0.74	0.62	0.83	0.76	0.85	0.78	0.70	0.57
Feb	0.92	0.93	0.57	0.27	0.52	0.16	0.81	0.69	0.81	0.79	0.65	0.49	0.75	0.64	0.85	0.76	0.68	0.50
Mar	0.93	0.95	0.48	0.18	0.50	0.17	0.80	0.78	0.73	0.70	0.55	0.36	0.67	0.52	0.86	0.82	0.61	0.34
Apr	0.90	0.90	0.40	0.09	0.47	0.16	0.77	0.77	0.64	0.58	0.48	0.27	0.69	0.53	0.88	0.89	0.65	0.44
May	0.95	0.91	0.44	0.13	0.47	0.17	0.80	0.75	0.63	0.48	0.48	0.17	0.76	0.66	0.82	0.72	0.73	0.67
Jun	0.91	0.88	0.43	0.05	0.51	0.20	0.80	0.76	0.62	0.38	0.54	0.28	0.81	0.77	0.71	0.48	0.79	0.78
Jul	0.87	0.80	0.60	0.39	0.49	0.16	0.78	0.75	0.72	0.54	0.64	0.46	0.69	0.53	0.53	-0.06	0.75	0.73
Aug	0.80	0.70	0.61	0.39	0.61	0.34	0.78	0.76	0.76	0.67	0.61	0.44	0.68	0.46	0.42	-0.25	0.80	0.77
Sept	0.96	0.97	0.53	0.25	0.60	0.32	0.79	0.77	0.71	0.63	0.61	0.43	0.76	0.72	0.66	0.39	0.83	0.84
Oct	0.95	0.90	0.57	0.29	0.66	0.43	0.82	0.73	0.81	0.73	0.70	0.55	0.79	0.67	0.81	0.76	0.89	0.88
Nov	0.85	0.79	0.58	0.29	0.71	0.51	0.75	0.61	0.80	0.77	0.64	0.49	0.77	0.66	0.69	0.50	0.80	0.67

Table C.6. East sub-region maximum temperature values of mean absolute error (MAE) and root mean square error (RMSE).

	MM5I-CCSM		RCM3-GFDL		ECP2-GFDL		WRFG-CCSM		WRFG-CGCM3		RCM3-CGCM3		CRCM-CGCM3		CRCM-CCSM		GFDL-TIMESLICE	
	MAE	RMSE	MAE	RMSE	MAE	RMSE	MAE	RMSE	MAE	RMSE	MAE	RMSE	MAE	RMSE	MAE	RMSE	MAE	RMSE
Dec	2.02	2.11	8.03	8.06	7.24	7.28	4.10	4.19	2.17	2.21	5.00	5.01	3.32	3.36	3.97	4.02	3.66	3.87
Jan	1.21	1.31	7.55	7.59	8.18	8.24	3.62	3.64	1.42	1.65	3.97	4.06	2.44	2.56	2.24	2.29	4.49	4.60
Feb	0.79	0.91	7.83	7.85	9.00	9.09	3.28	3.31	2.22	2.61	5.48	5.55	3.80	3.88	2.57	2.60	5.34	5.39
Mar	0.53	0.64	7.87	7.89	7.94	7.95	2.08	2.28	2.90	3.21	6.14	6.20	4.62	4.67	1.69	1.76	6.29	6.33
Apr	0.78	1.01	7.33	7.36	6.76	6.78	1.89	2.12	3.40	3.61	5.85	5.92	3.76	3.80	0.92	1.05	4.49	4.56
May	0.58	0.68	5.51	5.54	5.21	5.25	1.57	1.65	3.31	3.35	5.23	5.28	2.16	2.34	1.77	2.40	2.08	2.29
Jun	0.65	0.69	5.06	5.14	4.30	4.33	1.30	1.46	3.29	3.34	3.87	4.01	1.22	1.49	2.79	3.51	1.20	1.43
Jul	0.94	1.05	2.93	3.27	4.03	4.06	1.21	1.40	2.19	2.42	2.56	2.98	2.26	2.81	5.07	5.51	1.29	1.71
Aug	1.44	1.50	2.93	3.22	3.16	3.22	1.16	1.33	1.57	1.78	2.68	2.98	2.58	3.23	6.37	6.66	1.11	1.71
Sept	0.21	0.34	4.61	4.69	4.20	4.30	1.44	1.56	2.31	2.37	3.50	3.60	1.73	1.95	3.74	4.28	0.98	1.37
Oct	0.69	0.78	5.05	5.06	4.06	4.09	1.94	1.98	1.94	1.95	3.23	3.27	2.33	2.47	1.75	2.04	0.87	1.10
Nov	1.89	1.92	6.25	6.26	4.29	4.33	3.48	3.49	2.03	2.19	4.49	4.57	3.01	3.03	4.46	4.53	2.94	3.12

Table C.7. West sub-region maximum temperature values of Perkins' skill score (SS) and Willmott's index of agreement (W).

	MM5I-CCSM		RCM3-GFDL		ECP2-GFDL		WRFG-CCSM		WRFG-CGCM3		RCM3-CGCM3		CRCM-CGCM3		CRCM-CCSM		GFDL-TIMESLICE	
	SS	W	SS	W	SS	W	SS	W	SS	W	SS	W	SS	W	SS	W	SS	W
Dec	0.88	0.84	0.55	0.26	0.54	0.22	0.76	0.58	0.90	0.84	0.71	0.57	0.82	0.73	0.74	0.62	0.78	0.69
Jan	0.92	0.93	0.59	0.38	0.52	0.22	0.78	0.66	0.86	0.88	0.77	0.74	0.85	0.85	0.86	0.82	0.79	0.70
Feb	0.93	0.94	0.60	0.36	0.52	0.14	0.82	0.71	0.78	0.82	0.66	0.59	0.76	0.72	0.86	0.82	0.73	0.60
Mar	0.93	0.93	0.50	0.26	0.50	0.19	0.80	0.80	0.75	0.75	0.61	0.50	0.70	0.61	0.86	0.87	0.64	0.42
Apr	0.90	0.86	0.46	0.19	0.53	0.26	0.74	0.76	0.68	0.65	0.54	0.38	0.70	0.60	0.90	0.92	0.67	0.47
May	0.86	0.79	0.49	0.21	0.56	0.32	0.82	0.76	0.63	0.49	0.56	0.30	0.82	0.75	0.75	0.62	0.77	0.71
Jun	0.79	0.70	0.48	0.10	0.58	0.27	0.74	0.62	0.51	0.16	0.57	0.28	0.84	0.79	0.56	0.06	0.73	0.55
Jul	0.58	0.27	0.62	0.44	0.60	0.33	0.81	0.78	0.65	0.36	0.63	0.46	0.59	0.23	0.40	-0.42	0.58	0.03
Aug	0.50	0.05	0.63	0.44	0.68	0.43	0.79	0.73	0.82	0.71	0.63	0.44	0.57	0.09	0.40	-0.45	0.57	-0.07
Sept	0.76	0.64	0.52	0.28	0.66	0.43	0.90	0.92	0.80	0.74	0.63	0.48	0.81	0.79	0.59	0.25	0.70	0.49
Oct	0.90	0.90	0.58	0.34	0.68	0.48	0.88	0.80	0.87	0.82	0.72	0.59	0.82	0.77	0.78	0.71	0.82	0.76
Nov	0.89	0.87	0.59	0.40	0.70	0.53	0.79	0.66	0.83	0.85	0.65	0.60	0.81	0.79	0.71	0.56	0.86	0.79

Table C.8. West sub-region maximum temperature values of mean absolute error (MAE) and root mean square error (RMSE).

	MM5I-CCSM		RCM3-GFDL		ECP2-GFDL		WRFG-CCSM		WRFG-CGCM3		RCM3-CGCM3		CRCM-CGCM3		CRCM-CCSM		GFDL-TIMESLICE	
	MAE	RMSE	MAE	RMSE	MAE	RMSE	MAE	RMSE	MAE	RMSE	MAE	RMSE	MAE	RMSE	MAE	RMSE	MAE	RMSE
Dec	1.74	1.84	7.81	7.83	8.18	8.23	4.46	4.54	1.69	1.79	4.54	4.63	2.87	2.93	4.04	4.12	3.27	3.42
Jan	0.78	0.96	6.95	7.01	8.82	8.88	3.80	3.83	1.31	1.62	2.91	3.36	1.72	1.97	2.08	2.22	3.40	3.42
Feb	0.71	0.85	7.30	7.33	9.78	9.86	3.26	3.27	2.04	2.39	4.61	4.85	3.14	3.37	2.03	2.15	4.52	4.55
Mar	0.67	0.83	7.45	7.48	8.16	8.17	1.98	2.19	2.46	2.76	5.06	5.16	3.87	3.97	1.27	1.43	5.79	5.80
Apr	1.09	1.39	6.41	6.44	5.85	5.88	1.87	2.09	2.77	2.98	4.93	5.02	3.20	3.25	0.64	0.82	4.22	4.25
May	1.26	1.27	4.76	4.79	4.11	4.14	1.45	1.53	3.12	3.16	4.24	4.37	1.53	1.67	2.33	2.71	1.77	2.01
Jun	1.46	1.57	4.40	4.55	3.55	3.62	1.84	2.04	4.06	4.10	3.51	3.70	1.02	1.37	4.55	5.00	2.20	3.07
Jul	3.16	3.26	2.40	2.73	2.89	2.99	0.95	1.19	2.78	2.95	2.33	2.78	3.33	3.72	7.41	7.62	4.16	4.90
Aug	4.13	4.22	2.46	2.83	2.47	2.60	1.19	1.38	1.28	1.51	2.43	2.81	3.97	4.37	7.88	8.03	4.70	5.17
Sept	2.26	2.34	4.59	4.67	3.60	3.72	0.50	0.74	1.67	1.72	3.29	3.41	1.31	1.76	4.78	5.14	3.22	3.50
Oct	0.73	0.84	4.90	4.91	3.86	3.94	1.48	1.75	1.32	1.34	3.03	3.05	1.72	2.03	2.12	2.56	1.75	2.11
Nov	1.22	1.28	5.78	5.83	4.57	4.60	3.27	3.28	1.41	1.67	3.84	4.09	2.06	2.20	4.27	4.33	1.99	2.17

Table C.9. East sub-region mean precipitation values of Perkins' skill score (SS) and Willmott's index of agreement (W).

	MM5I-CCSM		RCM3-GFDL		ECP2-GFDL		WRFG-CCSM		WRFG-CGCM3		RCM3-CGCM3		CRCM-CGCM3		CRCM-CCSM		GFDL-TIMESLICE	
	SS	W	SS	W	SS	W	SS	W	SS	W	SS	W	SS	W	SS	W	SS	W
Dec	0.84	0.87	0.84	0.78	0.81	0.76	0.85	0.83	0.83	0.80	0.88	0.87	0.95	0.96	0.94	0.98	0.90	0.87
Jan	0.87	0.88	0.91	0.92	0.88	0.90	0.87	0.86	0.88	0.87	0.88	0.90	0.91	0.90	0.86	0.86	0.88	0.85
Feb	0.95	0.86	0.91	0.94	0.92	0.93	0.87	0.85	0.86	0.87	0.89	0.91	0.96	0.98	0.85	0.85	0.90	0.91
Mar	0.95	0.86	0.92	0.95	0.90	0.91	0.86	0.84	0.89	0.88	0.91	0.93	0.91	0.94	0.85	0.84	0.88	0.91
Apr	0.95	0.96	0.95	0.84	0.87	0.81	0.84	0.87	0.89	0.83	0.95	0.84	0.97	0.88	0.89	0.91	0.89	0.92
May	0.93	0.97	0.89	0.93	0.90	0.91	0.86	0.81	0.87	0.86	0.93	0.82	0.97	0.94	0.88	0.88	0.89	0.88
Jun	0.93	0.91	0.88	0.89	0.89	0.94	0.89	0.80	0.86	0.81	0.90	0.93	0.90	0.93	0.87	0.89	0.95	0.91
Jul	0.93	0.94	0.92	0.91	0.94	0.92	0.85	0.76	0.86	0.73	0.92	0.90	0.87	0.90	0.87	0.87	0.93	0.89
Aug	0.94	0.98	0.91	0.88	0.93	0.77	0.84	0.78	0.86	0.76	0.90	0.89	0.83	0.87	0.83	0.81	0.92	0.89
Sept	0.92	0.93	0.83	0.85	0.86	0.87	0.79	0.78	0.81	0.81	0.82	0.85	0.83	0.86	0.75	0.76	0.92	0.84
Oct	0.93	0.98	0.80	0.90	0.90	0.97	0.86	0.90	0.88	0.87	0.82	0.85	0.78	0.83	0.78	0.83	0.89	0.85
Nov	0.86	0.89	0.93	0.94	0.91	0.83	0.87	0.86	0.89	0.87	0.89	0.94	0.84	0.87	0.89	0.93	0.92	0.88

Table C.10. East sub-region mean precipitation values of mean absolute error (MAE) and root mean square error (RMSE).

	MM5I-CCSM		RCM3-GFDL		ECP2-GFDL		WRFG-CCSM		WRFG-CGCM3		RCM3-CGCM3		CRCM-CGCM3		CRCM-CCSM		GFDL-TIMESLICE	
	MAE	RMSE	MAE	RMSE	MAE	RMSE	MAE	RMSE	MAE	RMSE	MAE	RMSE	MAE	RMSE	MAE	RMSE	MAE	RMSE
Dec	10.07	14.15	4.40	8.84	7.53	12.26	10.21	15.63	10.75	18.01	5.19	10.01	5.12	9.39	3.77	8.50	8.98	14.75
Jan	9.48	13.17	7.99	13.23	9.49	14.25	10.04	14.98	10.41	15.16	9.25	14.12	2.69	8.61	4.22	10.11	10.16	15.95
Feb	8.96	12.52	5.76	11.91	9.12	14.61	9.80	15.34	11.73	17.39	8.65	14.36	3.82	9.47	4.10	10.30	8.58	15.15
Mar	9.54	13.93	6.18	12.52	10.05	15.88	9.77	15.43	11.34	18.15	7.65	14.24	4.72	10.12	4.39	11.35	9.36	16.32
Apr	7.32	12.73	8.02	14.87	4.40	11.67	8.67	15.14	5.33	12.05	7.88	14.47	7.84	12.13	6.38	10.48	5.26	12.51
May	4.14	9.17	6.01	10.77	7.49	12.75	7.05	11.33	8.50	15.22	7.21	15.12	5.20	9.95	2.33	5.84	5.08	12.52
Jun	3.70	10.64	6.73	12.96	5.20	10.37	6.97	11.06	8.35	14.51	6.14	12.58	3.72	8.58	3.93	8.06	6.28	15.95
Jul	3.14	8.52	4.53	13.34	5.90	10.80	6.46	10.82	8.14	15.17	3.98	11.50	2.25	8.08	2.60	8.36	6.01	16.15
Aug	2.42	8.94	5.05	13.60	7.02	11.03	7.59	13.47	7.70	15.54	3.36	11.00	2.82	6.53	3.83	10.54	2.97	14.96
Sept	3.39	12.39	5.10	13.85	7.35	15.73	7.49	12.90	10.80	20.90	5.84	15.17	5.92	12.64	5.92	13.84	9.71	19.80
Oct	8.65	16.78	3.84	8.29	8.16	16.29	11.15	21.33	12.93	22.44	7.94	16.72	6.11	11.51	6.64	12.07	11.02	20.01
Nov	10.37	15.49	3.45	10.83	5.85	15.31	10.09	16.79	9.67	17.08	3.53	9.73	4.60	8.77	6.99	10.96	9.79	16.22

Table C.11. West sub-region mean precipitation values of Perkins' skill score (SS) and Willmott's index of agreement (W).

	MM5I-CCSM		RCM3-GFDL		ECP2-GFDL		WRFG-CCSM		WRFG-CGCM3		RCM3-CGCM3		CRCM-CGCM3		CRCM-CCSM		GFDL-TIMESLICE	
	SS	W	SS	W	SS	W	SS	W	SS	W	SS	W	SS	W	SS	W	SS	W
Dec	0.89	0.91	0.90	0.96	0.91	0.94	0.89	0.88	0.85	0.86	0.90	0.95	0.92	0.93	0.88	0.88	0.92	0.92
Jan	0.89	0.86	0.90	0.92	0.90	0.93	0.87	0.87	0.87	0.87	0.89	0.92	0.93	0.91	0.85	0.87	0.87	0.88
Feb	0.95	0.83	0.91	0.94	0.93	0.93	0.87	0.85	0.90	0.88	0.93	0.93	0.93	0.93	0.83	0.83	0.88	0.91
Mar	0.97	0.82	0.94	0.90	0.92	0.94	0.86	0.83	0.92	0.89	0.92	0.92	0.91	0.91	0.84	0.82	0.90	0.93
Apr	0.96	0.93	0.94	0.93	0.88	0.85	0.79	0.88	0.89	0.90	0.94	0.90	0.95	0.90	0.86	0.88	0.86	0.92
May	0.94	0.87	0.85	0.91	0.94	0.95	0.76	0.78	0.82	0.87	0.91	0.83	0.94	0.94	0.81	0.82	0.80	0.84
Jun	0.97	0.91	0.86	0.87	0.90	0.94	0.78	0.76	0.74	0.80	0.88	0.89	0.93	0.95	0.85	0.82	0.87	0.87
Jul	0.94	0.88	0.92	0.90	0.94	0.87	0.82	0.69	0.79	0.70	0.88	0.90	0.86	0.82	0.83	0.76	0.82	0.81
Aug	0.94	0.91	0.92	0.96	0.96	0.80	0.83	0.77	0.85	0.75	0.89	0.93	0.84	0.85	0.83	0.81	0.86	0.82
Sept	0.91	0.93	0.88	0.92	0.84	0.80	0.82	0.77	0.82	0.78	0.86	0.88	0.81	0.83	0.75	0.77	0.88	0.78
Oct	0.95	0.96	0.81	0.88	0.87	0.93	0.86	0.87	0.85	0.83	0.81	0.84	0.79	0.83	0.82	0.84	0.87	0.82
Nov	0.91	0.90	0.91	0.94	0.91	0.93	0.85	0.86	0.85	0.86	0.91	0.91	0.87	0.86	0.88	0.89	0.93	0.88

Table C.12. West sub-region mean precipitation values of mean absolute error (MAE) and root mean square error (RMSE).

	MM5I-CCSM		RCM3-GFDL		ECP2-GFDL		WRFG-CCSM		WRFG-CGCM3		RCM3-CGCM3		CRCM-CGCM3		CRCM-CCSM		GFDL-TIMESLICE	
	MAE	RMSE	MAE	RMSE	MAE	RMSE	MAE	RMSE	MAE	RMSE	MAE	RMSE	MAE	RMSE	MAE	RMSE	MAE	RMSE
Dec	11.07	16.02	6.75	14.37	7.98	15.01	11.33	18.15	13.33	21.73	7.95	15.18	5.06	10.65	3.17	10.39	10.43	17.39
Jan	9.08	13.05	8.95	14.75	9.90	15.16	10.64	16.11	11.77	17.74	9.62	15.21	2.18	8.63	4.21	11.14	9.98	16.25
Feb	9.56	13.50	6.54	13.90	8.70	14.95	10.61	16.74	12.39	19.45	8.03	14.86	5.55	10.97	4.65	11.42	7.83	15.46
Mar	10.41	15.60	7.53	15.65	10.64	17.41	10.98	17.91	12.34	20.21	8.76	16.95	4.56	10.05	5.18	13.55	9.71	17.71
Apr	9.79	16.72	8.83	17.34	5.05	10.23	9.75	18.54	8.40	17.86	7.42	17.37	9.39	14.81	7.78	13.08	4.41	12.76
May	7.55	13.71	8.28	14.52	7.35	14.30	8.87	14.37	8.82	18.37	9.37	20.58	6.18	11.88	4.35	10.66	5.80	13.75
Jun	6.45	11.66	7.51	15.03	4.76	10.13	6.17	10.98	9.11	16.30	7.57	15.69	1.42	6.83	3.89	10.07	3.22	10.33
Jul	5.46	10.86	6.61	14.07	7.10	11.20	7.13	12.15	7.65	13.15	3.67	12.17	5.87	10.45	5.53	10.32	4.94	12.42
Aug	2.95	9.04	2.09	9.10	6.37	9.60	6.13	10.56	7.92	15.32	3.73	9.79	3.01	8.78	3.66	9.31	5.02	13.54
Sept	2.00	8.86	2.16	5.76	8.07	14.06	8.97	16.29	12.12	25.39	4.42	13.44	4.44	11.86	5.69	12.97	7.90	14.72
Oct	9.60	16.37	6.87	14.96	6.77	15.05	12.08	20.49	8.27	16.49	8.53	15.64	6.16	13.86	4.58	11.36	9.65	16.95
Nov	11.59	16.37	7.74	14.80	4.72	11.49	12.38	19.35	12.61	19.60	7.83	14.68	4.33	11.44	5.40	9.83	10.99	16.71

APPENDIX D – GRADS SCRIPTS

The following codes were used to create the plots showing future change in temperature and precipitation for the Southeast U.S. The first code is used to call in the control files (.ctl) created for each netCDF file which allows GrADS to read the data contained within the netCDF file. An example control file (.ctl) is provided first with a example GrADS script which plots the unweighted ensemble mean and standard deviation for all months and saves it as a PNG file.

```
#This code is saved as tas_ens_mean_fut-ref_min.ctl
DSET ^tas_ens_mean_fut-ref_min.nc
DTYPE netcdf
TITLE Temperature change for NARCCAP Ensemble
UNDEF 1.e+20 _FillValue
XDEF lon  43 LINEAR -94 0.5
YDEF lat  21 LINEAR 28 0.5
TDEF time  12 LINEAR 1JAN2069 1MO
VARS 1
tas=>tas 1 99 tas
ENDVARS

#This code is saves as tas_min_ensemble.gs
********* Grads script for plotting 12 figures in one plot ************

'reinit'
'xdfopen H:/Future_model_work/tas_ens_mean_fut-ref_min.ctl'
'xdfopen H:/Future_model_work/tas_ens_sd_fut-ref_min.ctl'


'set mproj scaled'
'set map 1 1 9'
'set rgb 16 0 0 155'
'set rgb 17 0 19 255'
'set rgb 18 60 130 255'
'set rgb 19 130 190 255'
'set rgb 20 150 255 255'
'set rgb 21 255 246 200'
'set rgb 22 255 225 100'
'set rgb 23 255 205 0'
'set rgb 24 255 180 0'
'set rgb 25 255 145 0'
'set rgb 26 255 100 0'
```

```
'set rgb 27 255 50 0'
'set rgb 28 236 0 0'
'set rgb 29 199 0 0'
'set rgb 30 159 34 34'



*****************
'set vpage 0 11 0 8'
'set parea 0.7 3.7 6.1 8.0'
'set gxout shaded'
'set mpdset hires'
'set mproj scaled'
'set lon -92 -75'
'set lat 28.9 37'
'set grid off'
'set xlab off'
'set ylab on'
'set xlopts 1 4 0.18'
'set ylopts 1 4 0.18'
'set xlint 2'
'set clevs -2 -1.5 -1 -0.5 0 0.5 1 1.5 2 2.5 3 3.5 4 5'
'set ccols 16 17 18 19 20 21 22 23 24 25 26 27 28 29 30'
'set t 1'
'set xlab off'
'set ylab on'
'set ylint 2'
'set digsiz 3'
'set grads off'
'd tas.1'
'set gxout contour'
'set clevs 0 0.25 0.5 0.75 1 1.5 2 2.5 3 3.5 4 4.5 5 5.5 6'
'set clab on'
#'set clskip 2'
'set cthick 2'
'set cterp on'
'd tas.2'
'set string 1 c 15 0'
'set strsiz 0.2'
'draw string 3.4 6.3 a)'
***********

'set vpage 0 11 0 8'
'set parea 3.7 6.7 6.1 8.0'
'set gxout shaded'
'set mpdset hires'
'set mproj scaled'
'set lon -92 -75'
'set lat 28.9 37'
'set grid off'
'set xlab off'
'set ylab off'
'set xlopts 1 4 0.18'
'set ylopts 1 4 0.18'
'set xlint 2'
'set clevs -2 -1.5 -1 -0.5 0 0.5 1 1.5 2 2.5 3 3.5 4 5'
'set ccols 16 17 18 19 20 21 22 23 24 25 26 27 28 29 30'
```

```
'set t 2'
'set gxout shaded'
'set grads off'
'set xlab off'
'set ylab off'
'set ylint 2'
'set digsiz 3'
'set grads off'
'd tas.1'
'set gxout contour'
'set clevs 0 0.25 0.5 0.75 1 1.5 2 2.5 3 3.5 4 4.5 5 5.5 6'
'set clab on'
#'set clskip 2'
'set cthick 2'
'set cterp on'
'd tas.2'
'set string 1 c 15 0'
'set strsiz 0.2'
'draw string 6.4 6.3 b)'
***********

'set vpage 0 11 0 8'
'set parea 6.7 9.7 6.1 8.0'
'set gxout shaded'
'set mpdset hires'
'set mproj scaled'
'set lon -92 -75'
'set lat 28.9 37'
'set grid off'
'set xlab off'
'set ylab off'
'set xlopts 1 4 0.18'
'set ylopts 1 4 0.18'
'set xlint 2'
'set clevs -2 -1.5 -1 -0.5 0 0.5 1 1.5 2 2.5 3 3.5 4 5'
'set ccols 16 17 18 19 20 21 22 23 24 25 26 27 28 29 30'
'set t 3'
'set gxout shaded'
'set grads off'
'set xlab off'
'set ylab off'
'set ylint 2'
'set digsiz 3'
'set grads off'
'd tas.1'
'set gxout contour'
'set clevs 0 0.25 0.5 0.75 1 1.5 2 2.5 3 3.5 4 4.5 5 5.5 6'
'set clab on'
#'set clskip 2'
'set cthick 2'
'set cterp on'
'd tas.2'
'set string 1 c 15 0'
'set strsiz 0.2'
'draw string 9.4 6.3 c)'
***********
```

```
'set vpage 0 11 0 8'
'set parea 0.7 3.7 4.2 6.1'
'set gxout shaded'
'set mpdset hires'
'set mproj scaled'
'set lon -92 -75'
'set lat 28.9 37'
'set grid off'
'set xlab off'
'set ylab on'
'set xlopts 1 4 0.18'
'set ylopts 1 4 0.18'
'set xlint 2'
'set clevs -2 -1.5 -1 -0.5 0 0.5 1 1.5 2 2.5 3 3.5 4 5'
'set ccols 16 17 18 19 20 21 22 23 24 25 26 27 28 29 30'
'set t 4'
'set gxout shaded'
'set grads off'
'set xlab off'
'set ylab on'
'set ylint 2'
'set digsiz 3'
'set grads off'
'd tas.1'
'set gxout contour'
'set clevs 0 0.25 0.5 0.75 1 1.5 2 2.5 3 3.5 4 4.5 5 5.5 6'
'set clab on'
#'set clskip 2'
'set cthick 2'
'set cterp on'
'd tas.2'
'set string 1 c 15 0'
'set strsiz 0.2'
'draw string 3.4 4.4 d)'
***********

'set vpage 0 11 0 8'
'set parea 3.7 6.7 4.2 6.1'
'set gxout shaded'
'set mpdset hires'
'set mproj scaled'
'set lon -92 -75'
'set lat 28.9 37'
'set grid off'
'set xlab off'
'set ylab off'
'set xlopts 1 4 0.18'
'set ylopts 1 4 0.18'
'set xlint 2'
'set clevs -2 -1.5 -1 -0.5 0 0.5 1 1.5 2 2.5 3 3.5 4 5'
'set ccols 16 17 18 19 20 21 22 23 24 25 26 27 28 29 30'
'set t 5'
'set gxout shaded'
'set grads off'
'set xlab off'
'set ylab off'
'set ylint 2'
```

```
'set digsiz 3'
'set grads off'
'd tas.1'
'set gxout contour'
'set clevs 0 0.25 0.5 0.75 1 1.5 2 2.5 3 3.5 4 4.5 5 5.5 6'
'set clab on'
#'set clskip 2'
'set cthick 2'
'set cterp on'
'd tas.2'
'set string 1 c 15 0'
'set strsiz 0.2'
'draw string 6.4 4.4 e)'
***********

'set vpage 0 11 0 8'
'set parea 6.7 9.7 4.2 6.1'
'set gxout shaded'
'set mpdset hires'
'set mproj scaled'
'set lon -92 -75'
'set lat 28.9 37'
'set grid off'
'set xlab off'
'set ylab off'
'set xlopts 1 4 0.18'
'set ylopts 1 4 0.18'
'set xlint 2'
'set clevs -2 -1.5 -1 -0.5 0 0.5 1 1.5 2 2.5 3 3.5 4 5'
'set ccols 16 17 18 19 20 21 22 23 24 25 26 27 28 29 30'
'set t 6'
'set gxout shaded'
'set grads off'
'set xlab off'
'set ylab off'
'set ylint 2'
'set digsiz 3'
'set grads off'
'd tas.1'
'set gxout contour'
'set clevs 0 0.25 0.5 0.75 1 1.5 2 2.5 3 3.5 4 4.5 5 5.5 6'
'set clab on'
#'set clskip 2'
'set cthick 2'
'set cterp on'
'd tas.2'
'set string 1 c 15 0'
'set strsiz 0.2'
'draw string 9.4 4.4 f)'
***********

'set vpage 0 11 0 8'
'set parea 0.7 3.7 2.3 4.2'
'set gxout shaded'
'set mpdset hires'
'set mproj scaled'
'set lon -92 -75'
```

```
'set lat 28.9 37'
'set grid off'
'set xlab on'
'set ylab on'
'set xlopts 1 4 0.18'
'set ylopts 1 4 0.18'
'set xlint 6'
'set clevs -2 -1.5 -1 -0.5 0 0.5 1 1.5 2 2.5 3 3.5 4 5'
'set ccols 16 17 18 19 20 21 22 23 24 25 26 27 28 29 30'
'set t 7'
'set gxout shaded'
'set grads off'
'set xlab on'
'set ylab on'
'set ylint 2'
'set digsiz 3'
'set grads off'
'd tas.1'
'set gxout contour'
'set clevs 0 0.25 0.5 0.75 1 1.5 2 2.5 3 3.5 4 4.5 5 5.5 6'
'set clab on'
#'set clskip 2'
'set cthick 2'
'set cterp on'
'd tas.2'
'set string 1 c 15 0'
'set strsiz 0.2'
'draw string 3.4 2.5 g)'
***********

'set vpage 0 11 0 8'
'set parea 3.7 6.7 2.3 4.2'
'set gxout shaded'
'set mpdset hires'
'set mproj scaled'
'set lon -92 -75'
'set lat 28.9 37'
'set grid off'
'set xlab on'
'set ylab off'
'set xlopts 1 4 0.18'
'set ylopts 1 4 0.18'
'set xlint 6'
'set clevs -2 -1.5 -1 -0.5 0 0.5 1 1.5 2 2.5 3 3.5 4 5'
'set ccols 16 17 18 19 20 21 22 23 24 25 26 27 28 29 30'
'set t 8'
'set gxout shaded'
'set grads off'
'set xlab on'
'set ylab off'
'set ylint 2'
'set digsiz 3'
'set grads off'
'd tas.1'
'set gxout contour'
'set clevs 0 0.25 0.5 0.75 1 1.5 2 2.5 3 3.5 4 4.5 5 5.5 6'
'set clab on'
```

```
#'set clskip 2'
'set cthick 2'
'set cterp on'
'd tas.2'
'set string 1 c 15 0'
'set strsiz 0.2'
'draw string 6.4 2.5 h)'
***********

'set vpage 0 11 0 8'
'set parea 6.7 9.7 2.3 4.2'
'set gxout shaded'
'set mpdset hires'
'set mproj scaled'
'set lon -92 -75'
'set lat 28.9 37'
'set grid off'
'set xlab on'
'set ylab off'
'set xlopts 1 4 0.18'
'set ylopts 1 4 0.18'
'set xlint 6'
'set clevs -2 -1.5 -1 -0.5 0 0.5 1 1.5 2 2.5 3 3.5 4 5'
'set ccols 16 17 18 19 20 21 22 23 24 25 26 27 28 29 30'
'set t 9'
'set gxout shaded'
'set grads off'
'set xlab on'
'set ylab off'
'set ylint 2'
'set digsiz 3'
'set grads off'
'd tas.1'
'set gxout contour'
'set clevs 0 0.25 0.5 0.75 1 1.5 2 2.5 3 3.5 4 4.5 5 5.5 6'
'set clab on'
#'set clskip 2'
'set cthick 2'
'set cterp on'
'd tas.2'
'set string 1 c 15 0'
'set strsiz 0.2'
'draw string 9.4 2.5 i)'

'run cbarn 1 1 10.1 3.9 7.2'
'set string 1 c 4 1'
'set strsiz 0.17'
'draw string 10.4 7.1 `3.`0C'

***********

'set vpage 0 11 0 8'
'set parea 0.7 3.7 0.4 2.3'
'set gxout shaded'
'set mpdset hires'
'set mproj scaled'
'set lon -92 -75'
```

```
'set lat 28.9 37'
'set grid off'
'set xlab on'
'set ylab on'
'set xlopts 1 4 0.18'
'set ylopts 1 4 0.18'
'set xlint 6'
'set clevs -2 -1.5 -1 -0.5 0 0.5 1 1.5 2 2.5 3 3.5 4 5'
'set ccols 16 17 18 19 20 21 22 23 24 25 26 27 28 29 30'
'set t 10'
'set gxout shaded'
'set grads off'
'set xlab on'
'set ylab on'
'set ylint 2'
'set digsiz 3'
'set grads off'
'd tas.1'
'set gxout contour'
'set clevs 0 0.25 0.5 0.75 1 1.5 2 2.5 3 3.5 4 4.5 5 5.5 6'
'set clab on'
#'set clskip 2'
'set cthick 2'
'set cterp on'
'd tas.2'
'set string 1 c 15 0'
'set strsiz 0.2'
'draw string 3.4 0.6 j)'


'set vpage 0 11 0 8'
'set parea 3.7 6.7 0.4 2.3'
'set gxout shaded'
'set mpdset hires'
'set mproj scaled'
'set lon -92 -75'
'set lat 28.9 37'
'set grid off'
'set xlab on'
'set ylab off'
'set xlopts 1 4 0.18'
'set ylopts 1 4 0.18'
'set xlint 6'
'set clevs -2 -1.5 -1 -0.5 0 0.5 1 1.5 2 2.5 3 3.5 4 5'
'set ccols 16 17 18 19 20 21 22 23 24 25 26 27 28 29 30'
'set t 11'
'set gxout shaded'
'set grads off'
'set xlab on'
'set ylab off'
'set ylint 2'
'set digsiz 3'
'set grads off'
'd tas.1'
'set gxout contour'
'set clevs 0 0.25 0.5 0.75 1 1.5 2 2.5 3 3.5 4 4.5 5 5.5 6'
'set clab on'
```

```
#'set clskip 2'
'set cthick 2'
'set cterp on'
'd tas.2'
'set string 1 c 15 0'
'set strsiz 0.2'
'draw string 6.4 0.6 k)'


'set vpage 0 11 0 8'
'set parea 6.7 9.7 0.4 2.3'
'set gxout shaded'
'set mpdset hires'
'set mproj scaled'
'set lon -92 -75'
'set lat 28.9 37'
'set grid off'
'set xlab on'
'set ylab off'
'set xlopts 1 4 0.18'
'set ylopts 1 4 0.18'
'set xlint 6'
'set clevs -2 -1.5 -1 -0.5 0 0.5 1 1.5 2 2.5 3 3.5 4 5'
'set ccols 16 17 18 19 20 21 22 23 24 25 26 27 28 29 30'
'set t 12'
'set gxout shaded'
'set grads off'
'set xlab on'
'set ylab off'
'set ylint 2'
'set digsiz 3'
'set grads off'
'd tas.1'
'set gxout contour'
'set clevs 0 0.25 0.5 0.75 1 1.5 2 2.5 3 3.5 4 4.5 5 5.5 6'
'set clab on'
#'set clskip 2'
'set cthick 2'
'set cterp on'
'd tas.2'
'set string 1 c 15 0'
'set strsiz 0.2'
'draw string 9.4 0.6 l)'

'printim H:/Future_model_work/tas_ens_min.png white'
```

APPENDIX E – RMSE VERSUS NORMALIZED RMSE

Presented in Appendix E is the comparison of raw RMSE values computed for each minimum temperature, maximum temperature, and mean precipitation for the east and west sub-regions. This Appendix is meant to show the relationship between the raw RMSE and normalized RMSE values has a correlation of one, indicating normalizing RMSE with Kramer's "normalized.vector" operator does not adversely impact the representation of RMSE. Also presented in this Appendix is the R script used to calculate normalized RMSE and create the plots illustrated below.

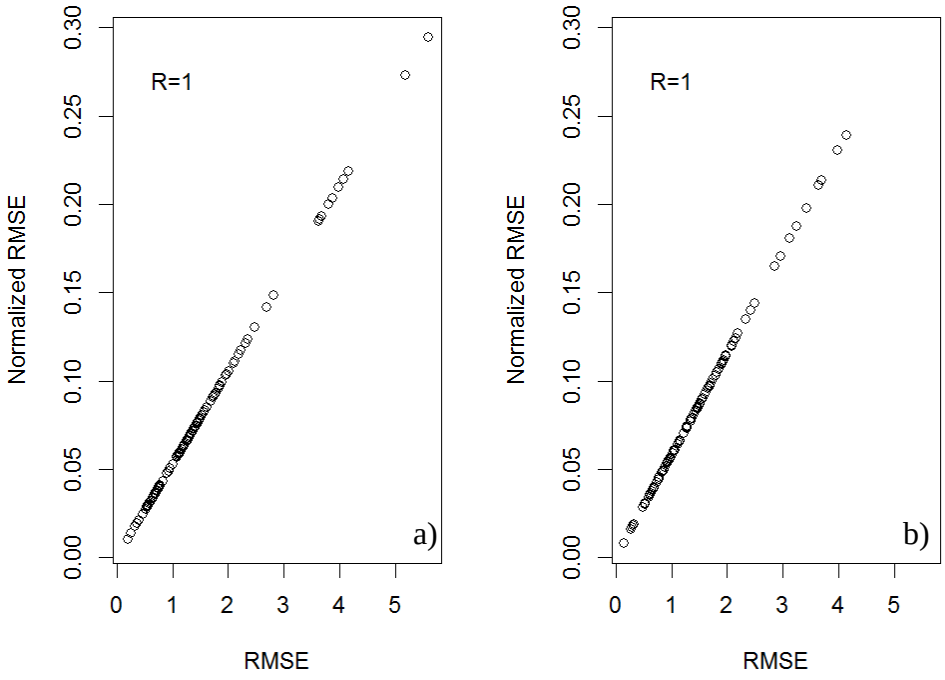

Figure E.1. Comparison of minimum temperature RMSE and normalized RMSE for the west (a) and east (b) sub-regions.

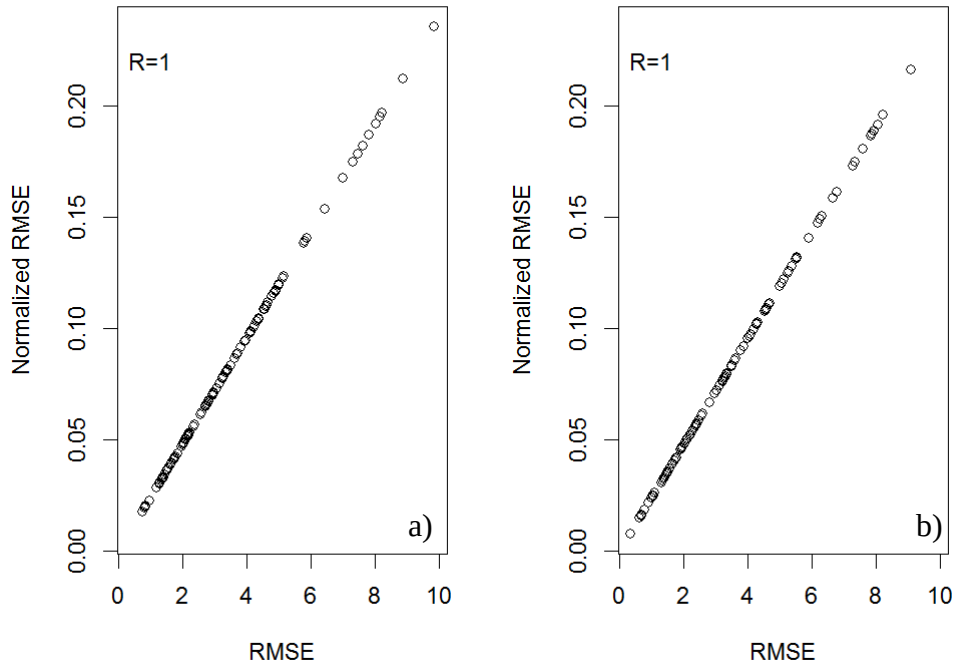

Figure E.2. Comparison of maximum temperature RMSE and normalized RMSE for the west (a) and east (b) sub-regions.

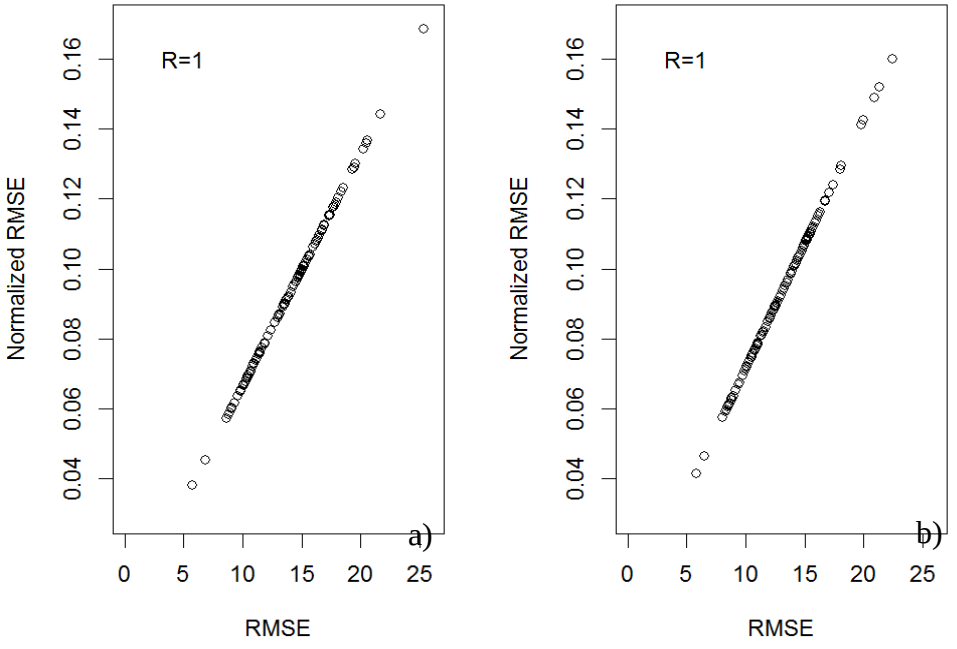

Figure E.3. Comparison of mean preciptiation RMSE and normalized RMSE for the west (a) and east (b) sub-regions.

```
library(ppls)

gg<-read.csv(file="H:\\Dissertation\\tasmax_west_rmse_all_models.csv",
sep=",",header=T)

ii<-read.csv(file="H:\\Dissertation\\tasmax_east_rmse_all_models.csv",
sep=",",header=T)

data_raw_west<-c(gg$MM5I_CCSM,gg$RCM3_GFDL,gg$ECP2_GFDL,gg$WRFG_CCSM,
gg$WRFG_CGCM3,gg$RCM3_CGCM3,gg$CRCM_CCSM,gg$CRCM_CGCM3,gg$GFDL_TS)
data_norm_west<-normalize.vector(data_raw_west)

data_raw_east<-c(ii$MM5I_CCSM,ii$RCM3_GFDL,ii$ECP2_GFDL,ii$WRFG_CCSM,
ii$WRFG_CGCM3,ii$RCM3_CGCM3,ii$CRCM_CCSM,ii$CRCM_CGCM3,ii$GFDL_TS)
data_norm_east<-normalize.vector(data_raw_east)

cor1<-cor(data_raw_west,data_norm_west)
cor2<-cor(data_raw_east,data_norm_east)


windows()

png(filename =
"H://Dissertation//tasmax_west_east_rmse_vs_norm_rmse.png", width =
1000, height = 800,units = "px", pointsize = 13.5, bg = "white",
res = 130,restoreConsole = TRUE)

par(mfrow=c(1,2))
plot(data_raw_west,data_norm_west,xlab="RMSE",ylab="Normalized
RMSE",xlim=c(min(data_raw_west,data_raw_east),max(data_raw_west,
data_raw_east)),ylim=c(min(data_norm_west,data_norm_east),
max(data_norm_west,data_norm_east)))
text(1,0.22,"R=")
text(1.5,0.22,cor1)


plot(data_raw_east,data_norm_east,xlab="RMSE",ylab="Normalized
RMSE",xlim=c(min(data_raw_west,data_raw_east),max(data_raw_west,
data_raw_east)),ylim=c(min(data_norm_west,data_norm_east),
max(data_norm_west,data_norm_east)))
text(1,0.22,"R=")
text(1.5,0.22,cor1)

dev.off()
```

APPENDIX F – GCM PERCENTILE PLOTS

Presented in Appendix F are the percentile plots created for the three global climate models used as boundary conditions for the NARCCAP RCM's. These percentile plots provide an insight into the bias each GCM has in comparison to observations. Additionally, these plots can aid in explaining the biases found in each of the NARCCAP ensemble members.

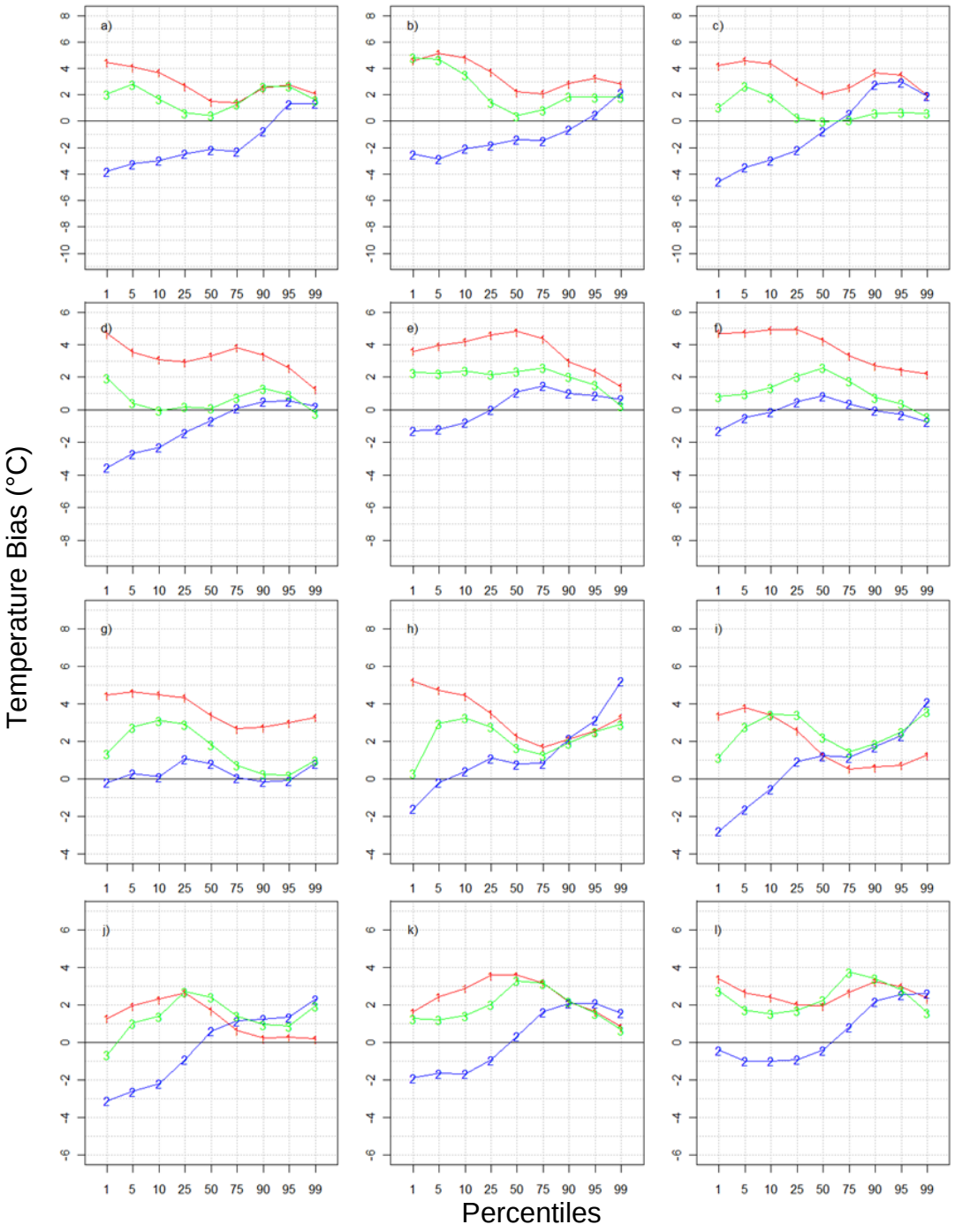

Figure F.1. Percentile plots of minimum temperature bias for the east sub-region from the GCMs used as boundary conditions in NARCCAP for December (a) through November (l). Labels for the GCMs are as follows: "1"=CCSM, "2"=GFDL, and "3"=CGCM3.

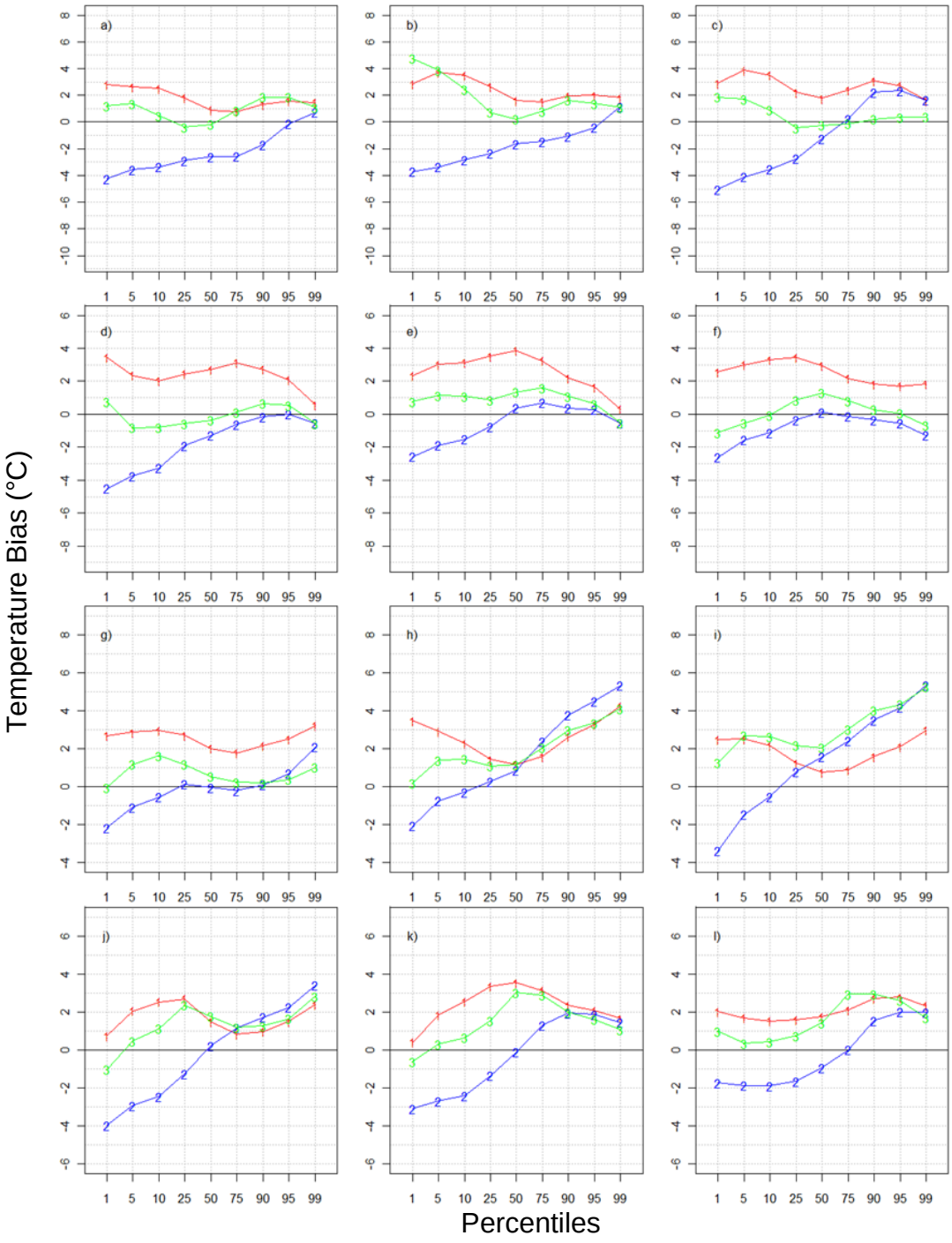

Figure F.2. Percentile plots of minimum temperature bias for the west sub-region from the GCMs used as boundary conditions in NARCCAP for December (a) through November (l). Labels for the GCMs are as follows: "1"=CCSM, "2"=GFDL, and "3"=CGCM3.

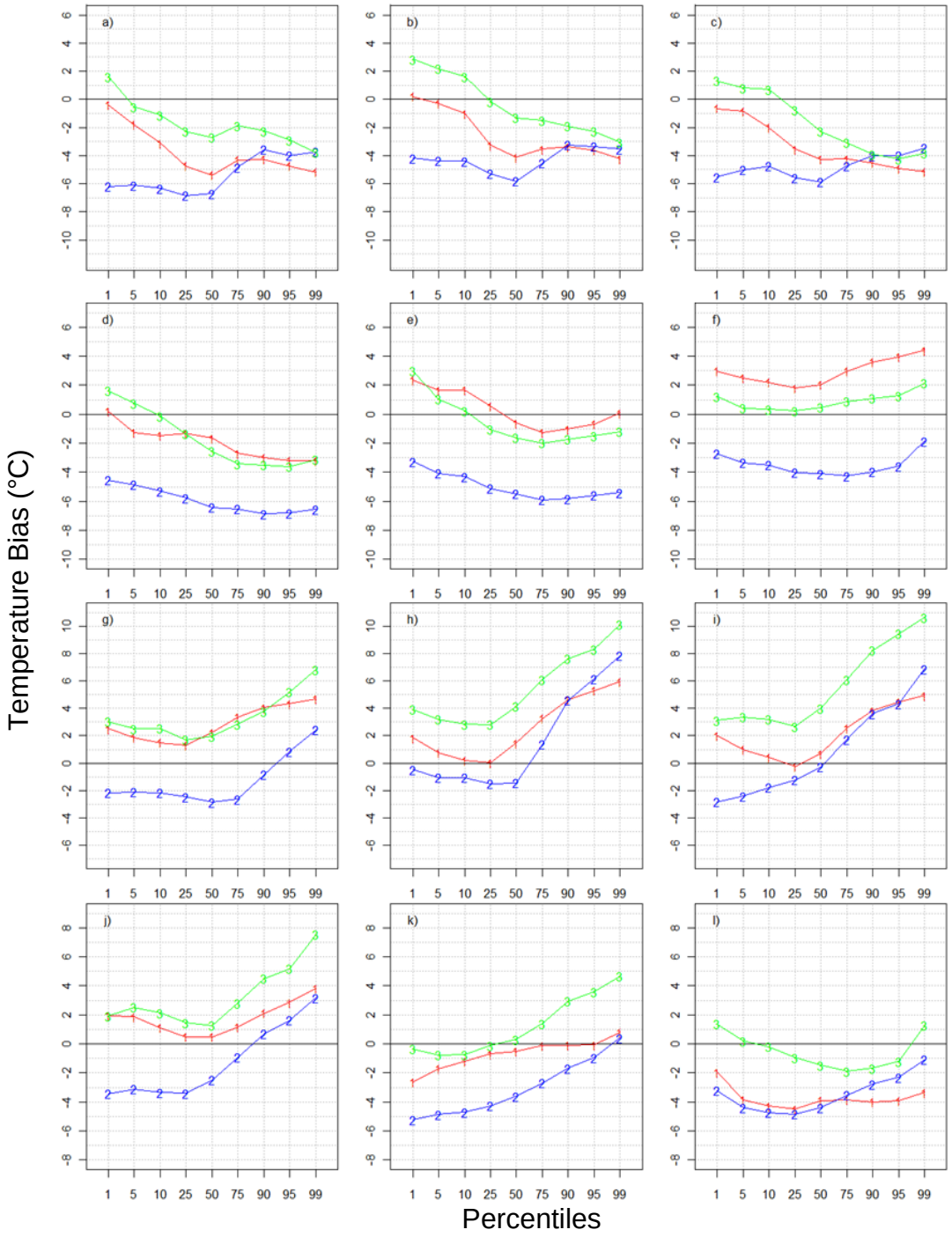

Figure F.3. Percentile plots of maximum temperature bias for the east sub-region from the GCMs used as boundary conditions in NARCCAP for December (a) through November (l). Labels for the GCMs are as follows: "1"=CCSM, "2"=GFDL, and "3"=CGCM3.

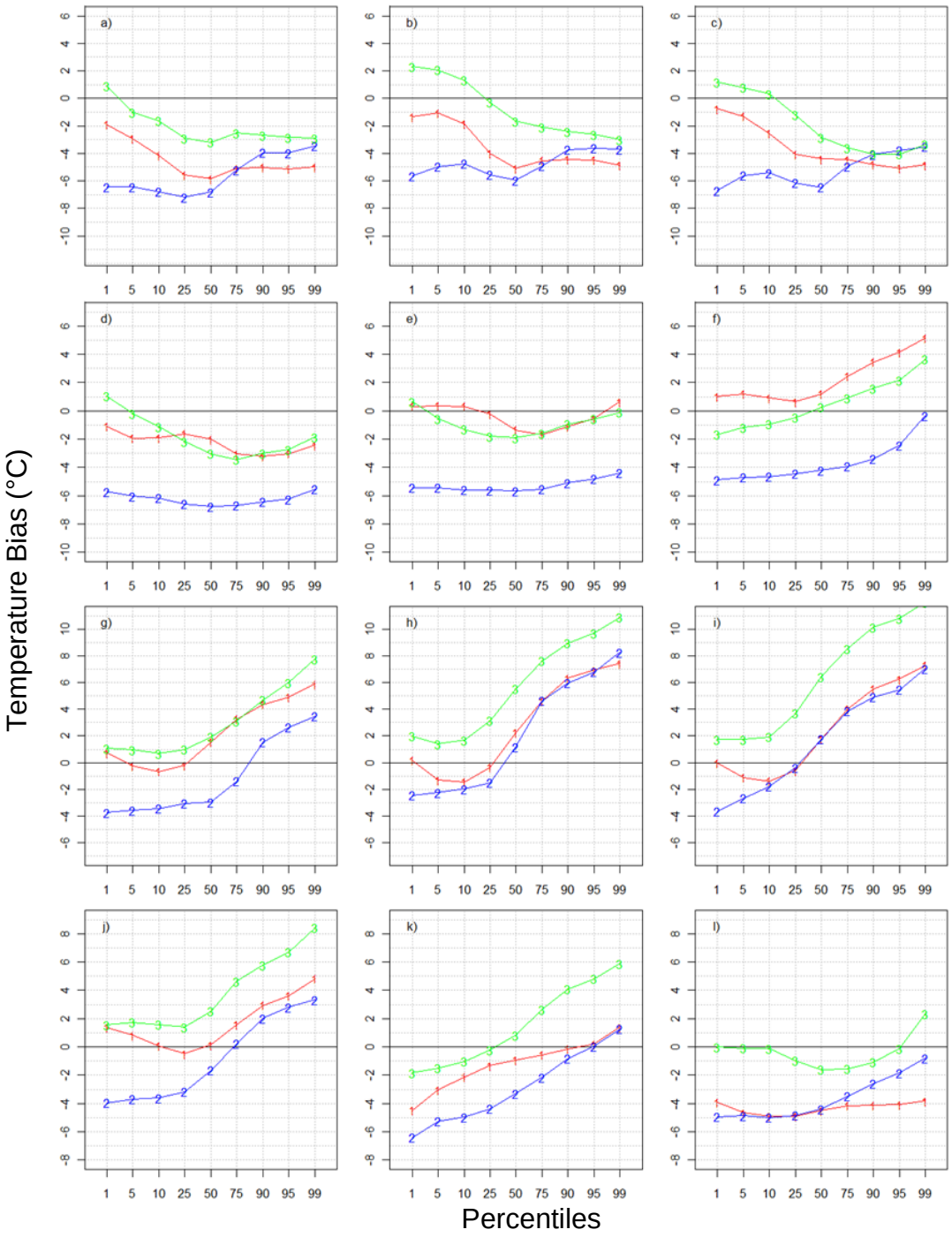

Figure F.4. Percentile plots of maximum temperature bias for the west sub-region from the GCMs used as boundary conditions in NARCCAP for December (a) through November (l). Labels for the GCMs are as follows: “1”=CCSM, “2”=GFDL, and “3”=CGCM3.

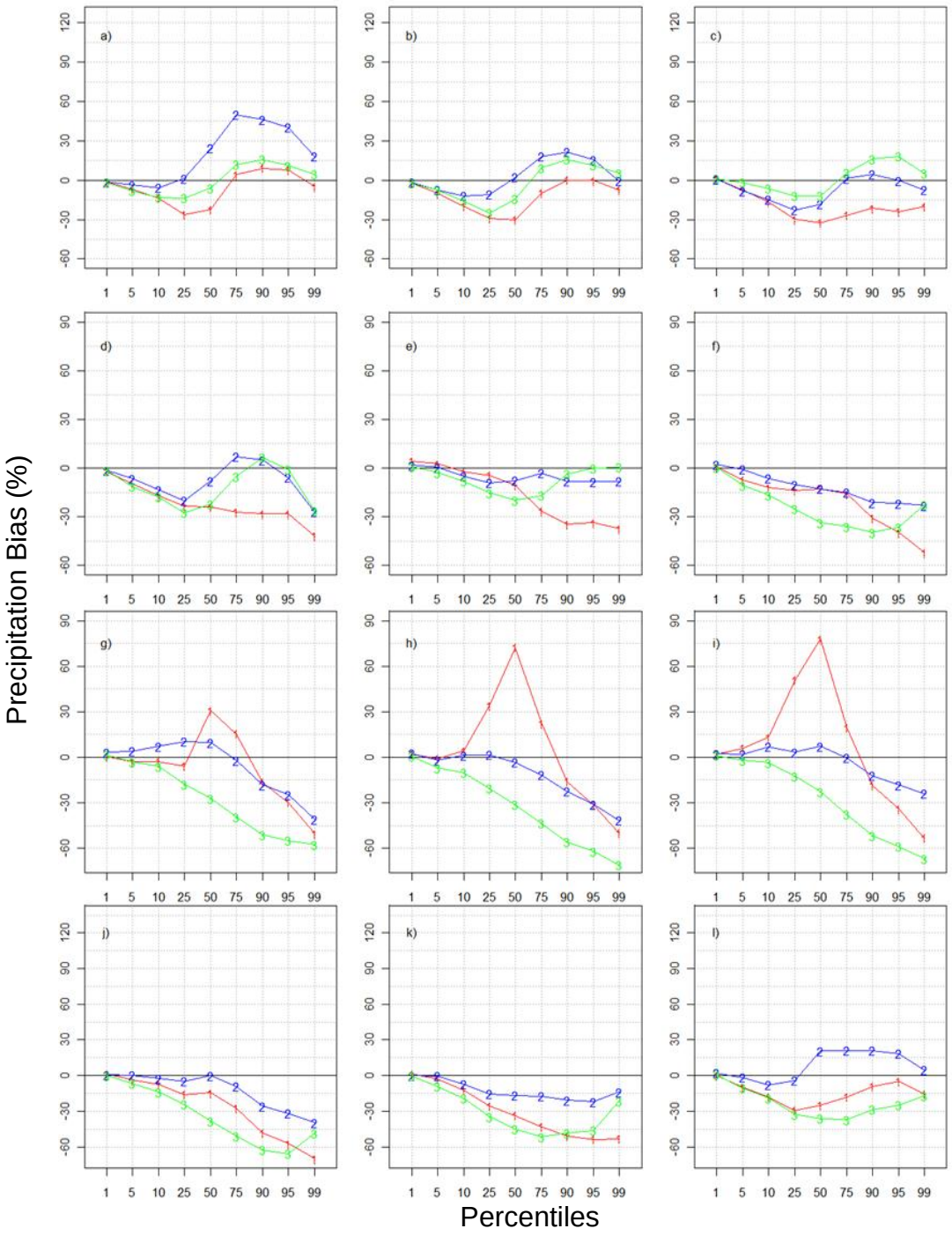

Figure F.5. Percentile plots of precipitation bias for the east sub-region from the GCMs used as boundary conditions in NARCCAP for December (a) through November (l). Labels for the GCMs are as follows: "1"=CCSM, "2"=GFDL, and "3"=CGCM3.

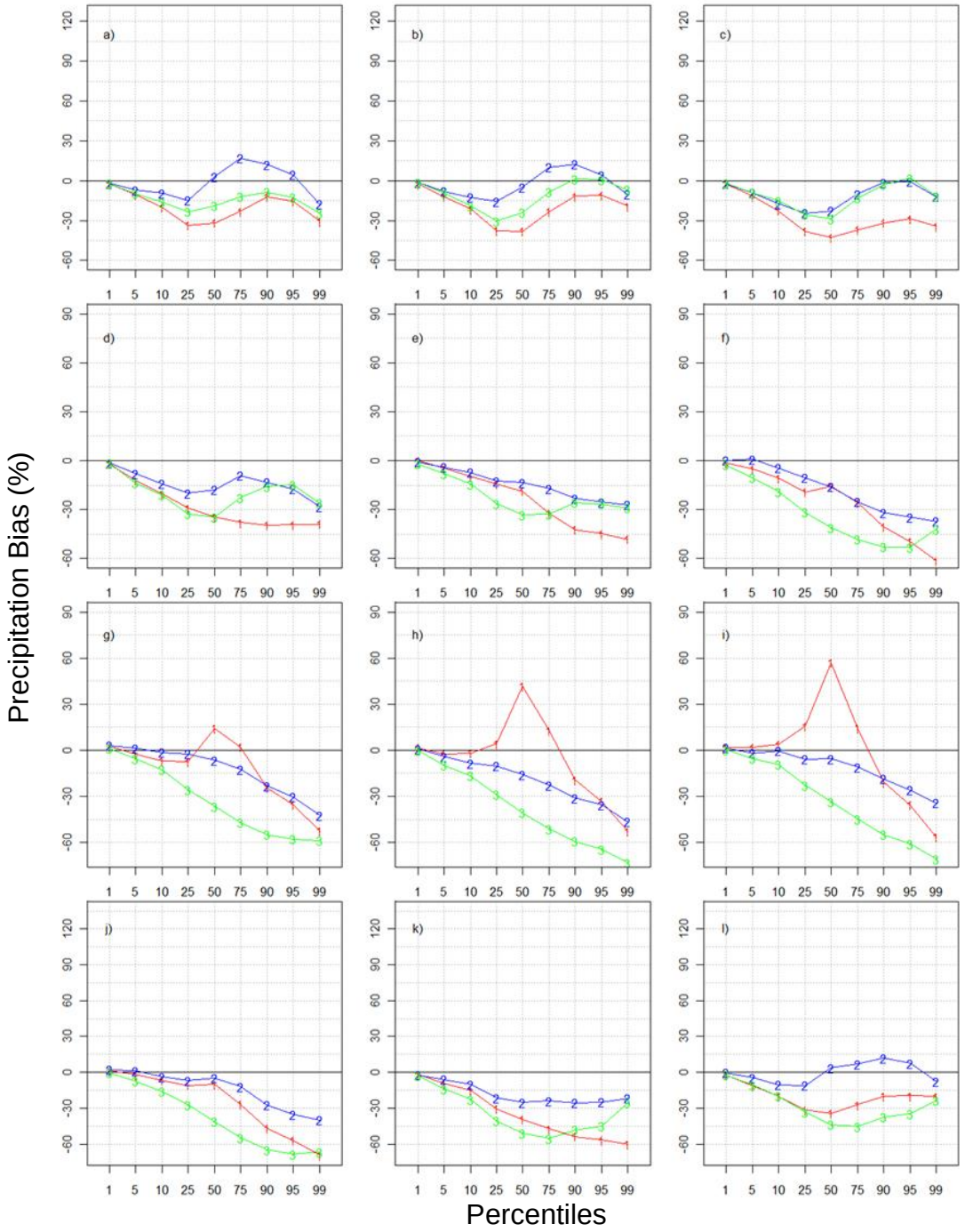

Figure F.6. Percentile plots of precipitation bias for the west sub-region from the GCMs used as boundary conditions in NARCCAP for December (a) through November (l). Labels for the GCMs are as follows: "1"=CCSM, "2"=GFDL, and "3"=CGCM3.

APPENDIX G – NARCCAP INDIVIDUAL ENSEMBLE MEMBER PROJECTIONS

Presented in Appendix G are the percentile plots created for the three global climate models used as boundary conditions for the NARCCAP RCM's. These percentile plots provide an insight into the bias each GCM has in comparison to observations. Additionally, these plots can aid in explaining the biases found in each of the NARCCAP ensemble members.

G.1 MINIMUM TEMPERATURE

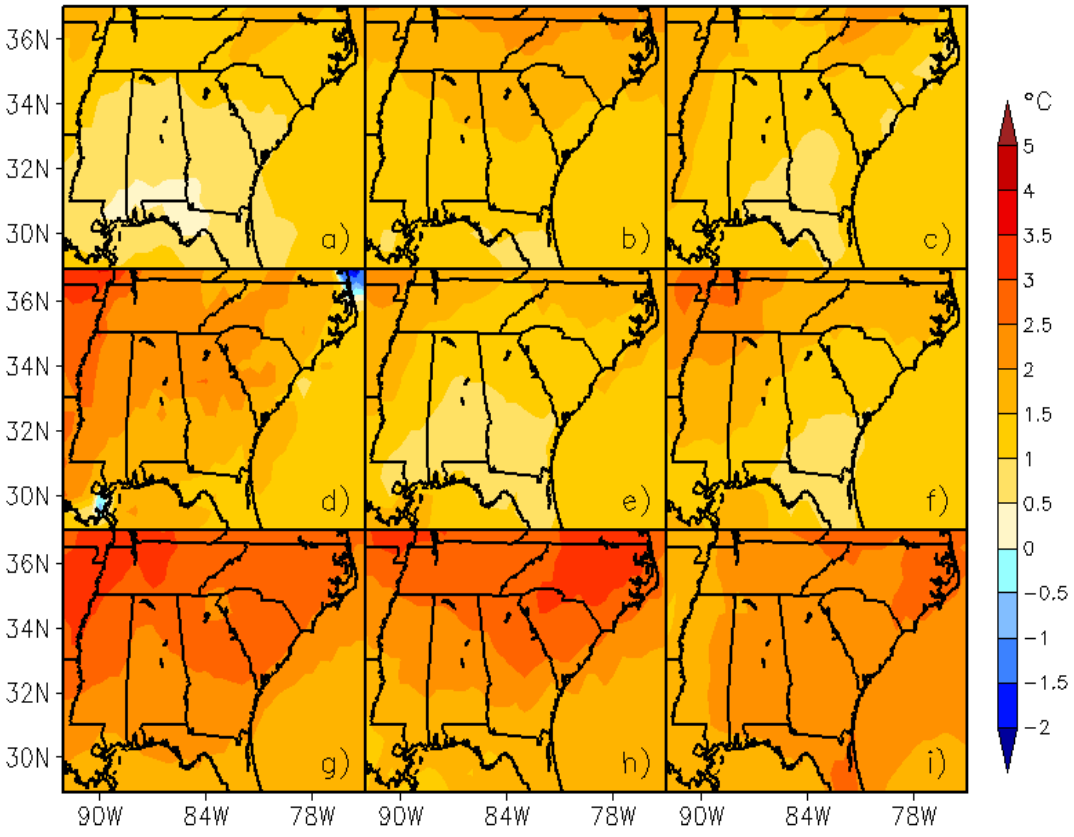

Figure G.1. Individual January minimum temperature change for the WRFG-CGCM3 (a), RCM3-CGCM3 (b), CRCM-CGCM3 (c), WRFG-CCSM (d), MM5I-CCSM (e), CRCM-CCSM (f), ECP2-GFDL (g), RCM3-GFDL (h), and GFDL-timeslice (i) NARCCAP models.

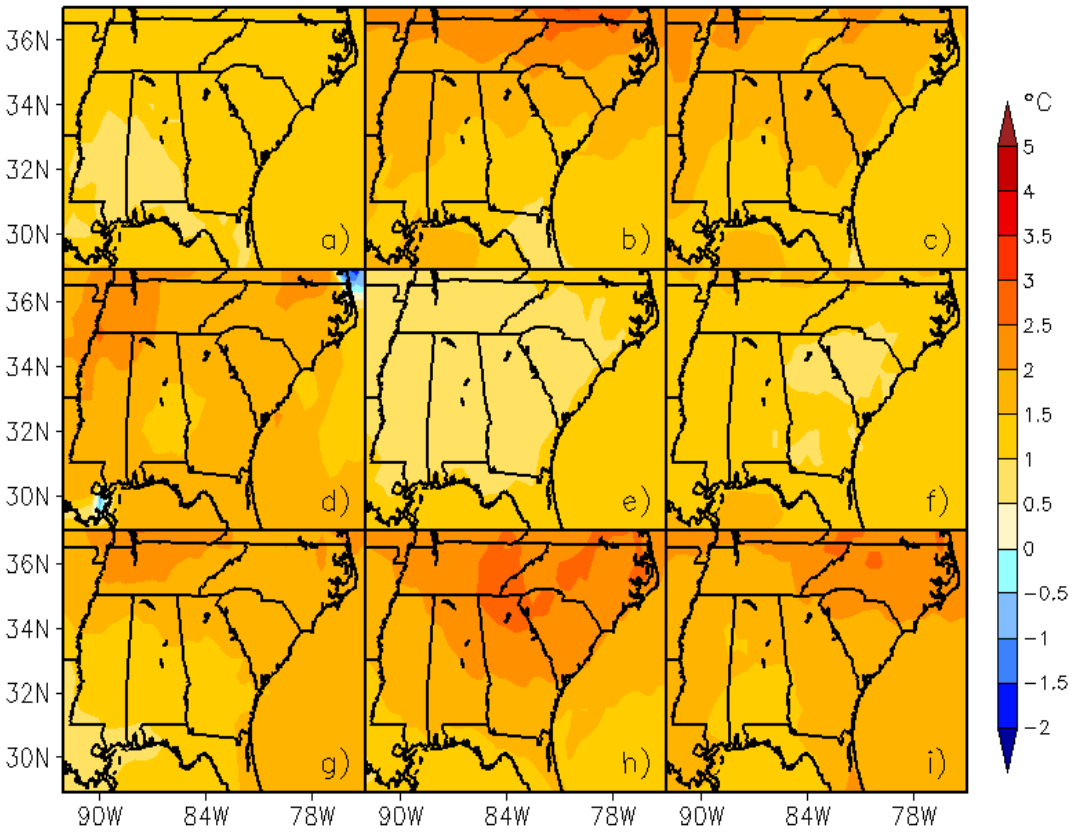

Figure G.2. Individual February minimum temperature change for the WRFG-CGCM3 (a), RCM3-CGCM3 (b), CRCM-CGCM3 (c), WRFG-CCSM (d), MM5I-CCSM (e), CRCM-CCSM (f), ECP2-GFDL (g), RCM3-GFDL (h), and GFDL-timeslice (i) NARCCAP models.

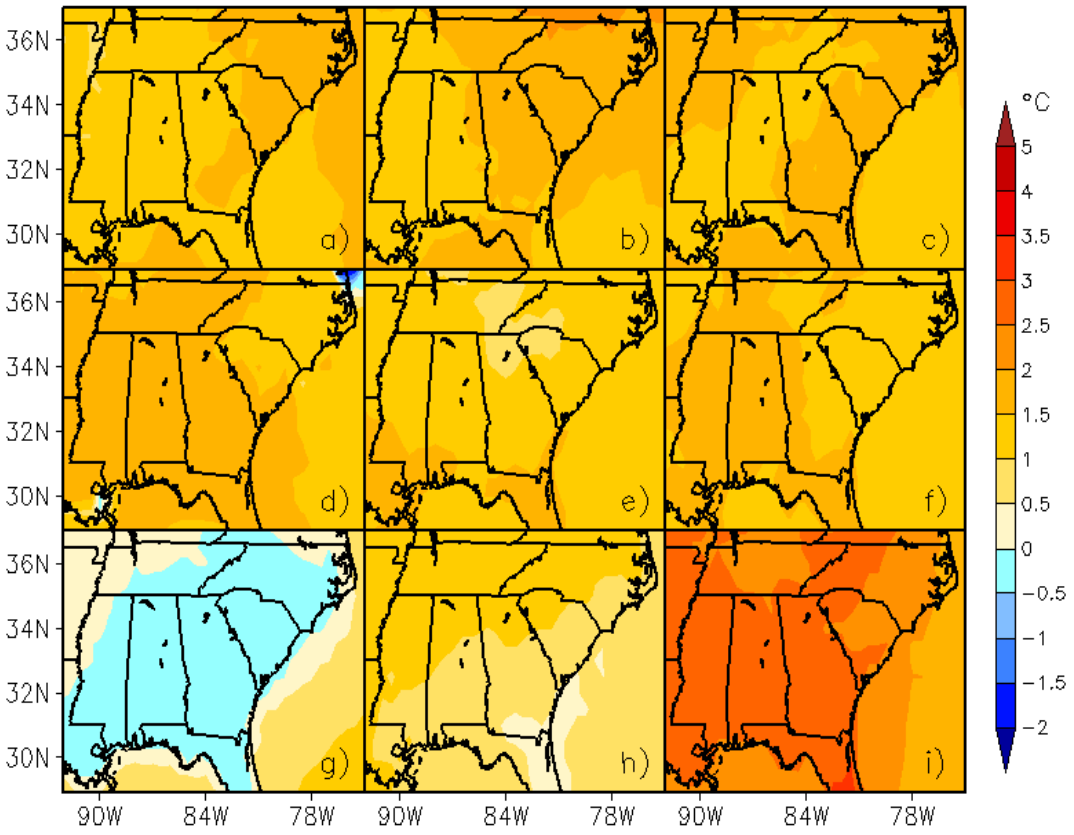

Figure G.3. Individual March minimum temperature change for the WRFG-CGCM3 (a), RCM3-CGCM3 (b), CRCM-CGCM3 (c), WRFG-CCSM (d), MM5I-CCSM (e), CRCM-CCSM (f), ECP2-GFDL (g), RCM3-GFDL (h), and GFDL-timeslice (i) NARCCAP models.

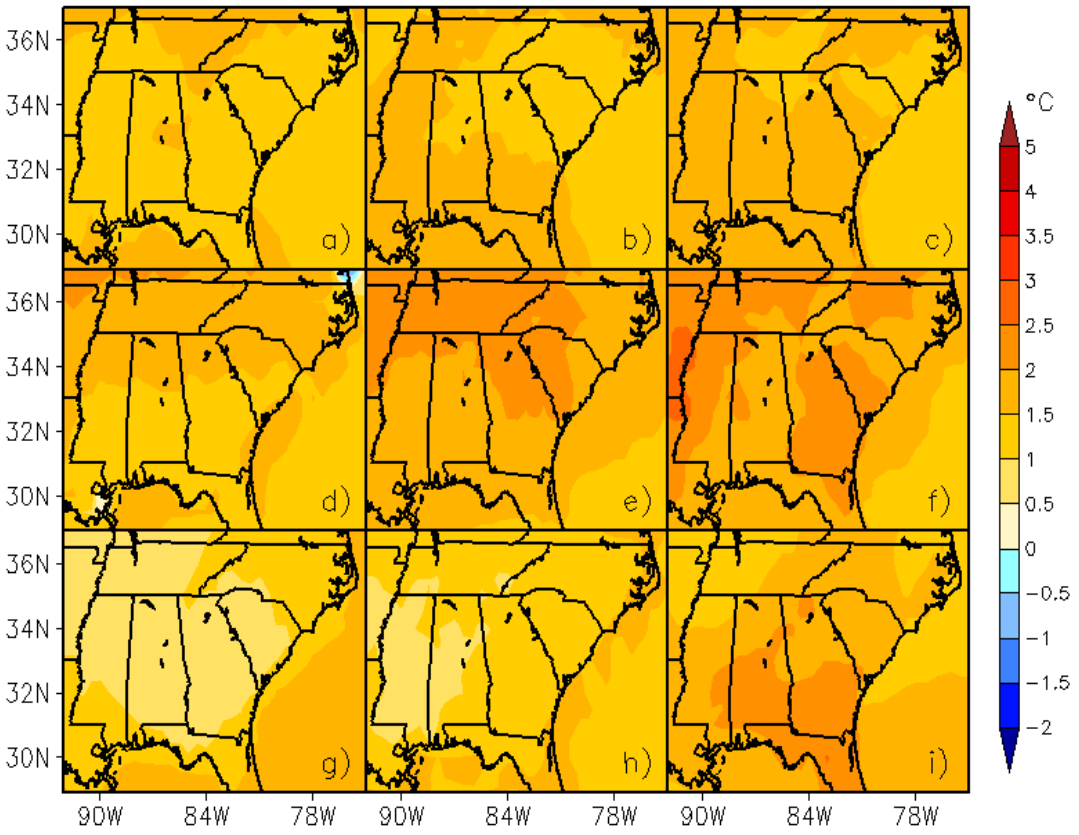

Figure G.4. Individual April minimum temperature change for the WRFG-CGCM3 (a), RCM3-CGCM3 (b), CRCM-CGCM3 (c), WRFG-CCSM (d), MM5I-CCSM (e), CRCM-CCSM (f), ECP2-GFDL (g), RCM3-GFDL (h), and GFDL-timeslice (i) NARCCAP models.

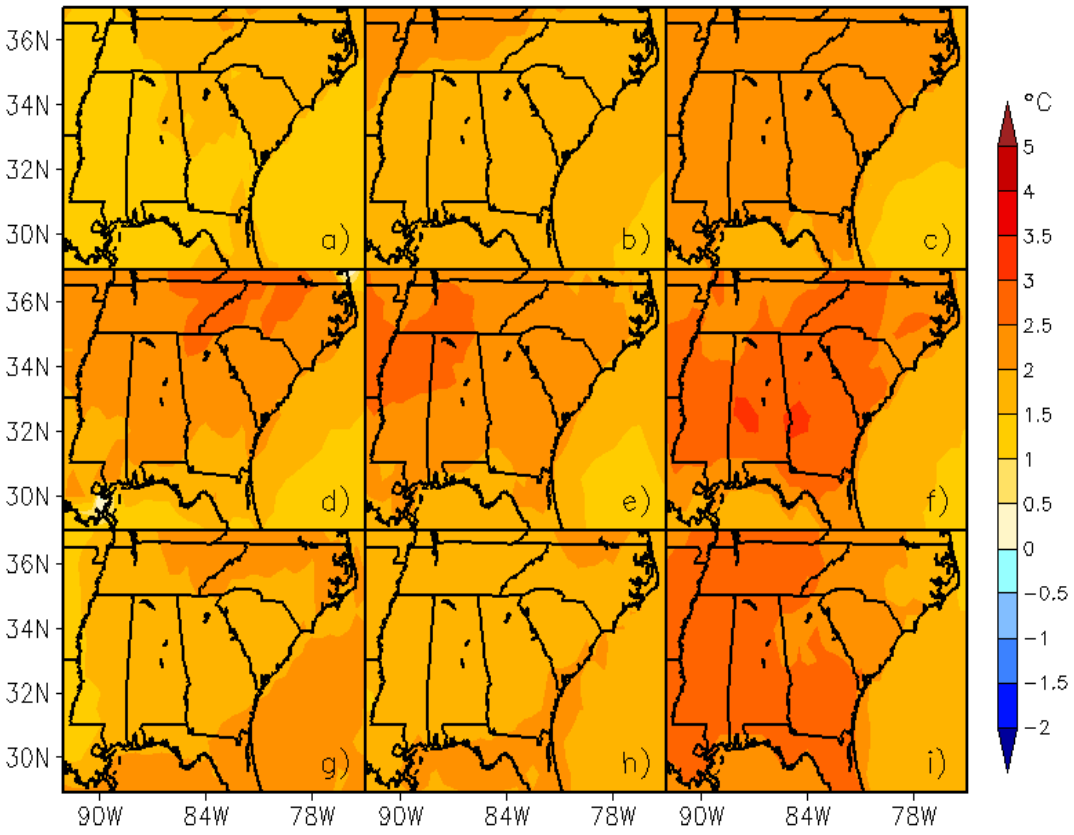

Figure G.5. Individual May minimum temperature change for the WRFG-CGCM3 (a), RCM3-CGCM3 (b), CRCM-CGCM3 (c), WRFG-CCSM (d), MM5I-CCSM (e), CRCM-CCSM (f), ECP2-GFDL (g), RCM3-GFDL (h), and GFDL-timeslice (i) NARCCAP models.

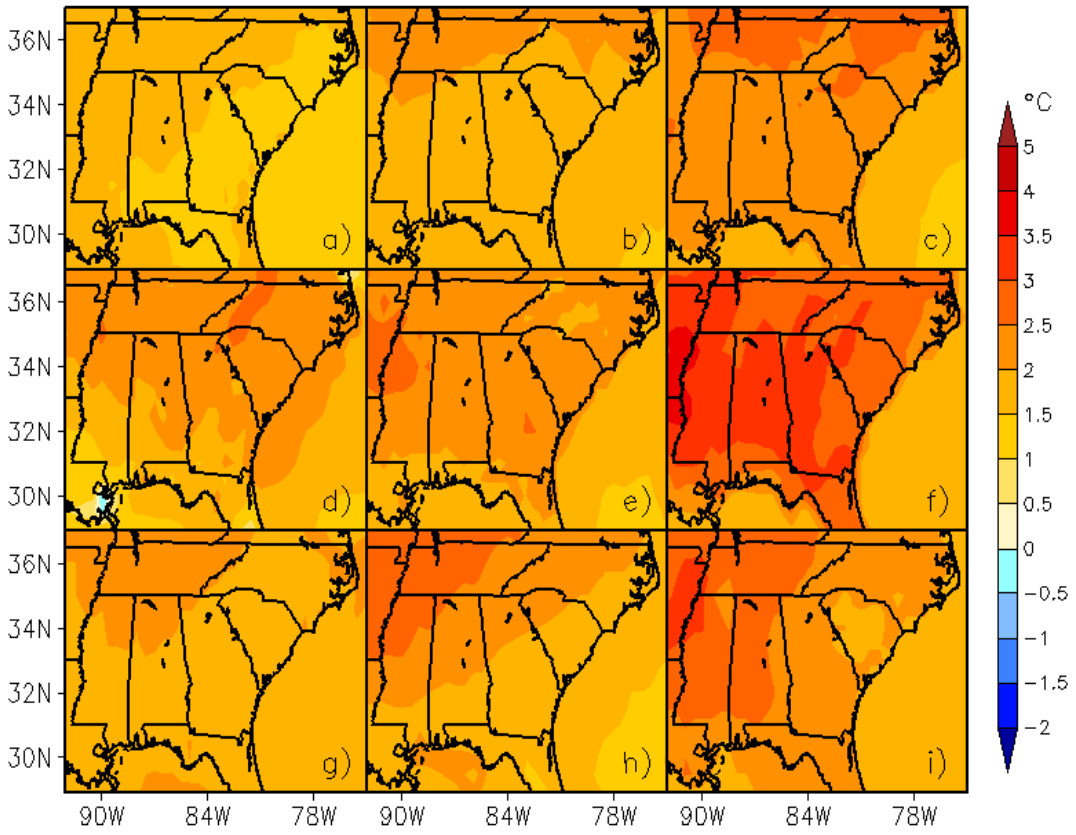

Figure G.6. Individual June minimum temperature change for the WRFG-CGCM3 (a), RCM3-CGCM3 (b), CRCM-CGCM3 (c), WRFG-CCSM (d), MM5I-CCSM (e), CRCM-CCSM (f), ECP2-GFDL (g), RCM3-GFDL (h), and GFDL-timeslice (i) NARCCAP models.

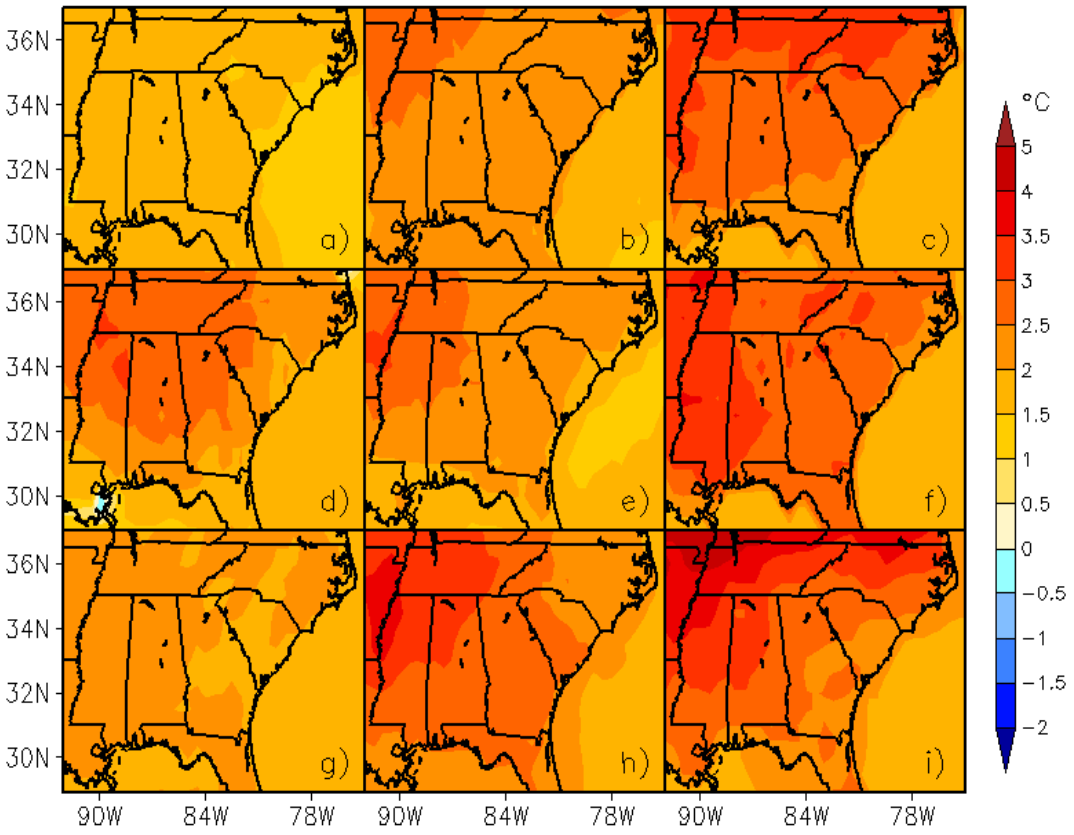

Figure G.7. Individual July minimum temperature change for the WRFG-CGCM3 (a), RCM3-CGCM3 (b), CRCM-CGCM3 (c), WRFG-CCSM (d), MM5I-CCSM (e), CRCM-CCSM (f), ECP2-GFDL (g), RCM3-GFDL (h), and GFDL-timeslice (i) NARCCAP models.

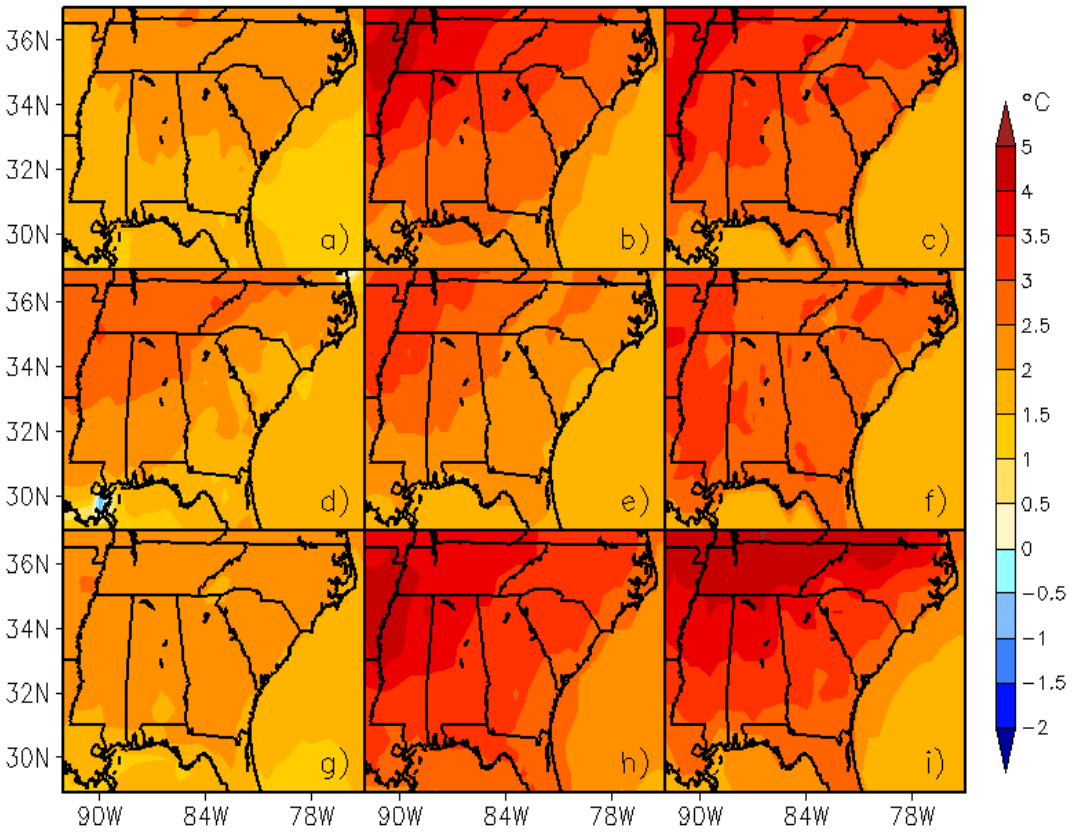

Figure G.8. Individual August minimum temperature change for the WRFG-CGCM3 (a), RCM3-CGCM3 (b), CRCM-CGCM3 (c), WRFG-CCSM (d), MM5I-CCSM (e), CRCM-CCSM (f), ECP2-GFDL (g), RCM3-GFDL (h), and GFDL-timeslice (i) NARCCAP models.

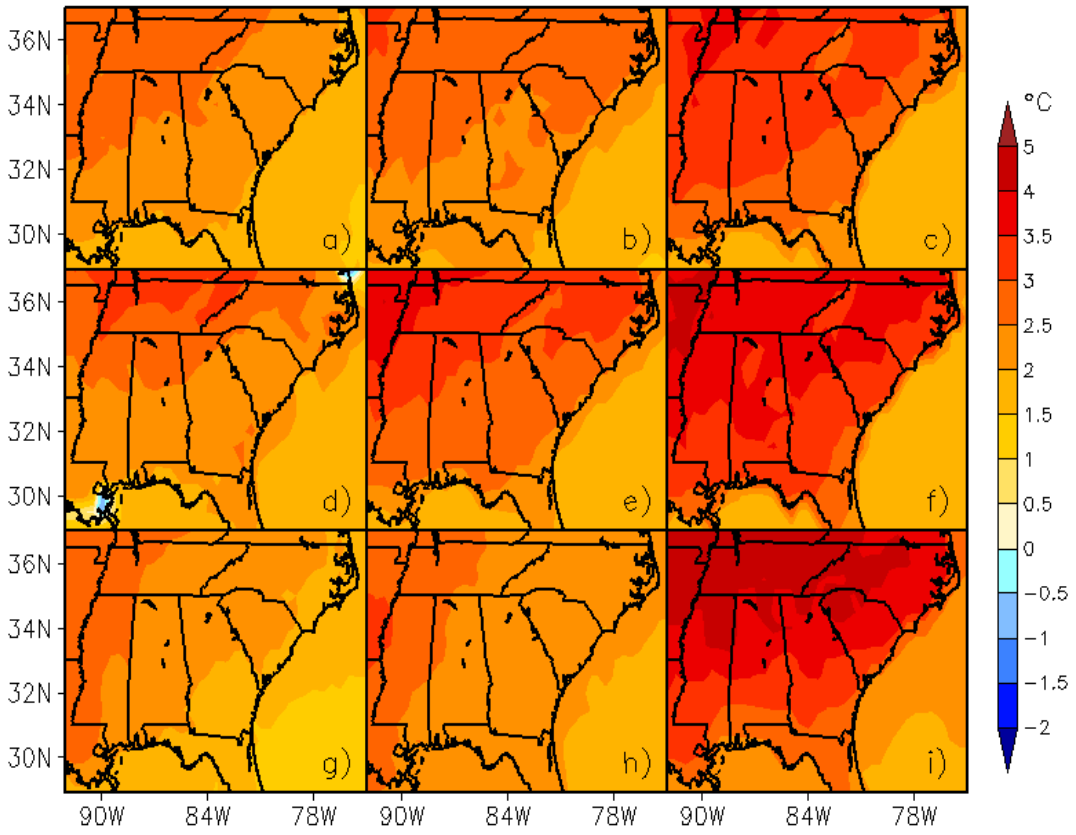

Figure G.9. Individual September minimum temperature change for the WRFG-CGCM3 (a), RCM3-CGCM3 (b), CRCM-CGCM3 (c), WRFG-CCSM (d), MM5I-CCSM (e), CRCM-CCSM (f), ECP2-GFDL (g), RCM3-GFDL (h), and GFDL-timeslice (i) NARCCAP models.

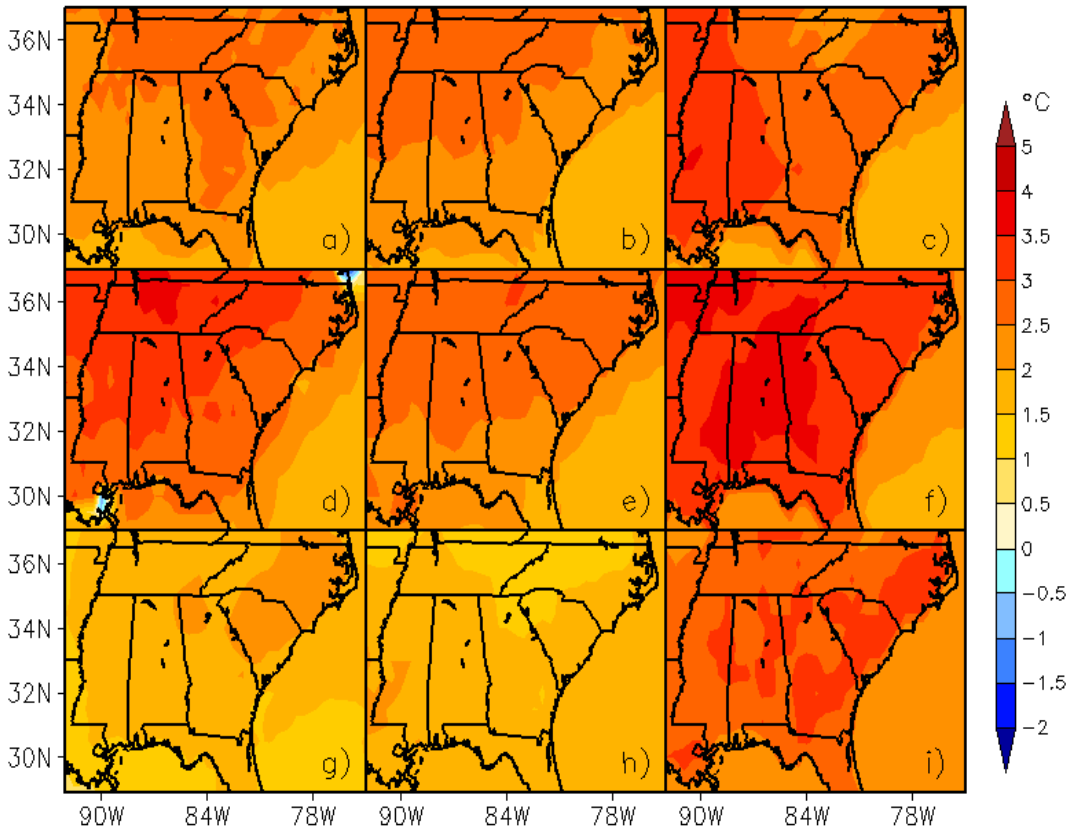

Figure G.10. Individual October minimum temperature change for the WRFG-CGCM3 (a), RCM3-CGCM3 (b), CRCM-CGCM3 (c), WRFG-CCSM (d), MM5I-CCSM (e), CRCM-CCSM (f), ECP2-GFDL (g), RCM3-GFDL (h), and GFDL-timeslice (i) NARCCAP models.

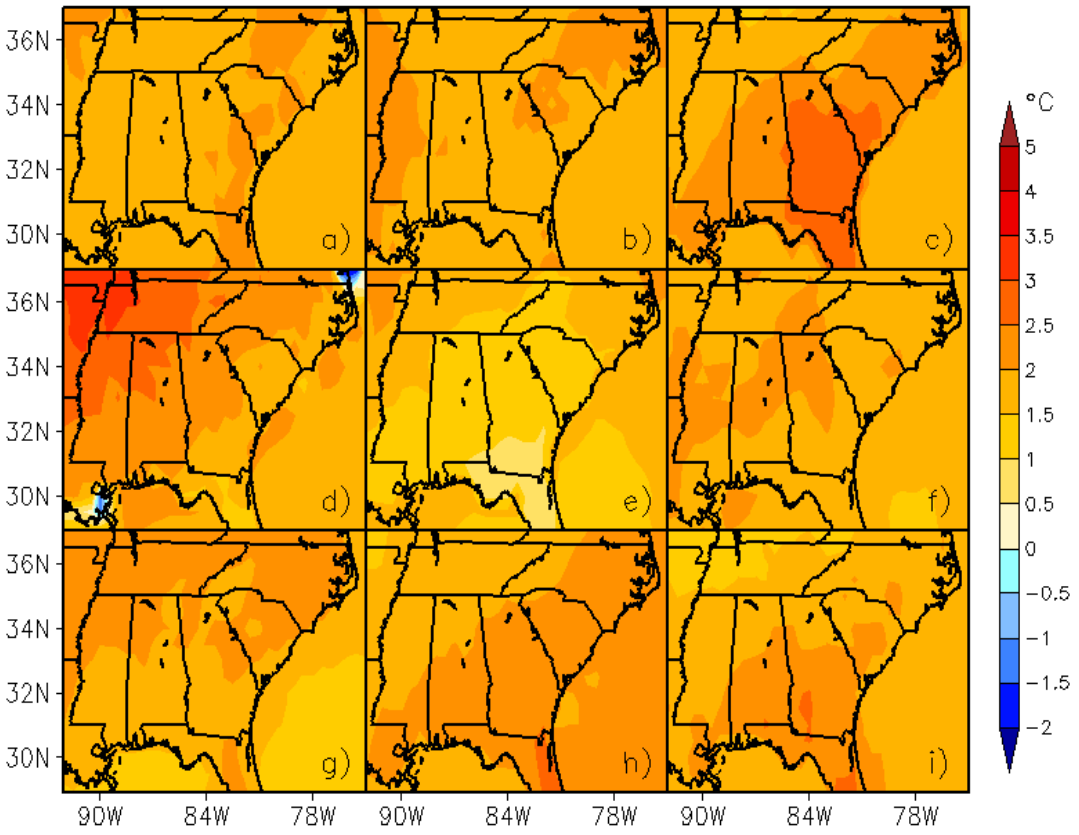

Figure G.11. Individual November minimum temperature change for the WRFG-CGCM3 (a), RCM3-CGCM3 (b), CRCM-CGCM3 (c), WRFG-CCSM (d), MM5I-CCSM (e), CRCM-CCSM (f), ECP2-GFDL (g), RCM3-GFDL (h), and GFDL-timeslice (i) NARCCAP models.

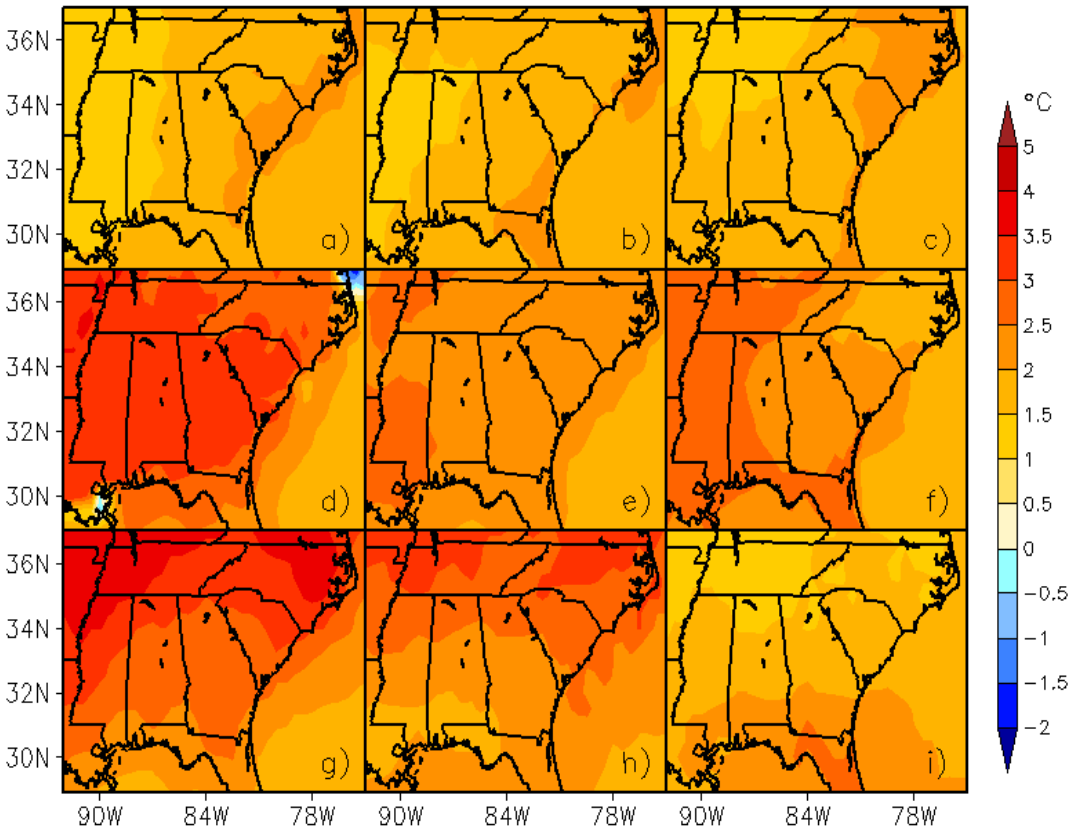

Figure G.12. Individual December minimum temperature change for the WRFG-CGCM3 (a), RCM3-CGCM3 (b), CRCM-CGCM3 (c), WRFG-CCSM (d), MM5I-CCSM (e), CRCM-CCSM (f), ECP2-GFDL (g), RCM3-GFDL (h), and GFDL-timeslice (i) NARCCAP models.

G.2 MAXIMUM TEMPERATURE

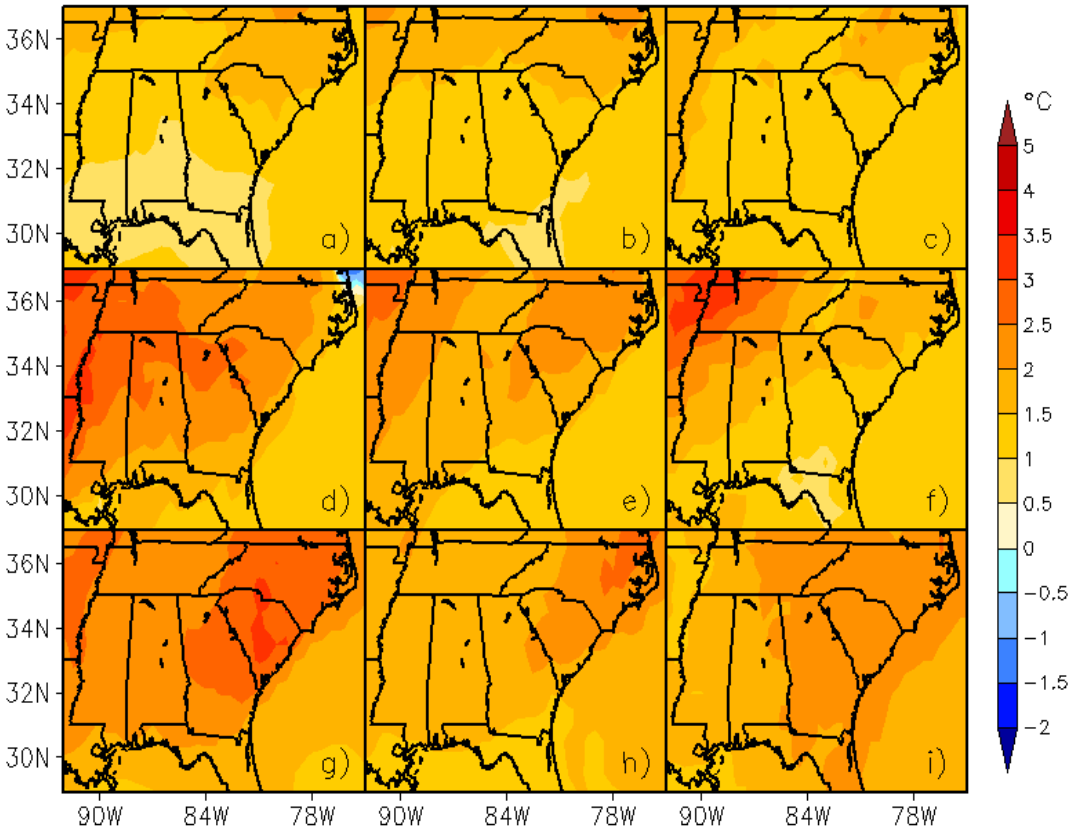

Figure G.13. Individual January maximum temperature change for the WRFG-CGCM3 (a), RCM3-CGCM3 (b), CRCM-CGCM3 (c), WRFG-CCSM (d), MM5I-CCSM (e), CRCM-CCSM (f), ECP2-GFDL (g), RCM3-GFDL (h), and GFDL-timeslice (i) NARCCAP models.

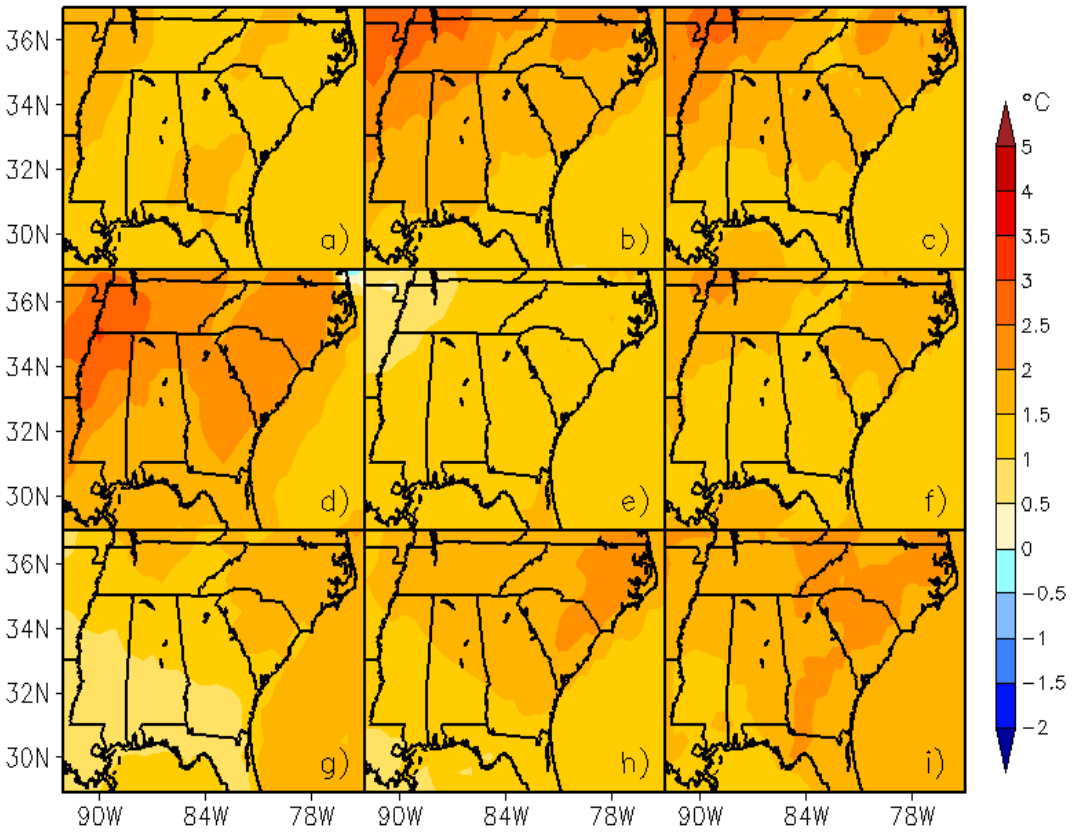

Figure G.14. Individual February maximum temperature change for the WRFG-CGCM3 (a), RCM3-CGCM3 (b), CRCM-CGCM3 (c), WRFG-CCSM (d), MM5I-CCSM (e), CRCM-CCSM (f), ECP2-GFDL (g), RCM3-GFDL (h), and GFDL-timeslice (i) NARCCAP models.

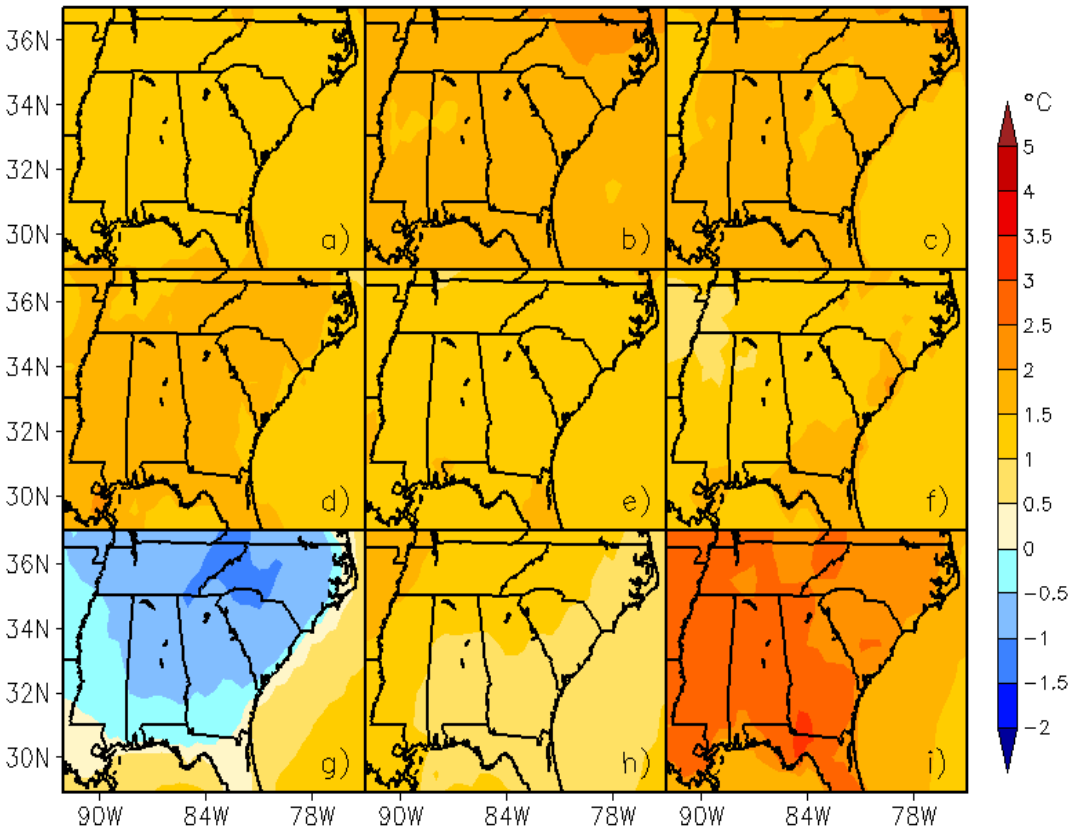

Figure G.15. Individual March maximum temperature change for the WRFG-CGCM3 (a), RCM3-CGCM3 (b), CRCM-CGCM3 (c), WRFG-CCSM (d), MM5I-CCSM (e), CRCM-CCSM (f), ECP2-GFDL (g), RCM3-GFDL (h), and GFDL-timeslice (i) NARCCAP models.

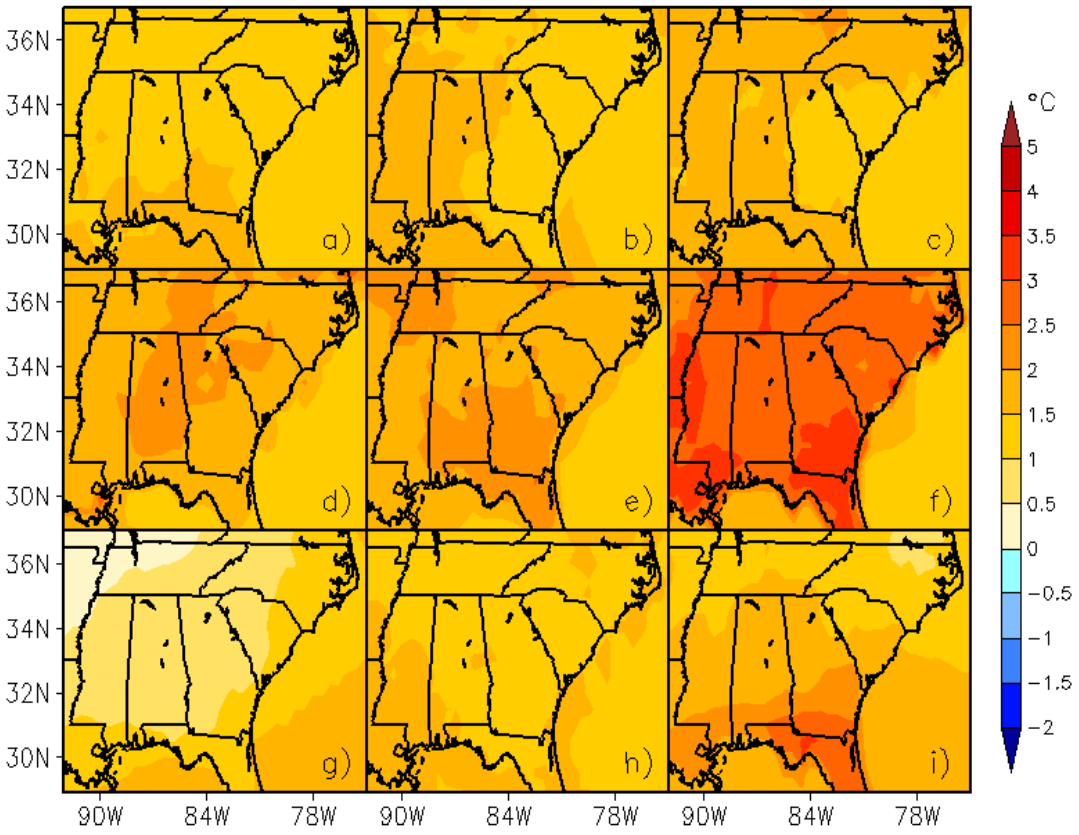

Figure G.16. Individual April maximum temperature change for the WRFG-CGCM3 (a), RCM3-CGCM3 (b), CRCM-CGCM3 (c), WRFG-CCSM (d), MM5I-CCSM (e), CRCM-CCSM (f), ECP2-GFDL (g), RCM3-GFDL (h), and GFDL-timeslice (i) NARCCAP models.

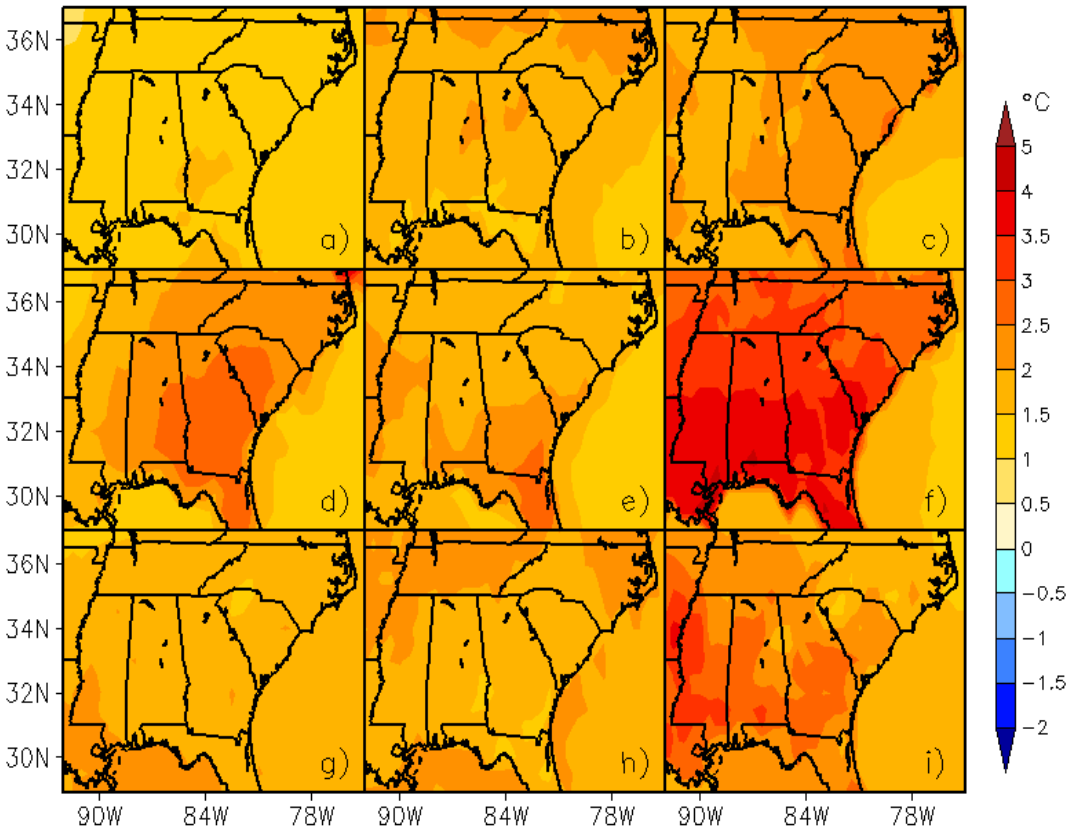

Figure G.17. Individual May maximum temperature change for the WRFG-CGCM3 (a), RCM3-CGCM3 (b), CRCM-CGCM3 (c), WRFG-CCSM (d), MM5I-CCSM (e), CRCM-CCSM (f), ECP2-GFDL (g), RCM3-GFDL (h), and GFDL-timeslice (i) NARCCAP models.

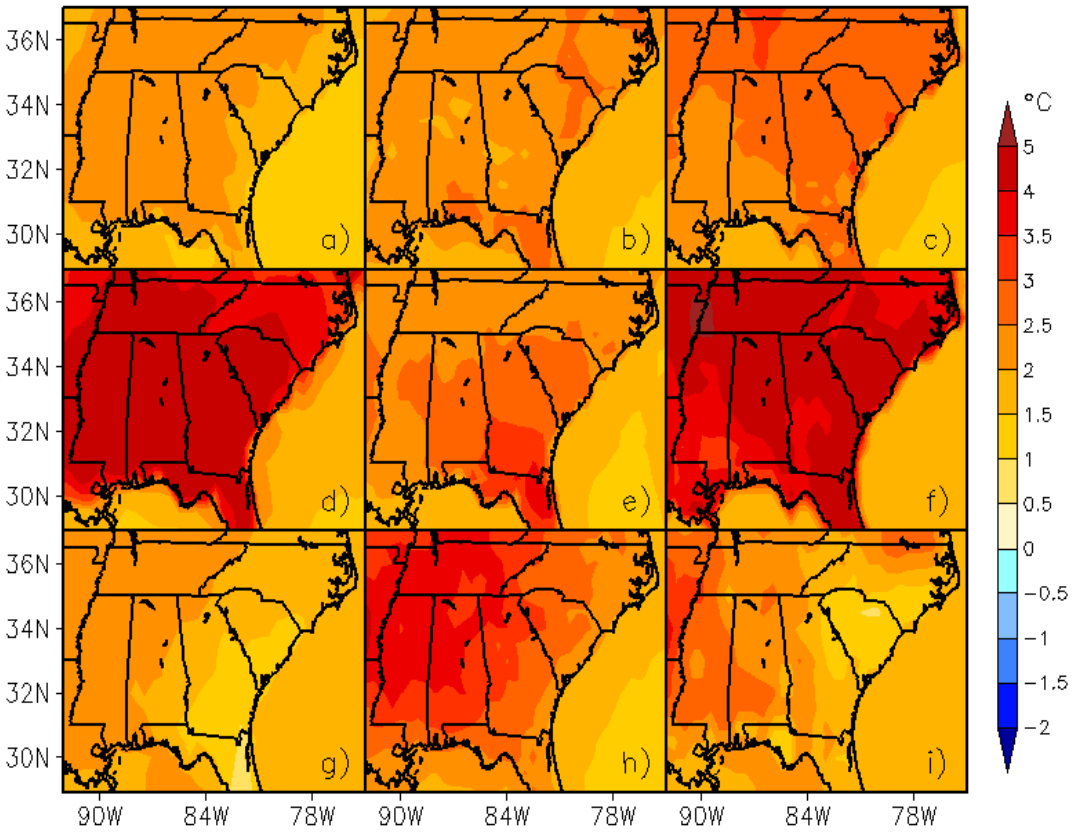

Figure G.18. Individual June maximum temperature change for the WRFG-CGCM3 (a), RCM3-CGCM3 (b), CRCM-CGCM3 (c), WRFG-CCSM (d), MM5I-CCSM (e), CRCM-CCSM (f), ECP2-GFDL (g), RCM3-GFDL (h), and GFDL-timeslice (i) NARCCAP models.

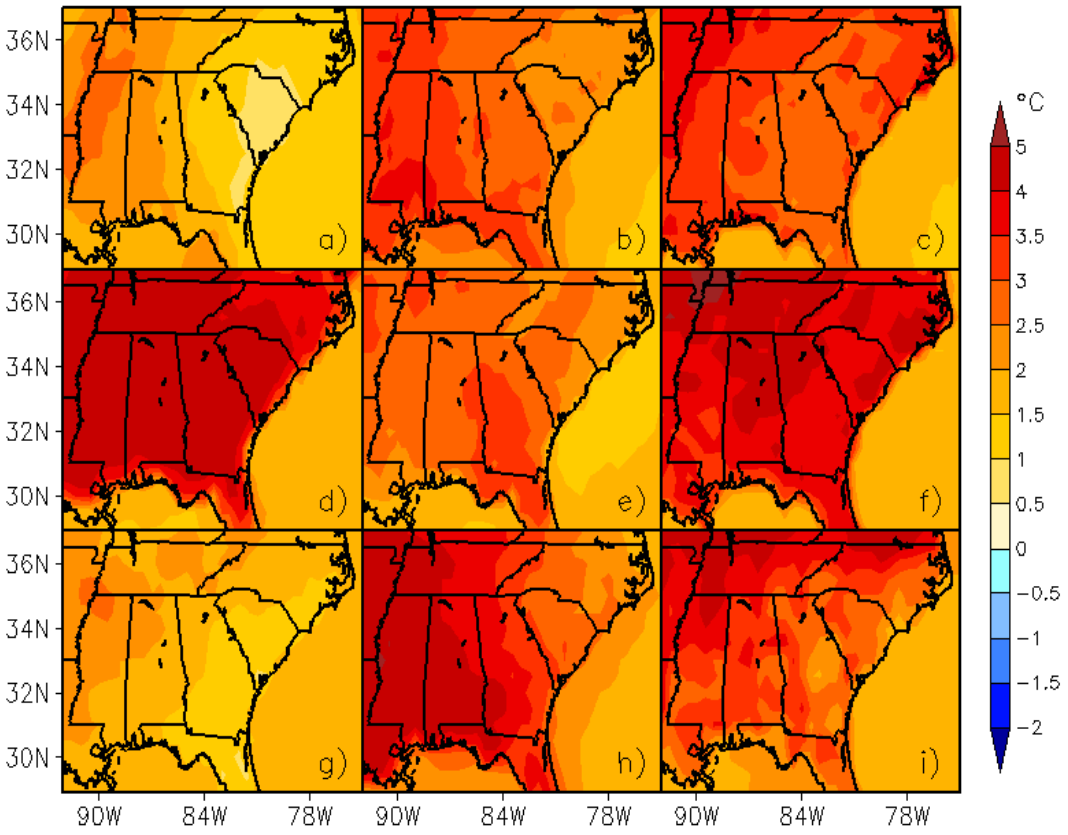

Figure G.19. Individual July maximum temperature change for the WRFG-CGCM3 (a), RCM3-CGCM3 (b), CRCM-CGCM3 (c), WRFG-CCSM (d), MM5I-CCSM (e), CRCM-CCSM (f), ECP2-GFDL (g), RCM3-GFDL (h), and GFDL-timeslice (i) NARCCAP models.

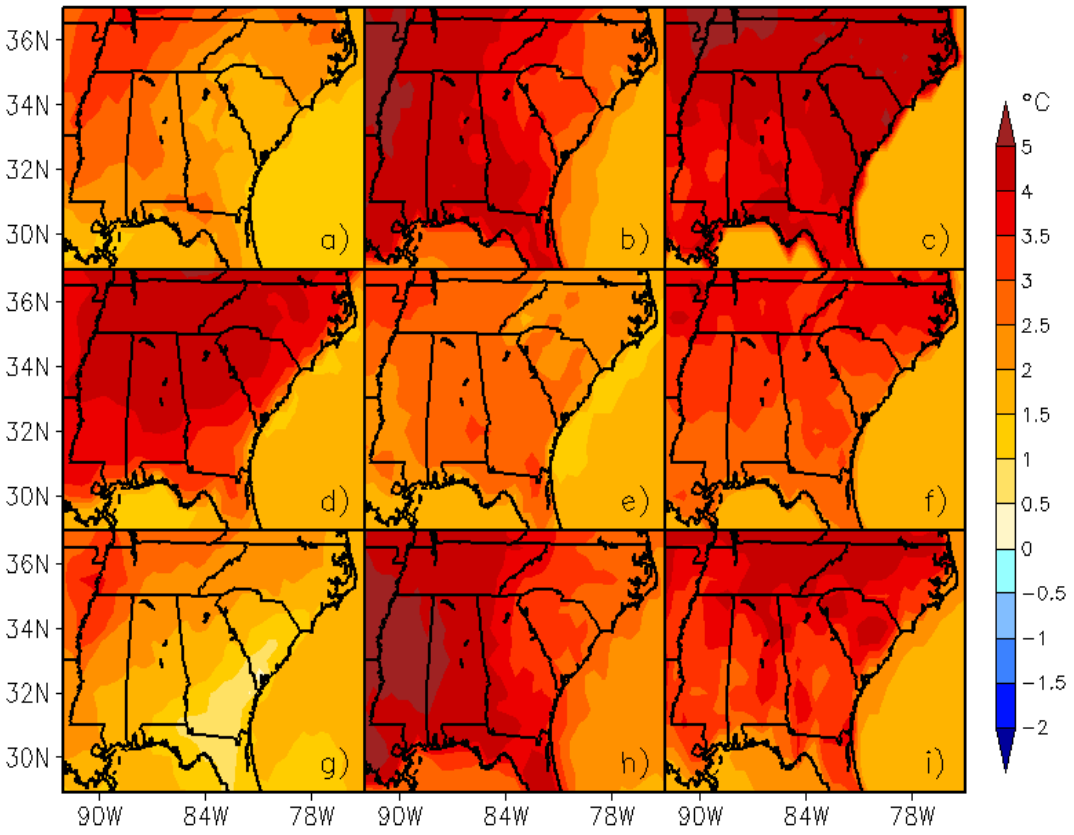

Figure G.20. Individual August maximum temperature change for the WRFG-CGCM3 (a), RCM3-CGCM3 (b), CRCM-CGCM3 (c), WRFG-CCSM (d), MM5I-CCSM (e), CRCM-CCSM (f), ECP2-GFDL (g), RCM3-GFDL (h), and GFDL-timeslice (i) NARCCAP models.

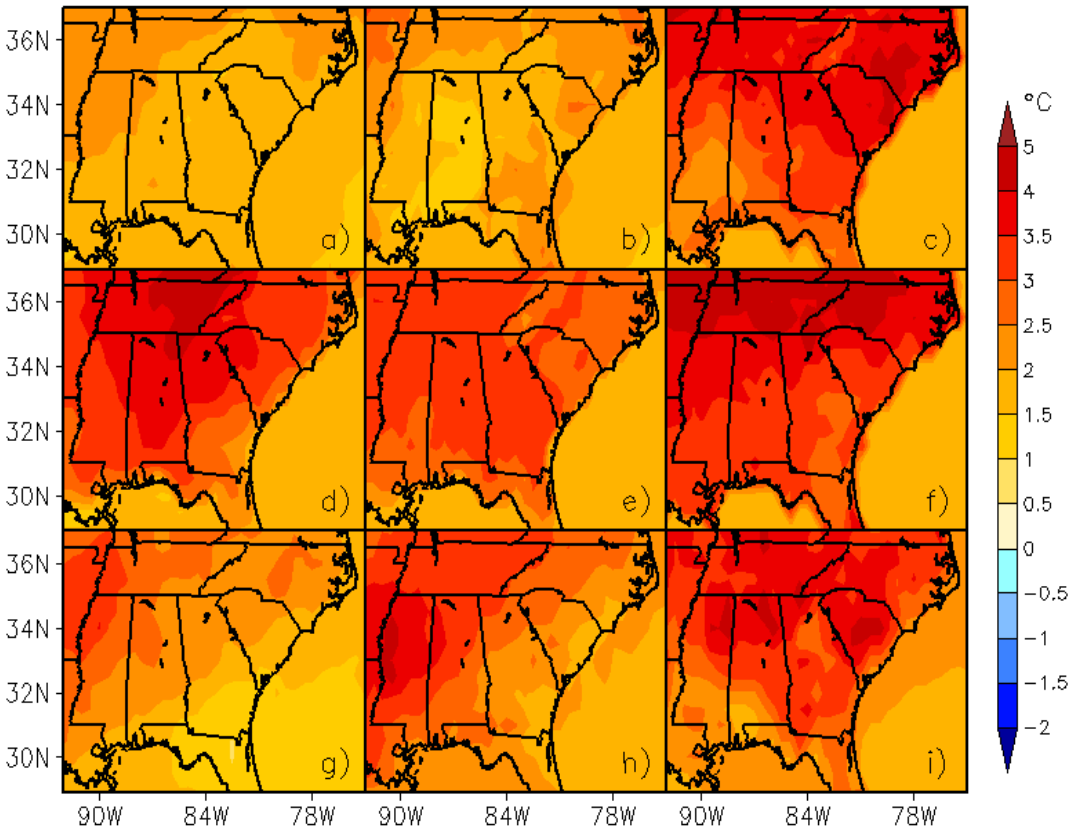

Figure G.21. Individual September maximum temperature change for the WRFG-CGCM3 (a), RCM3-CGCM3 (b), CRCM-CGCM3 (c), WRFG-CCSM (d), MM5I-CCSM (e), CRCM-CCSM (f), ECP2-GFDL (g), RCM3-GFDL (h), and GFDL-timeslice (i) NARCCAP models.

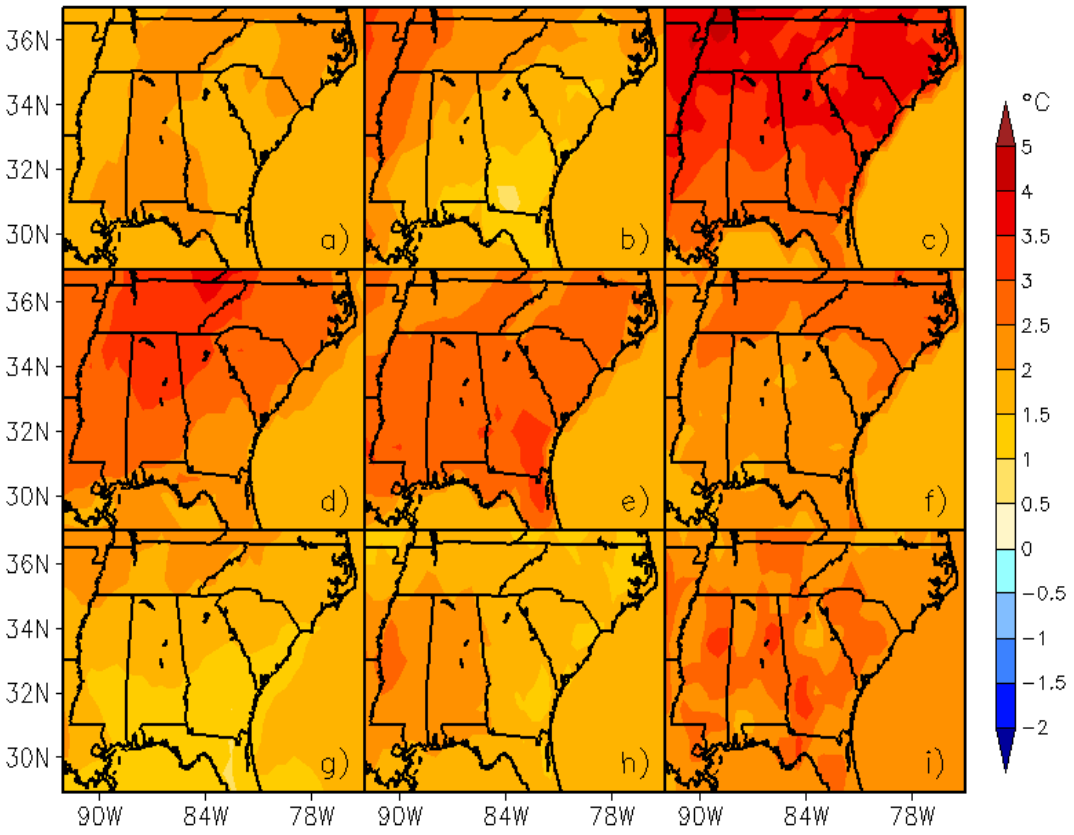

Figure G.22. Individual October maximum temperature change for the WRFG-CGCM3 (a), RCM3-CGCM3 (b), CRCM-CGCM3 (c), WRFG-CCSM (d), MM5I-CCSM (e), CRCM-CCSM (f), ECP2-GFDL (g), RCM3-GFDL (h), and GFDL-timeslice (i) NARCCAP models.

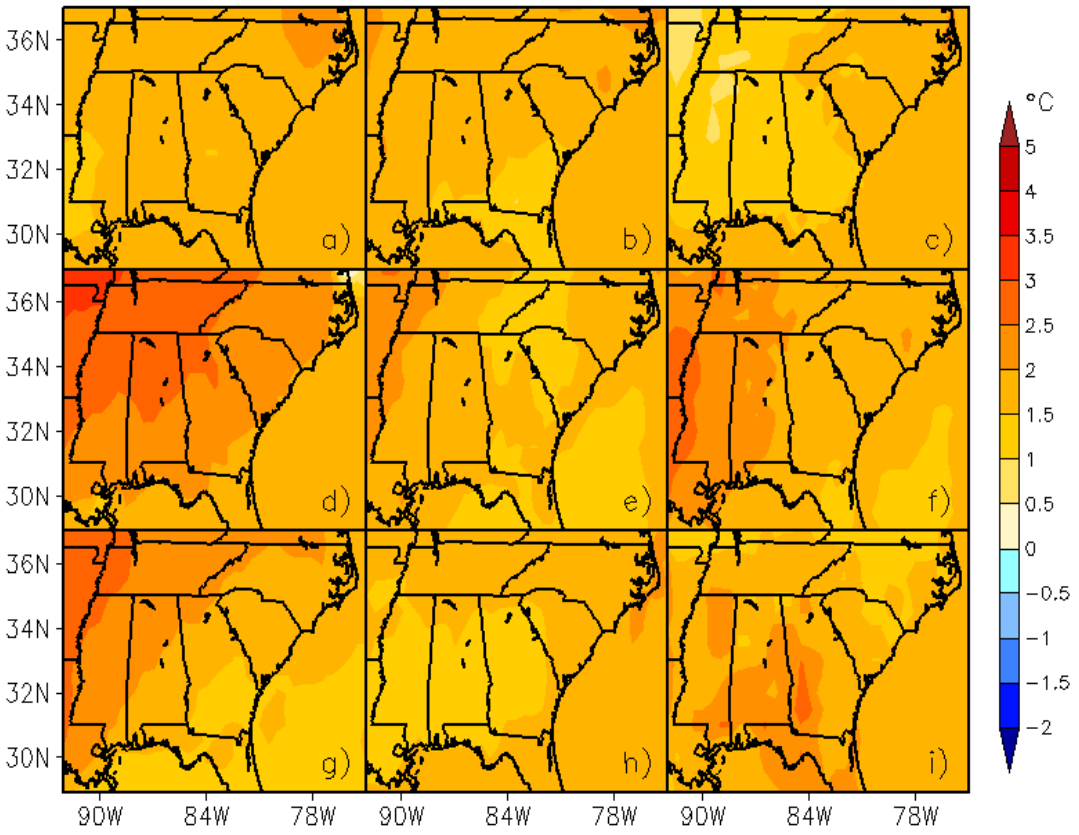

Figure G.23. Individual November maximum temperature change for the WRFG-CGCM3 (a), RCM3-CGCM3 (b), CRCM-CGCM3 (c), WRFG-CCSM (d), MM5I-CCSM (e), CRCM-CCSM (f), ECP2-GFDL (g), RCM3-GFDL (h), and GFDL-timeslice (i) NARCCAP models.

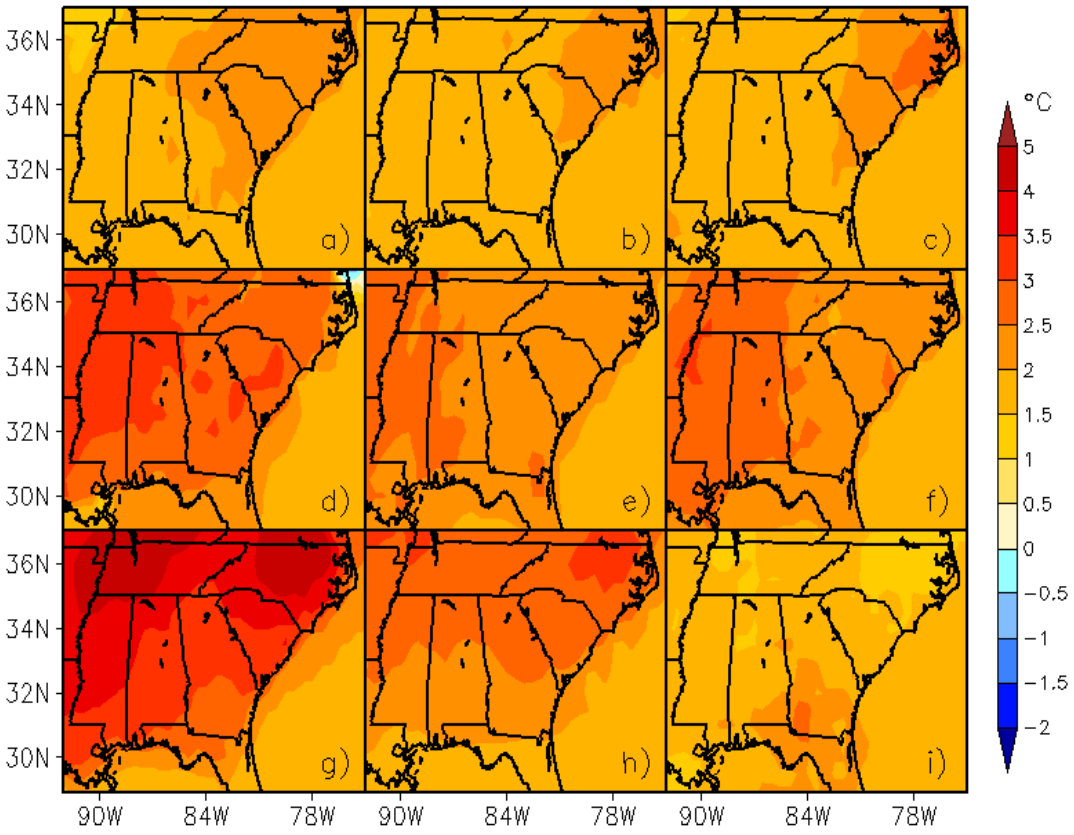

Figure G.24. Individual December maximum temperature change for the WRFG-CGCM3 (a), RCM3-CGCM3 (b), CRCM-CGCM3 (c), WRFG-CCSM (d), MM5I-CCSM (e), CRCM-CCSM (f), ECP2-GFDL (g), RCM3-GFDL (h), and GFDL-timeslice (i) NARCCAP models.

G.3 MEAN PRECIPITATION

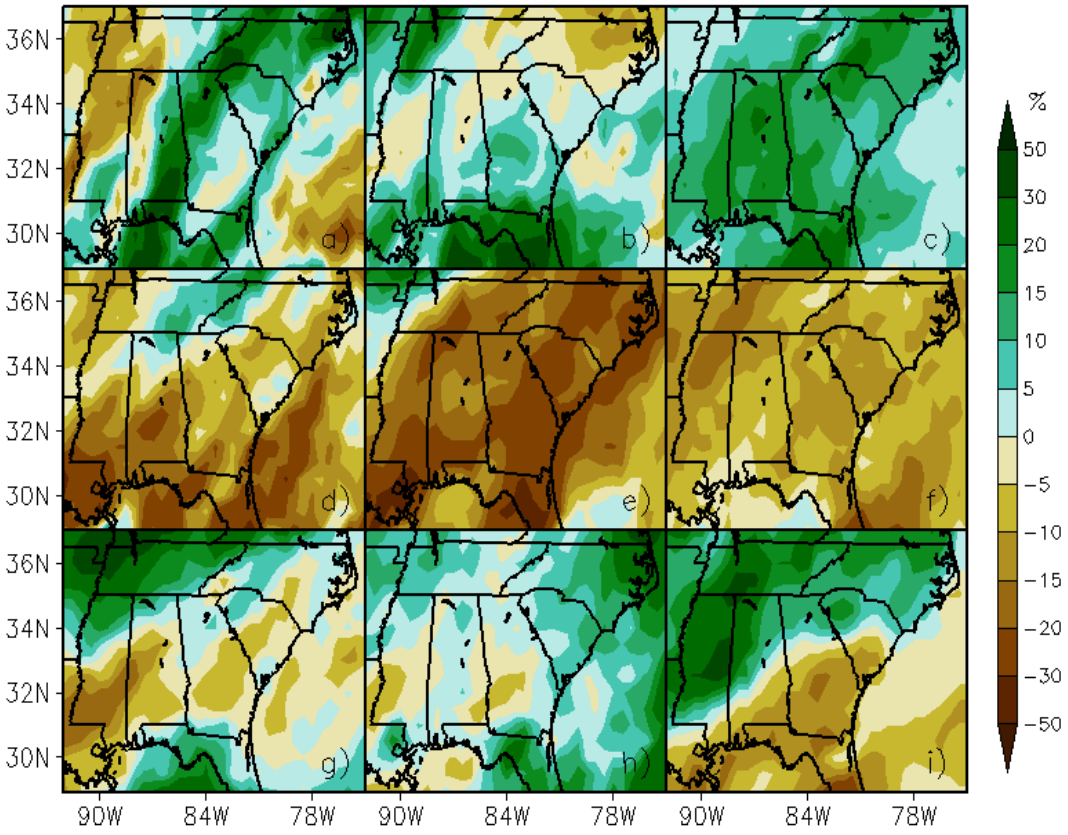

Figure G.25. Individual January mean precipitation change for the WRFG-CGCM3 (a), RCM3-CGCM3 (b), CRCM-CGCM3 (c), WRFG-CCSM (d), MM5I-CCSM (e), CRCM-CCSM (f), ECP2-GFDL (g), RCM3-GFDL (h), and GFDL-timeslice (i) NARCCAP models.

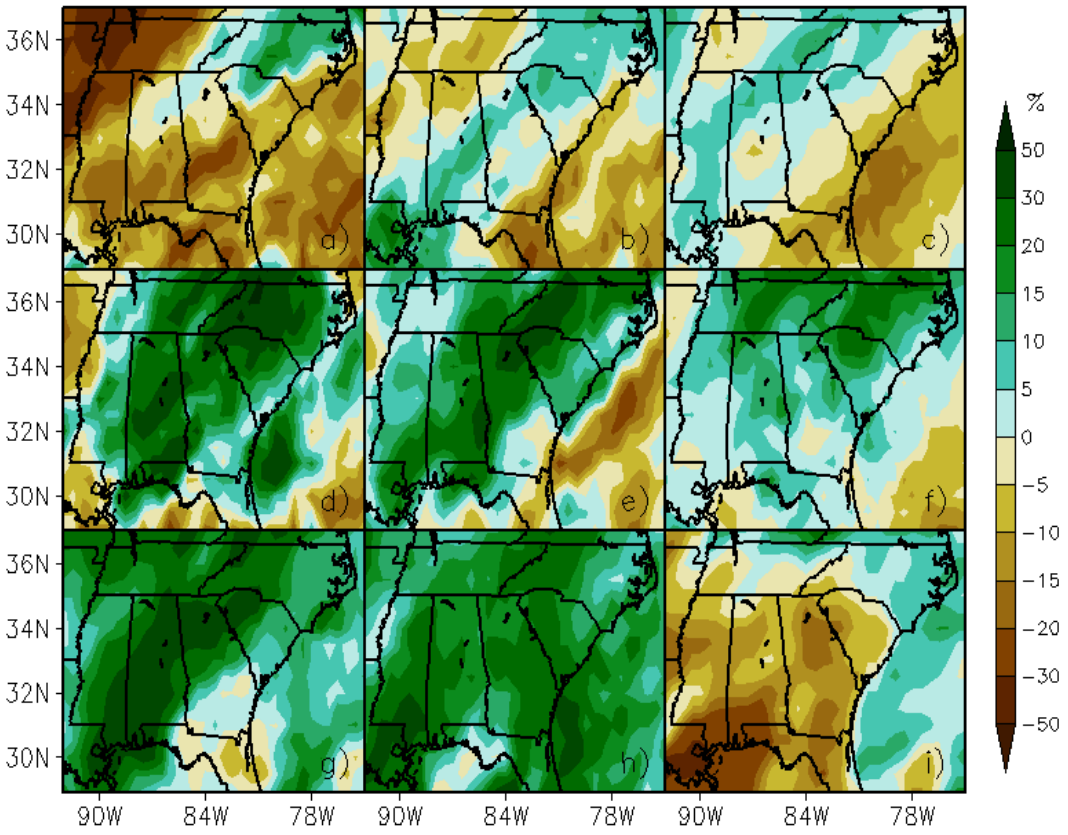

Figure G.26. Individual February mean precipitation change for the WRFG-CGCM3 (a), RCM3-CGCM3 (b), CRCM-CGCM3 (c), WRFG-CCSM (d), MM5I-CCSM (e), CRCM-CCSM (f), ECP2-GFDL (g), RCM3-GFDL (h), and GFDL-timeslice (i) NARCCAP models.

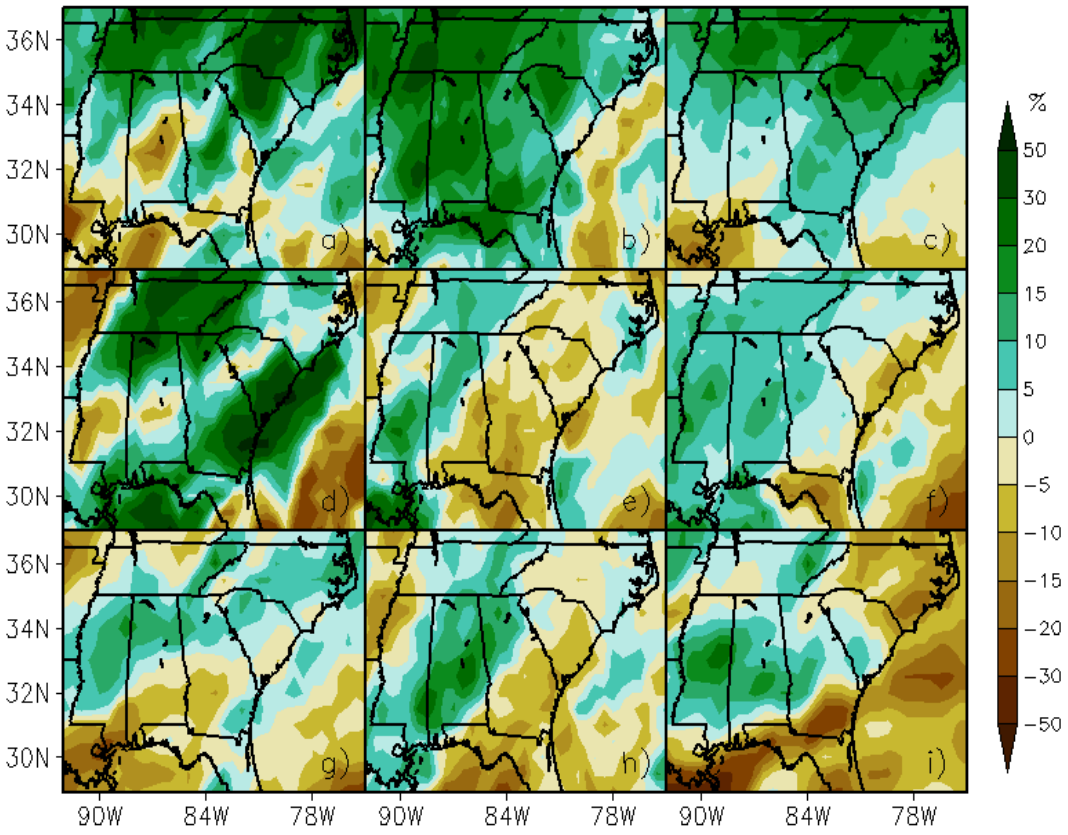

Figure G.27. Individual March mean precipitation change for the WRFG-CGCM3 (a), RCM3-CGCM3 (b), CRCM-CGCM3 (c), WRFG-CCSM (d), MM5I-CCSM (e), CRCM-CCSM (f), ECP2-GFDL (g), RCM3-GFDL (h), and GFDL-timeslice (i) NARCCAP models.

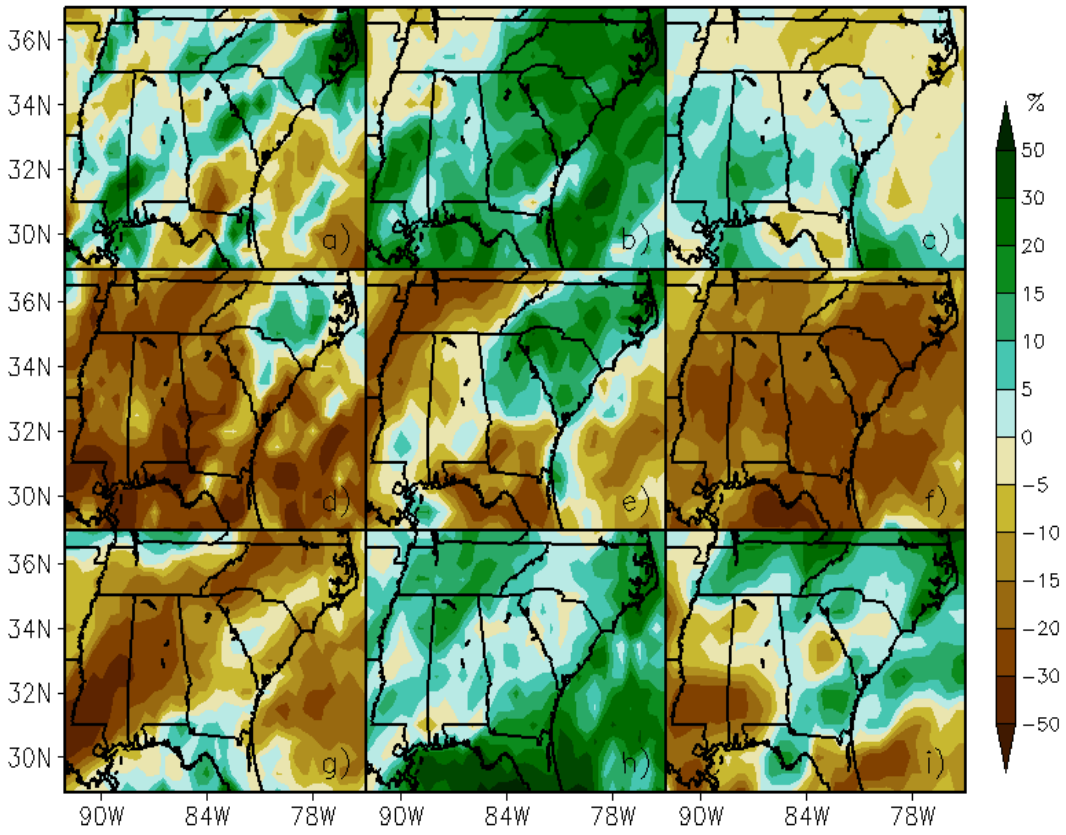

Figure G.28. Individual April mean precipitation change for the WRFG-CGCM3 (a), RCM3-CGCM3 (b), CRCM-CGCM3 (c), WRFG-CCSM (d), MM5I-CCSM (e), CRCM-CCSM (f), ECP2-GFDL (g), RCM3-GFDL (h), and GFDL-timeslice (i) NARCCAP models.

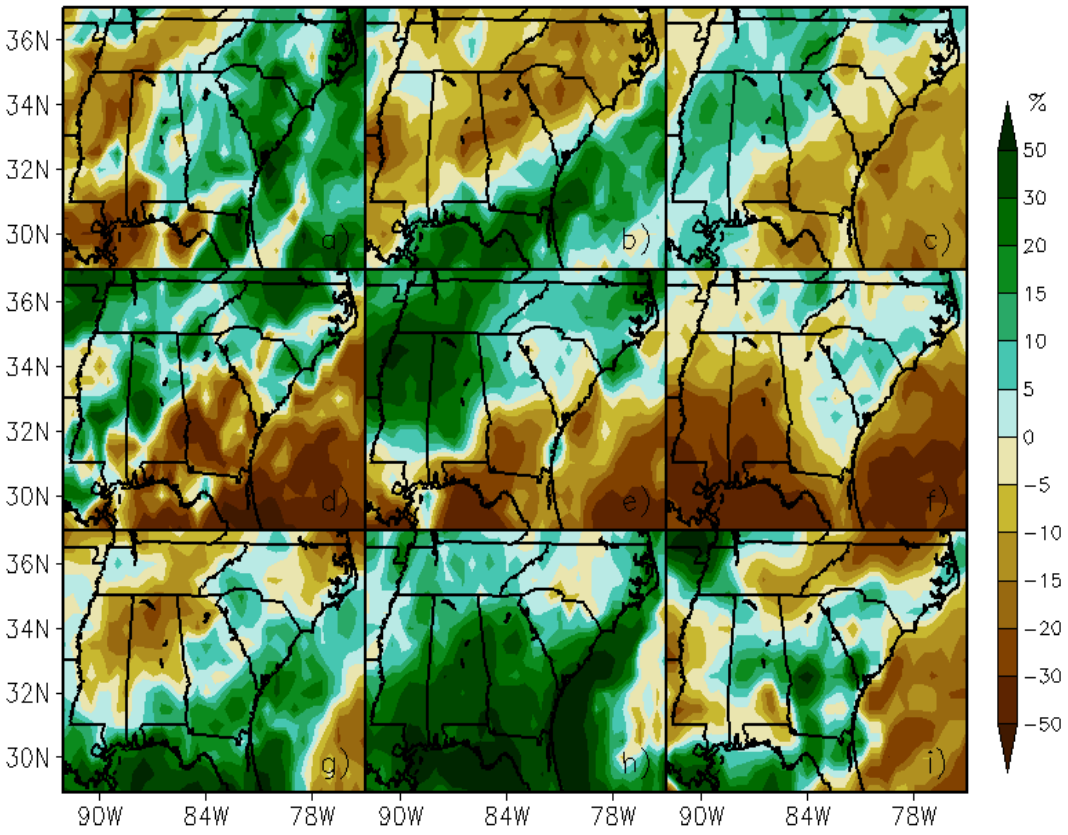

Figure G.29. Individual May mean precipitation change for the WRFG-CGCM3 (a), RCM3-CGCM3 (b), CRCM-CGCM3 (c), WRFG-CCSM (d), MM5I-CCSM (e), CRCM-CCSM (f), ECP2-GFDL (g), RCM3-GFDL (h), and GFDL-timeslice (i) NARCCAP models.

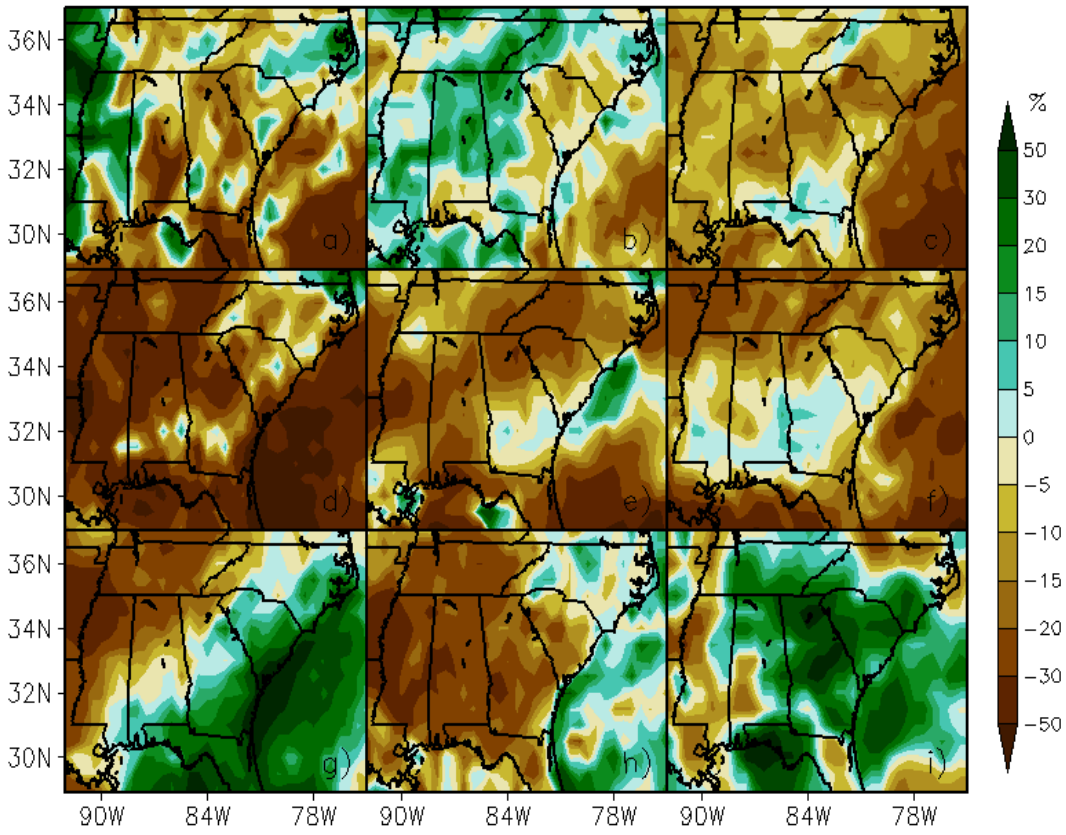

Figure G.30. Individual June mean precipitation change for the WRFG-CGCM3 (a), RCM3-CGCM3 (b), CRCM-CGCM3 (c), WRFG-CCSM (d), MM5I-CCSM (e), CRCM-CCSM (f), ECP2-GFDL (g), RCM3-GFDL (h), and GFDL-timeslice (i) NARCCAP models.

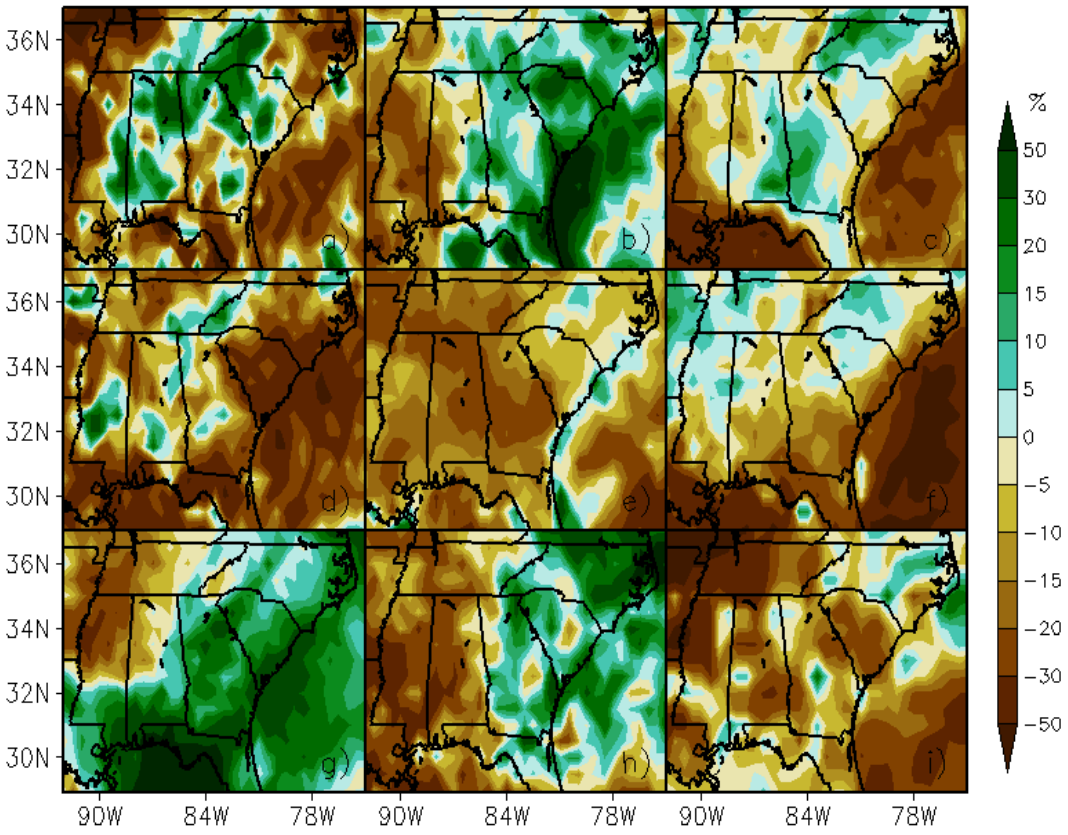

Figure G.31. Individual July mean precipitation change for the WRFG-CGCM3 (a), RCM3-CGCM3 (b), CRCM-CGCM3 (c), WRFG-CCSM (d), MM5I-CCSM (e), CRCM-CCSM (f), ECP2-GFDL (g), RCM3-GFDL (h), and GFDL-timeslice (i) NARCCAP models.

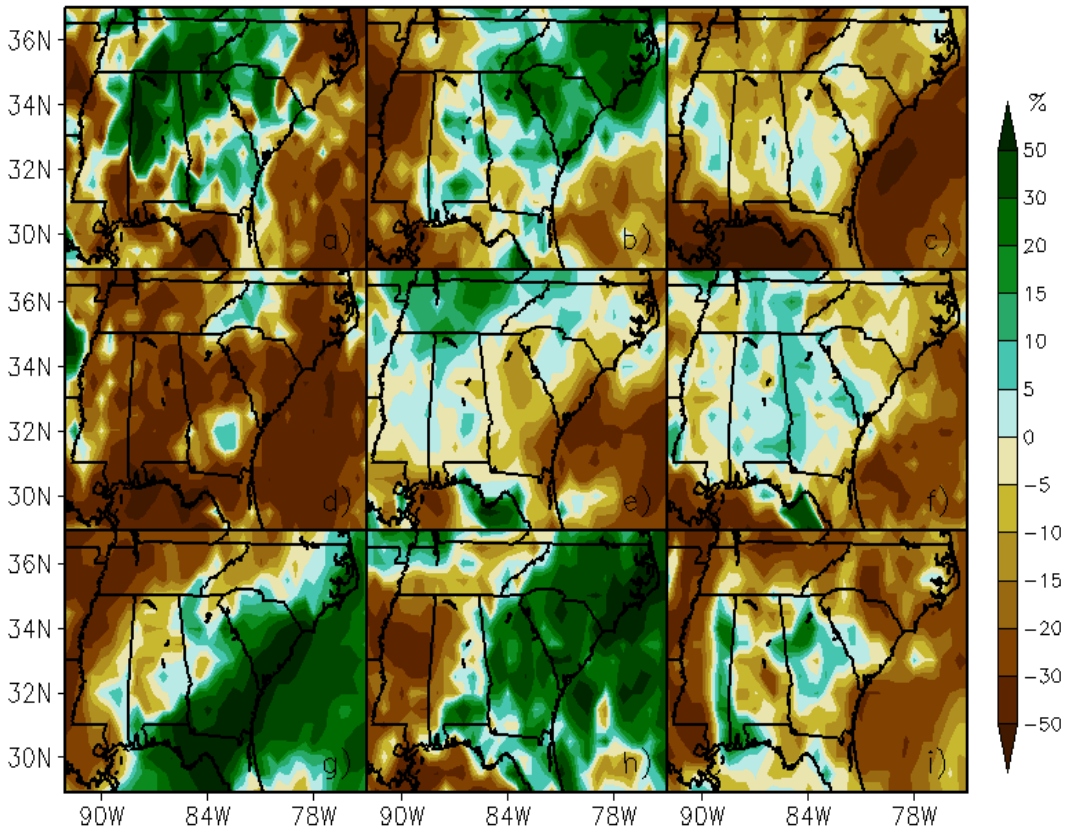

Figure G.32. Individual August mean precipitation change for the WRFG-CGCM3 (a), RCM3-CGCM3 (b), CRCM-CGCM3 (c), WRFG-CCSM (d), MM5I-CCSM (e), CRCM-CCSM (f), ECP2-GFDL (g), RCM3-GFDL (h), and GFDL-timeslice (i) NARCCAP models.

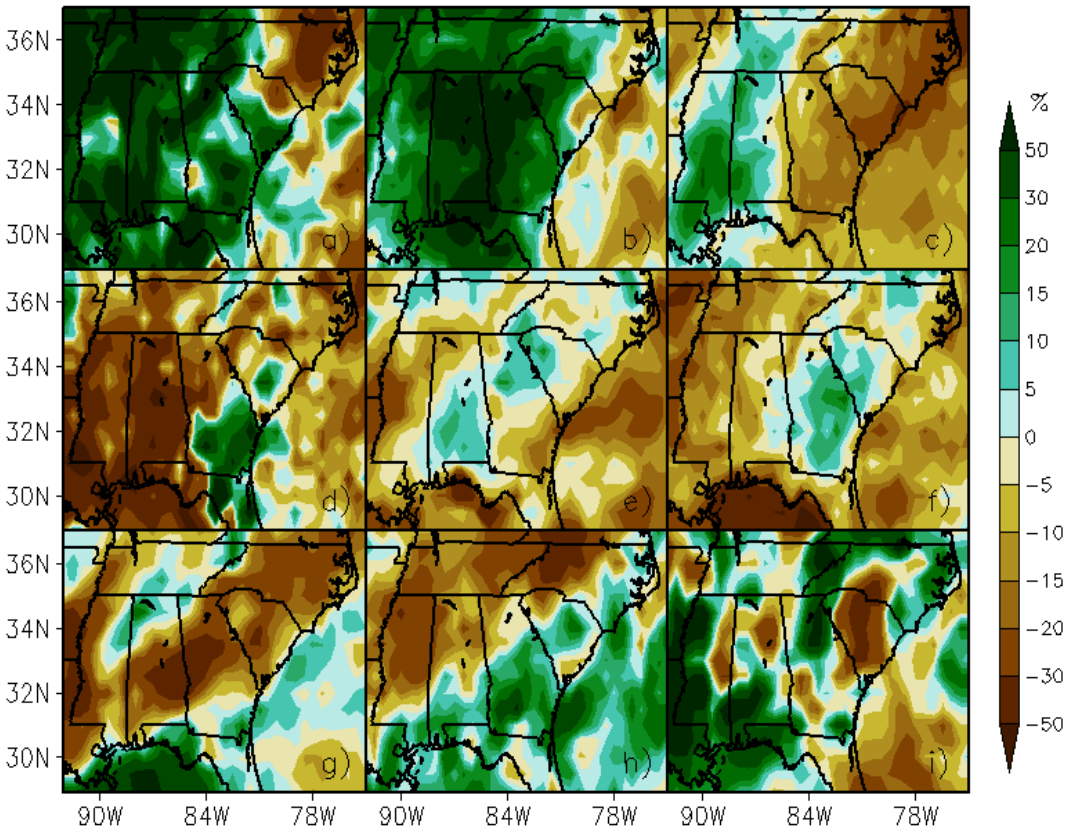

Figure G.33. Individual September mean precipitation change for the WRFG-CGCM3 (a), RCM3-CGCM3 (b), CRCM-CGCM3 (c), WRFG-CCSM (d), MM5I-CCSM (e), CRCM-CCSM (f), ECP2-GFDL (g), RCM3-GFDL (h), and GFDL-timeslice (i) NARCCAP models.

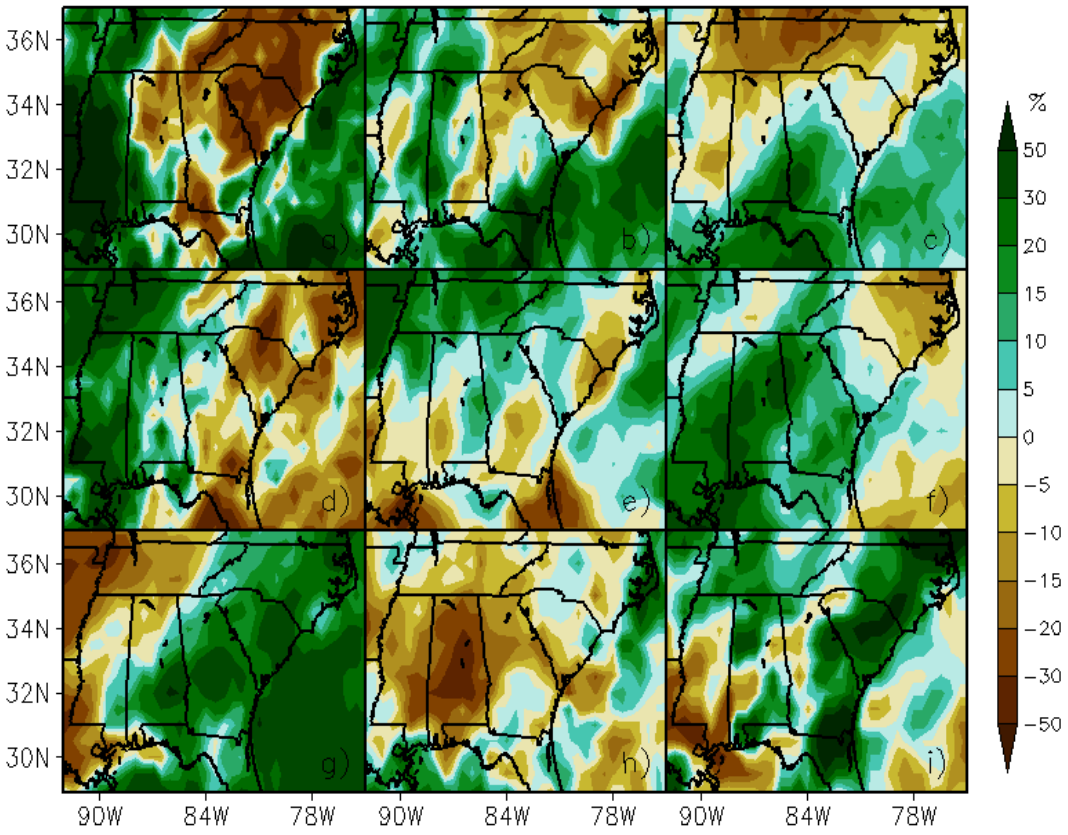

Figure G.34. Individual October mean precipitation change for the WRFG-CGCM3 (a), RCM3-CGCM3 (b), CRCM-CGCM3 (c), WRFG-CCSM (d), MM5I-CCSM (e), CRCM-CCSM (f), ECP2-GFDL (g), RCM3-GFDL (h), and GFDL-timeslice (i) NARCCAP models.

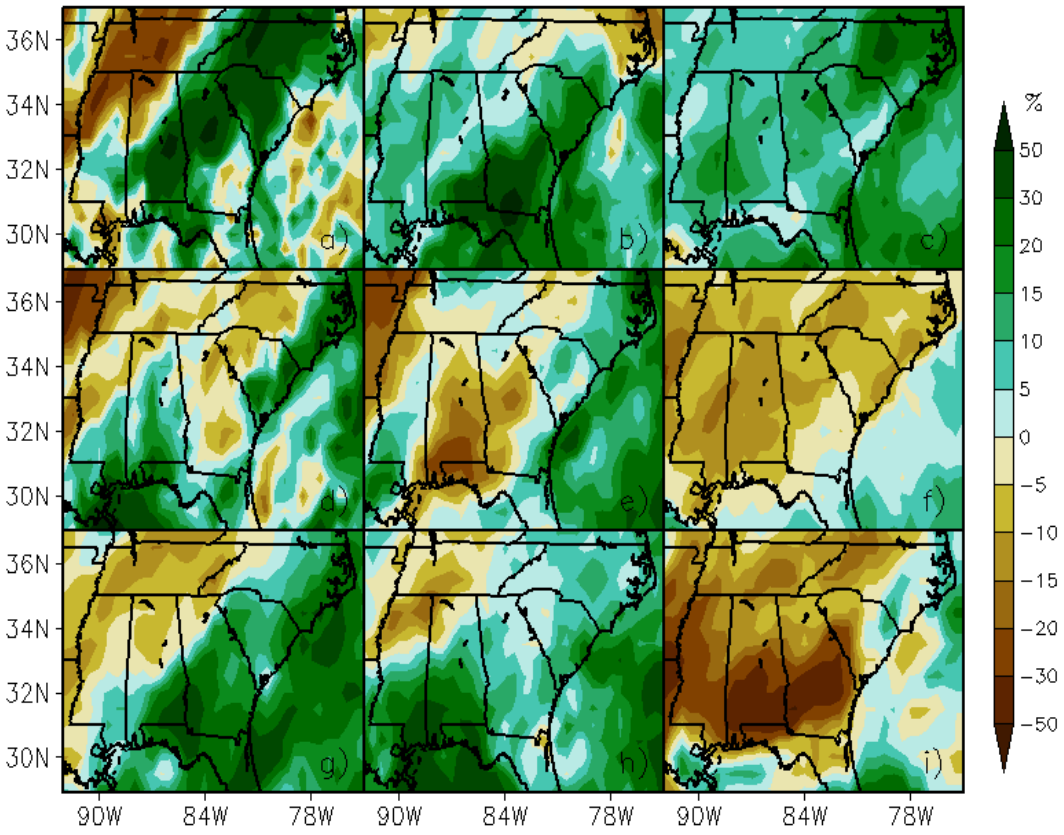

Figure G.35. Individual November mean precipitation change for the WRFG-CGCM3 (a), RCM3-CGCM3 (b), CRCM-CGCM3 (c), WRFG-CCSM (d), MM5I-CCSM (e), CRCM-CCSM (f), ECP2-GFDL (g), RCM3-GFDL (h), and GFDL-timeslice (i) NARCCAP models.

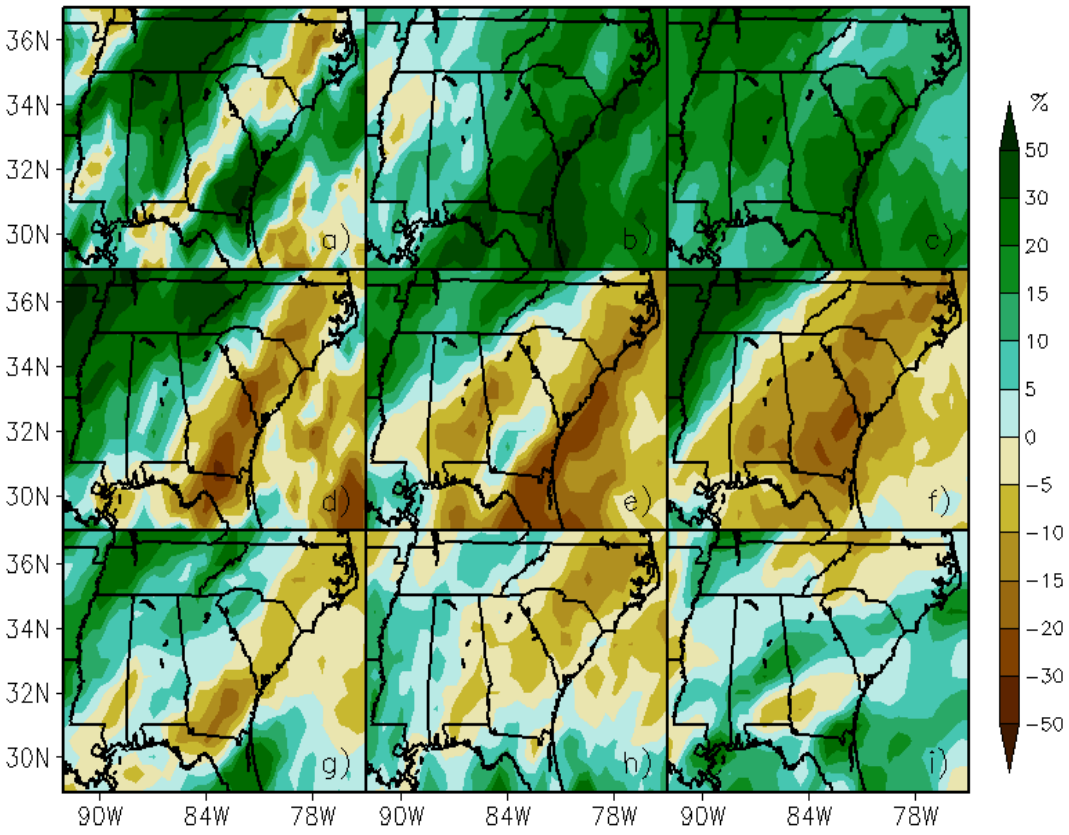

Figure G.36. Individual December mean precipitation change for the WRFG-CGCM3 (a), RCM3-CGCM3 (b), CRCM-CGCM3 (c), WRFG-CCSM (d), MM5I-CCSM (e), CRCM-CCSM (f), ECP2-GFDL (g), RCM3-GFDL (h), and GFDL-timeslice (i) NARCCAP models.

APPENDIX H – RCM-NCEP REANALYSIS

Presented in Appendix H are percentile plots of minimum temperature, maximum temperature, and mean precipitation for RCMs from NARCCAP run with NCEP Reanalysis boundary conditions. Additionally, monthly time series soil moisture, latent and sensible heat flux, 500mb height, and cloud cover are presented.

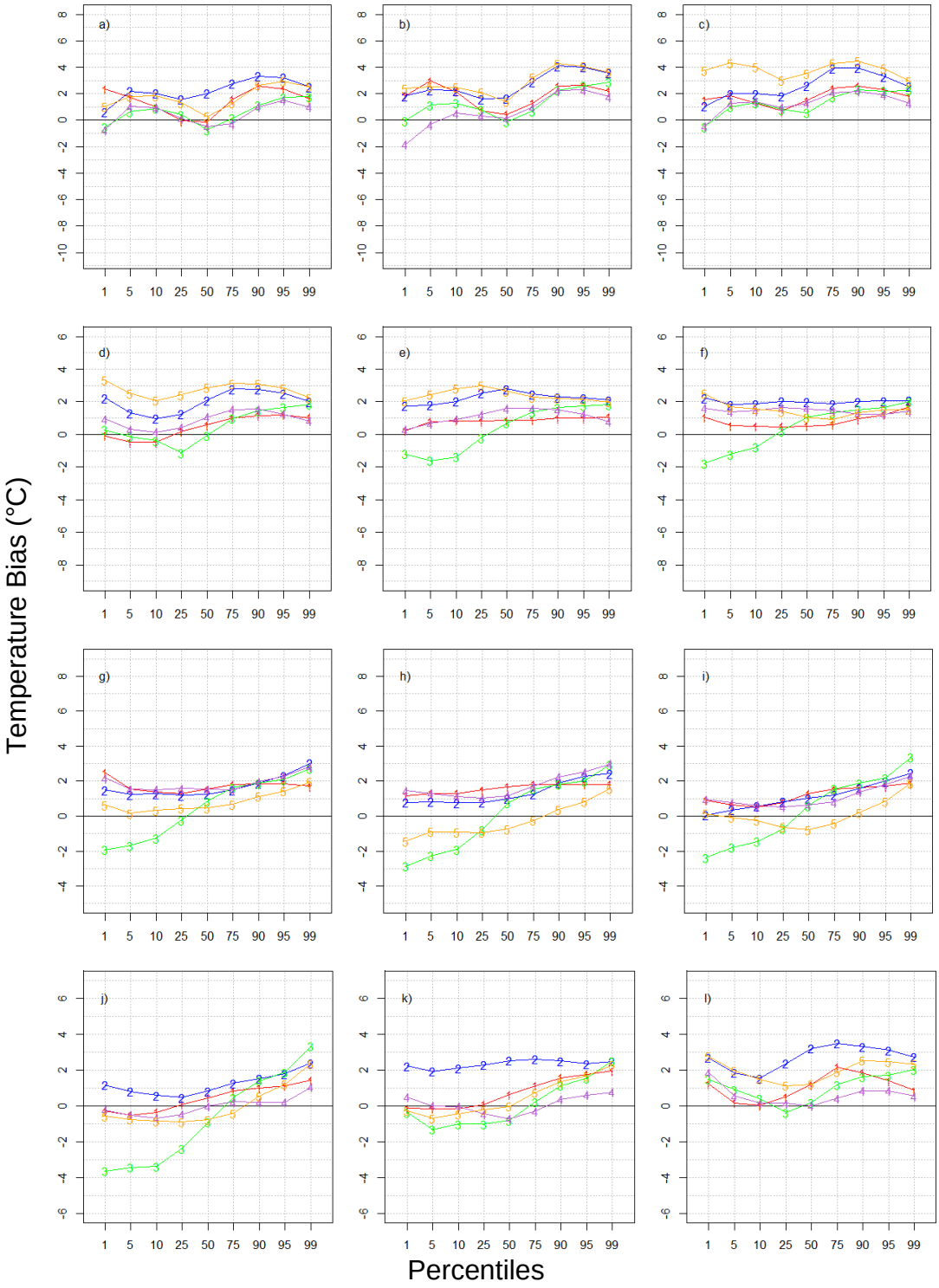

Figure H.1. Percentile plots of minimum temperature bias for the east sub-region from each NARCCAP RCMs run with NCEP reanalysis LBCs for December (a) through November (l). Labels for the RCMs are as follows: “1”=CRCM, “2”=ECP2, “3”=MM5I, “4”=RCM3, and “5”=WRFG.

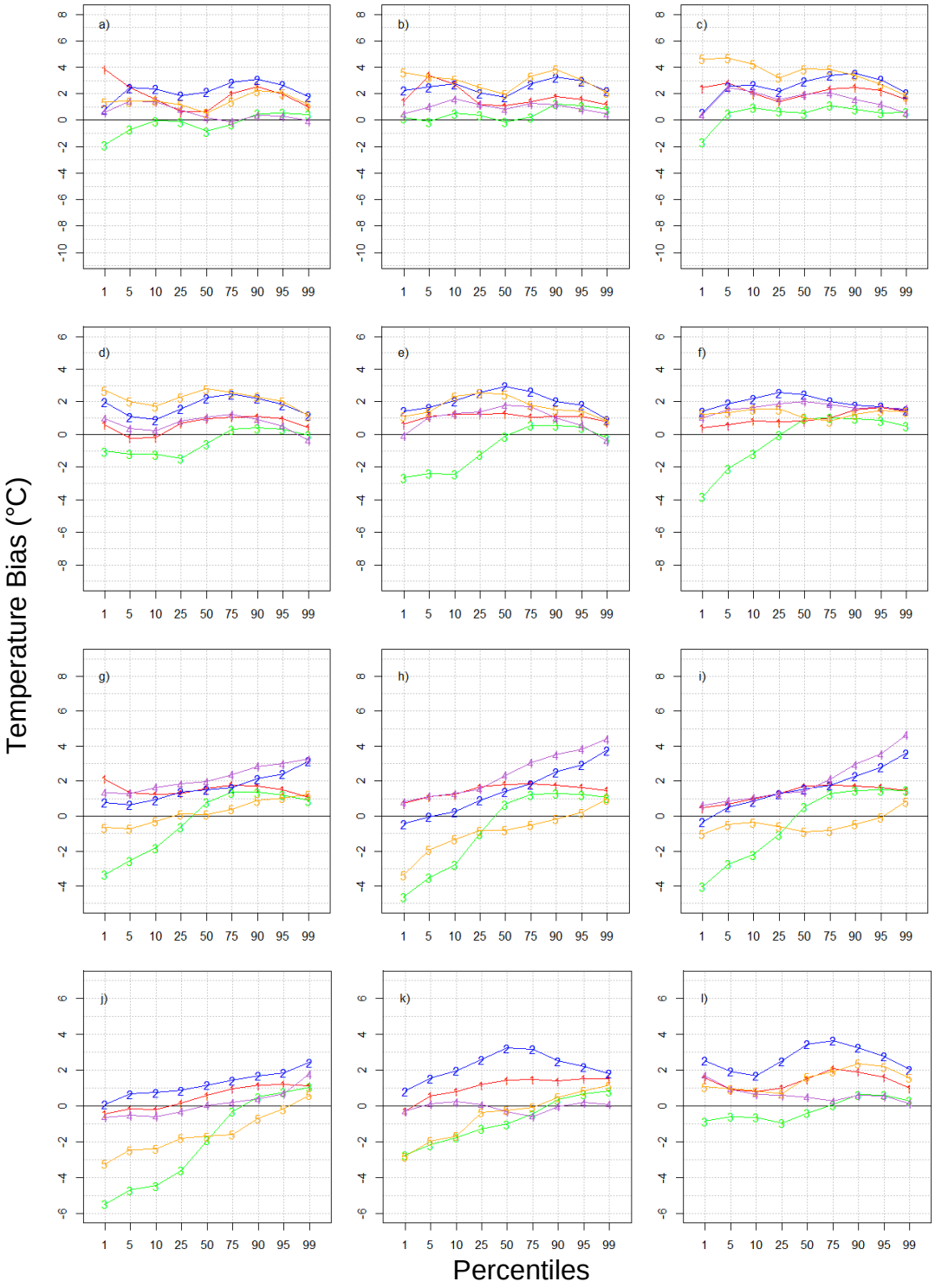

Figure H.2. Percentile plots of minimum temperature bias for the west sub-region from each NARCCAP RCMs run with NCEP reanalysis LBCs for December (a) through November (l). Labels for the RCMs are as follows: “1”=CRCM, “2”=ECP2, “3”=MM5I, “4”=RCM3, and “5”=WRFG.

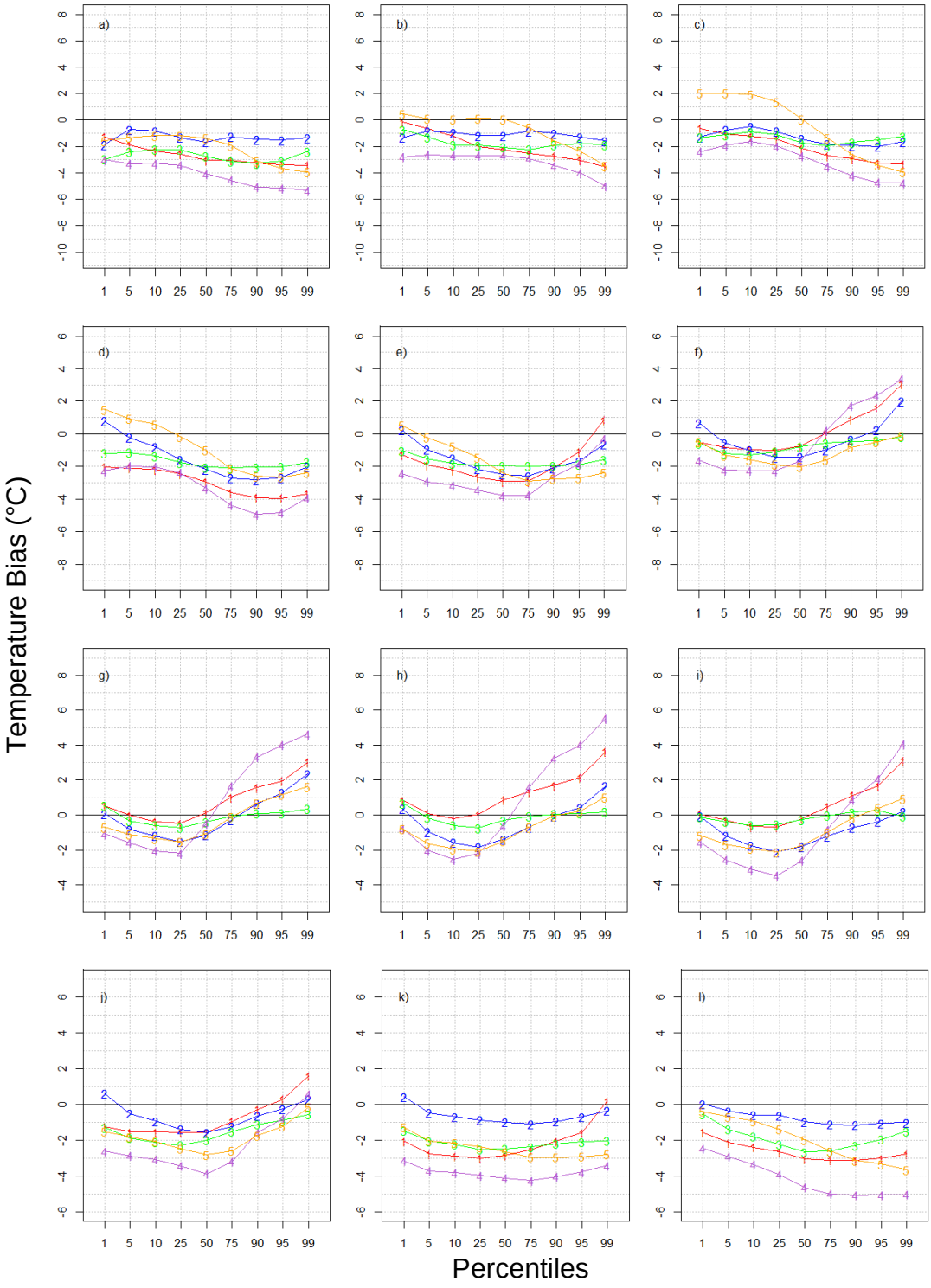

Figure H.3. Percentile plots of maximum temperature bias for the east sub-region from each NARCCAP RCMs run with NCEP reanalysis LBCs for December (a) through November (l). Labels for the RCMs are as follows: “1”=CRCM, “2”=ECP2, “3”=MM5I, “4”=RCM3, and “5”=WRFG.

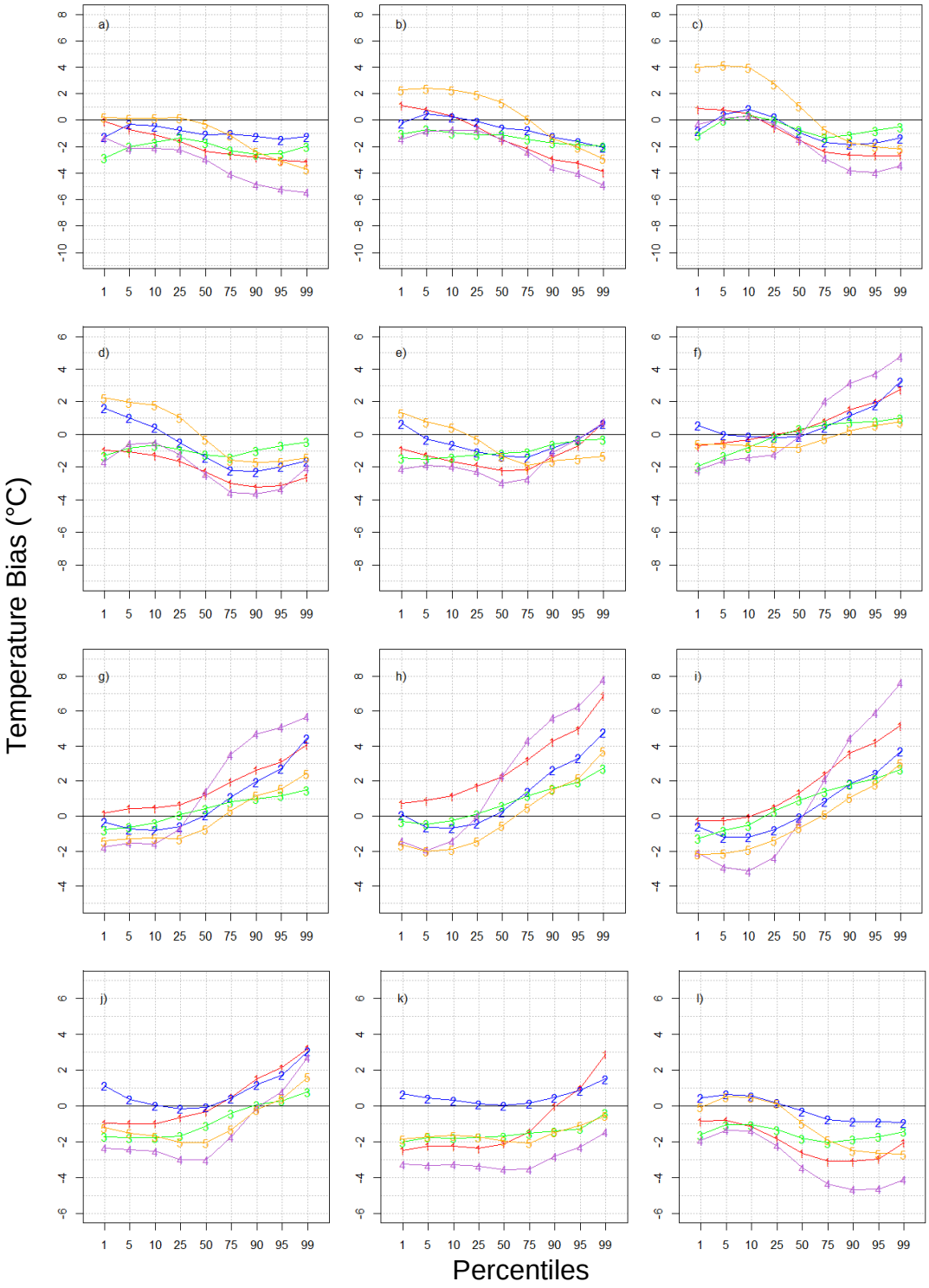

Figure H.4. Percentile plots of maximum temperature bias for the west sub-region from each NARCCAP RCMs run with NCEP reanalysis LBCs for December (a) through November (l). Labels for the RCMs are as follows: “1”=CRCM, “2”=ECP2, “3”=MM5I, “4”=RCM3, and “5”=WRFG.

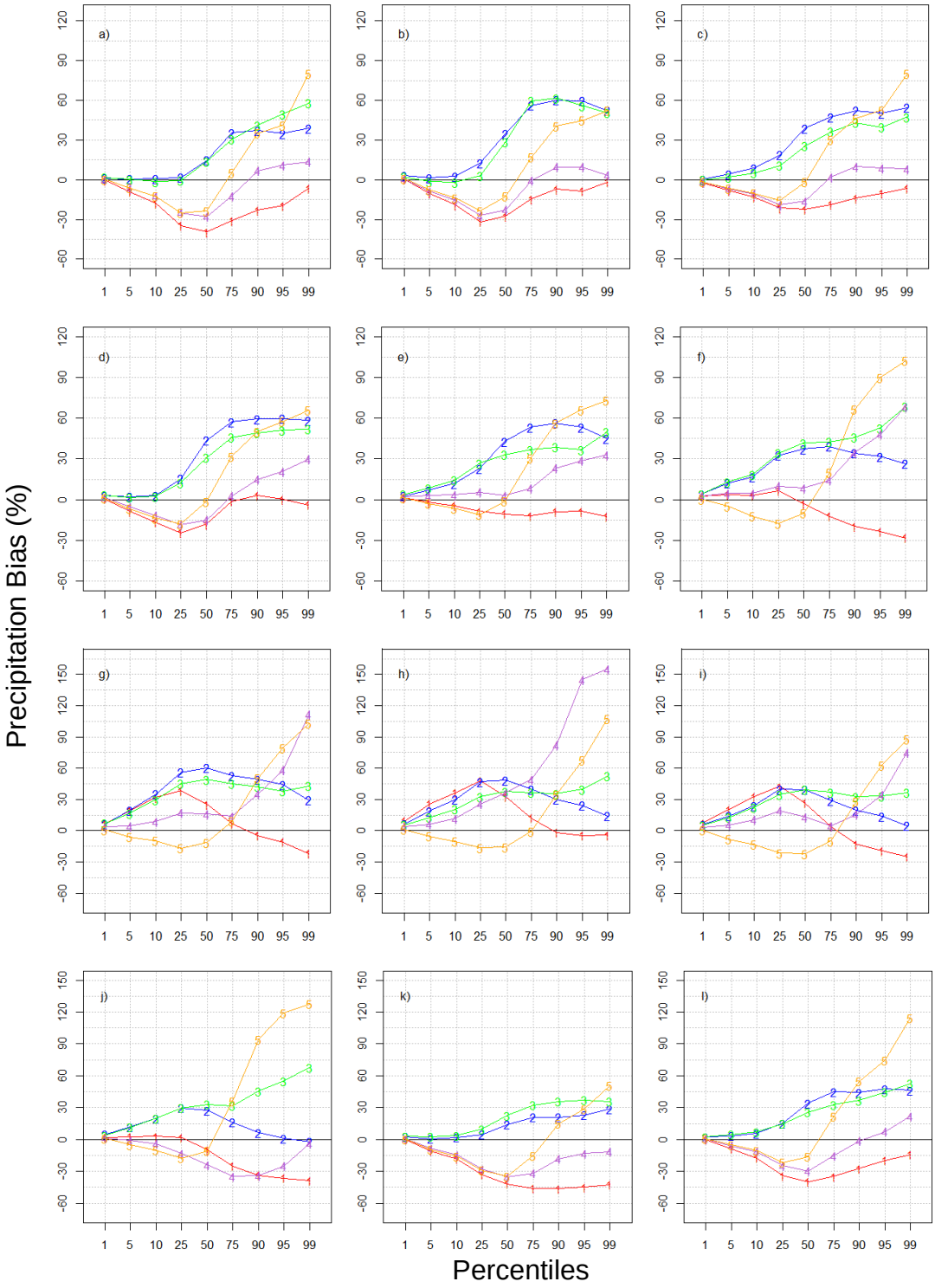

Figure H.5. Percentile plots of mean precipitation bias for the east sub-region from each NARCCAP RCMs run with NCEP reanalysis LBCs for December (a) through November (l). Labels for the RCMs are as follows: “1”=CRCM, “2”=ECP2, “3”=MM5I, “4”=RCM3, and “5”=WRFG.

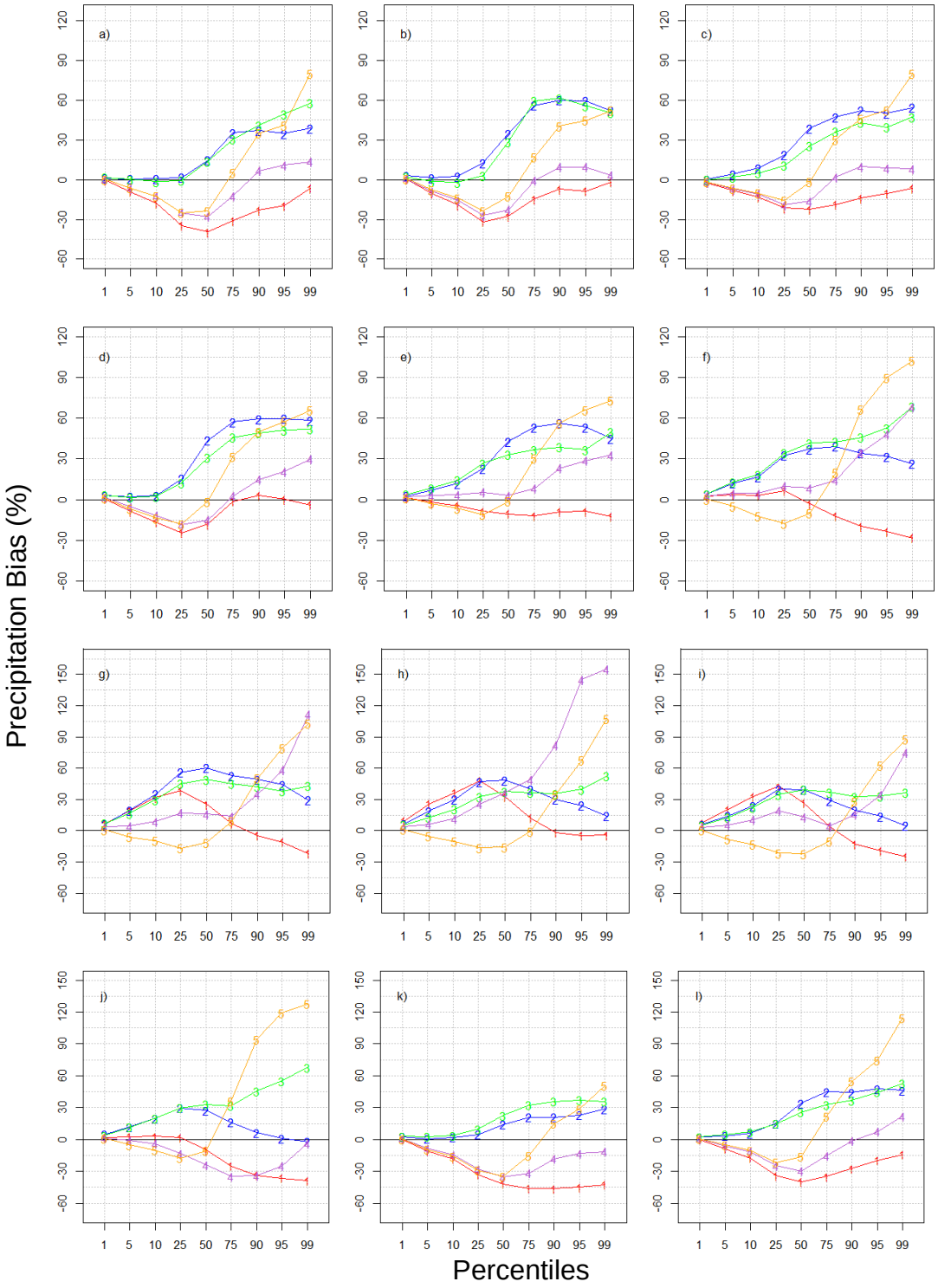

Figure H.6. Percentile plots of mean precipitation bias for the west sub-region from each NARCCAP RCMs run with NCEP reanalysis LBCs for December (a) through November (l). Labels for the RCMs are as follows: “1”=CRCM, “2”=ECP2, “3”=MM5I, “4”=RCM3, and “5”=WRFG.

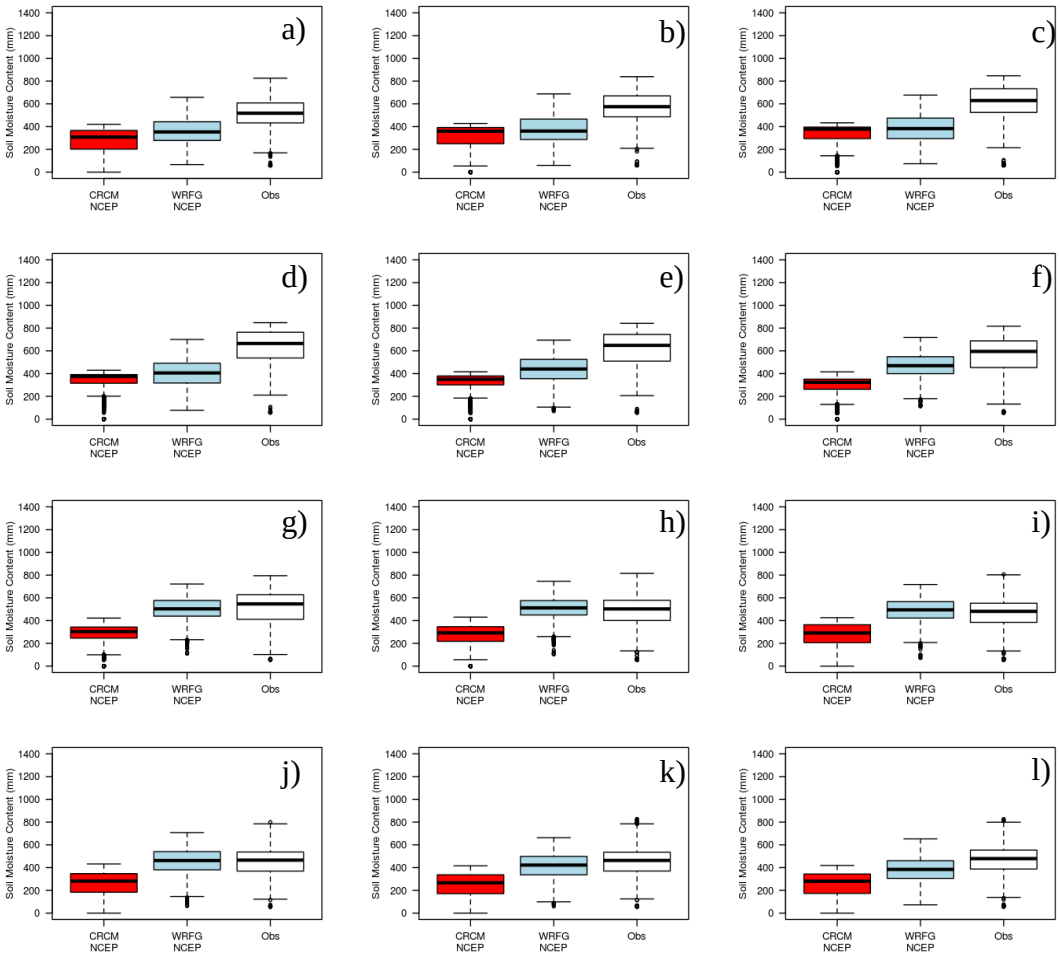

Figure H.7. Box and whisker plots of monthly soil moisture for RCMs run with NCEP reanalysis as boundary conditions for the east sub-regions for December (a) through November (l).

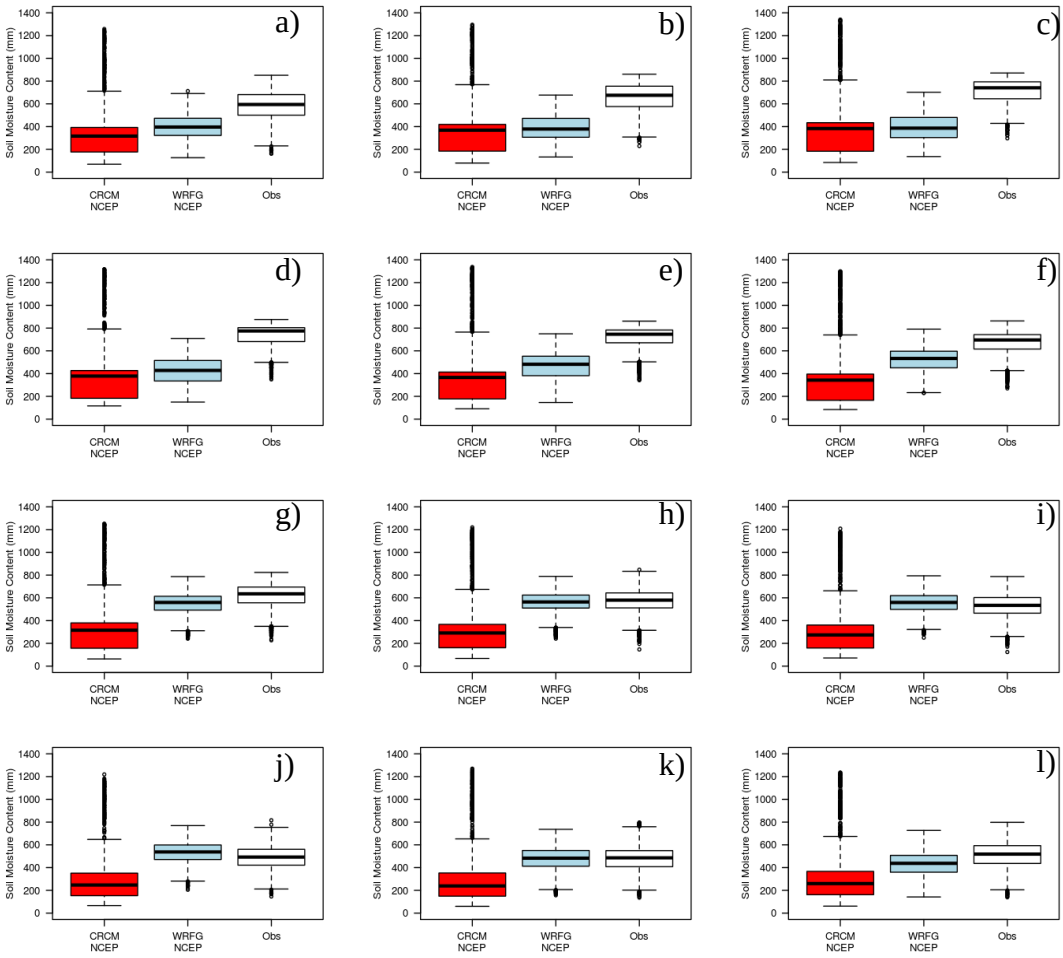

Figure H.8. Box and whisker plots of monthly soil moisture for RCMs run with NCEP reanalysis as boundary conditions for the west sub-regions for December (a) through November (l).

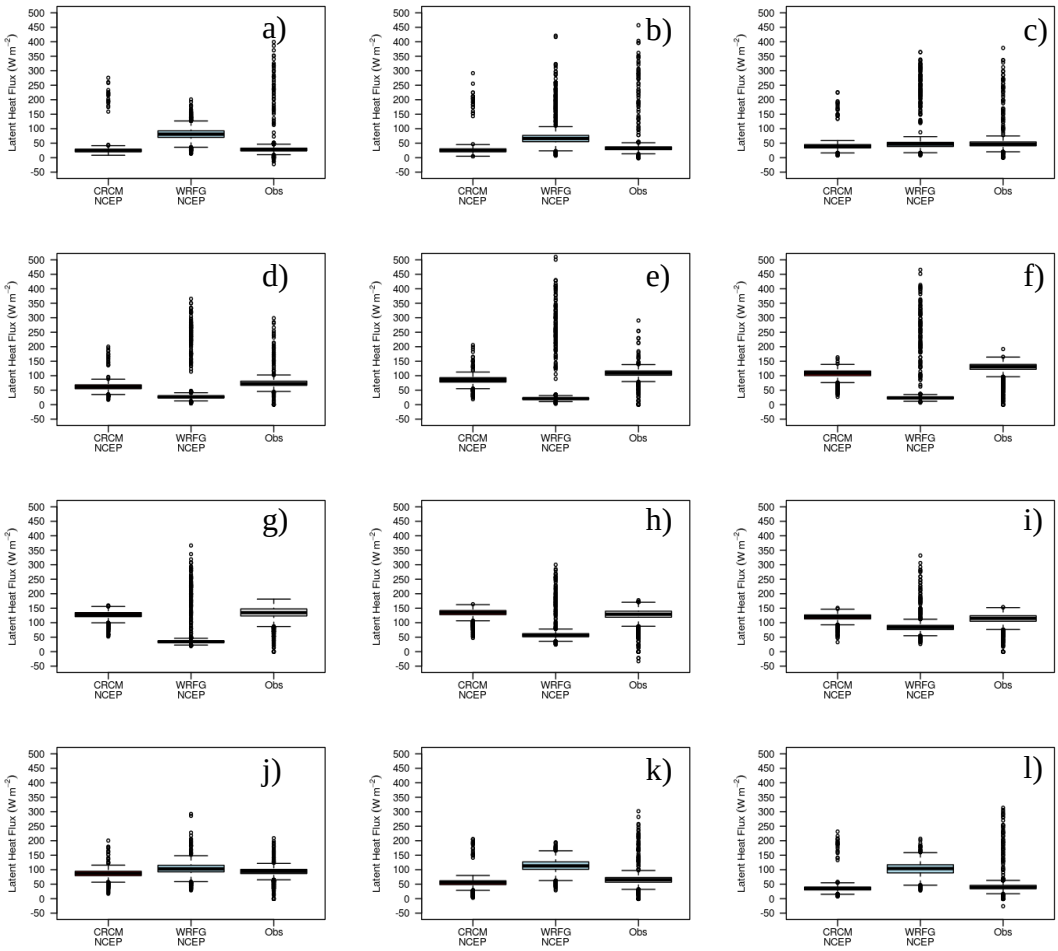

Figure H.9. Box and whisker plots of monthly latent heat flux for RCMs run with NCEP reanalysis as boundary conditions for the east sub-regions for December (a) through November (l).

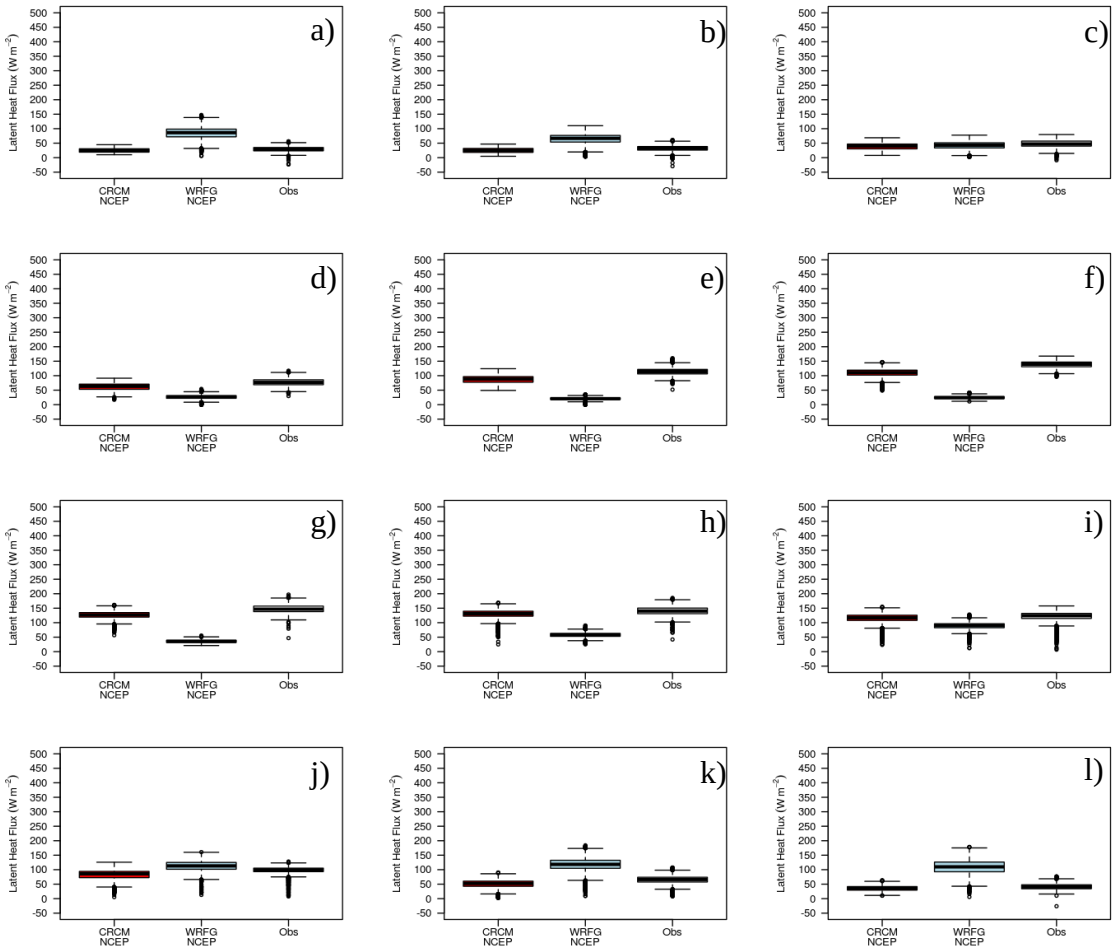

Figure H.10. Box and whisker plots of monthly latent heat flux for RCMs run with NCEP reanalysis as boundary conditions for the west sub-regions for December (a) through November (l).

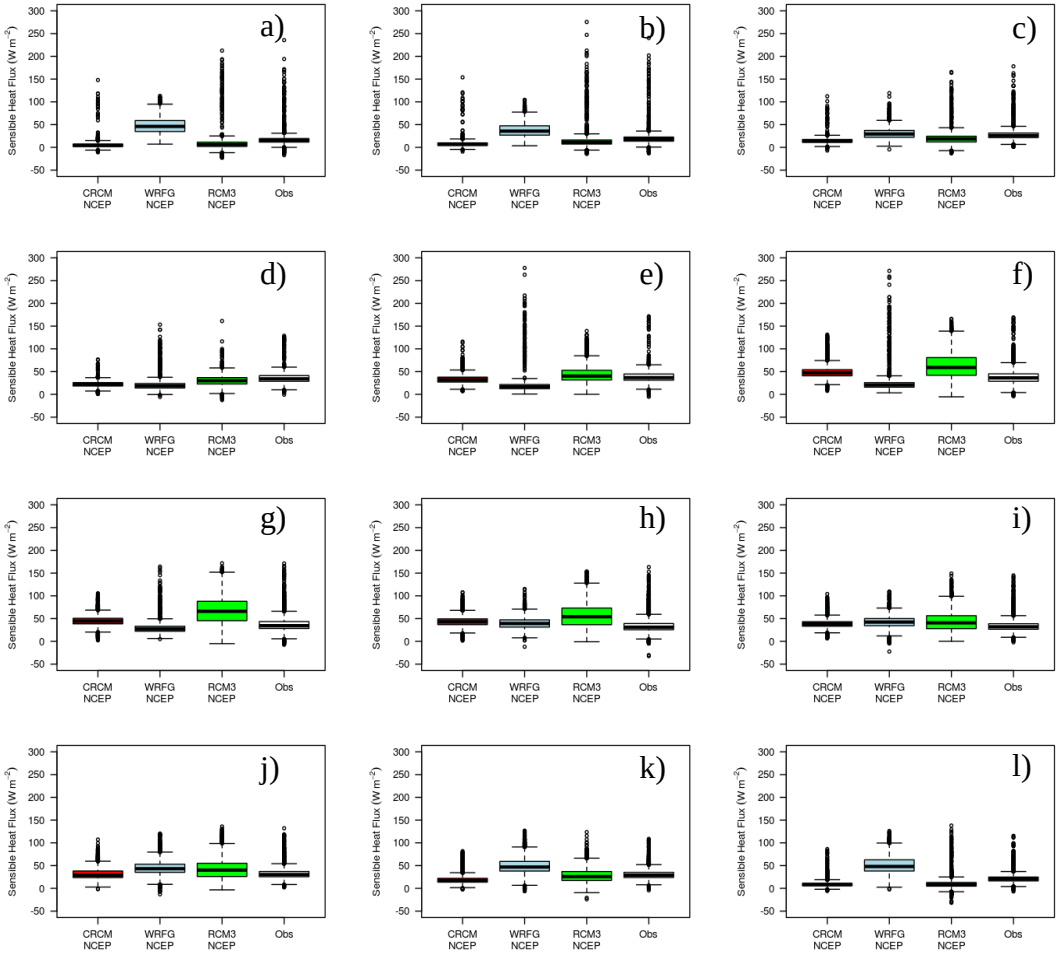

Figure H.11. Box and whisker plots of monthly sensible heat flux for RCMs run with NCEP reanalysis as boundary conditions for the east sub-regions for December (a) through November (l).

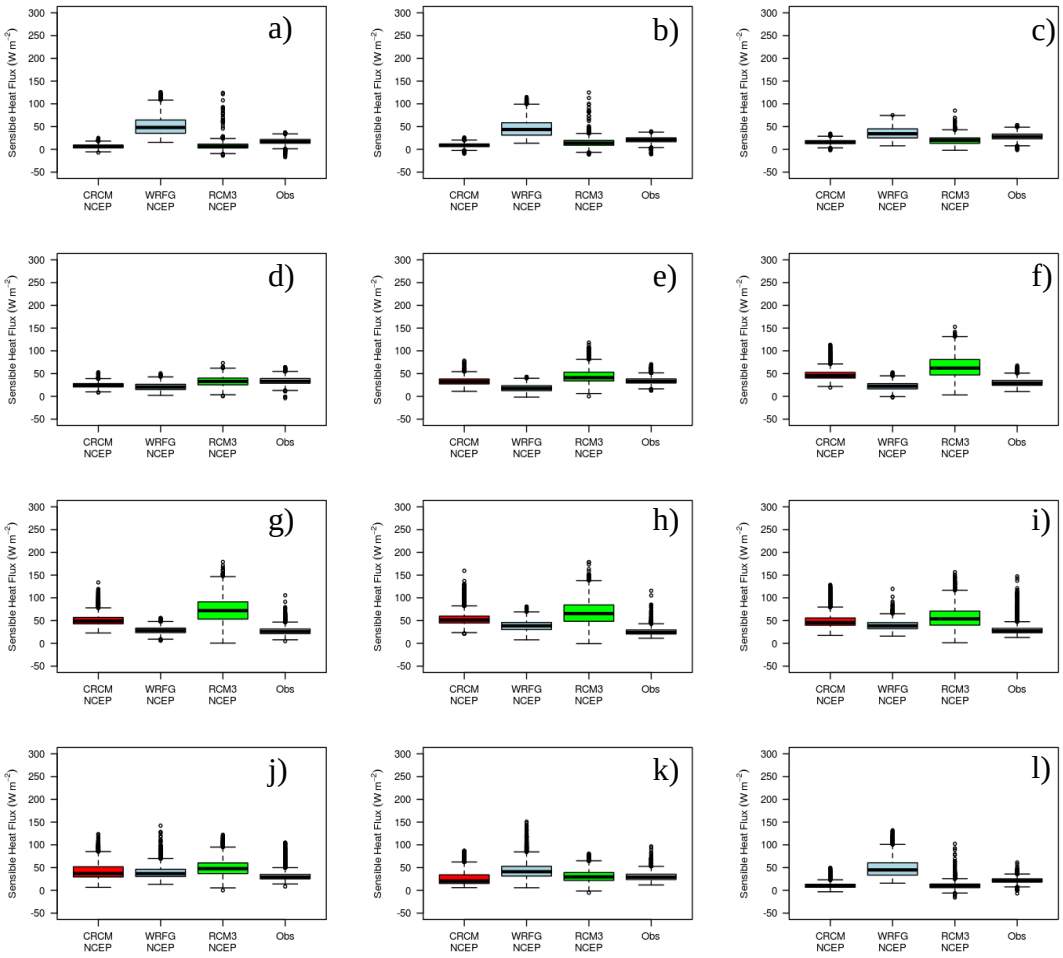

Figure H.12. Box and whisker plots of monthly sensible heat flux for RCMs run with NCEP reanalysis as boundary conditions for the west sub-regions for December (a) through November (l).

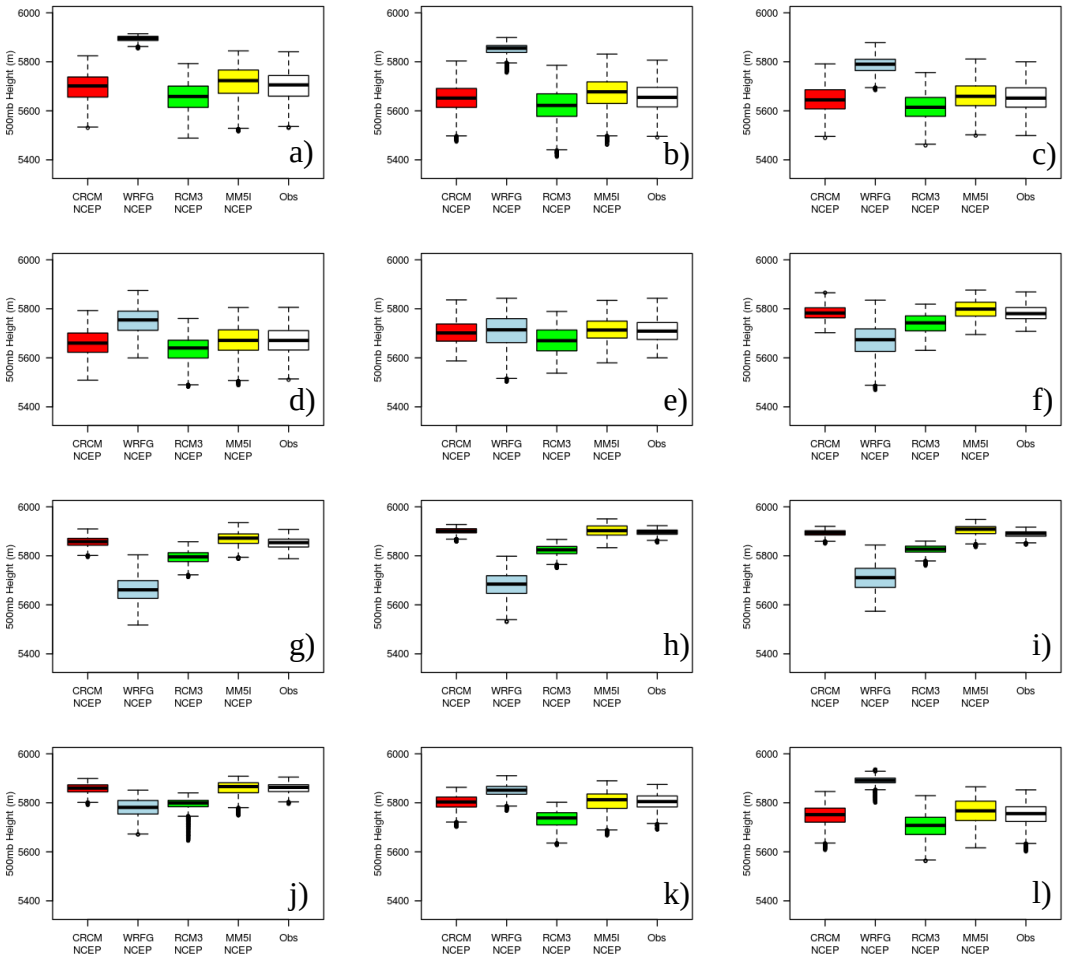

Figure H.13. Box and whisker plots of monthly 500-mb heights for RCMs run with NCEP reanalysis as boundary conditions for the east sub-regions for December (a) through November (l).

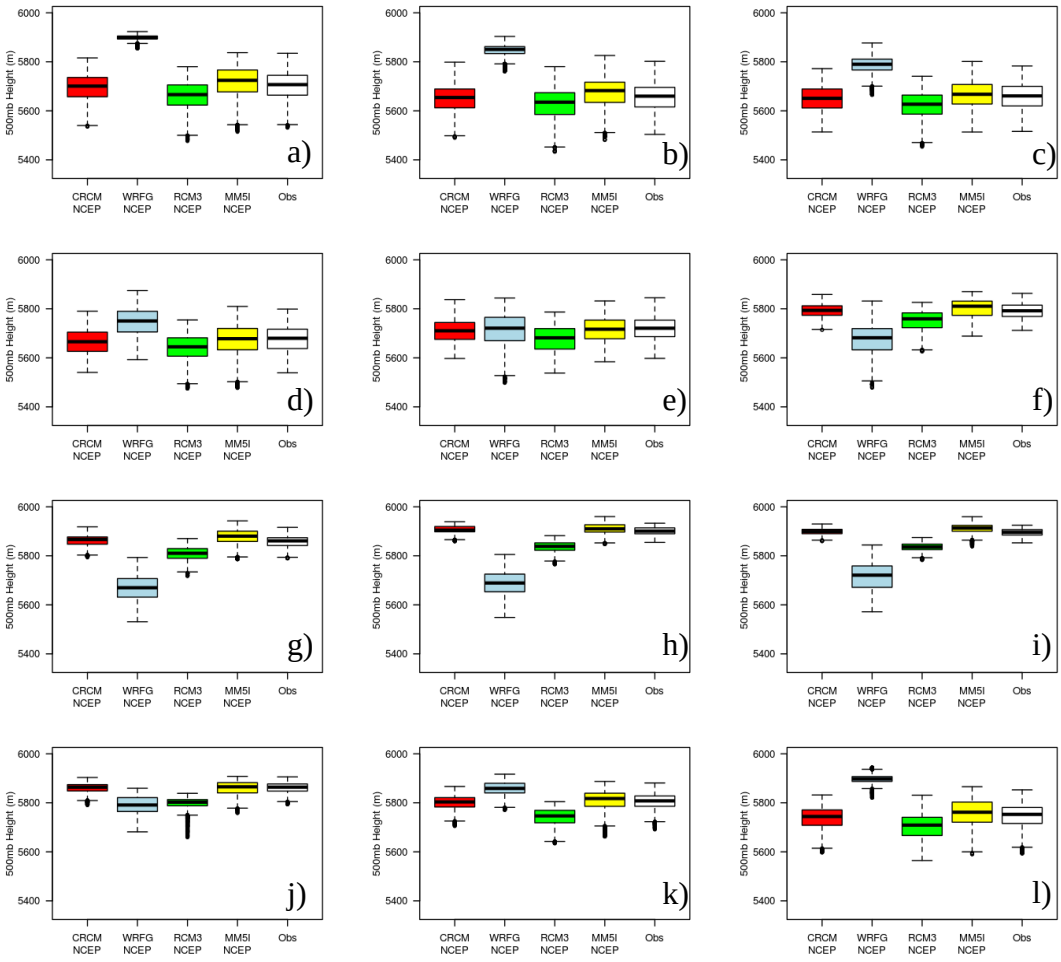

Figure H.14. Box and whisker plots of monthly 500-mb heights for RCMs run with NCEP reanalysis as boundary conditions for the west sub-regions for December (a) through November (l).

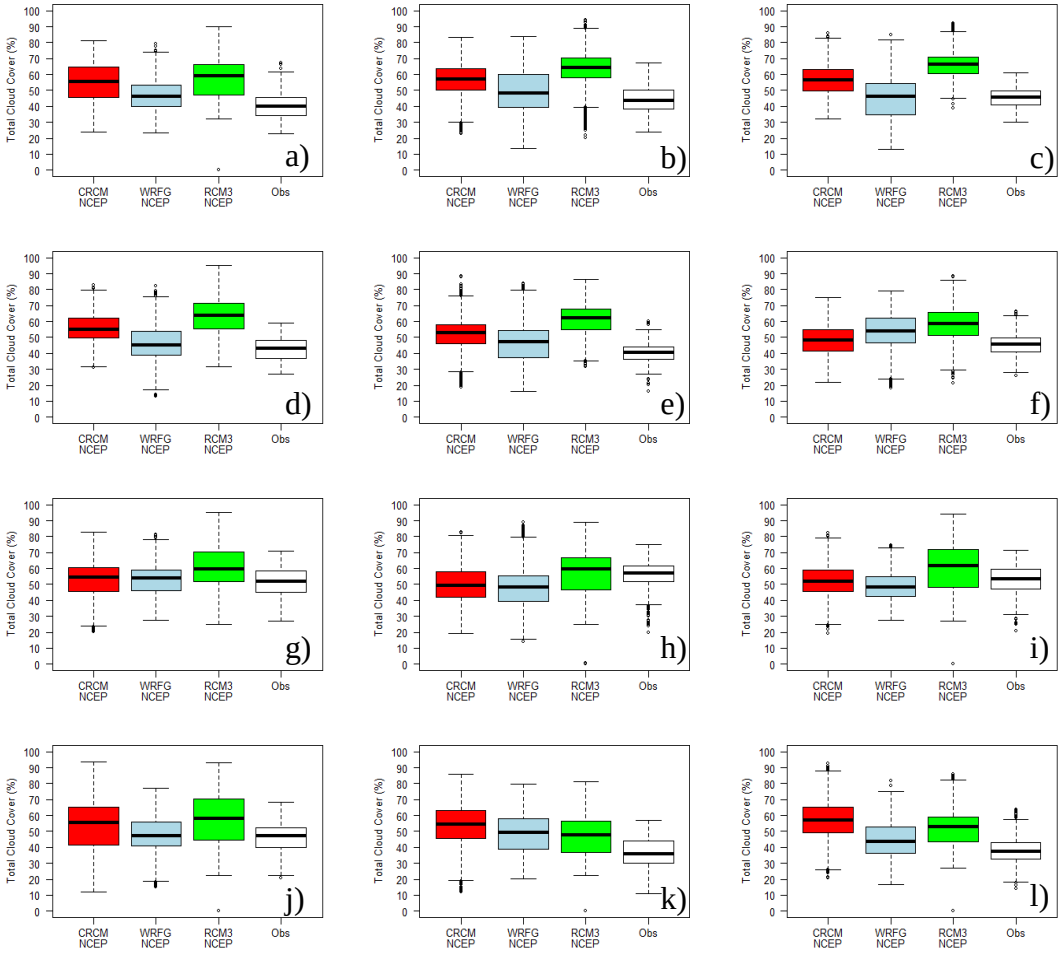

Figure H.15. Box and whisker plots of monthly total cloud cover for RCMs run with NCEP reanalysis as boundary conditions for the east sub-regions for December (a) through November (l).

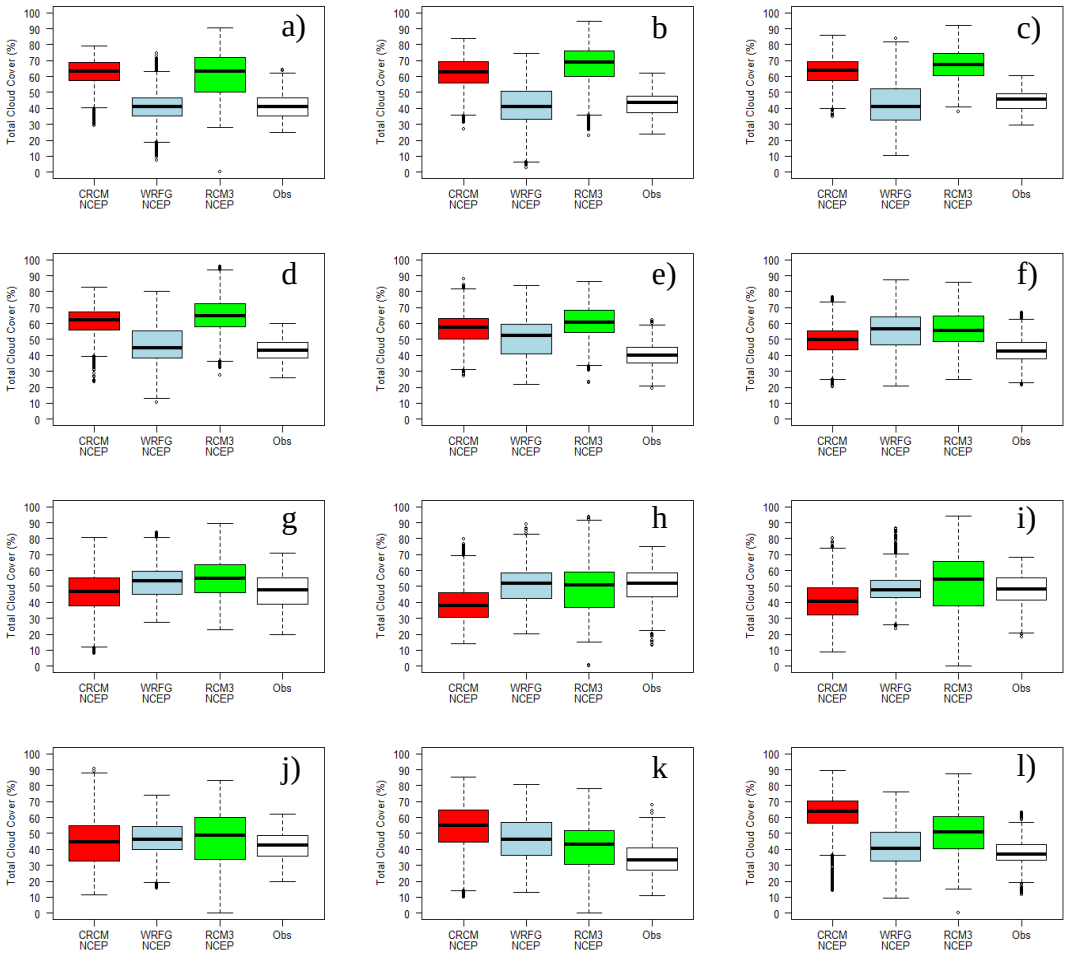

Figure H.16. Box and whisker plots of monthly total cloud cover for RCMs run with NCEP reanalysis as boundary conditions for the west sub-regions for December (a) through November (l).

APPENDIX I – MICRO-, MESO-, AND SYNOPTIC-SCALE SUPPLEMENTAL GRAPHICS

Presented in Appendix I are graphics providing enhanced insight into the the micro-, meso-, and synoptic-scale variables used to assess model deficiencies related to the energy- and moisture-budgets as well as surface and upper-level flow patterns.

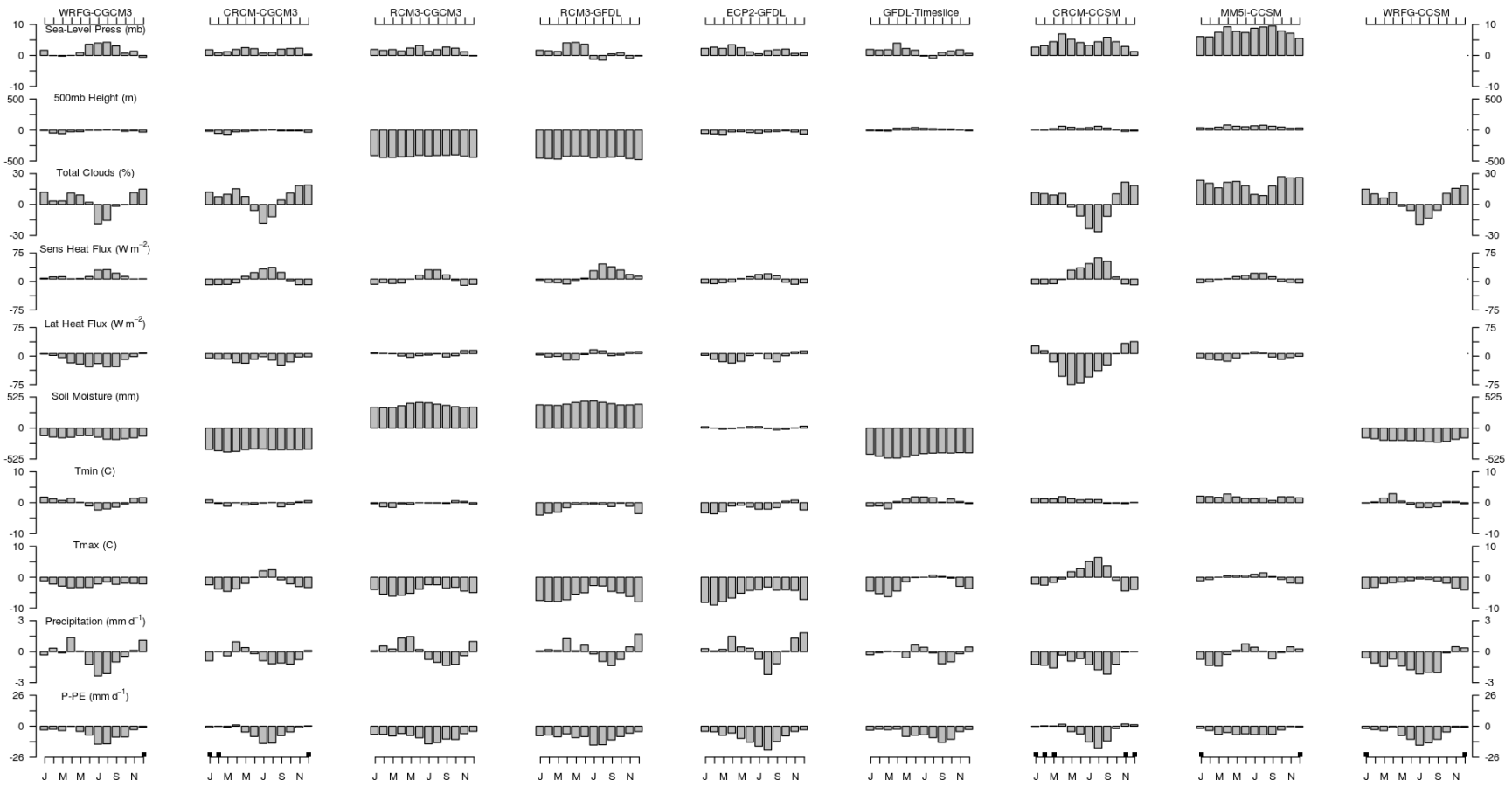

Figure I.1. Montly anomolies (RCM values minus observations) of micro-, meso-, and synoptic-scale components for grid points from the east sub-region. Black boxes on the precipitation minus potential evapotranspirtation (P-PE) histograms represent a model-predicted surplus of moisture for the respective month (P-PE before subtracting from observations). Each histogram begins with the month of January and ends with the month of December.

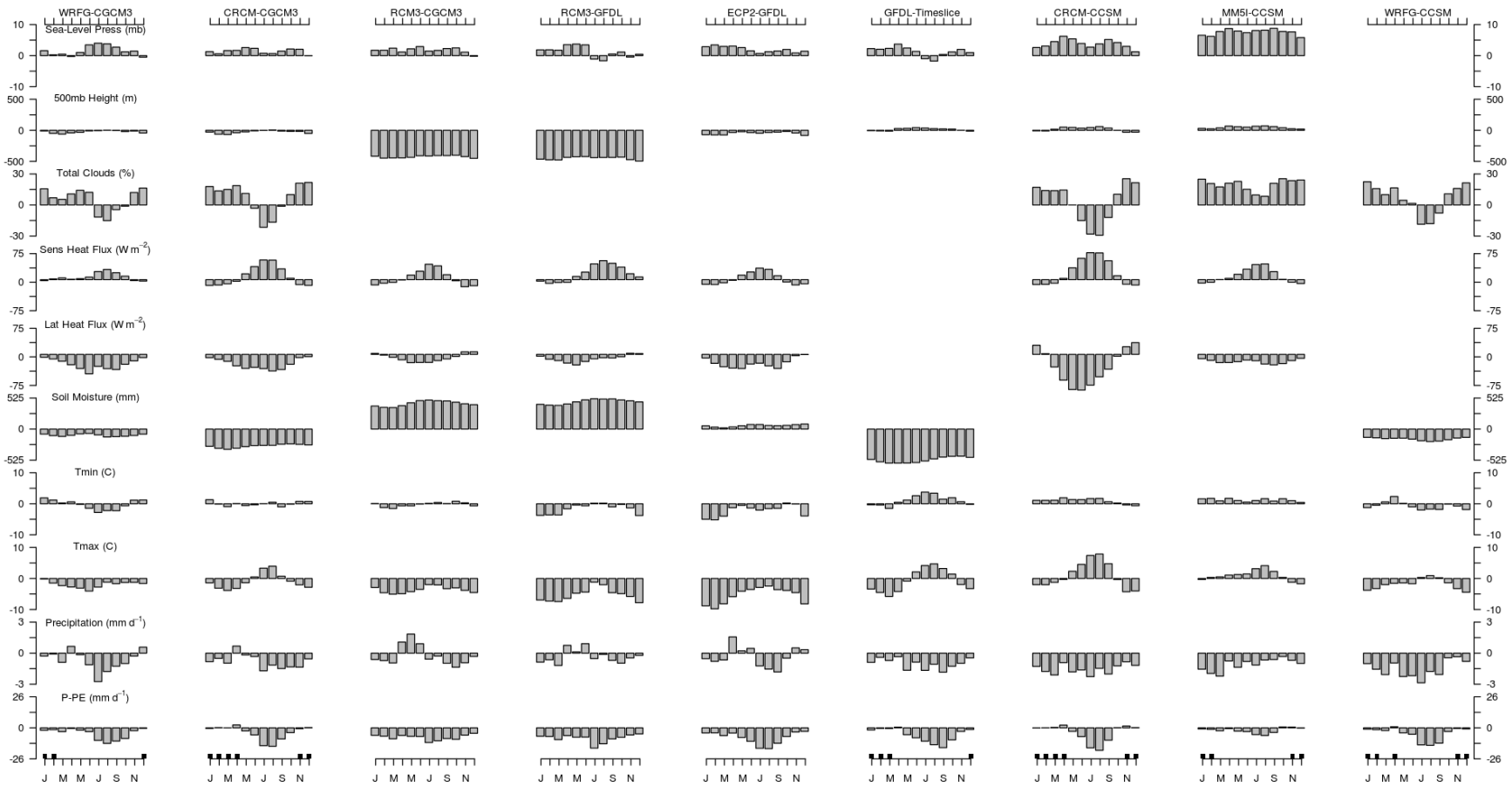

Figure I.2. Montly anomolies (RCM values minus observations) of micro-, meso-, and synoptic-scale components for grid points from the west sub-region. Black boxes on the precipitation minus potential evapotranspirtation (P-PE) histograms represent a model-predicted surplus of moisture for the respective month (P-PE before subtracting from observations). Each histogram begins with the month of January and ends with the month of December.

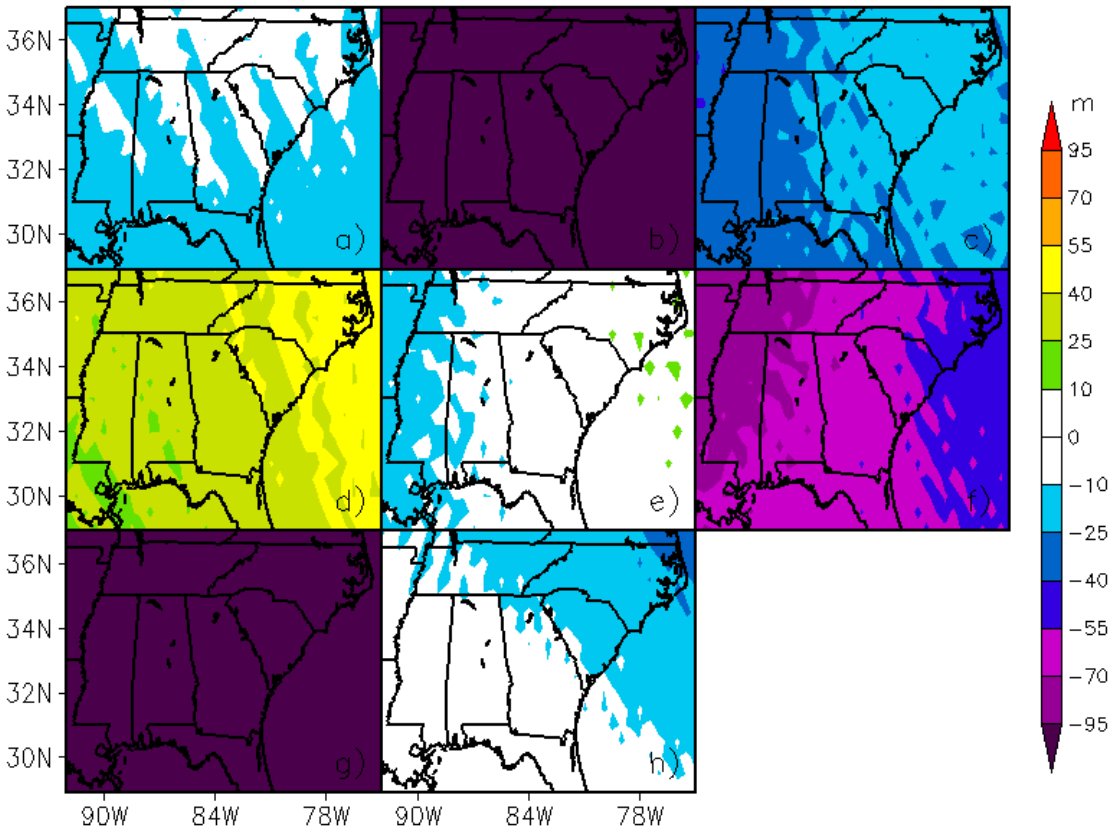

Figure I.3. Individual January 500-mb height anomolies for the WRFG-CGCM3 (a), RCM3-CGCM3 (b), CRCM-CGCM3 (c), MM5I-CCSM (d), CRCM-CCSM (e), ECP2-GFDL (f), RCM3-GFDL (g), and GFDL-timeslice (h) NARCCAP models.

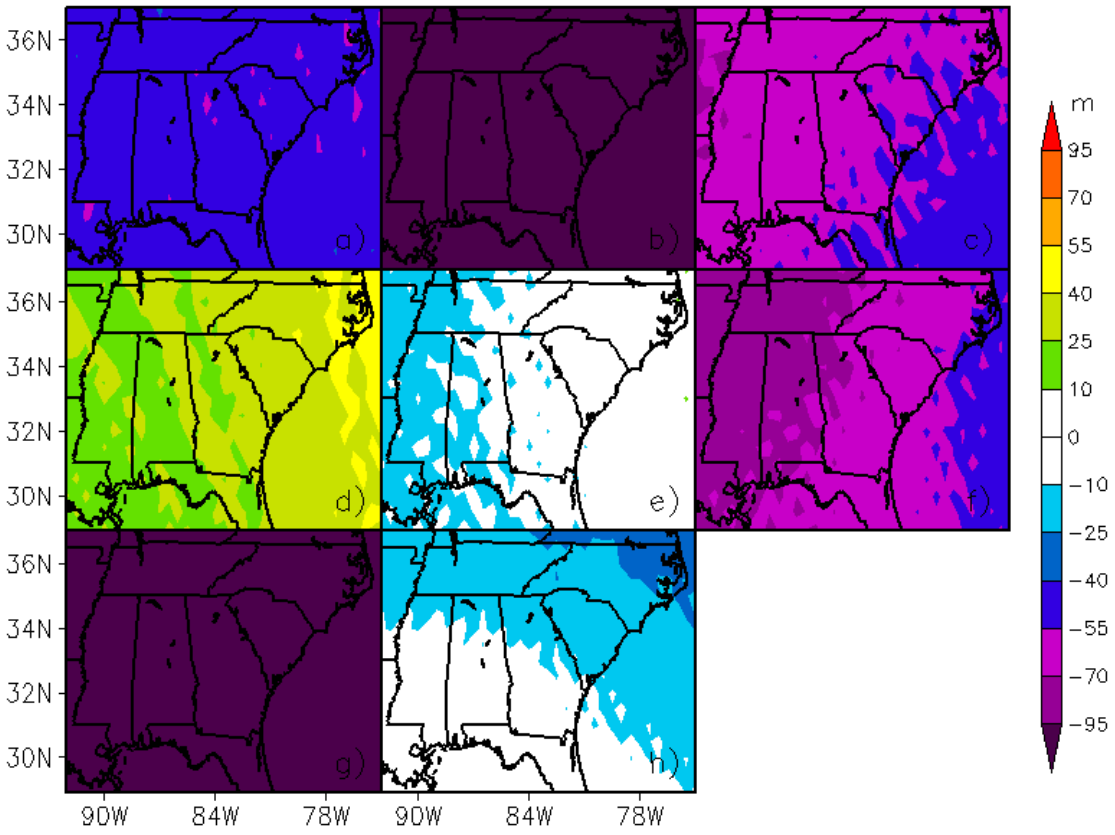

Figure I.4. Individual February 500-mb height anomolies for the WRFG-CGCM3 (a), RCM3-CGCM3 (b), CRCM-CGCM3 (c), MM5I-CCSM (d), CRCM-CCSM (e), ECP2-GFDL (f), RCM3-GFDL (g), and GFDL-timeslice (h) NARCCAP models.

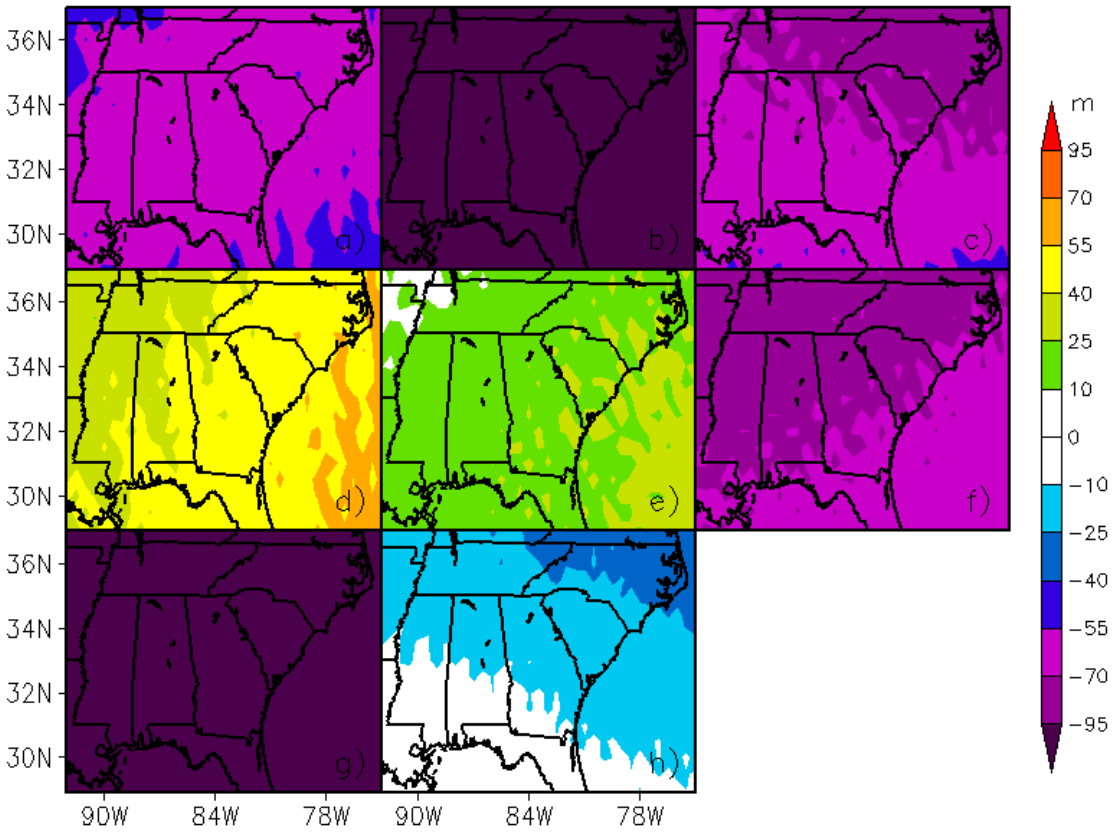

Figure I.5. Individual March 500-mb height anomolies for the WRFG-CGCM3 (a), RCM3-CGCM3 (b), CRCM-CGCM3 (c), MM5I-CCSM (d), CRCM-CCSM (e), ECP2-GFDL (f), RCM3-GFDL (g), and GFDL-timeslice (h) NARCCAP models.

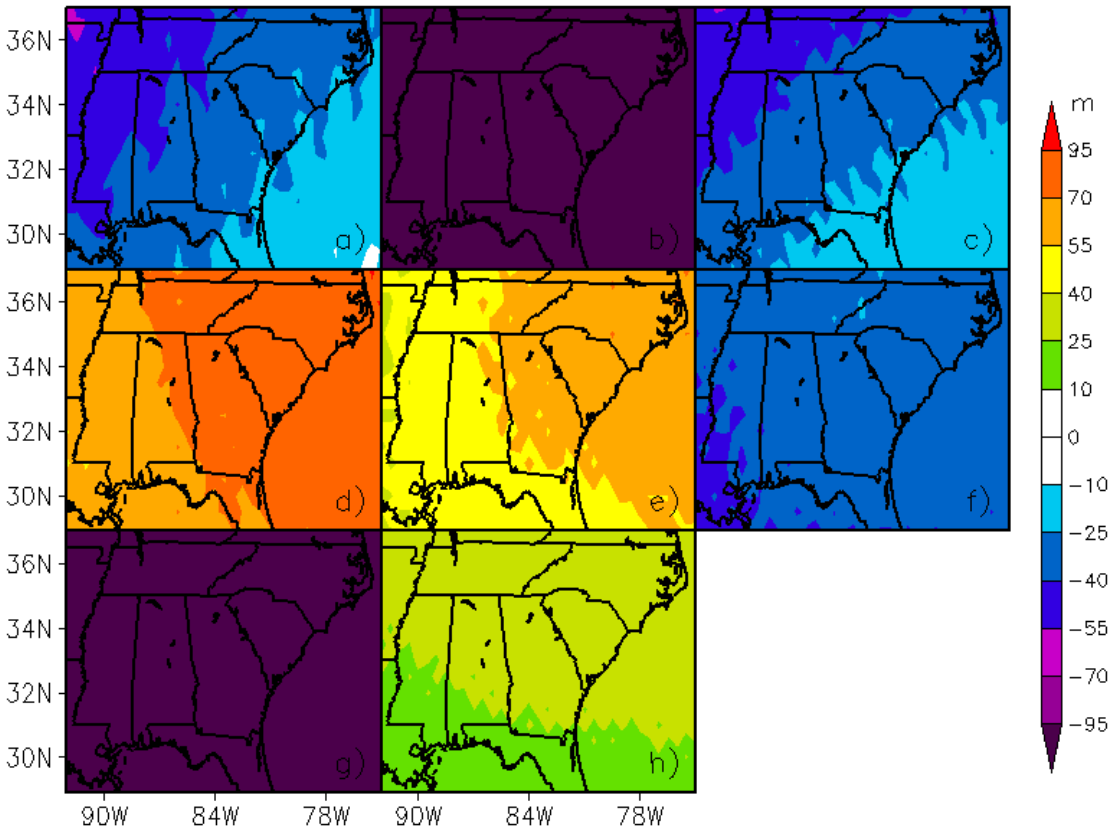

Figure I.6. Individual April 500-mb height anomolies for the WRFG-CGCM3 (a), RCM3-CGCM3 (b), CRCM-CGCM3 (c), MM5I-CCSM (d), CRCM-CCSM (e), ECP2-GFDL (f), RCM3-GFDL (g), and GFDL-timeslice (h) NARCCAP models.

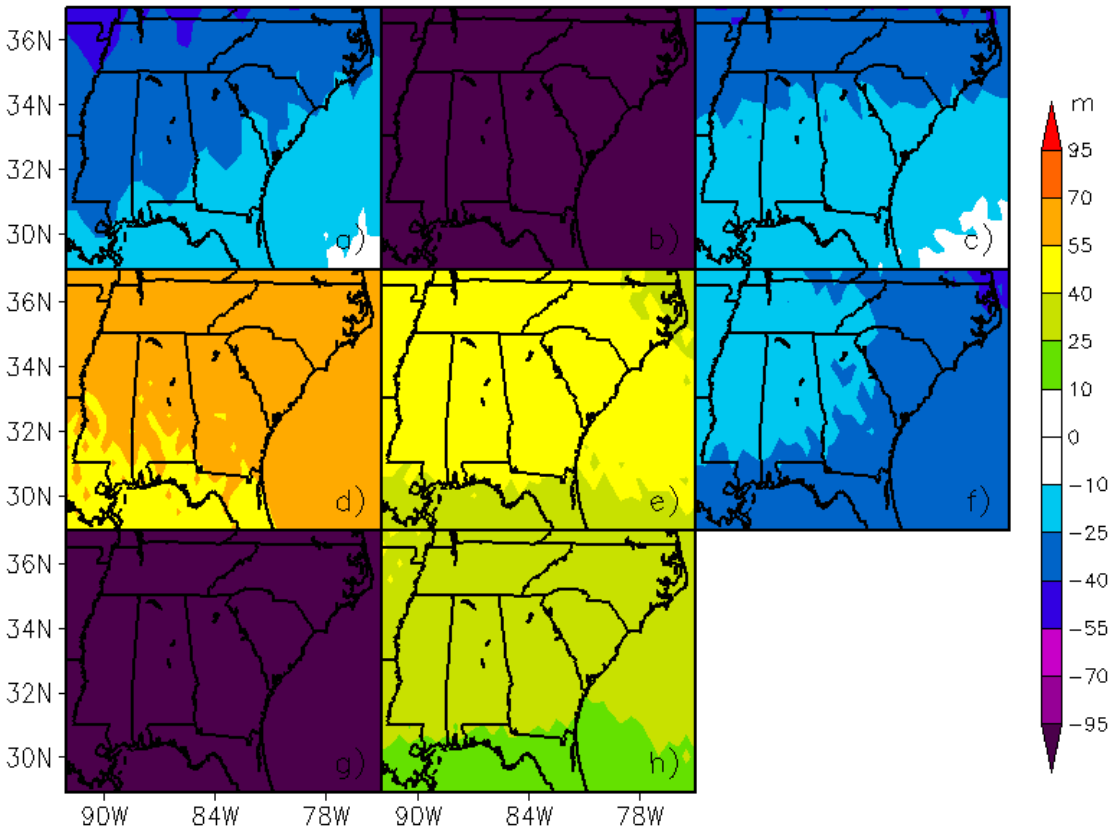

Figure I.7. Individual May 500-mb height anomolies for the WRFG-CGCM3 (a), RCM3-CGCM3 (b), CRCM-CGCM3 (c), MM5I-CCSM (d), CRCM-CCSM (e), ECP2-GFDL (f), RCM3-GFDL (g), and GFDL-timeslice (h) NARCCAP models.

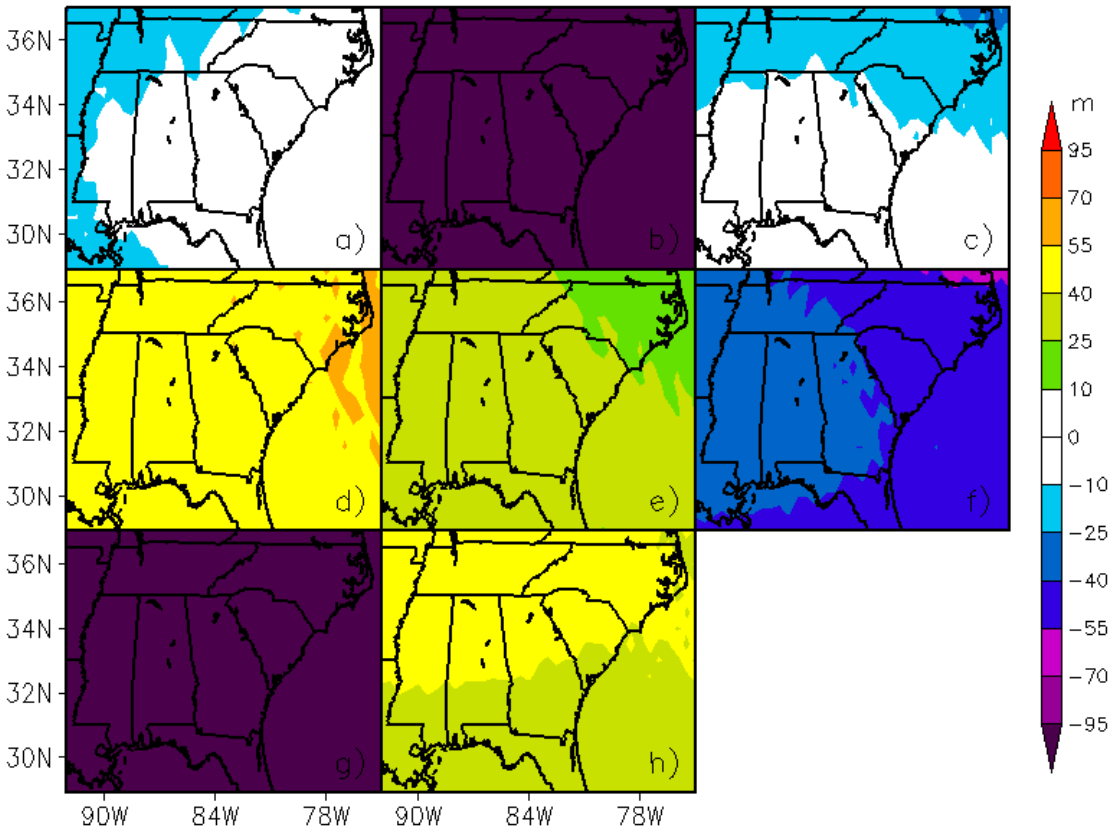

Figure I.8. Individual June 500-mb height anomolies for the WRFG-CGCM3 (a), RCM3-CGCM3 (b), CRCM-CGCM3 (c), MM5I-CCSM (d), CRCM-CCSM (e), ECP2-GFDL (f), RCM3-GFDL (g), and GFDL-timeslice (h) NARCCAP models.

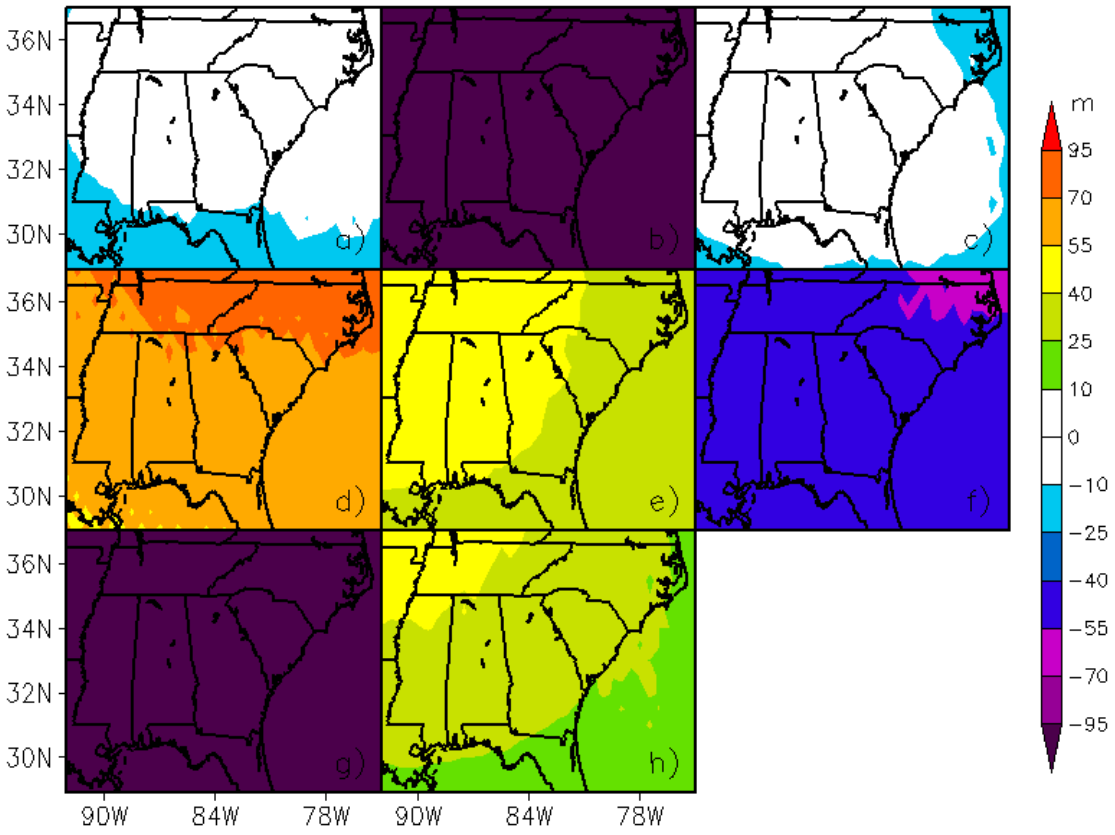

Figure I.9. Individual July 500-mb height anomolies for the WRFG-CGCM3 (a), RCM3-CGCM3 (b), CRCM-CGCM3 (c), MM5I-CCSM (d), CRCM-CCSM (e), ECP2-GFDL (f), RCM3-GFDL (g), and GFDL-timeslice (h) NARCCAP models.

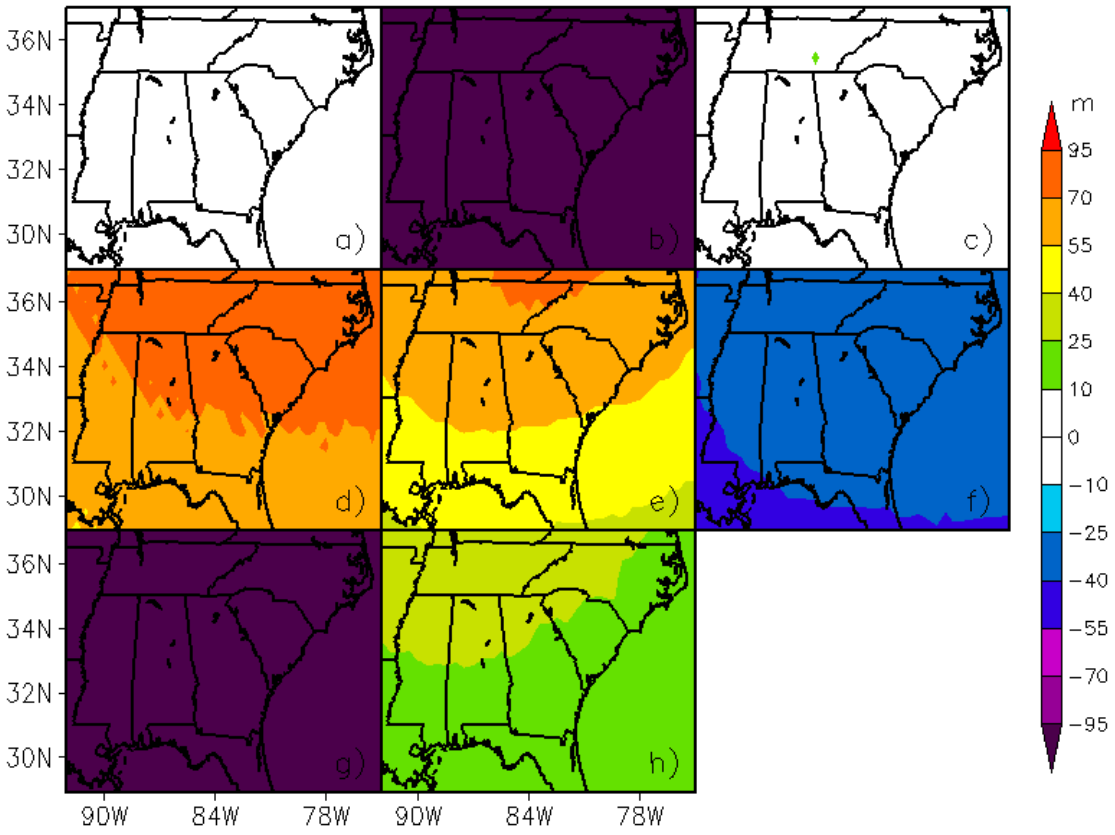

Figure I.10. Individual August 500-mb height anomolies for the WRFG-CGCM3 (a), RCM3-CGCM3 (b), CRCM-CGCM3 (c), MM5I-CCSM (d), CRCM-CCSM (e), ECP2-GFDL (f), RCM3-GFDL (g), and GFDL-timeslice (h) NARCCAP models.

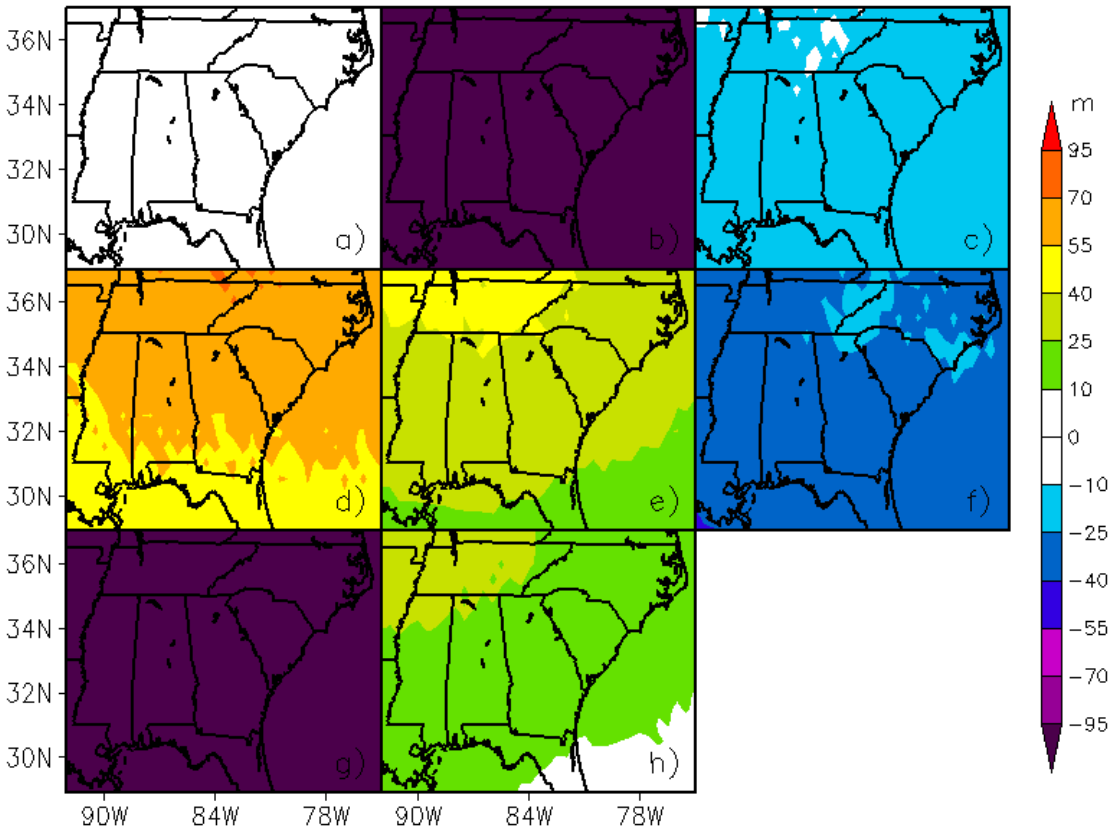

Figure I.11. Individual September 500-mb height anomolies for the WRFG-CGCM3 (a), RCM3-CGCM3 (b), CRCM-CGCM3 (c), MM5I-CCSM (d), CRCM-CCSM (e), ECP2-GFDL (f), RCM3-GFDL (g), and GFDL-timeslice (h) NARCCAP models.

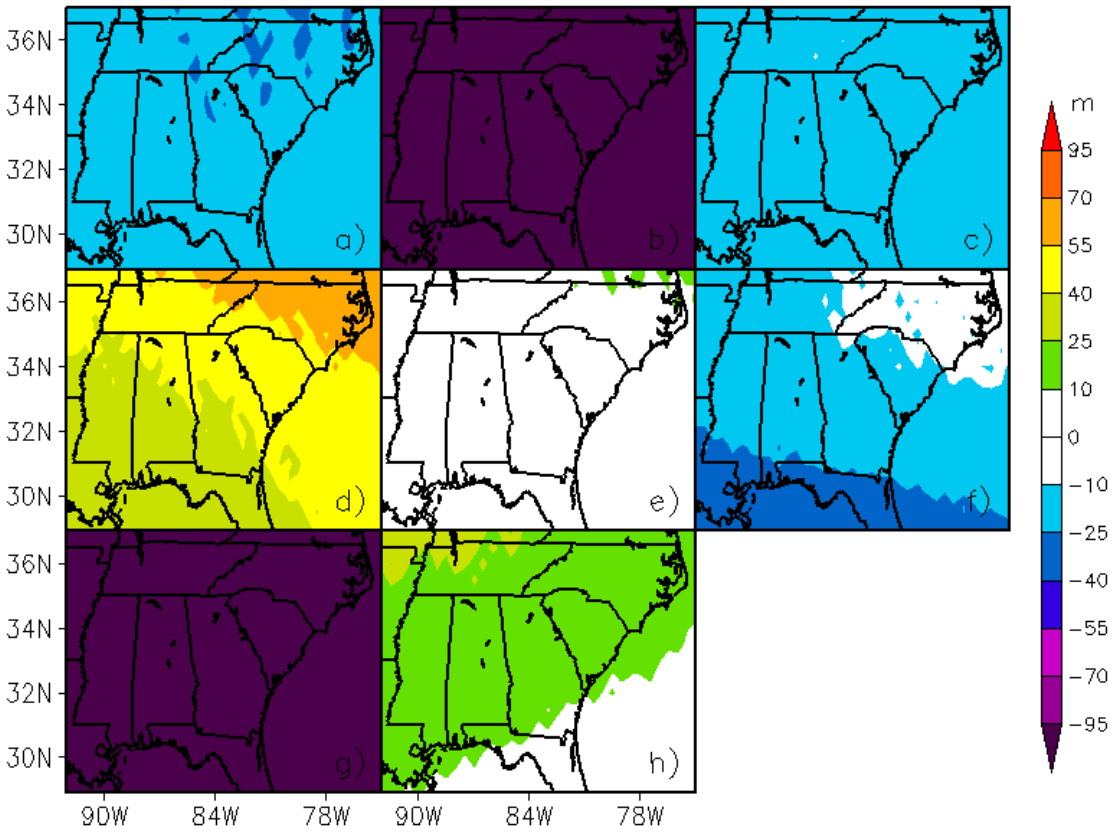

Figure I.12. Individual October 500-mb height anomolies for the WRFG-CGCM3 (a), RCM3-CGCM3 (b), CRCM-CGCM3 (c), MM5I-CCSM (d), CRCM-CCSM (e), ECP2-GFDL (f), RCM3-GFDL (g), and GFDL-timeslice (h) NARCCAP models.

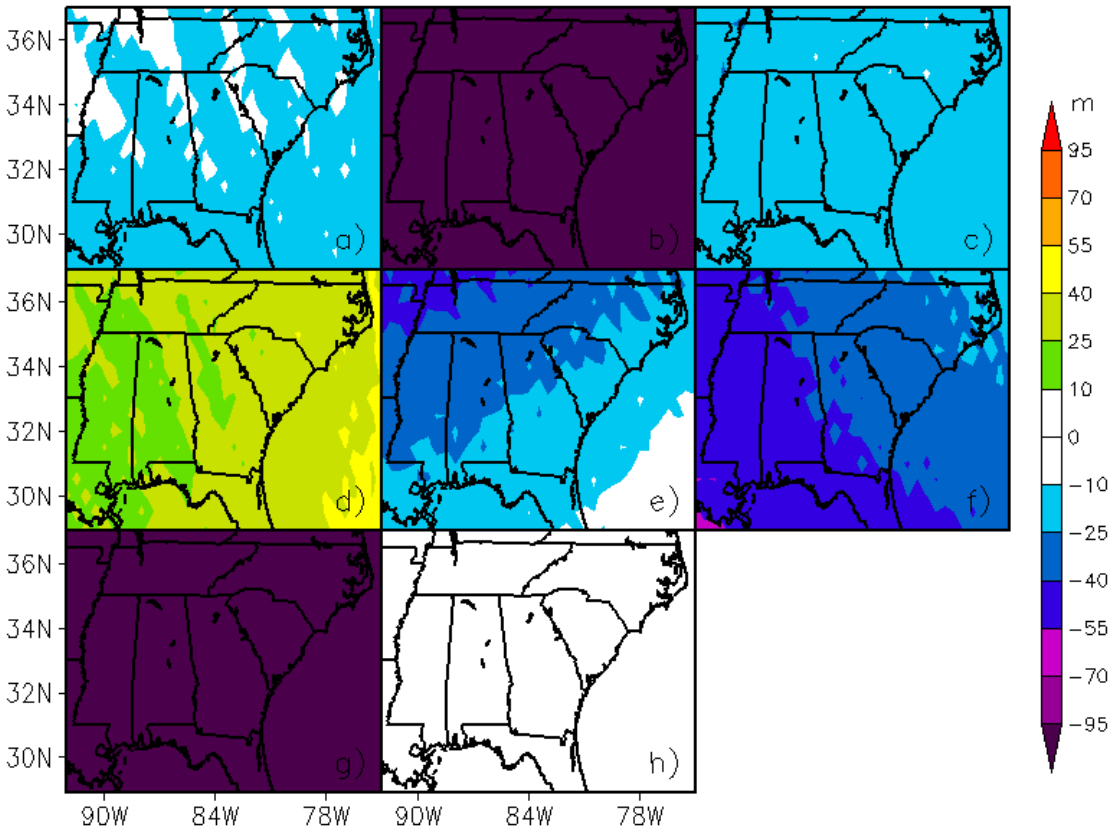

Figure I.13. Individual November 500-mb height anomolies for the WRFG-CGCM3 (a), RCM3-CGCM3 (b), CRCM-CGCM3 (c), MM5I-CCSM (d), CRCM-CCSM (e), ECP2-GFDL (f), RCM3-GFDL (g), and GFDL-timeslice (h) NARCCAP models.

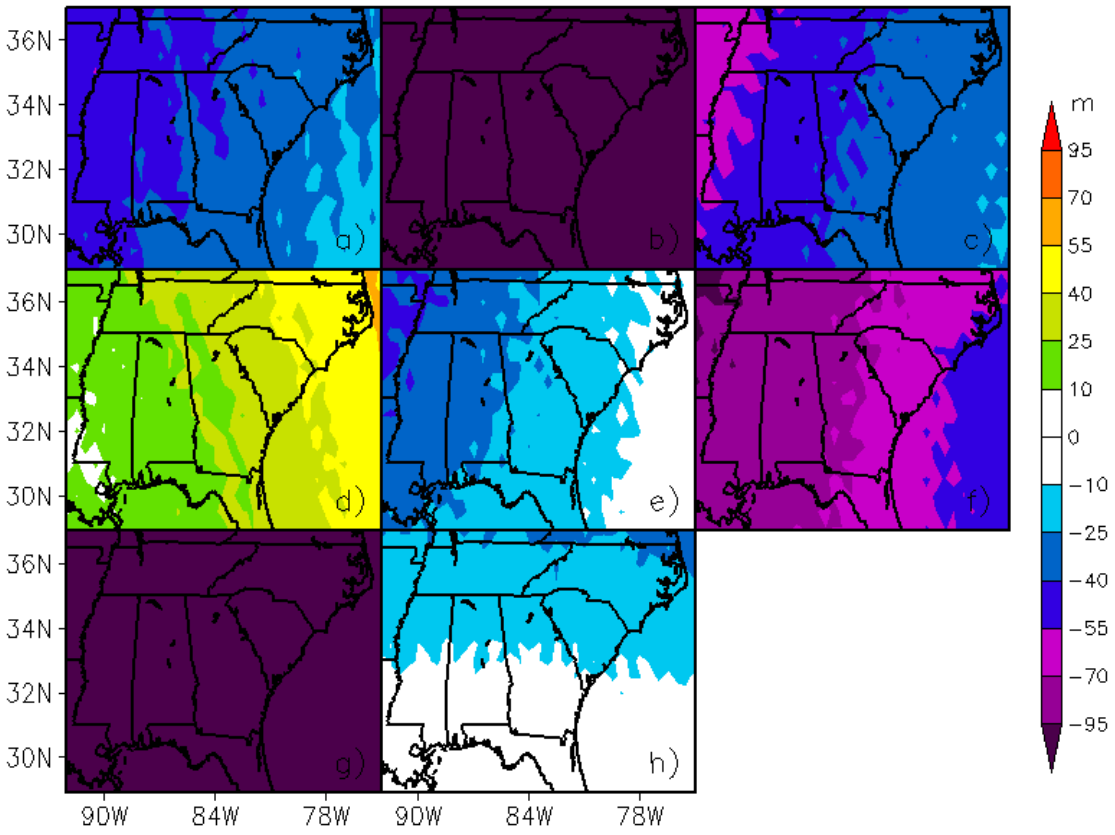

Figure I.14. Individual December 500-mb height anomolies for the WRFG-CGCM3 (a), RCM3-CGCM3 (b), CRCM-CGCM3 (c), MM5I-CCSM (d), CRCM-CCSM (e), ECP2-GFDL (f), RCM3-GFDL (g), and GFDL-timeslice (h) NARCCAP models.

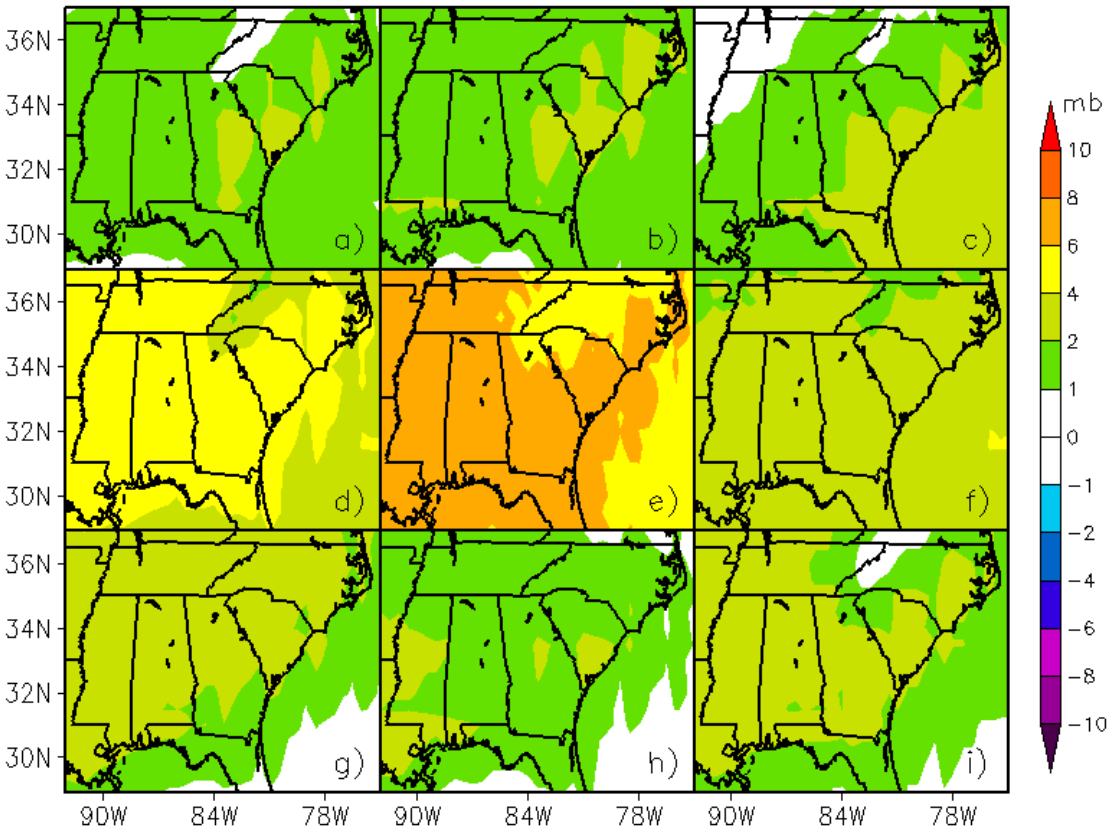

Figure I.15. Individual January sea-level pressure anomolies for the WRFG-CGCM3 (a), RCM3-CGCM3 (b), CRCM-CGCM3 (c), WRFG-CCSM (d), MM5I-CCSM (e), CRCM-CCSM (f), ECP2-GFDL (g), RCM3-GFDL (h), and GFDL-timeslice (i) NARCCAP models.

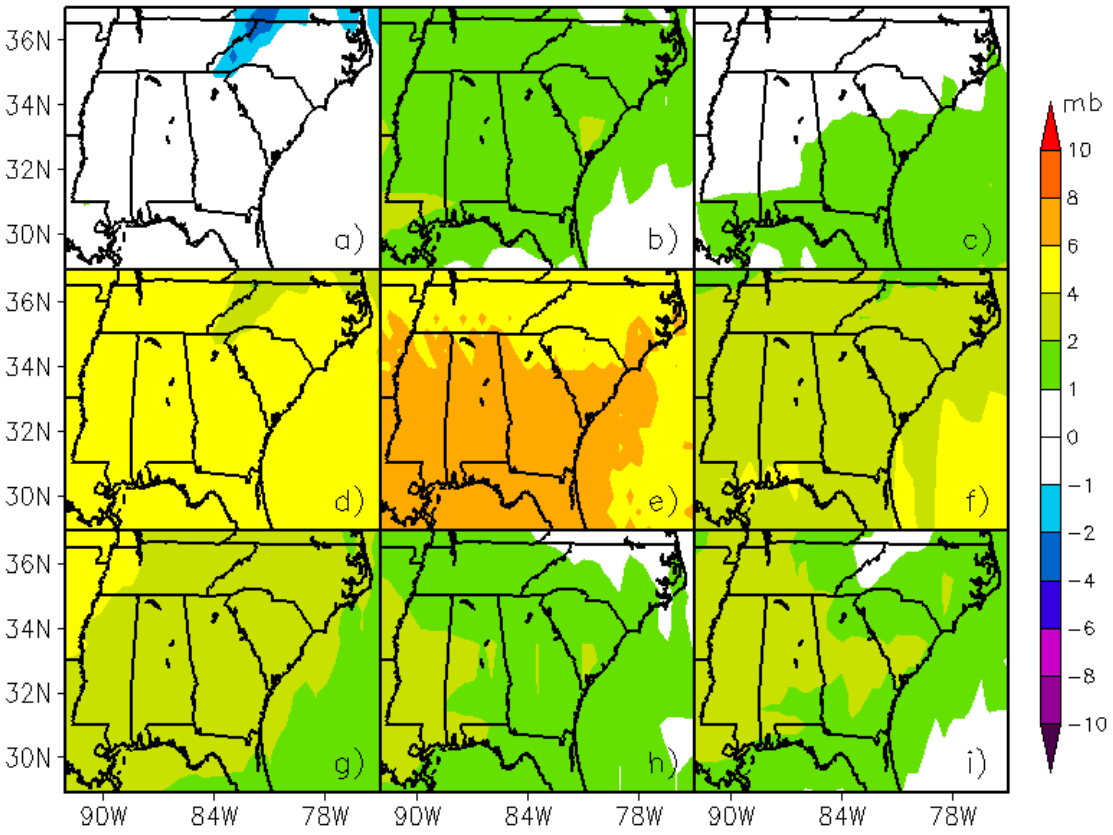

Figure I.16. Individual February sea-level pressure anomolies for the WRFG-CGCM3 (a), RCM3-CGCM3 (b), CRCM-CGCM3 (c), WRFG-CCSM (d), MM5I-CCSM (e), CRCM-CCSM (f), ECP2-GFDL (g), RCM3-GFDL (h), and GFDL-timeslice (i) NARCCAP models.

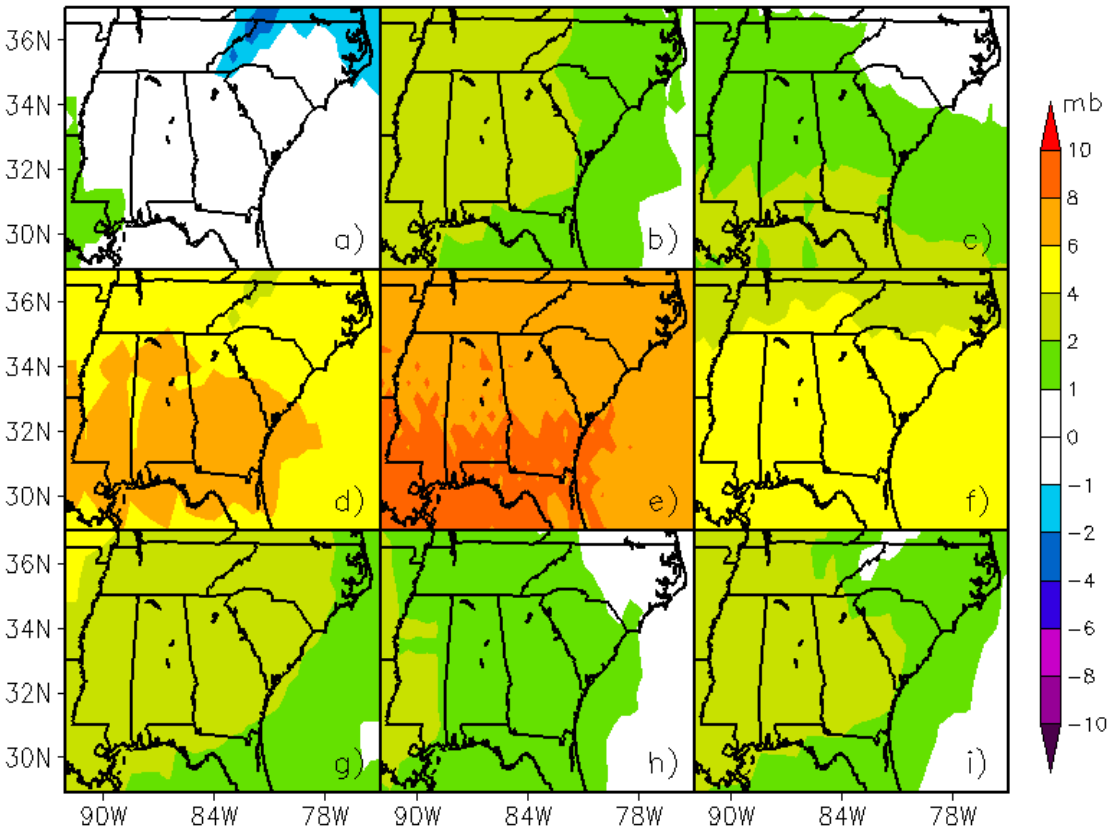

Figure I.17. Individual March sea-level pressure anomolies for the WRFG-CGCM3 (a), RCM3-CGCM3 (b), CRCM-CGCM3 (c), WRFG-CCSM (d), MM5I-CCSM (e), CRCM-CCSM (f), ECP2-GFDL (g), RCM3-GFDL (h), and GFDL-timeslice (i) NARCCAP models.

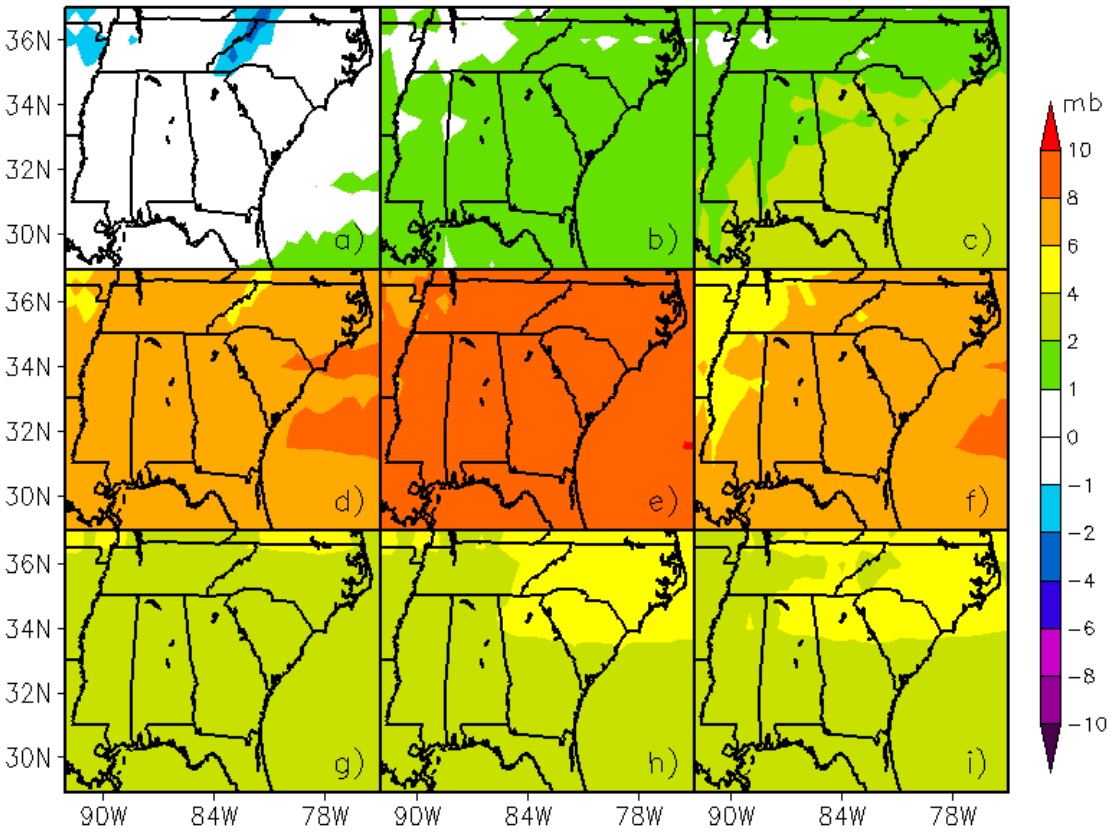

Figure I.18. Individual April sea-level pressure anomolies for the WRFG-CGCM3 (a), RCM3-CGCM3 (b), CRCM-CGCM3 (c), WRFG-CCSM (d), MM5I-CCSM (e), CRCM-CCSM (f), ECP2-GFDL (g), RCM3-GFDL (h), and GFDL-timeslice (i) NARCCAP models.

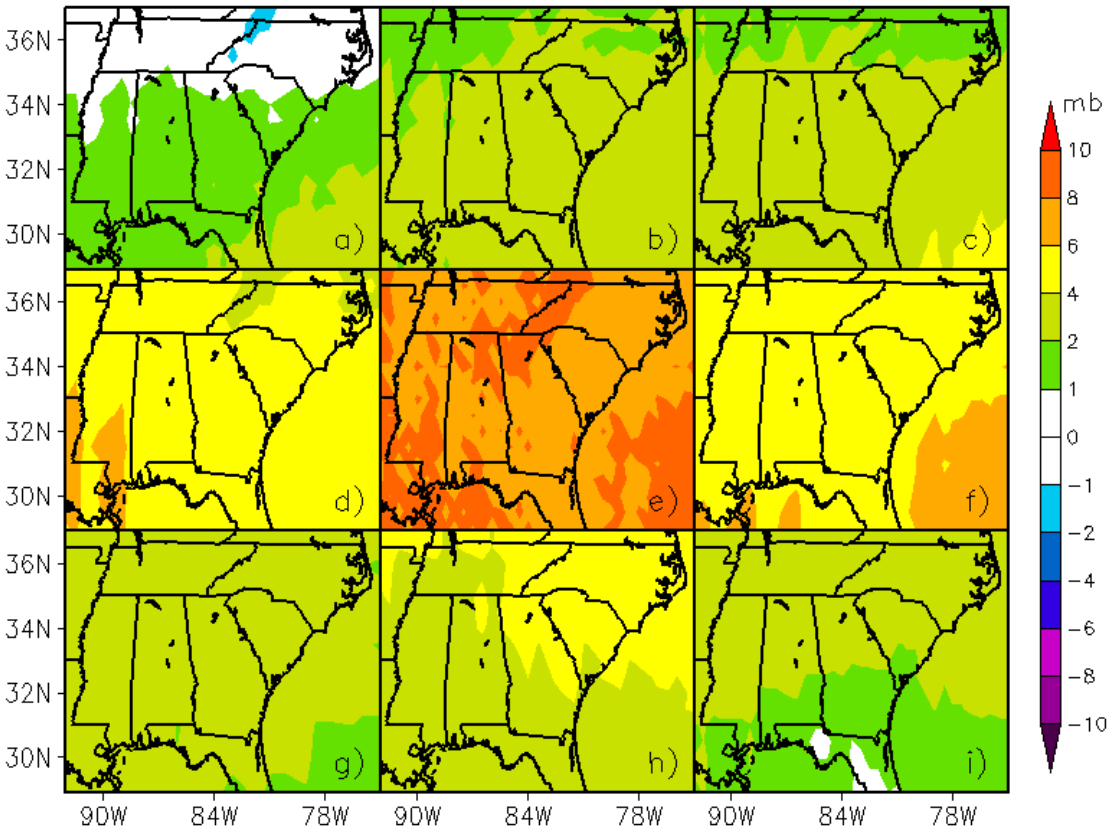

Figure I.19. Individual May sea-level pressure anomolies for the WRFG-CGCM3 (a), RCM3-CGCM3 (b), CRCM-CGCM3 (c), WRFG-CCSM (d), MM5I-CCSM (e), CRCM-CCSM (f), ECP2-GFDL (g), RCM3-GFDL (h), and GFDL-timeslice (i) NARCCAP models.

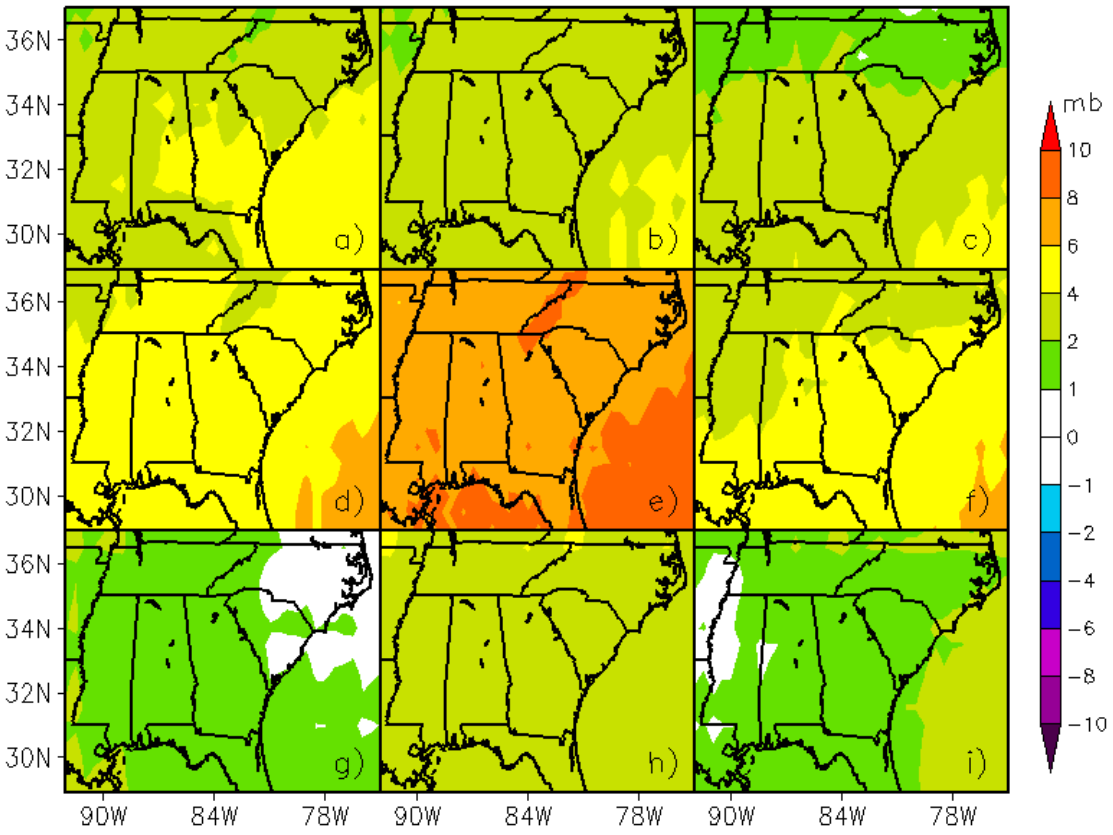

Figure I.20. Individual June sea-level pressure anomolies for the WRFG-CGCM3 (a), RCM3-CGCM3 (b), CRCM-CGCM3 (c), WRFG-CCSM (d), MM5I-CCSM (e), CRCM-CCSM (f), ECP2-GFDL (g), RCM3-GFDL (h), and GFDL-timeslice (i) NARCCAP models.

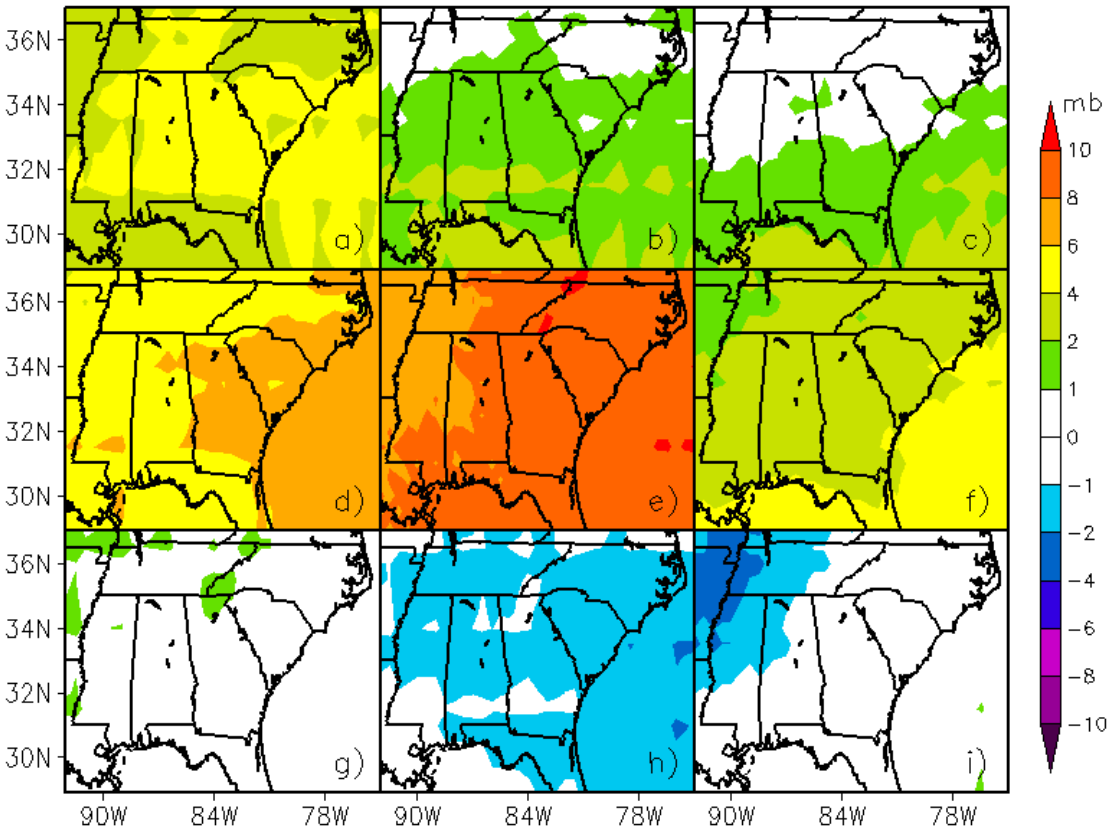

Figure I.21. Individual July sea-level pressure anomolies for the WRFG-CGCM3 (a), RCM3-CGCM3 (b), CRCM-CGCM3 (c), WRFG-CCSM (d), MM5I-CCSM (e), CRCM-CCSM (f), ECP2-GFDL (g), RCM3-GFDL (h), and GFDL-timeslice (i) NARCCAP models.

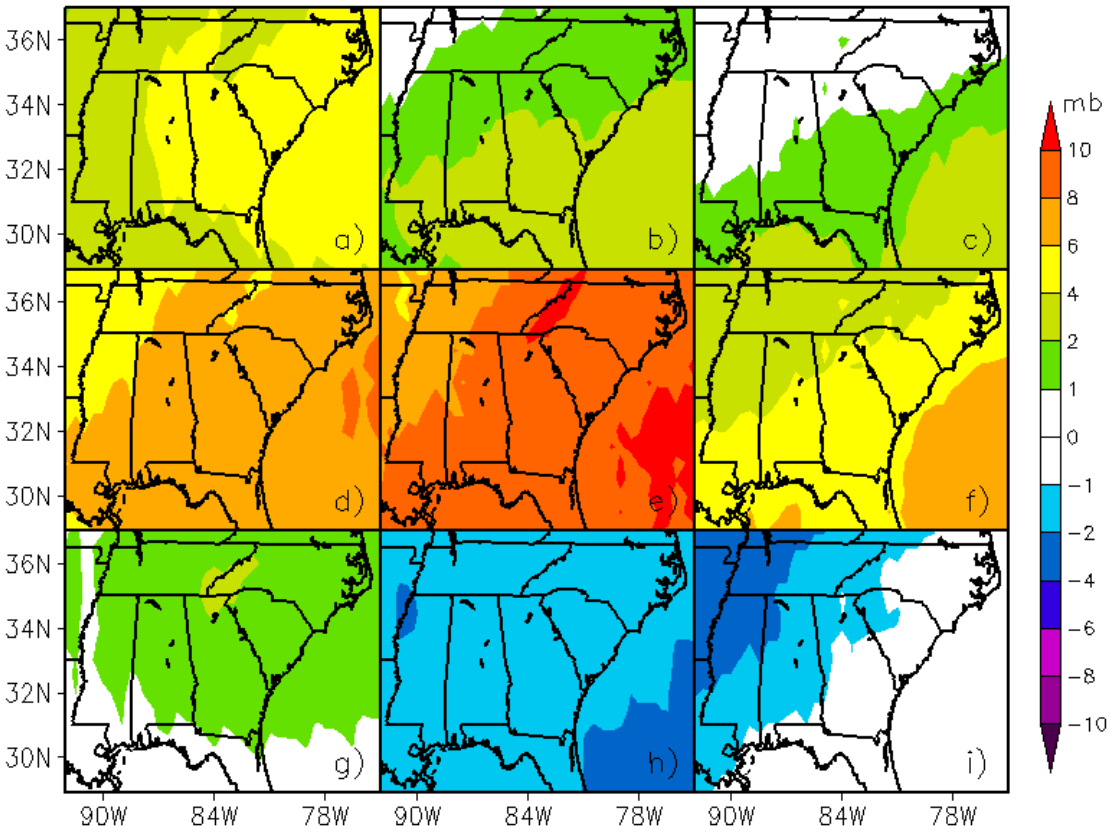

Figure I.22. Individual August sea-level pressure anomolies for the WRFG-CGCM3 (a), RCM3-CGCM3 (b), CRCM-CGCM3 (c), WRFG-CCSM (d), MM5I-CCSM (e), CRCM-CCSM (f), ECP2-GFDL (g), RCM3-GFDL (h), and GFDL-timeslice (i) NARCCAP models.

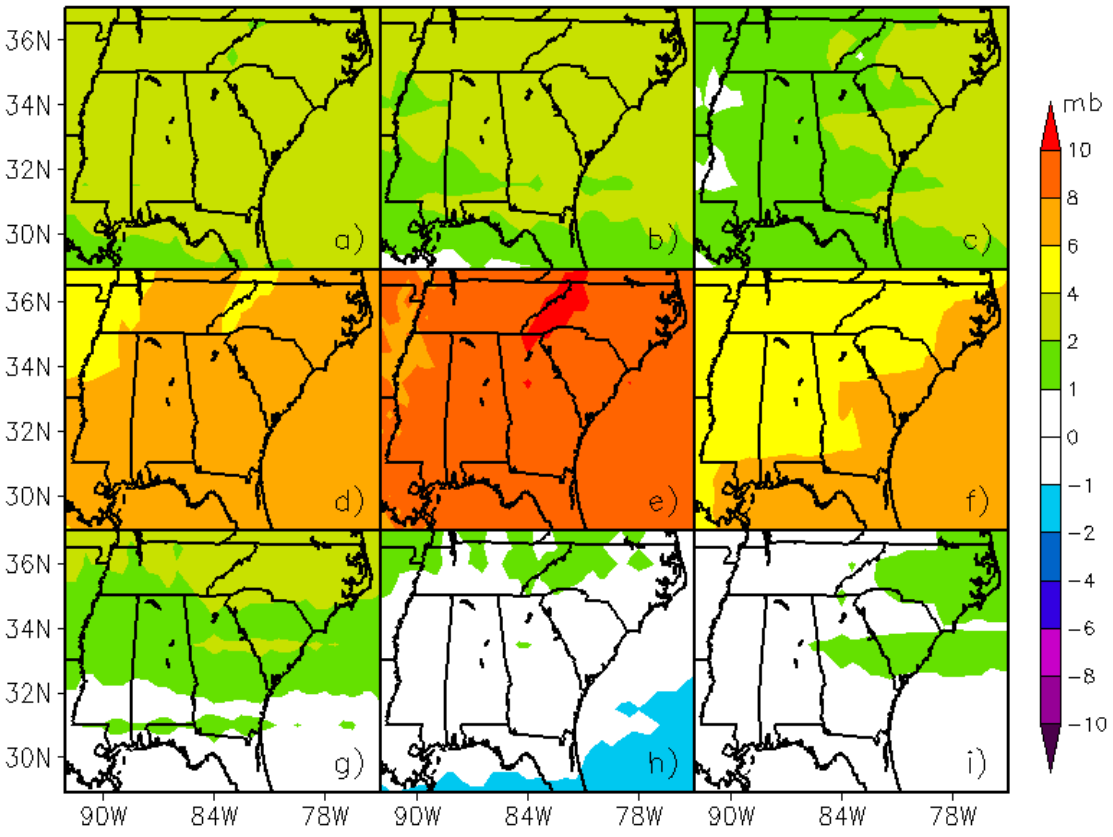

Figure I.23. Individual September sea-level pressure anomolies for the WRFG-CGCM3 (a), RCM3-CGCM3 (b), CRCM-CGCM3 (c), WRFG-CCSM (d), MM5I-CCSM (e), CRCM-CCSM (f), ECP2-GFDL (g), RCM3-GFDL (h), and GFDL-timeslice (i) NARCCAP models.

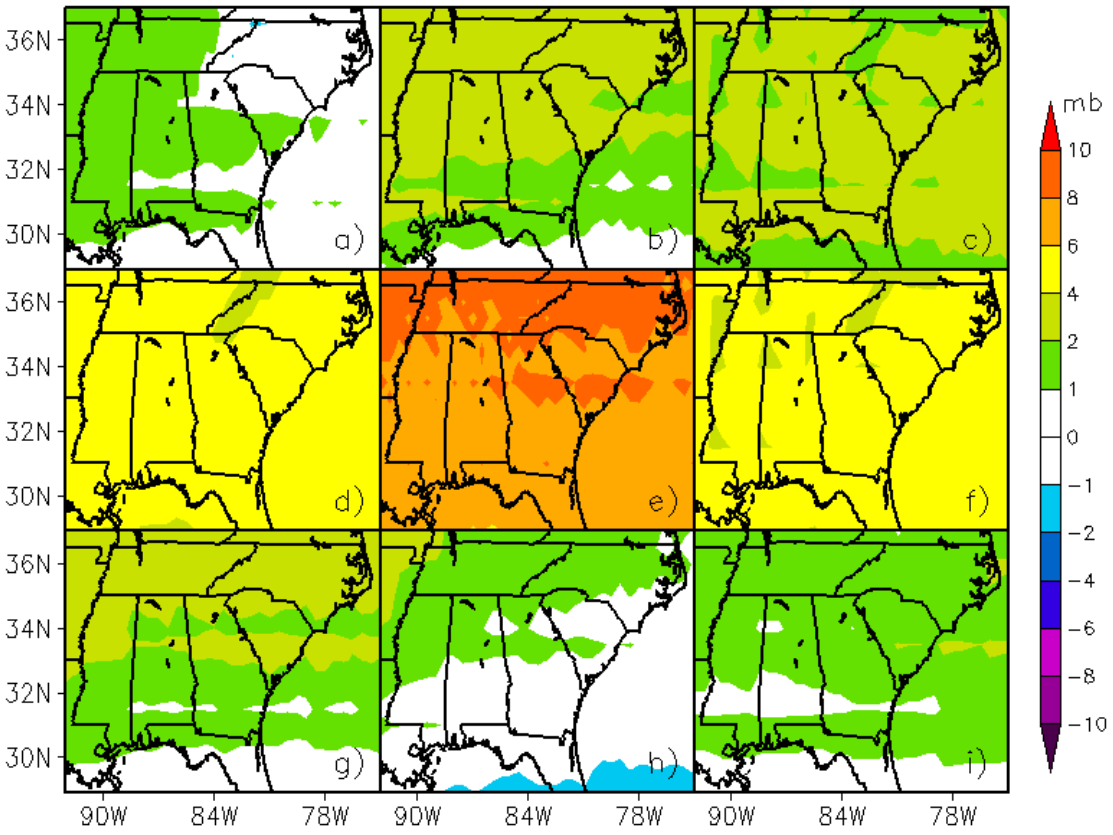

Figure I.24. Individual October sea-level pressure anomolies for the WRFG-CGCM3 (a), RCM3-CGCM3 (b), CRCM-CGCM3 (c), WRFG-CCSM (d), MM5I-CCSM (e), CRCM-CCSM (f), ECP2-GFDL (g), RCM3-GFDL (h), and GFDL-timeslice (i) NARCCAP models.

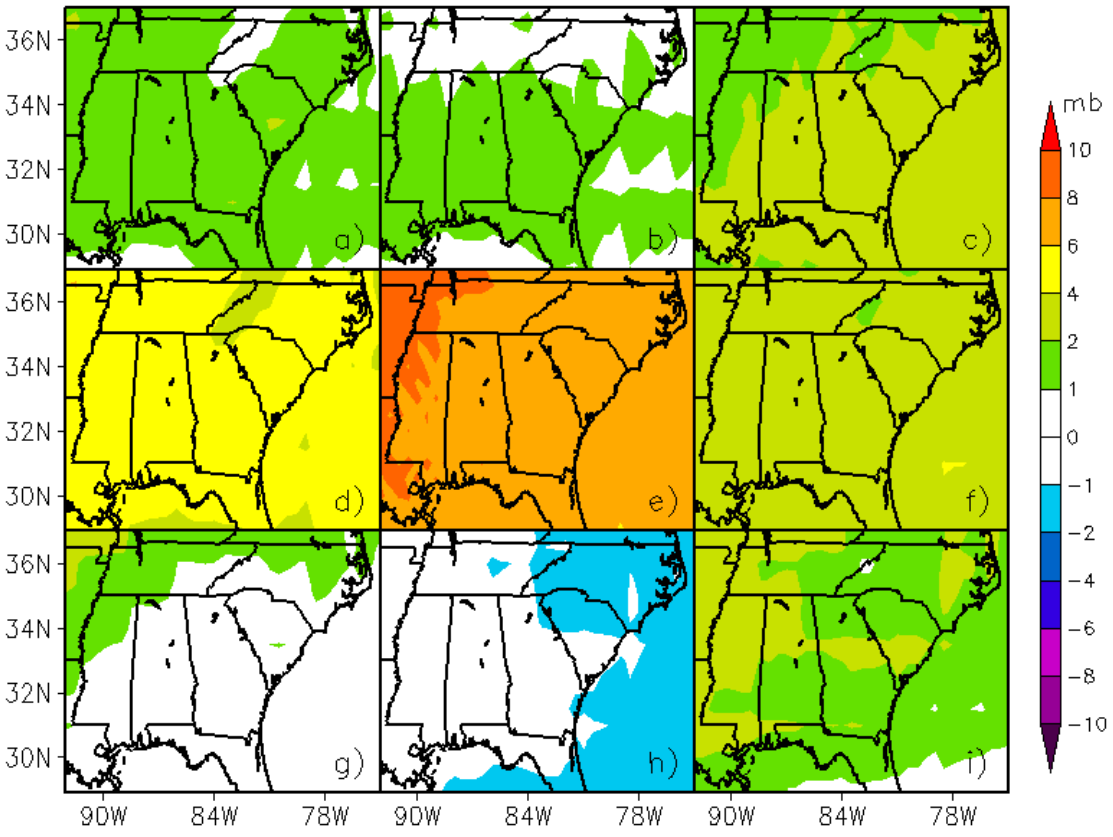

Figure I.25. Individual November sea-level pressure anomolies for the WRFG-CGCM3 (a), RCM3-CGCM3 (b), CRCM-CGCM3 (c), WRFG-CCSM (d), MM5I-CCSM (e), CRCM-CCSM (f), ECP2-GFDL (g), RCM3-GFDL (h), and GFDL-timeslice (i) NARCCAP models.

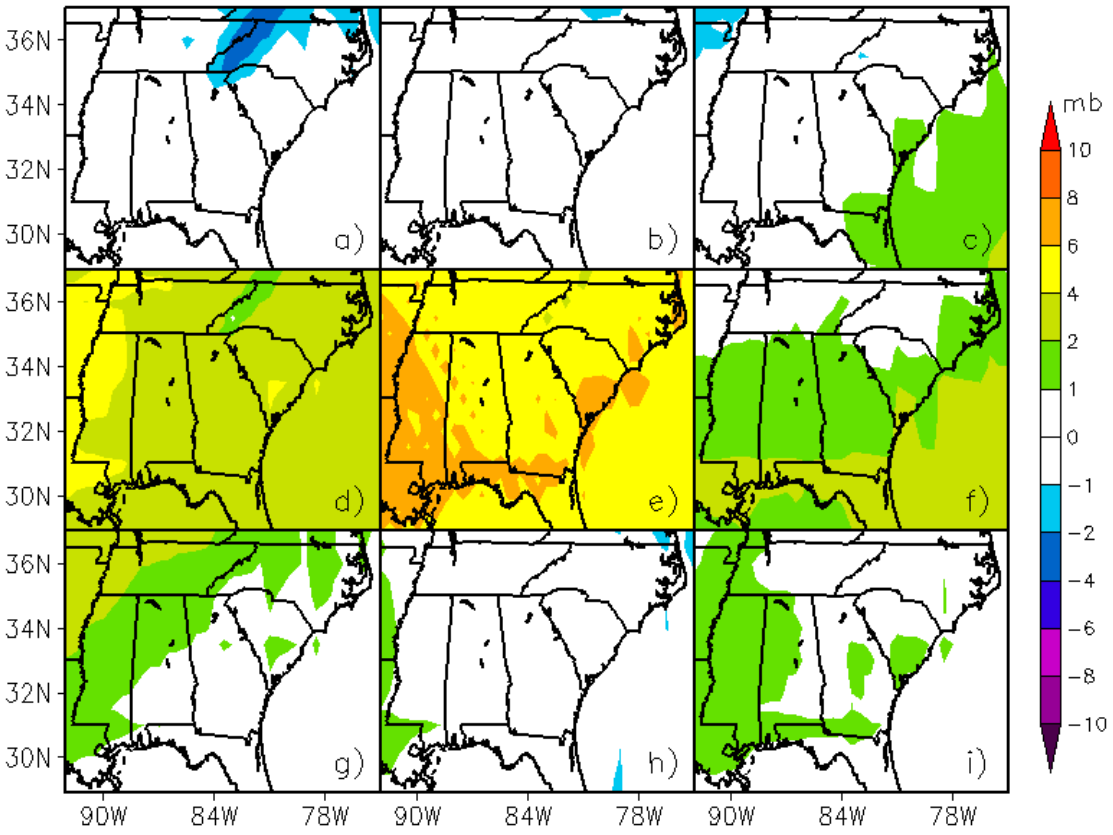

Figure I.26. Individual December sea-level pressure anomolies for the WRFG-CGCM3 (a), RCM3-CGCM3 (b), CRCM-CGCM3 (c), WRFG-CCSM (d), MM5I-CCSM (e), CRCM-CCSM (f), ECP2-GFDL (g), RCM3-GFDL (h), and GFDL-timeslice (i) NARCCAP models.